REPORT

ST15452 Flemish Pass Geotechnical Investigation

DATA INTERPRETATION AND EVALUATION

DOC.NO. 20140857-02-R
REV.NO. 1 / 2016-05-30

NORWEGIAN GEOTECHNICAL INSTITUTE
NGI.NO

Project

Project title:	ST15452 Flemish Pass Geotechnical Investigation
Document title:	Data interpretation and evaluation
Document no.:	20140857-02-R
Date:	2016-05-24
Revision no. /rev. date:	1 / 2016-05-30

Client

Client:	Benthic
Client contact person:	Mike Powell
Contract reference:	Sub-contract signed 26th March 2015

Operator

Operator:	Statoil Canada Ltd.
Contact person:	Martine Helena de Vries

for NGI

Project manager:	Victor Smith
Prepared by:	Victor Smith, Vishal Dantal, Siren Knudsen, Knut Schjetne, Maarten Vanneste, Carl Fredrik Forsberg
Reviewed by:	Tom Lunne

Summary

The Flemish Pass Geotechnical Investigation provides understanding of the geological history of the Flemish Pass and geotechnical input for use in studies and design work at the site. This report discusses the geological history including dating and geomorphological processes of the area with particular focus on submarine instabilities. It also discusses and analyses the geotechnical information and presents recommended representative profiles. The soil conditions are layered, lightly over consolidated silty clay. There are some sand layers and frequent stones, gravel and larger, throughout the area and depth. Mass transport deposits are encountered at various depths across the field.

ST15452 FLEMISH PASS GEOTECHNICAL INVESTIGATION

FIELD OPERATIONS AND PRELIMINARY RESULTS Reported by Benthic (Benthic 2015a & 2015b)	20140857-01-R MEASURED AND DERIVED GEOTECHNICAL PARAMETERS AND FINAL RESULTS	20140857-02-R DATA INTERPRETATION AND EVALUATION OF REPRESENTATIVE GEOTECHNICAL PARAMETERS
	A Investigated Locations and Scope of Work **B** List of Symbols and Terms Used **C** Soil Description and Geotechnical Boring Logs **D** Cone Penetration Tests (Benthic) **E** Classification Tests **F** Oedometer Tests **G** Triaxial Tests **H** Direct Simple Shear Tests **I** Bender Element Tests **J** Age dating Tests **K** Geochemical Tests **L** X-ray **M** Description of Laboratory Test Procedures **N** References	**A** Investigated Locations and Scope of Work **B** Intent of the Investigation **C** Summary of Soil Conditions **D** List of symbols and Terms Used **E** Interpretation of Geological and Geophysical Data **F** Interpretation and Evaluation of Geotechnical Data **G** Recommended Representative Geotechnical Parameters, Field centre **H** Recommended Representative Geotechnical Parameters, Slopes **I** Recommendations on additional data **J** References

White background means current report

Field operations and preliminary results are presented by Benthic

Section A

INVESTIGATED LOCATIONS AND SCOPE OF WORK

Contents

Table

Figures

A1 General

This section contains a description of the sites and the objective of the soil investigation carried out for the ST15452 Flemish Pass Soil Investigation on the Canadian continental shelf in the Atlantic Ocean. A map of the general area is shown in Figure A1.1.

A2 Investigated locations

A vicinity map and location plan of the Flemish Pass Geotechnical investigation are shown in Figure A2.1. All West Slope locations are shown in Figure A2.2 and all Field Centre and East Slope locations are shown in Figure A2.3.

The fieldwork was carried out in August and September 2015. The geotechnical sampling and testing was done using the remotely operated seabed system PROD 2 from the dynamically positioned vessel Mærsk Chancellor. The soil investigation consisted of 10 locations with a total of 24 investigated boreholes. The maximum investigated depth at each location range from 26.7 m to 101.0 m below mudline. The samples were sent to NGIs onshore laboratory in Oslo for the onshore laboratory testing.

Table A2-1 presents the coordinates and water depths at the investigated positions. The water depth varies between 675 m and 1172 m and is indicated by colour shading based on bathymetric data.

A3 Scope of work

The objective of the soil investigation is threefold. It is to provide an understanding of the geologic history of the area including the history of sliding, to provide parameters for a geohazard study and to provide parameters for design of installations in the Field Centre area connected to development of hydrocarbon fields in the area.

The offshore site investigation scope of work was designed and continuously updated to optimize the sample recovery and CPT coverage taking account of the in situ conditions and other external factors. Benthic (2015b) presents various operational details of the offshore site investigation.

The onshore laboratory work and reporting were designed to provide the necessary engineering parameters for a field development in the Field Centre area, while at the same time give necessary input for slope stability calculations in the East and West Slopes and the geological history of the area. This report present the interpretation of the geotechnical and geophysical data and present recommendations. All the factual geotechnical data is presented in NGI (2016).

Table A2-1 Coordinates and water depths at all investigated locations

Location	Eastings [m]	Northings [m]	Water depth [m]	Area designation
ST15452-CPT-02	820532.5	5330384.6	875.4	West Slope
ST15452-S-03	813893.6	5326044.8	758.2	West Slope
ST15452-CPT-03	813887.8	5326028.7	758.3	West Slope
ST15452-S-05	840871.0	5325480.4	1162.9	West Slope
ST15452-S-05a	840872.3	5325468.8	1163.9	Field Centre
ST15452-CPT-05	840868.0	5325472.5	1163.7	Field Centre
ST15452-S-07	810252.0	5324989.0	675.1	West Slope
ST15452-CPT-07	810246.0	5324972.7	675.4	West Slope
ST15452-CPT-07a	810248.2	5324968.4	675.9	West Slope
ST15452-CPT-07b	810255.0	5324978.7	675.9	West Slope
ST15452-BH-08a	815969.8	5317827.8	791.1	West Slope
ST15452-CPT-08	815960.5	5317822.4	791.1	West Slope
ST15452-CPT-08a	815973.8	5317817.0	791.1	West Slope
ST15452-BH-12	840770.5	5321194.5	1168.7	Field Centre
ST15452-CPT-12	840768.1	5321202.6	1168.8	Field Centre
ST15452-CPT-15	840773.5	5317131.8	1172.1	Field Centre
ST15452-S-15	840789.2	5317127.1	1172.6	Field Centre
ST15452-CPT-16	810739.5	5324925.3	697.4	West Slope
ST15452-BH-18a	866117.4	5327970.5	1003.4	East Slope
ST15452-CPT-18	866111.0	5327981.4	1004.0	East Slope
ST15452-BH-19	817 452.0	5326080.9	789.2	West Slope
ST15452-CPT-19	817447.3	5326081.2	789.1	West Slope
ST15452-PIEZ-18a	866104.6	5327978.0	1003.5	East Slope
ST15452-PIEZ-08	815959.1	5317830.8	789.1	West Slope

Note: All coordinates in NAD83 UTM Zone 22, CM 51°W,

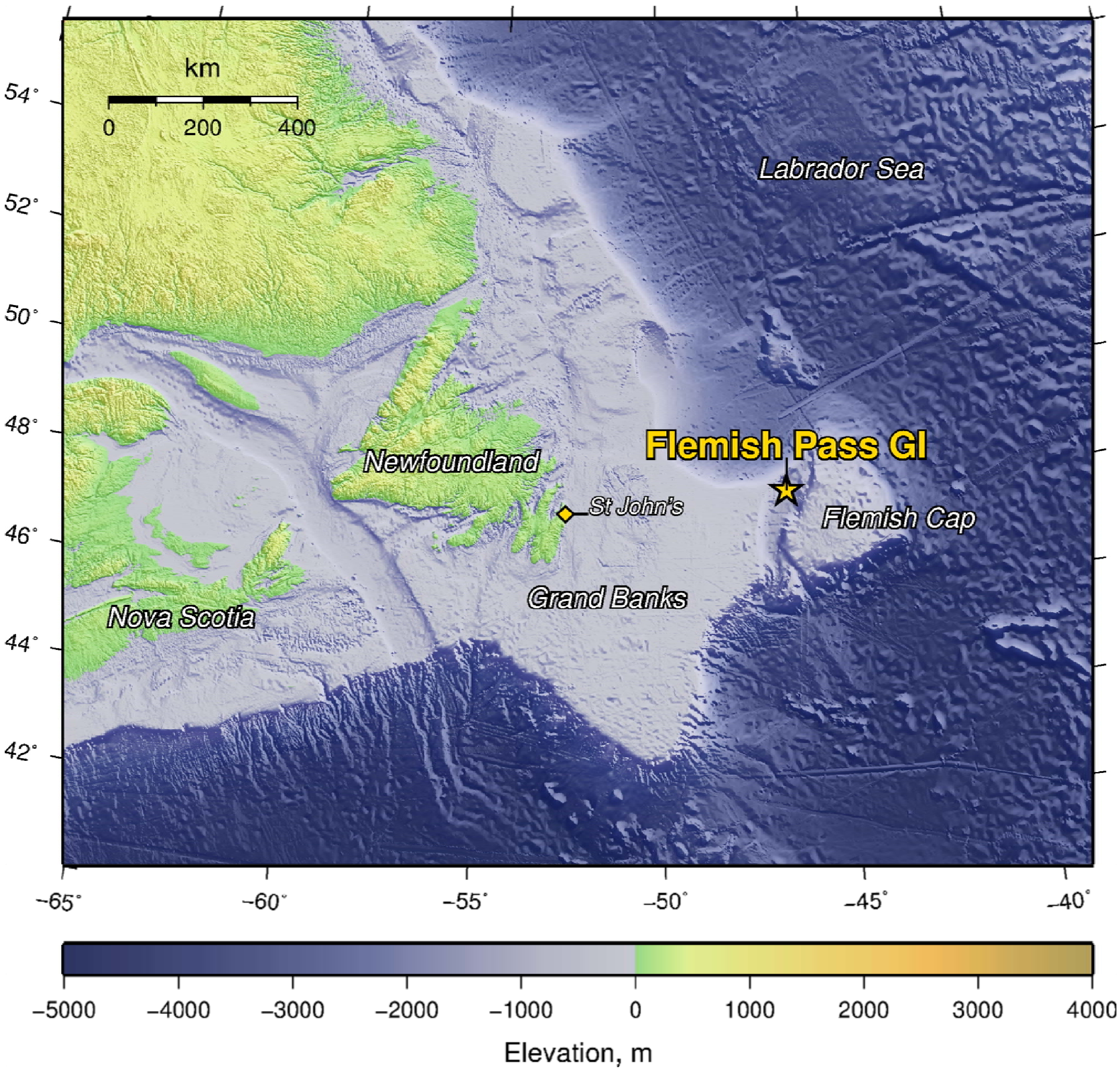

Date/Rev.: 2015-01-21/01

ST15452 Flemish Pass Geotechnical Investigation	Document No. 20140857-02-R	
Regional map	Figure No. A1.1	
	Date 2016-04-01	Drawn by VBS
Map data from ESRI ArcGIS Online World Imagery Basemap	NGI	

P:\2014\08\20140857\Leveransedokumenter\Rapport\20140857-02-R Data interpretation and evaluation\Figures\Section A\Figure A1.1-Regional_map.grf

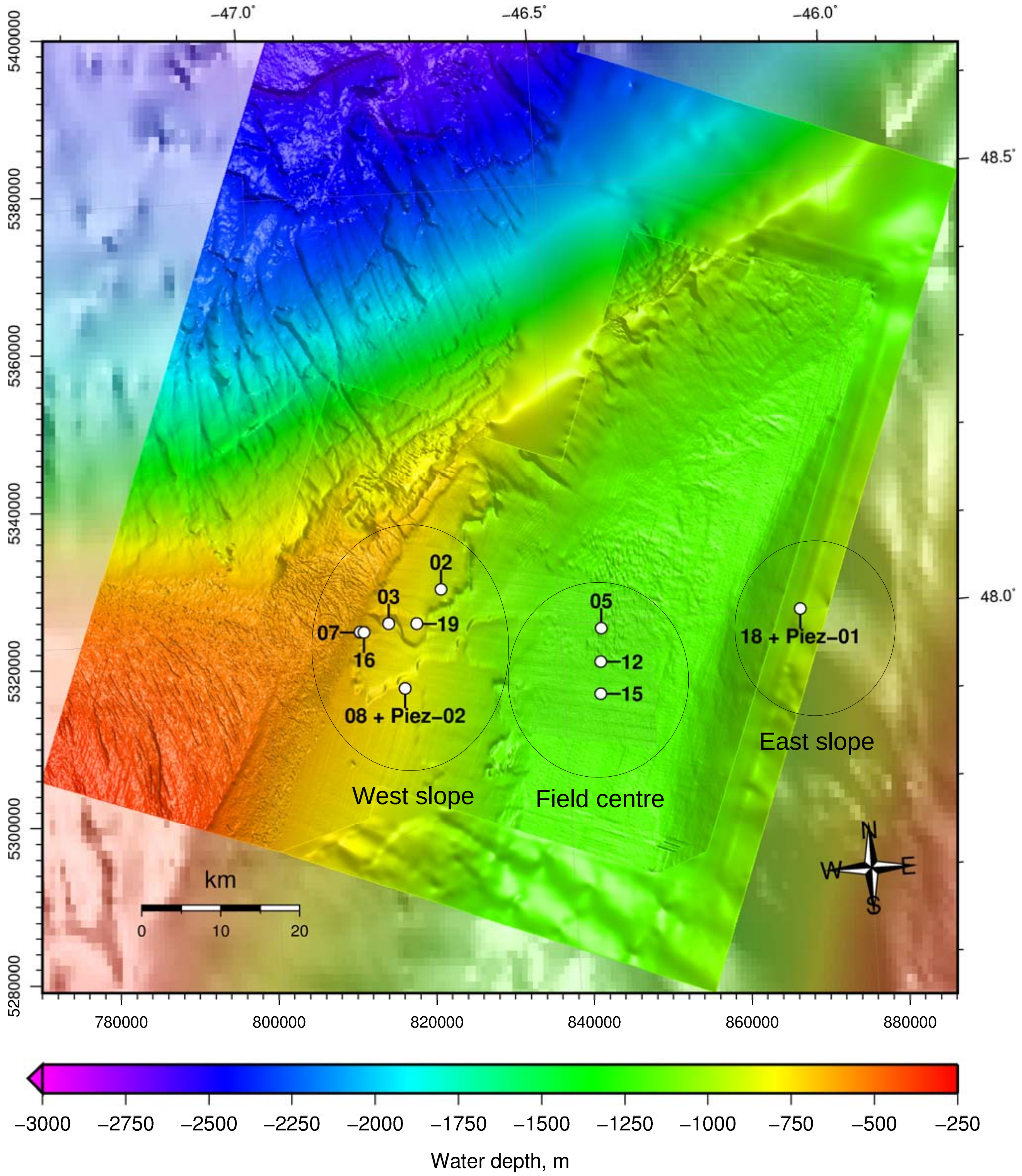

Date/Rev.: 2015-01-21/01

ST15452 Flemish Pass Geotechnical Investigation	Document No. 20140857-02-R
Location plan for Flemish Plass GI Numbers indicate location with the prefix ST15452- abbreviated Coordinate system NAD83 UTM zone 22N	Figure No. A2.1 Date 2016-04-01 / Drawn by VBS

P:\2014\08\20140857\Leveransedokumenter\Rapport\20140857-02-R Data interpretation and evaluation\Figures\Section A\Figure A2.1-Location_plan.grf

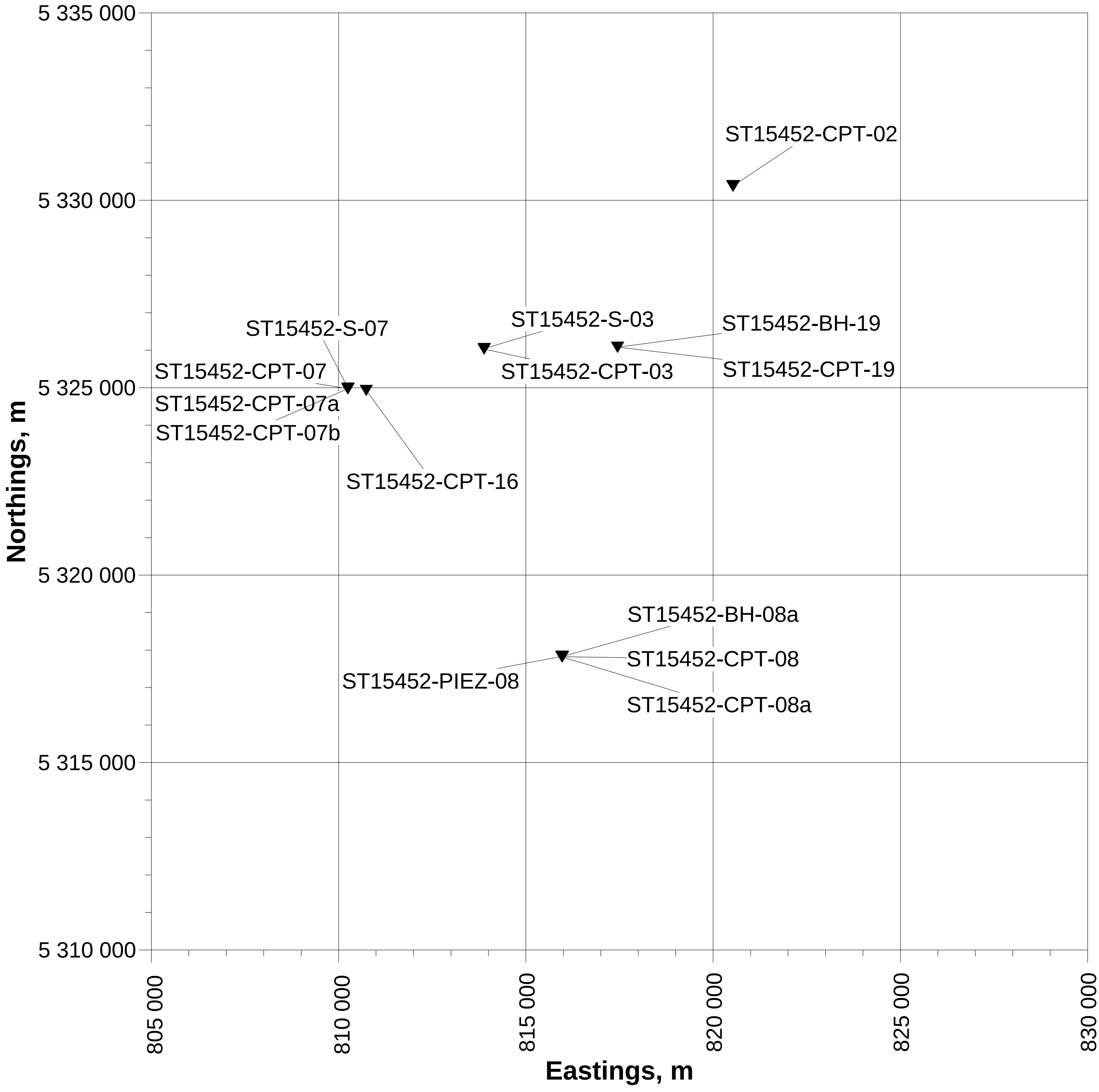

P:\2014\08\20140857\Leveransedokumenter\Rapport\20140857-02-R Data interpretation and evaluation\Figures\Section A\Figure A2.2-West_slope_locations.grf

Date/Rev.: 2015-01-21/01

ST15452 Flemish Pass Geotechnical Investigation	Document No. 20140857-02-R	
West slope locations Coordinate system NAD83 UTM zone 22N	Figure No. A2.2	
	Date 2016-04-01	Drawn by VBS
	NGI	

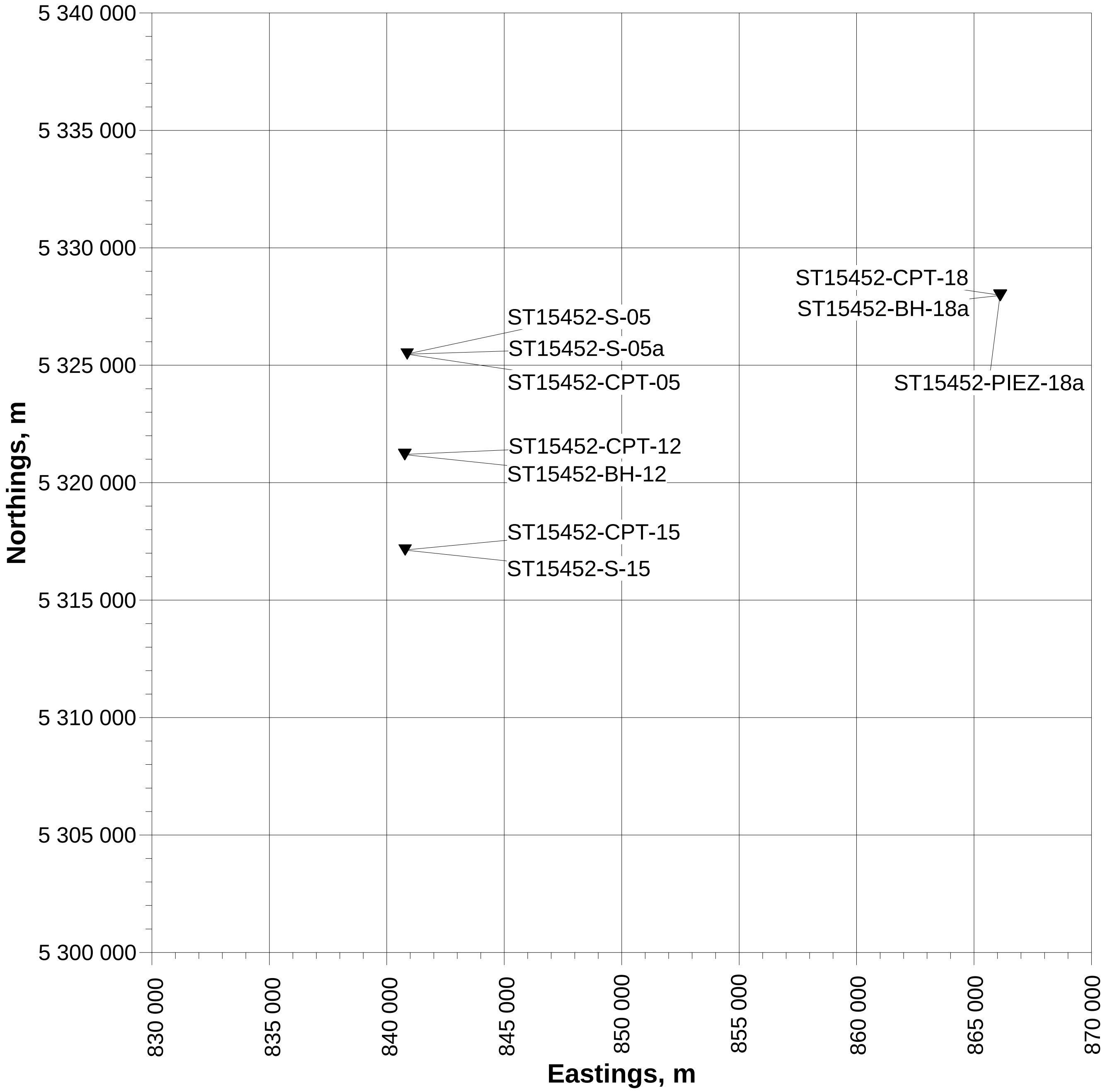

Date/Rev.: 2015-01-21/01

ST15452 Flemish Pass Geotechnical Investigation

Field Centre and East slope locations

Coordinate system NAD83 UTM zone 22N

Document No.	20140857-02-R
Figure No.	A2.3
Date	2016-04-01
Drawn by	VBS

P:\2014\08\20140857\Leveransedokumenter\Rapport\20140857-02-R Data interpretation and evaluation\Figures\Section A\Figure A2.3-Field_centre_and_East_locations.grf

Section B

INTENT OF INVESTIGATION

Contents

B1 General

This section contains a description of the intended use of this report, including the input to foundation design of possible structures and geohazard analyses.

B2 Intended structures

The Flemish Pass development area lies in approximately 1200 m of water. Developing hydrocarbon resources at this location will require installing a series of structures. It is not known at present exactly what will be installed. It is likely that some or all of the following will be part of a development:

- A floating platform anchored to seabed by suction anchors
- Riser bases either standing on seabed on suction caissons or a floating structure anchored to seabed
- Templates standing on suction caissons
- Pipelines, flowlines etc.
- Various structures associated with pipelines like PLETS

The above listed items focus on the foundations. This report presents geotechnical data also intended to form the basis of possible FEED design of such foundations.

B3 Geohazards

The Flemish pass is a gateway between the Great banks of Newfoundland and the Flemish Cap. The geophysical data from the area reveal clear evidence for submarine instabilities in the Flemish Pass, see Section E. The current understanding is that the landsliding spans several hundred thousand years. In relation to the development of the area, it is important to assess the hazard potential of future landslides.

This report discusses the geological and geophysical evidence of instabilities as well as the results of a series of age dating tests that were performed to understand the geomorphology and chronology of previous slide events, and – if possible – tie them to environmental pre-conditioning factors (e.g., variations in sedimentation rates related to climatic cycles) or triggers (e.g., seismicity).

The geological understanding in combination with the geotechnical data forms a basis for a subsequent in depth geohazard assessment, which is beyond the scope of this report.

Section C

SUMMARY OF SOIL CONDITIONS

Contents

Tables

C1 General

This section presents a short summary of the soil conditions found in the Flemish Pass Geotechnical Investigation. The comprehensive discussion of soil conditions and geotechnical parameters are given in Section F, with recommendations summarised in Sections G and H. A designer is referred to those sections.

C2 Soil conditions

The soil at Flemish Pass down to the maximum investigated depth of 100 m below seafloor is in general clay or silty clay. It is affected by the geological history. The soil units used to describe the soil are tied to the geological history, and the difference in geotechnical properties between the units is at times subtle. Four soil units have been defined in the Flemish Pass Geotechnical Investigation. Table C2-1 gives a general description of the four soil units.

Table C2-1 Summary of the generalised soil units

Unit	Soil description
I	CLAY, silty, extremely low to low strength, traces of fine to medium sand partings. Sandy in the upper 20 cm in some locations.
II	CLAY, low to medium strength, seams of sand and silt at different locations, few drop stones, gravel or larger, and pockets of sands.
III	CLAY, medium to high strength, seams of sand and silt at different locations, few drop stones, gravel or larger. Gas in solution. Probably affected by sliding.
IV	CLAY, medium to high strength, drop stones, gravel or larger. Possibly mass transport deposits.

Unit I is a late glacial to Holocene drape deposited in an environment with very slow deposition and is in general very soft. Unit II is layered and deposited after the previous sliding history. Unit III is very similar to Unit II, but is probably to some degree affected by sliding. It contains more gas dissolved in the pore water than Unit II. Unit IV contains mass transport deposits and is the most heterogeneous.

The upper three units are in general lightly overconsolidated (i.e. not mechanically overconsolidated) while the forth unit has some overconsolidation as a result of the sliding history.

The four units are found at different depths in the different locations Tables C2-2, C2-3 and C2-4 present the generalized soil conditions at the three areas, Field Centre, West Slope and East Slope.

C2-2 Summary of the generalised soil conditions encountered at the Field Centre locations

Unit	Depth below seafloor, m (indicative values)	Soil description
I	0 – 3.0	CLAY, silty, extremely low to low strength, traces of fine to medium sand partings and few shell fragments, greenish grey. Sandy in the upper 20 cm in some locations
II	3.0 – 20.0	CLAY, low to medium strength, low to medium plasticity, sand seams at different locations, few drop stones, gravel or larger, and pockets of sands, greenish grey to dark gray.
III	20.0 – 45.0[1)]	CLAY, medium to high strength, medium plasticity, traces of fine sub-angular to sub-rounded gravels and coarse shell fragments, dark gray, gas in solution
IV	45.0 – 61.2[2)]	CLAY, medium to high strength, medium plasticity, drop stones, gravel or larger. Possibly mass transport deposit, dark gray.

1) End of borehole for ST15452 –S-05 is at 26.7 m and for ST15452 –S-15 is at 26.7 m.
2) End of borehole for ST15452 –BH-12 is at 61.2 m.

Table C2-3 Summary of the generalised soil conditions encountered at the West Slope locations

Unit	Depth below seafloor, m (indicative values)	Soil description
I	0 – 3.0	CLAY, silty, extremely low to low strength, traces of fine to medium sand partings, medium to coarse sub-angular gravels and few shell fragments, greenish gray. Sandy in the upper 20 cm in some locations
II	3.0 – 25.0	CLAY, silty, low to medium strength, low to medium plasticity, sand seams at different locations, few drop stones, gravel or larger, and pockets of sands, greenish grey to dark gray.
III	25.0 – 45.0	CLAY, medium to high strength clay, medium plasticity, traces of fine sub-angular to sub-rounded gravels and coarse shell fragments, dark gray, gas in solution
IV	45.0 – 101.0[1)]	CLAY, medium to high strength, medium plasticity, drop stones, gravel or larger. Possibly mass transit deposit, dark gray.

1) End of borehole for ST15452 –02 = 101.0 m; ST15452 –03 = 62.5 m; ST15452 – 07 = 45.8 m; ST15452 –08 = 62.5 m; ST15452 –16 = 55.6 m; ST15452 –19 = 50.6 m.

Table C2-4 Summary of the generalised soil conditions encountered at the East Slope location

Unit	Depth below seafloor, m (indicative values)	Soil description
I	0 – 3.0	CLAY, silty, extremely low to low strength.
II	3.0 – 50.0	CLAY, low to medium strength, low to medium plasticity, sand seams at different locations, few drop stones, gravel or larger, and pockets of sands.
III	50.0 – 70.0	CLAY, medium to high strength clay, medium plasticity, traces of fine sub-angular to sub-rounded gravels and coarse shell fragments, dark gray, gas in solution
IV	70.0 – 98.2[1)]	CLAY, medium to high strength, medium plasticity, drop stones, gravel or larger. Possibly mass transit deposit, dark greenish gray.

1) End of borehole for ST15452 –18 = 98.2 m.

C3 Summary of soil parameters

The geotechnical parameters of the four units are given in Tables C3-1, C3-2 and C3-3 below for Field Centre, West Slope and East Slope locations respectively.

The tables include the representative characteristics, but also the range of measured data as all units are layers with some parameters changing significantly over short depth ranges. A designer should refer to the text in Sections G or H for further details on classification data including profiles of recommended representative basic soil parameters and advanced parameters that are presented in Section F.

Table C3-1 Soil units and representative characteristics relevant for 0 – 61 m depth, Field Centre locations. The range of measured data is given in brackets to show variability.

Unit	Typical depth below seafloor, m	Soil type	Water content, w, %	Total unit weight, γ, kN/m^3	Plasticity index[2)], I_p, %	Fines content[3)], %	Corrected cone resistance[4)], q_t, MPa	Undrained shear strength[4)], s_{uC}, kPa
I	0 – 3.0	CLAY	55 (31-76)	16.5 (15.3 – 19.0)	22 (20 – 24)	92 - 96 (42 - 46)	0.05 – 0.1	1 – 8
II	3.0 – 20.0	CLAY	35 (15 – 72)	18.5 (15.0 – 22.5)	12 (6 – 30)	55 - 94 (18 - 44)	0.1 - 1	8 -55
III	20.0 – 45.0	CLAY	27-40 (17 – 73)	18.0-19.6 (15.5 – 22.0)	20 (9 – 35)	60 - 96 (19 - 50)	1 - 2	55 – 125
IV	45.0 – 61.2[1)]	CLAY	27 (20-33)	19.6 (17.8 – 20.8)	14 (14 – 16)	79 - 81 (34 - 36)	2.2 – 3.5	125 - 170

1) End of borehole for ST15452 –BH-12 is at 61.2 m
2) Only relevant for clay material
3) Range of values (range of clay content in brackets)
4) Low representative values or range of values

Table C3-2 Soil units and representative characteristics relevant for 0 – 101 m depth. West Slope locations. The range of measured data is given in brackets to show variability.

Unit	Typical depth below seafloor, m	Soil type	Water content, w, %	Total unit weight, γ, kN/m^3	Plasticity index[2)], I_p, %	Fines content[3)], %	Corrected cone resistance[4)], q_t, MPa	Undrained shear strength[4)], s_{uC}, kPa
I	0 – 3.0	Clay	35 (29-38)	18.5 (18.2-19.2)	12 (6-12)	67-76 (19-34)	0.1-0.2	0.2 - 10
II	3.0 – 25.0	Clay	25 (18-48)	20 (17.2-22.8)	15 (4-18)	50-86 (10-46)	0.2-1	10-70
III	25.0 – 45.0	Clay	20 (15-42)	21 (17.5-23.0)	15 (8-24)	52-87 (20-33)	1-2	70-125
IV	45.0 – 101 [1)]	Clay	25 (19-33)	20 (18.5-21.0)	12 (5-17)	63-90 (15-32)	2-7	125-350

[1)] End of borehole for ST15452 –02 = 101.0 m
[2)] Only relevant for clay material
[3)] Range of values (range of clay content in brackets)
[4)] Low representative values or range of values

Table C3-3 Soil units and representative characteristics relevant for 0 – 98 m depth. East Slope location. The range of measured data is given in brackets to show variability.

Unit	Typical depth below seafloor, m	Soil type	Water content, w, %	Total unit weight, γ, kN/m^3	Plasticity index[2)], I_p, %	Fines content[3)], %	Corrected cone resistance[4)], q_t, MPa	Undrained shear strength[4)], s_{uC}, kPa
I	0 – 3.0	Clay	25 (n.a)	20.0 (n.a)	15 (n.a.)	n.a. (n.a.)	0.08-0.2	0.2 - 10
II	3.0 – 50.0	Clay	25 (18-36)	20.0 (18.3-21.0)	15 (n.a.)	91 (38)	0.2-2.3	10-140
III	50.0 – 70.0	Clay	31 (22-50)	19.0 (17.0-20.9)	10 (6-28)	49-94 (15-55)	2.1-2.8	140-200
IV	70.0 – 98.2[1)]	Clay	31 (22-36)	19.0 (17.9-20.5)	15 (5-18)	65-91 (9-30)	3-4	200-280

[1)] End of borehole for ST15452 –18 = 98.2 m
[2)] Only relevant for clay material
[3)] Range of values (range of clay content in brackets)
[4)] Low representative values or range of values

Section D

LIST OF SYMBOLS AND TERMS USED

Contents

D1 General

According to ISO 19901-8 (E):

a	net area ratio of a cone penetrometer
c_v	coefficient of consolidation
C_s	swelling index (for consolidation tests)
h_{sf}	height of reference point above seafloor
f_s	sleeve friction
G	specific gravity of solid particles
G_{max}	initial (small strain) shear modulus
I_L	liquidity index
I_P	plasticity index
I	Inclination
K_0	coefficient of earth pressure at rest (= $\sigma'_{h0} / \sigma'_{v0}$)
m_v	coefficient of compressibility
p_0'	in situ vertical effective stress (=σ'_{v0})
q_c	cone resistance
q_t	cone resistance corrected for pore water pressure effects
s	vane blade thickness
$s_u = c_u$	undrained (undisturbed) shear strength of soil
s_{uC}	static triaxial compression undrained shear strength
s_{uD}	static DSS undrained shear strength
s_{uE}	static triaxial extension undrained shear strength
s_{ufv}	shear strength by field vane testing
$s_{ufv,rem}$	remoulded shear strength by field vane testing
$s_{ufv,res}$	residual shear strength by field vane testing
S_t	soil sensitivity
u_2	pore pressure measured through a filter location in the cylindrical cone part just above conical part
V_p	compression wave velocity
V_s	shear wave velocity
V_{vh}	vertically (v) propagated, horizontally (h) polarized shear wave velocity
ξ	material damping ratio
Z	height above seafloor for drilling mode *in situ* probe zero reference readings
γ'	submerged unit weight of soil
ν	Poisson's ratio
σ	stress
σ'_{v0}	*in situ* vertical effective stress (= p_0')

σ'_{h0}	*in situ* horizontal effective stress
σ'_p	preconsolidation stress
$\Delta\sigma_v'$	Change in effective vertical stress
ϕ'	effective angle of internal friction

D2 Units

According to ISO 19901-8 (E):

Units to be used may vary somewhat from one clause to another based on historical use. For example, a CPT cone cross-sectional area should be given in units of square millimetres (mm^2) as used today, and not for example in square metres (m^2). However, if there are no special historical reasons for deviating from the units listed below, then the units to be used are:

force	kN
moment	kNm
density	kg/m^3
unit weight	kN/m^3
stress, pressure, strength and stiffness	kPa
coefficient of permeability	m/s
coefficient of consolidation	m^2/s

D3 Abbreviated terms

According to ISO 19901-8 (E):

BHA	bottom hole assembly
CCV	consolidated constant volume
CD	consolidated drained
CPT	cone penetration test
CPTU	electrical CPT with measurement of the pore pressures around the cone
CRS	controlled rate of strain
CT	computerized tomography
CU	consolidated undrained
DGPS	differential global positioning system
DS	direct shear
DSS	direct simple shear
ERP	emergency response plan
FVT	field vane test
GIS	geographical information system
GNSS	global navigation satellite system

HAZID	hazard identification
HAZOP	hazard and operability
HSE	health, safety and environment
HVAC	heating, ventilation and air conditioning
IL	incremental loading
JSA	job safety analysis
LAT	lowest astronomical tide
LBL	long baseline
MSCL	multi-sensory core logging
MSL	mean sea level
OCR	over-consolidation ratio
PEP	project execution plan
PPE	personal protective equipment
QA	quality assurance
QC	quality control
RFID	radio-frequency identification
ROP	rate of penetration
ROV	remotely operated vehicle
RS	ring shear
SCPT	seismic CPT
SH	shear waves
SHANSEP	stress history and normalized soil engineering parameters
SIMOPS	simultaneous operations
SOW	scope of work
SRB	sulphate-reducing bacteria
SWL	safe working load
TC	triaxial compression
TE	triaxial extension
TOC	total organic content
UCT	unconfined compression test
USBL	ultra-short baseline
UU	Unconsolidated-undrained
VSP	vertical seismic profiling
WGS	world geographic system
YSR	yield stress ratio

Additional abbreviated terms:

ASTM	American Standard for Testing and Materials
CAD	Consolidated Anisotropic Drained
CAU	Consolidated Anisotropic Undrained
CRSC	Constant Rate of Strain Consolidation
ISO	International Organization for Standardization
NGF	Norsk Geoteknisk Forening (Norwegian Geotechnical Society)
NS	Norsk Standard (Norwegian Standard)
PGA	Peak Ground Acceleration
PSV	Pseudo Velocity

D4 Classification system

D4.1 Shear strength of clays or density of sands (ISO 14688-2:2004(E))

Undrained shear strength, $s_u = c_u$, of clays (in kPa)		Density index, I_D, of sands (in %)	
Extremely low	<10	Very loose	0 to 15
Very low	10 to 20	Loose	15 to 35
Low	20 to 40	Medium dense	35 to 65
Medium	40 to 75	Dense	65 to 85
High	75 to 150	Very dense	85 to 100
Very high	150 to 300		
Extremely high*)	>300		

*) Materials with shear strength greater than 300 kPa may behave as weak rock. Can be described according to ISO 14689-1

D4.2 Terms characterizing soil structure (NGI standard practice)

PARTING(S)	Horizontal inclusion(s) of different sediment type less than 3 mm thick
SEAM(S)	Horizontal inclusion(s) of different sediment type 3 mm to 75 mm thick
LAYER(S)	Horizontal inclusion(s) of different sediment type greater than 75 mm thick
POCKET(S)	Inclusion of different sediment type that is smaller than the diameter of the sample
BLOCKY	Containing discrete blocks of sediment set in a non-structured matrix
PSEUDO-BLOCKY	Block structures formed by intersecting fissures
PLATY	Containing discrete platelets with one dimension (vertical) limited and less than the other two
SLICKENSIDED	Having (inclined) planes of weakness that are slick and glossy in appearance
FISSURED	Containing small scale discontinuities in sediment fabric
LAMINATED	Composed of thin seams or partings of varying colour and texture
FOLIATED	Containing small scale laminar structure with no colour or textural variations
INTERLAYERED	Composed of alternate layers of different sediment types
WELL GRADED	Having a wide range of grain sizes. Similar to poorly sorted
POORLY GRADED	Predominantly of one grain size. Similar to well sorted

D4.3 Grain size distribution (ISO 14688-1:2002(E))

The grain size distribution is presented as percentages of the various grain sizes present in the soil as determined by sieving and sedimentation. The terms used to describe grain sizes are:

Soil fractions	**Sub-fractions**	**Particle size (in mm)**
Very coarse soil	Large boulder Boulder Cobble	> 630 200 to 630 63 to 200
Coarse soil	Gravel Coarse gravel Medium gravel Fine gravel	2 to 63 20 to 63 6.3 to 20 2.0 to 6.3
	Sand Coarse sand Medium sand Fine sand	0.063 to 2.0 0.63 to 2.0 0.2 to 0.63 0.063 to 0.2
Fine soil	Silt Coarse silt Medium silt Fine silt	0.002 to 0.063 0.02 to 0.063 0.0063 to 0.02 0.002 to 0.0063
	Clay	< 0.002

D4.4 Soil description

The general soil description (borehole logs, soil unit etc) is according to ISO 14688-1:2002(E) and ISO 14688-2:2004(E). The soil description based on grain size distributions is according to NGF (2011).

D4.5 Plasticity

The soil classification system used is described in NGF (2011).

Descriptions	I_p (%)
Low plasticity	< 10
Medium plasticity	10 – 20
High plasticity	> 20

Section E

INTERPRETATION OF GEOLOGICAL AND GEOPHYSICAL DATA FOR GEOHAZARD ASSESSMENT AT FLEMISH PASS

Contents

Tables

Figures

Figure E2.2.14	Slice, extracted from a similarity cube derived from the 3D seismic data (survey ST14001), from 95 m below the present seafloor. Light colours correspond to high similarity between the neighbouring traces, whereas dark colours correspond to low similarity. The data clearly illustrate the presence of blocks of various dimensions, from small to large, at this depth interval. The similarity is high close to the flanks of the Flemish Pass, but low at the centre (e.g., field development area). The red line shows the location of the seismic profile presented in Figure E2.2.11.
Figure E2.2.15	3D seismic data examples (survey ST14001) showing buried landslide complexes along the eastern flank of the site investigations, across site BH-18 (yellow line). The profile at the top shows two headwalls. The profile at the bottom focuses on the location of the geotechnical borehole.
Figure E2.2.16	Various geotechnical parameters (corrected tip resistance q_t, pore pressure parameter B_q, normalized tip resistance Q_t, OCR, and undrained shear strength s_u) derived from the measured CPTU data set at BH-18, eastern flank, down to about 100 m. The grey shading marks the interval where the CPTU penetrates the deformation zone of the upper MTD (see Figure E2.2.15).
Figure E2.3.1	Age-depth model derived from 6 radiocarbon dates from the field development area (BH12) and the western flank (other data points). The dashed light blue line represents the best-fit linear regression equation for the 6 data points. The thick dark blue markers along the y-axis indicate the timing of Heinrich events 1 (youngest) to 5 (oldest).
Figure E2.3.2	Multi-sensor core logging results from BH-05 and BH-05a, Field Development area, showing P-wave velocity (left panel), bulk density (middle panel) and volumetric magnetic susceptibility (right panel) versus depth. The labels to the right represent the core sections. The yellow circles and crosses on the bulk density plot are densities from laboratory measurements, determined from the bulk sample dimensions and water contents, respectively.
Figure E2.3.3	Various logs derived from sedimentological and paleoceanographic analyses from a sediment core from the Orphan Knoll (Weber et al., 2001). The Heinrich layers are typically characterised by high carbonate content and positive anomalies in the density and magnetic susceptibility data. For location of the core, see Figure E1.1.1.
Figure E2.3.4	Bulk density from MSCL from BH-05 as well as three reference cores (Orphan Basin, data downloaded from https://www.pangaea.de/; for location, see Figure E1.1.1). The interpretation of Heinrich layers on the Marion Dufresne cores is based on Weber et al., 2001.
Figure E2.3.5	Volumetric magnetic susceptibility as well as three reference cores (Orphan Basin, data downloaded from https://www.pangaea.de/; for location, see Figure E1.1.1). The interpretation of Heinrich layers on the Marion Dufresne cores is based on Weber et al., 2001.

Figure E2.3.6 Plot of Ca/Ti ratio from XRF measurements in borehole S-05/05a showing clear peaks in the Ca content corresponding to the carbonate pulses associated with Heinrich Events. The colour scans of the cores on the left show that the Heinrich Events are associated with lighter colours of the sediment. The annotations indicate which Heinrich Event the individual peaks are interpreted to have been derived from.

Figure E2.3.7 Age vs. depth model including both radiocarbon dates and interpreted Heinrich Events.

Figure E2.3.8 Cross-plots of geochemical test results of the tephra shards found in cores BH12 (Field Development, diamonds) and BH19 (western flank, squares). The yellow vs. green colouring indicates the light or dark colours of the shards, respectively. The background data (black dots) are compiled from a larger database, with documented geochemical provinces (see Brendryen et al., 2010 and others).

E1 Geological setting

E1.1 Location and physiography

The study area lies within the northern part of the Flemish Pass, a narrow gateway between the continental shelves of the Grand Banks of Newfoundland and the Flemish Cap (Figure E1.1.1, Figure E1.1.2), the latter being a submarine basement high representing the easternmost extension of the North American continental crust (Mao et al., 2014). The Flemish Pass enters northwards into the deeper Orphan Basin (Figure E1.1.1).

The northern Flemish Pass is about 50 km wide, and about 1200 m deep at the Field Development location (Figure E1.1.2). The water depth along the shelves at either side is about 300 m. The eastern and western slopes of the northern Flemish Pass are relatively gentle, typically only a few degrees steep (Figure E1.1.3). The flanks of the northern Flemish Pass are characterised by the occurrence of several escarpments, illustrating that submarine landsliding has affected the area (Figure E1.1.2). The escarpments are up to 10° steep, which is modest (Figure E1.1.3).

Towards the west and north-west, the northern Flemish Pass is bordered by the Sackville Spur, a prominent southwest-northeast trending sedimentary ridge which becomes narrower towards the Orphan Basin (Figure E1.1.2). Sackville Spur is an elongated sediment drift, i.e., a sedimentary deposit influenced by bottom currents. Sackville Spur is of Neogene-Quaternary age (e.g., Piper, 2005). Sackville Spur is characterised by moraines and scouring (Figure E1.1.2), due to glacial movement and the ploughing of icebergs crossing the area at the end of glacial periods (e.g., Huppertz and Piper, 2009). The flank of Sackville Spur towards the Orphan Basin is steeper than the flanks of the Flemish Pass (Figure E1.1.3). This area is characterized by various instabilities, like smaller-scale slope failures, channels and gullies (e.g., Piper, 2005; Tripsanas et al., 2008).

According to the *Levitus94* ocean climatology database, the present-day bottom water temperature is around 3-4°C, with sea surface temperature around 8°C. Present-day draft of the icebergs crossing the area and primarily derived from Greenland or Baffin Bay is about 200 m at the Grand Banks (Piper, 2005).

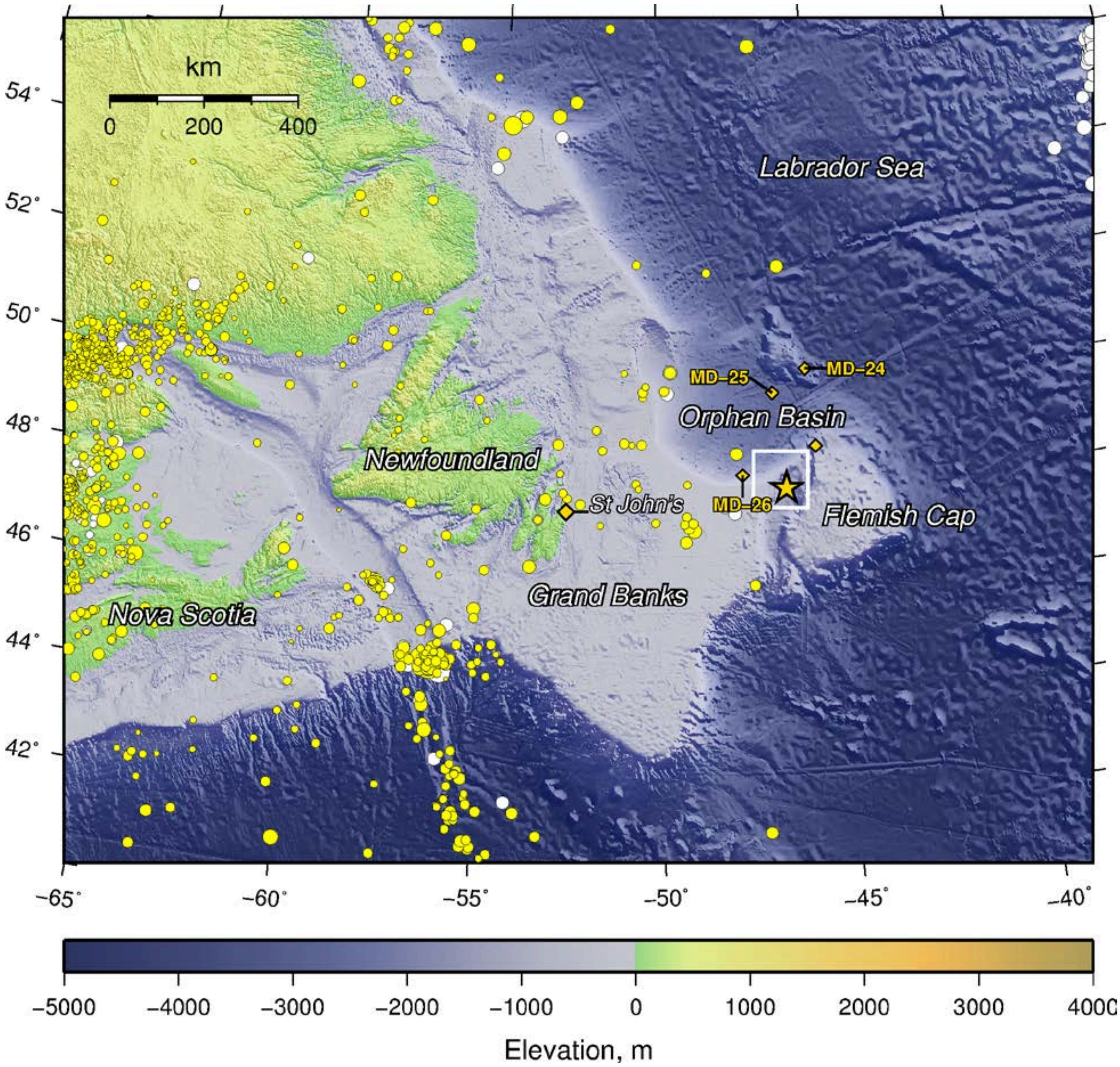

Figure E1.1.1 Regional topographic map showing the location of the performed geotechnical site investigation (golden star) in the northern Flemish Pass, a narrow strait between the Grand Banks of Newfoundland and the Flemish Cap. The elevation data used is the GEBCO_2014 public-domain data set. Labels MD-2 refer to the locations where sediment cores were taken onboard R/V Marion Dufresne in 1995, on which various sedimentological tests were conducted. The white box is the outline of the map presented underneath. The circles represent historical earthquake epicentre locations (white: USGS data; yellow: Canadian Composite Seismicity Catalogue, CCSC 2011). These are scaled with earthquake magnitude.*

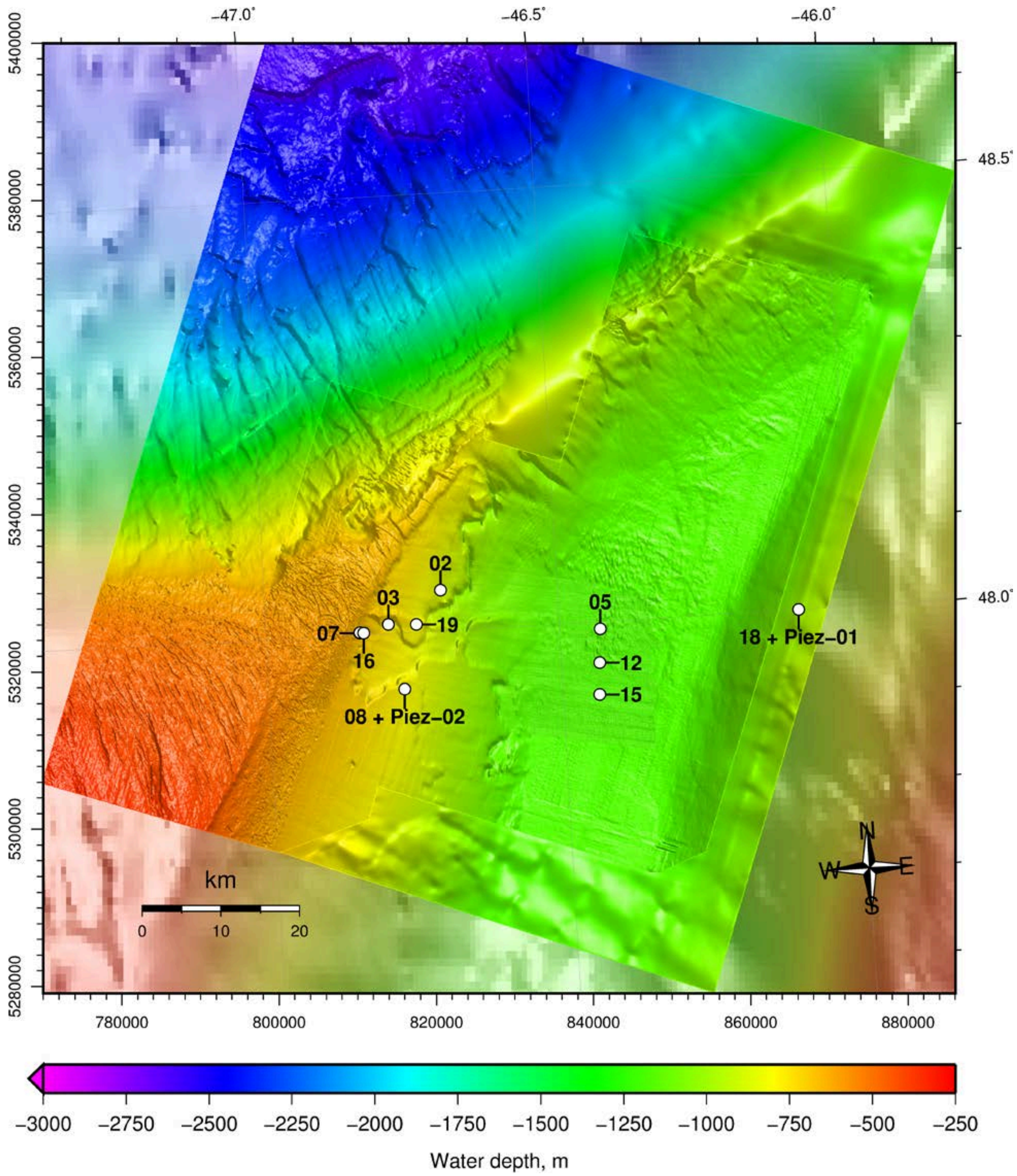

Figure E1.1.2 Location of the 2015 geotechnical investigation sites within the Flemish Pass. The circles are geotechnical boreholes or CPT locations. Piezometers were installed at sites 8 and 18. Note the difference in resolution of the various bathymetric datasets available. The prominent ridge trending SW-NE is the Sackville Spur.

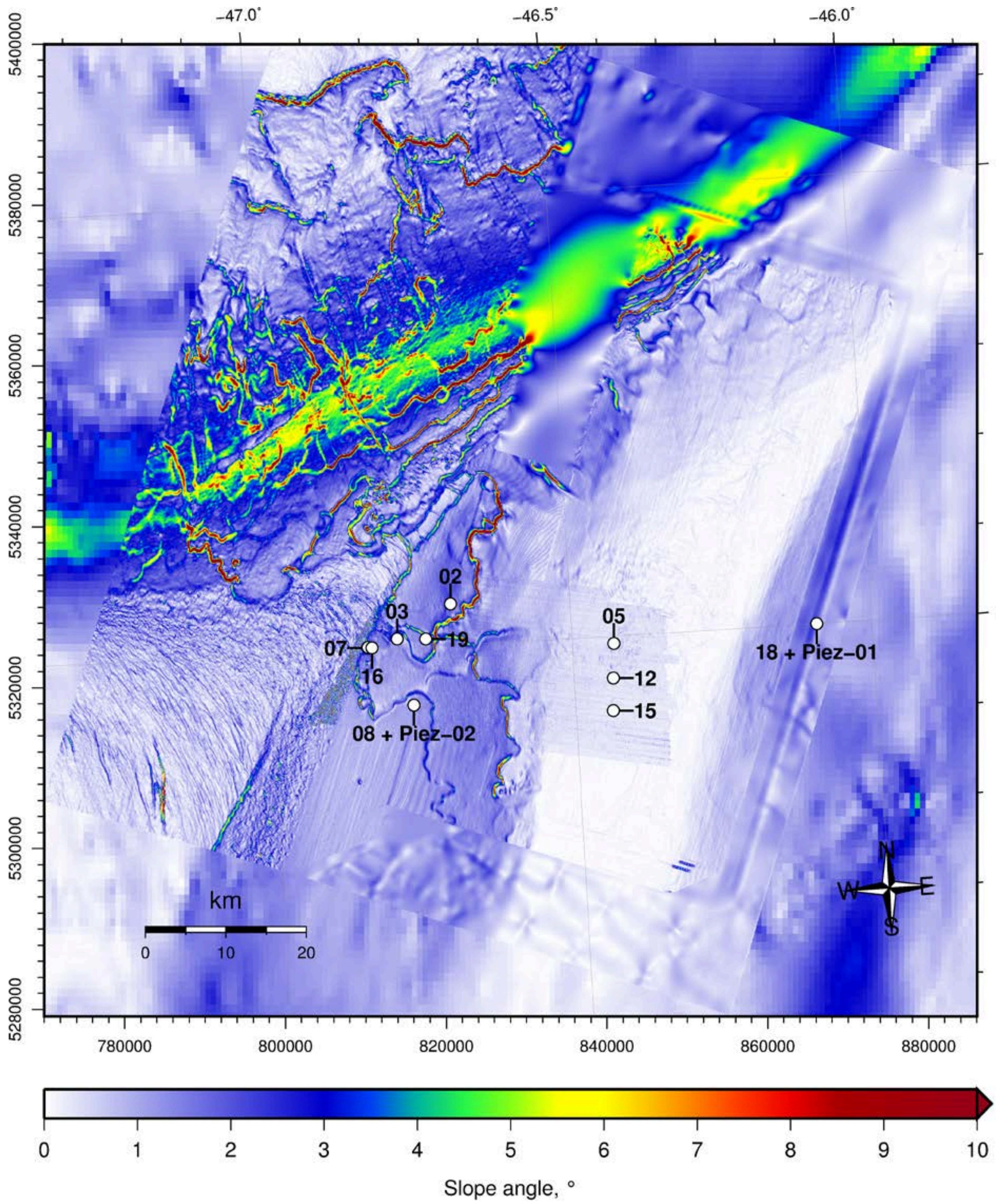

Figure E1.1.3 Slope angle map derived from the composite bathymetry data.

E1.1.1 Discoveries in the northern Flemish Pass

At least three significant discoveries lie within the Flemish Pass since 2009. These are, from South to North, the Bay du Nord (discovered in 2013), Harpoon (discovered in 2013) and Mizzen (discovered in 2009). Bay du Nord lies approximately 500 km NE of St. John's. The Bay du Nord field is a high-quality Jurassic reservoir containing mainly light crude oil. Discovered volumes are estimated at 300 to 600 million barrels of recoverable oil (source: Statoil). It is the largest discovery off the coast of Newfoundland and Labrador of the last three decades.

E1.2 Tectonic setting and seismicity

A detailed description of the tectonic setting of the Flemish Pass area is provided by Golder Associates (2014) and C-CORE (2012).

In summary, the Flemish Pass is an elongated sedimentary basin located between the Grand Banks of Newfoundland (W) and a structural basement high the Flemish Cap (E), on the eastern Canadian continental margin (Figure E1.1.1). It is of Mesozoic-Cenozoic age, governed by passive margin tectonics. The Flemish Pass was created during initial rifting and spreading region during the early Cretaceous (145-100 Ma), but the extension was short-lived in the Flemish Pass, therefore interpreted as a failed rift. Nevertheless, sedimentation continued in response to changes in the regional tectonic regime (rifting, thermal subsidence) during the opening of the North Atlantic Ocean. The post-rift sediment thickness in Flemish Pass is variable, with a maximum of over 10 km (Golder Associates, 2014).

During the mid- to late-Cenozoic, the Flemish Pass became progressively infilled by prograding sequences derived from the Grand Banks area or Flemish Cap. Muds and sands have been in places reworked by bottom currents, or contourite deposits (see underneath) (Piper, 2005; Marshall et al., 2014). A major change in sedimentation style coincided with the onset of the large scale glaciations characterising the Quaternary (last 2.6 million years, see underneath). The Quaternary succession consists primarily of muds with interbedded turbidites, as well as mass transport deposits and glacigenic debris flows (Piper, 2005).

According to Piper (2005), there is evidence of neotectonic activity during the Quaternary off the eastern Canadian margin, including faulting around the Flemish Cap.

Figure E1.1.1 includes the epicentres of historical earthquakes in the larger area, obtained from the public-domain data base from the USGS and the Canadian Composite Seismicity Catalogue. Whereas there are swarms of epicentres, particularly concentrated along alignments through which ice streams moved, their magnitudes are relatively low. Historically, the area has thus low activity, and even lower close to the geotechnical site investigation location. The most significant seismic event was the infamous 7.2 magnitude Grand Banks event at the outlet of the Laurentian Channel that triggered an important submarine instability and turbidity current (Piper et al., 1999).

Some of the seismic profiles show evidence of polygonal faults, a non-tectonic class of faults that may be due to dewatering of sediments (Berndt et al., 2003).

E1.3 Quaternary Geology: glaciations and oceanography

E1.3.1 Glacial history and Marine Isotope Stages

The Quaternary (last 2.6 Ma) is characterised by large-scale climatic variations exemplified by the cyclic waxing and waning of continental ice sheets. Almost the entire eastern Canadian continental shelf has been glaciated, which is reflected in its geomorphology (Piper, 2005). During the glacial periods, the glaciers have reached across the shelf, but not necessarily always reaching the shelf breaks. For example, the ice sheet only reached the mid-shelf during the Last Glacial Maximum (LGM), but did extend to the shelf break during the Early Wisconsinan (around 100 kyr ago). The shelf is characterised by cross-shelf troughs, through which fast-flowing ice moved during glacial times, and shallower banks with different types of moraines (Figure E1.1.1). The two dominant ice-stream pathways were the Laurentian Channel (South) and the Hudson Strait (North), but there were several locations where secondary ice stream discharge took place (Figure E1.3.1).

This change in environmental conditions affected the sedimentation style offshore, including shelf progradation (Figure E1.3.2), the occurrence of stacked debris lobes (Figure E1.3.3), meltwater plume deposits, and turbidites. When icebergs drift across the shelf and upper slope under the influence of the ocean currents, their keels may scour the seafloor, leaving behind a criss-crossing pattern of curvi-linear depressions, called iceberg ploughmarks. During the glacial periods, the iceberg draft was up to 500-650 m, i.e., significantly deeper that the iceberg draft at present (Piper, 2005). The seafloor geomorphology of the Sackville Spur shows iceberg imprints from glacial times (Figure E1.1.2). The fact that these relict features remain visible implies that the post-glacial sedimentation rate was quite low, as sediment infill tends to smoothen irregularities on the seafloor.

There is also abundant evidence of the occurrence of recent and older submarine landslides in the area (see underneath).

Often, dating in the Quaternary period is expressed in the Marine Isotope Scale (MIS) system. The system has alternating periods of warm (odd numbers) and cold periods (even numbers), and are deduced from detailed oxygen isotope analysis which reflect variations in temperatures from pollen and foraminifera. Table E1.3-1 gives the start time of the last 10 MIS stages, covering approximately the last 400 ka.

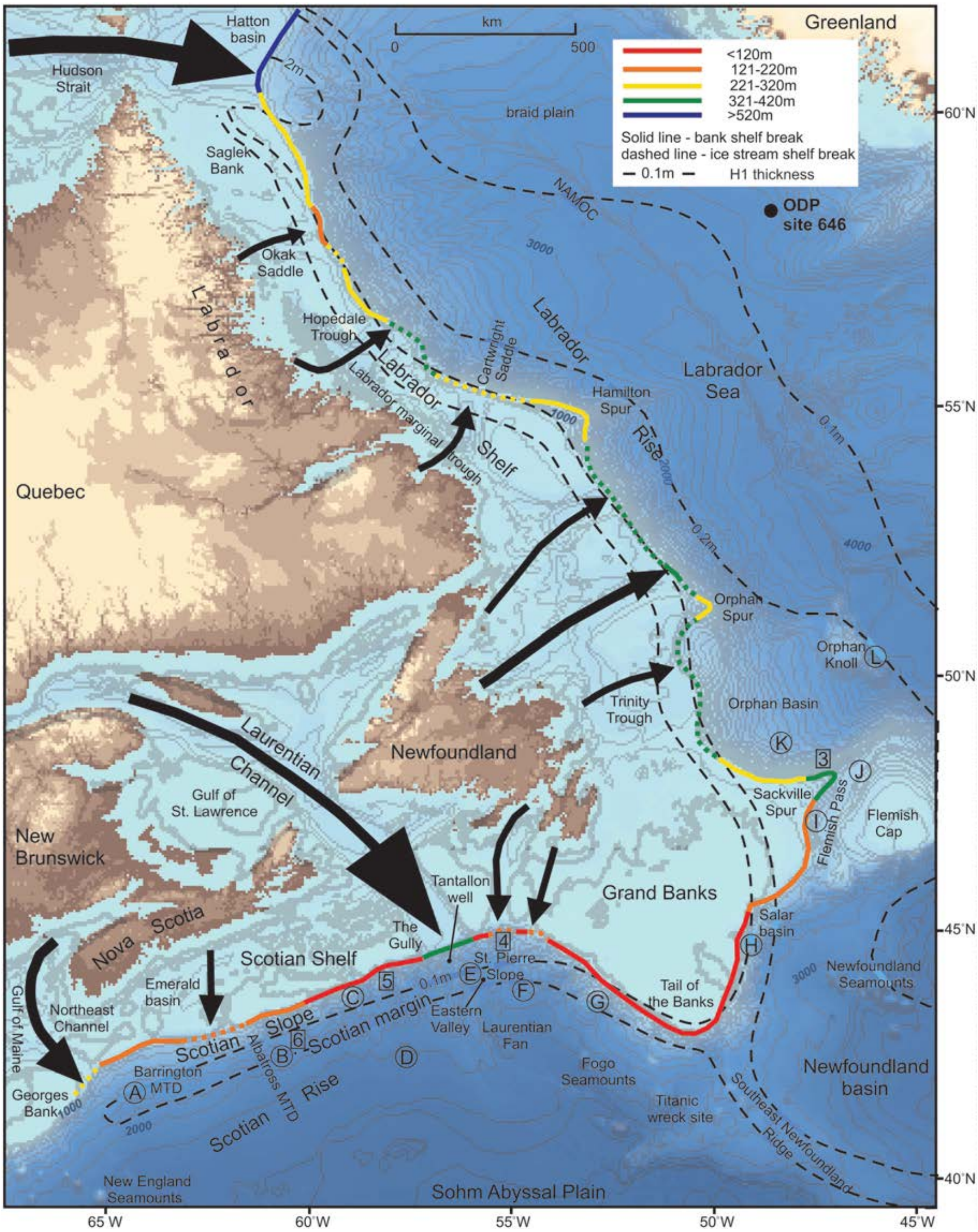

Figure E1.3.1 Topography of the south-eastern Canadian margin, showing the locations of the paleo-ice streams (bold arrows). The coloured line segments are indicative of the water depth at the shelf break. The dashed lines are isopachs for Heinrich Event H1. Source: Piper, 2005.

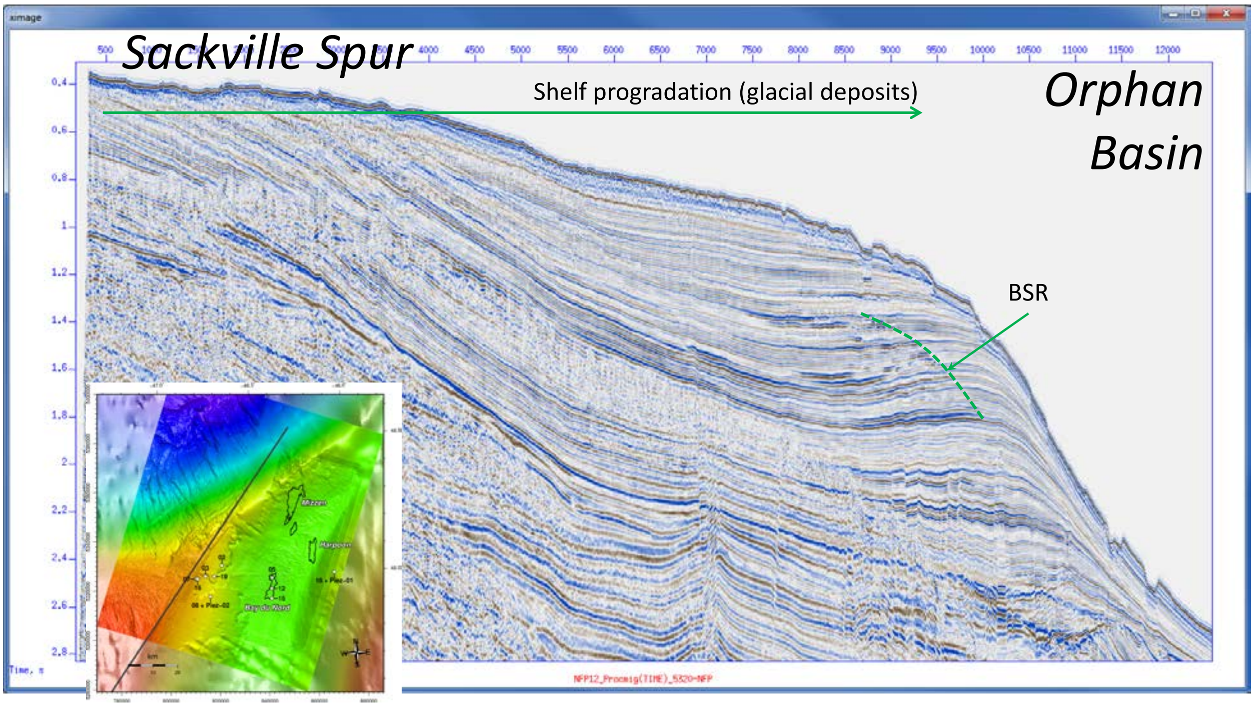

Figure E1.3.2 *Regional 2D seismic line from Sackville Spur to the Orphan Basin margin showing shelf progradational sequences. Note the weak BSR along the steepest part of the slope.*

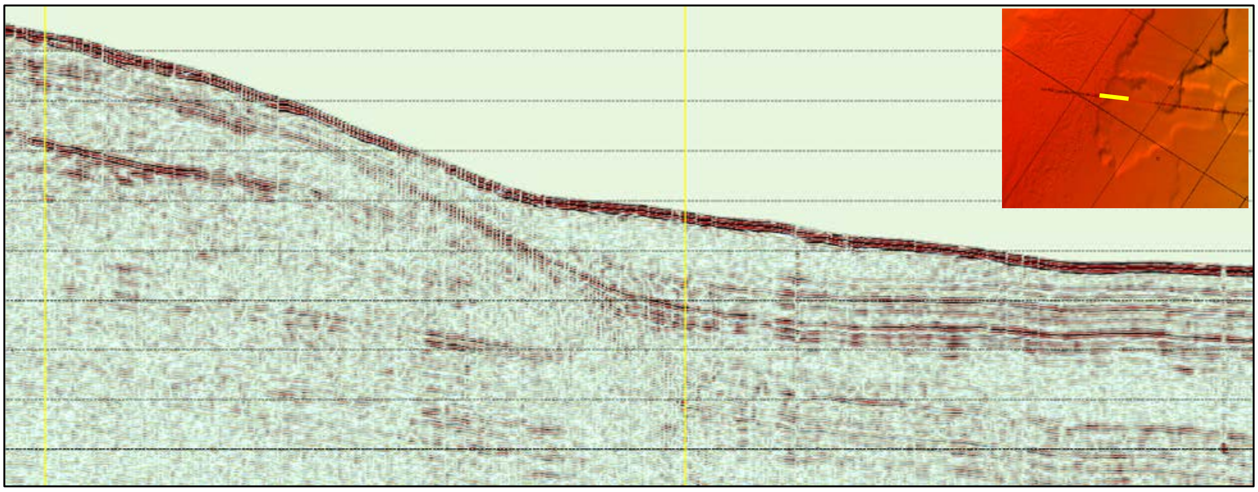

Figure E1.3.3 *Sparker line across one of the escarpments on the western flank of the Flemish Pass. The distance between the horizontal lines is 10 ms (two-way traveltime).*

Table E1.3-1 Marine Isotope stages for the last 400 ka. The stages with blue background colour correspond to cold periods, whereas those with orange background colour are warmer periods.

MIS	age ka (start)
1	14
2	29
3	57
4	71
5	130
6	191
7	243
8	300
9	337
10	374

E1.3.2 Oceanography

The current system in the study area is part of the Atlantic Meridional Overturning Circulation (AMOC) (Figure E1.3.4). For the northern hemisphere, AMOC is a major current pattern in the Atlantic Ocean characterised by the northwards flow of warm and saline waters (shallow), which supplies the formation of the North Atlantic Deep Water (NADW) flowing southwards at larger depth. This current transports substantial amounts of heat from tropical areas towards the North Atlantic, where transfer to the atmosphere takes place, and is therefore a controlling factor for the Earth's climate (e.g., Hebbeln et al., 1998). This current pattern is also important for sediment reworking (e.g., contourites) as well as distributing ice-rafted debris (IRD) across significant parts of the North Atlantic (see underneath).

On the eastern Canadian margin and the Flemish Pass region, the surface water currents originate from the polar water derived from the Arctic Ocean and the more temperate waters from the North Atlantic Drift. These currents form a boundary circulation pattern in the Labrador Sea, of which the Labrador Current is the southernmost segment (Figure E1.3.5). The Labrador Current flows southwards along the continental margin (Piper, 2005; Marshall et al., 2014; Mao et al., 2014). This current splits in the Orphan Basin into an inner branch that flows into the Flemish Pass at speeds of 0.25 to 1.20 m/s (slower at depth), and an outer branch that flows around the Flemish Cap. It is known to have varied in intensity as well as temperature on a variety of timescales (Marshall et al., 2014). The Labrador Current was more vigorous during interglacial periods (Piper, 2005). The Labrador Current erodes and scours the seabed down to about 1300 m (Piper, 2005).

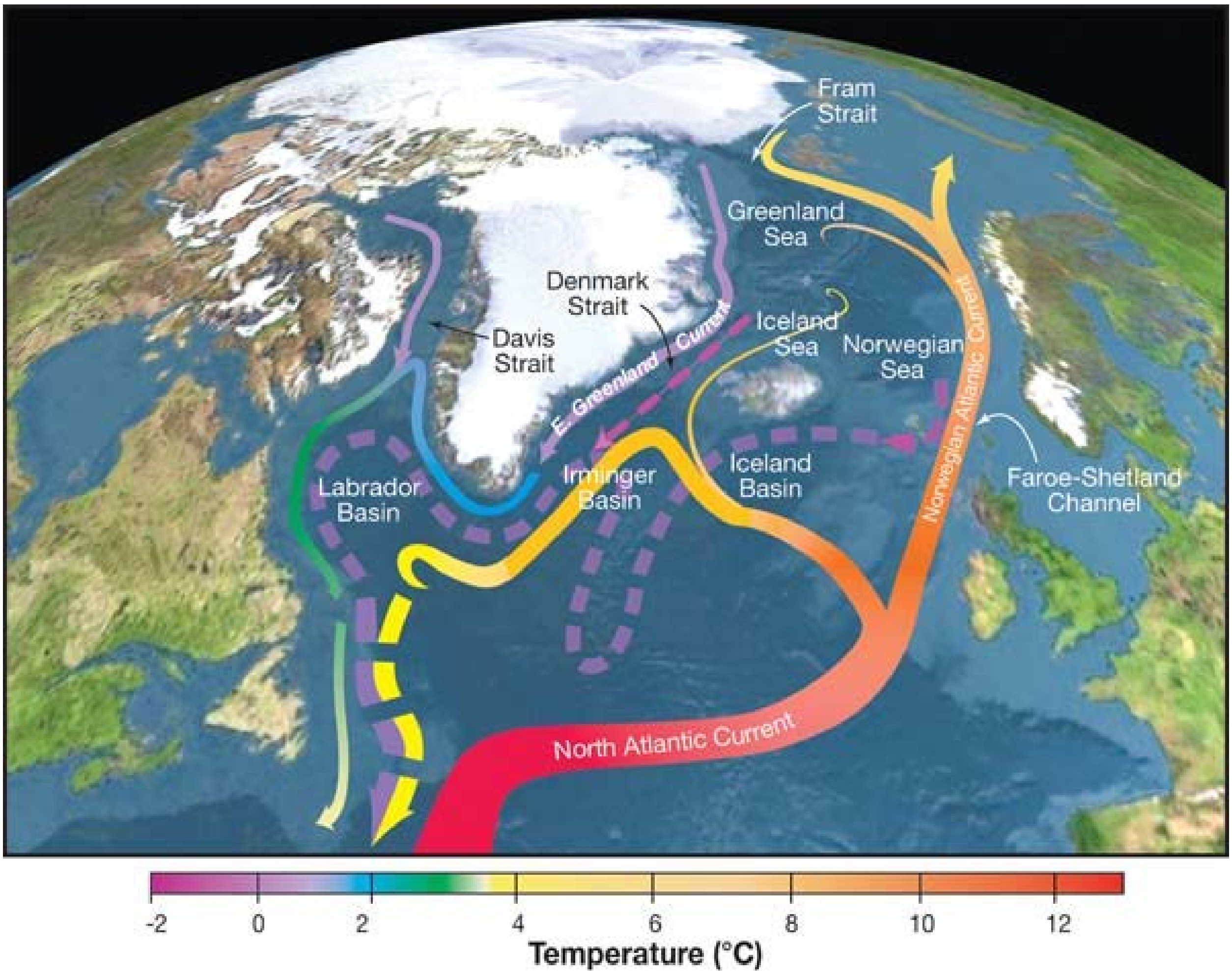

Figure E1.3.4 Topography of the North Atlantic Region with the Atlantic Meridional Overturning Circulation pattern. The solid lines represent surface currents, whereas the dashed lines represent deep currents. The colours are indicative of the temperature of the water masses. Source: http://www.eoearth.org/view/article/150290/

Furthermore, currents sweeping the seafloor are capable of reworking the sediment, causing various bedforms typically called sediment drift or contourites. The shape and extent depends on the current intensity and sediment supply. Contourites are described from across the Orphan Basin as well as the Flemish Pass (Marshall et al., 2014). Bottom current activity has taken place since the Late Miocene (Piper et al., 2005). The Labrador Current played a significant role in constructing the shallow water drift deposit of Sackville Spur, intensified since the onset of widespread cross-shelf glaciation and the resulting increased supply of sediment (Piper, 2005). An example from the Sackville Spur is shown in Figure E1.3.6. Contourite deposits may play a role as pre-conditioning factor in submarine landsliding.

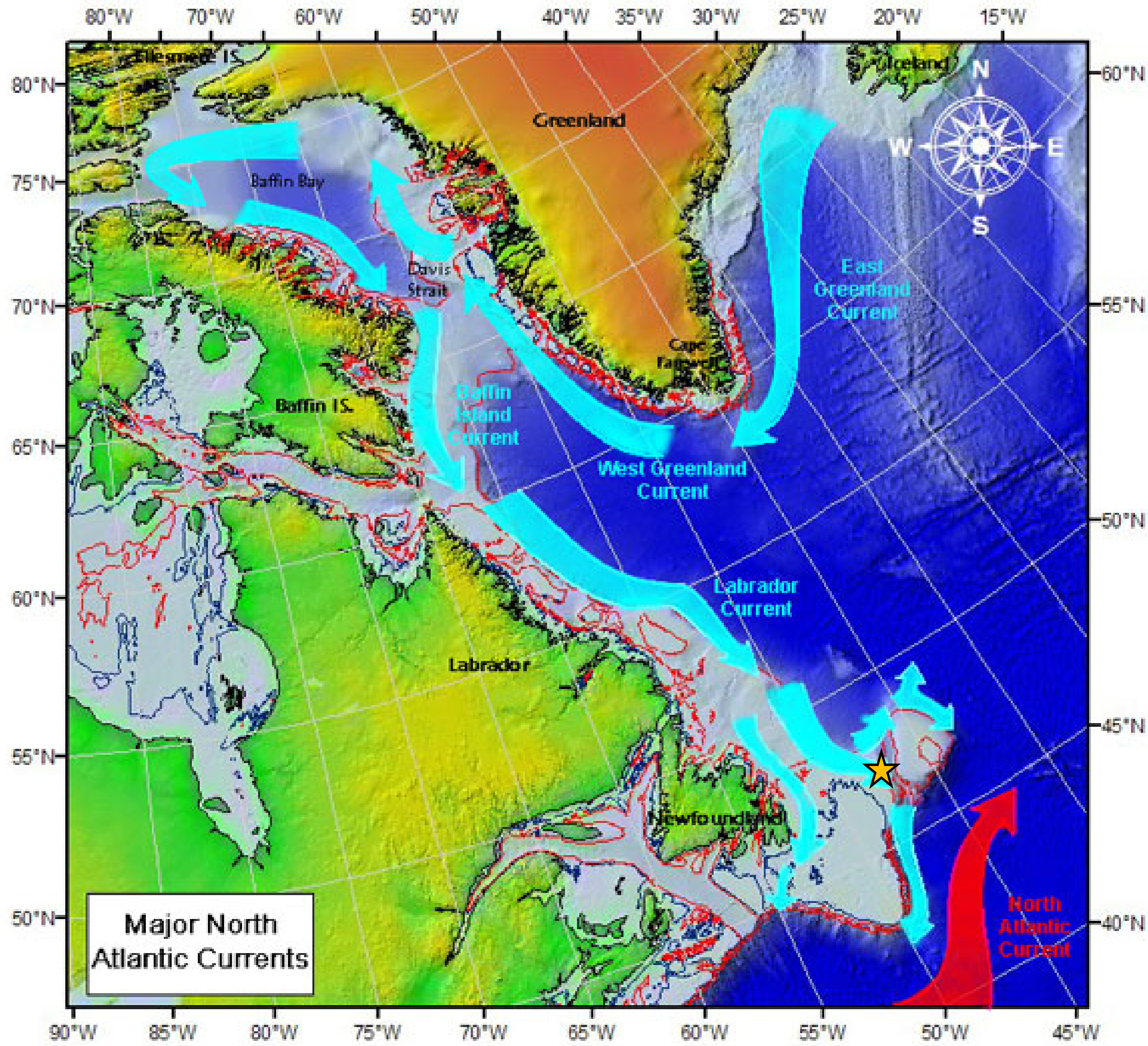

Figure E1.3.5 Overview of the major current systems off the eastern Canadian margin, with the southwards flowing Labrador Current the dominant current within and close to the Flemish Pass area. The golden star marks the location of the 2015 geotechnical site investigation. Source: Wikipedia, image provided by United States Coast Guard.

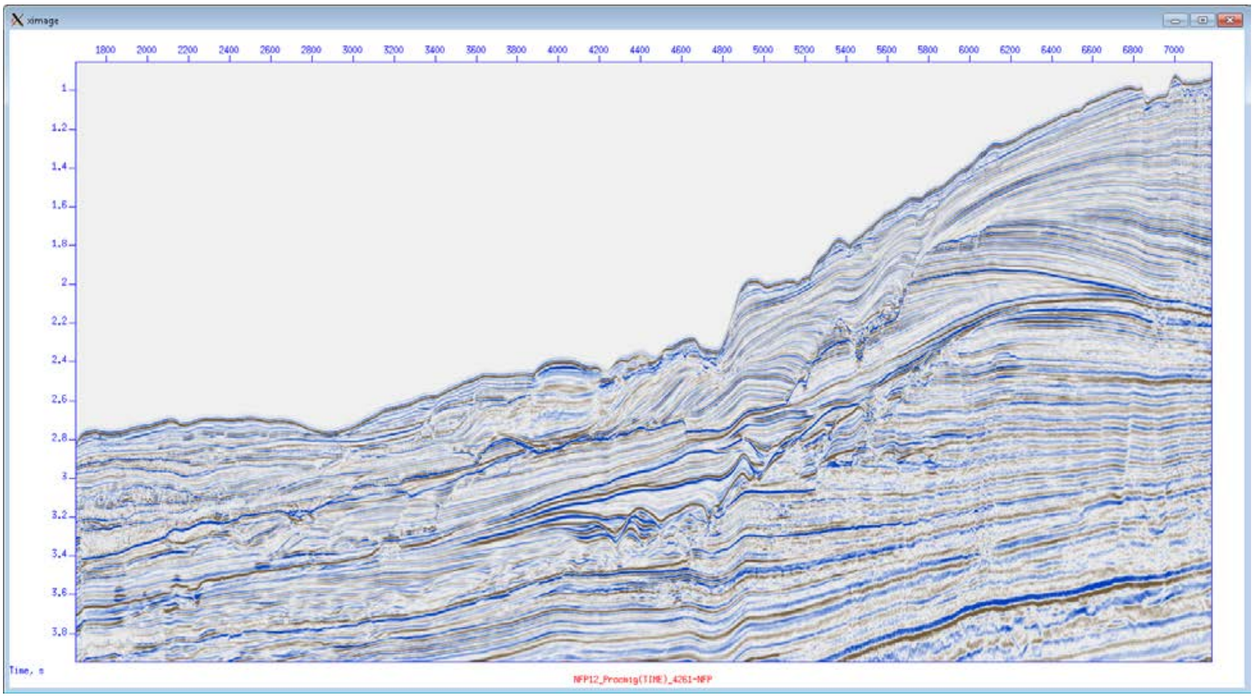

Figure E1.3.6 2D seismic profile across the northwestern margin of Sackville Spur towards the Orphan Basin, west of the geotechnical site investigation area, showing typical wavy sedimentary sequences, attributed to the influence of ocean currents (contourites). Vertical exaggeration is approximately 10.

E1.3.3 Heinrich events and layers

Heinrich events are short periods of time during which large amounts of icebergs break off from ice sheets and glaciers, and start drifting across the northern North Atlantic. Gradually, the icebergs melt and discharge their sediment load across the ocean basins. The subsequent deposit is known as a Heinrich layer (e.g., Rasmussen et al., 2003; Alvarez-Solar and Ramstein, 2011) which are typically found in sediment cores across the North Atlantic region.

The Heinrich layers are characteristic deposits, with often a unique signature. The layers contain large amount of clasts and ice-rafted debris. Often, the soil has high volumes of carbonate rocks. As a result, they have a different grain size distribution (larger fraction of coarser soils), have higher bulk density, and higher magnetic susceptibility (for examples, see Figure E2.3.3). Furthermore, the signature yields information of the provenance of the glaciers, considering that glacier movement are highly erosive and entrain the bedrock particles upon their movement. Spectrophotometry (colour scanning using CIElab colour space) may also help identifying, correlating and differentiating the origin of the Heinrich layers (e.g., Marshall et al., 2014).

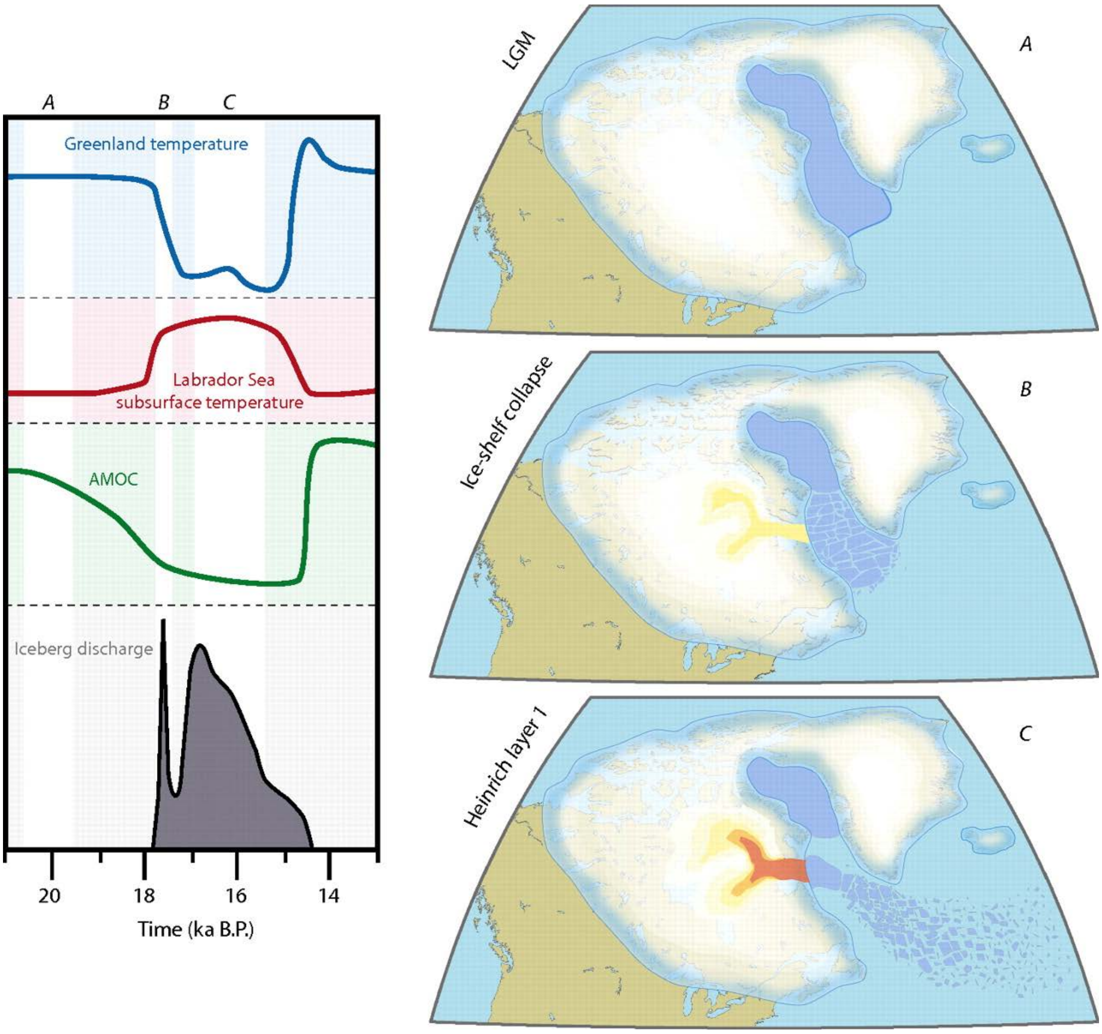

Figure E1.3.7 Schematics of the processes causing Heinrich event 1, leading to the deposition of characteristic deposits in the study area and abroad. Source: Alvarez-Solas and Ramstein, 2011.

As the collapse of the glaciers and the melting of the icebergs takes place rapidly (on the geological timescale), the Heinrich layers may be found over large regions and used as a proxy for sediment dating purposes, as long as continuous records are available and the signature can be unambiguous identified. At the same time, the melting causes a freshwater pulse into the oceans, which may contribute to changes in the global thermohaline circulation due to the difference in density between the seawater and water released by the ice masses.

Heinrich events are known to occur at the end of glacial or stadial periods, but their signature and magnitude varies, depending on the intensity of the cold stage and iceberg release. Table E1.3-2 gives an overview of the timing of the best-documented Heinrich events.

Figure E1.3.7 (Alvarez-Solas and Ramstein, 2011) sketches the processes leading to the latest major Heinrich event, occurring at the Last Glacial Maximum (LGM), coupling ice sheet dynamics with oceanography. At the end of the glacial period, there was a slow-down of the AMOC and a reduction in the formation of the NADW. The reduced convection resulted in the progressive warming of the subsurface ocean layer, which amplified the rate of basal melting underneath the Labrador Sea ice shelf. The effect is thinning of the ice shelf and possibly collapse, which in turn facilitates ice stream acceleration. The latter is the main source of detritus transport from land into the oceans. The melting of ice also initiates sea level rise.

All evidence from sediment cores suggests that the study area was in the direct pathways of the glacier movement after the ice sheet collapses, and therefore, one would expect Heinrich layers to be found in the boreholes. They are positively identified in sediment cores from both north and south of the study area (see Weber et al., 2001; Marshall et al., 2014).

In a similar way, the occurrence of red mud deposits can assist in establishing the chronology off Eastern Canada. Also these deposits have a regional extent, and are likely interpreted as a meltwater plume deposit with possible origin from sandstones and siltstones beneath the NE Newfoundland shelf (e.g., Marshall et al., 2014). An example from the Flemish Pass is shown in Figure E1.3.8.

Table E1.3-2 Approximate timing of the last 9 Heinrich events.

Event	age ka
H0	12
H1	17
H2	24
H3	31
H4	38
H5	45
H5a	53
H6	58
H7	70
H8	75
H9	84

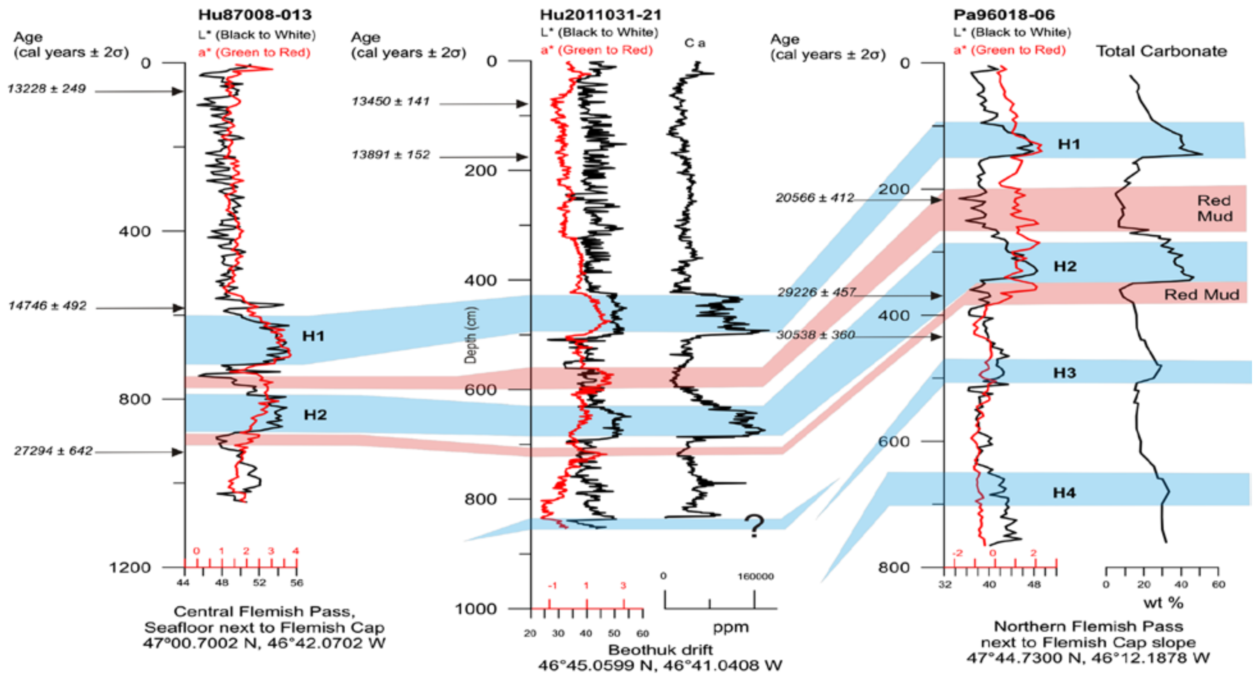

Figure E1.3.8 An example of the occurrence of Heinrich events red mud deposits, the latter likely the result of meltwater plumes, from the Flemish Pass, based on spectrophotometry and carbonate abundance (Marshall et al., 2014).

E1.4 Occurrence of gas and gas hydrates

C-CORE (2012, 2014) present the current state-of-the-art on gas hydrates and their occurrence along the Newfoundland Continental margin. Gas hydrates are ice-like mixtures of low-molecular weight gas – predominantly methane – that are trapped within cages formed by water molecules. For hydrates to be stable, one requires sufficient high pressures, sufficiently low temperatures, sufficient hydrate forming components (typically methane) and sufficient water to form the hydrate structure (Sloan, 1998). The transition between partially gas hydrate saturated sediments (above) and free gas containing sediments (below) often gives rise to a prominent bottom-simulating reflection (BSR) on seismic data, even though its expression depends on a number of factors (e.g., Vanneste et al., 2001).

The dissolution or dissociation of gas hydrates under environmental (e.g., climate change) or anthropogenic influences (e.g., radial heat flow from warm wells) are often mentioned as a potential triggers or pre-conditioning factors for slope instability (e.g., Sultan et al., 2004). However, there is only indirect evidence of the causal role of gas hydrates in setting off submarine failures (e.g., Vanneste et al., 2014). Also the presence of gas is often mentioned as a potential factor facilitating slope failures or as zones where excess pore pressure may occur.

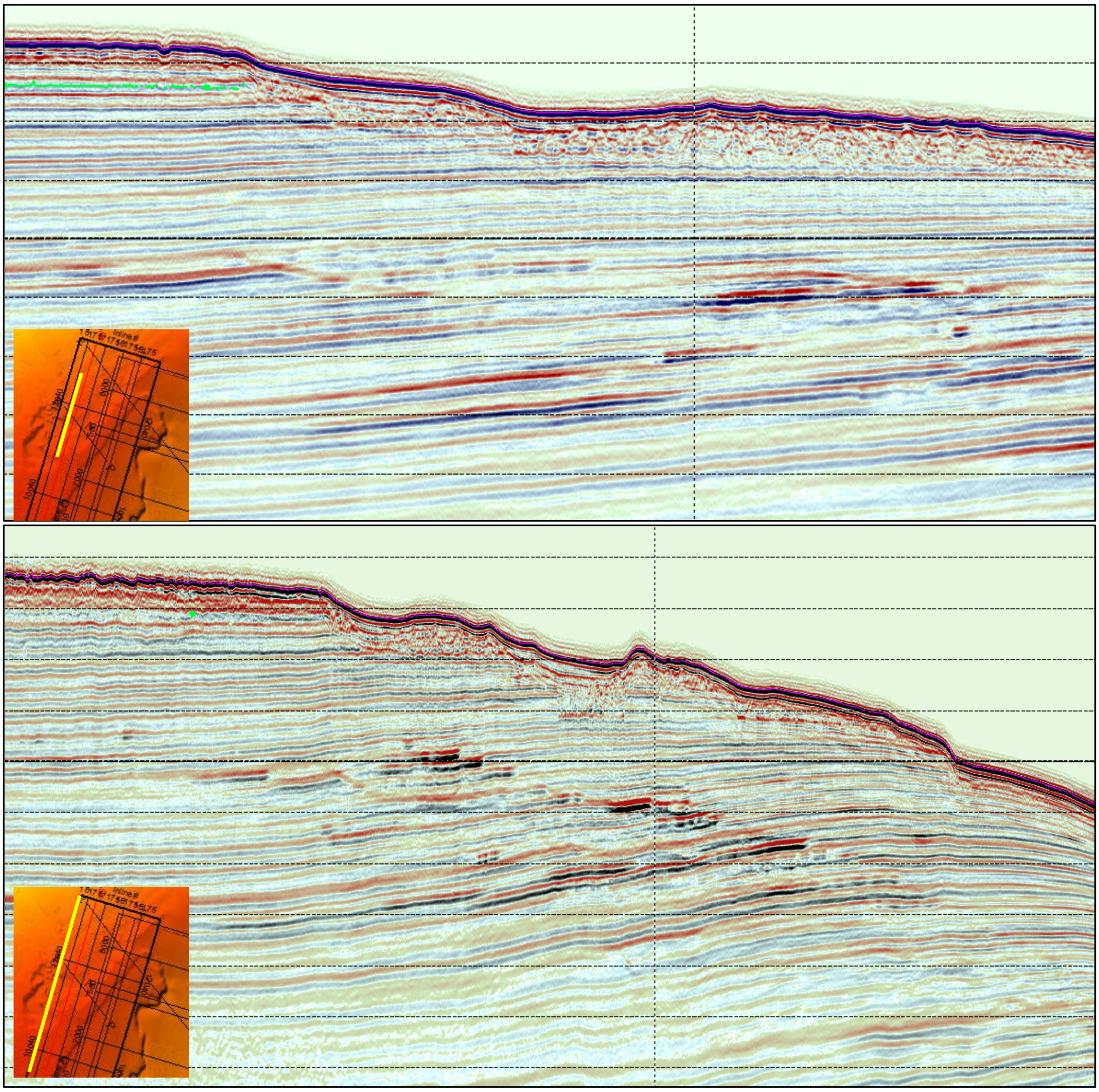

Figure E1.4.1 3D seismic sections from across the Sackville Spur showing a BSR-like feature, albeit weak and irregular. The horizontal lines mark 100 m depth intervals.

From inspection of the geophysical data from the northern Flemish Pass, it appears that BSRs occur across the northern part of Sackville Spur. Examples from 3D and 2D data are shown in Figure E1.4.1 and Figure E1.4.2. The BSRs are not too clear, and is not really a reflection. Rather, it stands out due to its cross-cutting behaviour and the change in amplitude of the stratigraphy across this reflection. The data suggest that gas has a preferential accumulation within the strata, presumably coarser sediment units through which gas and pore water migrate easier along the stratification. Along these seismic profiles, there is evidence of shallow instabilities close to the seafloor. There is no indirect evidence of gas hydrates in the immediate vicinity of the geotechnical site investigations. However, hydrates likely occur to the north and northwest of the site investigation area (see Figure E1.4.1, Figure E1.4.2). The seismic data do not indicate the presence of shallow gas pockets in the shallow sub-surface either. At these settings, shallow gas would typically be converted into gas hydrates. Also beyond the hydrate stability conditions, there is little evidence of free gas presence.

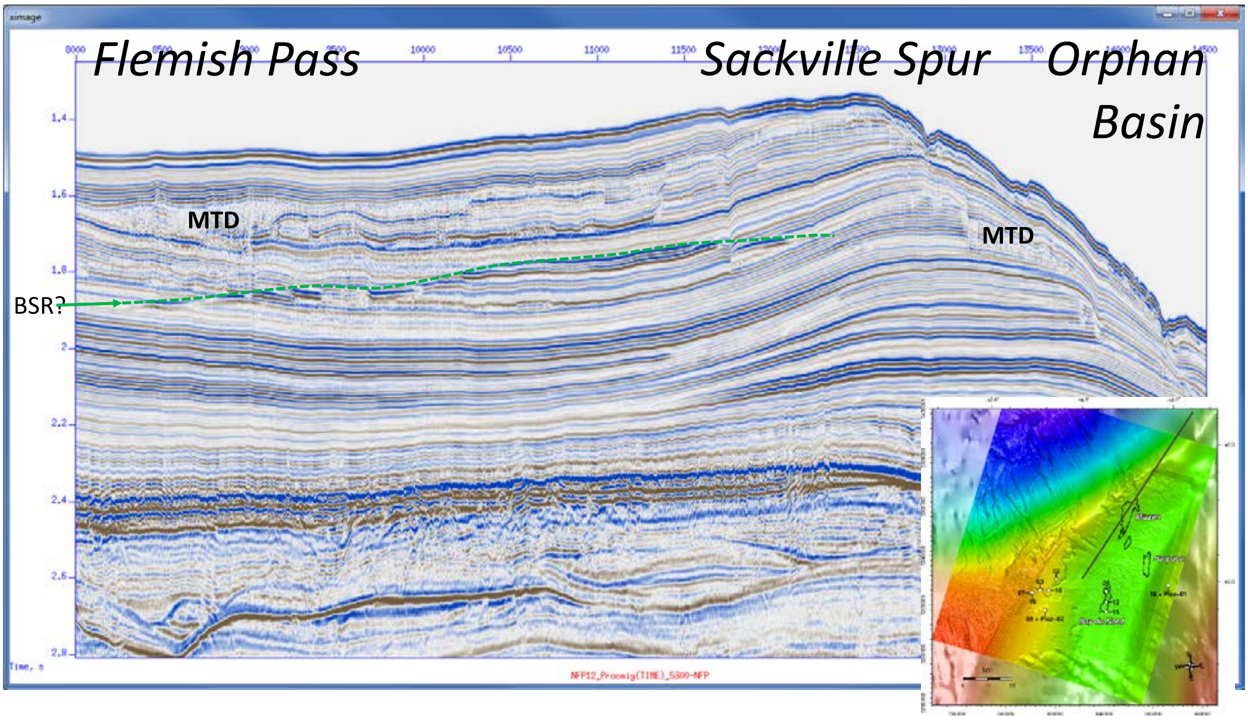

Figure E1.4.2 2D regional seismic data, oblique to Sackville Spur, connecting the Flemish Pass to the Orphan Basin slope. The profile shown starts in between the western slope and the Field Development of the 2015 geotechnical site investigation. Also along this line, one can see enhanced strata, of which the terminations appear as a BSR-like feature. There are MTDs on different levels in the stratigraphy along the Orphan Basin slope as well as the Flemish Pass.

The samples and geotechnical data collected during the 2015 site investigations did not reveal unambiguous and direct evidence of *in situ* gas or gas hydrates. For the latter, one should note that the coring procedure would not allow keeping the hydrate stable, as controlled pressure coring would be a necessity. Indirect evidence for the presence of gas comes from the observation of significant cracks in the core visible through the liners (for an example, see Figure E1.4.3). Whereas the cracks are abundant in certain depth intervals, their volume compared to the sample as a whole remains fairly small. Hydrate dissociation would also release additional fresh water, often resulting in a "soupy" sediment, which is not observed. Note that the presence of cracks or soupy sediment, however, does not imply that free gas and/or gas hydrate is present *in situ*. The release of pressure during sample retrieval from the seabed to the vessel will induce gas coming out of solution or hydrate dissociation to take place. The result of the gas exsolution due to pressure release causes sample cracking, particularly within fine-grained soils (NGI, 2016b). Our interpretation is that methane is dissolved into the pore water, and that no hydrate was present in the recovered samples. From a preliminary analysis, at the typical depths of the hydrate stability limit in the area, a minimum of 8 l of methane could be released upon sample retrieval (1 m long), before giving evidence for *in situ* hydrate occurrence.

Gas analyses indicate that the gas is predominantly methane of biogenic origin, suggesting that it is not migrating from large depths towards the shallow sub-surface. Chlorinity measurements (see Table K2-1 in NGI, 2016) from boreholes BH-12, 18 and 19 yield values typically around 30 to 35 g/l. One value has higher chlorinity (37.2 g/l) and two values are lower (26.5 and 28.4 g/l). These are not considered as abnormal values, taking into account uncertainties in the measurements. Therefore, these data are not further used to derive potential hydrate saturation values.

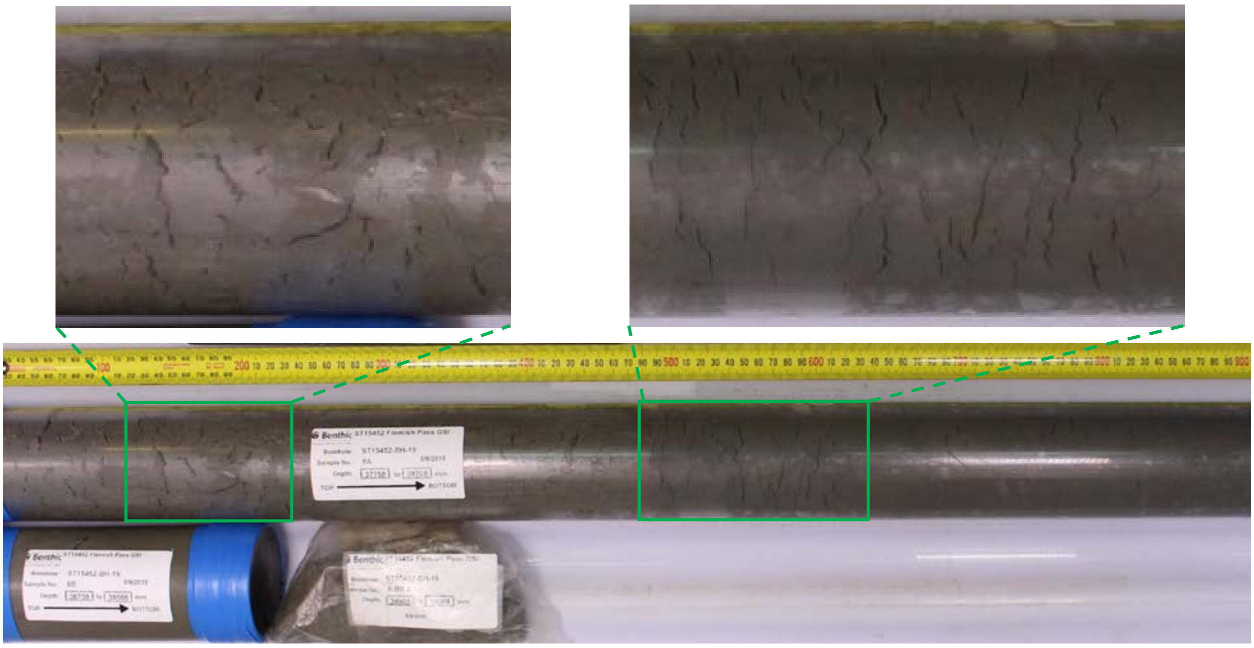

Figure E1.4.3 Example of cracks found in the cores (BH-19, western flank) during the offshore investigation. Pictures courtesy of Benthic Ltd.

E2 Evaluation of slope instabilities

E2.1 Data received

NGI has received various data and reports, essentially through Statoil. The following data and reports were used in this study:

Swath bathymetry:
- EC_Regional_Seabed_utm22_xyz_historic, 100 m by 100 m bins
- Jdex+BDN2014psdmstk_RENEWS, 100 m by 100 m bins
- 20150016_PrelimBathy_5m_Jun26, 5 m by 5 m bins

2D seismic data – all in time-domain:
- NFP12_Procmig survey, airgun-array data
- SO1500, sparker data and sub-bottom profiler data

3D seismic data – depth-domain:
- ST14001 survey
- ST12002 Renews_Cambriol_hr_degh_3trace_stackr

Well logs:
- Bay du Nord P 78, from about 1260 to 1970 m below RKB

E2.2 Sediment reworking and instabilities in the Flemish Pass region

The Geological Survey of Canada has conducted extensive research into the mapping and understanding of seafloor instabilities and sediment deformation in the area. Figure E2.2.1 presents a geomorphological interpretation of the different processes affecting various areas in the northern Flemish Pass. The features include landslide escarpments, exposed landslide deposits, and buried mass-transport deposits within the Flemish Pass. The flank of Sackville Spur towards the Orphan Basin also reveals evidence of submarine canyon systems, channels, and gullies (e.g., Piper, 2005; Tripsanas et al., 2008). Most of the recent failures are relatively small; however, larger-scale buried features are documented on exploration seismic data (Piper, 2005; see underneath).

The landslide complex to the NE of the study area is probably best studied. Piper and co-workers have identified 4 different phases, occurring over the past 28 kyr, with recurrence approximately every 7 kyr. The instabilities are clustered, and involved different slip planes with some of the more recent feature cutting the older features (Figure E2.2.2).

Factors contributing to the failures mentioned in literature include sediment load due to glacial processes, generation of overpressures, effect of gas, but mainly seismicity (Piper, 2005). For the latter, the simultaneous triggering of different landslides is used as a key indicator. Piper (2005) reports recurrence intervals of 5000 years for smaller-scale failures and more than 200 000 years for larger failures.

E2.3 Slope failures at the geotechnical site investigation area

In this section, we further describe the instabilities in the immediate vicinity of the site investigation. The discussion is split into the western flank, the field centre and the eastern flank.

E2.3.1 Western Flank of Flemish Pass

The bathymetry data from the western flank of the Flemish Pass clearly show the presence of multiple escarpments at different water depths (Figure E2.2.3). The upper headwalls lie in water depths around 600 m. The water depth at the deepest escarpments is about 1150 m. Some of the escarpments are arcuate-shaped. At the location of the headwalls and sidewalls, the present-day seafloor slopes are not very steep (Figure E2.2.4). The area between the landslides is fairly flat (Figure E2.2.3, Figure E2.2.4).

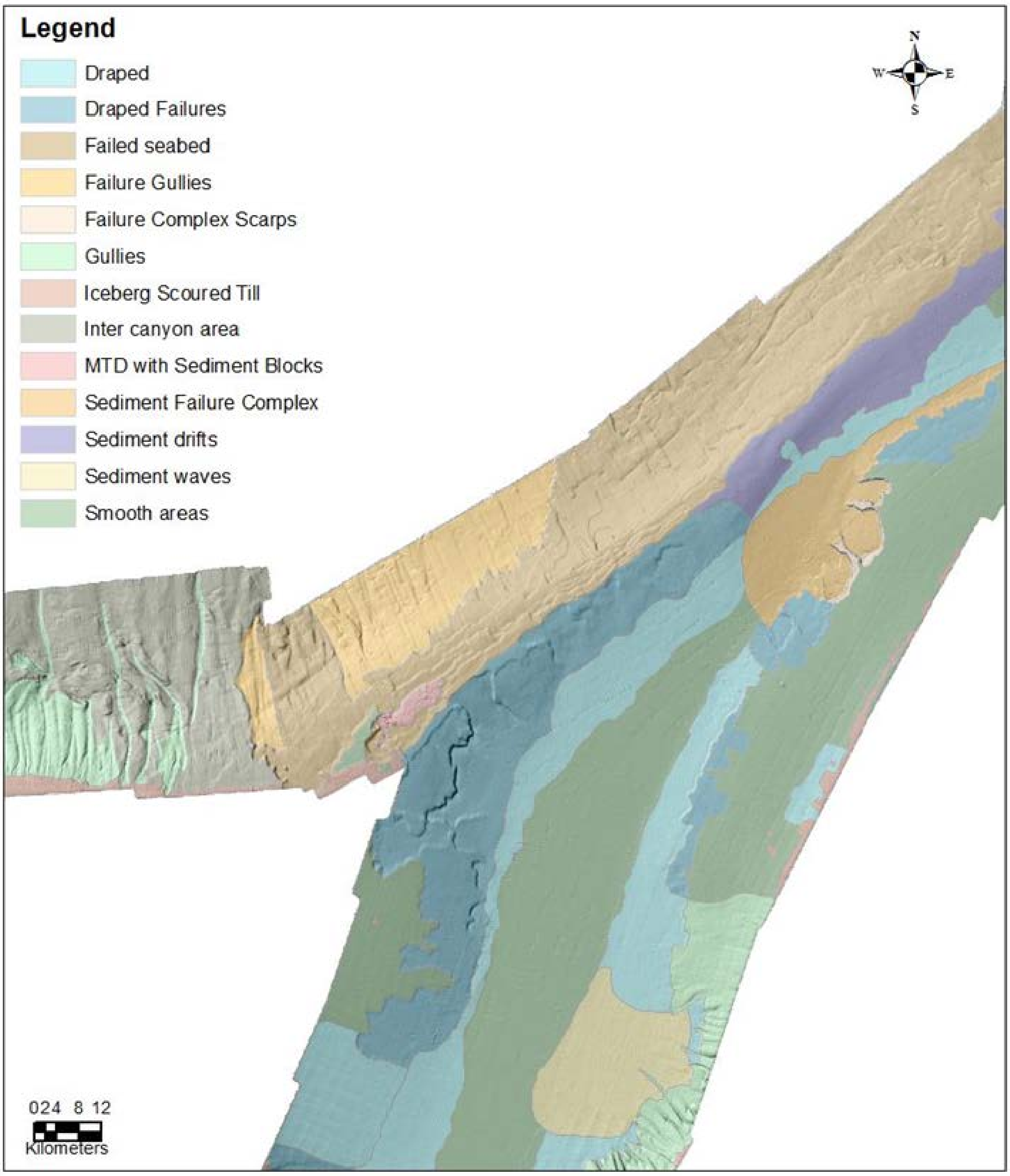

Figure E2.2.1 Geomorphological interpretation of the seabed in the northern part of the Flemish Pass and adjacent Sackville Spur area, showing ample evidence of sediment instabilities. Figure courtesy Cameron et al., 2013.

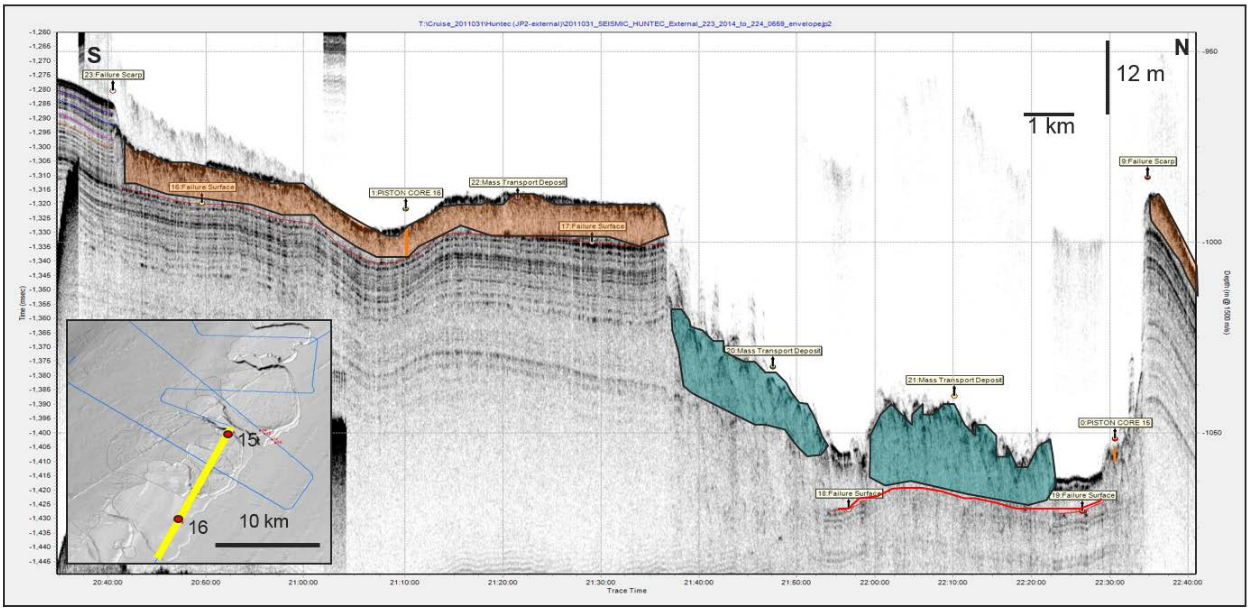

Figure E2.2.2 Sub-bottom profile across the recent landslide complexes NE of the 2015 site investigation area. Note that there are different landsliding episodes in the area. These landslides occurred at 21 ka (blue-green) and 28 ka (orange). Data courtesy of the Geological Survey of Canada. Vertical exaggeration is approximately 100. Source: Cameron et al., 2014.

These data suggest that the buried landslide complex is the result of a multi-phase and likely retrogressive failure development. The age of the landslides is currently not known. There is indirect evidence of glacigenic sediment infill from the Sackville Spur area into the outline of the upper escarpments (see Figure E1.3.3).

There is a nearly intact sediment drape present covering (nearly) the entire area (e.g., Figure E2.2.5; Figure E2.2.6; Figure E2.2.7), suggesting that the area is quiet over recent geological times. Considering the low sedimentation rates (see underneath), this part of the margin has apparently not failed over several tens of thousands of years.

The evolution of the landslides is not well constrained. From the seismic data, we identify a number of discrete slip planes that were involved in the landslides (Figure E2.2.8). At least two major slip planes have been involved, with some smaller slip planes locally. Whether or not the pink area is an undisturbed margin segment remains to be seen. A random line connecting this area to the shelf and towards the undisturbed area south of the landslide may suggest so.

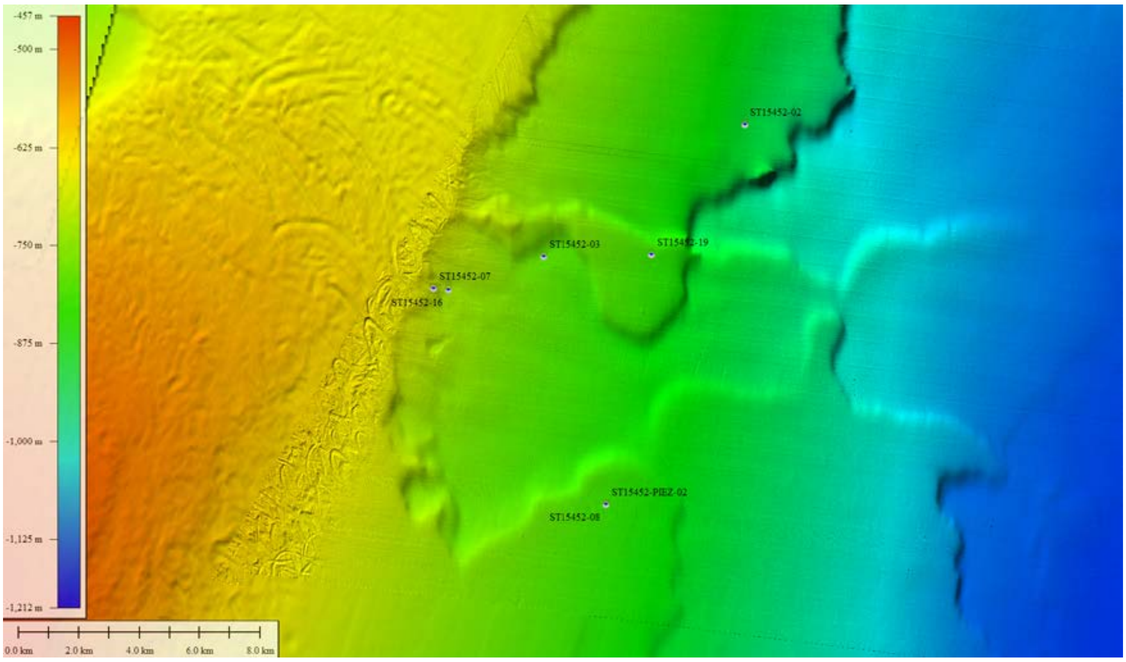

Figure E2.2.3 Bathymetry map over part of the western flank of the northern Flemish Pass, showing a multitude of escarpments. These are interpreted to be the result of several submarine instabilities. The shallower areas to the west reveal glacial imprints on the Sackville Spur, caused by iceberg ploughing.

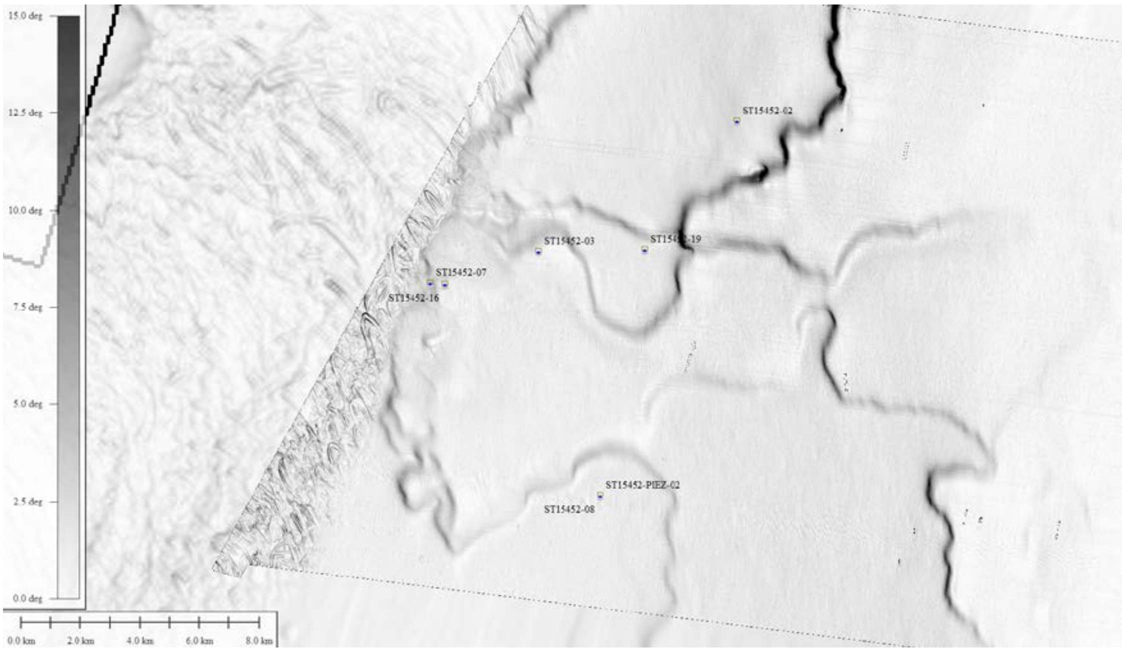

Figure E2.2.4 Corresponding slope map derived from the bathymetry data.

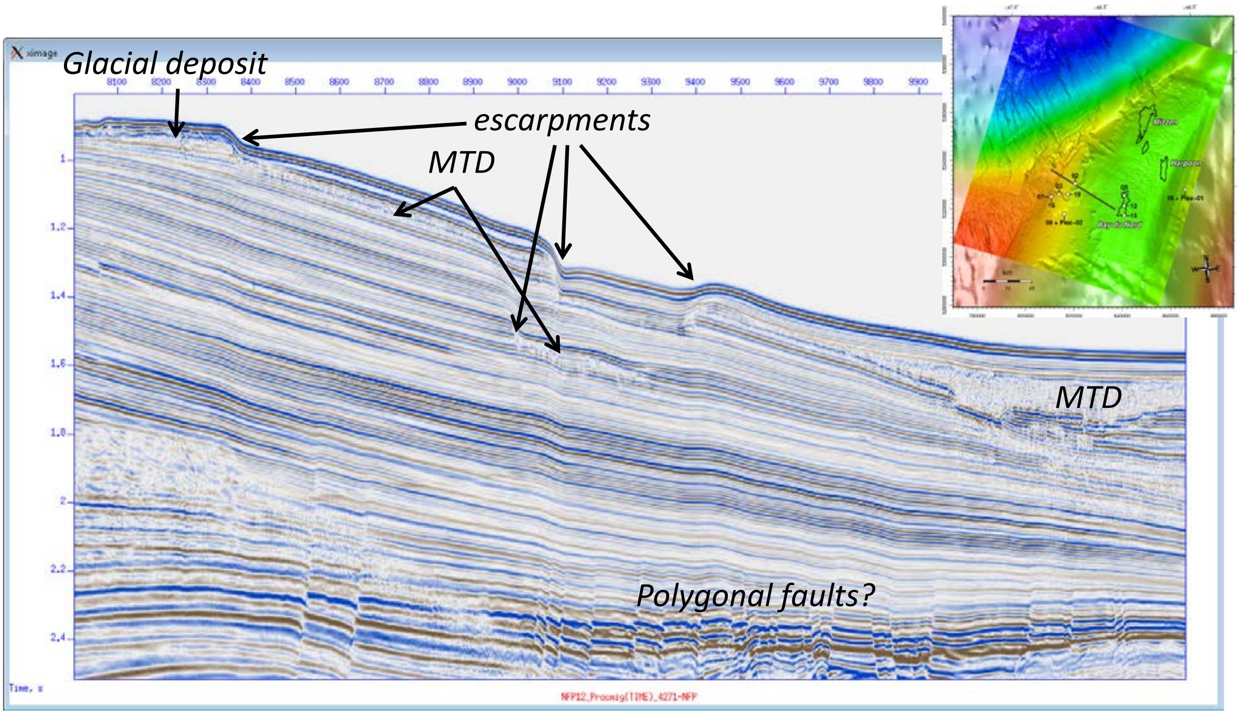

Figure E2.2.5 Seismic profile (NFP12_Procmig_4271) across the western flank and terminating at the development area. There is a nearly intact sediment drape along the entire line.

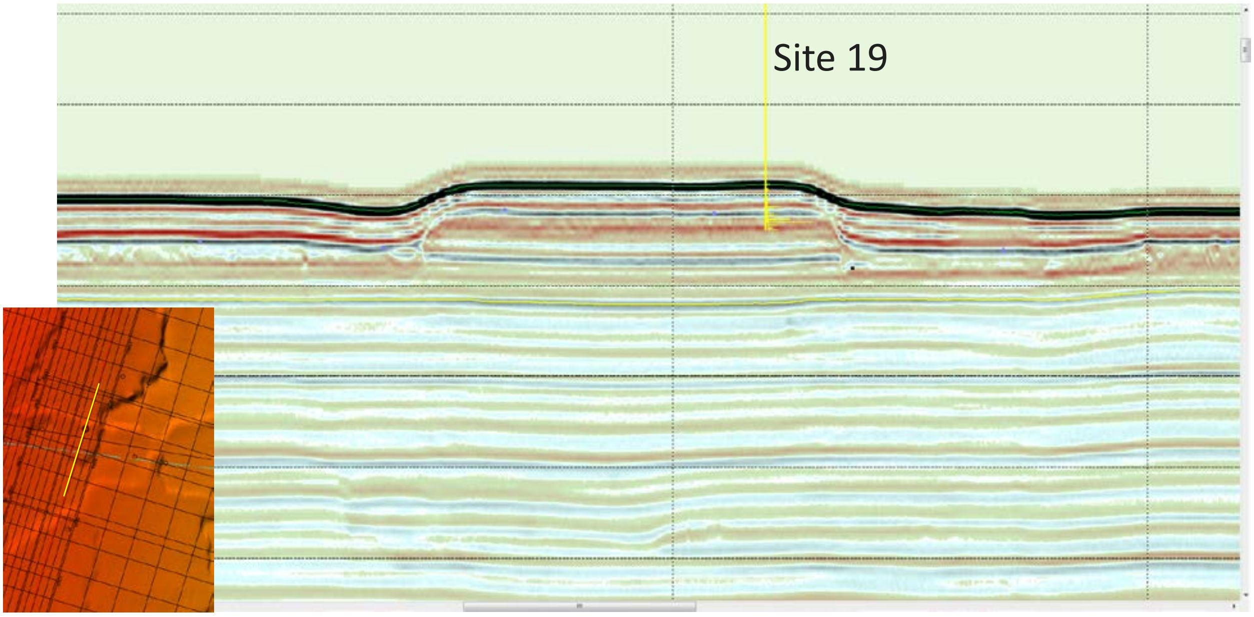

Figure E2.2.6 Seismic profile across site 19, located on a local high (survey ST14001). There is a nearly intact sediment drape along the entire line. The horizontal lines mark 100 m depth intervals.

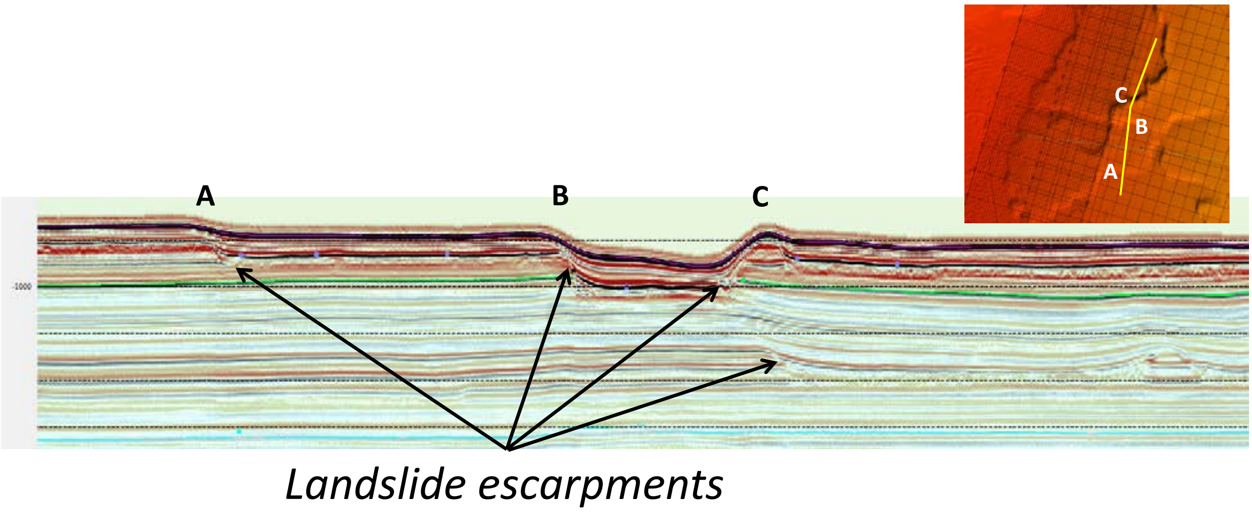

Figure E2.2.7 Random 3D seismic profile (survey ST14001) across a series of seabed irregularities, illustrating the occurrence of different buried escarpments. There is a nearly intact sediment drape across the entire line. The horizontal lines mark 100 m depth intervals.

E2.3.2 Field Development area

The bathymetry data from the Field Development area show no distinct evidence of recent instabilities (Figure E2.2.9). The seafloor morphology is essentially flat, with subtle irregularities in the northern half of the field outline. These undulations are likely the surface expression as a results of differential sediment infill on top of irregular landslide deposits. The latter become very clear on the 3D seismic data, and they appear as hummocky or semi-transparent units in between well-stratified sediments (Figure E2.2.10; Figure E2.2.11). The deposits are very thick, in places beyond 200 m, thus indicating that large-scale landsliding has affected this area significantly. They are also extensive, as these deposits can be identified along most of the seismic data from the field development area (Figure E2.2.10, Figure E2.2.11).

Considering the relatively low sedimentation rates obtained (see later), and the presence of an undisturbed sediment infill of about 80 m, then the timing of the last phase of basin wide failure would be approximately 265 000 years. There is, however, large uncertainty on this estimate.

We used the 3D seismic data to create a similarity cube, an attribute which highlights how similar neighbouring traces are. This attribute can be used to delineate the deformation characteristics at given depths.

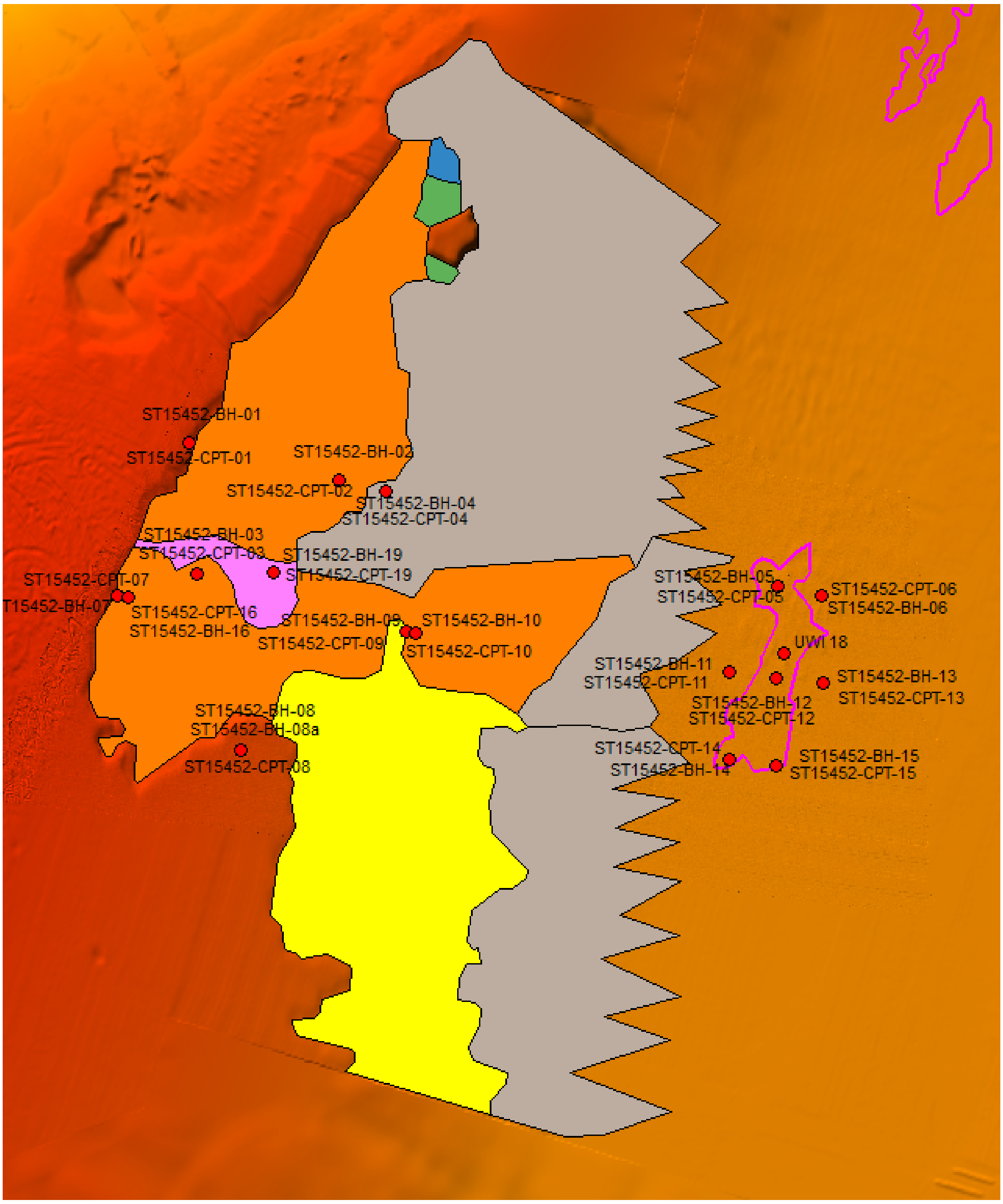

Figure E2.2.8 Slip planes in the investigation area. Colours represent identical slip planes. These are stratigraphically deeper towards the east. The saw tooth edge on the eastern side indicates that the slip plane is deeply buried, but continues eastwards.

Figure E2.2.14 shows a sub-surface depth slice (at 95 mbsf) of this similarity cube. This depth was selected as is corresponds to approximately the largest penetration of the geotechnical site investigation programme, while it also lies within the youngest, basin-wide MTD. On this figure, the light colours correspond to high similarity, and dark colour to low similarity. At this sub-surface depth, the central northern Flemish Pass is characterised by low similarity, typical for the seismo-acoustic signature of MTDs. This map also confirms the large spatial extent of the uppermost failure deposit.

Towards the western flank, we note the presence of a few slabs at this depth as well, originating at the location of the observed escarpments or paleo-headwalls expressed on the present-day seafloor. There is virtually no deformation along the upper slope. On the eastern flank, the site investigations also appear to lie within slab like failure zones, with somewhat higher dissimilarity compared to the western flank (see underneath).

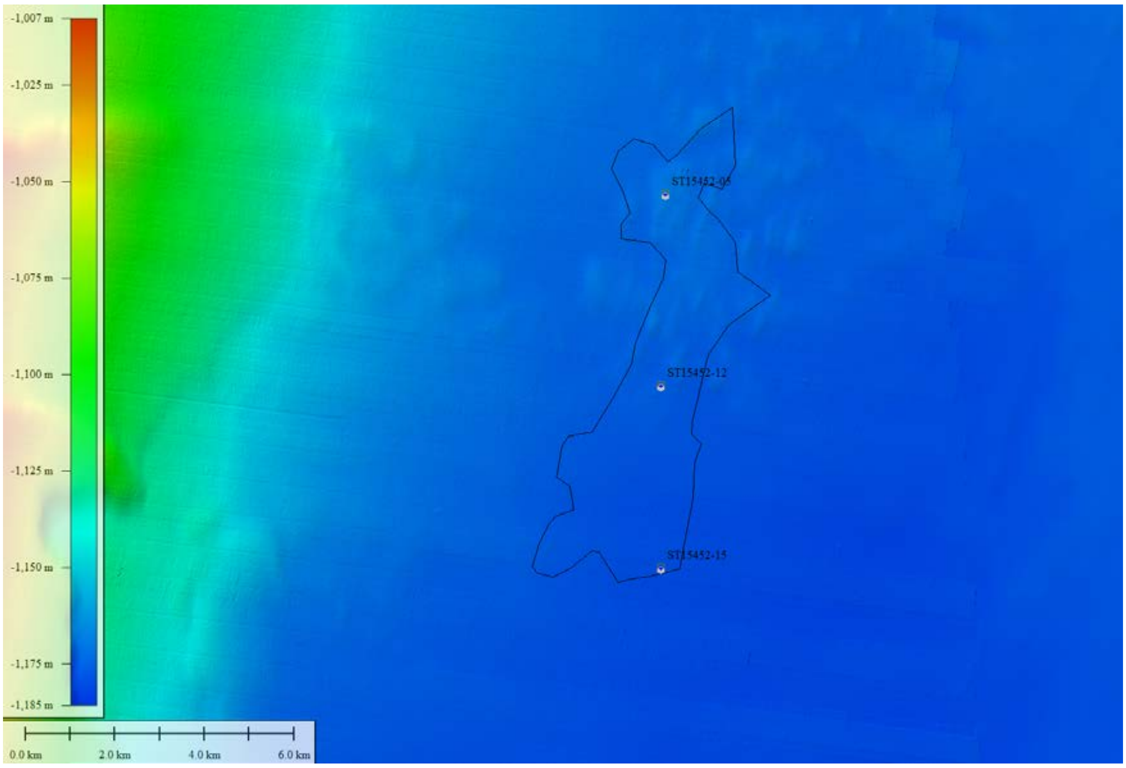

Figure E2.2.9 Bathymetry map over the Field Development area showing a fairly flat seafloor morphology. There are some irregularities around the northern part of the field, which are the result of sediment infill over paleo-landslide deposits.

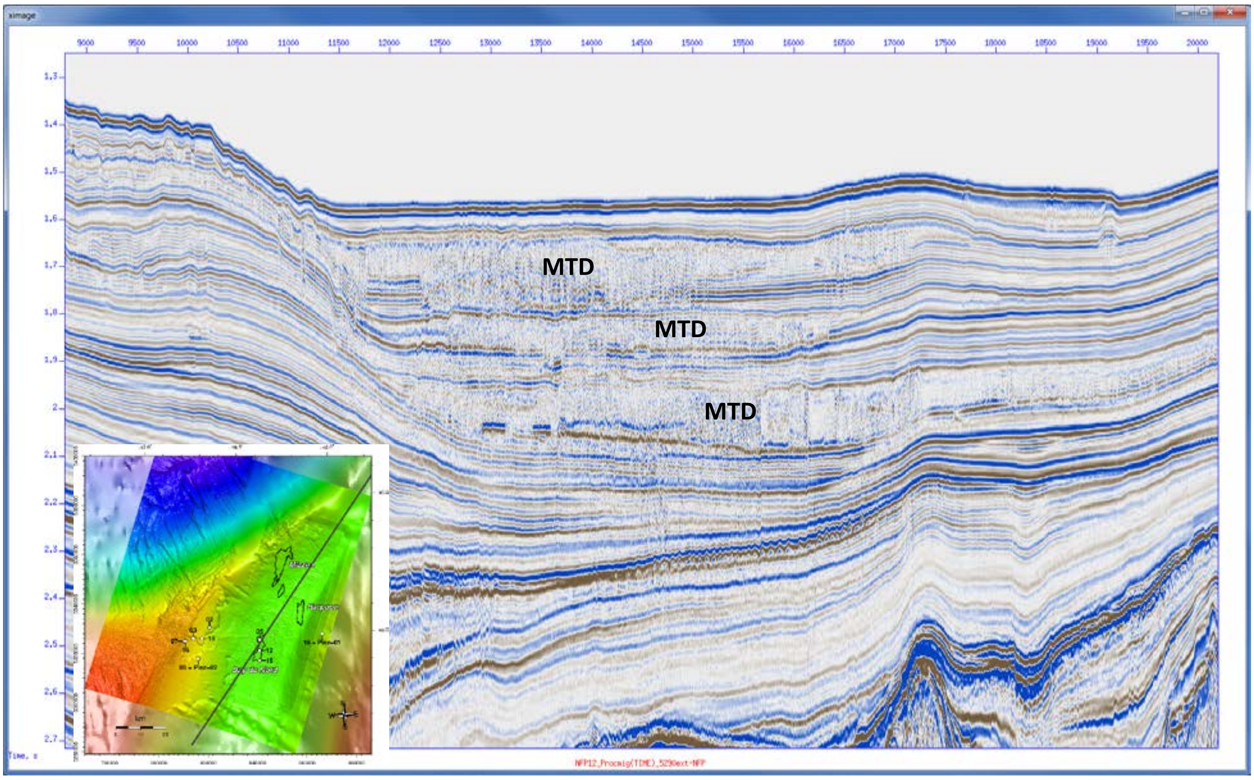

Figure E2.2.10 Time-migrated seismic profile (SW-NE, NFP12_Procmig_5290) across the Field Centre in the Flemish Pass. These data show that there have been at least 3 major submarine landslide episodes with nearly basin-wide deposits.

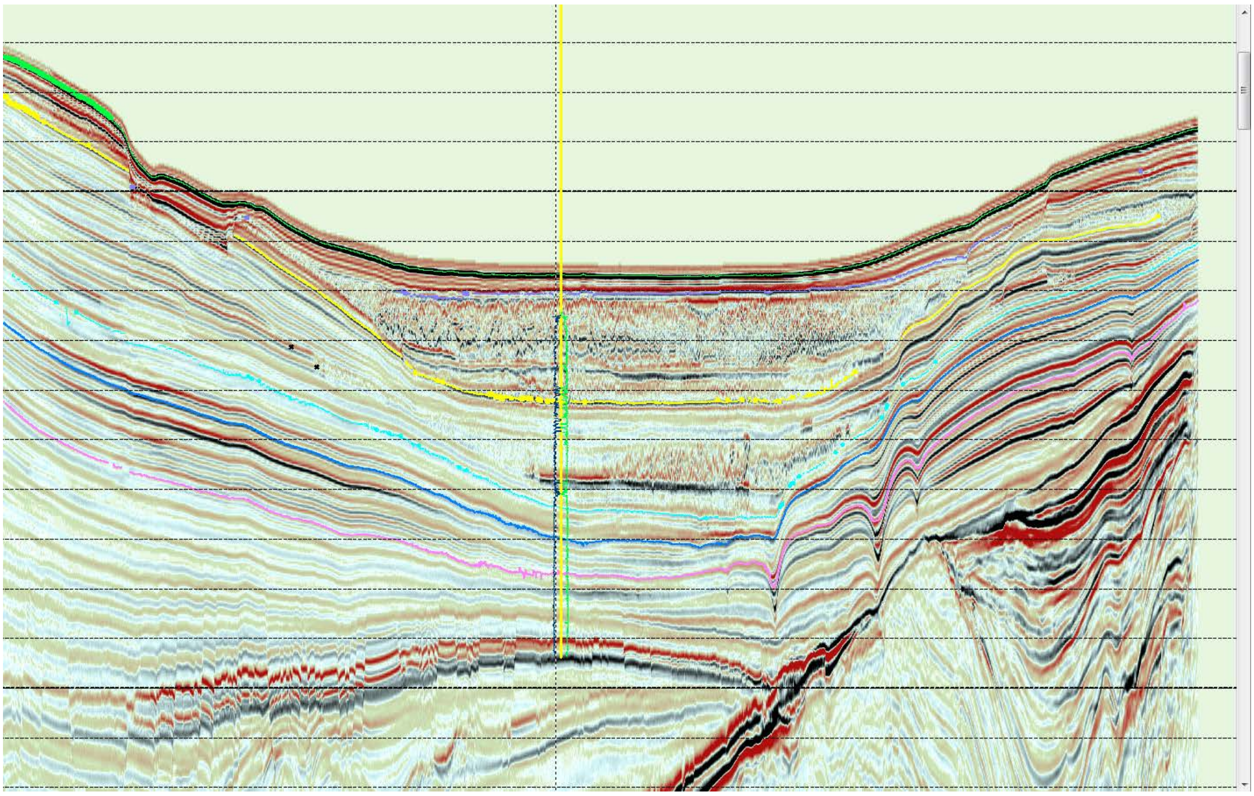

Figure E2.2.11 Depth-migrated seismic profile across the northern Flemish Pass (ST14001). For location, see Figure E2.2.14. Note the occurrence of various escarpments at the seafloor and buried within the stratigraphy. At the centre, there is evidence of several massive landslide deposits, of which the chaotic seismic response is an indicator. The yellow and green lines are well data. The horizontal lines mark 100 m depth intervals.

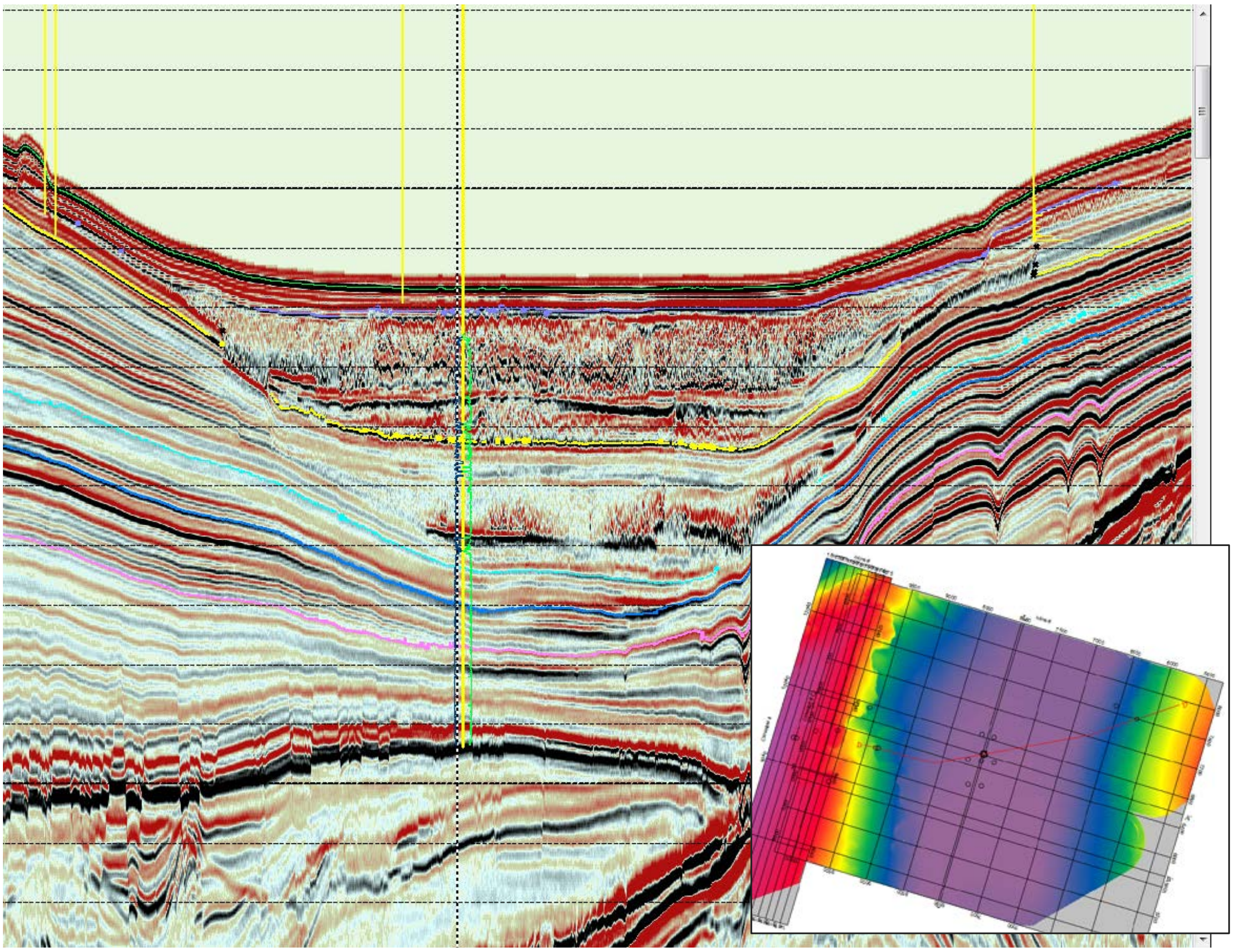

Figure E2.2.12 Random seismic line across the northern Flemish Pass extracted from the depth-migrated 3D volume (ST14001). For location, see the inset. Note the occurrence of various escarpments at the seafloor and buried within the stratigraphy. At the centre, there is evidence of several massive landslide deposits, of which the chaotic seismic response is an indicator. The yellow and green lines are well data (Field Centre) or CPTU data (flanks). The horizontal lines mark 100 m depth intervals.

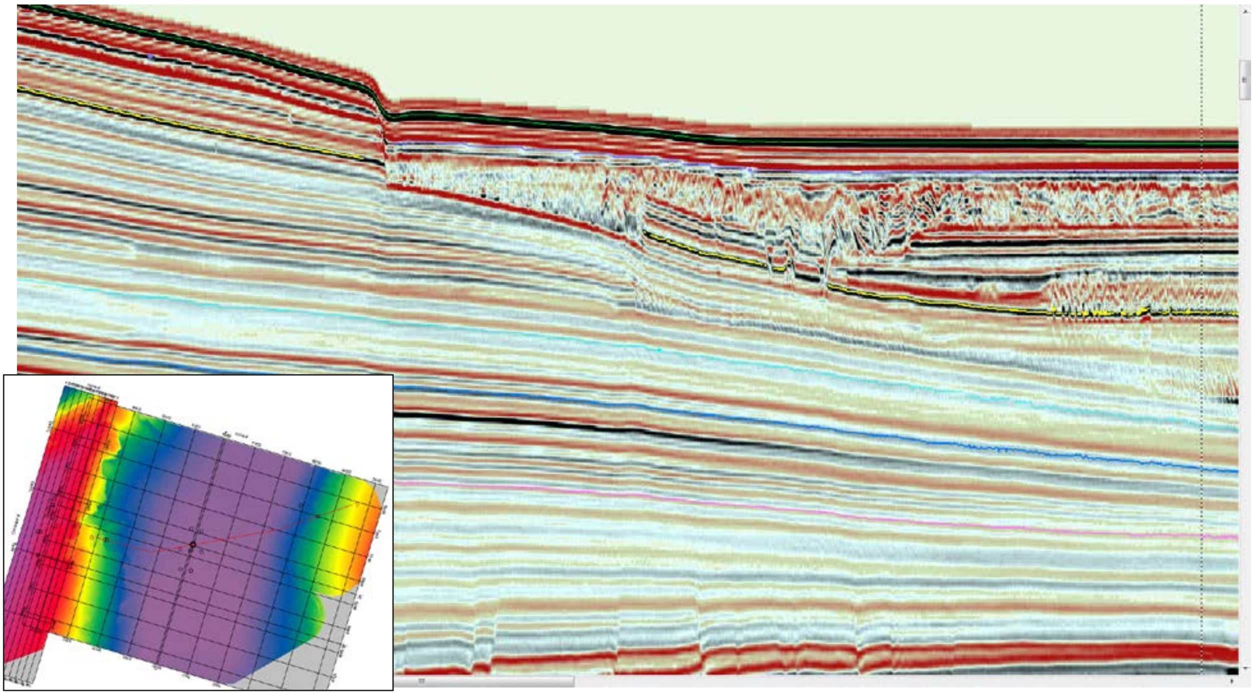

Figure E2.2.13 Seismic profile connecting the western flank and field development area (ST14001). Note the occurrence of landslide deposits at different levels in the stratigraphy, as well as an area characterized by overthrusting. The horizontal lines mark 100 m depth intervals.

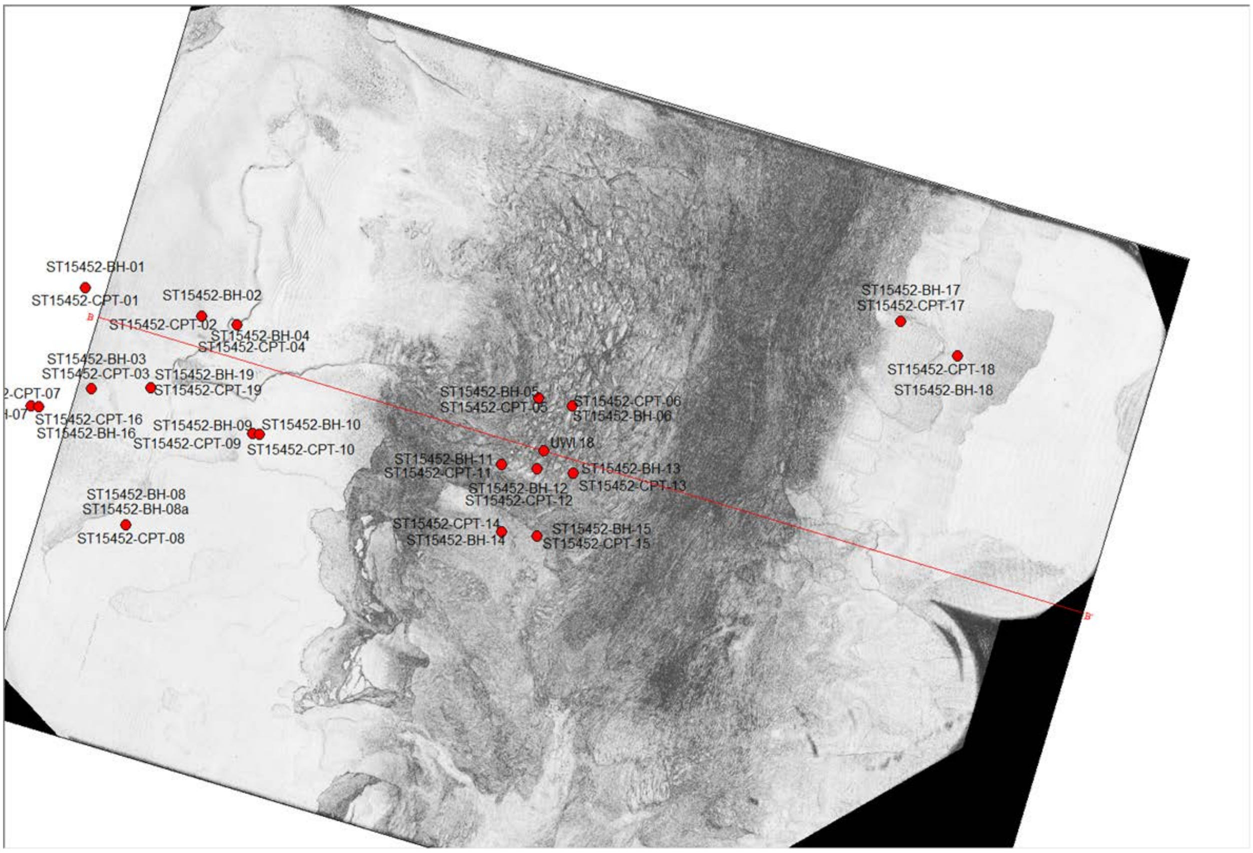

Figure E2.2.14 Slice, extracted from a similarity cube derived from the 3D seismic data (survey ST14001), from 95 m below the present seafloor. Light colours correspond to high similarity between the neighbouring traces, whereas dark colours correspond to low similarity. The data clearly illustrate the presence of blocks of various dimensions, from small to large, at this depth interval. The similarity is high close to the flanks of the Flemish Pass, but low at the centre (e.g., field development area). The red line shows the location of the seismic profile presented in Figure E2.2.11.

E2.3.3 Eastern Flank of Flemish Pass

The bathymetry data from the eastern part of the site investigation data are not conclusive for identifying recent slope failures, as the sites lie too close to the termination of the higher-resolution data available. The seismic data indicate, however, that there have been several episodes of failures in the geological past in that area (Figure E2.2.15), which is also evident from the similarity cube (Figure E2.2.14). The acoustic signature of the MTDs is probably affected by the relatively low resolution of the geophysical data.

The failures appear different than those on the western flank. The MTDs are draped by post-slide sediments of about 50 m, but the MTDs themselves are relatively thin deposits. The seismic line reveals deformation at two different levels in the stratigraphy, each with a headwall or sidewall expression. BH-18 appears to terminate close to or at the top of the deeper MTD, and it has penetrated the tail or downslope part of the deformation zone of the upper MTD (Figure E2.2.15).

Various geotechnical parameters derived from the measured CPTU data at BH-18 are shown in Figure E2.2.16. The data indicates that the soil is essentially a normally-consolidated clay to silty clay. The data show a subtle variation in trend in q_t and derived parameters between 52 and 70 mbsf, which corresponds to the tail of the upper MTD observed on the seismic data. This behaviour can thus probably be attributed to the deformation or remoulding effect retained in the landslide deposit. It is not clear whether or not the second MTD was penetrated.

A standpipe piezometer was installed at this location at a sub-surface depth of approximately 85 m. The piezometer is monitoring the long-term evolution of pore pressure, and will likely be retrieved in the late Spring to Summer of 2016.

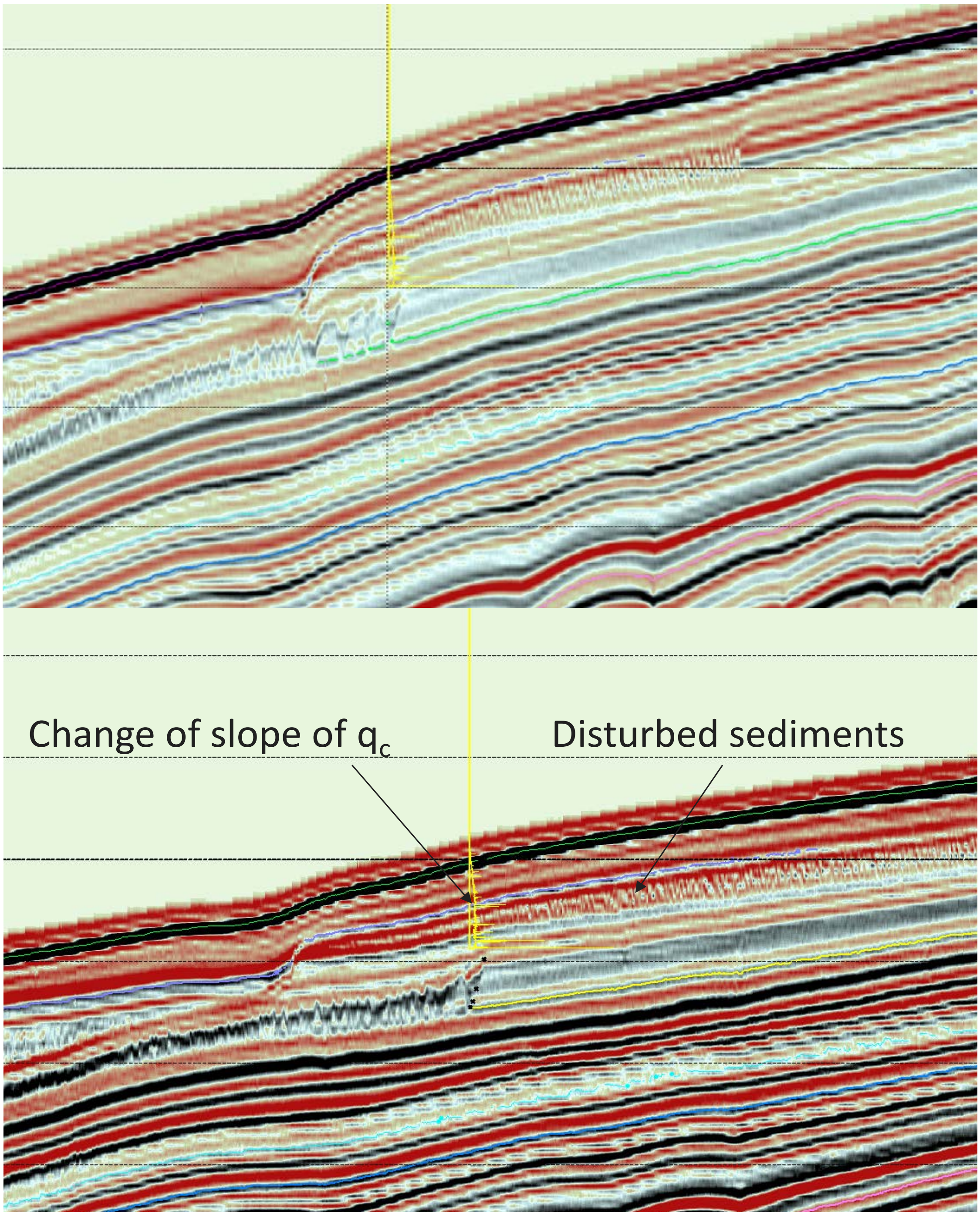

Figure E2.2.15 3D seismic data examples (survey ST14001) showing buried landslide complexes along the eastern flank of the site investigations, across site BH-18 (yellow line). The profile at the top shows two headwalls. The profile at the bottom focuses on the location of the geotechnical borehole.

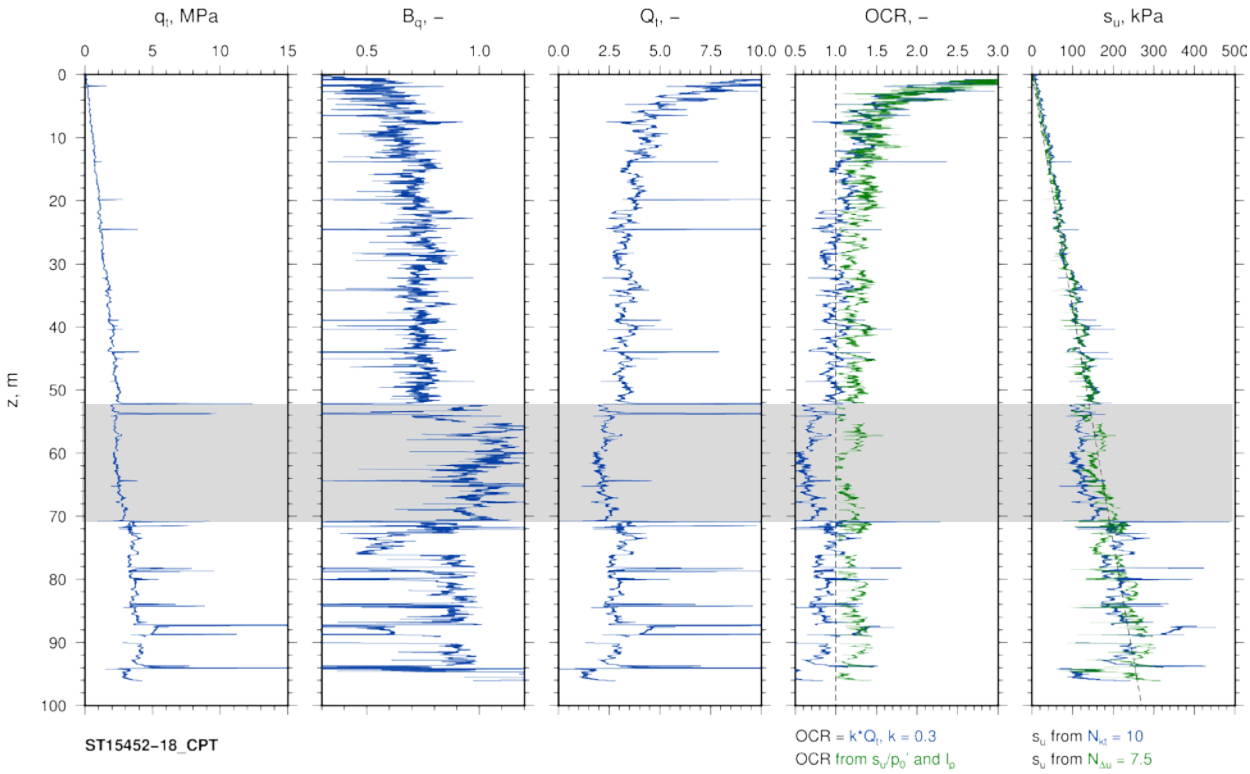

Figure E2.2.16 Various geotechnical parameters (corrected tip resistance q_t, pore pressure parameter B_q, normalized tip resistance Q_t, OCR, and undrained shear strength s_u) derived from the measured CPTU data set at BH-18, eastern flank, down to about 100 m. The grey shading marks the interval where the CPTU penetrates the deformation zone of the upper MTD (see Figure E2.2.15).

E2.4 Age control

With respect to hazard assessment, it is of critical importance to obtain reliable information of (1) when the slope instabilities took place and (2) how large the affected area is. For the latter, a combination of seismic data and bathymetry data can often be used to obtain reasonable estimates of the impact of the instability. For the former, one can use a number of direct and indirect methods, each having their advantages and disadvantages. The methods adopted here and the obtained results are briefly explained in the following sub-sections.

E2.4.1 Radiocarbon dating

Radiocarbon dating is the most used dating method for geotechnical site investigation approaches. However, the method cannot be used for soils that were deposited prior to about 45000 years ago, and the soils should have sufficient amount of organic material that can be used for dating.

Of the ten (10) analyses performed, four (4) fell outside the reliable age range of the radiocarbon method. The other six (6) samples gave results with relatively low uncertainty (small standard deviations, see NGI, 2016). The results are shown in Figure E2.3.1, and indicate that the radiocarbon method is only suitable for dating the top 7 to 8 metres of soil across the Flemish Pass site investigation area.

The average gross sedimentation rate (i.e., not correcting for compaction) is around 30 cm per 1000 years, which is low. Similar values were reported from the area (Huppertz, 2007). Sedimentation rates are likely variable across the area. However, in deeper waters, the sedimentation is controlled by the Labrador Current system flowing through the Flemish Pass (Mao et al., 2014). In shallower waters and closer to the paleo-ice margins, sedimentation rates may well be significantly higher, particularly at the end of glacial periods.

The linear regression of the obtained depth-age data also indicate that there was little sedimentation in the Holocene. The fact that iceberg ploughmarks remain visible on the bathymetry data from the Sackville Spur west of the study area confirms this, as sedimentation tends to smoothen the irregularities in the seafloor.

The low sedimentation rates suggest that the soils will be normally-consolidated, except where there is a significant input of glacial sediments or erosion and deposition related to submarine instabilities.

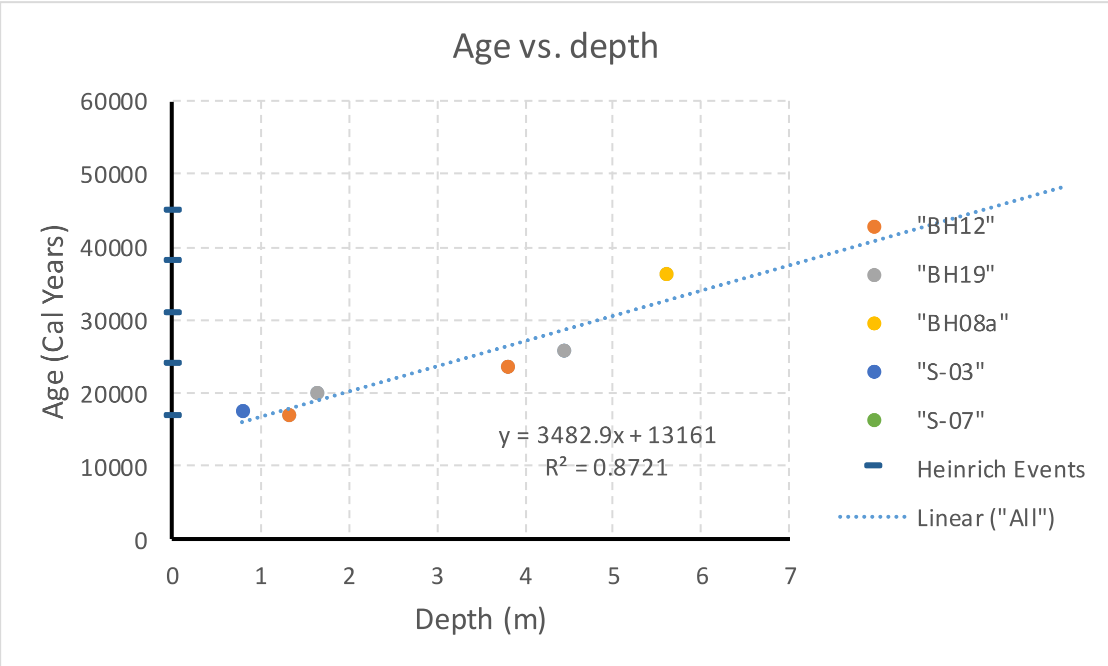

Figure E2.3.1 Age-depth model derived from 6 radiocarbon dates from the field development area (BH12) and the western flank (other data points). The dashed light blue line represents the best-fit linear regression equation for the 6 data points. The thick dark blue markers along the y-axis indicate the timing of Heinrich events 1 (youngest) to 5 (oldest).

E2.4.2 Micro-fossil descriptions

Micro-fossil description is necessary to (i) identify specific targets for further analysis, (ii) assess similarities between the species from different core sites, and (iii) identify potential climatic signals based on the type of species. Considering that the occurrence of species depends on the ambient environmental conditions, their presence (or absence) can be used as a proxy.

Table E2.3-1 summarizes the micro-fossil descriptions on the samples available. The first ten on the list are those that were selected for radiocarbon dating. The table is essentially compiled by the University of Bergen in collaboration with NGI.

Table E2.3-1 Micro-fossil description of the samples retrieved from the site investigations, including the 10 samples targeted for radiocarbon dating and additional samples from BH12 and BH19. As with the MIS table, the cells with blue shading refer to cold conditions, and those with orange shading to warmer conditions.

Borehole	Tube	Depth interval (m) sieved	Age, ^{14}C	Age, cal	Description of micro-fossils
S-03	1A	0.78	14770	17513	*N. labradoricum* dominant *E.excavatum* with other cold-water benthic species Few planktonic species
BH12	1B	1.30	14380	16970	*N. labradoricum dominant*
BH19	1B	1.62	16930	19945	Small amounts of benthic species; *E. Excavatum* dominant
BH12	2B	3.78	20040	23663	Mainly planktonic species, with few benthic species.
BH19	2C	4.42	21950	25840	Small amounts of planktonic species
BH-08a	1A	5.58	32920	36443	Abundance of *E. Magellum*; few planktonic species Some smaller shell fragments Sea urchin fragments larger than 1 mm occur Likely shallow marine evironmental conditions
BH12	3B	6.68	>43500	NA	Many planktonic specimens. Plenty of *N. labradoricum* and *E. Magellum* Open ocean conditions of temperature to cold water masses
BH19	3C	7.20	>43500	NA	Many planktonic specimens, but also plenty benthic of species indicative of cold conditions. Abundant sponge spicules.
BH19	01C	10.00	>43500	NA	Many planktonic specimens. Only few cold water benthic specimens.
BH12	5A	10.10	>43500	NA	Many planktonic specimens. Few benthic specimens. Numerous diatoms. Shell fragments larger than 1 mm occur.
BH12	8C	18.13	NA	NA	Relatively rich in planktonic forams, dominated by *N. Pachyderma* (*sin*), but also *N. Quinquelobe* and *G. Bulloides*. Benthic species also occur, e.g., *Wüllerstorfi*, *N. Labradorica* and reworked *E. Excavatum*. Also contains sponge spicules. Indicative of interstadial and/or interglacial environmental conditions
BH12	15A	31.72	NA	NA	Virtually no planktonic specimens. Some benthic specimens, mostly *N. labradorica*, but also *B. marginata* and sporadically *E. Magellum*. **Occurrence of volcanic shards**. Abundance of pyritised grains and burrows. Glaciomarine conditions or cold interstadial conditions
BH12	19B	42.28	NA	NA	Mainly terrigeneous material, with few planktonic forams of which >99 % were *N. pachyderma* (*sin*). Sporadic occurrence of *G. Bulloides*. Virtually no benthic forams, some *B. Marginata sp.* *Glacial or glaciomarine conditions*
BH19	4C	15.43	NA	NA	Rich in planktonic forams, mainly *N. Pachyderma* (*sin*). Many *B. marginata*, *M. barleeanum*, *C. laevigata*, *N. labradorica* og *C. lobatulus*. Interstadial or interglacial conditions
BH19	5C	26.20	NA	NA	High abundance of diatoms, composing almost the entire grain size fraction of 100 microns. **Many basaltic volcanic shards of various sizes** Virtually no planktonic forams, and very few benthic forams (mainly *N. Labradorica*) or planktonic forams. Nutrient-rich environment in open ocean conditions, with cold temperatures; cold but not extreme
BH19	8C	31.95	NA	NA	Somewhat smaller amounts of planktonic species than in sample BH19 4C. Almost exclusively N. Pachyderma (sin). Of the benthic species, B. Marginata is most abundant with little M. Barleeanum. Relatively warm conditions; interstadial or cold interglacial

E2.4.3 Multi-sensor core logging

The University of Bergen has logged borehole ST15452-S-05 and -05a (field centre) using a GEOTEK multi-sensor core logging tool, using the whole-round core (not split). The logs, shown in Figure E2.3.2, consist of:

a. *P*-wave velocity and quality, using transducers on the core liner and frequencies around 230 kHz. Low quality typically indicates that the P-wave velocities are less reliable, e.g., due to the presence of fractures, gaps, or gas.
b. Gamma-ray density, using a narrow collimated beam of gamma rays emitted from a 137Cs source and energy of 0.662 MeV. Photons pass through the core and are detected at the other side. Gamma ray attenuation at these frequencies is dominated by Compton scattering on electrons in the core. Therefore, the attenuation depends on the number of electrons in the beam, which yields a proxy for the bulk density of the soil.
c. Magnetic susceptibility (MS), i.e., the degree of magnetization of a soil in response to an applied magnetic field. Variations in MS are typically used to infer changes in the sedimentary environments, provenance and/or diagenetic environment. Values reported here are either the *measured volumetric magnetic susceptibility* or the *mass specific magnetic susceptibility* (i.e., the volumetric MS divided by the measured bulk density).

NGI has applied a correction to the depths of the logs as the logs received from Bergen did not take into account the gaps due to intervals removed for geotechnical analyses. The data with values that were considered to be unrealistic were subsequently removed. For the *P*-wave velocity data, only points where the amplitude quality was above 80 were retained.

Correlations of magnetic susceptibility, and potentially the density, between different cores/boreholes may provide a relative dating of the soils. When the sediments are deposited under similar environmental conditions (e.g., oceanography, glacial input), the provenance of the sediments would imply that there are similarities in the MS records. Thus, the comparison of logs with well-calibrated cores from nearby areas on which a full-scale sedimentological, climatic and paleoceanographic analysis (e.g., oxygen isotope analysis or $\delta^{18}O$ records) is conducted in high vertical resolution (e.g., iODP) may provide an indirect proxy for the sedimentary history and a litho-stratigraphic framework in the study area when only little information can otherwise be extracted (e.g., Weber et al., 2001; Rasmussen et al., 2003). Furthermore, Heinrich layers may have a significant signature on both the density (positive anomalies) and MS logs (also positive anomalies). An example from the relatively nearby Marion Dufresne (MD) core 2024 (for location, see Figure E1.1.1), from the Orphan Knoll is shown in Figure E2.3.3.

As mentioned above, the northern Flemish Pass is swept by the Labrador Current which is one of the main controlling factors for the sedimentation history in the area. Also the ice cover history should be fairly similar across the region. The three MD cores from the

Orphan Basin (for location, see Figure E1.1.1) and BH-05 are thus from relatively similar oceanographic environments. Therefore, it is of interest to evaluate and compare the records from the different sites to check whether or not one can extend the age dating across the area using the core logs as proxies.

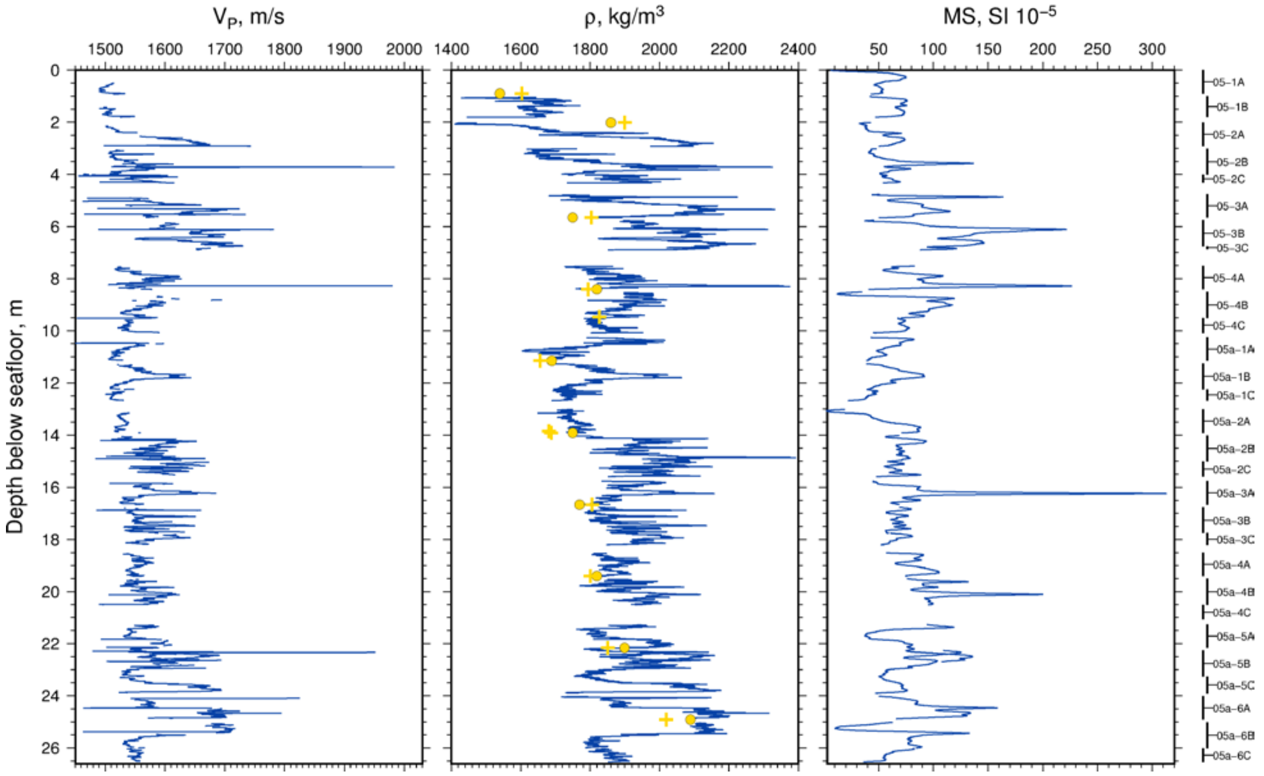

Figure E2.3.2 Multi-sensor core logging results from BH-05 and BH-05a, Field Development area, showing P-wave velocity (left panel), bulk density (middle panel) and volumetric magnetic susceptibility (right panel) versus depth. The labels to the right represent the core sections. The yellow circles and crosses on the bulk density plot are densities from laboratory measurements, determined from the bulk sample dimensions and water contents, respectively.

The critical units are the Heinrich layers, considering their peculiar signature on the MSCL data. Whereas the Heinrich layers stand out on the logs from the Orphan Basin, they are less distinct on the logs from the Field Development area, for both the density (Figure E2.3.4) and magnetic susceptibility (Figure E2.3.5). A tentative interpretation, taking into account the radiocarbon dates and the MSCL results, is added to the BH-05 logs (Figure E2.3.4, Figure E2.3.5). Even though there is large uncertainty, the first 8 Heinrich layers may occur in the top 15 m of soil, going back to approximately 75000 years. Underneath, no distinct patterns are present to the naked eye, and comparison is thus complicated.

In order to establish an improved and less biased numerical match between the different logs and further extend the chronology, NGI is currently investigating the use of a numerical technique developed to match time series, known as the concept of dynamic time warping (e.g., Giorgino, 2009). The underlying philosophy is to use the cores on which (nearly-continuous) oxygen isotope analysis was conducted as a reference, and optimally match the records from BH-05 by compressing and/or stretching various segments of the data. To this end, NGI is testing an open-source library *dtw* (*dynamic time warping)* developed for the statistical software package *R* (Giorgino, 2009). This method appears promising, but requires further testing, as there are a number of challenges:

1. There are inconsistencies between the presented reference logs in literature (e.g., Weber et al., 2001) and the actual data available in the public-domain Pangaea database (https://www.pangaea.de/). The discrepancies lie in the continuity (or discontinuity) of the data (e.g., compare Figure E2.3.3 with Figure E2.3.4 and Figure E2.3.5, around the H5 event).
2. The occurrence of gaps or invalid data points introduces uncertainties, which need to be addressed.
3. As the logs from the different areas do not necessarily represent the same time span, one needs to be cautious on allowing relaxing the start and end point for the comparison.
4. NGI has also contacted the Geological Survey of Canada (Dr. David Piper) to verify whether or not more suitable data are available from the area.

This is a novel approach and needs further work. NGI only became aware of this method recently.

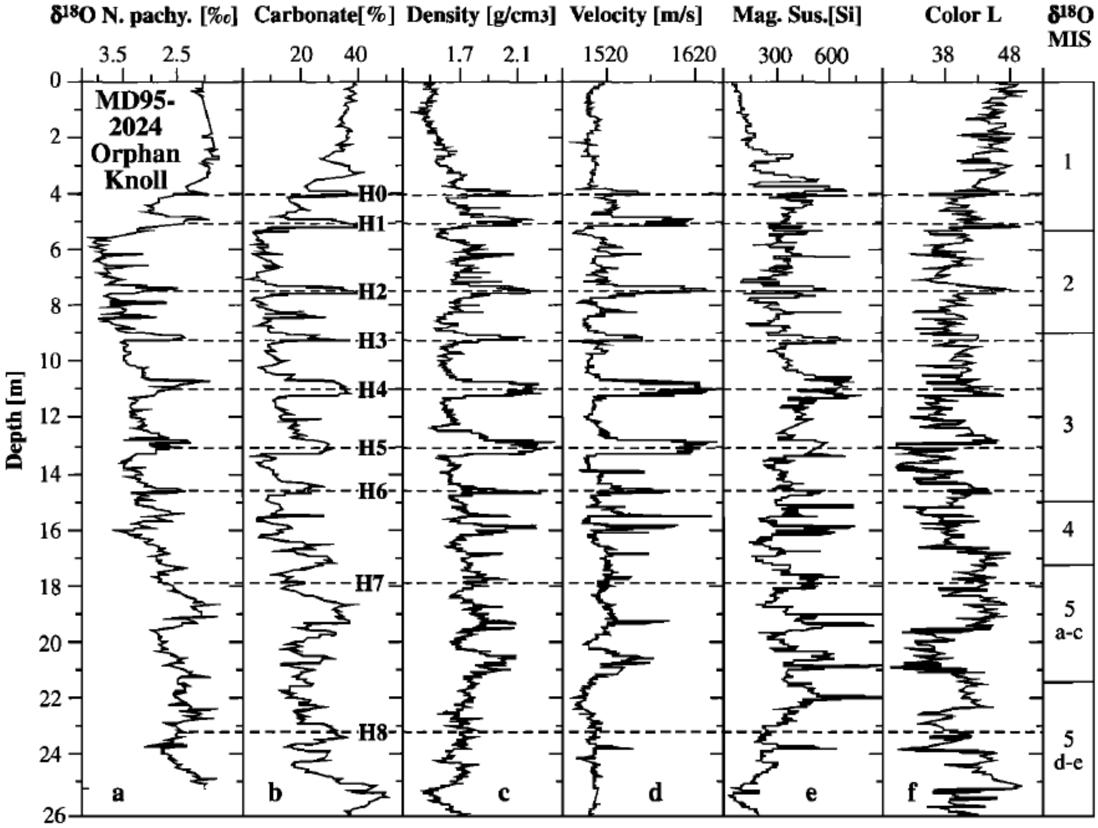

Figure E2.3.3 Various logs derived from sedimentological and paleoceanographic analyses from a sediment core from the Orphan Knoll (Weber et al., 2001). The Heinrich layers are typically characterised by high carbonate content and positive anomalies in the density and magnetic susceptibility data. For location of the core, see Figure E1.1.1.

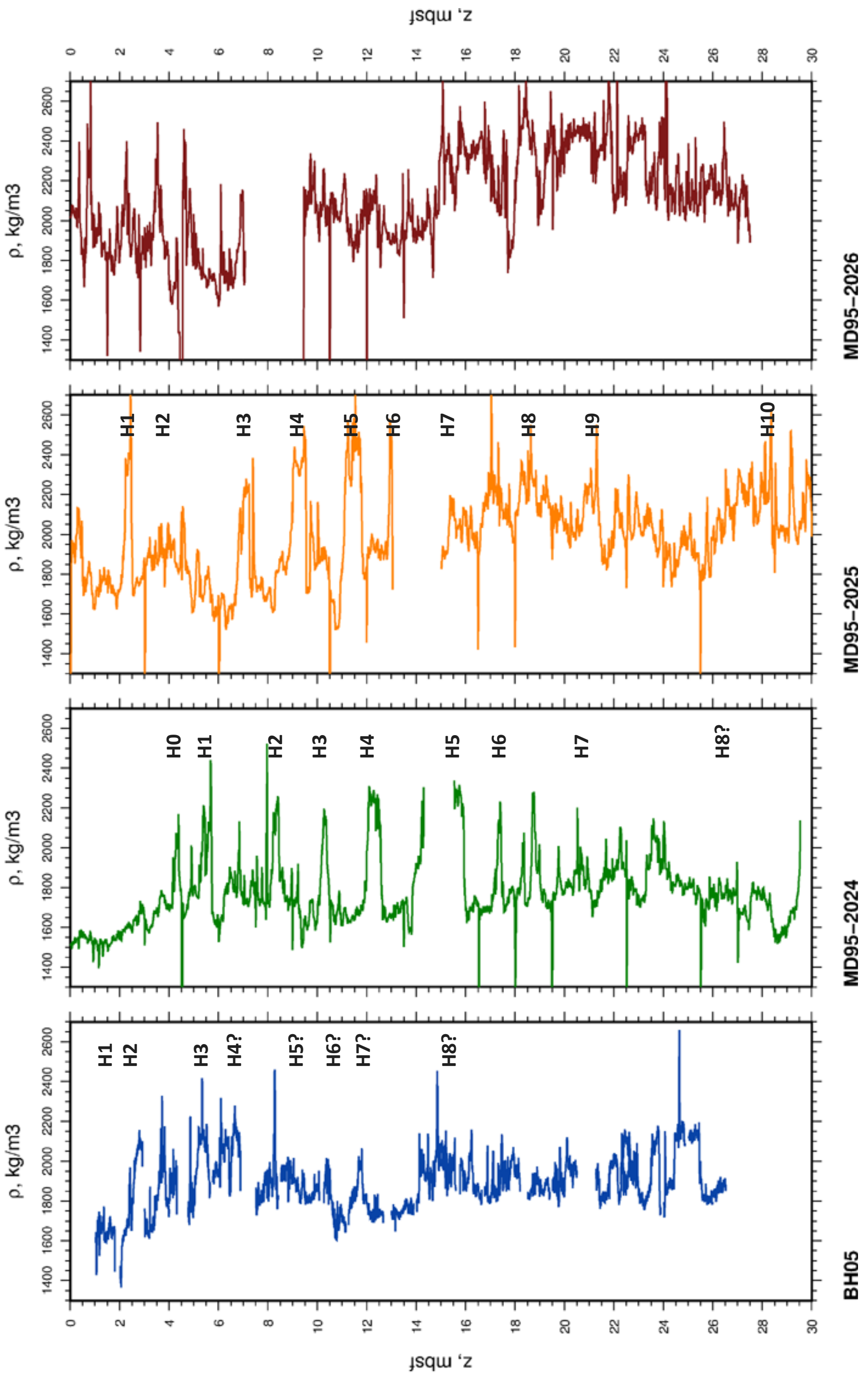

Figure E2.3.4 Bulk density from MSCL from BH-05 as well as three reference cores (Orphan Basin, data downloaded from https://www.pangaea.de/; for location, see Figure E1.1.1). The interpretation of Heinrich layers on the Marion Dufresne cores is based on Weber et al., 2001.

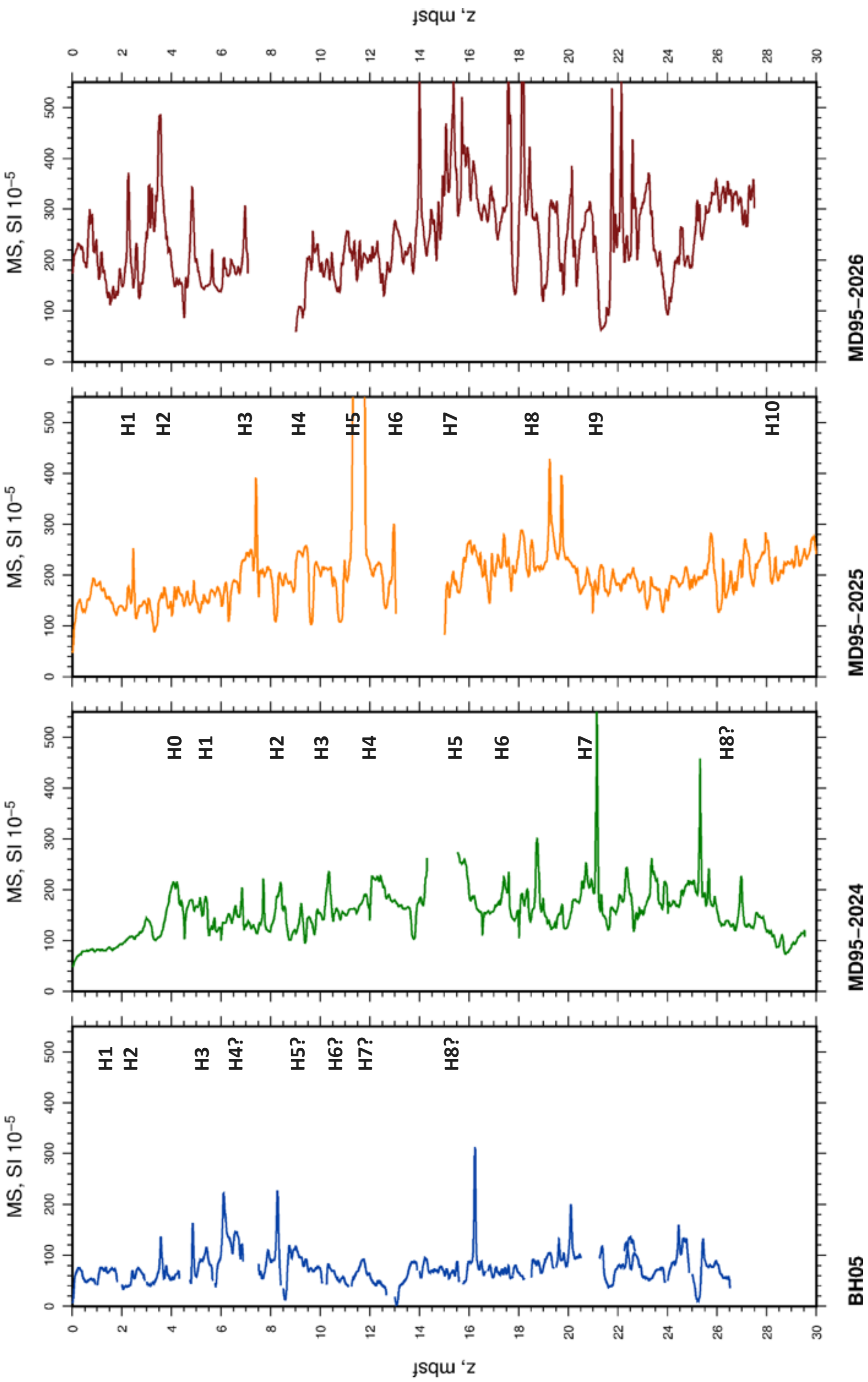

Figure E2.3.5 Volumetric magnetic susceptibility as well as three reference cores (Orphan Basin, data downloaded from https://www.pangaea.de/; for location, see Figure E1.1.1). The interpretation of Heinrich layers on the Marion Dufresne cores is based on Weber et al., 2001.

Because Heinrich layers characteristically contain a large proportion of carbonates, *XRF* (*X*-ray fluorescence) scanning was performed at the University of Bergen on borehole S-05/05a to better identify where they occur (Figure E2.3.6). The *XRF* scans provide relative quantities of 28 elements every 2 mm along the length of the split samples.

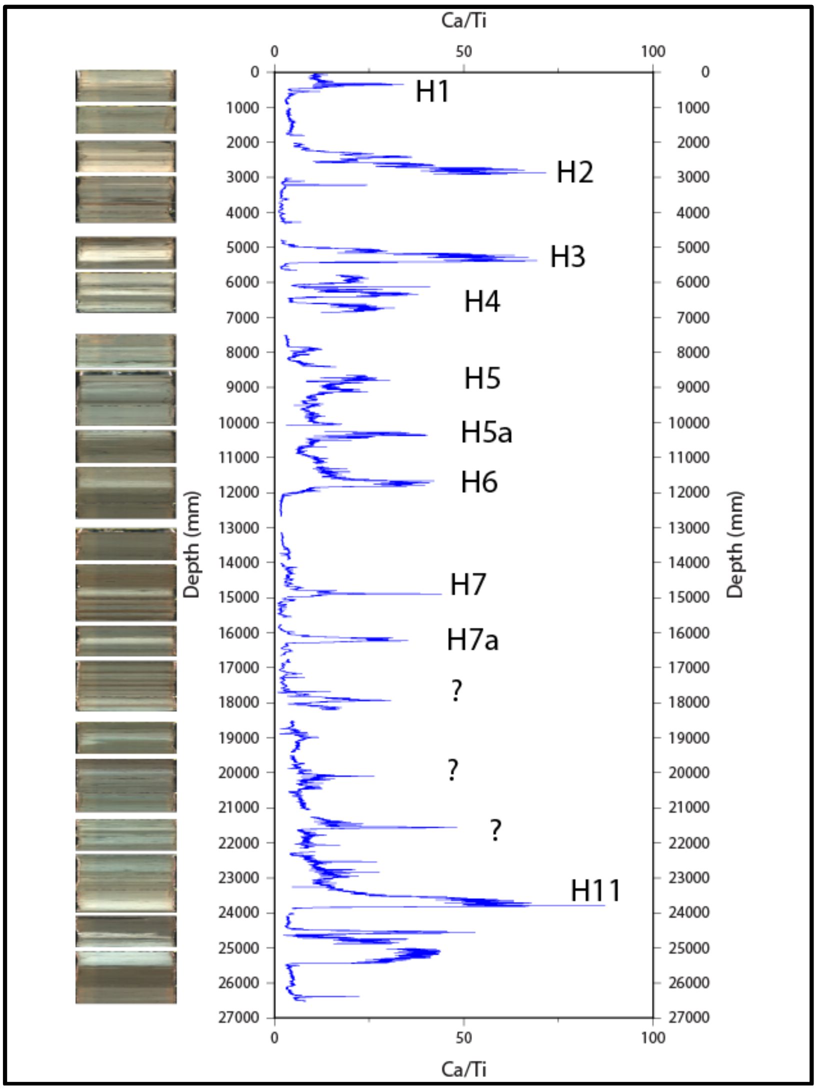

Figure E2.3.6 Plot of Ca/Ti ratio from XRF measurements in borehole S-05/05a showing clear peaks in the Ca content corresponding to the carbonate pulses associated with Heinrich Events. The colour scans of the cores on the left show that the Heinrich Events are associated with lighter colours of the sediment. The annotations indicate which Heinrich Event the individual peaks are interpreted to have been derived from.

Using the ages of the Heinrich Events and their depths in borehole S-05/05a allows extension of Figure E2.3.1 back in time to about 130 kyr BP (Figure E2.3.7) which shows that there have not been any great changes in sedimentation rate.

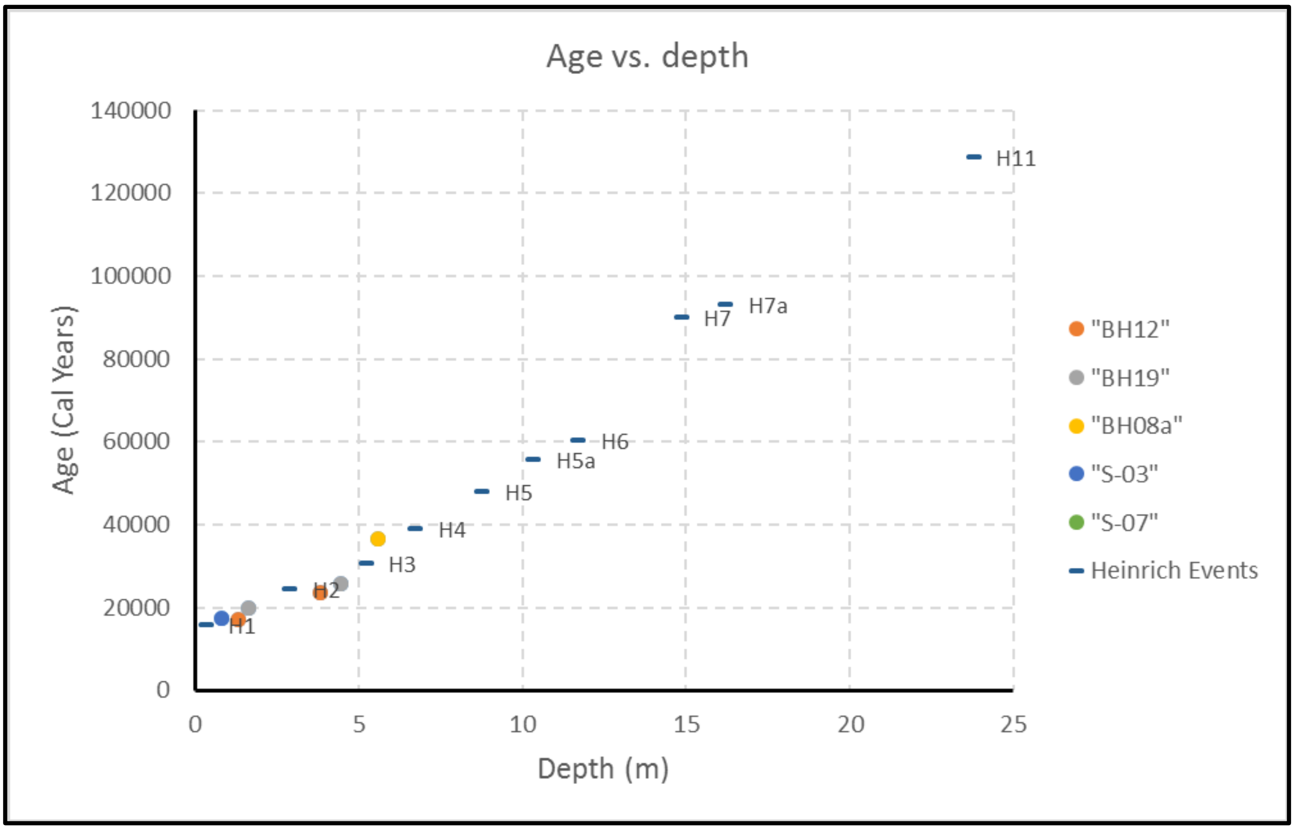

Figure E2.3.7 Age vs. depth model including both radiocarbon dates and interpreted Heinrich Events.

E2.4.4 Tephra stratigraphy

Tephrachronology can also be used for correlating the occurrence of tephra layers on land and offshore, and assist when dating is otherwise difficult. In essence, volcanic ash layers have often a very specific geochemical signature typical for volcanic source zone. Following volcanic activity, ash falls on land, ice, lakes and ocean, forming primary tephra deposits with fairly large spatial coverage. However, when the ash falls on sea ice and glaciers, it may take time before the deposition takes place. Once one knows the origin and the timing of the volcanic eruption, the presence of the ash layer is a proxy for the age of the sediments. For further reference, see for example, Brendryen et al., 2010.

Segments rich in tephra were selected at Bergen University from two boreholes (field centre, borehole 12, 31.7 mbsf; western slope, borehole 19, 26.2 mbsf). In total, 40 shards were handpicked from the 106 micron fraction in core BH 19-5c (26.2 m), split into 20 light brown and dark brown coloured shards. From the >106 micron fraction in core BH 12-15a (31.8 m), a total of 39 shards were handpicked, of which 18 were light brown and 21 dark brown. All the samples were mounted on a tape for preparation of a polished thin section for geochemical analyses using a microprobe. All the grains were therefore cut so the morphological bias of the single grains could be ignored. The shards were analysed using the EDS facilities on the SEM Zeiss supra VP electron microscope at the University of Bergen. Here, the analytical settings were 15 kV, 10 mA for probe current and 20–60 s for the counting time. All picked grains were analysed. The method normalizes all totals to 100%.

Figure E2.3.8 presents cross-plots of the fraction of given geochemical elements for the two ash layers analysed. The geochemical signatures cannot unambiguously be matched to one volcano system. The results illustrate basically that each sample consists of a mixture of tephra from different volcanic systems in Iceland and grain from BH19-5c is coming from Jan Mayen or possibly from one of the west coast USA volcanoes. All are of a basaltic type of origin and commonly not necessary explosive. So the volcanoes have not transported much material into the stratosphere and to reach the site area – with the present circulation system – the material needs to be transported around the northern hemisphere. The mixed composition and the large grain size means that this has been transported by ice. Colour discrimination did not yield significantly different results.

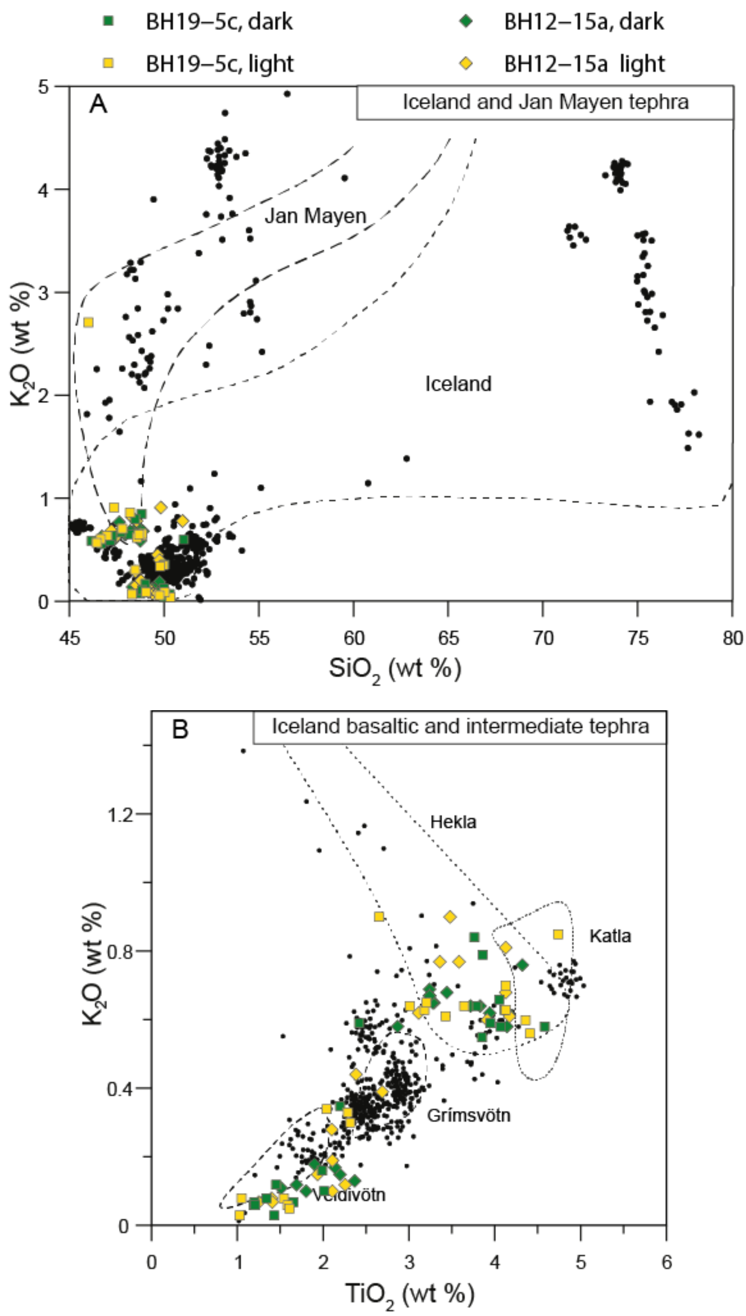

Figure E2.3.8 Cross-plots of geochemical test results of the tephra shards found in cores BH12 (Field Development, diamonds) and BH19 (western flank, squares). The yellow vs. green colouring indicates the light or dark colours of the shards, respectively. The background data (black dots) are compiled from a larger database, with documented geochemical provinces (see Brendryen et al., 2010 and others).

E2.4.5 Amino-acid analysis

Amino-acid dating uses the ratio of isomers or configurations of organic compounds in biological tissue. The method requires abundance of foraminifera (e.g., *N. Pachyderma sinistral*), but also knowledge of environmental conditions (e.g., water temperature). Using this method, one can go back to approximately 500 to 700 kyr, and thus it provides suitable extension to the radiocarbon method.

The amino-acid analysis is currently on hold, due to logistical issues with the laboratory in Colorado. Forsberg et al. (2003) applied this method to a sediment core from glacial environments off Antarctica.

E3 Summary and suggested further work

E3.1 Geohazard assessment

A full geohazard assessment, with particular focus on submarine instabilities, requires understanding of the magnitude (extent, thickness, source areas) as well as timing of paleo-landslides as well as determining the pre-conditioning and triggering factors that have brought the margin close to failure or set off the failure (Vanneste et al., 2014). Thus, it is of critical importance to obtain a reliable timeframe for the occurrence of the paleo-landslides.

With respect to magnitudes, the data reveal various scales of landsliding in the larger area, from relatively small failures to large-scale instabilities resulting in basin-wide MTDs. The instabilities have involved different stratigraphic units, but the dynamics remain poorly constrained. Processes include retrogression and slab failures.

The seismic data should also be interpreted in more detail for the slope stability assessment. A number of key seismic horizons should be traced across the entire area. The focus should be on a better correlation of the MTDs and slip planes across the Flemish Pass. Seismic attribute analysis should then also be conducted for various target depths (e.g., MTDs). These techniques will assist in better outlining the occurrence, history and development of the various instabilities. In addition, it would be helpful to obtain data from well logs penetrating through the undisturbed strata, to check for changes in the sedimentary record (e.g., between pre-Quaternary and Quaternary).

The presence of a continuous sediment drape across the entire area, from the western slope across the field development and onto the eastern slope, indicates that recent failures have not occurred in the immediate vicinity of the site investigations. The observed MTDs are probably more than 200 kyr old. Nevertheless, an in-depth analysis and modelling should be conducted for both the western and eastern flank, particularly as there is clear evidence for repeated failures further north (eastern flank) with

4 episodes of failure during the last 28 kyr with an approximate 7 kyr recurrence interval (Piper, 2005). The same author suggests that the oldest landslides in the area are probably about 1 Myr old.

None of the dating so far is conclusive for determining the ages of the larger-scale landslides. An improved age model is thus paramount for further elucidating the hazard potential of the area. One of the key limitations is that continuous borehole data is limited to the upper 25 m below the seabed.

Samples have been dispatched for amino acid analyses, but because the laboratory it is currently being moved, results are still pending.

XRF (*X*-Ray Fluorescence) and colour spectrophotometry have been conducted on the BH-05/05a core. These data provide further information on the chemical elements as well as colour space of the sediments and allow the correlation to reference cores and the identification of probable Heinrich Events. A reasonable age vs depth model has been established using such interpreted Heinrich Event levels and radiocarbon ages. However, refinement of this model can be performed when amino acid analyses become available. Furthermore, dynamic time warping on XRF and MSCL data to correlate with well dated boreholes in the area can be used to supplement the amino acid results.

E3.2 Pre-conditions and triggers

Even though an in-depth evaluation of the pre-conditioning factors and triggers for the submarine slope failures falls beyond the scope of this report, we briefly report current findings and interpretations as input to follow-up studies.

Submarine mass movements of various scales are quite common on formerly glaciated continental margins. Key drivers for the instabilities are the climatic cycles, their influence in sedimentation patterns and the variations in geotechnical properties of the deposits, e.g., marine clays deposited as contourites, turbidites, glacial clays deposited as glacigenic debris flows. From the Norwegian margin, and the Storegga Slide in particular, the alternation of rapidly deposited glacial units on top of marine deposits (contourites) was a prime pre-conditioning factor. The sediment load also caused the generation of excess pore pressure and subsequent sub-lateral fluid migration in deeper oozes. The actual trigger is believed to have been an earthquake (Bryn et al., 2005; Kvalstad et al., 2005a; Kvalstad et al., 2005b).

The present-day sedimentation rates are quite low and the sediments are close to normally-consolidated. As a result, the present-day conditions are very unlikely to generate excess pore pressures. There are currently two long-term piezometers installed (western flank at 66 mbsf, eastern flank at 85 mbsf). These data will have a 1-yr record (approximately) and should be investigated in detail to shed light on the *in situ* pore pressures. From the eastern flank, the piezometer lies very close to a MTD evidenced on the seismic reflection profiles.

The entire area was heavily affected by glacial processes during the Quaternary. During peak glacial periods, ice streams may deliver large volumes of sediments from inland and the shelf towards the slope, where they become deposited as glacigenic debris flows, which may trigger turbidites. During the LGM, the ice margin did not reach the shelf break, and therefore, less sediment was delivered to the study area compared to previous glaciations. The relationship between glacial advances and the occurrence of the paleo-landslides deserves further interest, but may explain why there was no major failure following the LGM from the Grand Banks area.

The present-day slope angles are relatively low in the area. As such, the gravitational force is small too. It would therefore require additional energy to force instability.

Seismicity is one of the prime triggering factors to set off submarine instabilities. The reason is that seismic events can release significant amount of energy over a fairly large area. The occurrence of landslides that apparently happened synchronously (Orphan Basin) would indeed suggest that seismicity is an important factor. Historical data, however, only reveal low seismicity in the area. It is nevertheless likely that seismicity was higher at the end of glacial periods and early interglacials, when the crust had to balance the loss of ice loads (isostacy). Magnitudes could well have been significantly higher then. The minimum required seismic load will have to be determined from dynamic slope stability analyses. Considering the occurrence of silts, one should include liquefaction in a follow-up study. We currently do not know whether or not the slip planes have a tendency for liquefaction. The CPTU data from the eastern flank, where a slip plane was penetrated, may shed light on this. The influence of silt is clearly a topic for further investigations.

Gas and hydrates cannot be excluded from the area, but neither the geophysical data nor the geotechnical data unambiguously proves that gas or hydrates occur in the immediate vicinity of the development areas. However, there is indirect evidence of hydrates – through the presence of a BSR – to the N-NE of the study area. Whether or not hydrate dissociation is an actual pre-conditioning or trigger remains highly debated (Vanneste et al., 2014). The geophysical data from the area here illustrate that there is a BSR well underneath shallow failures on the Sackville Spur, with little to no evidence of fluid migration through the hydrate stability zone.

Another aspect of the geohazard assessment is that, in the case of failure, how far the deposit will run out. Debris flow modelling requires input from the geotechnical data and rheology. NGI has developed a new generation of run-out models, which can be applied to this area in a follow up study, using both 1.5D and 2.5D (depth-averaged) dynamic landslide models.

E4 References

Alvarez-Solar, J., Ramstein, G., 2011. On the triggering mechanism of Heinrich events. PNAS 108, E1359-E1360.

Berndt, C., Bünz, S., Mienert, J., 2003. Polygonal fault systems on the Mid-Norwegian margin: a long-term source for fluid flow, in: Rensbergen, P.V., Hillis, R., Maltman, A., Morley, C. (Eds.), Origin, Processes, and Effects of Subsurface Sediment Mobilization on reservoir to regional scale. Geological Society of London, Special Publication, pp. 283-290.

Brendryen, J., Haflidason, H., Sejrup, H.P., 2010. Norwegian Sea tephrostratigraphy of marine isotope stages 4 and 5: Prospects and problems for tephrochronology in the North Atlantic region. Quaternary Science Reviews 29, 847-864.

Bryn, P., Berg, K., Forsberg, C.F., Solheim, A., Kvalstad, T.J., 2005. Explaining the Storegga Slide. Marine and Petroleum Geology 22, 11-19.

Cameron, G.D.M., Campbell, C., Saint-Ange, F., Jiménez García, P., Piper, D.J.W., MacKillop, K., 2013. The anatomy of a submarine slide complex in the northeast Flemish Pass, offshore Newfoundland and Labrador. Geological Survey of Canada, Scientific Presentation 21, 1 ppt. doi:10.4095/293154

Cameron, G.D.M., Piper, D.J.W., MacKillop, K., 2014. Sediment failures in northern Flemish Pass. Geological Survey of Canada, Open File 7566, pp. 141.

C-CORE, 2012. Gas hydrate characterization of the Newfoundland Continental Margin: Resources and Geohazards - M1 report. C-Core, St. John's, NL, p. 146.

C-CORE, 2014. M2 Report - Gas hydrate characterization of the Newfoundland Margin: Resources and Geohazards. C-Core, St. John's, NL, p. 60.

Forsberg, C.F., Løvlie, R., Jansen, E., Solheim, A., Sejrup, H.P., Lie, H.E., 2003. A 1.3-Myr palaeoceanographic record from the continental margin off Dronning Maud Land, Antarctica. Palaeogeography, Palaeoclimatology, Palaeoecology 198, 223-235.

Giorgino, T., 2009. Computing and visualizing dynamic time warping alignments in R: the dtw package. Journal of Statistical Software 31, 24.

Golder Associates, 2014. Flemish Pass Geotechnical and Geological Desktop Study - Neogene/Quaternary Geology of the Flemish Pass. Golder Associates, p. 26.

Golder Associates, 2014. Site-specific seismic hazard analysis - Flemish Pass Project Site, Newfoundland, Canada. Golder Associates, p. 52.

Hebbeln, D., Henrich, R., Baumann, K.-H., 1998. Paleoceanography of the Last Interglacial/Glacial cycle in the Polar North Atlantic. Quaternary Science Reviews 17, 125-153.

Huppertz, T.J., 2007. Late Quaternary history of the Flemish Pass, southeast Canadian continental margin, Department of Earth Sciences. Dalhousie University, Halifax, Nova Scotia, p. 137.
Huppertz, T.J., Piper, D.J.W., 2009. The influence of shelf-crossing glaciation on continental slope sedimentation, Flemish Pass, eastern Canadian continental margin. Marine Geology 265, 67-85.

Huppertz, T.J., Piper, D.J.W., 2010. Interbedded Late Quaternary turbidites and contourites in Flemish Pass, off southeast Canada: Their recognition, origin and temporal variation. Sedimentary Geology 228, 46-60.

Kvalstad, T.J., Andresen, L., Forsberg, C.F., Berg, K., Bryn, P., Wangen, M., 2005a. The Storegga slide: evaluation of triggering sources and slide mechanics. Marine and Petroleum Geology 22, 245-256.

Kvalstad, T.J., Nadim, F., Kaynia, A.M., Mokkelbost, K.H., Bryn, P., 2005. Soil conditions and slope stability in the Ormen Lange area. Marine and Petroleum Geology 22, 299-310.

Levitus94. http://iridl.ldeo.columbia.edu/SOURCES/.LEVITUS94/index.html

Mao, L., Piper, D.J.W., Saint-Ange, F., Andrews, J.T., Kienast, M., 2014. Provenance of sediment in the Labrador Current: a record of hinterland glaciation over the past 125 ka. Journal of Quaternary Science 29, 650-660.

Marshall, N., Piper, D.J.W., Saint-Ange, F., Campbell, D.C., 2014. Late Quaternary history of contourite drifts and variations in Labrador Current flow, Flemish Pass, offshore eastern Canada. Geo-Marine Letters 34, 457-470.
NGI, 2016. Effects of sample cracking and gas exsolution on deepwater samples - Interpretation and recommendation report. NGI, Oslo, p. 83.

Piper, D.J.W., 2005. Late Cenozoic evolution of the continental margin of eastern Canada. Norwegian Journal of Geology 85, 305-318.

Piper, D.J.W., Cochonat, P., Morrison, M.L., 1999. The sequence of events around the epicentre of the 1929 Grand Banks earthquake: initiation of debris flows and turbidity current inferred from sidescan sonar. Sedimentology 46, 79-97.

Rasmussen, T.L., Oppo, D.W., Thomsen, E., Lehman, S.J., 2003. Deep sea records from the southeast Labrador Sea: Ocean circulation changes and ice-rafting events during the last 160,000 years. Paleoceanography 18.

Sloan, E.D.J., 1998. Clathrate Hydrates of Natural Gases, Second edition ed. Marcel Dekker Inc., New York & Basel.

Sultan, N., Cochonat, P., Foucher, J.P., Mienert, J., 2004. Effect of gas hydrates melting on seafloor slope instability. Marine Geology 213, 379-401.

Tripsanas, E.K., Piper, D.J.W., Campbell, D.C., 2008. Evolution and depositional structure of earthquake-induced mass movements and gravity flows: Southwest Orphan Basin, Labrador Sea. Marine and Petroleum Geology 25, 645-662.

Vanneste, M., De Batist, M., Golmshtok, A., Kremlev, A., Versteeg, W., 2001. Multi-frequency seismic study of gas hydrate-bearing sediments in Lake Baikal, Siberia. Marine Geology 172, 1-21.

Vanneste, M., Sultan, N., Garziglia, S., Forsberg, C.F., L'Heureux, J.-S., 2014. Seafloor instabilities and sediment deformation processes: The need for integrated, multi-disciplinary investigations. Marine Geology 352, 183-214.

Weber, M.E., Mayer, L.A., Hillaire-Marcel, C., Bilodeau, G., Rack, F., Hiscott, R.N., Aksu, A.E., 2001. Derivation of δ18O from sediment core log data: Implications for millennial-scale climate change in the Labrador Sea. Paleoceanography 16, 503-514.

Section F

INTERPRETATION AND EVALUATION OF GEOTECHNICAL DATA

Contents

Tables

Figures

F1 General

This section presents the interpretation of all the geotechnical data obtained from the 2015 Flemish Pass geotechnical site investigation. The data include the in situ CPTU testing and the offshore and onshore laboratory testing performed on samples from the 2015 offshore campaign.

The locations are shown on maps in Section A. The water depth varies between 675 m and 1172 m at the investigated locations, deepest at the Field Centre. Sections G and H present the recommended soil parameters for the Field Centre and slopes, respectively.

Data from all three areas investigated, Field Centre, West Slope and East Slope, are interpreted below. Parameters are presented for the three areas individually, but interpretation was done in light of the full dataset. In some cases there are limited (few or no data), but suggested representative profiles are still presented based on the general trend encountered across the site. However, these profiles are best guess or indicative profiles and shall be seen in light of the number of measured data. Hence, further information is needed to confirm profiles based on limited data.

Several figures presented in this report contain a soil column with the main soil units and average layering versus depth. This soil column is an idealisation for illustration purposes and the individual borehole logs (NGI, 2016) should be consulted for specific details.

This section refers to locations, and not to individual boreholes. As an example, the CPTU and lab data from the boreholes ST15452-CPT-03 and ST15452-S-03 are both referred to as location ST15452-03. Each data point can be traced to the individual results in the tables and borehole logs presented in NGI (2016).

F2 Soil stratigraphy

F2.1 Soil units

The various locations include in situ testing and sampling to a depth below seafloor of between 26.7 m and 101 m. The soil within this depth range can be divided into four main units. The same four units describe the conditions at all the investigated locations (Table F2-1). The units are in agreement with the geophysical interpretation presented in Section E.

Table F2-1 Summary of the generalised soil units

Unit	Soil description
I	CLAY, silty, extremely low to low strength, traces of fine to medium sand partings. Sandy in the upper 20 cm in some locations.
II	CLAY, low to medium strength, seams of sand and silt at different locations, few drop stones, gravel or larger, and pockets of sands.
III	CLAY, medium to high strength, seams of sand and silt at different locations, few drop stones, gravel or larger. Gas in solution. Probably affected by sliding.
IV	CLAY, medium to high strength, drop stones, gravel or larger. Possibly mass transport deposits.

F2.2 Soil descriptions

The four units described above occur at all areas investigated. Table F2-2, Table F2-3 and Table F2-4 present the depths to the units and the descriptions for the three areas respectively. The depths given are indicative as the investigated depths and the range of depths to the units vary substantially across the sites. Depths to specific layers at single locations can be found in NGI (2016). The depths given in Table F2-2, Table F2-3 and Table F2-4 are the same as those presented in the units column in the figures later in this section.

The soil classification from normalised CPTU parameters after Robertson (1990) show that the soil units are in general clays, clay to silty clay, with some layers of silt mixtures, clayey silt to silty clay (Figures F2.2.1 – F2.2.10).

Table F2-2 Summary of the generalised soil conditions encountered at the Field Centre locations

Unit	Depth below seafloor, m (indicative values)	Soil description
I	0 – 3.0	CLAY, silty, extremely low to low strength, traces of fine to medium sand partings and few shell fragments, greenish gray. Sandy in the upper 20 cm in some locations
II	3.0 – 20.0	CLAY, low to medium strength, low to medium plasticity, sand seams at different locations, few drop stones, gravel or larger, and pockets of sands, greenish grey to dark gray.
III	20.0 – 45.0 1)	CLAY, medium to high strength, medium plasticity, traces of fine sub-angular to sub-rounded gravels and coarse shell fragments, dark gray, gas in solution
IV	45.0 – 61.2 2)	CLAY, medium to high strength, medium plasticity, drop stones, gravel or larger. Possibly mass transport deposit, dark gray.

1) End of borehole for ST15452 –S-05 is at 26.7 m and for ST15452 –S-15 is at 26.7 m.
2) End of borehole for ST15452 –BH-12 is at 61.2 m.

Table F2-3 Summary of the generalised soil conditions encountered at the West slope locations

Unit	Depth below seafloor, m (indicative values)	Soil description
I	0 – 3.0	CLAY, silty, extremely low to low strength, traces of fine to medium sand partings, medium to coarse sub-angular gravels and few shell fragments, greenish gray. Sandy in the upper 20 cm in some locations
II	3.0 – 25.0	CLAY, silty, low to medium strength, low to medium plasticity, sand seams at different locations, few drop stones, gravel or larger, and pockets of sands, greenish grey to dark gray.
III	25.0 – 45.0	CLAY, medium to high strength clay, medium plasticity, traces of fine sub-angular to sub-rounded gravels and coarse shell fragments, dark gray, gas in solution
IV	45.0 – 101.0[1)]	CLAY, medium to high strength, medium plasticity, drop stones, gravel or larger. Possibly mass transit deposit, dark gray.

1) End of borehole for ST15452 –02 = 101.0 m; ST15452 –03 = 62.5 m; ST15452 – 07 = 45.8 m; ST15452 –08 = 62.5 m; ST15452 –16 = 55.6 m; ST15452 –19 = 50.6 m.

Table F2-4 Summary of the generalised soil conditions encountered at the East Slope location

Unit	Depth below seafloor, m (indicative values)	Soil description
I	0 – 3.0	CLAY, silty, extremely low to low strength.
II	3.0 – 50.0	CLAY, low to medium strength, low to medium plasticity, sand seams at different locations, few drop stones, gravel or larger, and pockets of sands.
III	50.0 – 70.0	CLAY, medium to high strength clay, medium plasticity, traces of fine sub-angular to sub-rounded gravels and coarse shell fragments, dark gray, gas in solution
IV	70.0 – 98.2[1)]	CLAY, medium to high strength, medium plasticity, drop stones, gravel or larger. Possibly mass transit deposit, dark greenish gray.

1) End of borehole for ST15452 –18 = 98.2 m.

The descriptions given above give a good sense of the soil that is encountered in a given depth interval. However, the soil is highly layered, and in places laminated. All data indicate that there is a high degree of variability within a very short down-hole depth range. Table F2-5 presents index measurements from a small depth range in ST15452-18. The data clearly show a considerable variation in some parameters, but not in all. The content of clay varies from 31.1 to 54.8 % within 10 cm, whereas the measured content of fines remains virtually unchanged. Variation can also be seen in some of the parameters presented below. Figure F3.1.1 shows the water content measurements done, the bulk of the data in the upper 15 m fall between 18 and 55 % with some measurements outside even this range. A continuous profile of density can be found in Section J of NGI

(2016) confirming the variability described above. In summary, most of the index tests reveal significant variability with depth.

Table F2-5 Example index data from ST15452-18

Depth, m	s_u from fall cone, kPa	Plasticity index, %	Clay content, %	Fines content, %
62.80			32.9	91.5
62.82		27.3		
62.86	80	26.5	47.3	93.6
62.91	74	28.3	54.8	90.2
63.09			31.1	92.7
63.11		25.8		
63.14		22.7		
63.16	77	26.1	51.9	88.6
63.17			37.1	92.8
63.19		24.4	37.8	92.7
63.21	67	23.2	47.8	89.5

Trends can be found in many parameters in spite of this variation. For most structural design tasks such trends give sufficiently detailed information. For geo-hazard evaluation purposes such trends and representative lines may not capture thin layers with deviating properties that may be key to the analyses in question. It follows that the engineer using the data must pay special attention to the variability and possible effects this can have on the analysis.

At most locations, samples retrieved below a certain threshold are cracked. There is no evidence of gas hydrates in the geophysical data in the immediate vicinity of the geotechnical sites or the samples (see also Section E). The cracks are believed to be the result of gas dissolved in the pore water coming out of solution as a result of the pressure relief the samples are subject to during retrieval to the vessel.

F3 Basic soil parameters

F3.1 Water content

Water content was measured offshore and onshore. Onshore water content is measured on all advanced tests. All the measurements of water content are shown in Figure F3.1.1. The water content lies between 15 % and 75 % in the top, and between 20 % and 40 % at 100 m depth.

The measured water contents show no systematic change from the offshore to the onshore measurements. The mean of all offshore measurements is 32.3% (standard deviation = 11.5), whereas the mean of all onshore measurements is 33.5% (standard deviation = 10.8).

Figures F3.1.2 – F3.1.4 show the water content measurements as a function of depth from the Field Centre, West slope and East slope locations respectively. Each figure include a representative profile.

F3.2 Total unit weight of soil

The total unit weight of the soil was determined offshore and onshore. In addition, the total unit weight was calculated from all water content values assuming 100 % saturation and a unit weight of solid particles, γ_s = 26.8 kN/m^3. Figure F3.2.1 shows the results. The total unit weight typically lies between 15 and 22 kN/m^3 in the top with some measurements falling outside this range. The range becomes smaller with depth.

In general there is no systematic difference between the total unit weight of soil as determined from the bulk dimensions and as derived from the measured water content, either for all measurements combined, or for the measurements in specific depth intervals. However, in some instances the derived values appear to be higher than those derived from the bulk dimensions. It is unknown if this is due to the variability with depth, or if it is connected to gas coming out of solution in specific samples.

Figures F3.2.2 – F3.2.4 show the total unit weight as a function of depth from the Field Centre, West slope and East slope locations respectively. Each figure includes a representative profile.

F3.3 Plasticity data

The liquid (w_L) and plastic (w_p) limits and the corresponding plasticity indices ($I_p = w_L - w_p$) were determined on a number of clay and clayey samples from Field Centre, West Slope and East Slope locations.

All plasticity indices are shown in Figure F3.3.1. The data typically fall between 6 and 25 %, with some values above 25 %. A series of measurements at around 63 m depth in ST15452-18 illustrates the variability. It also illustrate the sensitivity of the method due to the large uncertainty connected to determinations of the liquidity index as the plasticity and water content measurements is not done on the same material.

Figures F3.3.2 – F3.2.4 show the plasticity indices from the Field Centre, West slope and East slope locations respectively. Each figure includes a representative profile.

The plasticity index is plotted versus the liquid limit, w_L, on the plasticity chart in Figure F3.3.5. For all samples tested, with one exception, the results plot above the A-line. According to "The Unified Soil Classification System" (ASTM, D2487) the large majority of the measurements classifies as *"inorganic clays of low to medium plasticity, gravelly clays, sandy clays, silty clays, lean clays"*. Some samples classify as *"Inorganic clays of high plasticity, fat clays"* while some samples classify as *"Inorganic silts, very fine sands, rock flour, silty or clayey fine sands"*. There is no apparent correlation between what is seen from the CPTU data and where the data plot in the plasticity chart.

F3.4 Unit weight of solid particles

The unit weight of solid particles, γ_s, was determined on selected samples from Field Centre, West and East Slope locations. The results are presented in Figure F3.4.1. The measured values vary between 26.2 kN/m^3 and 27.0 kN/m^3.

A suggested representative value of γ_s = 26.8 kN/m^3 is included in the figure. This was used for calculation of total unit weight from water content.

F3.5 Grain size distribution

The grain size characteristics were determined in the onshore laboratory. Samples from all three areas were tested. The individual grain size distribution curves are presented in NGI (2016).

The soil classification system is according to NGF (2011) where a soil is classified as CLAY if the clay content is 30 % or higher. A soil is classified as SAND if the sand content is 60% or higher <u>and</u> the clay content is less 15%. A soil is classified as SILT if the content of fines is more than 45 % <u>and</u> the clay content is less than 15%.

In Figure F3.5.1 one set of data represents the clay fraction (particles less than 0.002 mm), a second set of data represents the fines content (particles less than 0.063 mm) and a third set of data represents the sand content (particles less than 2 mm) versus depth for all locations. Figures F3.5.2 – F3.5.4 show the same data for each of the three areas respectively. Figure F3.5.5 show the soil classification triangle according to the NGF classification system.

The data show that most of the tested material is *"CLAY"*. Some material is *"CLAY, silty, sandy"* or *"CLAY, silty"*. A single point fall within *"SILT, sandy, clayey"* and one in *"MATERIAL"*. There is generally good consistency between this classification and the Soil Behaviour Type given by Robertson (1990) (Figures F2.2.1 – F2.2.10).

F3.6 Remoulded shear strength

Remoulded shear strength measurements were carried out using index shear strength tests on a number of remoulded clay samples. A small number of remoulded UU tests were also performed offshore. Whereas the sensitivity of a clay sample is influenced by sample disturbance, the remoulded strength is not, provided that the water content is unchanged. Standard practice at NGI is to use the fall cone test to obtain remoulded strength values. Both the fall cone and other index measurements are influenced by nearby layers with more silt or sand and by coarser particles in the clay. All the measurements of remoulded shear strength, s_{ur}, are shown in Figure F3.6.1.

There is large scatter in the s_{ur} measurements. The scatter reflects the variability in the soil conditions and the fact that s_{ur} varies with test type used as shown in a JIP at NGI that Statoil participated in (De Groot et al., 2012). Some data points will be affected by the gravel that is known to be spread throughout the boreholes and some may be affected by more silty or sandy layers.

Figures F3.6.2 – F3.6.4 show the measured values of s_{ur} at the Field Centre, West Slope and East Slope locations. The figures include representative high and low profiles based on the measured data. The designer should carefully evaluate whether the profiles are suitable for use in a specific analysis and if the relevant details are captured.

For installation analyses it is recommended to use $s_{ur} = s_{uD}/S_t$ (Andersen et al., 2008). Since there are more measurements of s_{uC}, the anisotropy ratio s_{uD}/s_{uC} can be applied, see Section F6.3.

F3.7 Sensitivity

Sensitivity was determined from index shear strength tests on intact and remoulded samples. The sensitivity is calculated as $S_t = s_u/s_{ur}$, where s_u and s_{ur} are the shear strengths for the intact and the remoulded samples, respectively. Most data come from lab vane and fall cone test. All measurements are presented on the borehole logs in NGI (2016) for each individual borehole. A summary plot of all sensitivity values, including UU tests, is presented in Figure F3.7.1.

As sensitivity depend on both the intact and remoulded strength. There is significant spread in the results, with values ranging from 1 to 10, and single values exceeding 10. There is no direct indication or evidence that single sensitivity value could be erroneous. However, as discussed in Section F6.3, the intact index measurements are lower than the profiles of index shear strength. Given that the remoulded strength is reliable, the sensitivities will be too low.

Figures F3.7.2 – F3.7.4 present the sensitivity at the Field Centre, West Slope and East Slope locations respectively. Each figure includes a suggested representative profile with depth. Because the intact index measurements are considered less reliable, the profiles are found from the average representative profiles of s_{ur} and s_{uD} with depth with $S_t = s_{uD}^{avg}/s_{ur}^{avg}$. The profiles found in this way are within or slightly to the high side of the measured index sensitivities.

F3.8 Thixotropy

Thixotropy is the regain of undrained shear strength in clay with time after remoulding, when the soil is allowed to rest with constant water content. Thixotropy is one factor governing the "set-up" effect observed on pile or skirt capacity shortly after installation. Two sets of thixotropy tests were performed on samples from the Field Centre. The results can be found in NGI (2016).

The two tests were done at approximately 3.3 m and 12.5 m depth at ST15452-12. The water content is somewhat variable in the test at 3.2 m depth, whereas the re-remoulded strength is close to constant.

The thixotropy ratios from the two tests at selected times are compared to data from literature (Andersen et al. 2008) in Figure F3.8.1. The activity has been chosen based on Figure F3.9.1, but the value for each test is uncertain due to the scatter in the data. It is evident that the thixotropy results are very high compared to the published data. However, the number of datapoints is low for the activity in question. It is recommended that thixotropy closer to the published values are used in design if further data is not available.

F3.9 Mineralogy and activity

Mineralogy was determined on five samples by x-ray diffraction analysis. Bulk samples were analysed at the Norwegian Geological Survey (NGU). The detailed results are given in NGI (2016).

The methodology used can detect all clay minerals in larger quantity than the detection limits in the bulk sample. The bulk sample contain both clay, silt and some sand before preparation. The different samples show varying results, with quartz content between 21 and 51 % and plagioclase content between 16 and 22 %. Two samples have 4 and 5 % calcite while three other samples have 20, 23 and 25 % calcite. There are no swelling minerals detected. The large variability in calcite is matched by similar variability in carbonate and by the changing reaction to dilute HCL found offshore. This is discussed in Section E and not likely to affect the geotechnical properties outside the range reported.

Skempton (1953) defined activity of a clay as the plasticity index divided by the content of clay and showed that this parameter is in a way linked to clay mineralogy. Figure F3.9.1 show the activity from all locations. The range is large, which is however not uncommon for offshore clays.

In summary, it appears that the mineralogy of the sediment is varied, but that special minerals like swelling minerals are not present in significant quantities

F3.10 Thermal conductivity

Thermal conductivity was measured on three samples from the Field Centre. The factual results are given in NGI (2016). The thermal conductivity can also be calculated by the method from Johansen (1976).

The measured date is shown versus depth in Figure F3.10.1. Lines are also included in the figure indicating the range found by applying relevant parameters to the method by Johansen (1975). The main variables are given in the figure.

A value of $\lambda = 1.3$ W/mK is representative. There is limited data available and important that the user evaluates what is the appropriate value to apply to any specific analysis.

F4 In situ stresses and stress history

F4.1 In situ effective vertical stress

The representative profile of effective vertical stress, p_0', is presented in Figures F4.1.1 – F4.1.3 for the Field Centre, West slope and East slope locations respectively. Each figure includes a representative profile. The profiles are derived from the representative total unit weight profiles in Figures F3.2.1 – F3.2.3 assuming hydrostatic pore pressure in situ. The in situ vertical stress p_0' (in kPa) at the locations can be calculated as:

Field Centre

$0 < z < 3.0$ m:	$p_0' = 6.5z$
$3.0 < z < 20.0$ m:	$p_0' = -6 + 8.5z$
$20.0 < z < 30.0$ m:	$p_0' = -16 + 9z$
$30.0 < z < 40.0$ m:	$p_0' = 14 + 8z$
$40.0 < z < 60.0$ m:	$p_0' = -50 + 9.6z$

West Slope

$0 < z < 3.0$ m:	$p_0' = 5.5z$
$3.0 < z < 25.0$ m:	$p_0' = -4.5 + 10z$
$25.0 < z < 45.0$ m:	$p_0' = -29.5 + 11z$
$45.0 < z < 100.0$ m:	$p_0' = 15.5 + 10z$

East Slope

$0 < z < 50.0$ m:	$p_0' = 10z$
$50.0 < z < 100.0$ m:	$p_0' = 50 + 9z$

where z is depth below seafloor in metres.

F4.2 Preconsolidation stress and overconsolidation ratio

The interpretation of preconsolidation stress, p_c', is based on results from oedometer tests on undisturbed clay samples using the interpretation methods recommended by Casagrande (1936), Becker et al. (1987) and Janbu (1970).

The overconsolidation ratio, OCR = p_c'/p_0', is calculated directly using the estimates of p_c' and the estimated in situ effective stress.

A second method for estimating p_c' and OCR for a clay material is to use empirical correlations between s_{uC}/σ'_v, OCR and I_p (Andresen et al., 1979), as presented in Lunne et al. (1997). This can be applied to results from CAUC and to CPTU data (applying relevant N_{kt} or $N_{\Delta u}$ factor).

Figure F4.2.1shows all determinations of p_c' from oedometer tests plotted together with the empirical correlation of CAUC and CPTU data using (Andresen et al., 1979) with a constant I_p = 15%. Equations used by NGI do not include values under OCR = 1.0, giving an erroneous impression of a cut off. The equivalent data is plotted in Figures F4.2.2 – F4.2.4 for the Field Centre, West slope and East slope locations, respectively. The same data was transformed to OCR and is shown in Figures F4.2.5 – F4.2.8.

The interpretations of the oedometer data should be seen together when estimating the in situ p_c'. For the present samples the Casagrande interpretation tends to give a p_c' on the low side, whereas the Janbu interpretation as implemented tend to give a p_c' to the high side. The Becker interpretation could be implemented for fewer samples than the other methods. Taken together, p_c' from oedometer test interpreted by the different methods fits well with the p_c' found by Andresen's correlation applied to the CPTU data with s_u interpreted using an $N_{\Delta u}$ as discussed in Section F6.3.

The result is a soil exhibiting a slight apparent overconsolidation as expected for aged normally consolidated deposits. As discussed in Section E, the sediment that has not experienced sliding has not been mechanically overconsolidated. The figures of p_c' and OCR for each of the three areas include profiles of p_c' and OCR. The apparent overconsolidation is maybe a result of various effects such as ageing.

F4.3 Coefficient of earth pressure at rest

No tests to determine the coefficient of earth pressure at rest, K_0, were carried out.

Evaluation of K_0 is based on the empirical correlation between OCR, K_0 and I_p (Brooker and Ireland, 1965). OCR used in the correlation is estimated from the CPTU data, according to Section F4.2. Equations used by NGI do not include values of K_0 in the range 0.5 – 0.6, giving an erroneous impression of a cut off at 0.6.

Figures F4.3.2 - F4.3.4 present the resulting K_0 data for the Field Centre, West slope and East slope locations, respectively. A representative profile based on engineering judgement of the data herein is included in the figure. Note that the suggested profiles are drawn schematically. Figure F4.3.1 shows the K_0 data for all locations.

F5 Consolidation parameters

F5.1 General

A total of 26 oedometer tests were performed on clay samples from Flemish Pass. The results are reported in NGI (2016). The consolidation parameters are presented for the three areas individually, but interpretation was done in light of the full dataset. Shear modulus relevant for immediate settlement evaluations are presented in Section F8.

F5.2 Immediate settlements

Immediate settlements may be estimated by elastic theory using the shear modulus, G. The G-value will typically vary from soil element to soil element and depends on the degree of strength mobilization, the degree of overconsolidation, the strength and general soil characteristics. Based on the undrained triaxial and DSS tests, the secant shear modulus versus strength mobilization can be established from the tests performed on samples.

Figures F8.2.1 – F8.2.2 present the results from triaxial tests for Field Centre and Slopes respectively. The figures show the secant shear modulus, G, versus shear stress, τ, normalised to the undrained shear strength in triaxial compression, s_{uC}. The figures present results from the triaxial compression and extension tests carried out, and include representative profiles.

Similarly, Figures F8.2.3 – F8.2.4 give values of secant shear modulus, G, versus horizontal shear stress, τ_h, normalised to the undrained shear strength in DSS, s_{uD}, from the static direct simple shear tests for Field Centre and Slopes respectively.

The figures include suggested representative profiles.

F5.3 Primary consolidation settlements

The soil parameters necessary for evaluating the consolidation settlement and its time dependency are the constrained modulus, M, the coefficient of vertical consolidation, c_v, and the drainage length, H.

The primary consolidation settlements are generally influenced by the relationship between the stress increase imposed by the structure, the initial in situ stresses, and the preconsolidation stress, p_c'. The representative p_c' profiles are shown in in Figures F4.2.2 – F4.2.4 for the Field Centre, West slope and East slope locations, respectively.

The consolidation settlements can be calculated using the Janbu modulus concept (Janbu, 1963), see Figure F5.3.1. For effective stresses below p_c' the constrained modulus, M, is assumed to be constant and is denoted M_0. For effective stresses exceeding p_c', the deformation modulus will be stress dependent. This stress dependency is approximately linear above p_c'. The stress dependent constrained modulus is expressed as a function of the modulus number and reference stress:

$$M = m \cdot (\sigma_{v0}' + \Delta p - p_r')$$

where p_r' = reference stress
Δp = additional stress, exceeding p_c'

Consolidation tests were performed on samples from all three locations (i.e. Field Centre, West slope, and East slope location). The results from CRSC tests are presented in Table F2-1 (NGI, 2016). Most of the CRSC tests performed on samples from this site investigation were loaded beyond assumed p_c' to evaluate OCR and estimate p_c' using four different methods. A total of five samples from different locations were tested with two unloading/reloading loops to evaluate unload/reload modulus.

Figure F5.3.2 shows the interpreted M_0 values for all locations. Figures F5.3.3 – F5.3.5 present the interpreted M_0 values for the Field Centre, West slope and East slope locations, respectively. A representative profile based on engineering judgement of the data herein is included in the figure for calculation of settlements for stresses less than p_c'. Note that the suggested profiles are drawn schematically. In soil units with limited or no measured data, an indicative profile has been included based on the full dataset from this site investigation.

Figure F5.3.6 shows the interpreted modulus number and reference stress (m and p_r') from the tests for all locations. Typically the m values lie between 13 and 25, with p_r' in the range 0 kPa to 400 kPa. The m values are within the expected range for a clay with water content in the range 20-40% (Janbu, 1970). Figures F5.3.7 – F5.3.9 present the m and p_r' data for the Field Centre, West slope and East slope locations, respectively. A representative profile based on engineering judgement of the data herein is included in the figure. In units with limited or no measured data, an indicative profile has been included based on the full dataset from this site investigation.

For all locations values of m = 20 and p_r' =0 kPa are included as indicative for Unit I, based on the test at 3.35 m depth at the Field Centre.

At the Field Centre it is assumed that Unit IV has similar consolidation parameters as Unit IV of the West and East slopes. Hence, values of m = 15 and p_r' =200 kPa are included as indicative for Unit IV at the Field Centre.

For the East slope, the one measurement in Unit II has the highest m value reported herein. For this specimen, the clay content is 39% which is somewhat to the high side compared to the other oedometer tests whereas the water content of 28% is within the typical range. This data point may be due to the observed variability that is observed within small depth intervals across the site. Alternatively, the reesult may simply be an outlier. Therefore, only an indicative profile is given for Unit II at the East slope, based on the full dataset from this site investigation.

F5.4 Coefficient of vertical permeability

Generally the coefficient of vertical permeability is determined from CRSC oedometer tests. The values given for the vertical permeability in Figures F5.4.1 - F5.4.4 are at zero axial strain from CRSC tests. In addition, four constant head permeability test were performed in triaxial specimens for Field Centre and West slope locations. The results from these constant head tests are shown in Figure F5.4.2 and Figure F5.4.3.

The vertical permeabilities are all between 1.6E-10 m/s and 3.0E-10 m/s. These values are within the expected range (Andersen and Schjetne, 2013). The permeability from constant head testing in the triaxial cell gives somewhat lower values than the permeability reported at zero axial strain in the oedometer tests. In the suggested representative profiles, the constant head test results are given more weight than the results at zero axial strain.

For all locations, a value of k = 1.0E-9 m/s is included as indicative for Unit I, based on the test at 3.35 m depth at the Field Centre.

At the Field Centre it is assumed that Unit IV has similar permeability as Unit IV of the West and East slopes. Hence, a value of k = 2.5E-10 m/s is included as indicative for Unit IV at the Field Centre.

Representative profile based on engineering judgement of the data herein is included in Figures F5.4.2 - F5.4.4 for the Field Centre, West slope and East slope locations, respectively.

F5.5 Coefficient of vertical consolidation

The coefficient of vertical consolidation at p_0', c_{v0}, was determined in the CRSC oedometer tests on clay. The vertical consolidation coefficients are calculated using:

$$c_v = \frac{k_v \cdot M}{\rho_w \cdot g}$$

Figure F5.5.1 shows the interpreted c_v values for all locations. Figures F5.5.2 – F5.5.4 present the interpreted c_v values for the Field Centre, West slope and East slope locations, respectively.

For all locations a value of c_v = 5.0E-8 m^2/s is included as indicative for Unit I, based on the test at 3.35 m depth at the Field Centre.

A representative profile based on engineering judgement of the data herein is included in the figure. Note that the suggested profiles are drawn schematically.

F6 Static soil strength parameters

F6.1 General

The static strength of the soil has been measured by means of CPTU tests at all locations. Lab testing include offshore and onshore index strength measurements in all samples taken, and consolidated undrained triaxial compression (CAUC) and extension (CAUE) tests and direct simple shear (DSS) tests at selected locations in the onshore laboratory. All the individual measurements are given in NGI (2016). The static strength measured by CPTU is found by correlation to the advanced lab tests with a pore pressure factor $N_{\Delta u}$ as discussed below.

All measured values of undrained shear strength are summarised on the borehole logs as presented in NGI (2016).

F6.2 CPTU measurements

The CPTU measures the cone resistance, q_c, pore pressure, u_2, and sleeve friction, f_s with depth. Figure F6.2.1 shows the corrected cone resistance, q_t, for all locations. For ease of reading, a filter has been applied to the data to remove spikes and smooth the curve (Figure F6.2.2). The filter selected is a moving average Gausian filter with 0.5 m depth interval as window length, and excluding outliers. It is important to note that the filter removes real variation in the data so that the full dataset shall always be consulted for design. Figures F6.2.3 – F6.2.6 give the corrected cone resistance for the Field Centre, West Slope and East slope locations respectively. Figure F6.2.4 shows the Field Centre data to a maximum depth of 20 m and includes a representative high and low profile.

Figure F6.2.7 shows the sleeve friction, f_s, for all locations. As for q_t, the same Gausian filter was applied with outlier removal to remove spikes and smooth the curve (Figure F6.2.8). It is important to note that the filter removes real variation in the data so that the full dataset shall always be consulted for design. Figures F6.2.9 – F6.2.11 give the sleeve friction for the Field Centre, West Slope and East slope locations respectively.

Figure F6.2.12 shows the pore pressure response, u_2, for all locations. Also for u_2, the filter was applied to the data to remove spikes and smooth the curve (Figure F6.2.13). It is important to note that the filter removes real variation in the data so that the full dataset shall always be consulted for design. Figures F6.2.14 – F6.2.16 give the pore pressure for the Field Centre, West Slope and East slope locations respectively.

It can be observed that the scatter is less in the pore pressure measurements (Figure F6.2.12) compared to the q_t data (Figure F6.2.1). The f_s profiles show the largest scatter (Figure F6.2.5).

F6.3 Interpretation of undrained shear strength, total stress

F6.3.1 Correlation of CPTU to lab tests

The CPTU measurements need to be correlated to lab measurements in order to be interpreted in terms of the undrained shear strength, s_u. This is commonly done by applying a cone factor $N_{kt} = s_{uC.}/q_{net}$. A N_{kt} factor is selected for each CAUC test by picking a value of q_t believed to represent the same depth as the CAUC test. Figure F6.3.1 shows all the N_{kt} values versus the quality of the triaxial tests as measured by the change in void ratio relative to initial void ratio when consolidating the specimens back to the best estimate of in situ stresses $\Delta e/e_{0.}$ There is no apparent trend in the N_{kt} versus $\Delta e/e_0$.

s_u can also be interpreted from the CPTU data by applying a pore pressure factor $N_{\Delta u} = (u_2 - u_0)/s_u$ where u_0 is the hydrostatic pore pressure. Values of $N_{\Delta u}$ were selected for each CAUC by selecting representative values of u_2 for each test. Figure F6.3.2 shows $N_{\Delta u}$ versus $\Delta e/e_0$. The value with $N_{\Delta u}$ below 2 is considered an outlier and is not given any weight in the following.

Figures F6.3.3 and F6.3.4 present the N_{kt} and $N_{\Delta u}$ values versus the pore pressure parameter B_q ($\Delta u/q_{net}$), respectively. The plots reveal a trend of falling N_{kt} versus B_q whereas there is no clear trend in $N_{\Delta u}$ versus B_q. Figures F6.3.5 and F6.3.6 show the N_{kt} and $N_{\Delta u}$ values versus depth. The scatter in the N_{kt} values is significant compared to the scatter in $N_{\Delta u}$ values.

Collated profiles of q_t, B_q, Q_t, s_u and OCR for each location are shown in Figures F6.3.7 – F6.3.16. There are clear shifts in B_q in most of the locations. The s_{uC} is plotted in terms of a constant N_{kt} and constant $N_{\Delta u}$ with depth. As observed in Section F6.2 there is less scatter in the u_2 profiles compared to q_t profiles.

The most practical and appropriate correlation between CPTU and s_u is considered to be a constant $N_{\Delta u}$ taken as the mean of the values = 7.5. This has been implemented in the strength profiles below and in the borehole logs in NGI (2016). It should be noted that a value of $N_{\Delta u}$ = 7.5 also fits well with correlations presented by Karlsrud et al. (2005) based on high quality CAUC tests in block samples of soft Norwegian clays.

F6.3.2 Profiles of undrained shear strength

All measurements of s_u shown in Figure F6.3.17 include all the index measurements, the advanced lab tests and the CPTU measurements interpreted as discussed above. Figure F6.3.18 shows the advanced test results and the CPTU data from all locations down to a depth of 50 m. The index data fall in general below the strengths obtained from the above discussed correlation of the CPTU data and below a $s_u/p_0' = 0.3$. Therefore, NGI recommends that the index data is taken into account when selecting design strength profiles. The $s_u/p_0' = 0.3$ is a commonly accepted value for normally consolidated clay and assumed to represent a lower bound of the strength under hydrostatic pore pressure conditions.

Two pairs of two SHANSEP tests were run to increase the understanding of the material behaviour and stress influence. One test was run at a lab-created OCR = 1.0 and the second at a lab-created OCR = 1.5 in each pair. Key data from the tests are given in Table F6-1. The normalised strength is conventionally interpreted via the equation $(s_u/\sigma_{ac}')_{OC} = (s_u/\sigma_{ac}')_{NC} \cdot OCR^m$ where m is an empirical constant. The two sets of tests give m of 0.919 and 0.674, and $(s_u/\sigma_{ac}')_{NC}$ of 0.31 and 0.35 respectively. These values are within the reported range, but the differences are large if assumed to represent the same material. The tests have very different water contents and failure modes. This is probably a reflection of the layering discussed previously. The two sets of tests give s_u/σ_{ac}' for OCR = 1.3 of 0.39 and 0.42. In the p_0' consolidated CAUC tests the mean s_u/p_0' = 0.36.

For easy reference, Figures F6.3.23 – F6.3.26 show the s_{uC}/p_0' for all locations, the Field Centre and West and East Slopes respectively.

Table F6-1 Key data for SHANSEP tests

Sample	Depth m	w_i %	σ_{ac}' max kPa	σ_{ac}' kPa	OCR	s_u kPa	ε_f %	s_u/σ_{ac}'
BH-12-7C-1	15.11	31.0	255.5	255.0	1.0	79.1	0.446	0.31
BH-12-8A-1	15.98	43.7	269.9	180.1	1.5	80.9	1.286	0.45
S-03-5A-1	18.96	16.3	370.3	370.3	1.0	131	10	0.35
S-03-5A-2	18.85	23.0	369.0	245.9	1.5	112.8	0.685	0.46

The variability of the tested material means that great caution should be applied in applying the SHANSEP equation based on only four tests. However, the results increase the confidence that the p_0' consolidated CAUC tests provide a sound foundation for interpretation of the CPT data and profiles of shear strength, and that the sample disturbance is reducing the measured strength as compared to the in situ value. The sample disturbance is discussed further below.

Figures F6.3.19, F6.3.21 and F6.3.22 show the data at the Field Centre, West Slope and East Slope locations respectively. Figure F6.3.20 shows the Field Centre data to a depth of 5 m.

Figures F6.3.19 – F6.3.22 include high and low representative profiles of s_{uC}. These representative profiles provide a good indication of the trend and variation of strength with depth. For the user of strength profiles it is important to note that:

- Some advanced strength test results plot well above the representative high profile. These are test of material that is significantly more silty or sandy than the bulk of material. It is important to note that these are reliable and valid measurements that may be important for installation analyses. Layers of sand typically 0.5 – 1 m thickness occur at various depths and across boreholes. In some places, the sand layers are up to 2 m thick. They are shown in terms of q_t in Figures F6.2.1 – F6.2.6.
- The CPTU data indicate that there are layers with strength below the general trend in the data and the low representative strength profiles. Some are below $s_u/p_0' = 0.3$ which may suggest that the data should be disregarded. However, it is possible that layers of lower strength are present as indicated by the data. Typical layers are 1 m thick and has a strength 10 % below the low representative profile. For certain analyses, e.g. of slope stability, such layers may be of importance. The designer should evaluate the impact of such layers by assuming a layer is present at any depth below 5 m depth
- The seismic data (see Section E) show that mass transport deposits occur at various depths across the investigated area. As an example, the deposit occurs at 52 m depth at ST15452-03 and results in a clear shift in shear strength behaviour. At many locations the geotechnical data do not reach the depth where the mass

transport deposits start, and the user should evaluate how the shear strength is affected.

- *In the design the soil parameters should be carefully selected and evaluated by the user to ensure that the parameters used are valid for the analysis in question.*

F6.3.3 Strength anisotropy

Undrained shear strength anisotropy was investigated by CAUE triaxial tests and DSS tests performed close to CAUC tests. All the results are shown in Figure F6.3.27. The data from Field Centre, West Slope and East Slope locations are given in Figure F6.3.28 – F6.3.30.

The data indicate representative values of s_{uD}/s_{uC} = 0.8 and s_{uE}/s_{uC} = 0.75. There are data from approximately 30 m depth indicating lower values of anisotropy in Unit II at the Field Centre and West Slope of s_{uD}/s_{uC} = 0.6 and s_{uE}/s_{uC} = 0.45. The figures include representative profiles and the low representative profiles. The designer can take the representative profiles as a baseline but should assess the effect of applying the low representative profiles.

F6.4 Interpretation of undrained shear strength, effective stress

The triaxial compression and extension tests (CAUC and CAUE) on clayey material plotted in terms of the stress path define the strength in effective stresses. The stress path of each individual tests is given in NGI (2016).

The failure envelope defined by the effective stress paths can be represented by two parameters, the effective stress friction angle ϕ' and the attraction intercept, a. The intercept, a, is related to the internationally used cohesion, c, as

$$c = a \cdot \tan \phi'$$

Figure F6.4.1 presents the effective stress paths from the undrained triaxial tests performed on clay material from the Field Centre, whereas Figure F6.4.2 presents the equivalent from both East and West Slope locations.

A range of a = 0 kPa and ϕ' between 30° and 36° is appropriate for the tested material.

F7 Cyclic soil strength parameters

F7.1 General

Both cyclic DSS and cyclic triaxial tests were performed in order to provide data for assessing the cyclic behaviour of soil units at Flemish Pass. The tests were performed with both symmetric and non-symmetric cyclic shear stresses, i.e. with and without average shear stress during cycling. In the case of an average shear stress, $\Delta\tau_a$ was applied under undrained conditions. Cyclic tests performed on samples from the field centre location were for determination of cyclic behaviour of soil elements when subjected to wave loading. Therefore, a cyclic period of 10 s was used on the tests performed on field centre location samples.

A special type of cyclic DSS tests was performed on samples from the East Slope location. The objective of these tests was to determine the soil behaviour subjected to earthquake loading and to quantify the post-cyclic strength for slope stability analysis. The tests were performed with a cyclic period of 2 s. All the cyclic tests performed at East slope location were consolidated with horizontal shear stress to simulate an infinite sloping ground of 4°.

In general, a static test was performed on an adjacent sample in order to provide the relevant reference static undrained shear strength used for the normalisation of the cyclic tests. Identical consolidation procedures were used for the cyclic and the adjacent static tests.

A total of 4 cyclic DSS tests and 4 cyclic triaxial tests were performed on samples from Field centre location and a total of 3 special cyclic DSS tests were performed on samples from East slope location.

All but one cyclic test were terminated at 15% average shear strain, 15% cyclic shear strain or at 1500 cycles, whichever occurred first. Definition of average shear strain, cyclic shear strain and permanent shear strain are as follows:

$\gamma_a = (\gamma_{max} + \gamma_{min}) / 2$

$\gamma_{cy} = (\gamma_{max} - \gamma_{min}) / 2$

γ_p (permanent shear strain) is equal to the shear strain at $\tau = \tau_a$

Failure is defined as the number of cycles at which either γ_a or γ_{cy} exceeds 15%. For undrained triaxial tests, the shear strain is computed as $\gamma = 1.5\ \varepsilon_a$.

One cyclic triaxial test (ST15452-BH-12-6B-2) continued beyond 1500 cycles to fail at 15 % average shear strain. The number of cycles to failure for this test was 2724 cycles.

The cyclic triaxial and DSS tests are summarised in contour diagrams. The contour diagrams are based on a limited number of tests, and extrapolations and interpolations were made to draw the curves over a wide range of cyclic shear stress levels. Thus, there are some uncertainties in the exact shapes of the contours. Principles of how the various contour diagrams are established is described in Andersen (2015).

F7.2 Interpretation of cyclic strength for structural design

F7.2.1 Cyclic DSS tests (DSScy)

Cyclic DSS tests were performed on samples from the Field Centre location. The results from all 4 cyclic DSS tests are summarized in Table H2-1 (NGI, 2016). The average and cyclic shear stresses are normalised by the undrained shear strength, s_{uD}, from the nearest static DSS.

For the Field Centre Figure F7.2.1 presents a summary plot with contours of number of cycles to failure. Figure F7.2.2 presents cyclic shear strain versus normalised cyclic shear stress and number of cycles at $\tau_a / s_{uD} = 0.0$.

In the summary plot, the number of cycles to failure, cyclic and average shear strains at failure for each of the tests are included in the figure. The results from cyclic tests on Drammen clay, OCR = 1, with a period of T = 10 s are shown in the background (Andersen, 2004). Drammen clay contours are based on normally consolidated conditions. Drammen clay with OCR = 1 is a normally consolidated contracting clay. As can be seen from Figures F7.2.1 and F7.2.2 the Flemish Pass DSS results compare fairly well with the Drammen clay test results. This suggests that for a possible future soil investigation at Flemish Pass, the number of additional cyclic tests can be reduced.

F7.2.2 Cyclic triaxial tests (CAUcy)

The results from all cyclic triaxial tests are summarized in Table G2-1 (NGI, 2016). Cyclic triaxial tests were performed on samples from the Field Centre location. The average and cyclic shear stresses are normalised by the undrained shear strength in compression, s_{uC} from static triaxial compression tests close to cyclic triaxial tests.

The following diagrams are shown for the Field Centre from cyclic triaxial tests:

- Figure F7.2.3: A summary plot with contours of number of cycles to failure.
- Figure F7.2.4: Cyclic shear strain versus normalised cyclic shear stress and number of cycles at $\tau_a / s_{uC} = 0.3$.

In the summary plot, the number of cycles to failure, cyclic and average shear strains at failure for each of the tests are included in the figure. The results from cyclic tests on Drammen clay, OCR = 1, with a period of T = 10 s are shown in the background (Andersen, 2004). As can be seen from Figures F7.2.3 and F7.2.4 the Flemish Pass triaxial test results show higher strength and stiffness than Drammen clay. The comparison with Drammen clay results is still a useful exercise. With the limited number of tests performed, the comparison serves as a quality control of the shape of the cyclic failure contours.

F7.3 Interpretation of Cyclic strength for slope stability

F7.3.1 Special cyclic DSS tests (DSSeq)

A special type of cyclic DSS tests was performed on samples from the East Slope location. The objective of these tests was to determine the soil behaviour subjected to earthquake loading and to quantify the cyclic and post-cyclic strength for slope stability assessment.

Three cyclic DSS tests were performed with a cyclic period of T = 2s. The tests were first consolidated to a vertical stress equal to p_0', and a shear stress of τ_c representing a slope angle of 4^o. The aim was to apply 10 cycles at three different cyclic stress levels. One test, however, failed after 9 cycles. The second test was terminated after 10 cycles and the third after 14 cycles. Due to the high frequency of cycling it is challenging to stop the test exactly at the predetermined point. The cyclic stage was followed by a period of undrained creep followed by undrained static shearing to failure. The stresses applied are illustrated on Figure F7.3.1. The shear stresses are normalised to the strength of a nearby static test (BH-18a 3A-2) with identical consolidation conditions as the cyclic tests.

F7.3.2 Results of the tests

The results from the three cyclic DSS tests are summarised in Table H2-1 in the factual report (NGI, 2016) and illustrated on Figures F7.3.1, F7.3.2 and F7.3.3. Some comments to the tests are as follows,

> Test BH18a 3A-3: This test failed after 9 cycles. The test was terminated after the cyclic stage.
>
> Test BH18a 3A-4: The cyclic stage was terminated after 14 cycles. It was then subjected to 143 hours$^{*)}$ of undrained creep at τ_a and practically no creep was observed. Finally, the specimen was sheared statically to failure as illustrated on Figure F7.3.2. At a shear strain of about 6%, the post-cyclic stress-strain curve approaches that of the static test, BH18a 3A-2. The post cyclic strength was approximately 98% of the static strength of the soil.
>
> Test BH18a 3A-5: The cyclic stage was terminated after 10 cycles. It was then subjected to 97 hours$^{*)}$ of undrained creep at τ_a. The measured creep was less than 1%. Finally, the specimen was sheared statically to failure as illustrated on Figure F7.3.3. At a shear strain of about 9%, the post-cyclic stress-strain curve

approaches that of the static test, BH18a 3A-2. The post cyclic strength was approximately 89% of the static strength of the soil.

*) The creep stage was terminated when enough time had elapsed without observing any increase of creep rate. With the insignificant amount of creep observed in both tests, the difference in creep duration is unlikely to affect the final static strength.

Figure F7.3.4 illustrates the effect of the special cyclic tests with a cyclic period of 10 s. The upper graph illustrates the strain developed after 5 cycles as a function of the cyclic shear stress normalised to the static strength, $\tau_{cy}/s_{uD,\tau c}$, where $s_{uD,\tau c}$ is the strength of a static test consolidated with a shear stress as explained above. The fact that 5 cycles with a cyclic shear stress equal to the static strength generates less than 3% strain is attributed to rate effect. A cyclic test with a period of 2 s, has a rate of shear stress in the order of 10^4 faster than a standard static DSS test.

The lower graph in Figure F7.3.4 shows the measured strains after 10 cycles. In both graphs the initial slope of the stress-strain relationship is illustrated by the G_{max} from a bender element test performed on the static reference test.

Based on the limited number of cyclic tests performed, one conclusion may to be that for an earthquake-induced shear stress ratio $\tau_{cy}/s_{uD,\tau c}$ less than 0.8, the soil shear strains will be small (for 10 cycles or less).

F8 Stiffness and damping parameters

F8.1 General

This section describes the results and interpretation of results from the test performed to obtain stiffness and damping parameters. The samples from East slope were tested using special cyclic DSS criteria in order to obtain parameters which can be used for dynamic slope stability analyses.

F8.2 Normalised shear moduli

The G-value will typically vary from soil element to soil element and depends on the degree of strength mobilization, the degree of overconsolidation, the strength and general soil characteristics. Based on the undrained triaxial and DSS tests, the secant shear modulus versus strength mobilization can be established from the tests performed on samples.

Figures F8.2.1 – F8.2.2 present the results from triaxial tests for Field Centre and Slopes respectively. The figures show the secant shear modulus, G, versus shear stress, τ, normalised to the undrained shear strength in triaxial compression, s_{uC}. The figures present results from the triaxial compression and extension tests carried out, and include representative profiles.

Similarly, Figures F8.2.3 – F8.2.4 give values of secant shear modulus, G, versus horizontal shear stress, τ_h, normalised to the undrained shear strength in DSS, s_{uD}, from the static direct simple shear tests for Field Centre and Slopes respectively.

The figures include suggested representative profiles.

F8.3 Maximum shear modulus

G_{max} measurements were performed on samples in the laboratory using piezo-ceramic bender elements (NGI, 2016). Bender element tests were performed in a DSS apparatus in connection with static DSS tests. Further, these G_{max} measurements are compared with correlation established with CPT cone resistance proposed by Robertson and Cabal (2010).

In uncemented soils of Holocene and Pleistocene age, Robertson and Cabal (2010) suggested the correlation of shear wave velocity to the CPT cone resistance as a function of soil type and I_c (Normalized Soil Behaviour Type chart):

$$V_s = [\alpha_{vs}(q_t-\sigma_v)/p_a]^{0.5} \text{ (m/s)};$$

where: $\alpha_{vs} = 10^{(0.55\,I_c+1.68)}$

$I_c = ((3.47 - \log Q_t)^2 + (\log F_r + 1.22)^2)^{0.5}$

Q_t = normalised cone penetration resistance (dimensionless)
$= (q_t - \sigma_{v0})/\sigma_{v0}'$

F_r = normalised friction ratio, in %
$= (f_s/(q_t - \sigma_{v0}))\cdot 100\%$

From the shear wave velocity the shear modulus may then be estimated from

$$G_{max} = \rho V_s^2$$

To present an overview of measured G_{max} and validity of the correlation for the entire site, all the data from the different locations are presented in Figure F8.3.1. For the Field Centre locations, interpretation of G_{max} from CPT correlation along with measured G_{max} in laboratory using bender elements are presented in Figure F8.3.2. For West Slope and East Slope locations data is presented in Figure F8.3.3 and Figure F8.3.4 respectively. It should be noted that one of the static DSS tests from the East slope location was consolidated with horizontal shear stress to emulate infinite sloping ground of 4^0. Therefore, the G_{max} measurement for this DSS test is lower than other G_{max} measurements.

For the clay layers, Figure F8.3.5 shows G_{max}/s_{uD} measured in the laboratory tests versus plasticity index, I_p. Data from Andersen et al. (2008) are included with black symbols and OCR-values whenever OCR > 1.5. The clay at the Flemish Pass site has a medium plasticity according to NGF (2011). The results show some scatter, but $G_{max}/s_{uD} = 1000$ seems to be a low representative value. Profiles of $G_{max} = 1000 \cdot s_{uD}$ are included in Figures F8.3.2 – F8.3.4 in order to compare with directly measured values and the values derived from Robertson and Cabal (2010).

Representative high and low profiles of G_{max} with depth are given in Figures F8.3.2 – F8.3.4. The representative profiles are intended for the bulk material, and the G_{max} will be higher in the sand layers. A designer has to evaluate whether this is of importance in his specific application.

F8.4 Variation of shear modulus with shear strain

Figure F8.4.1 and Figure F8.4.2 present the normalised shear modulus, G/G_{max}, versus shear strain during the first quart cycle for all cyclic DSS tests that were performed on specimens from Field centre and East slope location respectively. The cyclic DSS tests performed on specimens from the East slope location were all consolidated with a shear stress to simulate a 4^o slope. The details of these tests are presented in Section H2.4 (NGI 2016).

For each DSS test in question, the normalisation is by the G_{max} value either from the closest bender element test, or from a value based on the correlation by Robertson and Cabal (2010). A comparison of G/G_{max} versus shear strain for clay (Vucetic and Dobry, 1991 and Darendeli, 2001) is included in the background.

The results of the tests from the Field centre as presented on Figure F8.4.1 are normalised to G_{max} = 39.3 MPa, a value based on the correlation by Robertson and Cabal (2010). A suggested range of G/G_{max} versus shear strain, i.e. modulus reduction, for the clay is included in the figure.

On Figure F8.4.2, the results from East slope are normalised to G_{max} = 61.6 MPa a value taken from a nearby bender element test. The curves representing the cyclic DSS tests, are from tests consolidated with a shear stress, τ_c = 38.8 kPa. The curves based on literature (Vucetic and Dobry, 1991 and Darendeli, 2001) are from tests consolidated without a shear stress (τ_c = 0) and are consequently not directly comparable with the actual cyclic DSS tests. The suggested range of G/G_{max} versus shear strain included in the figure is in principle a range for shear stress consolidated conditions.

F8.5 Damping

Shear wave damping is a parameter required in dynamic analysis. The damping ratio, D, is computed for each cyclic stress-strain loop of the all symmetric cyclic DSS tests performed for the Field Centre location and the East Slope location. A summary of the results is presented in Figure F8.5.1 and Figure F8.5.2. For comparison, damping versus shear strain for a clay with plasticity index, I_p = 25 % are also included on the figures (Vucetic and Dobry, 1991 and Darendeli, 2001).

Suggested damping versus shear strain profiles have been included on the figures for N =1 and N =10.

F9 Comments on sample quality

The sample quality was evaluated based on the results of all the advanced tests (triax, direct simple shear and oedometer) is evaluated in terms of the change in void ratio, (Δe), relative to initial void ratio when consolidating the specimens back to the best estimate of in situ stresses according to the recommendations given by Lunne et al. (1998).

Figure F9.1.1 shows all the measurements. It includes the sample quality criteria proposed by Lunne et al. (1998) for OCR 1 – 2. The sample quality varies from "Very good to Excellent" to "Very Poor", with most of the samples are of quality "Poor" or "Very Poor".

The sample liners have an inner diameter of 75 mm. This is slightly larger than the sampler opening, see Benthic (2016a) for details. Triaxial tests were mounted in equipment for 72 mm requiring some marginal trimming. Two samples were trimmed to 54 mm diameter to see if this could increase the sample quality (indicated in Figure F9.1.1). The trimming process is made difficult by gravel in the samples. This probably adversely affects the sample quality. It does not appear that trimming improves the sample quality of the present material.

The method for evaluating sample quality is dependent on the water content, and hence the initial void ratio, of the tested specimen. The measurements show that the water content may change significantly over small depth ranges. This can result in apparent larger variability of the sample quality than normally expected for homogenous clay as the initial void ratio is derived from a water content measurement that is not part of the tested specimen. There is no reason to believe however, that there is a systematic tendency that this either increases or decreases the measure.

Many samples have cracks. The unit weight determinations indicate that the gas coming out of solution has not expanded the bulk material, but has rather cracked the sample, likely in places with lower plasticity or less clay. All samples used for advanced testing were transported and stored vertically in the transparent liners. The lab operators, in discussion with the engineers, selected the exact depth at which to perform advanced tests in order to avoid being too close to a crack or sample ends. In spite of the attempts to select material with minimal influence from gas cracks for testing, there is probably an effect of the gas crack on the sample quality.

The poor sample quality leaves some uncertainty to the interpreted data. The area ratio of the sampler is one factor playing a role in the quality of the samples (e.g. Tjelta & Yetginer, 2010 and NGI 2010) that should be considered in a future investigation.

However, the OCR data from consolidation tests (CRS) show values close to what should be expected for sediments that have not been subjected to mechanical overloading, i.e. only apparent overconsolidation due to ageing. Similarly, the average s_{uC}/p_0' = 0.36 from triaxial tests is in the range that is expected for lightly overconsolidated sediments.

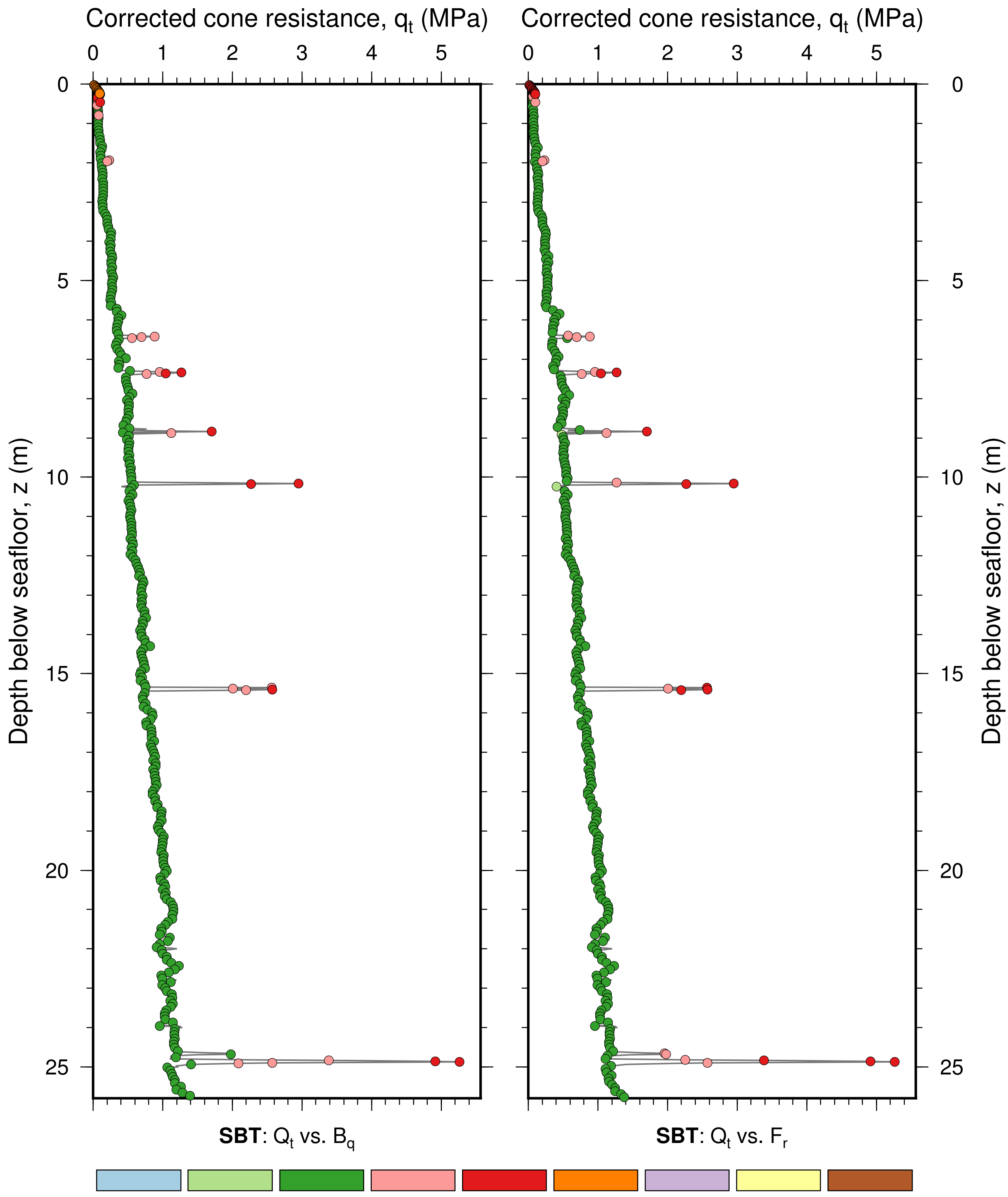

1: Sensitive, fine grained
2: Organic soils, peats
3: Clays; Clay to silty clay
4: Silt mixtures; Clayey silt to silty clay
SBT according to Robertson, 1990

5: Sand mixtures; Silty sand to sandy silt
6: Sand; Clean sand to silty sand
7: Gravelly sand to sand
8: Very stiff sand to clayey sand
9: Very stiff fine grained

ST15452 − Flemish Pass Geotechnical Investigation	Document No. 20140857−02−R
	Figure No. F2.2.1
Soil behaviour type (SBT) versus depth (after Robertson, 1990). Borehole: ST15452−05	Date 2016−04−07 / Drawn by MVa

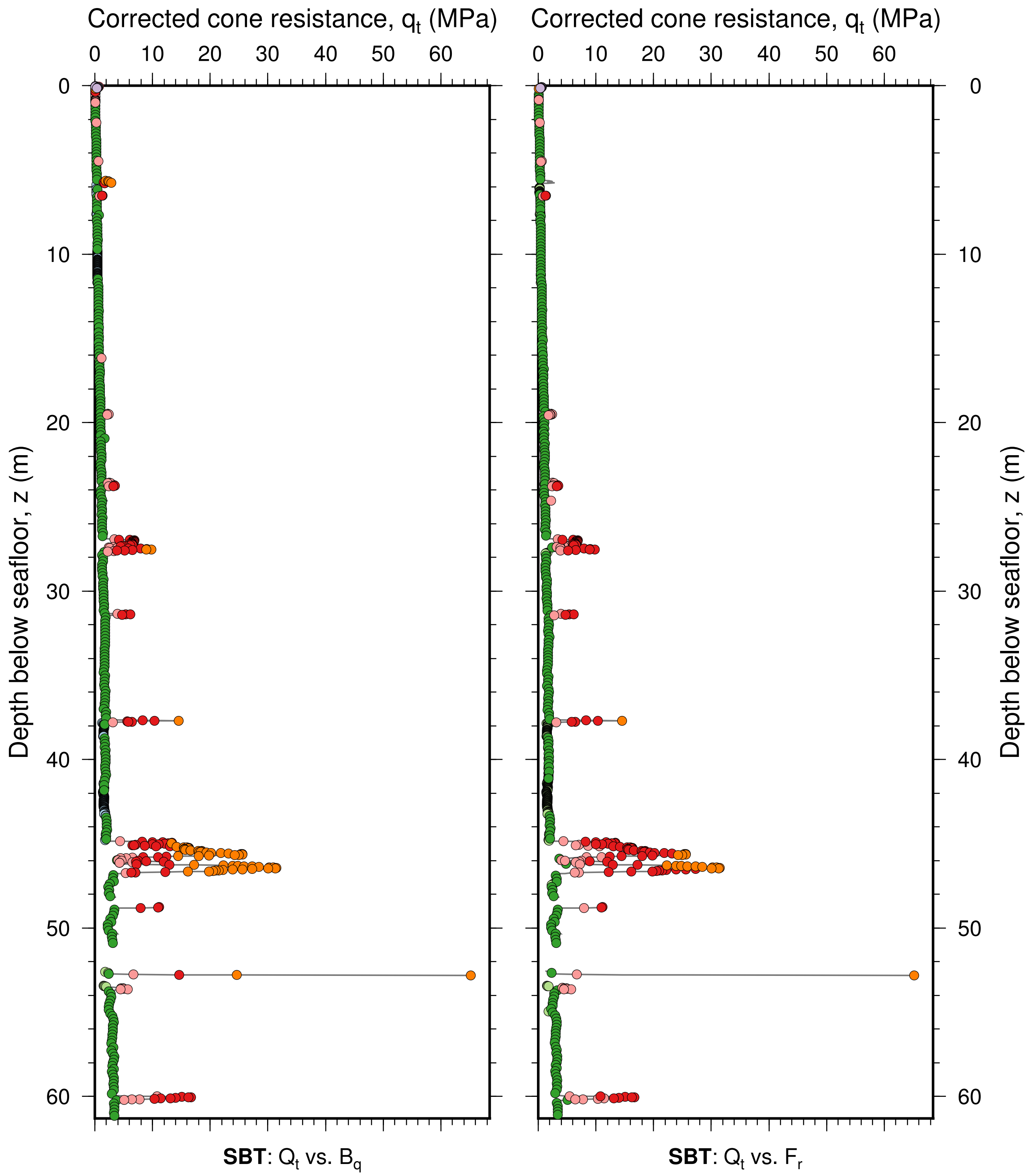

1: Sensitive, fine grained
2: Organic soils, peats
3: Clays; Clay to silty clay
4: Silt mixtures; Clayey silt to silty clay
SBT according to Robertson, 1990

5: Sand mixtures; Silty sand to sandy silt
6: Sand; Clean sand to silty sand
7: Gravelly sand to sand
8: Very stiff sand to clayey sand
9: Very stiff fine grained

ST15452 − Flemish Pass Geotechnical Investigation

Soil behaviour type (SBT) versus depth (after Robertson, 1990).
Borehole: ST15452−12

Document No.	
20140857−02−R	
Figure No. F2.2.2	
Date 2016−04−07	Drawn by MVa

NGI

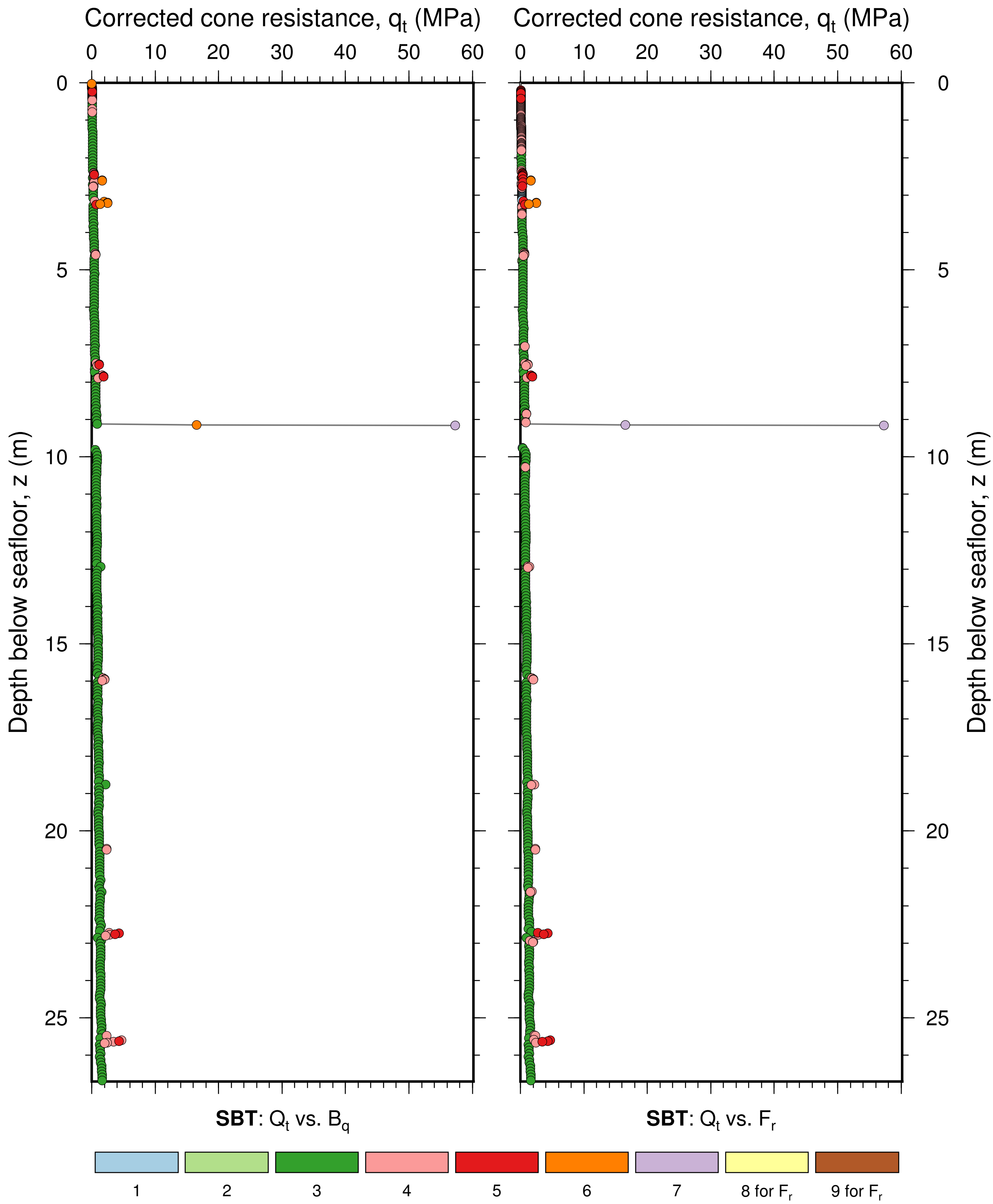

1: Sensitive, fine grained
2: Organic soils, peats
3: Clays; Clay to silty clay
4: Silt mixtures; Clayey silt to silty clay
5: Sand mixtures; Silty sand to sandy silt
6: Sand; Clean sand to silty sand
7: Gravelly sand to sand
8: Very stiff sand to clayey sand
9: Very stiff fine grained

SBT according to Robertson, 1990

trepak:/grouphome/gmtapp/20140857_Flemish/CPT/SoilClassification/DecimationTests/03-ST15452-15_CPT-SBT-depthprofile1-BqFrvsQt.ps

ST15452 − Flemish Pass Geotechnical Investigation	Document No. 20140857−02−R	
	Figure No. F2.2.3	
Soil behaviour type (SBT) versus depth (after Robertson, 1990). Borehole: ST15452−15	Date 2016−04−07	Drawn by MVa
	NGI	

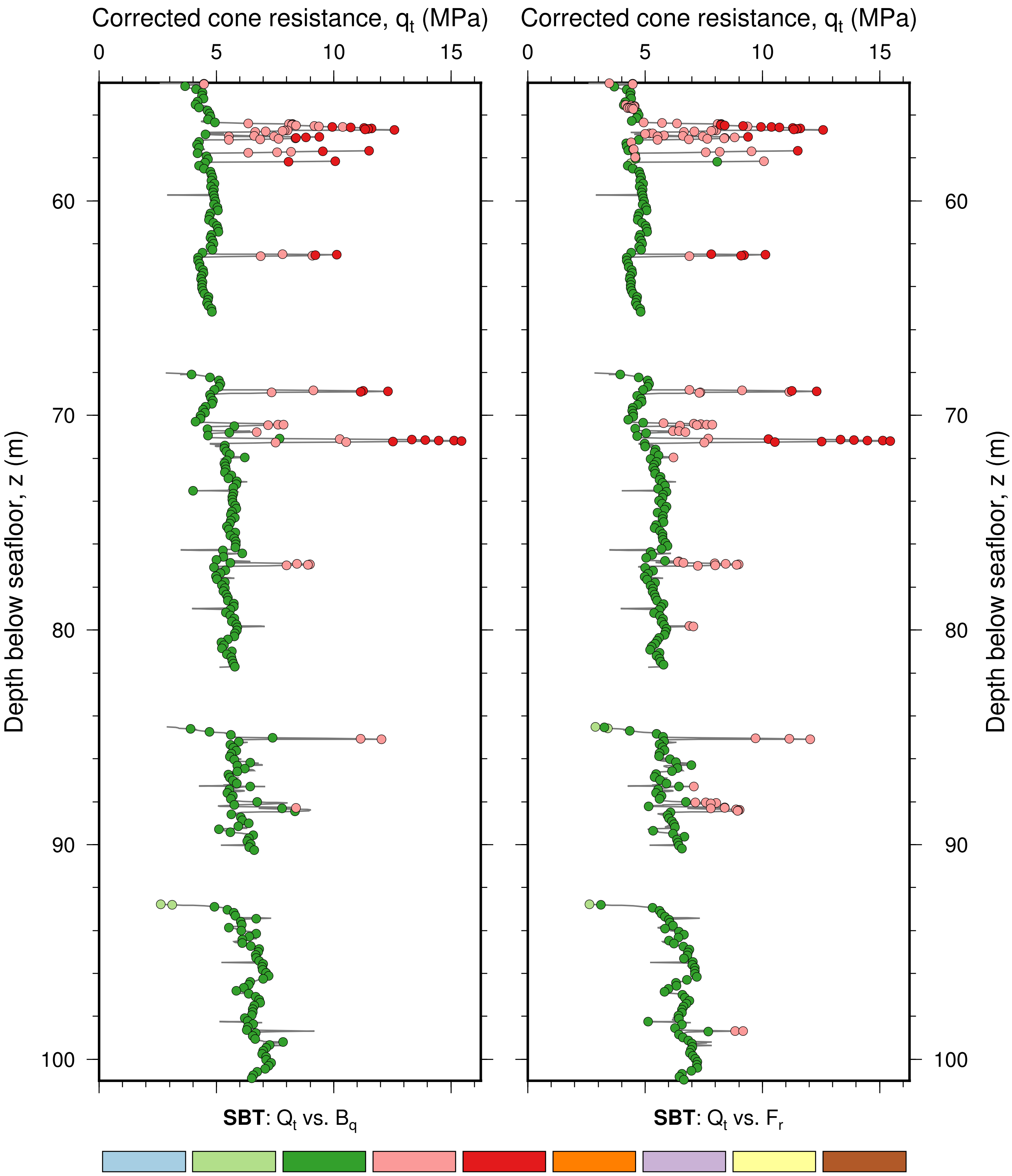

1: Sensitive, fine grained
2: Organic soils, peats
3: Clays; Clay to silty clay
4: Silt mixtures; Clayey silt to silty clay
5: Sand mixtures; Silty sand to sandy silt
6: Sand; Clean sand to silty sand
7: Gravelly sand to sand
8: Very stiff sand to clayey sand
9: Very stiff fine grained

SBT according to Robertson, 1990

trepak:/grouphome/gmtapp/20140857_Flemish/CPT/SoilClassification/DecimationTests/04−ST15452−02_CPT−SBT−depthprofile1−BqFrvsQt.ps

ST15452 − Flemish Pass Geotechnical Investigation	Document No. 20140857−02−R
Soil behaviour type (SBT) versus depth (after Robertson, 1990). Borehole: ST15452−02	Figure No. F2.2.4
	Date 2016−04−07 / Drawn by MVa
	NGI

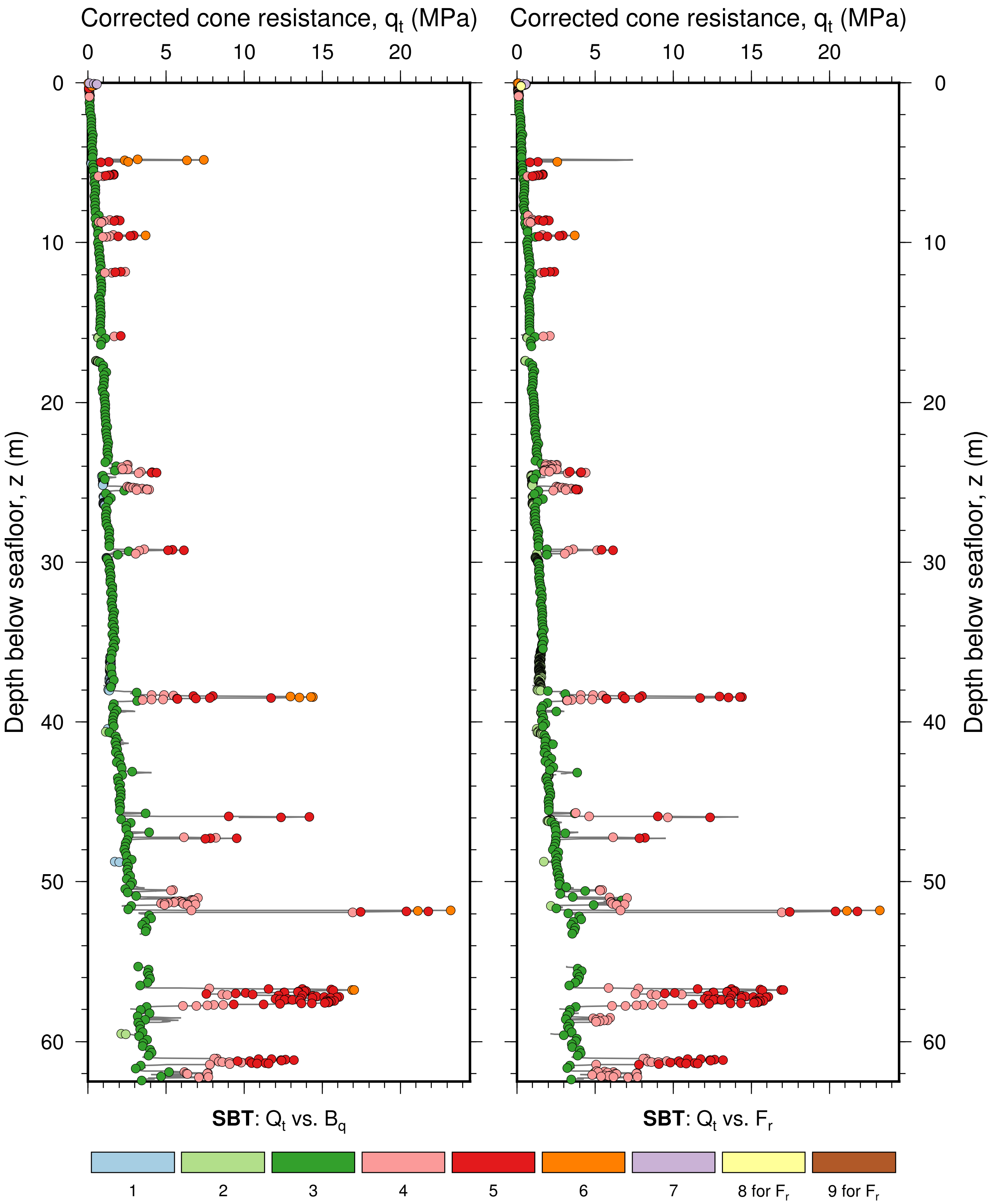

1: Sensitive, fine grained
2: Organic soils, peats
3: Clays; Clay to silty clay
4: Silt mixtures; Clayey silt to silty clay
SBT according to Robertson, 1990

5: Sand mixtures; Silty sand to sandy silt
6: Sand; Clean sand to silty sand
7: Gravelly sand to sand
8: Very stiff sand to clayey sand
9: Very stiff fine grained

ST15452 − Flemish Pass Geotechnical Investigation

Soil behaviour type (SBT) versus depth (after Robertson, 1990).
Borehole: ST15452−03

Document No. 20140857−02−R	
Figure No. F2.2.5	
Date 2016−04−07	Drawn by MVa

NGI

trepak:/grouphome/gmtapp/20140857_Flemish/CPT/SoilClassification/DecimationTests/05−ST15452−03_CPT−SBT−depthprofile1−BqFrvsQt.ps

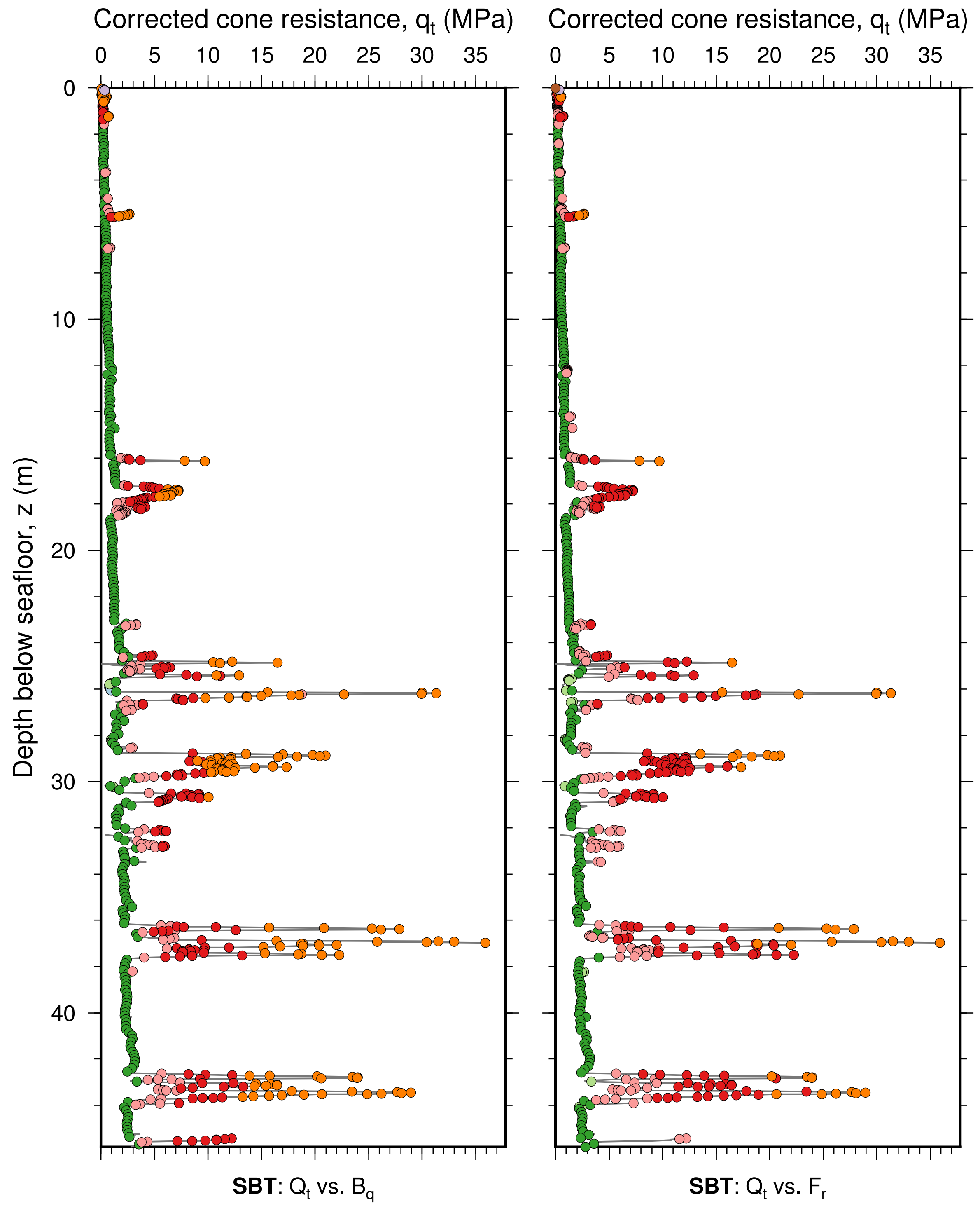

1: Sensitive, fine grained

2: Organic soils, peats

3: Clays; Clay to silty clay

4: Silt mixtures; Clayey silt to silty clay

SBT according to Robertson, 1990

5: Sand mixtures; Silty sand to sandy silt

6: Sand; Clean sand to silty sand

7: Gravelly sand to sand

8: Very stiff sand to clayey sand

9: Very stiff fine grained

trepak:/grouphome/gmtapp/20140857_Flemish/CPT/SoilClassification/DecimationTests/06−ST15452−07_CPT−SBT−depthprofile1−BqFrvsQt.ps

ST15452 − Flemish Pass Geotechnical Investigation	Document No. 20140857−02−R	
Soil behaviour type (SBT) versus depth (after Robertson, 1990). Borehole: ST15452−07	Figure No. F2.2.6	
	Date 2016−04−07	Drawn by MVa

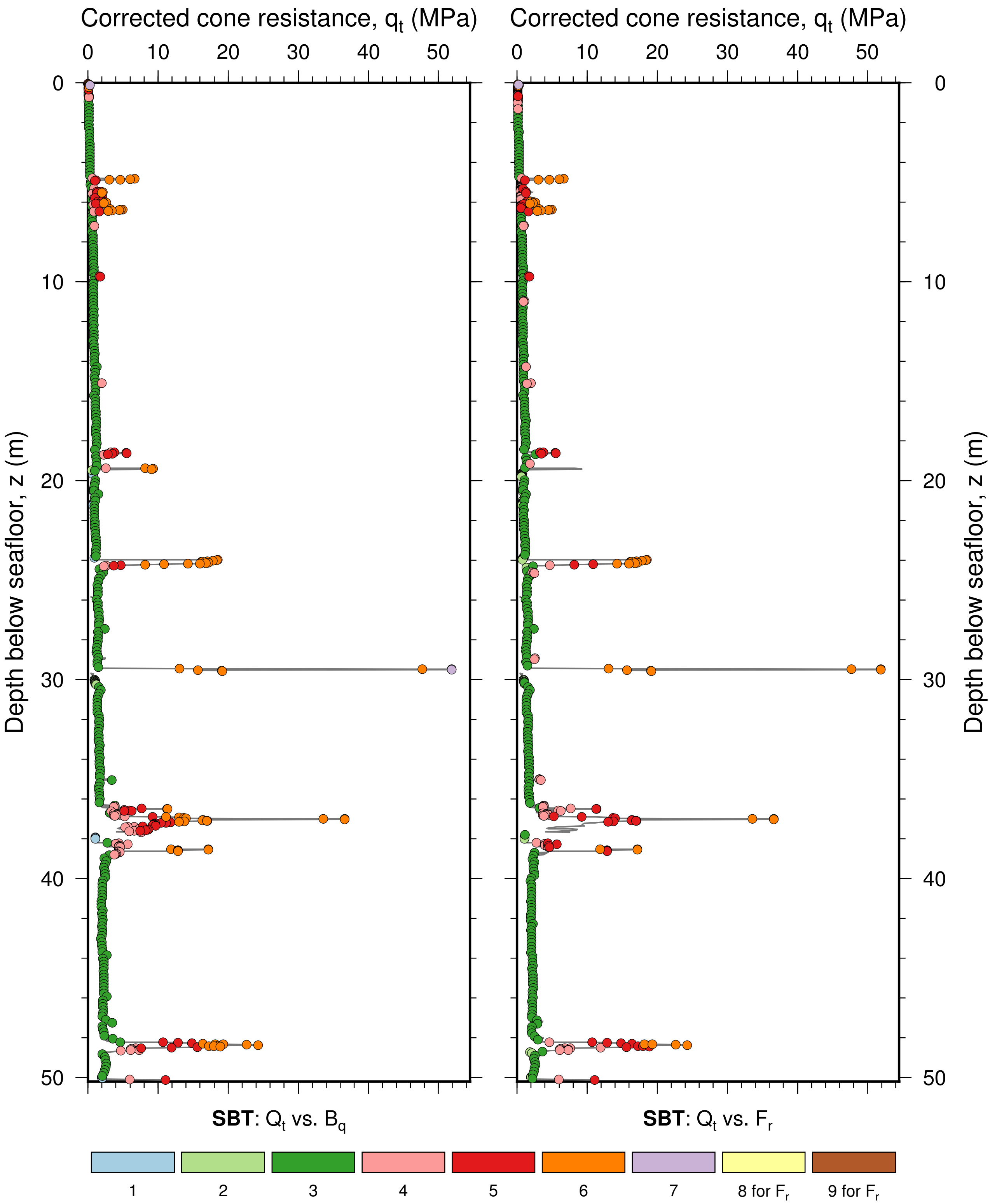

1: Sensitive, fine grained

2: Organic soils, peats

3: Clays; Clay to silty clay

4: Silt mixtures; Clayey silt to silty clay

SBT according to Robertson, 1990

5: Sand mixtures; Silty sand to sandy silt

6: Sand; Clean sand to silty sand

7: Gravelly sand to sand

8: Very stiff sand to clayey sand

9: Very stiff fine grained

ST15452 − Flemish Pass Geotechnical Investigation	Document No. 20140857−02−R
	Figure No. F2.2.7
Soil behaviour type (SBT) versus depth (after Robertson, 1990). Borehole: ST15452−08	Date 2016−04−07 / Drawn by MVa

NGI

trepak:/grouphome/gmtapp/20140857_Flemish/CPT/SoilClassification/DecimationTests/07−ST15452−08_CPT−SBT−depthprofile1−BqFrvsQt.ps

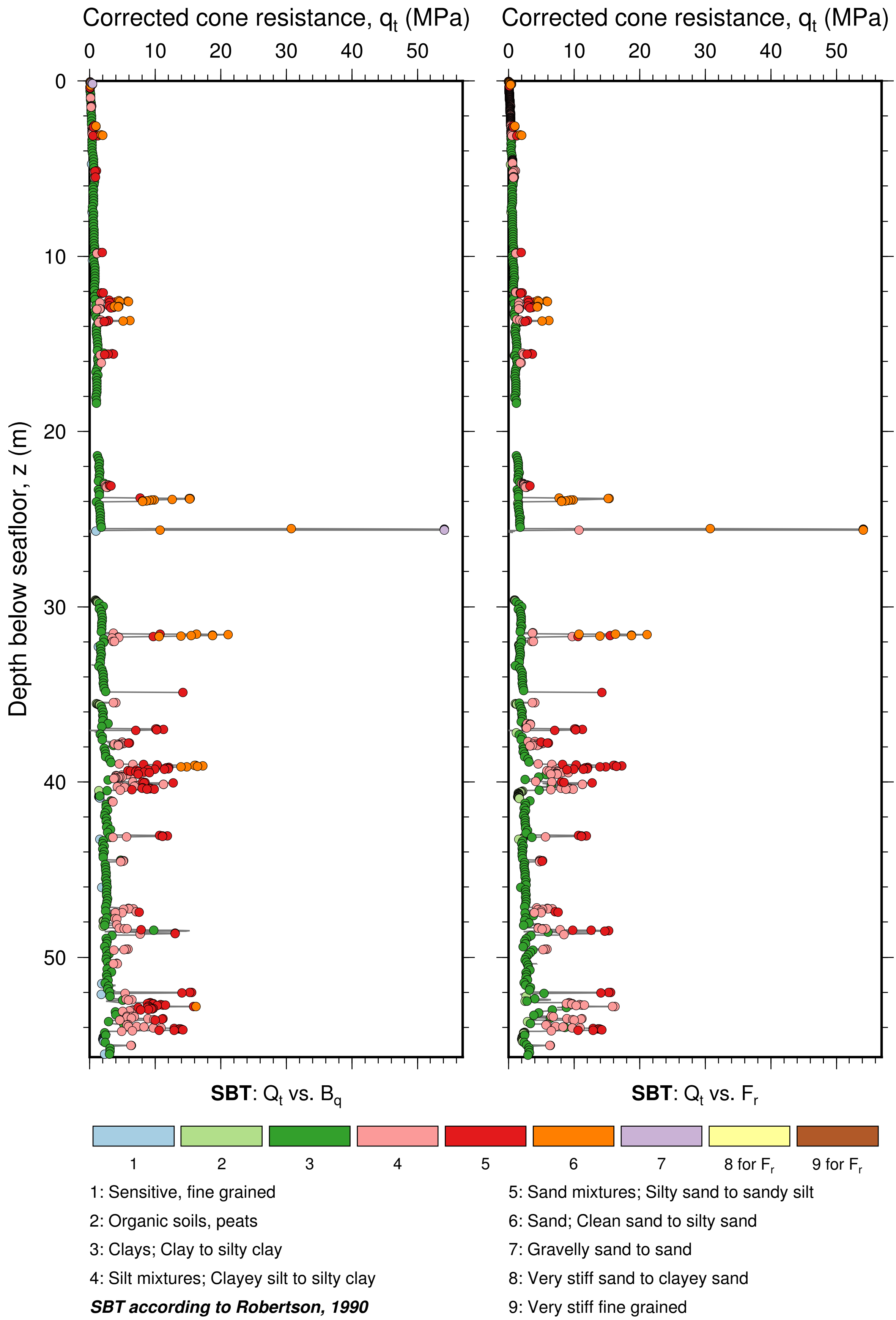

trepak:/grouphome/gmtapp/20140857_Flemish/CPT/SoilClassification/DecimationTests/08-ST15452-16_CPT-SBT-depthprofile1-BqFrvsQt.ps

ST15452 − Flemish Pass Geotechnical Investigation

Soil behaviour type (SBT) versus depth (after Robertson, 1990).
Borehole: ST15452−16

Document No.	20140857−02−R
Figure No.	F2.2.8
Date: 2016−04−07	Drawn by: MVa

NGI

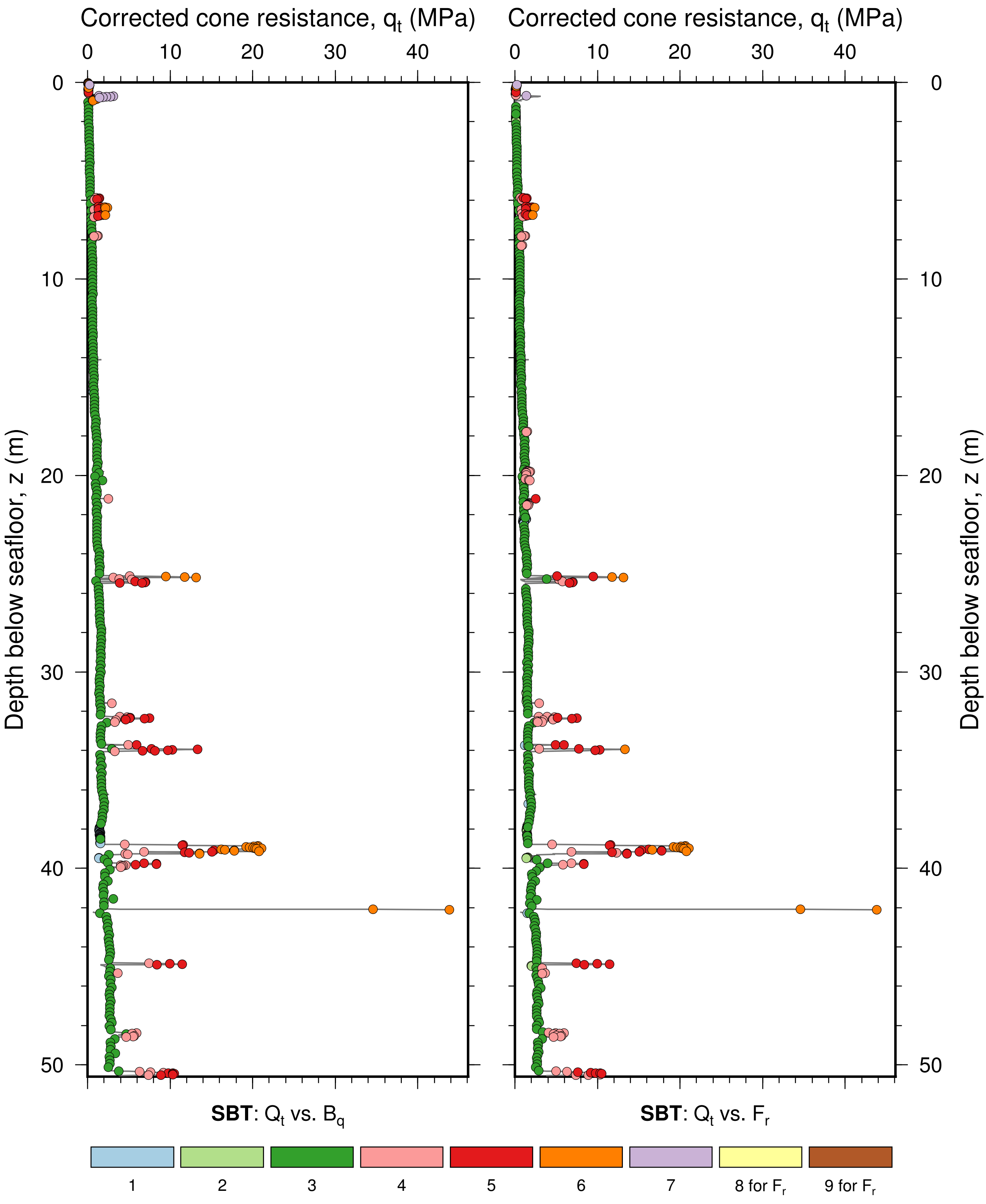

1: Sensitive, fine grained
2: Organic soils, peats
3: Clays; Clay to silty clay
4: Silt mixtures; Clayey silt to silty clay
5: Sand mixtures; Silty sand to sandy silt
6: Sand; Clean sand to silty sand
7: Gravelly sand to sand
8: Very stiff sand to clayey sand
9: Very stiff fine grained

SBT according to Robertson, 1990

trepak:/grouphome/gmtapp/20140857_Flemish/CPT/SoilClassification/DecimationTests/09−ST15452−19_CPT−SBT−depthprofile1−BqFrvsQt.ps

ST15452 − Flemish Pass Geotechnical Investigation	Document No. 20140857−02−R
	Figure No. F2.2.9
Soil behaviour type (SBT) versus depth (after Robertson, 1990). Borehole: ST15452−19	Date 2016−04−07 / Drawn by MVa

NGI

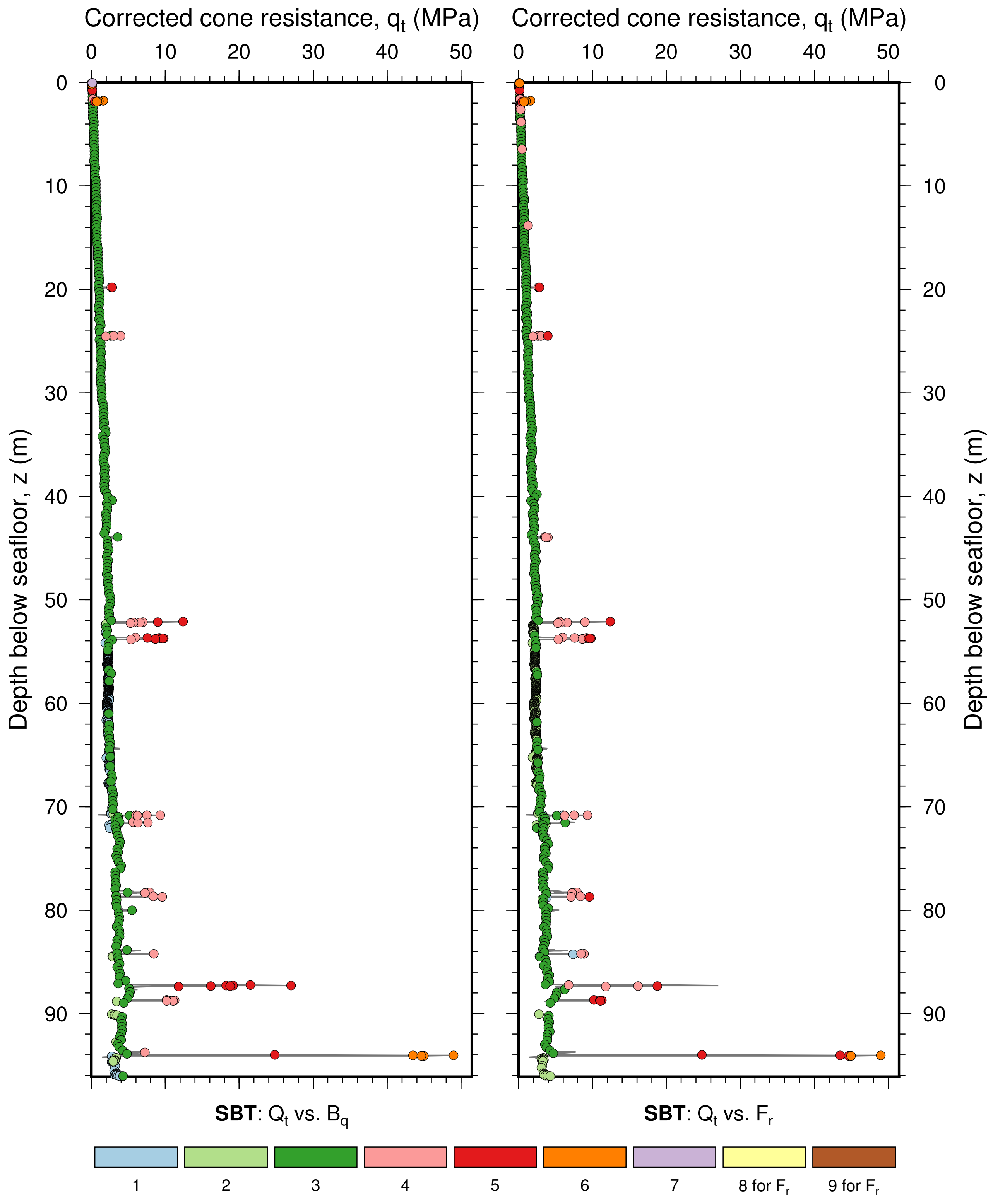

1: Sensitive, fine grained

2: Organic soils, peats

3: Clays; Clay to silty clay

4: Silt mixtures; Clayey silt to silty clay

SBT according to Robertson, 1990

5: Sand mixtures; Silty sand to sandy silt

6: Sand; Clean sand to silty sand

7: Gravelly sand to sand

8: Very stiff sand to clayey sand

9: Very stiff fine grained

ST15452 − Flemish Pass Geotechnical Investigation	Document No. 20140857−02−R	
	Figure No. F2.2.10	
Soil behaviour type (SBT) versus depth (after Robertson, 1990). Borehole: ST15452−18	Date 2016−04−07	Drawn by MVa
	NGI	

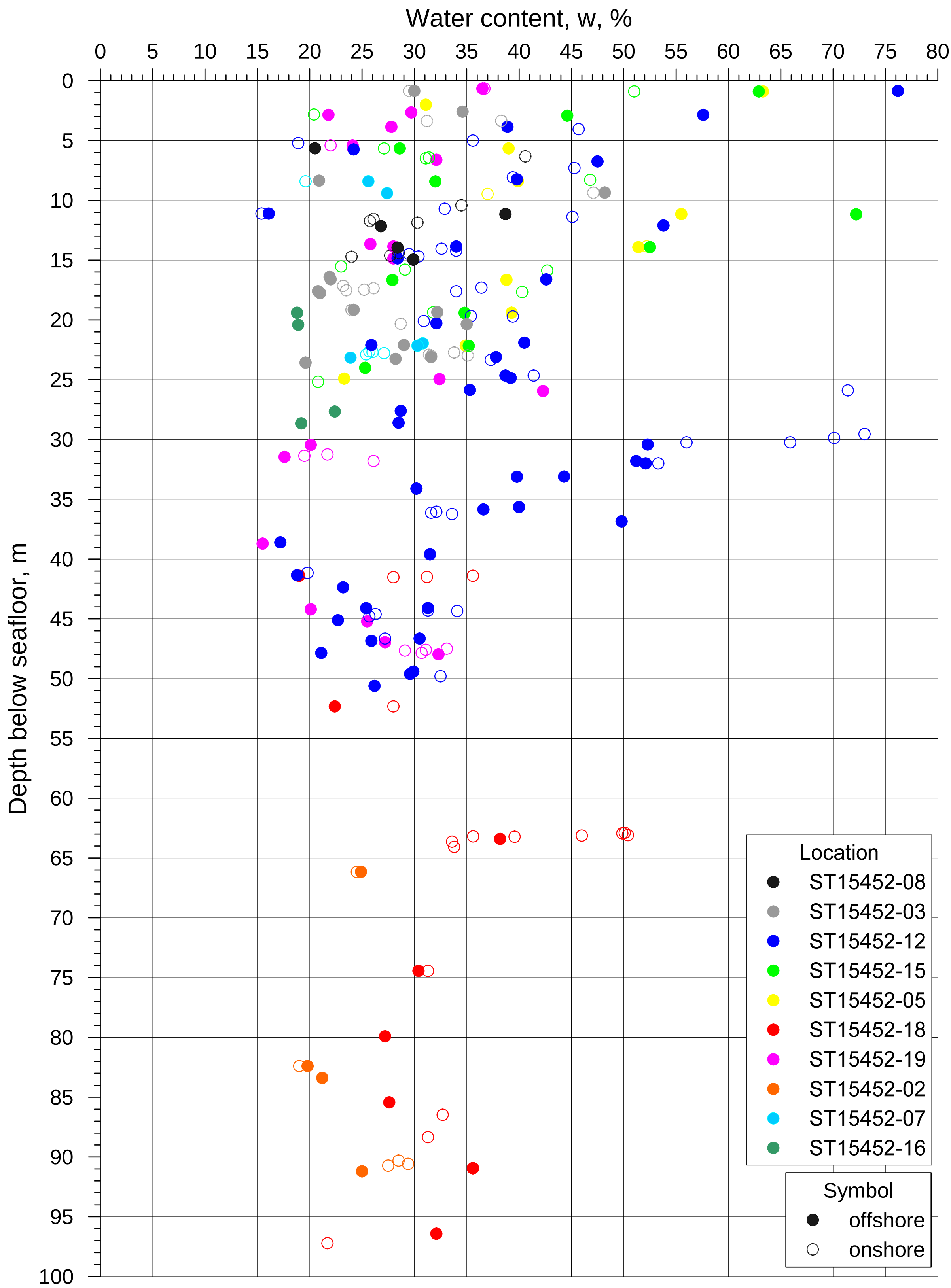

P:\2014\08\20140857\Leveransedokumenter\Rapport\20140857-02-R Data interpretation and evaluation\Figures\Section F\Figure F_03_01_01, water content versus depth.grf

Date/Rev.: 2015-01-21/01

ST15452 Flemish Pass Geotechnical Investigation	Document No. 20140857-02-R
Water content versus depth All locations	Figure No. F3.1.1
	Date 2016-04-03 / Drawn by VBS
	NGI

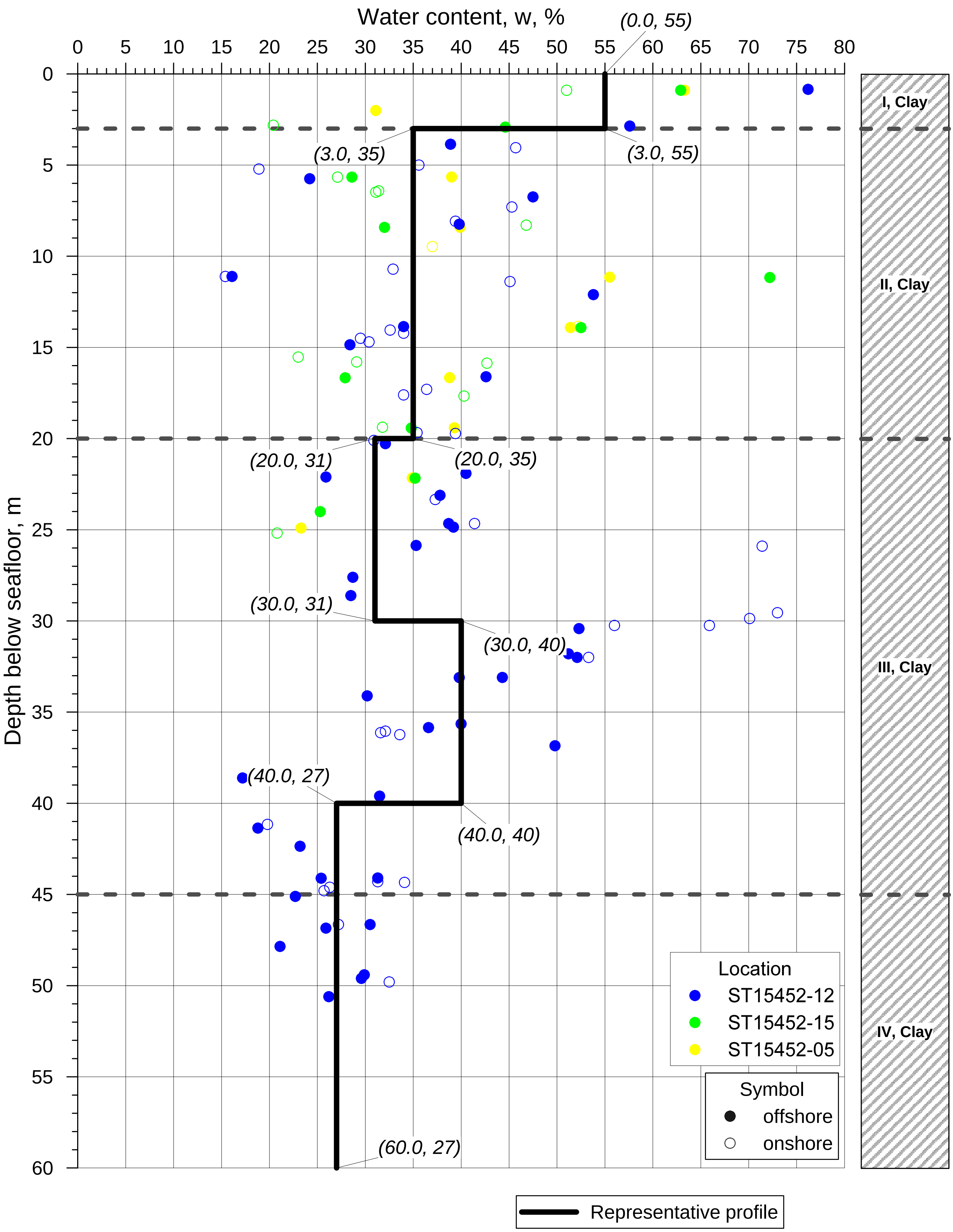

Label: *(depth, value)*

Date/Rev.: 2015-01-21/01

P:\2014\08\20140857\Leveransedokumenter\Rapport\20140857-02-R Data interpretation and evaluation\Figures\Section F\Figure F_03_01_02, water content versus depth-Fieldcentre.grf

ST15452 Flemish Pass Geotechnical Investigation	Document No. 20140857-02-R
Water content versus depth Field Centre	Figure No. F3.1.2
	Date 2016-04-03
	Drawn by VBS

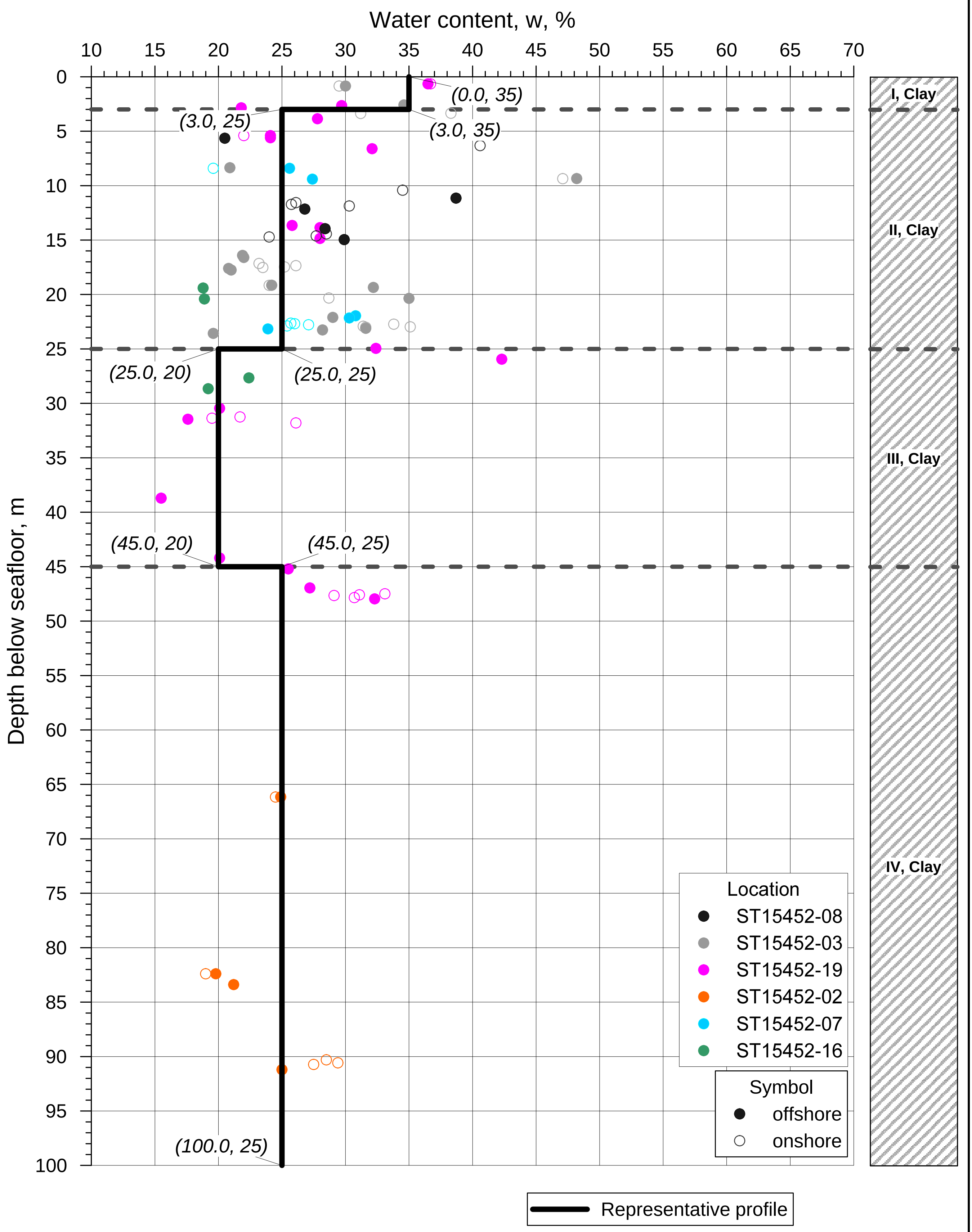

Label: *(depth, value)*

Date/Rev.: 2015-01-21/01

P:\2014\08\20140857\Leveransedokumenter\Rapport\20140857-02-R Data interpretation and evaluation\Figures\Section F\Figure F_03_01_03, water content versus depth-West.grf

ST15452 Flemish Pass Geotechnical Investigation	Document No. 20140857-02-R	
Water content versus depth West Slope	Figure No. F3.1.3	
	Date 2016-04-03	Drawn by VBS
	NGI	

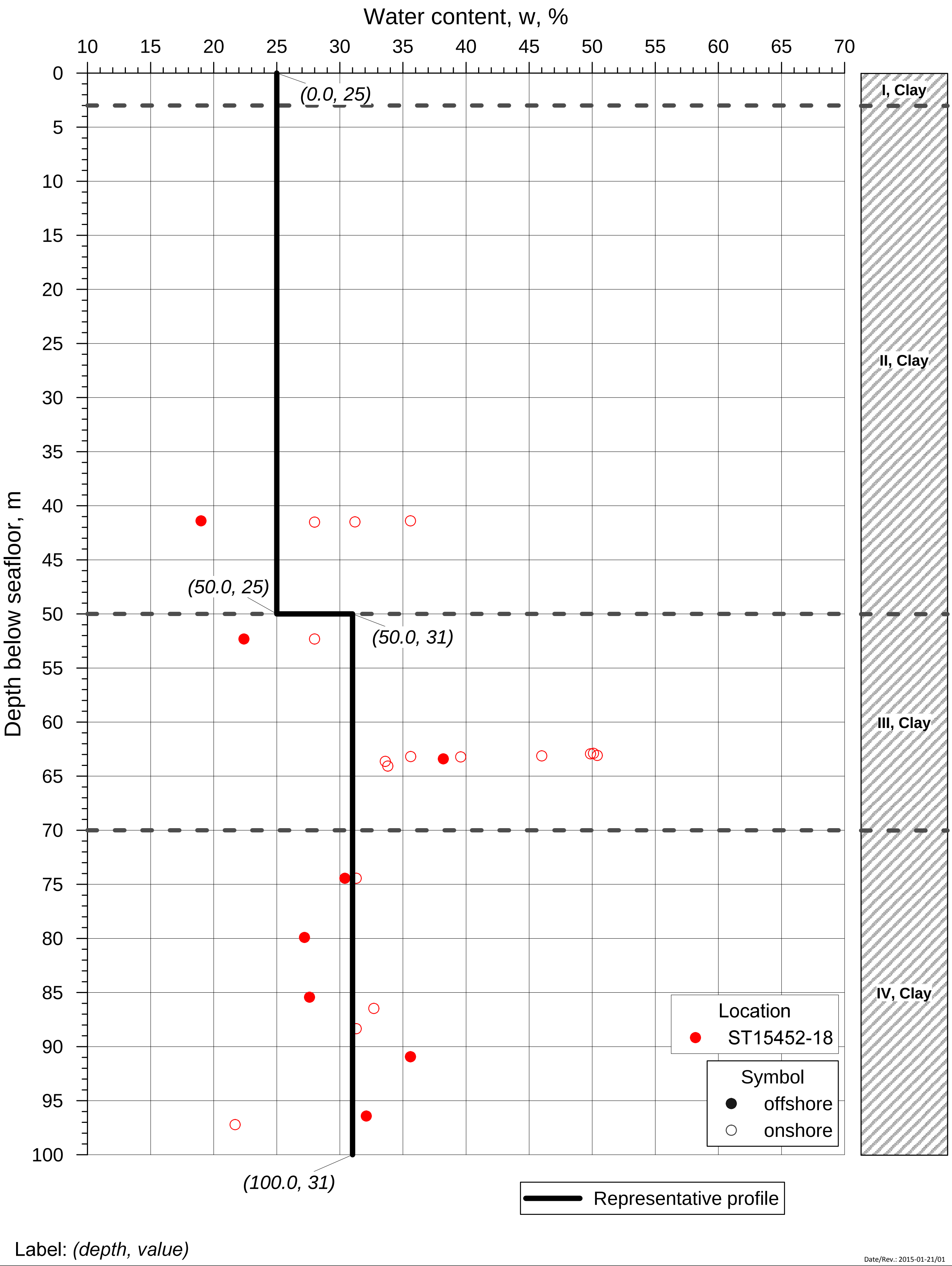

Date/Rev.: 2015-01-21/01

ST15452 Flemish Pass Geotechnical Investigation	Document No. 20140857-02-R
Water content versus depth East Slope	Figure No. F3.1.4
	Date 2016-04-03 / Drawn by VBS

P:\2014\08\20140857\Leveransedokumenter\Rapport\20140857-02-R Data interpretation and evaluation\Figures\Section F\Figure F_03_01_04, water content versus depth-East.grf

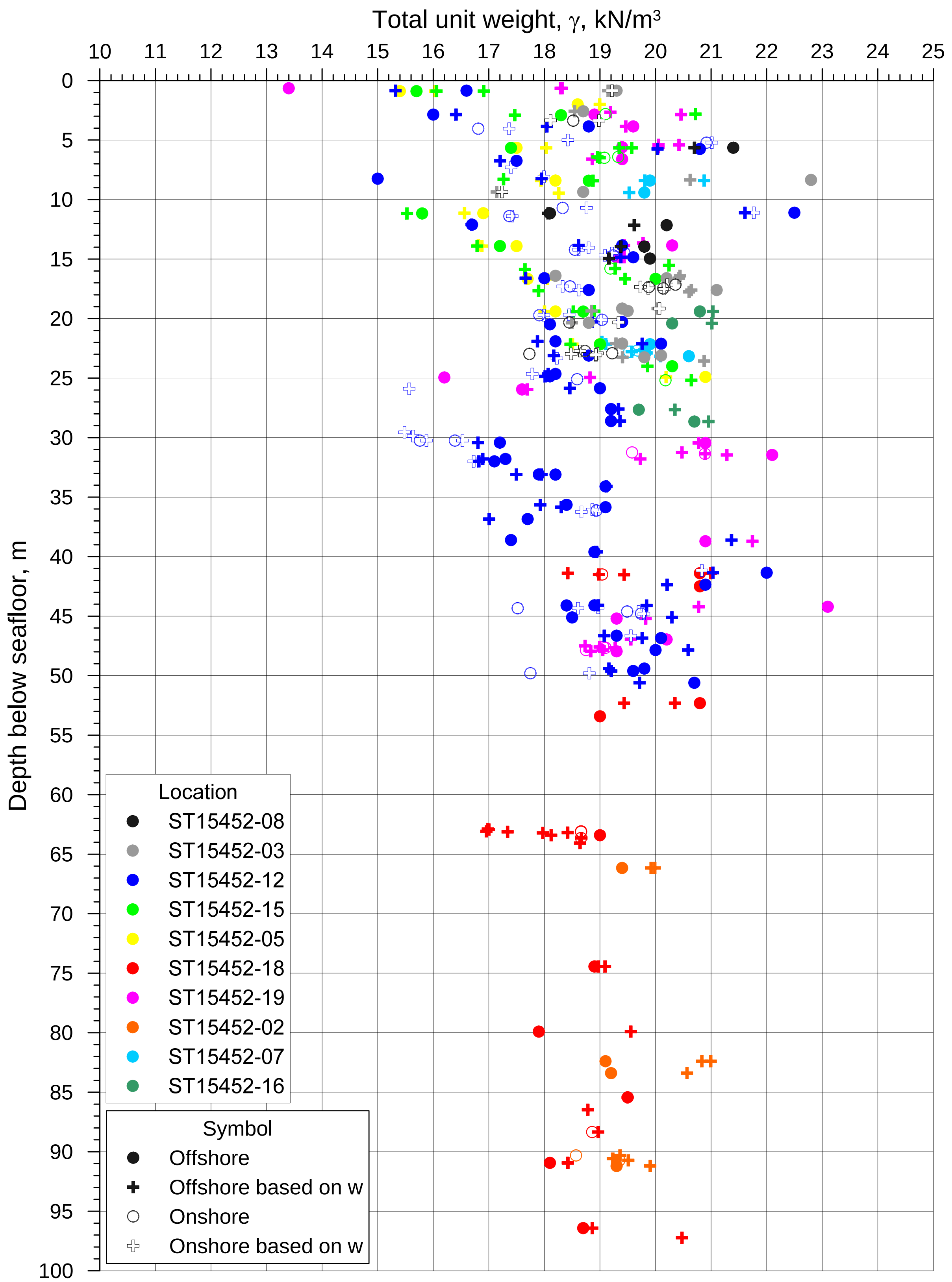

NOTE:
γ based on w is calculated assuming S_r = 100%
and using γ_s = 26.8 kN/m³

Date/Rev.: 2015-01-21/01

P:\2014\08\20140857\Leveransedokumenter\Rapport\20140857-02-R Data interpretation and evaluation\Figures\Section F\Figure F_03_02_01, total unit weight versus depth.grf

ST15452 Flemish Pass Geotechnical Investigation	Document No. 20140857-02-R	
Total unit weight versus depth All locations	Figure No. F3.2.1	
	Date 2016-04-03	Drawn by VBS

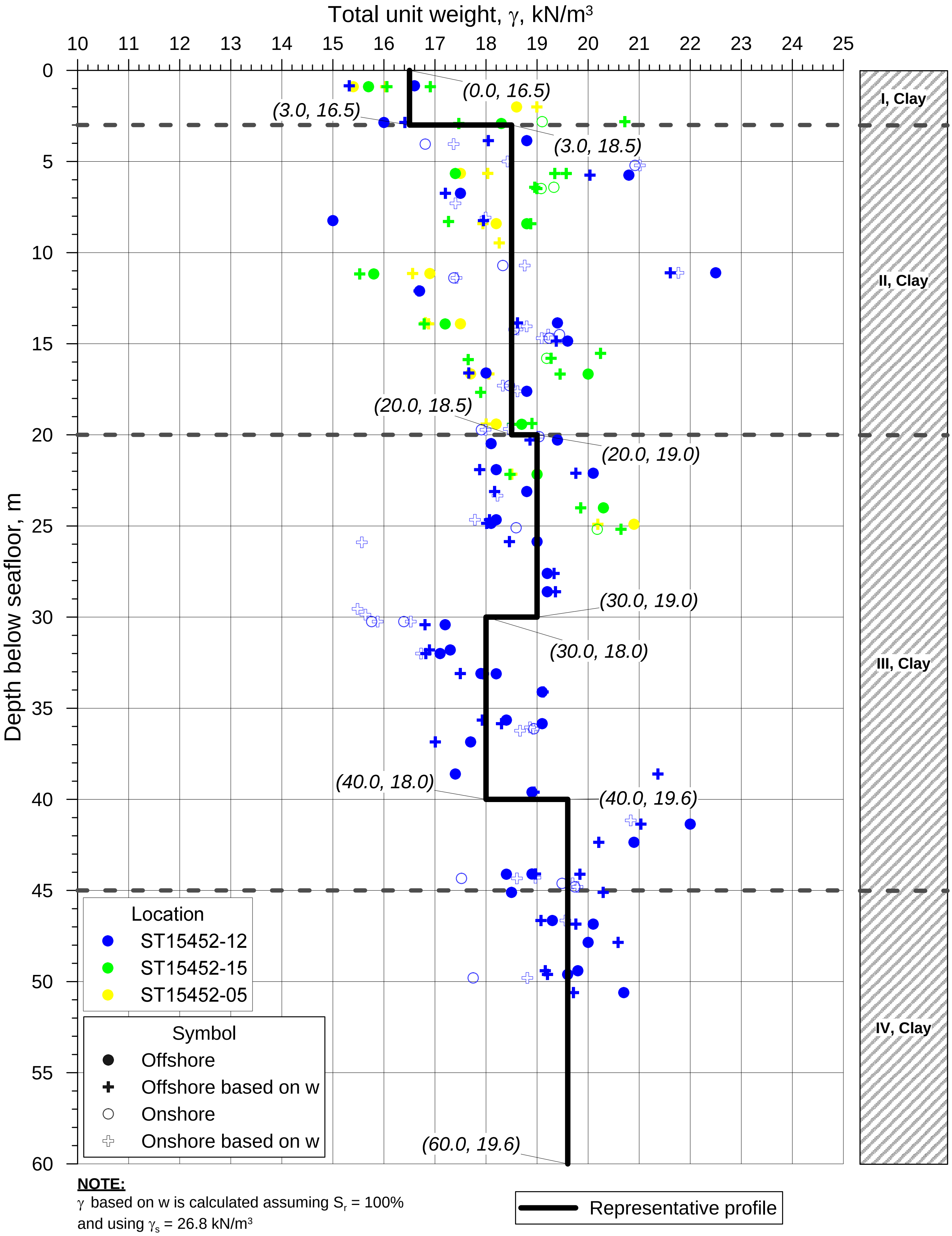

NOTE:
γ based on w is calculated assuming S_r = 100%
and using γ_s = 26.8 kN/m³

Label: *(depth, value)*

Date/Rev.: 2015-01-21/01

P:\2014\08\20140857\Leveranseddokumenter\Rapport\20140857-02-R Data interpretation and evaluation\Figures\Section F\Figure F_03_02_02, total unit weight versus depth-Fieldcentre.grf

ST15452 Flemish Pass Geotechnical Investigation	Document No. 20140857-02-R
Total unit weight versus depth Field Centre	Figure No. F3.2.2
	Date: 2016-04-03 — Drawn by: VBS
	NGI

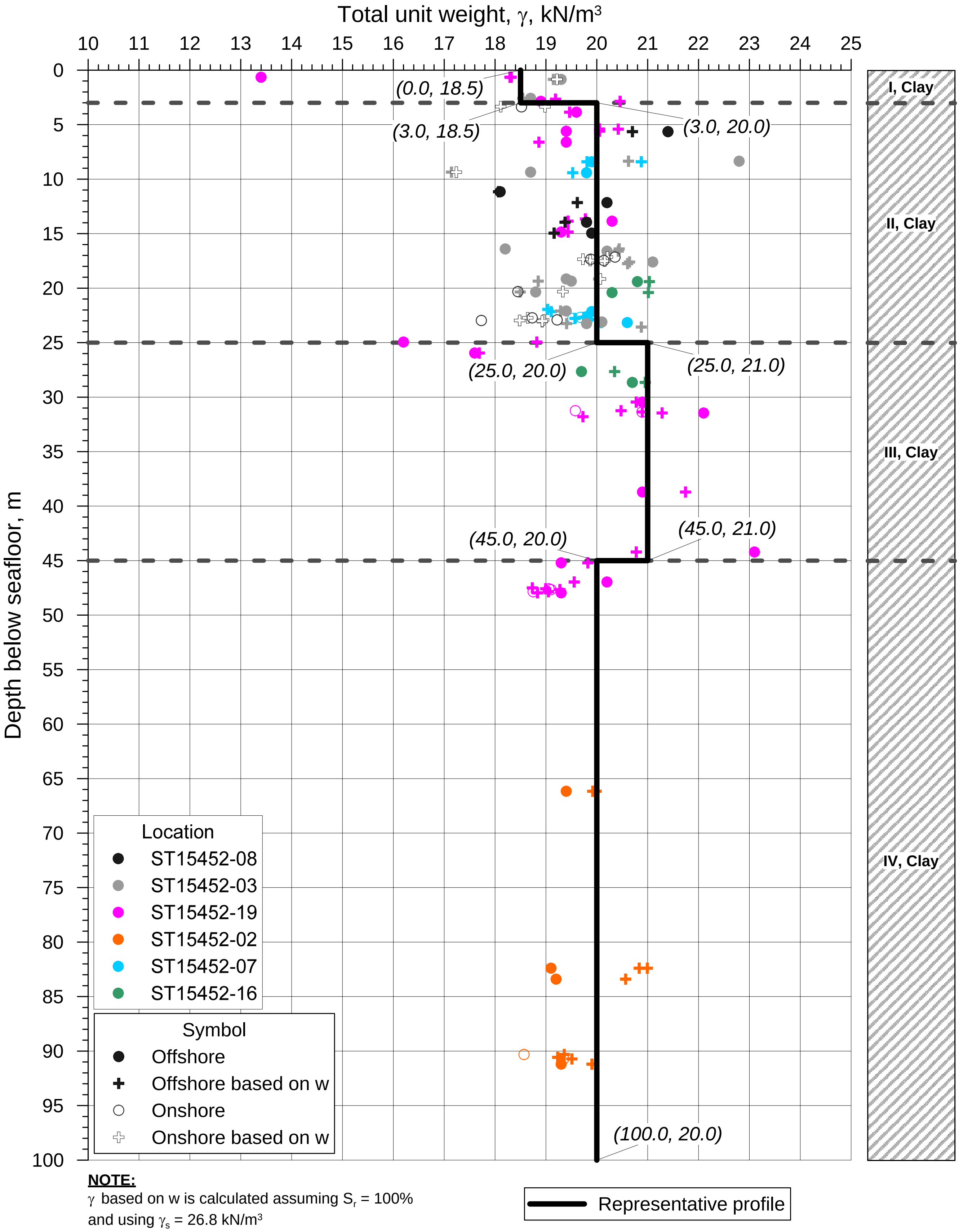

NOTE:
γ based on w is calculated assuming S_r = 100%
and using γ_s = 26.8 kN/m³

Label: *(depth, value)*

Date/Rev.: 2015-01-21/01

P:\2014\08\20140857\Leveransedokumenter\Rapport\20140857-02-R Data interpretation and evaluation\Figures\Section F\Figure F_03_02_03, total unit weight versus depth-West.grf

ST15452 Flemish Pass Geotechnical Investigation

Total unit weight versus depth
West Slope

Document No.	20140857-02-R
Figure No.	F3.2.3
Date	2016-04-03
Drawn by	VBS

NGI

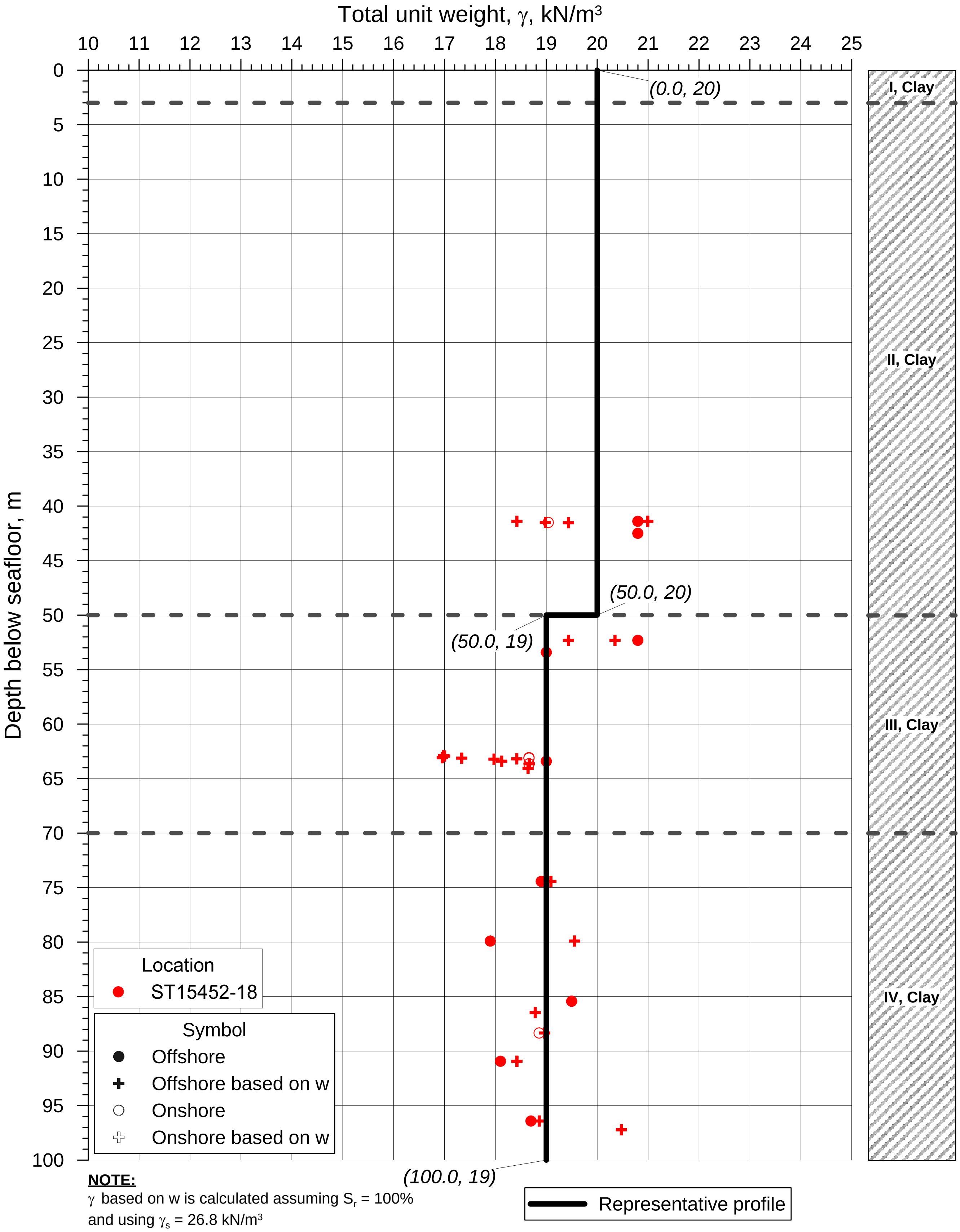

NOTE:
γ based on w is calculated assuming S_r = 100%
and using γ_s = 26.8 kN/m³

Label: *(depth, value)*

Date/Rev.: 2015-01-21/01

P:\2014\08\20140857\Leveransedokumenter\Rapport\20140857-02-R Data interpretation and evaluation\Figures\Section F\Figure F_03_02_04, total unit weight versus depth-East.grf

ST15452 Flemish Pass Geotechnical Investigation	Document No. 20140857-02-R
Total unit weight versus depth East Slope	Figure No. F3.2.4
	Date 2016-04-03 / Drawn by VBS
	NGI

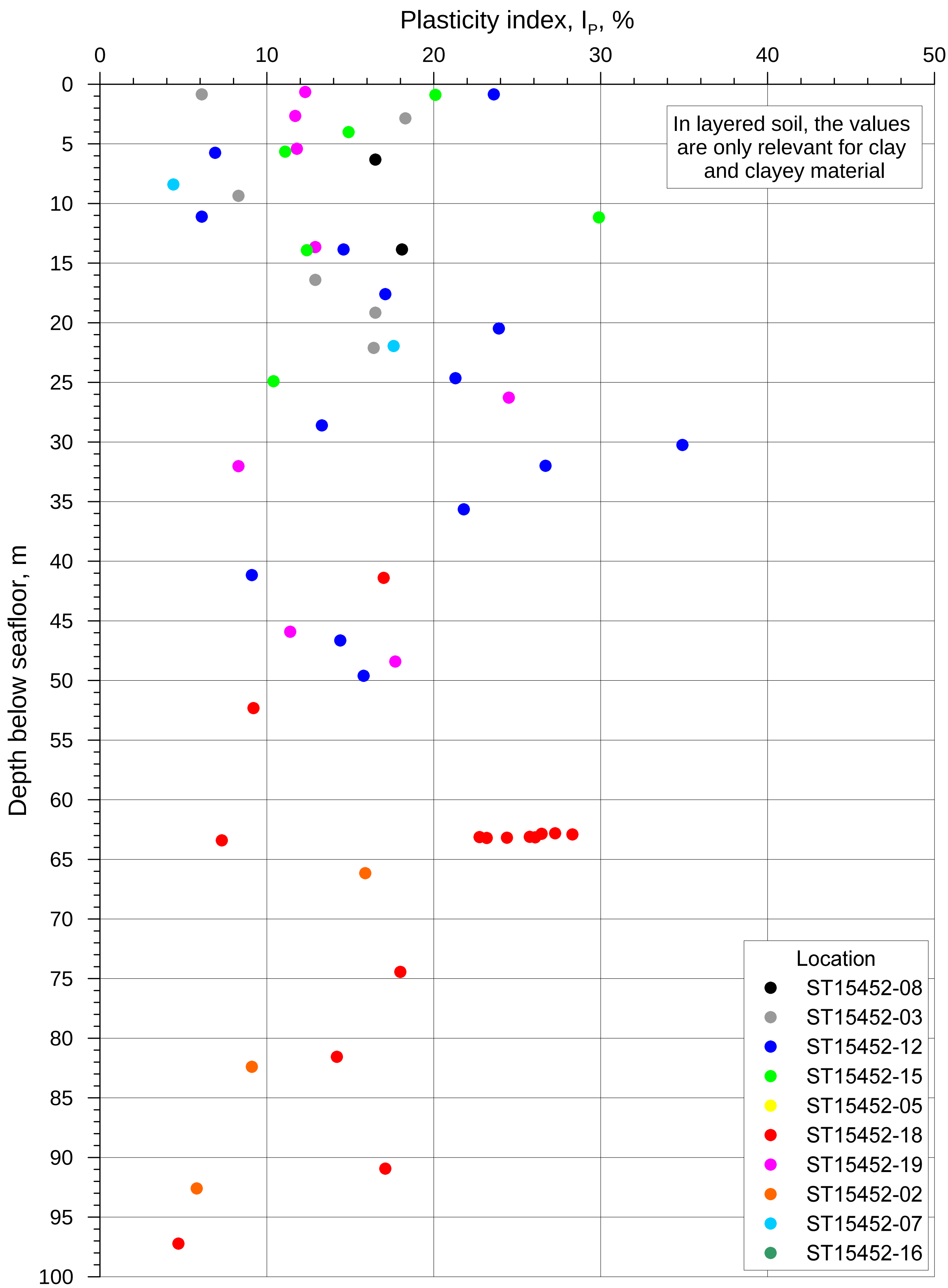

Date/Rev.: 2015-01-21/01

ST15452 Flemish Pass Geotechnical Investigation	Document No. 20140857-02-R
Plasticity index versus depth All locations	Figure No. F3.3.1
	Date 2016-04-03 / Drawn by VBS

P:\2014\08\20140857\Leveransedokumenter\Rapport\20140857-02-R Data interpretation and evaluation\Figures\Section F\Figure F_03_01, plasticity index versus depth.grf

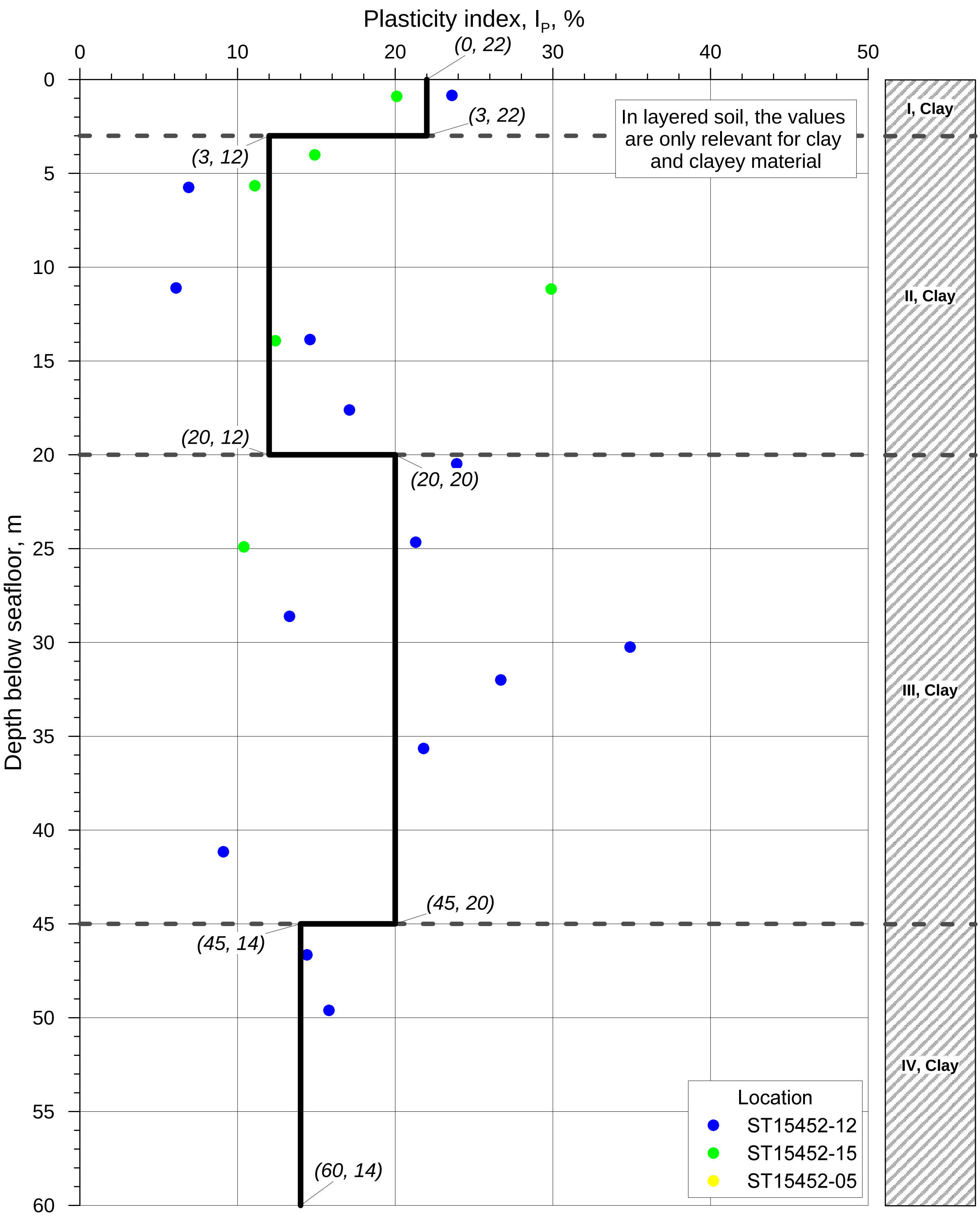

NOTE:
Representative profile based on engineering judgement.

Representative profile

Label: *(depth, value)*

Date/Rev.: 2015-01-21/01

P:\2014\08\20140857\Leveransedokumenter\Rapport\20140857-02-R Data interpretation and evaluation\Figures\Section F\Figure F_03_02, plasticity index versus depth-Fieldcentre.grf

ST15452 Flemish Pass Geotechnical Investigation	Document No. 20140857-02-R	
Plasticity index versus depth Field Centre	Figure No. F3.3.2	
	Date 2016-04-03	Drawn by VBS
	NGI	

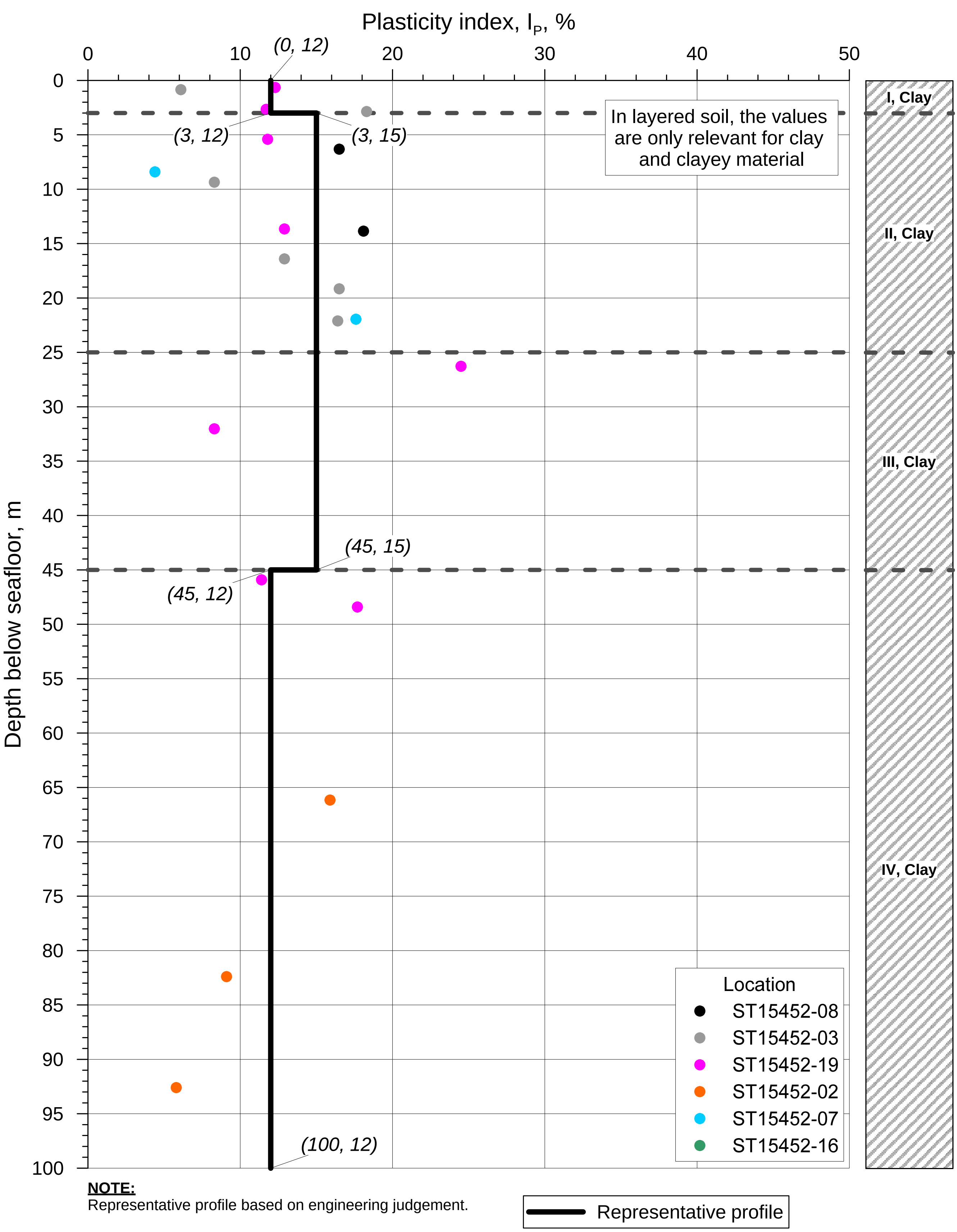

NOTE:
Representative profile based on engineering judgement.

Label: *(depth, value)*

Date/Rev.: 2015-01-21/01

ST15452 Flemish Pass Geotechnical Investigation	Document No. 20140857-02-R
Plasticity index versus depth West Slope	Figure No. F3.3.3
	Date 2016-04-03 / Drawn by VBS

NGI

P:\2014\08\20140857\Leveransedokumenter\Rapport\20140857-02-R Data interpretation and evaluation\Figures\Section F\Figure F_03_03_03, plasticity index versus depth-West.grf

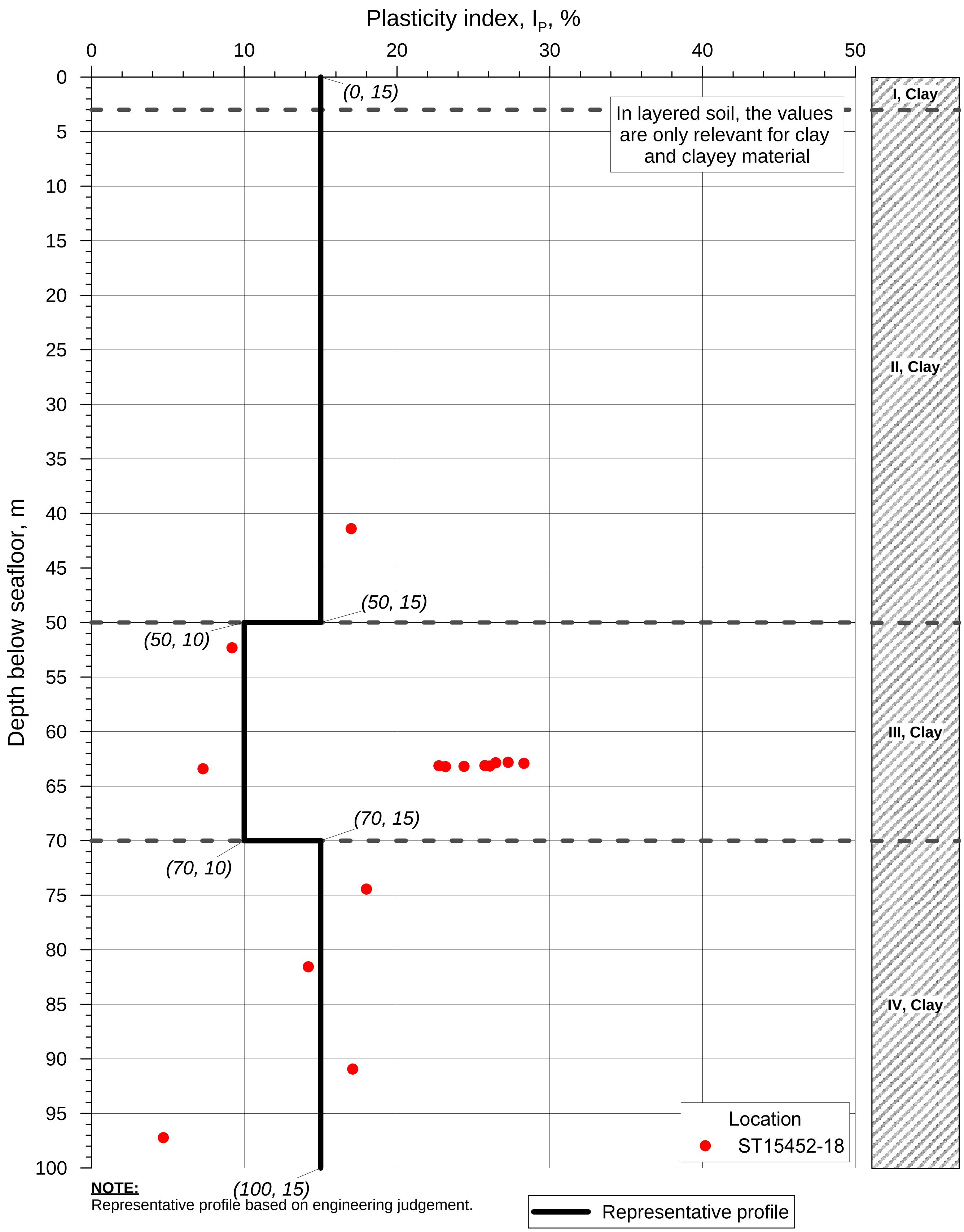

Label: *(depth, value)*

Date/Rev.: 2015-01-21/01

ST15452 Flemish Pass Geotechnical Investigation	Document No. 20140857-02-R	
Plasticity index versus depth East Slope	Figure No. F3.3.4	
	Date 2016-04-03	Drawn by VBS

P:\2014\08\20140857\Leveransedokumenter\Rapport\20140857-02-R Data interpretation and evaluation\Figures\Section F\Figure F_03_03_04, plasticity index versus depth-East.grf

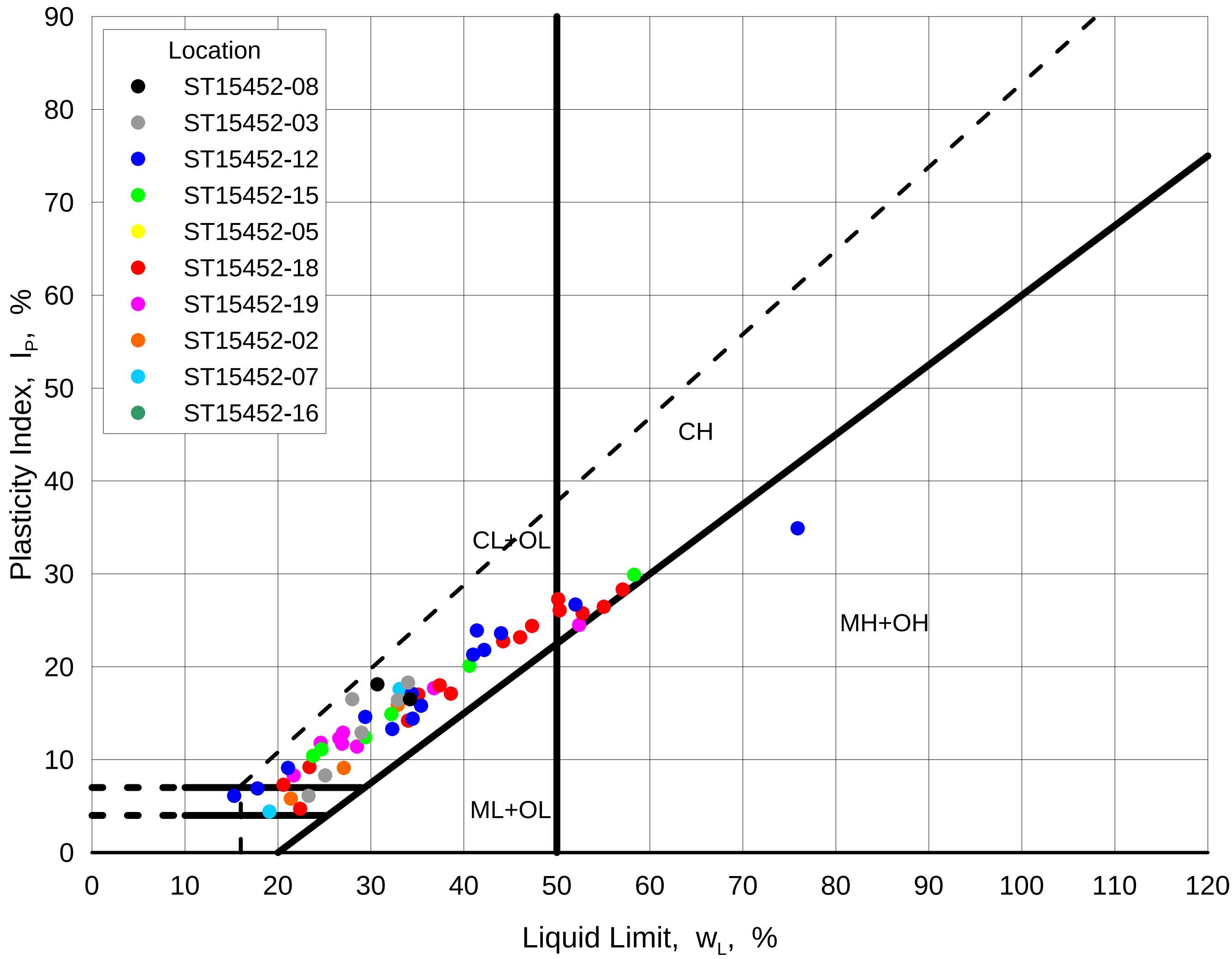

UNIFIED SOIL CLASSIFICATION

ML	Inorganic silts, very fine sands, rock flour, silty or clayey fine sands
MH	Inorganic silts, micaceous fine sands or silts, elastic silts
CL	Inorganic clays of low to medium plasticity, gravelly clays, sandy clays, silty clays, lean clays
CH	Inorganic clays of high plasticity, fat clays
OL	Organic silts and organic silty clays of low plasticity
OH	Organic clays of medium to high plasticity
PT	Peat, muck and other highly organic soils

Date/Rev.: 2015-01-21/01

ST15452 Flemish Pass Geotechnical Investigation

Plasticity Chart. Unified soil classification (from ASTM D2487).
All locations

Document No.	20140857-02-R
Figure No.	F3.3.5
Date	2016-04-03
Drawn by	VBS

P:\2014\08\20140857\Leveransedokumenter\Rapport\20140857-02-R Data interpretation and evaluation\Figures\Section F\Figure F_03_03_05, plasticity chart.grf

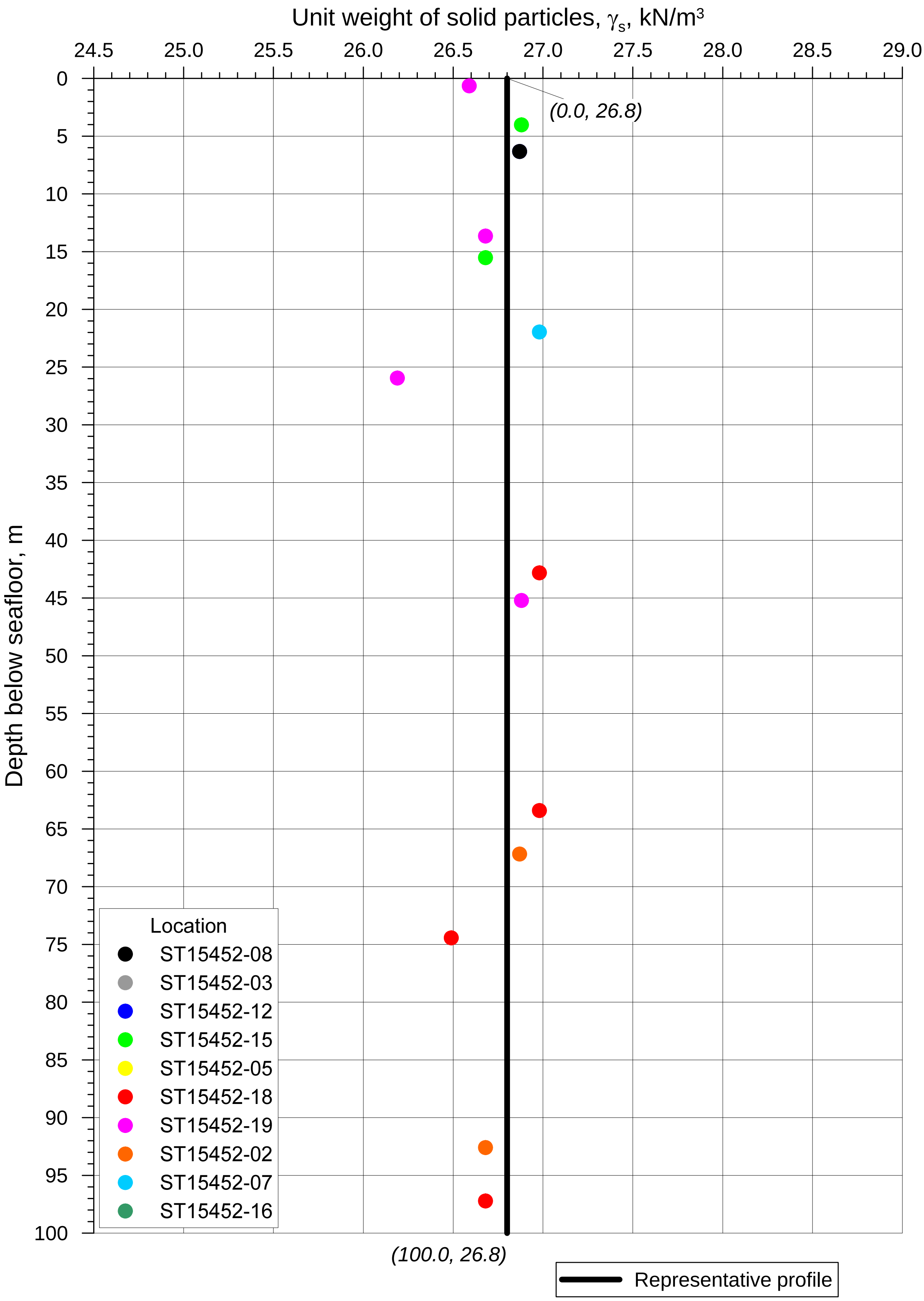

Label: *(depth, value)*

Date/Rev.: 2015-01-21/01

ST15452 Flemish Pass Geotechnical Investigation

Unit weight of solid particles versus depth
All locations

Document No. 20140857-02-R	
Figure No. F3.4.1	
Date 2016-04-03	Drawn by VBS

P:\2014\08\20140857\Leveransedokumenter\Rapport\20140857-02-R Data interpretation and evaluation\Figures\Section F\Figure F_03_04_01, unit weight of solid particles versus depth.grf

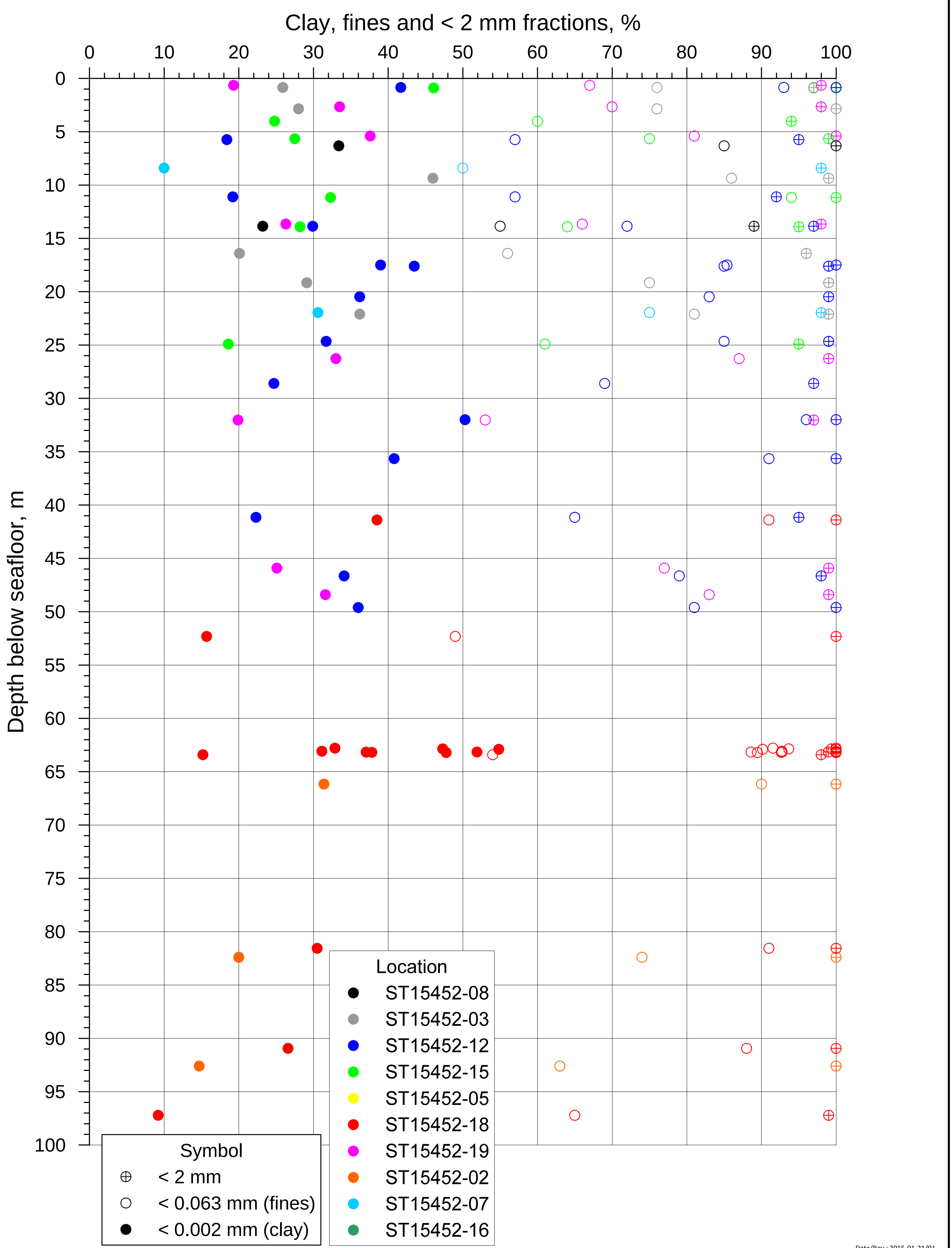

P:\2014\08\20140857\Leveransedokumenter\Rapport\20140857-02-R Data interpretation and evaluation\Figures\Section F\Figure F_03_05_01, grain size versus depth.grf

Date/Rev.: 2015-01-21/01

ST15452 Flemish Pass Geotechnical Investigation	Document No. 20140857-02-R
Clay, fines and <2 mm fractions versus depth All locations	Figure No. F3.5.1
	Date 2016-04-03 / Drawn by VBS

NGI

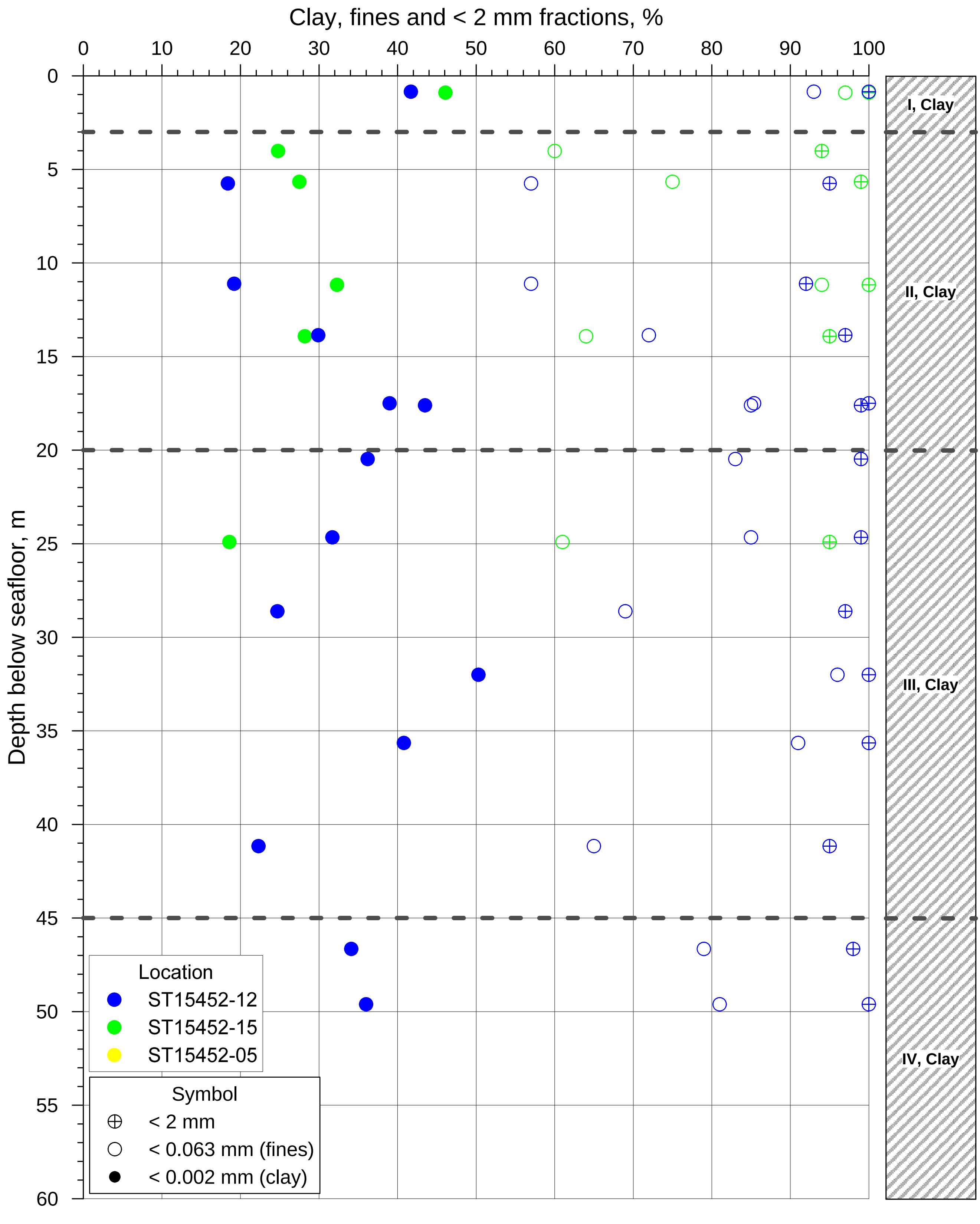

P:\2014\08\20140857\Leveransedokumenter\Rapport\20140857-02-R Data interpretation and evaluation\Figures\Section F\Figure F_03_05_02, grain size versus depth-Fieldcentre.grf

Date/Rev.: 2015-01-21/01

ST15452 Flemish Pass Geotechnical Investigation	Document No. 20140857-02-R
Clay, fines and <2 mm fractions versus depth Field Centre	Figure No. F3.5.2
	Date 2016-04-03 / Drawn by VBS
	NGI

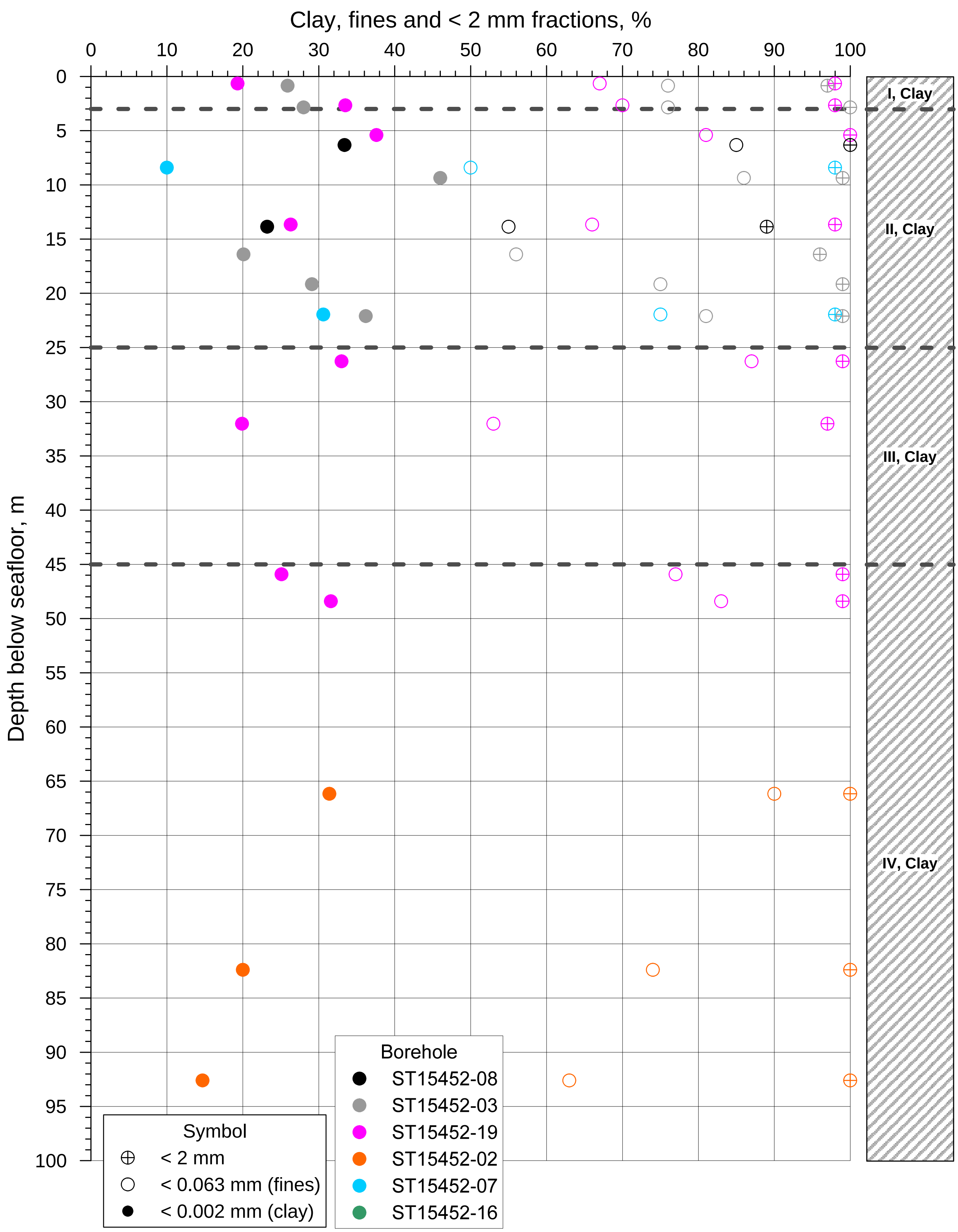

ST15452 Flemish Pass Geotechnical Investigation

Clay, fines and <2 mm fractions versus depth
West Slope

Document No. 20140857-02-R	
Figure No. F3.5.3	
Date 2016-04-03	Drawn by VBS

NGI

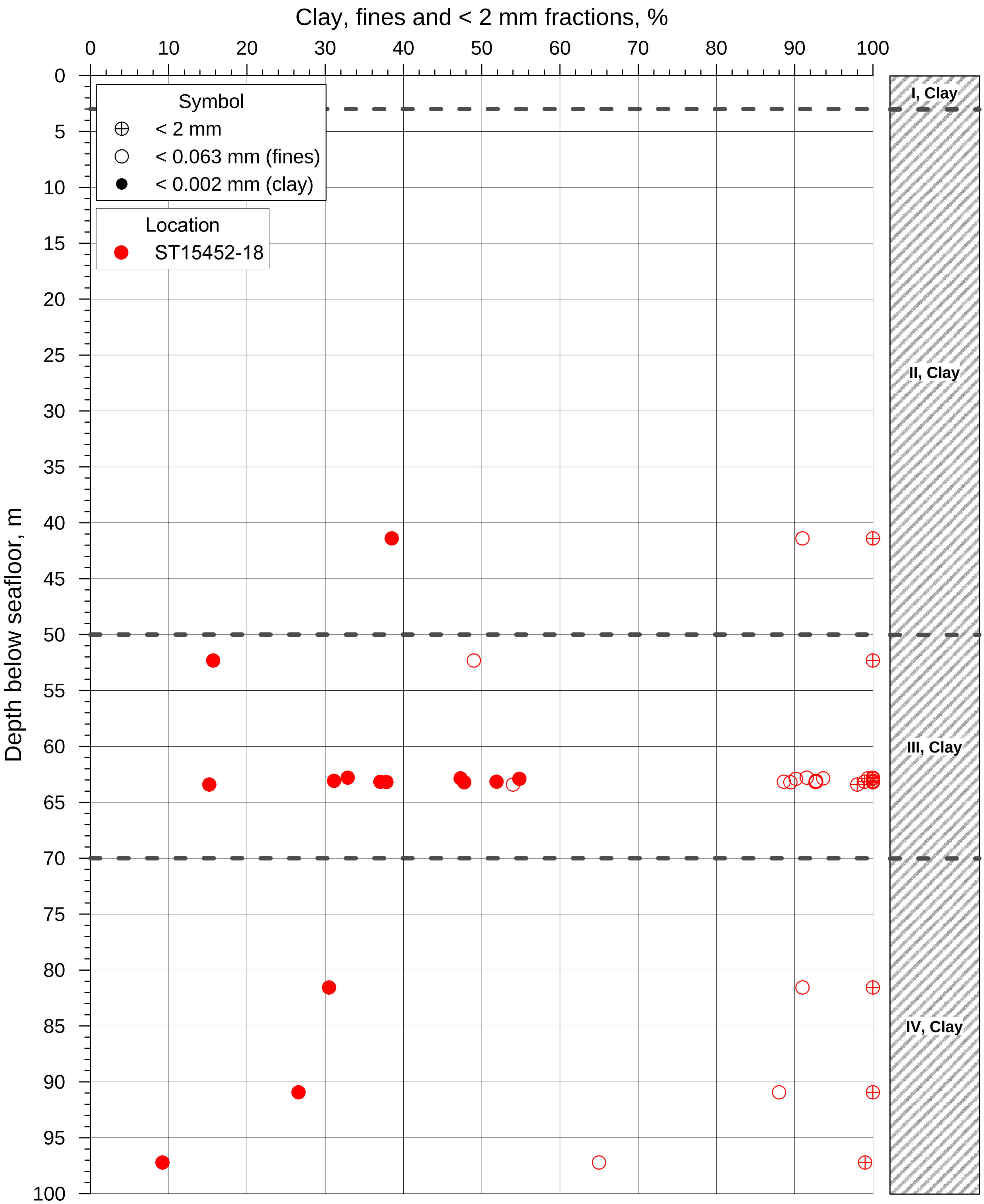

P:\2014\08\20140857\Leveransedokumenter\Rapport\20140857-02-R Data interpretation and evaluation\Figures\Section F\Figure F_03_05_04, grain size versus depth-East.grf

Date/Rev.: 2015-01-21/01

ST15452 Flemish Pass Geotechnical Investigation	Document No. 20140857-02-R
Clay, fines and <2 mm fractions versus depth East Slope	Figure No. F3.5.4
	Date 2016-04-03 / Drawn by VBS

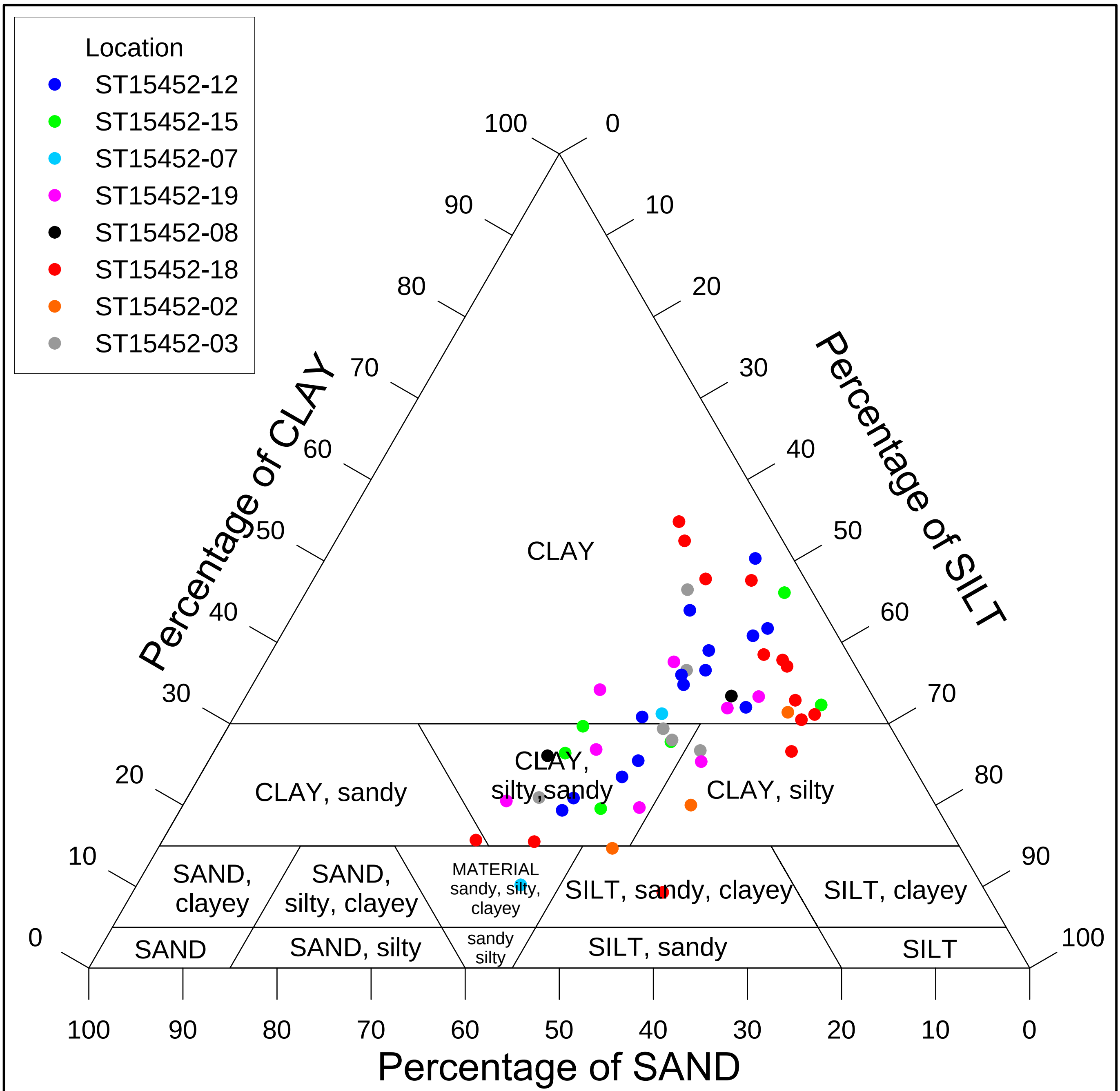

Classification according to NGF (2011)

Date/Rev.: 2015-01-21/01

ST15452 Flemish Pass Geotechnical Investigation	Document No. 20140857-02-R	
Soil classification triangle All locations	Figure No. F3.5.5	
	Date 2016-04-04	Drawn by VBS

NGI

P:\2014\08\20140857\Leveransedokumenter\Rapport\20140857-02-R Data interpretation and evaluation\Figures\Section F\Figure F_03_05_05 Classification Triangle.grf

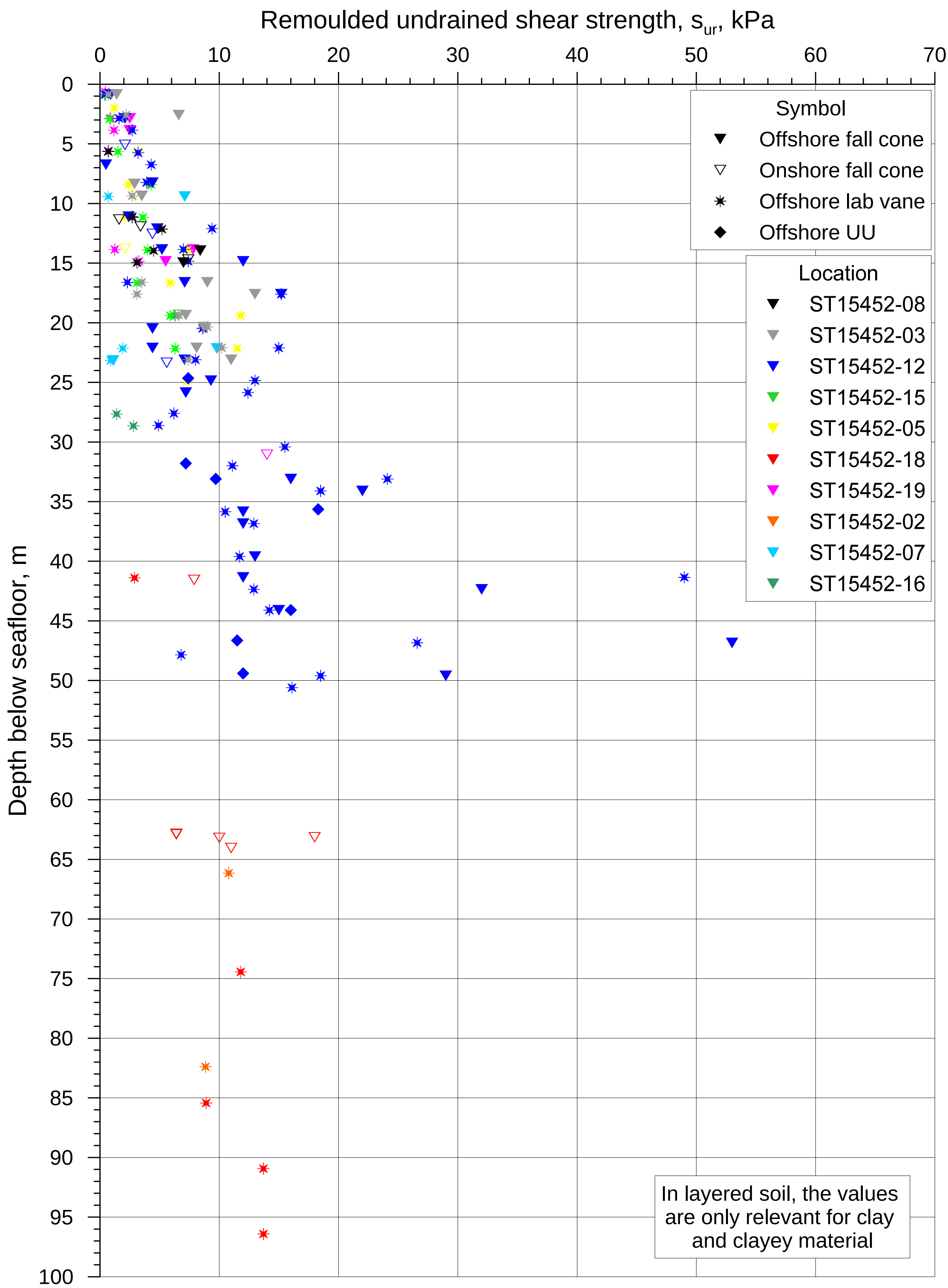

Date/Rev.: 2015-01-21/01

P:\2014\08\20140857\Leveransedokumenter\Rapport\20140857-02-R Data interpretation and evaluation\Figures\Section F\Figure F_03_06_01, su_rem versus depth.grf

ST15452 Flemish Pass Geotechnical Investigation	Document No. 20140857-02-R	
Remoulded undrained shear strength versus depth All locations	Figure No. F3.6.1	
	Date 2016-04-03	Drawn by VBS
	NGI	

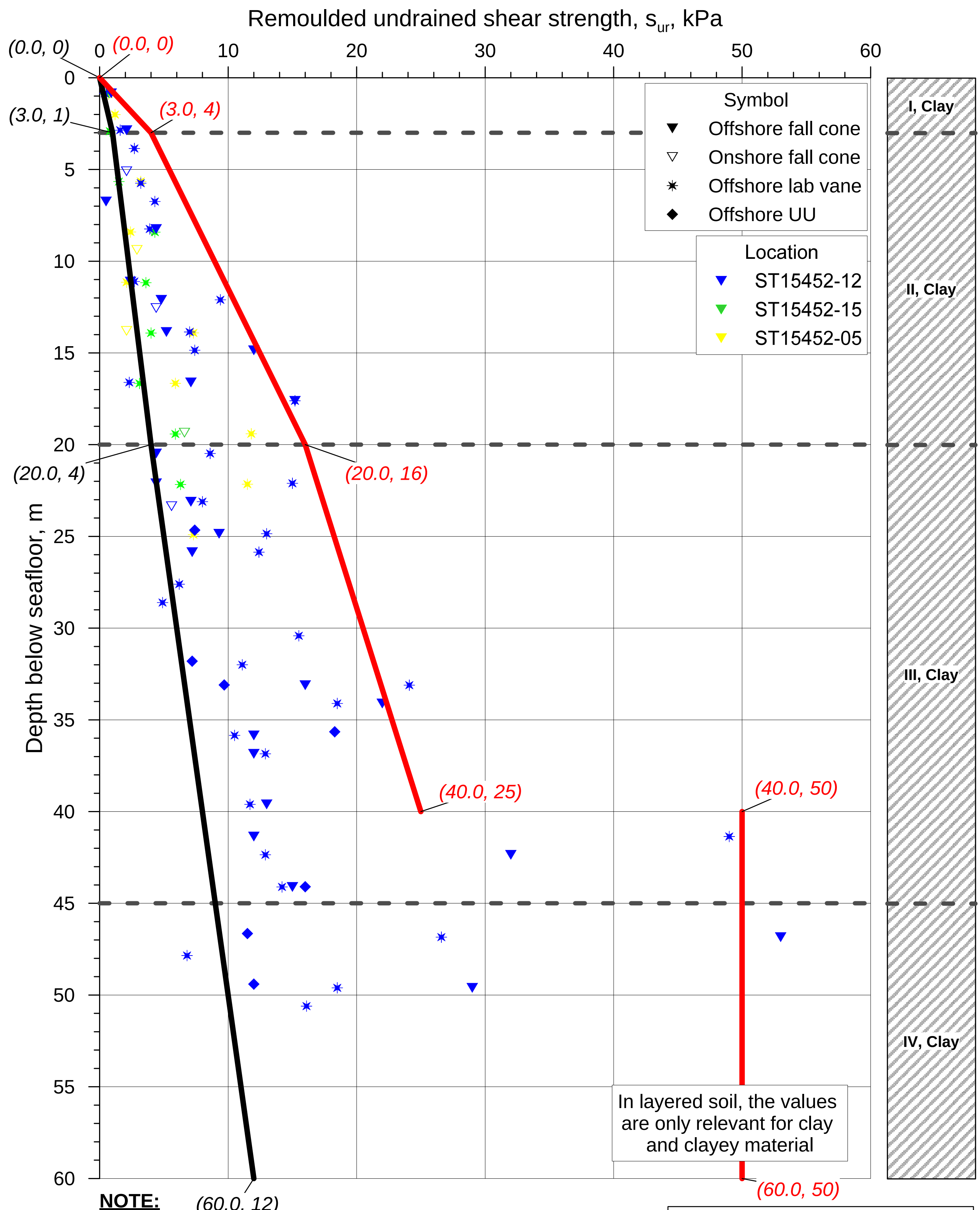

NOTE:
Representative profile based on engineering judgement

Label: *(depth, value)*

Date/Rev.: 2015-01-21/01

ST15452 Flemish Pass Geotechnical Investigation	Document No. 20140857-02-R
Remoulded undrained shear strength versus depth Field Centre	Figure No. F3.6.2
	Date 2016-04-03 / Drawn by VBS

P:\2014\08\20140857\Leveransedokumenter\Rapport\20140857-02-R Data interpretation and evaluation\Figures\Section F\Figure F_03_06_02, su_rem versus depth-Fieldcentre.grf

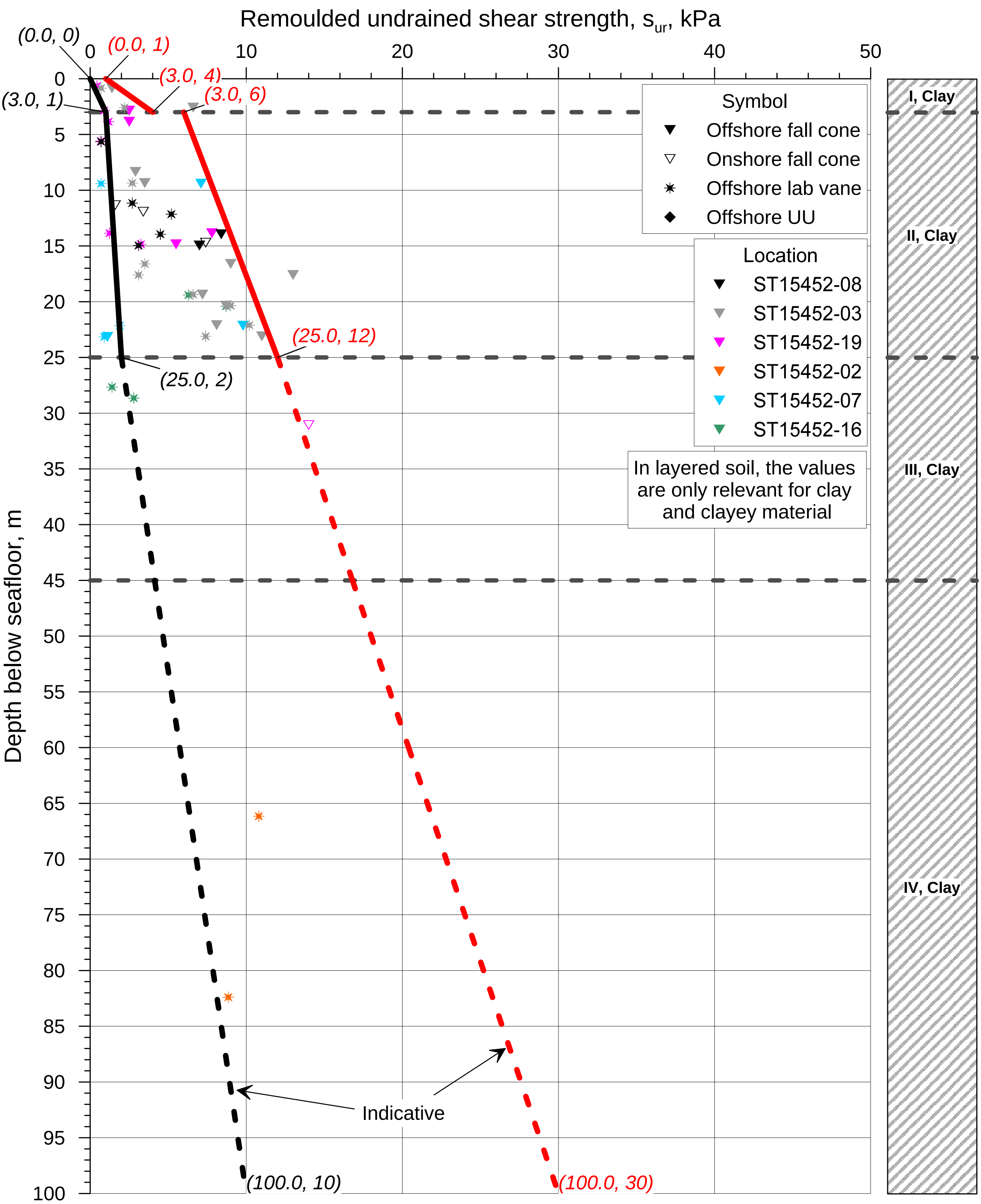

NOTE:
Representative profile based on engineering judgement

Representative high profile
Representative low profile

Label: *(depth, value)*

Date/Rev.: 2015-01-21/01

ST15452 Flemish Pass Geotechnical Investigation	Document No. 20140857-02-R	
Remoulded undrained shear strength versus depth West Slope	Figure No. F3.6.3	
	Date 2016-05-30	Drawn by VBS
	NGI	

P:\2014\08\20140857\Leveransedokumenter\Rapport\20140857-02-R Data interpretation and evaluation\Figures\Section F\Figure F_03_06_03, su_rem versus depth-West.grf

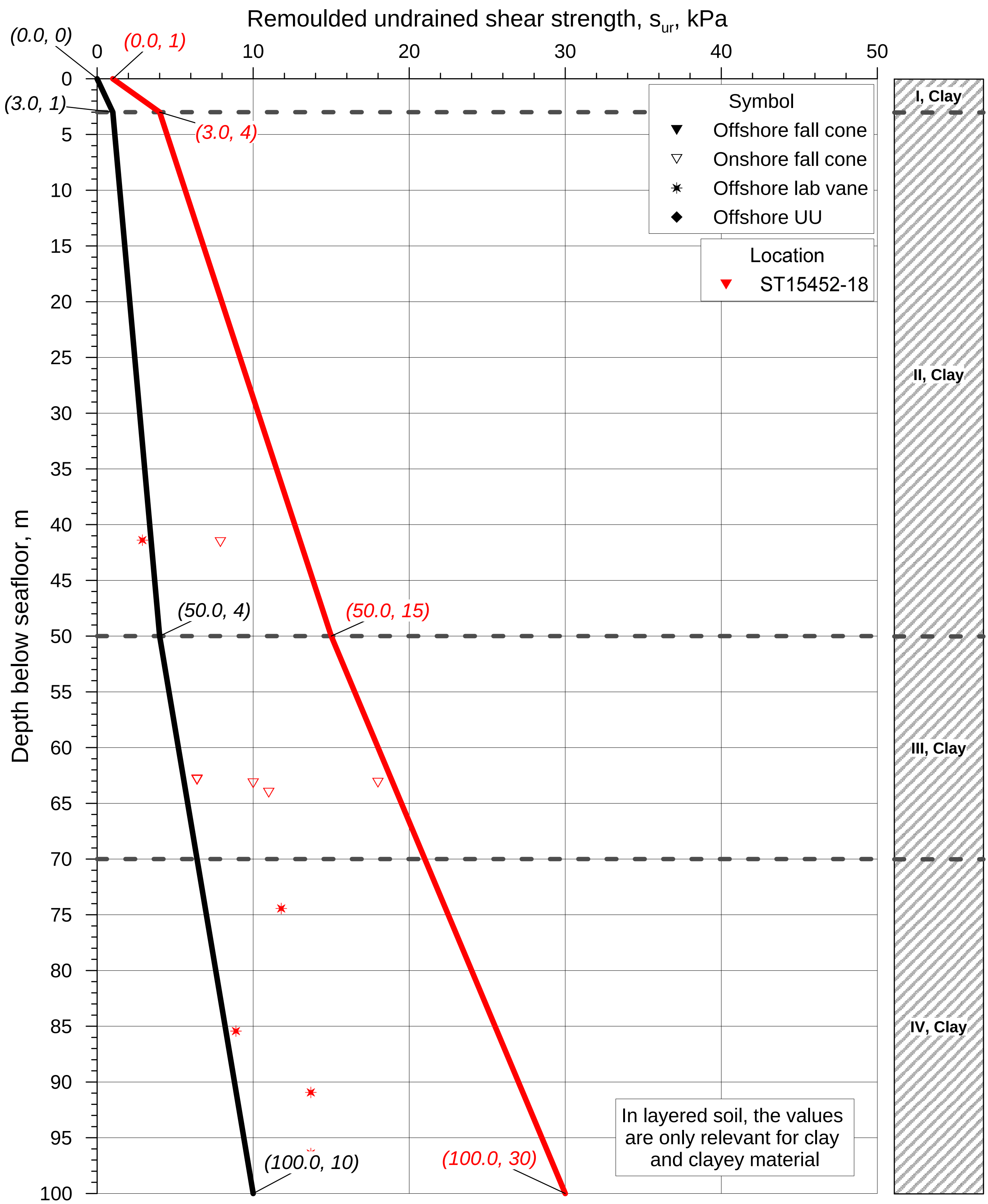

NOTE:
Representative profile based on engineering judgement

Label: *(depth, value)*

Date/Rev.: 2015-01-21/01

P:\2014\08\20140857\Leveransedokumenter\Rapport\20140857-02-R Data interpretation and evaluation\Figures\Section F\Figure F_03_06_04, su_rem versus depth-East.grf

ST15452 Flemish Pass Geotechnical Investigation	Document No. 20140857-02-R
Remoulded undrained shear strength versus depth East Slope	Figure No. F3.6.4
	Date 2016-04-03 / Drawn by VBS
	NGI

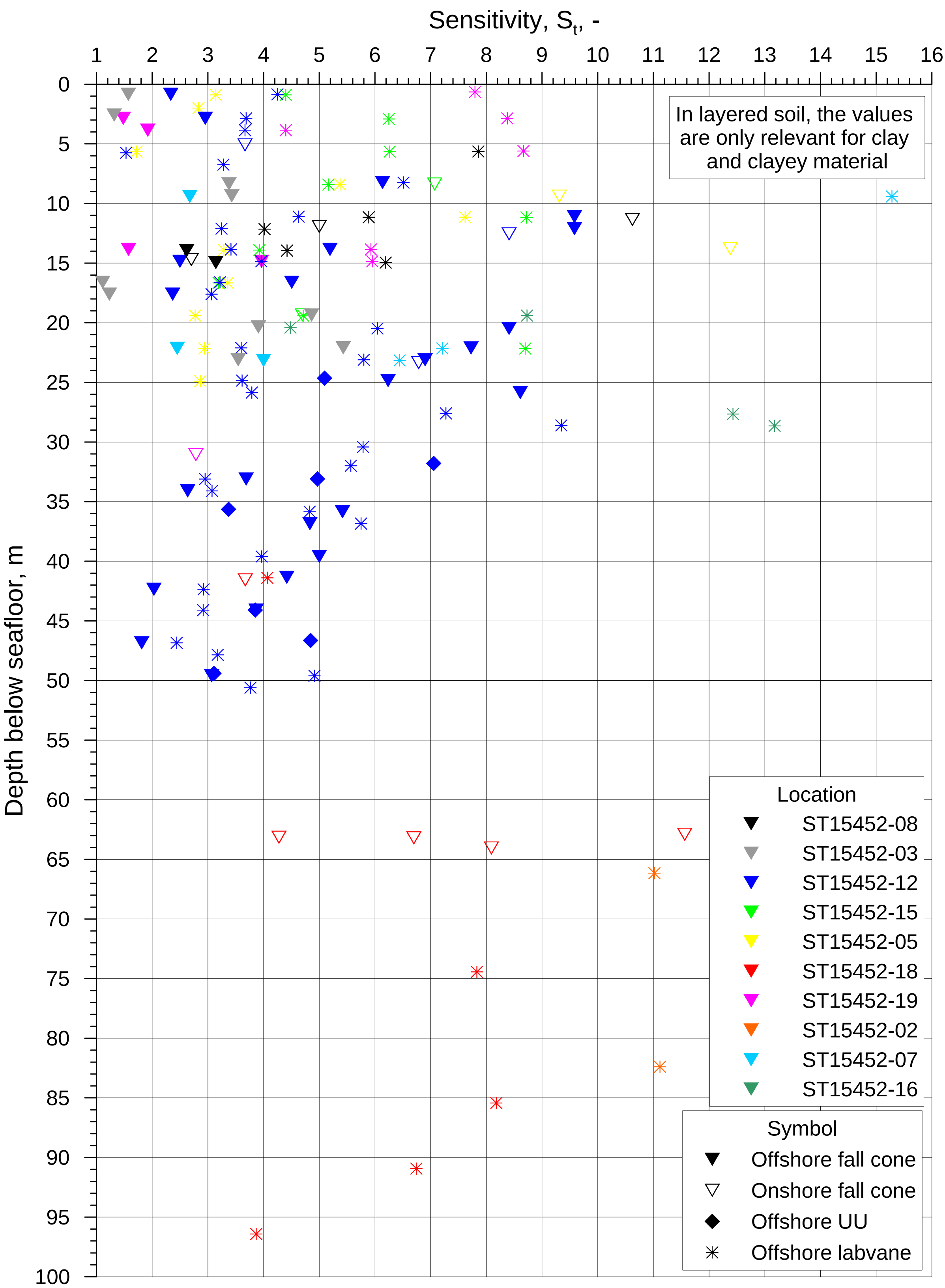

P:\2014\08\20140857\Leveransedokumenter\Rapport\20140857-02-R Data interpretation and evaluation\Figures\Section F\Figure F_03_07_01, sensitivity versus depth.grf

Date/Rev.: 2015-01-21/01

ST15452 Flemish Pass Geotechnical Investigation	Document No. 20140857-02-R
Sensitivity versus depth All locations	Figure No. F3.7.1
	Date 2016-04-03 / Drawn by VBS
	NGI

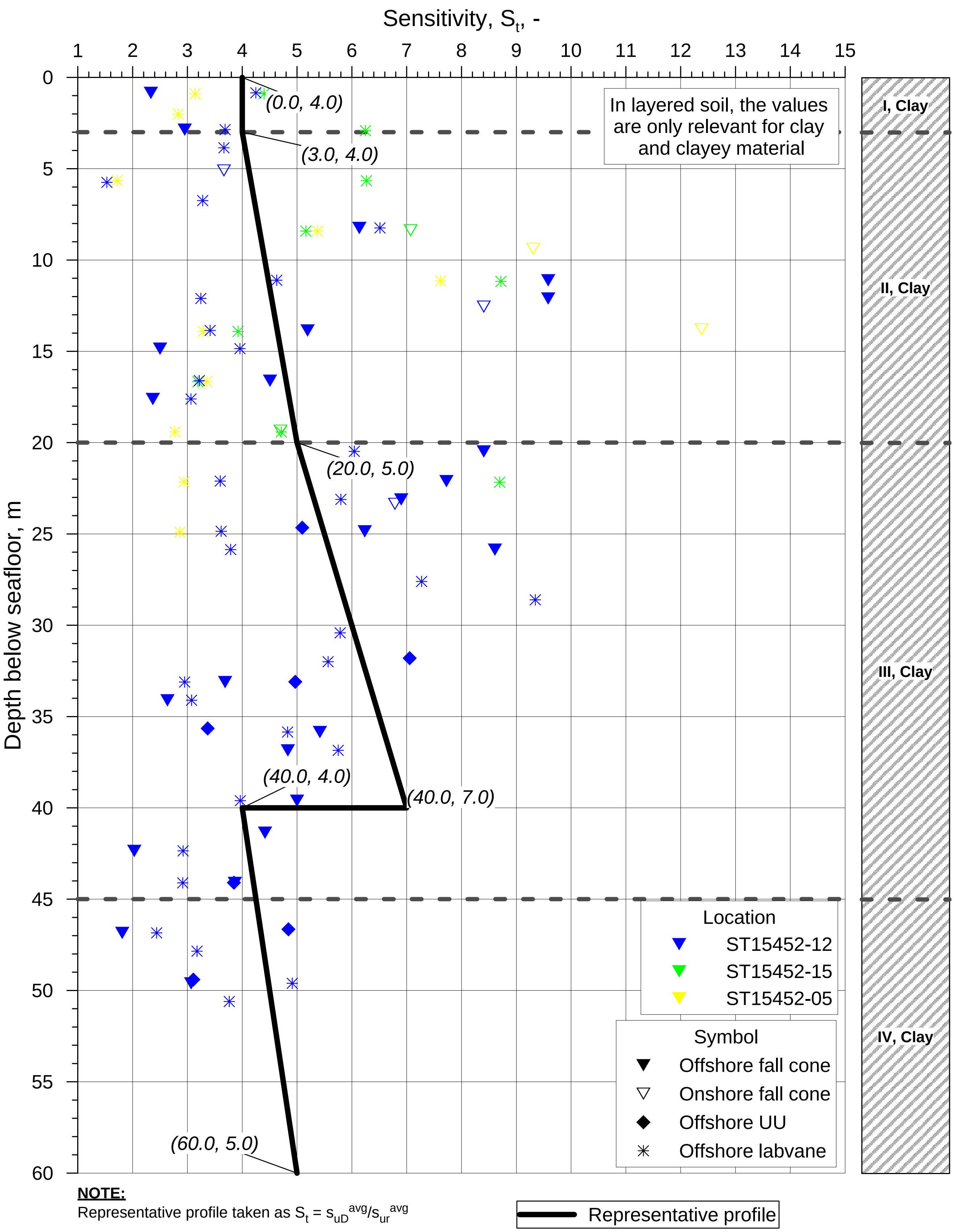

NOTE:
Representative profile taken as $S_t = s_{uD}^{avg}/s_{ur}^{avg}$

Label: *(depth, value)*

Date/Rev.: 2015-01-21/01

P:\2014\08\20140857\Leveransedokumenter\Rapport\20140857-02-R Data interpretation and evaluation\Figures\Section F\Figure F_03_07_02, sensitivity versus depth-Fieldcentre.grf

ST15452 Flemish Pass Geotechnical Investigation	Document No. 20140857-02-R	
Sensitivity versus depth Field Centre	Figure No. F3.7.2	
	Date 2016-04-04	Drawn by VBS
	NGI	

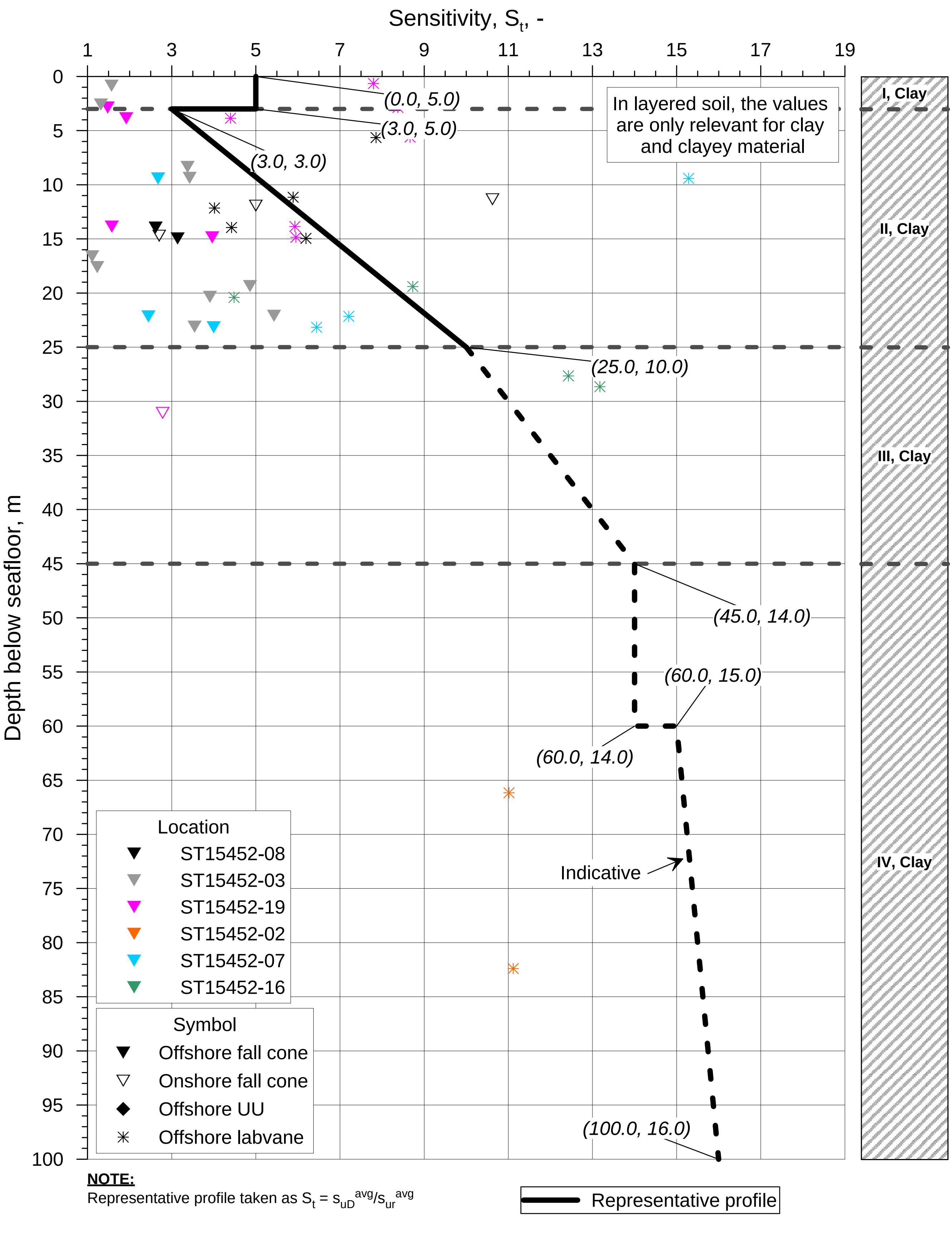

P:\2014\08\20140857\Leveransedokumenter\Rapport\20140857-02-R Data interpretation and evaluation\Figures\Section F\Figure F_03_07_03, sensitivity versus depth-West.grf

Date/Rev.: 2015-01-21/01

ST15452 Flemish Pass Geotechnical Investigation	Document No. 20140857-02-R	
Sensitivity versus depth West Slope	Figure No. F3.7.3	
	Date 2016-05-30	Drawn by VBS

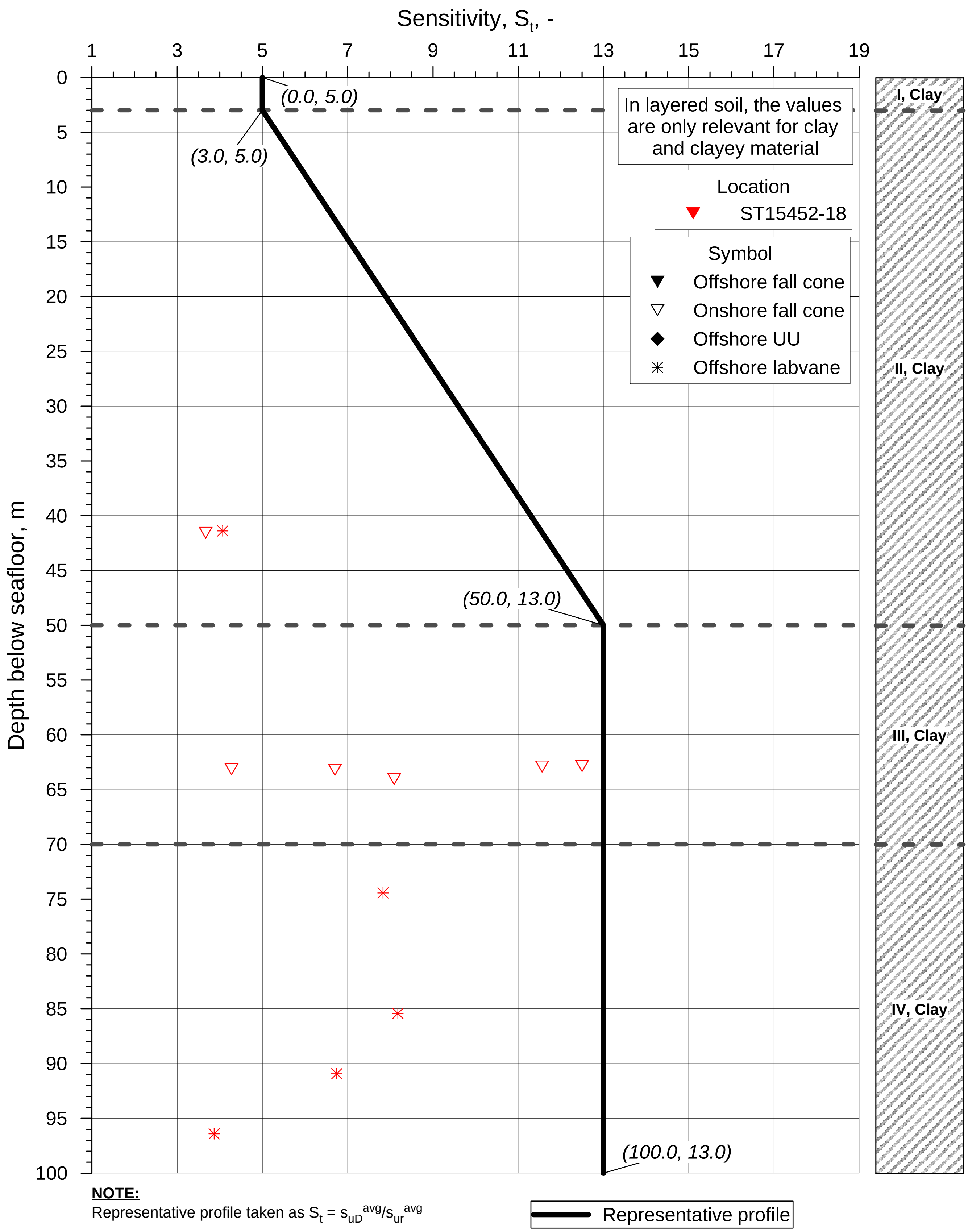

NOTE:
Representative profile taken as $S_t = s_{uD}^{avg}/s_{ur}^{avg}$

Representative profile

Label: *(depth, value)*

Date/Rev.: 2015-01-21/01

P:\2014\08\20140857\Leveransedokumenter\Rapport\20140857-02-R Data interpretation and evaluation\Figures\Section F\Figure F_03_07_04, sensitivity versus depth-East.grf

ST15452 Flemish Pass Geotechnical Investigation	Document No. 20140857-02-R
Sensitivity versus depth East Slope	Figure No. F3.7.4
	Date 2016-04-04 / Drawn by VBS
	NGI

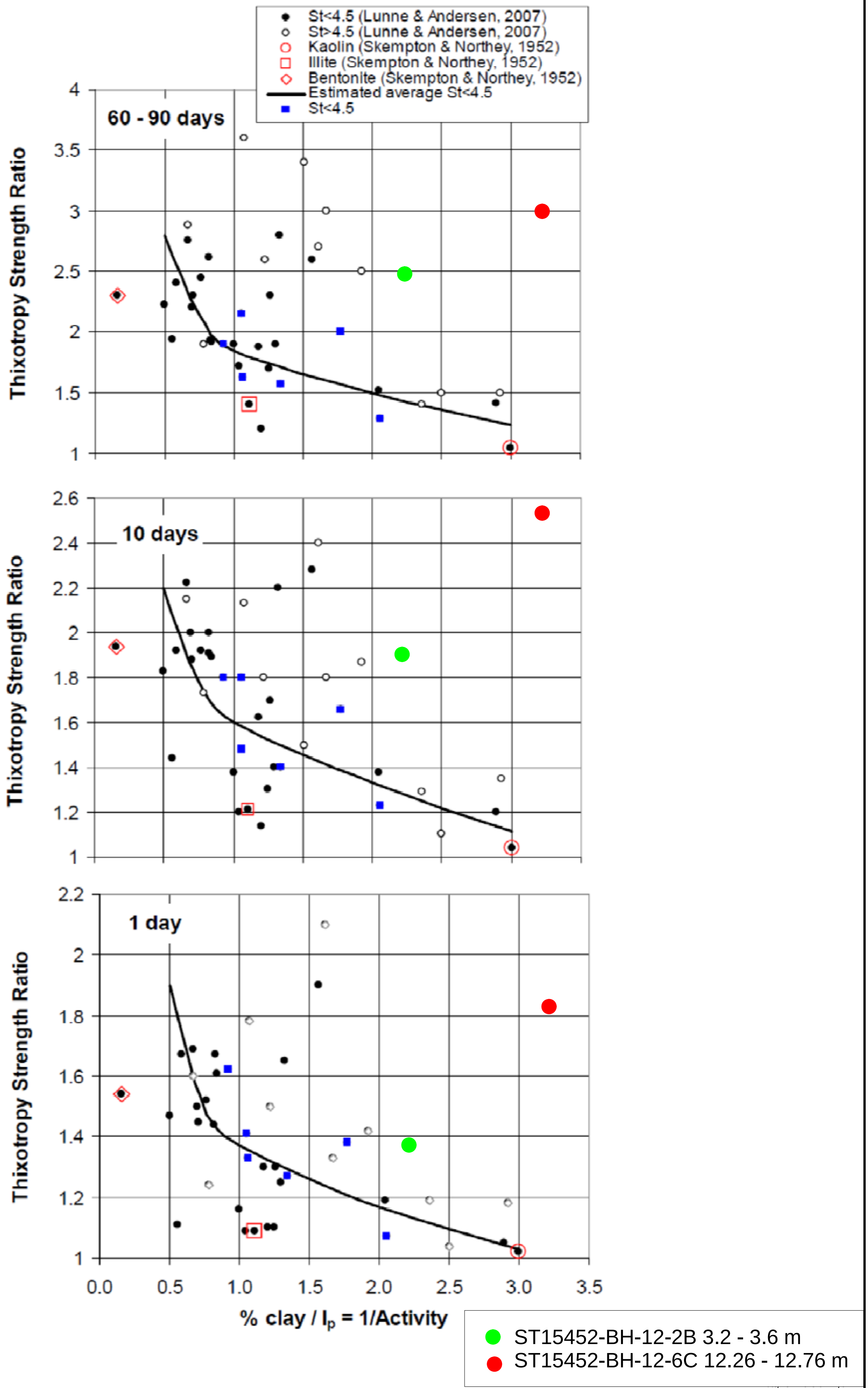

P:\2014\08\20140857\Leveransedokumenter\Rapport\20140857-02-R Data interpretation and evaluation\Figures\Section F\Figure F_03_08_01, thixotropy ratio.grf

ST15452 Flemish Pass Geotechnical Investigation	Document No. 20140857-02-R	
Thixotropy ratio measured at Flemish Pass Field Centre Compared to data from literature (Andersen et al. 2008)	Figure No. F3.8.1	
	Date 2016-04-03	Drawn by VBS

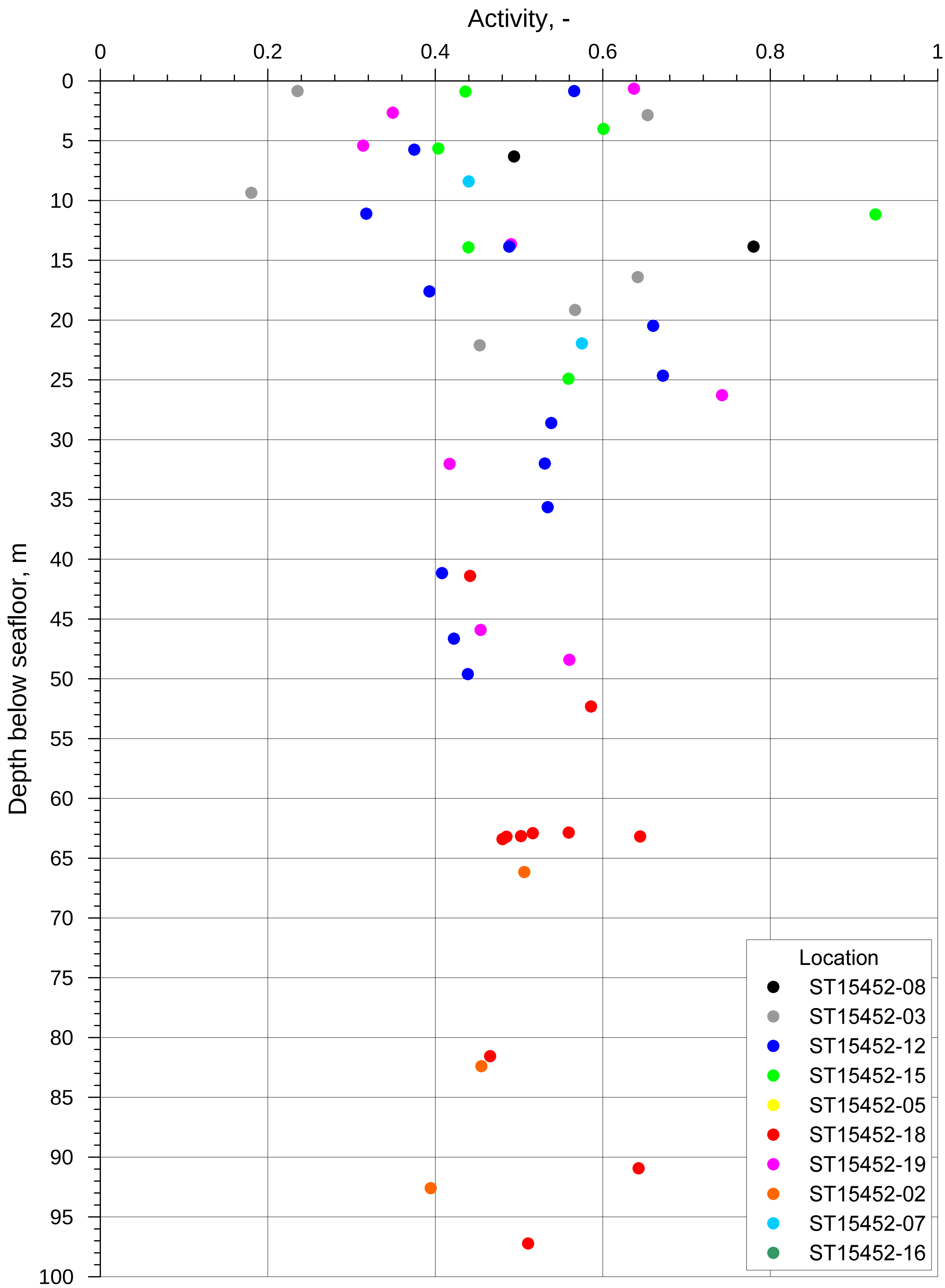

P:\2014\08\20140857\Leveransedokumenter\Rapport\20140857-02-R Data interpretation and evaluation\Figures\Section F\Figure F_03_09_01, activity versus depth.grf

Date/Rev.: 2015-01-21/01

ST15452 Flemish Pass Geotechnical Investigation	Document No. 20140857-02-R
Mineralogy All locations Activity defines as Ip/(% clay)	Figure No. F3.9.1
	Date 2016-04-03 / Drawn by VBS

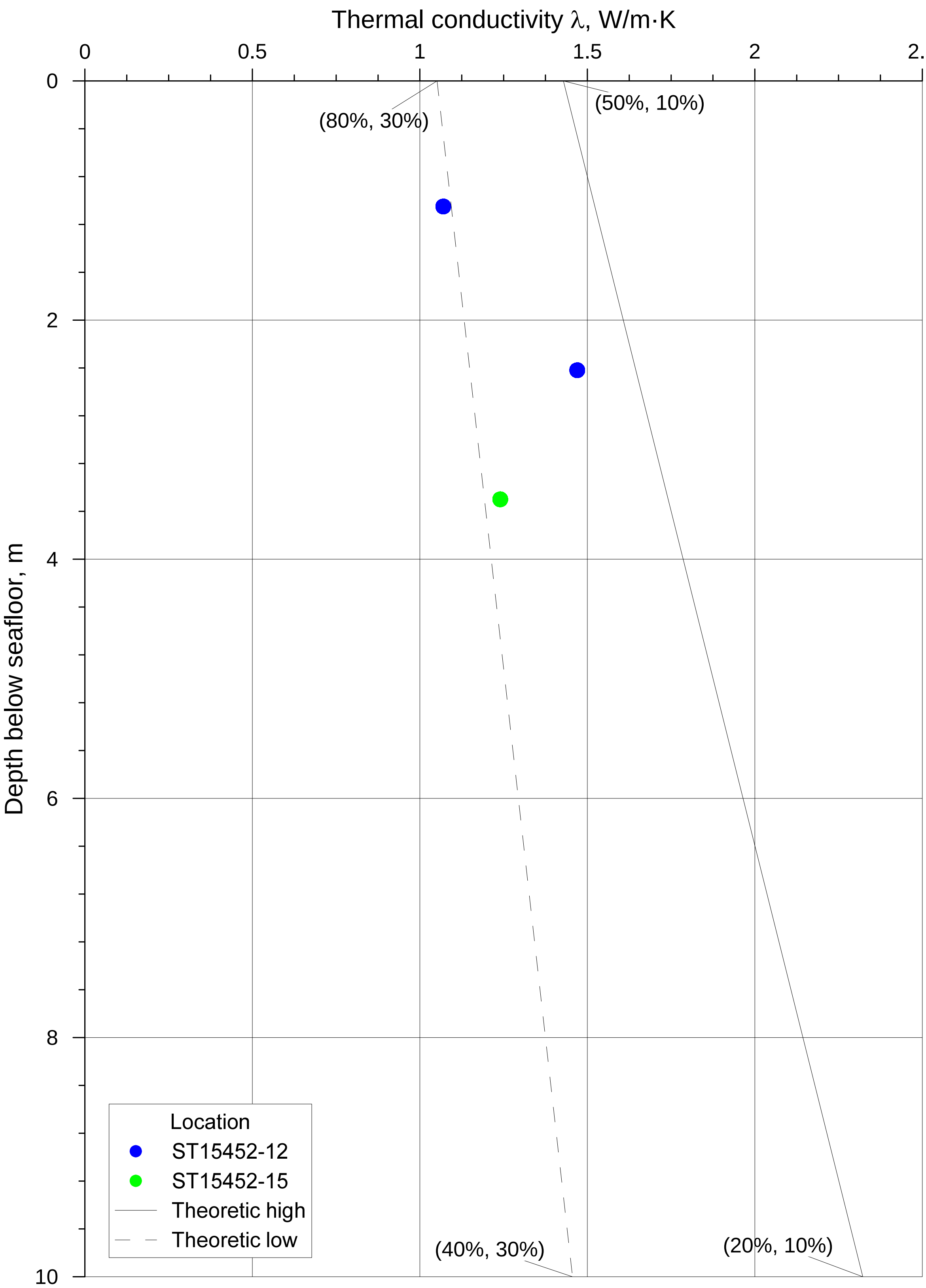

Theoretic calculation based on Johansen (1975)

Label: *(Assumed water content, assumed clay content)*

ST15452 Flemish Pass Geotechnical Investigation	Document No. 20140857-02-R
Thermal conductivity versus depth Field Centre	Figure No. F3.10.1
	Date 2016-04-04
	Drawn by VBS
	NGI

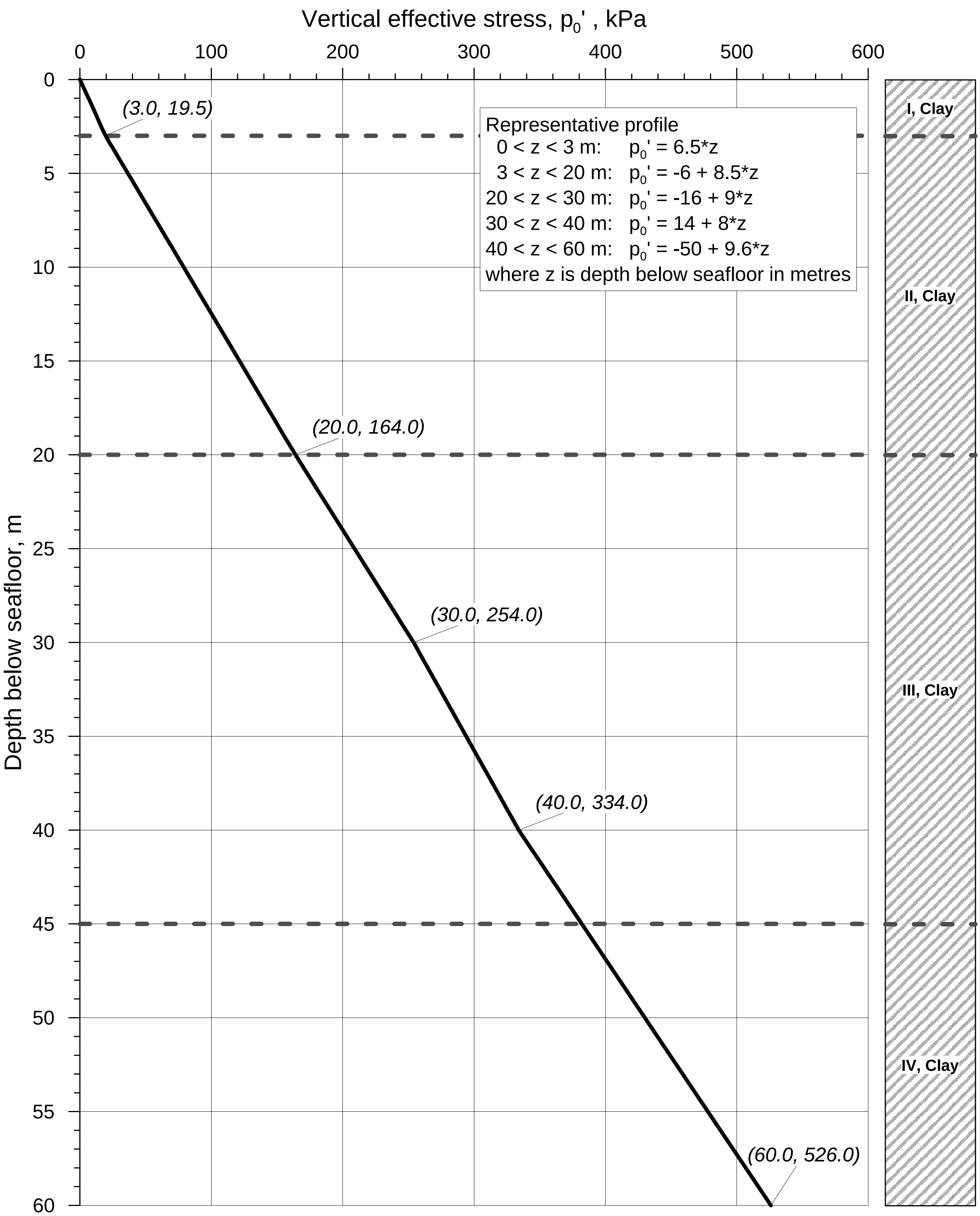

NOTE:
Representative profile based on
representative total unit weight profile

Label: *(depth, value)*

Date/Rev.: 2015-01-21/01

P:\2014\08\20140857\Leveransedokumenter\Rapport\20140857-02-R Data interpretation and evaluation\Figures\Section F\Figure F_04_01_01, p0 versus depth-Fieldcentre.grf

ST15452 Flemish Pass Geotechnical Investigation	Document No. 20140857-02-R
Vertical effective stress versus depth Field Centre	Figure No. F4.1.1
	Date 2016-04-03 / Drawn by VBS
	NGI

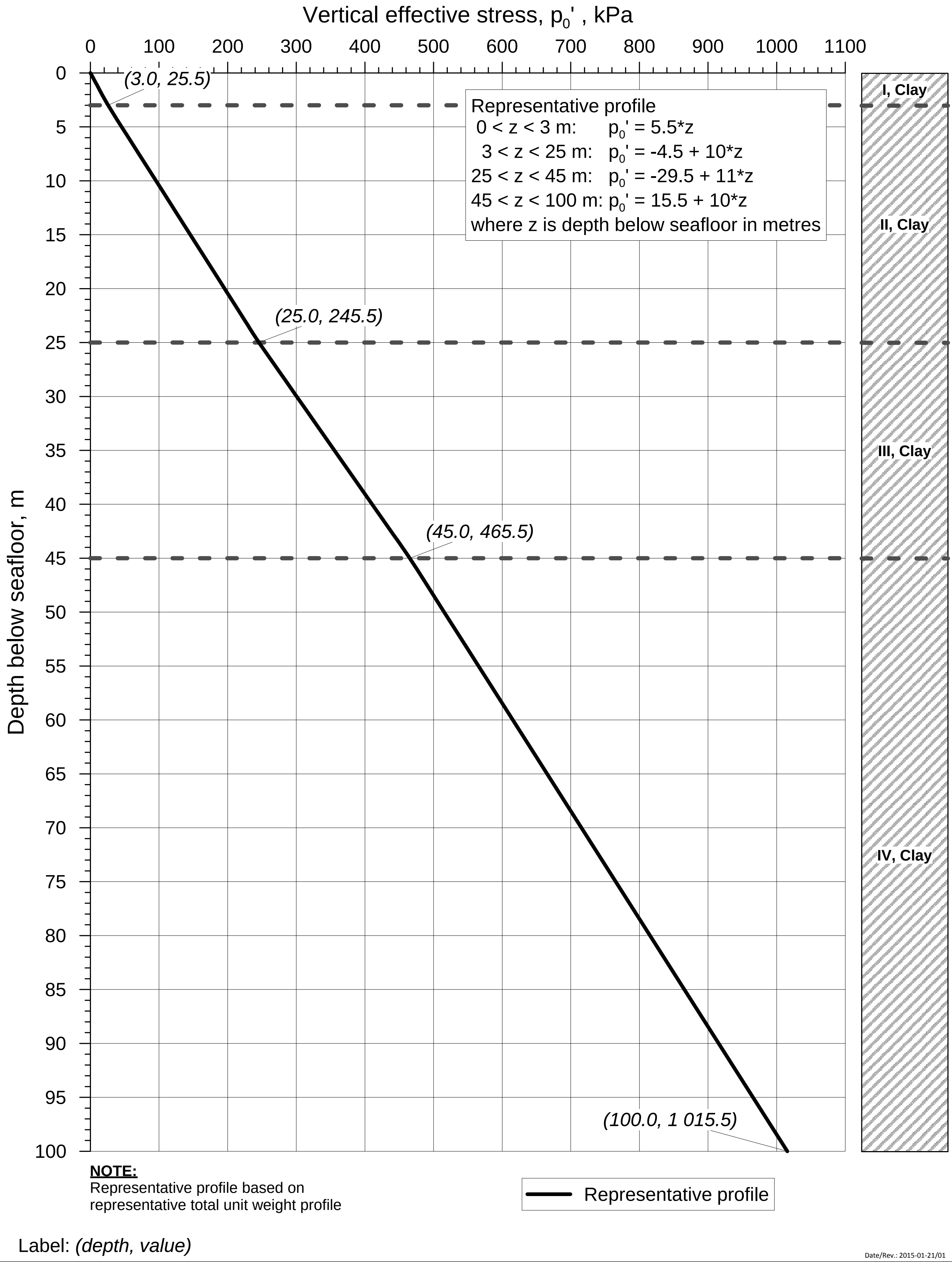

Date/Rev.: 2015-01-21/01

P:\2014\08\20140857\Leveransedokumenter\Rapport\20140857-02-R Data interpretation and evaluation\Figures\Section F\Figure F_04_01_02, p0 versus depth-West.grf

ST15452 Flemish Pass Geotechnical Investigation	Document No. 20140857-02-R
Vertical effective stress versus depth West Slope	Figure No. F4.1.2
	Date: 2016-04-03 / Drawn by: VBS

NGI

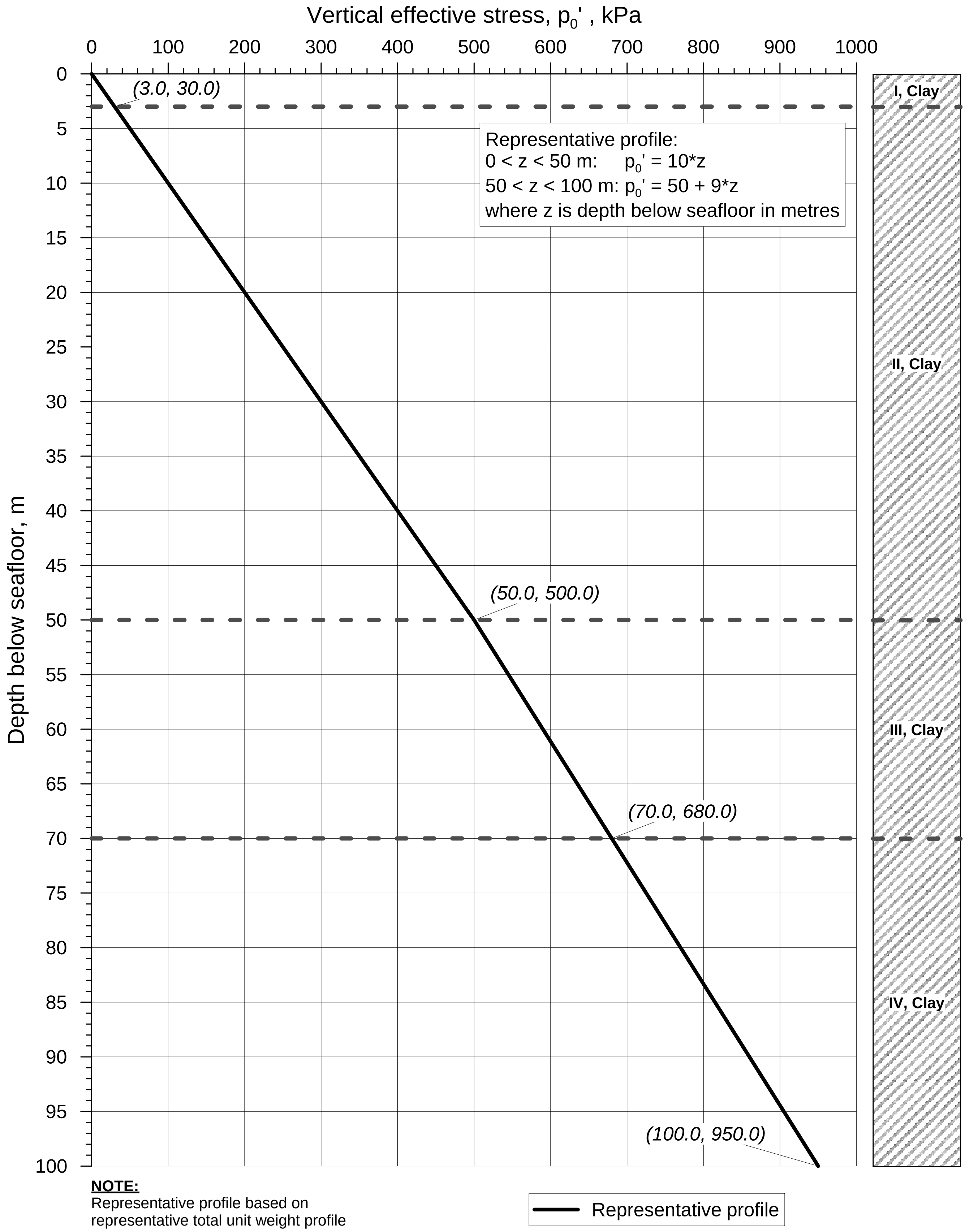

Label: *(depth, value)*

Date/Rev.: 2015-01-21/01

ST15452 Flemish Pass Geotechnical Investigation

Vertical effective stress versus depth
East Slope

Document No. 20140857-02-R	
Figure No. F4.1.3	
Date 2016-04-03	Drawn by VBS

NGI

P:\2014\08\20140857\Leveransedokumenter\Rapport\20140857-02-R Data interpretation and evaluation\Figures\Section F\Figure F_04_01_03, p0 versus depth-East.grf

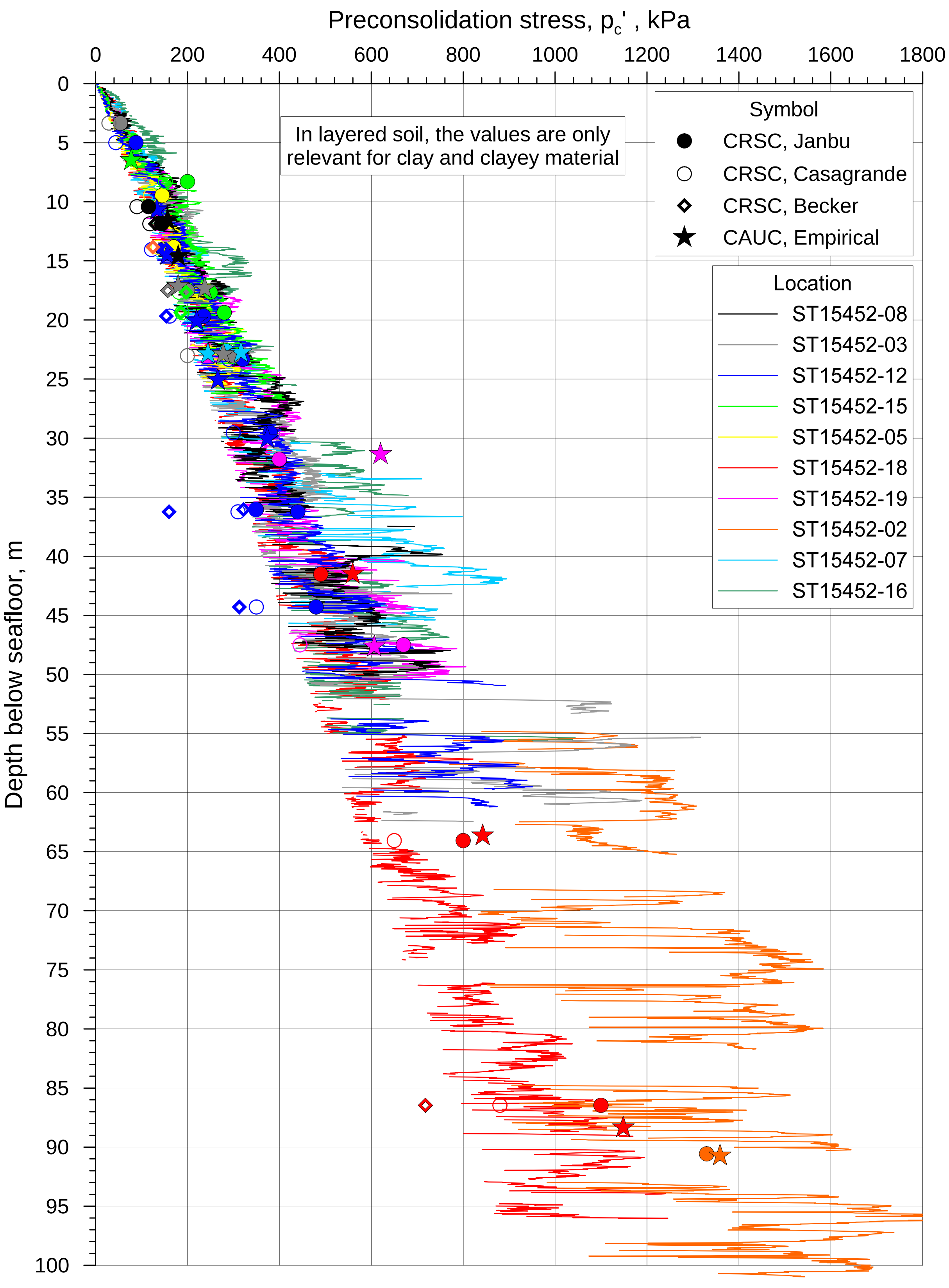

NOTE: p_c' in clay from CPTU based on Andresen et al. (1979)
$p_c'=p_0'xOCR(I_p;\ s_{uC}/p_0')$ using γ = 19 kN/m³, $N_{\Delta u}$ = 7.5 and I_p = 15%
Representative profile based on engineering judgement.

Date/Rev.: 2015-01-21/01

P:\2014\08\20140857\Leveransedokumenter\Rapport\20140857-02-R Data interpretation and evaluation\Figures\Section F\Figure F_04_02_01, pc versus depth.grf

ST15452 Flemish Pass Geotechnical Investigation	Document No. 20140857-02-R
Preconsolidation stress versus depth All locations	Figure No. F4.2.1
	Date 2016-05-30 — Drawn by SK

NGI

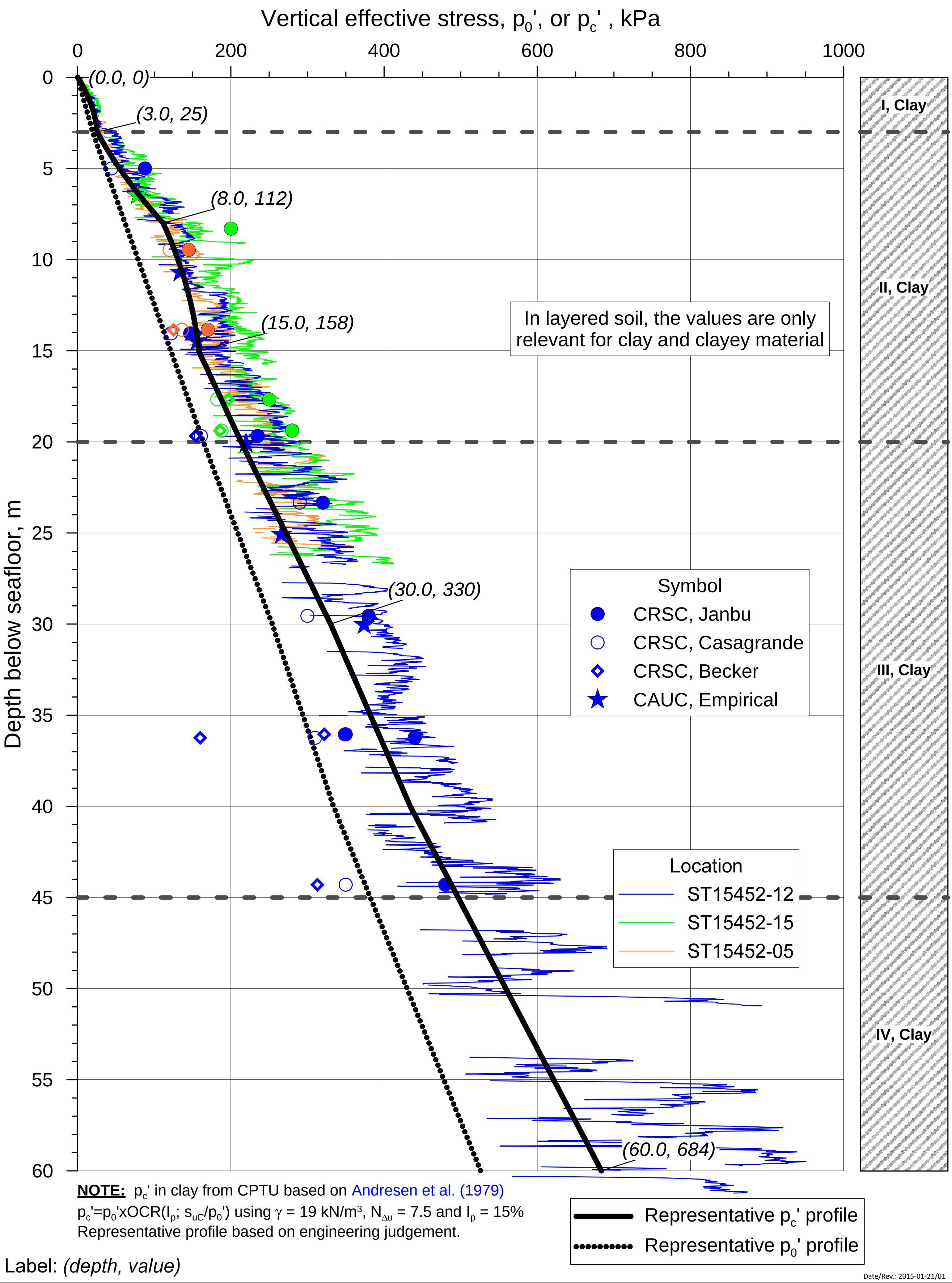

Date/Rev.: 2015-01-21/01

P:\2014\08\20140857\Leveransedokumenter\Rapport\20140857-02-R Data interpretation and evaluation\Figures\Section F\Figure F_04_02_02, pc' versus depth-Fieldcentre.grf

ST15452 Flemish Pass Geotechnical Investigation	Document No. 20140857-02-R
Preconsolidation stress versus depth Field Centre	Figure No. F4.2.2
	Date 2016-04-03 / Drawn by SK

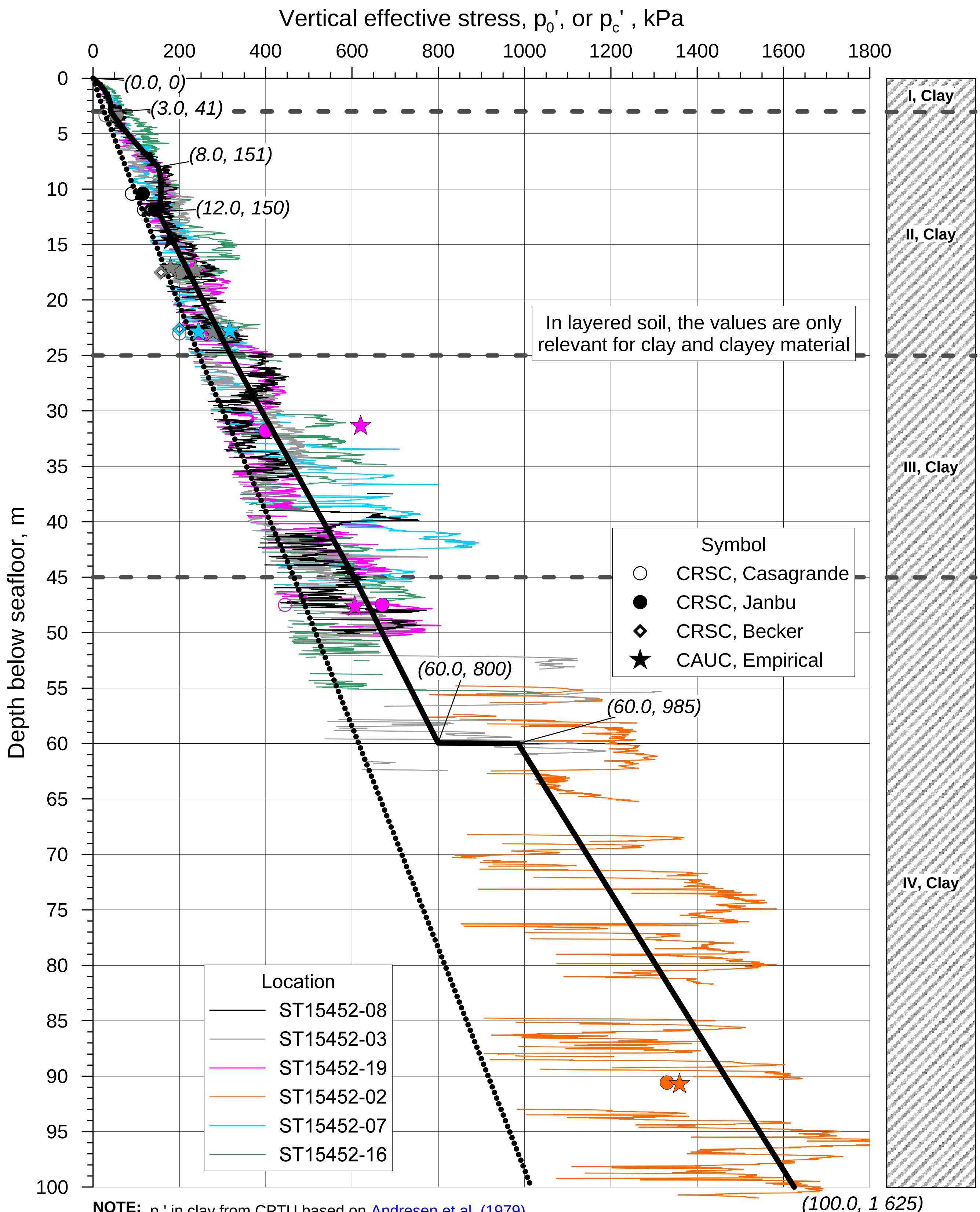

NOTE: p_c' in clay from CPTU based on Andresen et al. (1979)
$p_c' = p_0' \times OCR(I_p; s_{uC}/p_0')$ using γ = 19 kN/m³, $N_{\Delta u}$ = 7.5 and I_p = 15%
Representative profile based on engineering judgement.

Representative p_c' profile
Representative p_0' profile

Label: *(depth, value)*

Date/Rev.: 2015-01-21/01

ST15452 Flemish Pass Geotechnical Investigation

Preconsolidation stress versus depth
West Slope

Document No. 20140857-02-R	
Figure No. F4.2.3	
Date 2016-04-03	Drawn by SK

NGI

P:\2014\08\20140857\Leveransedokumenter\Rapport\20140857-02-R Data interpretation and evaluation\Figures\Section F\Figure F_04_02_03, pc versus depth-West.grf

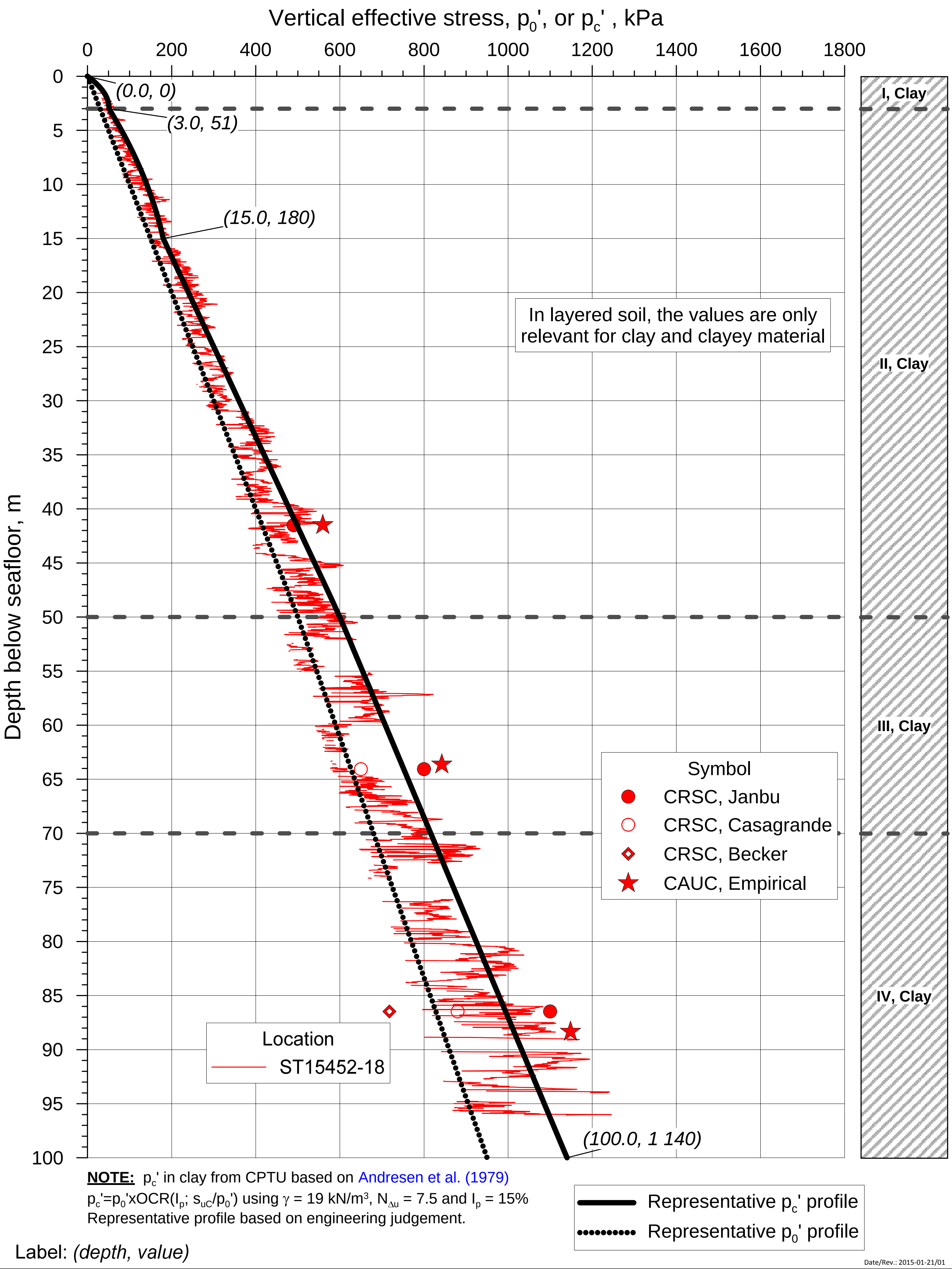

NOTE: p_c' in clay from CPTU based on Andresen et al. (1979)
$p_c'=p_0'\text{x}OCR(I_p;\ s_{uC}/p_0')$ using γ = 19 kN/m³, $N_{\Delta u}$ = 7.5 and I_p = 15%
Representative profile based on engineering judgement.

Representative p_c' profile
Representative p_0' profile

Label: *(depth, value)*

Date/Rev.: 2015-01-21/01

P:\2014\08\20140857\Leveranseddokumenter\Rapport\20140857-02-R Data interpretation and evaluation\Figures\Section F\Figure F_04_02_04, pc versus depth-East.grf

ST15452 Flemish Pass Geotechnical Investigation	Document No. 20140857-02-R	
Preconsolidation stress versus depth East Slope	Figure No. F4.2.4	
	Date 2016-04-03	Drawn by SK
	NGI	

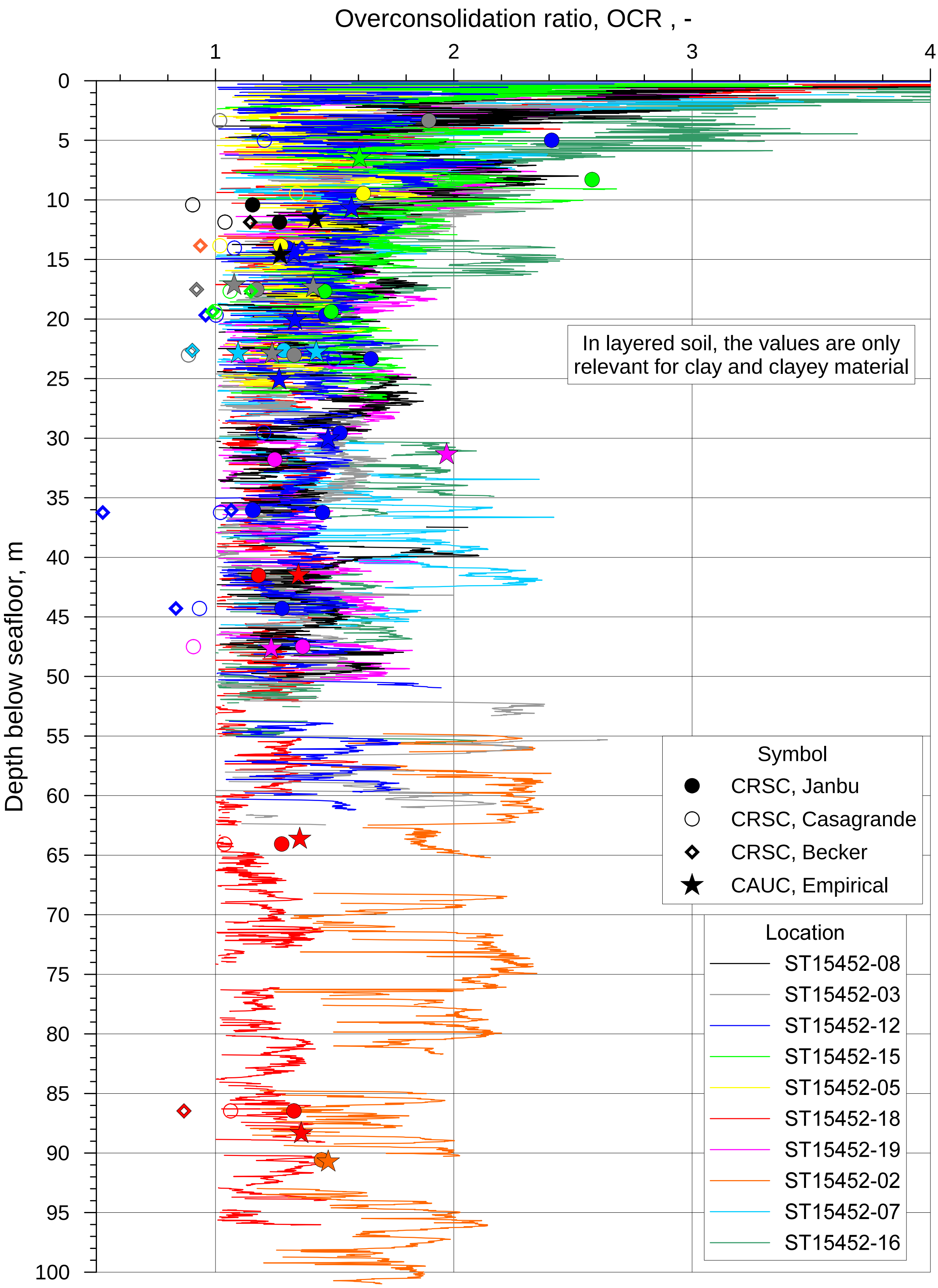

NOTE: p_c' in clay from CPTU based on Andresen et al. (1979)
OCR(I_p; s_{uC}/p_0') using γ = 19 kN/m³, $N_{\Delta u}$ = 7.5 and I_p = 15%
Representative profile based on engineering judgement.

Date/Rev.: 2015-01-21/01

ST15452 Flemish Pass Geotechnical Investigation	Document No. 20140857-02-R
Overconsolidation ratio versus depth All locations	Figure No. F4.2.5
	Date 2016-04-04 / Drawn by SK

NGI

P:\2014\08\20140857\Leveransedokumenter\Rapport\20140857-02-R Data interpretation and evaluation\Figures\Section F\Figure F_04_02_05, OCR versus depth.grf

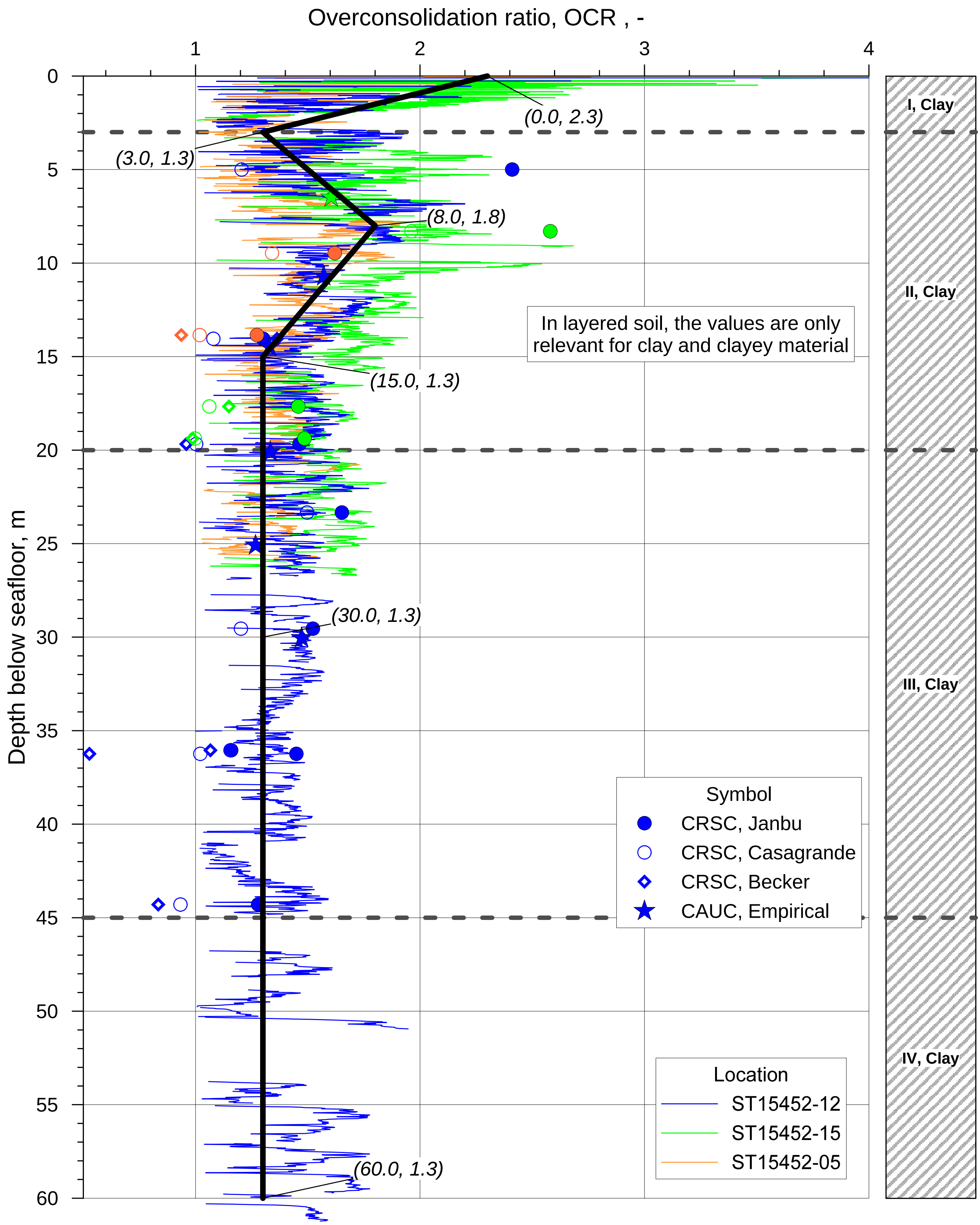

NOTE: p_c' in clay from CPTU based on Andresen et al. (1979)
OCR(I_p; s_{uC}/p_0') using γ = 19 kN/m³, $N_{\Delta u}$ = 7.5 and I_p = 15%
Representative profile based on engineering judgement.

Label: *(depth, value)*

Date/Rev.: 2015-01-21/01

P:\2014\08\20140857\Leveransedokumenter\Rapport\20140857-02-R Data interpretation and evaluation\Figures\Section F\Figure F_04_02_06, OCR versus depth-Fieldcentre.grf

ST15452 Flemish Pass Geotechnical Investigation	Document No. 20140857-02-R
Overconsolidation ratio versus depth Field Centre	Figure No. F4.2.6
	Date 2016-04-03 / Drawn by KS/SK
	NGI

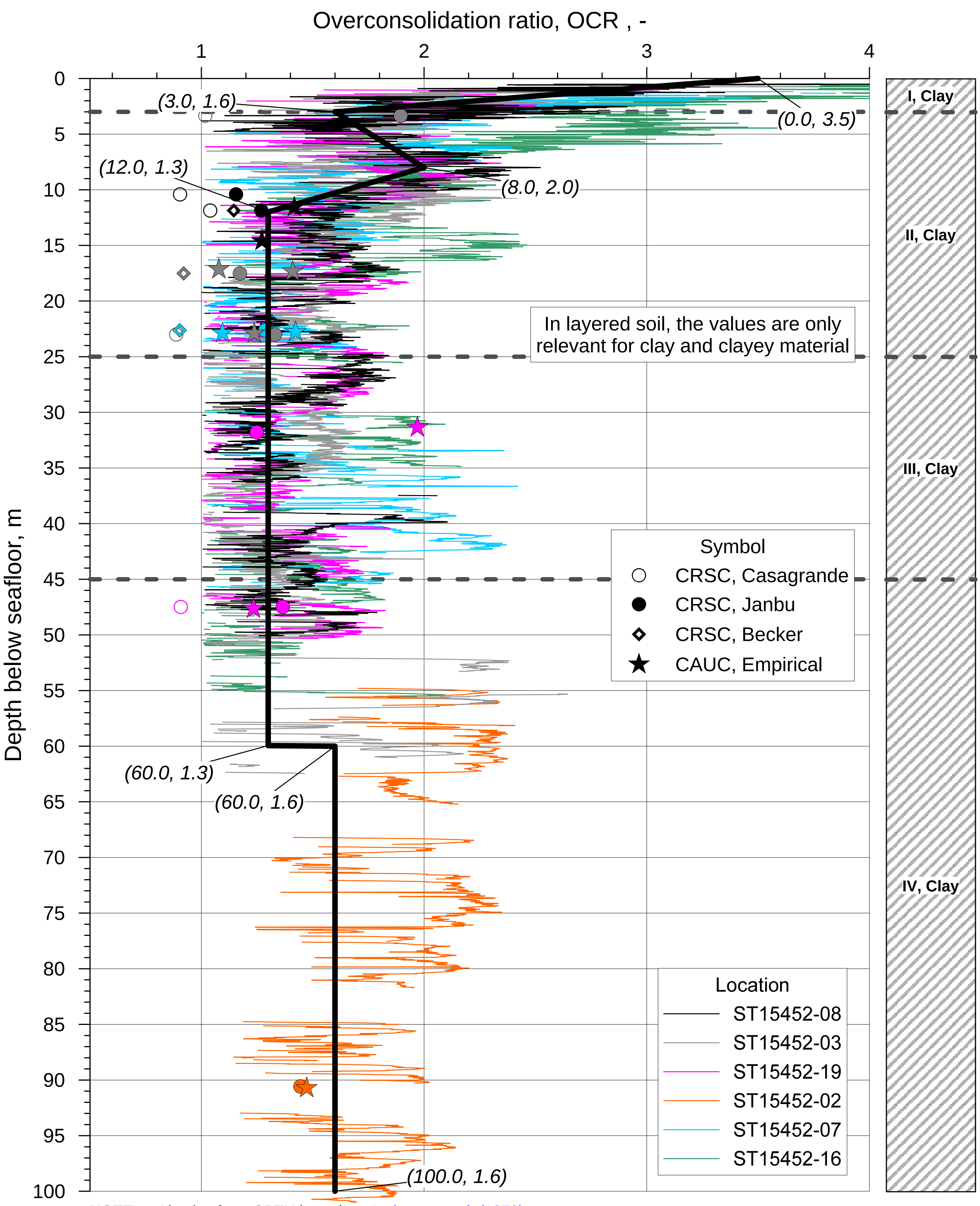

NOTE: p_c' in clay from CPTU based on Andresen et al. (1979)
OCR(I_p; s_{uC}/p_0') using γ = 19 kN/m³, $N_{\Delta u}$ = 7.5 and I_p = 15%
Representative profile based on engineering judgement.

Representative profile

Label: *(depth, value)*

Date/Rev.: 2015-01-21/01

ST15452 Flemish Pass Geotechnical Investigation

Overconsolidation ratio versus depth
West Slope

Document No. 20140857-02-R	
Figure No. F4.2.7	
Date 2016-04-03	Drawn by KS/SK

NGI

P:\2014\08\20140857\Leveransedokumenter\Rapport\20140857-02-R Data interpretation and evaluation\Figures\Section F\Figure F_04_02_07, OCR versus depth-West.grf

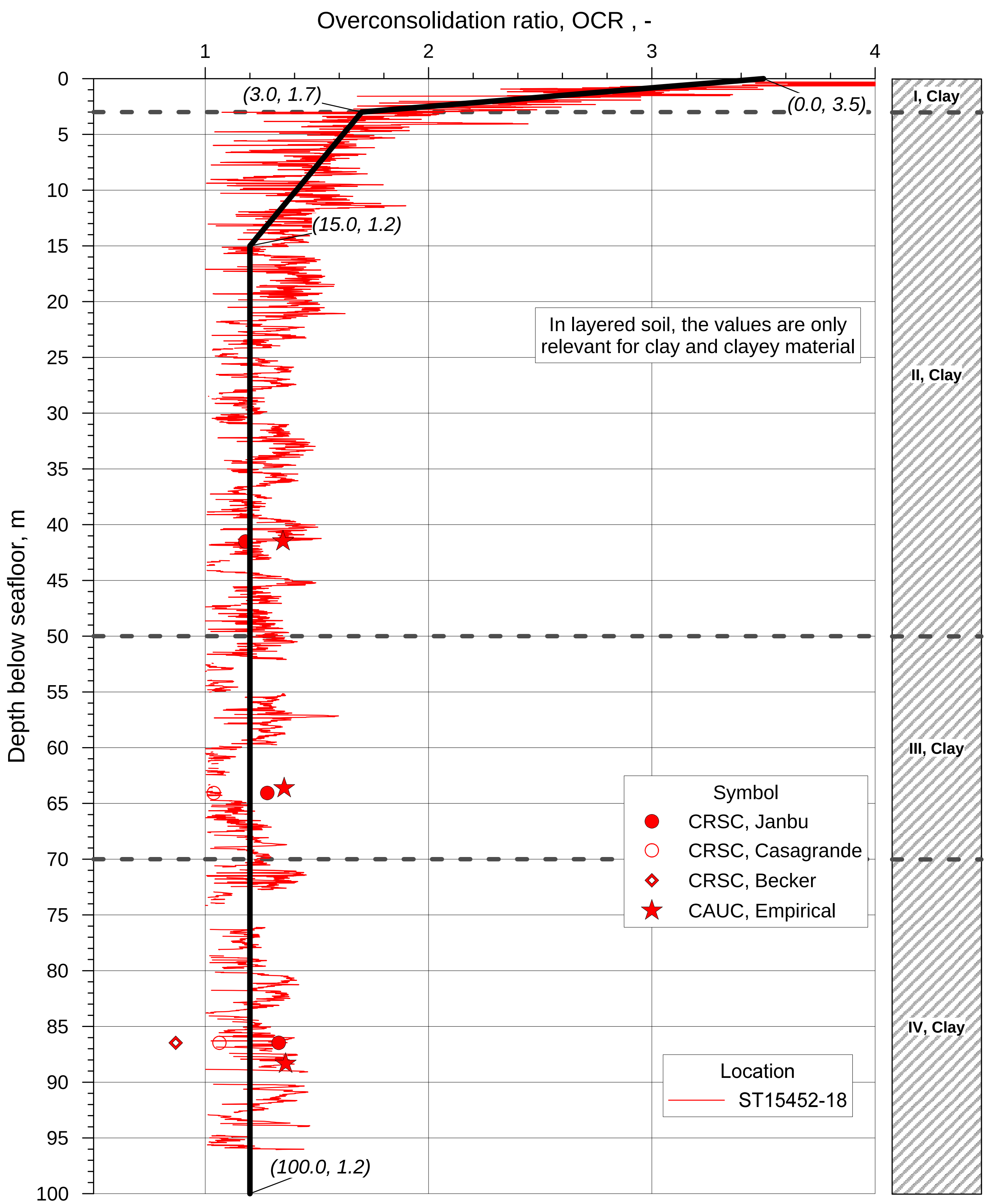

NOTE: p_c' in clay from CPTU based on Andresen et al. (1979)
OCR(I_p; s_{uC}/p_0') using γ = 19 kN/m³, $N_{\Delta u}$ = 7.5 and I_p = 15%
Representative profile based on engineering judgement.

Representative profile

Label: *(depth, value)*

Date/Rev.: 2015-01-21/01

ST15452 Flemish Pass Geotechnical Investigation	Document No. 20140857-02-R	
Overconsolidation ratio versus depth East Slope	Figure No. F4.2.8	
	Date 2016-04-03	Drawn by KS/SK

P:\2014\08\20140857\Leveransedokumenter\Rapport\20140857-02-R Data interpretation and evaluation\Figures\Section F\Figure F_04_02_08, OCR versus depth-East.grf

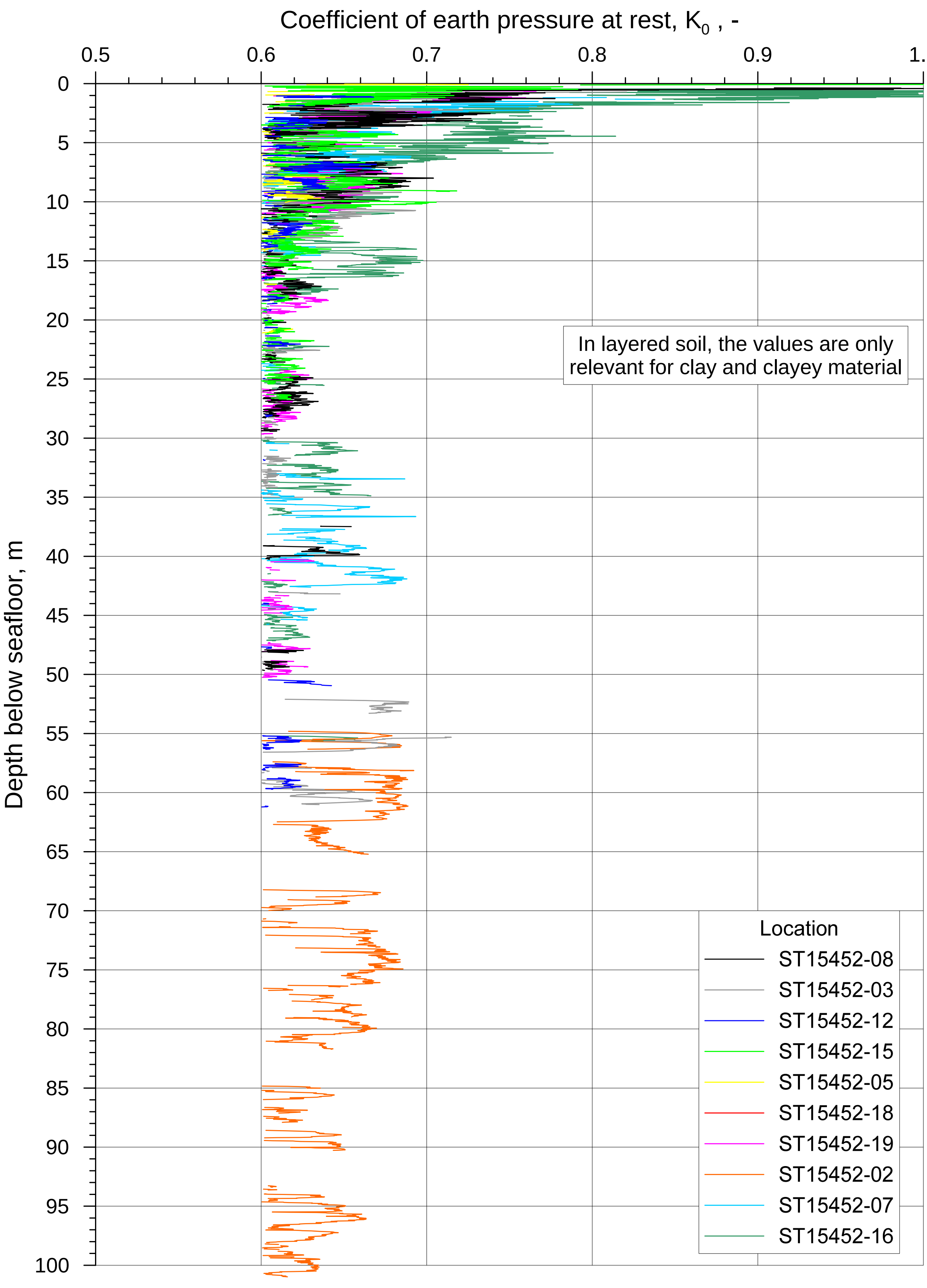

NOTE: K_0 in clay from CPTU using Brooker and Ireland (1965).
$K_0(I_p;\ s_{uC}/p_0')$ using γ = 19 kN/m³, $N_{\Delta u}$ = 7.5 and I_p = 15%.
Representative profile based on engineering judgement.

Date/Rev.: 2015-01-21/01

P:\2014\08\20140857\Leveransedokumenter\Rapport\20140857-02-R Data interpretation and evaluation\Figures\Section F\Figure F_04_03_01, K0 versus depth.grf

ST15452 Flemish Pass Geotechnical Investigation	Document No. 20140857-02-R
Coefficient of earth pressure at rest versus depth All locations	Figure No. F4.3.1
	Date 2016-04-04 / Drawn by SK

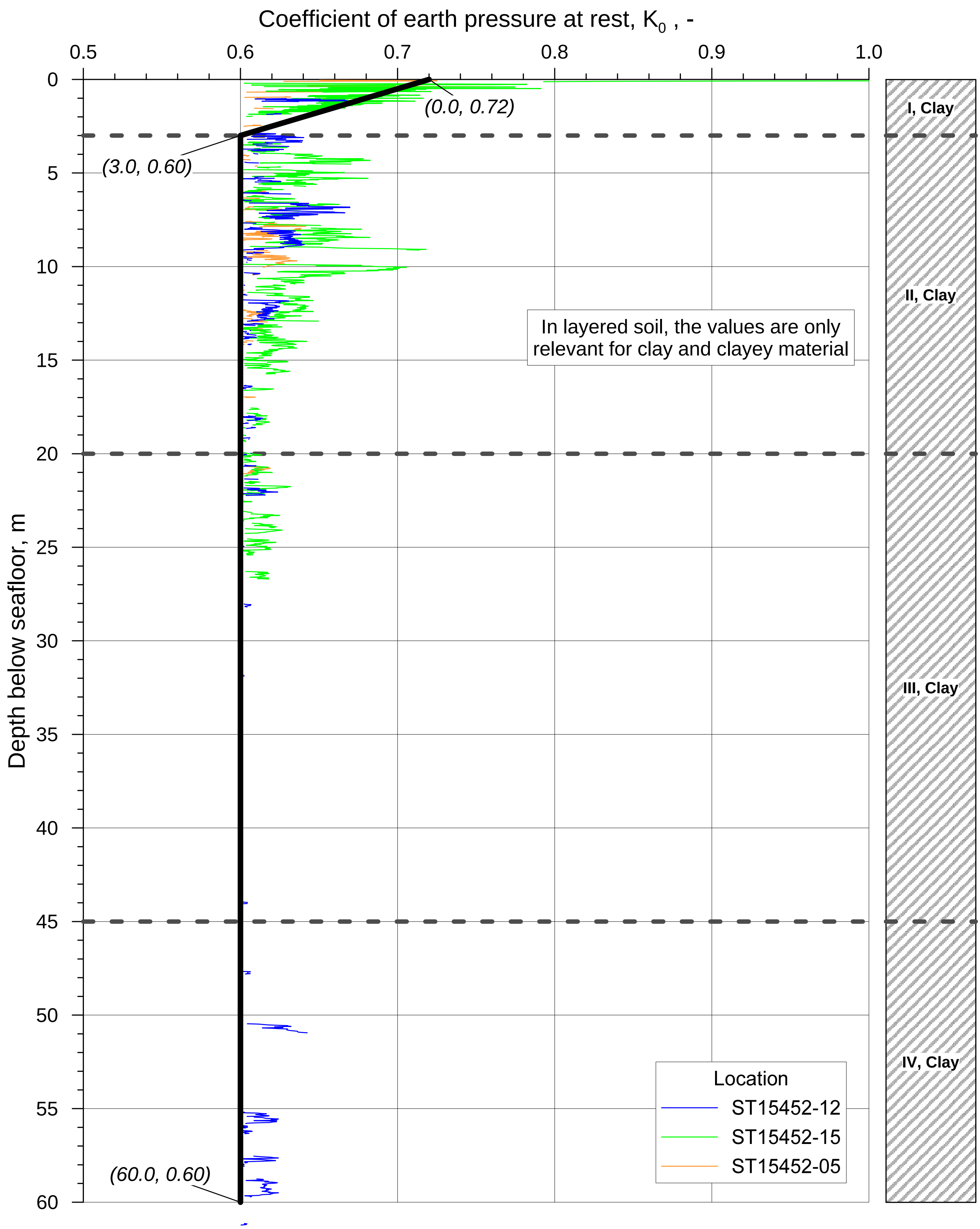

NOTE: K_0 in clay from CPTU using Brooker and Ireland (1965).
$K_0(I_p; s_{uC}/p_0')$ using γ = 19 kN/m³, $N_{\Delta u}$ = 7.5 and I_p = 15%.
Representative profile based on engineering judgement.

Label: *(depth, value)*

Date/Rev.: 2015-01-21/01

ST15452 Flemish Pass Geotechnical Investigation	Document No. 20140857-02-R	
Coefficient of earth pressure at rest versus depth Field Centre	Figure No. F4.3.2	
	Date 2016-04-03	Drawn by SK

P:\2014\08\20140857\Leveransedokumenter\Rapport\20140857-02-R Data interpretation and evaluation\Figures\Section F\Figure F_04_03_02, K0 versus depth-Fieldcentre.grf

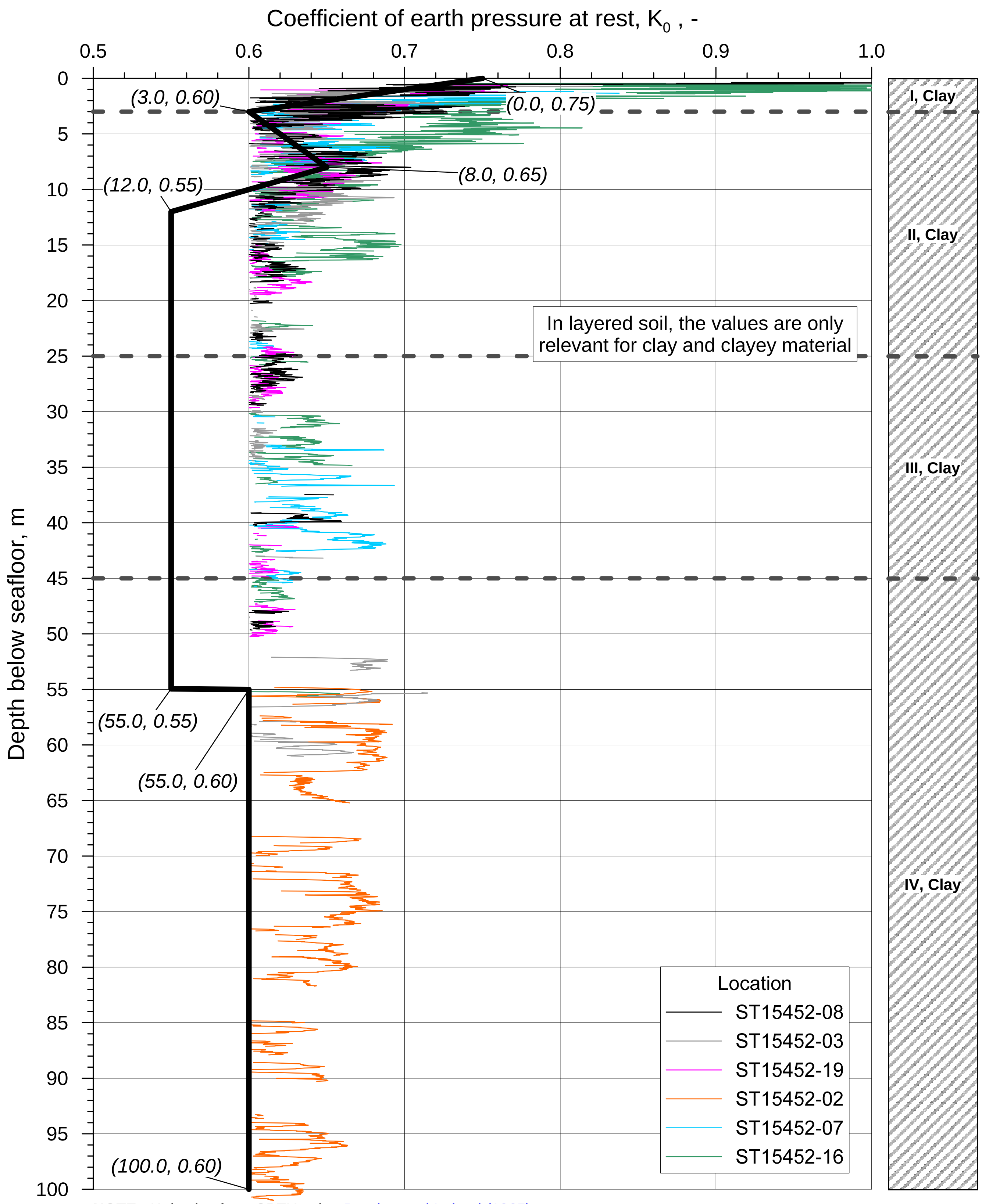

NOTE: K_0 in clay from CPTU using Brooker and Ireland (1965).
$K_0(I_p; s_{uC}/p_0')$ using γ = 19 kN/m³, $N_{\Delta u}$ = 7.5 and I_p = 15%.
Representative profile based on engineering judgement.

Label: *(depth, value)*

Date/Rev.: 2015-01-21/01

P:\2014\08\20140857\Leveransedokumenter\Rapport\20140857-02-R Data interpretation and evaluation\Figures\Section F\Figure F_04_03_03, K0 versus depth-West.grf

ST15452 Flemish Pass Geotechnical Investigation	Document No. 20140857-02-R	
Coefficient of earth pressure at rest versus depth West Slope	Figure No. F4.3.3	
	Date 2016-04-03	Drawn by SK
	NGI	

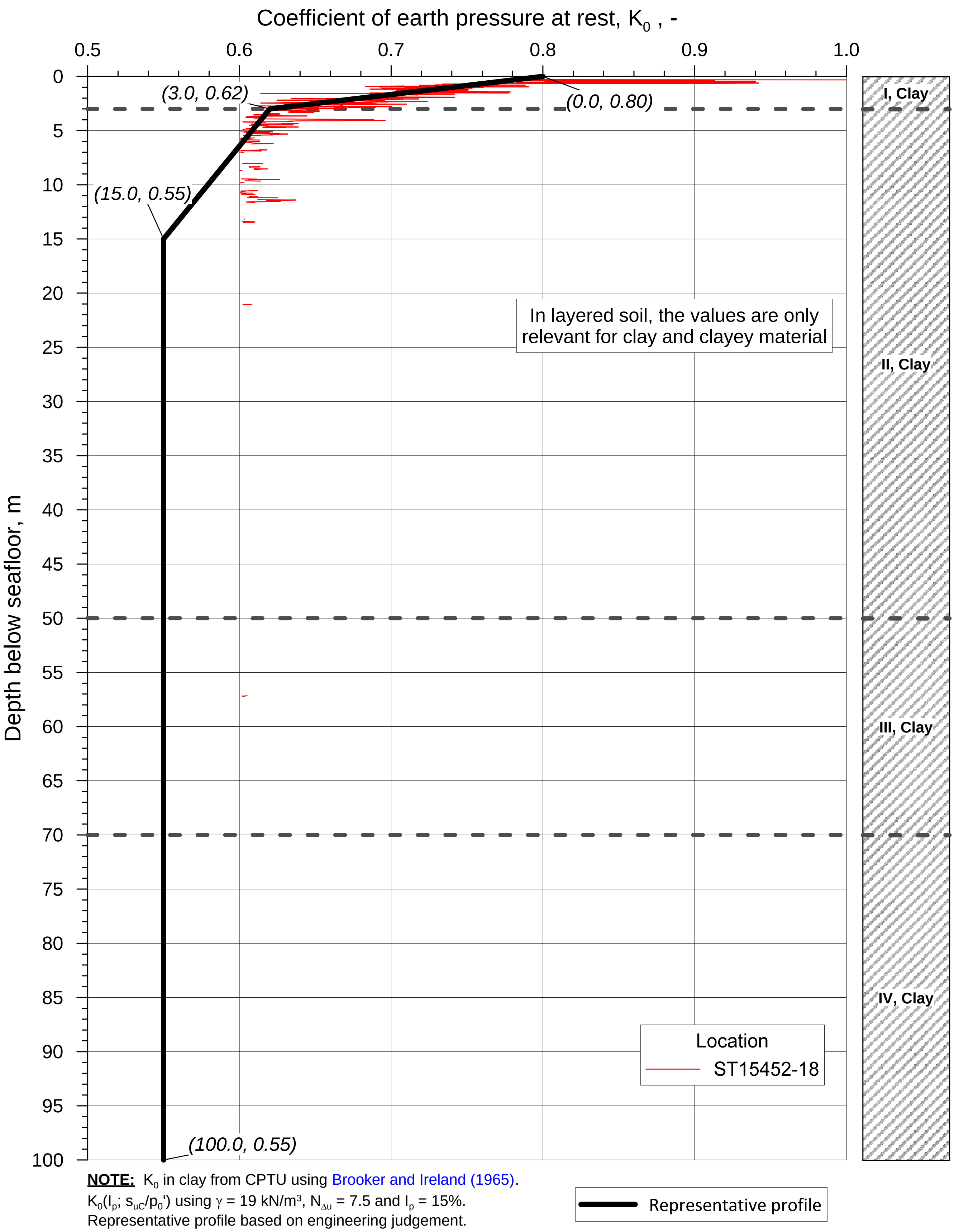

NOTE: K_0 in clay from CPTU using Brooker and Ireland (1965).
$K_0(I_p; s_{uC}/p_0')$ using γ = 19 kN/m³, $N_{\Delta u}$ = 7.5 and I_p = 15%.
Representative profile based on engineering judgement.

Label: *(depth, value)*

Date/Rev.: 2015-01-21/01

ST15452 Flemish Pass Geotechnical Investigation	Document No. 20140857-02-R
Coefficient of earth pressure at rest versus depth East Slope	Figure No. F4.3.4
	Date 2016-04-03 — Drawn by KS/SK

P:\2014\08\20140857\Leveransedokumenter\Rapport\20140857-02-R Data interpretation and evaluation\Figures\Section F\Figure F_04_03_04, K0 versus depth-East.grf

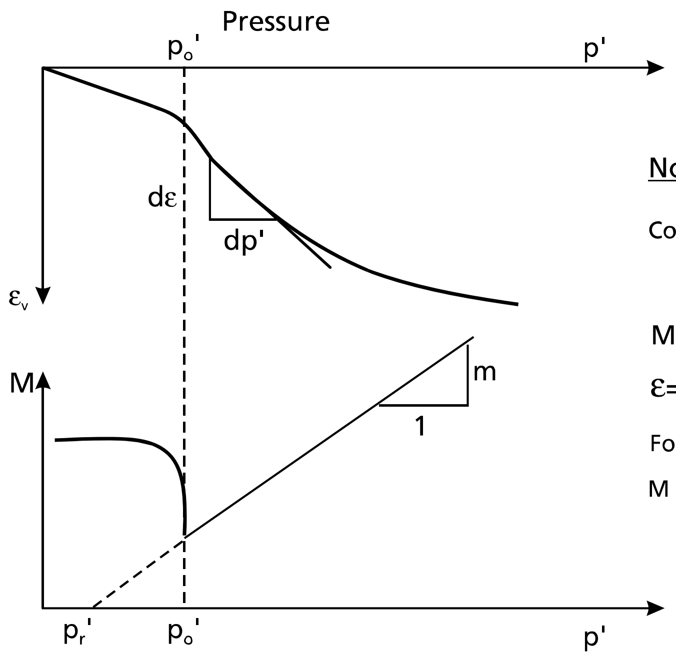

Normally consolidated clay

Constrained tangent modulus

$$M=\frac{dp'}{d\varepsilon}$$

$$\varepsilon=\int_{p'}\frac{1}{M}\,dp'$$

For $p'>p_o'$

$M = m(p'-p_r')$

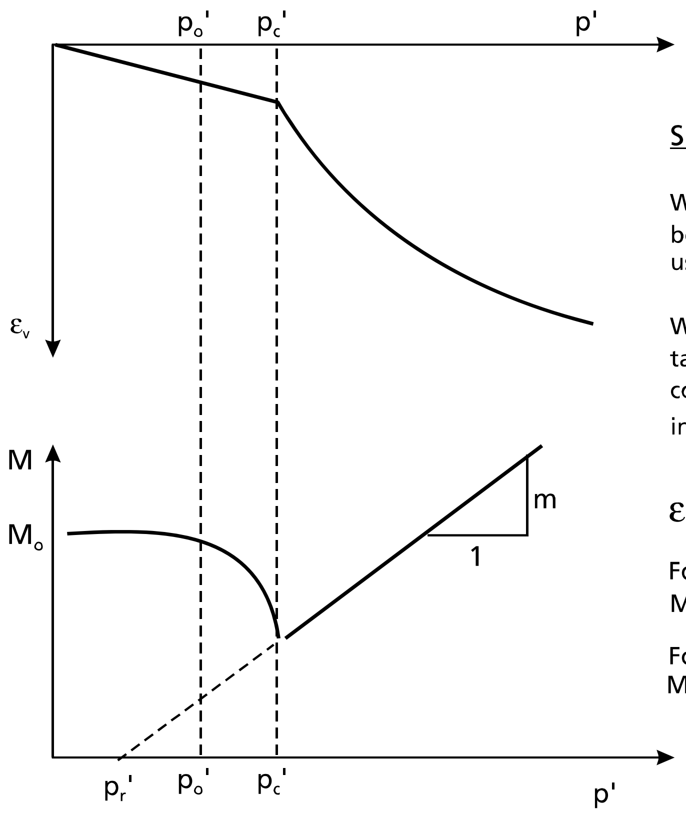

Slightly overconsolidated clay

When $p_c'-p_o'<<\Delta p$ the settlements may be approximately given by the model used for normally consolidated clay (above).

When p_c' is well defined, the constrained tangent modulus may be defined by a constant M from p_o' to p_c' and a linearly increasing M for stresses > p_c'.

$$\varepsilon=\int_{p'}\frac{1}{M}\,dp'$$

For $p_o'<p'\leq p_c'$
$M = M_o$ (constant)

For $p'>p_c'$
$M = m(p'-p_r')$

Date/Rev.: 2015-01-21/01

ST15452 Flemish Pass Geotechnical Investigation	Document No. 20140857-02-R	
Principles of using constrained deformation moduli in settlement calculations	Figure No. F5.3.1	
	Date 2016-04-03	Drawn by VBS

P:\2014\08\20140857\Leveransedokumenter\Rapport\20140857-02-R Data interpretation and evaluation\Figures\Section F\Figure F_05_03_01, Janbu principles.grf

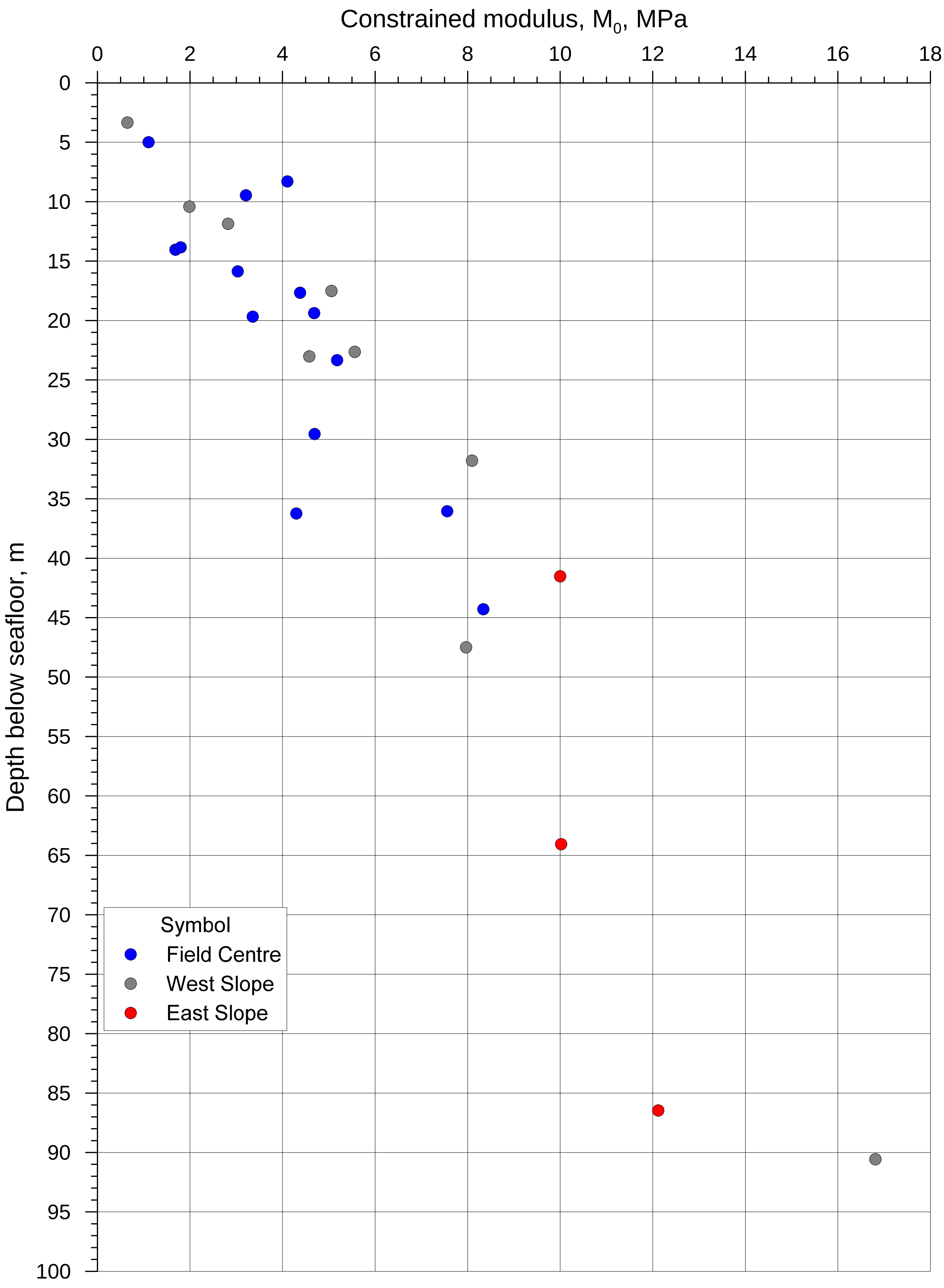

Date/Rev.: 2015-01-21/01

ST15452 Flemish Pass Geotechnical Investigation

Constrained modulus at in-situ vertical effective stress versus depth
All locations

Document No.	20140857-02-R
Figure No.	F5.3.2
Date	2016-04-03
Drawn by	VDa

P:\2014\08\20140857\Leveransedokumenter\Rapport\20140857-02-R Data interpretation and evaluation\Figures\Section F\Figure F_05_03_02, Constrained modulus versus depth.grf

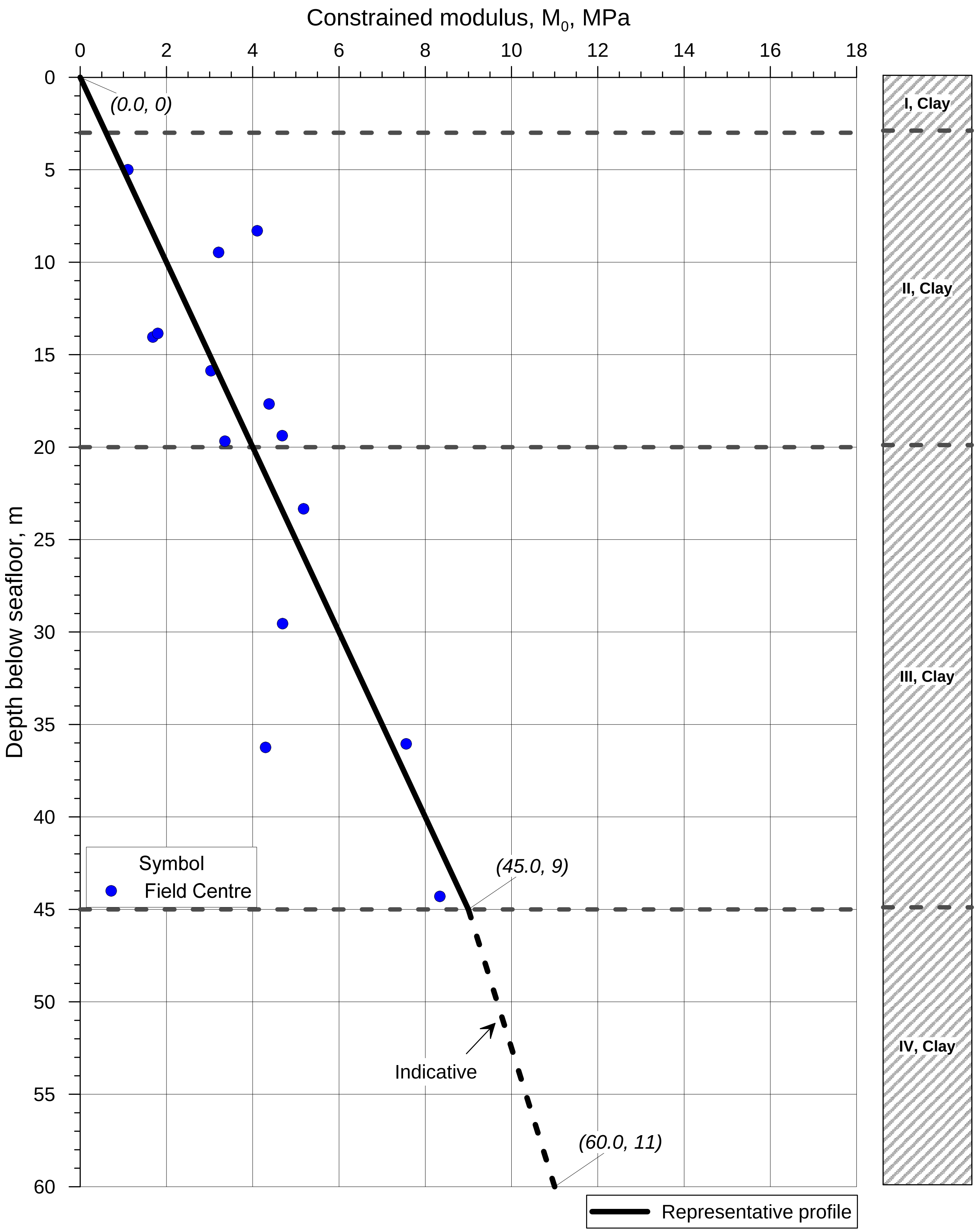

Label: *(depth, value)*

ST15452 Flemish Pass Geotechnical Investigation	Document No. 20140857-02-R
Constrained modulus at in-situ vertical effective stress versus depth Field Centre	Figure No. F5.3.3
	Date 2016-04-03 / Drawn by VDa

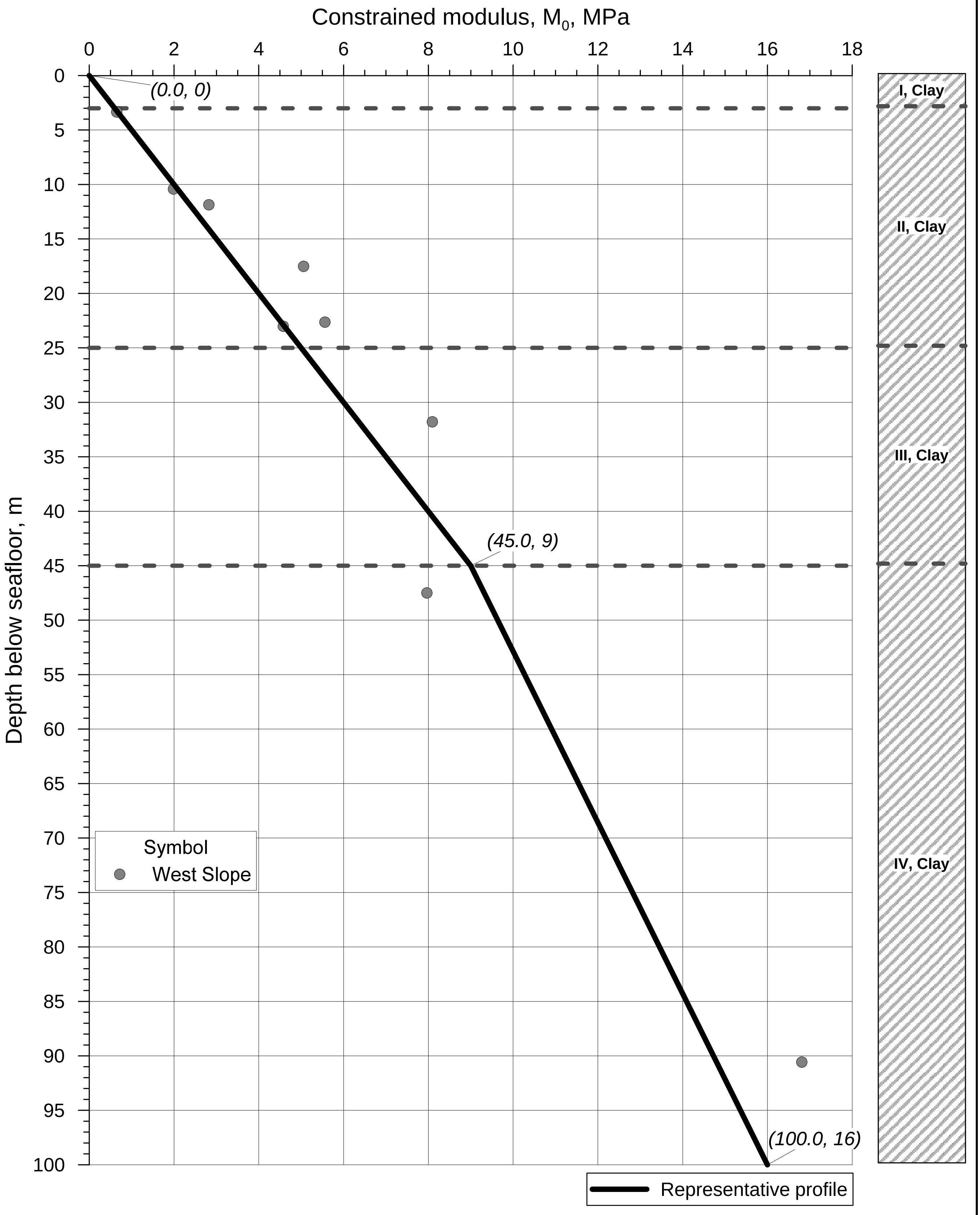

Label: *(depth, value)*

P:\2014\08\20140857\Leveransedokumenter\Rapport\20140857-02-R Data interpretation and evaluation\Figures\Section F\Figure F_05_03_04, Constrained modulus versus depth_West.grf

Date/Rev.: 2015-01-21/01

ST15452 Flemish Pass Geotechnical Investigation	Document No. 20140857-02-R
Constrained modulus at in-situ vertical effective stress versus depth West Slope	Figure No. F5.3.4
	Date 2016-04-03 · Drawn by VDa
	NGI

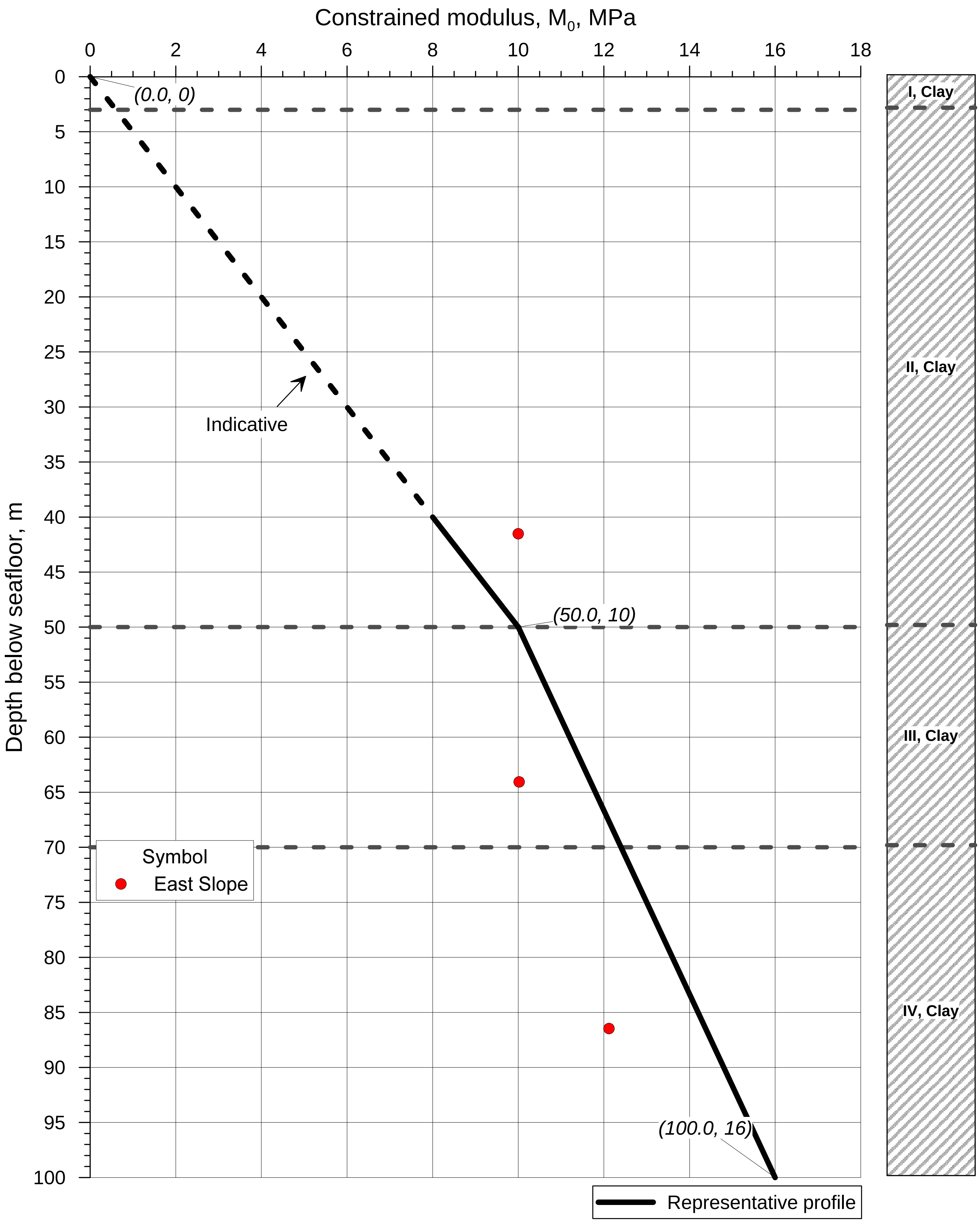

Label: *(depth, value)*

P:\2014\08\20140857\Leveransedokumenter\Rapport\20140857-02-R Data interpretation and evaluation\Figures\Section F\Figure F_05_03_05, Constrained modulus versus depth_East.grf

Date/Rev.: 2015-01-21/01

ST15452 Flemish Pass Geotechnical Investigation	Document No. 20140857-02-R
Constrained modulus at in-situ vertical effective stress versus depth East Slope	Figure No. F5.3.5
	Date 2016-04-03 / Drawn by VDa

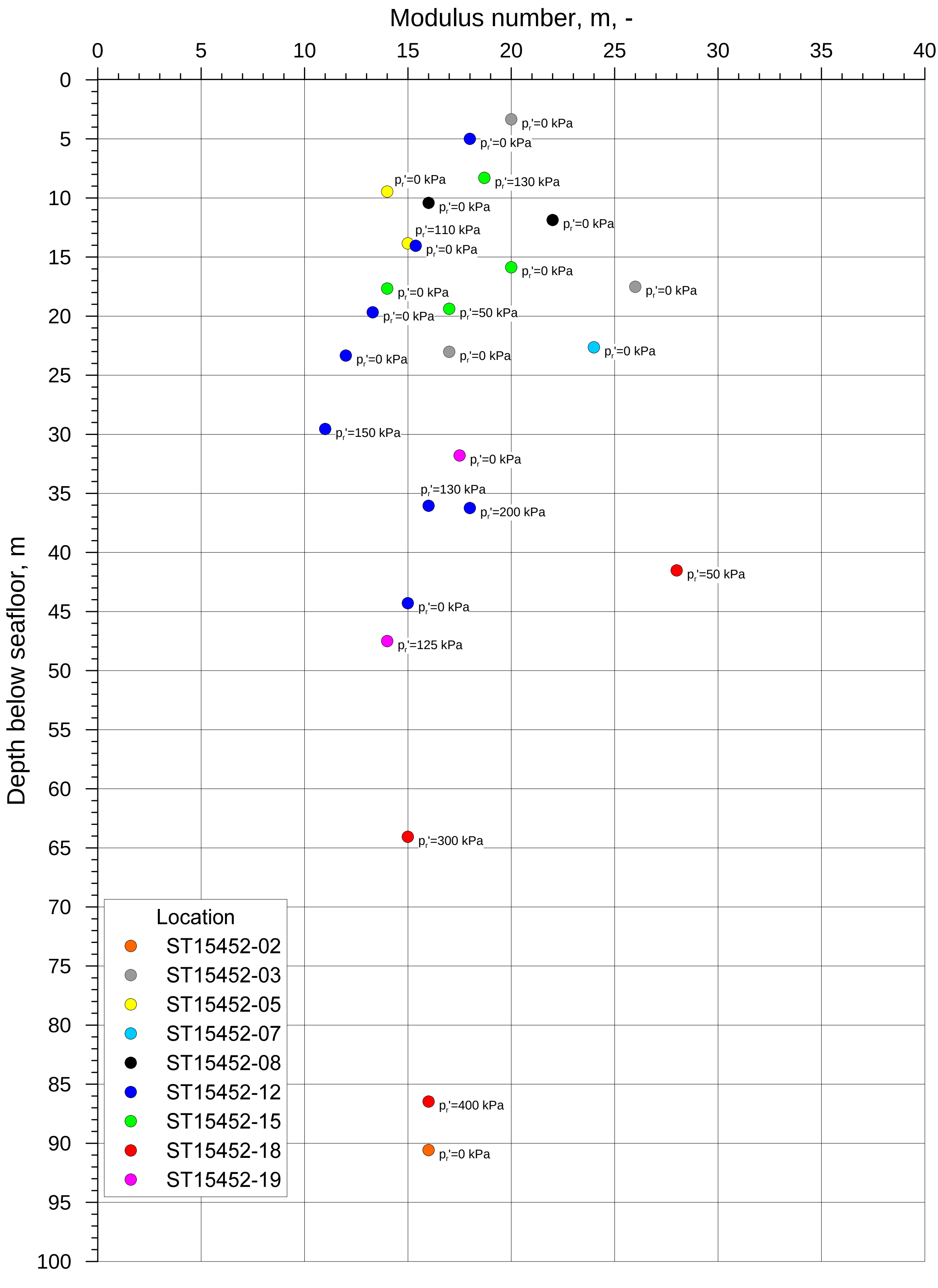

P:\2014\08\20140857\Leveransedokumenter\Rapport\20140857-02-R Data interpretation and evaluation\Figures\Section F\Figure F_05_03_06, modulus number versus depth.grf

Date/Rev.: 2015-01-21/01

ST15452 Flemish Pass Geotechnical Investigation	Document No. 20140857-02-R
Modulus number and reference stress versus depth All locations	Figure No. F5.3.6
	Date 2016-04-03 / Drawn by VDa

NGI

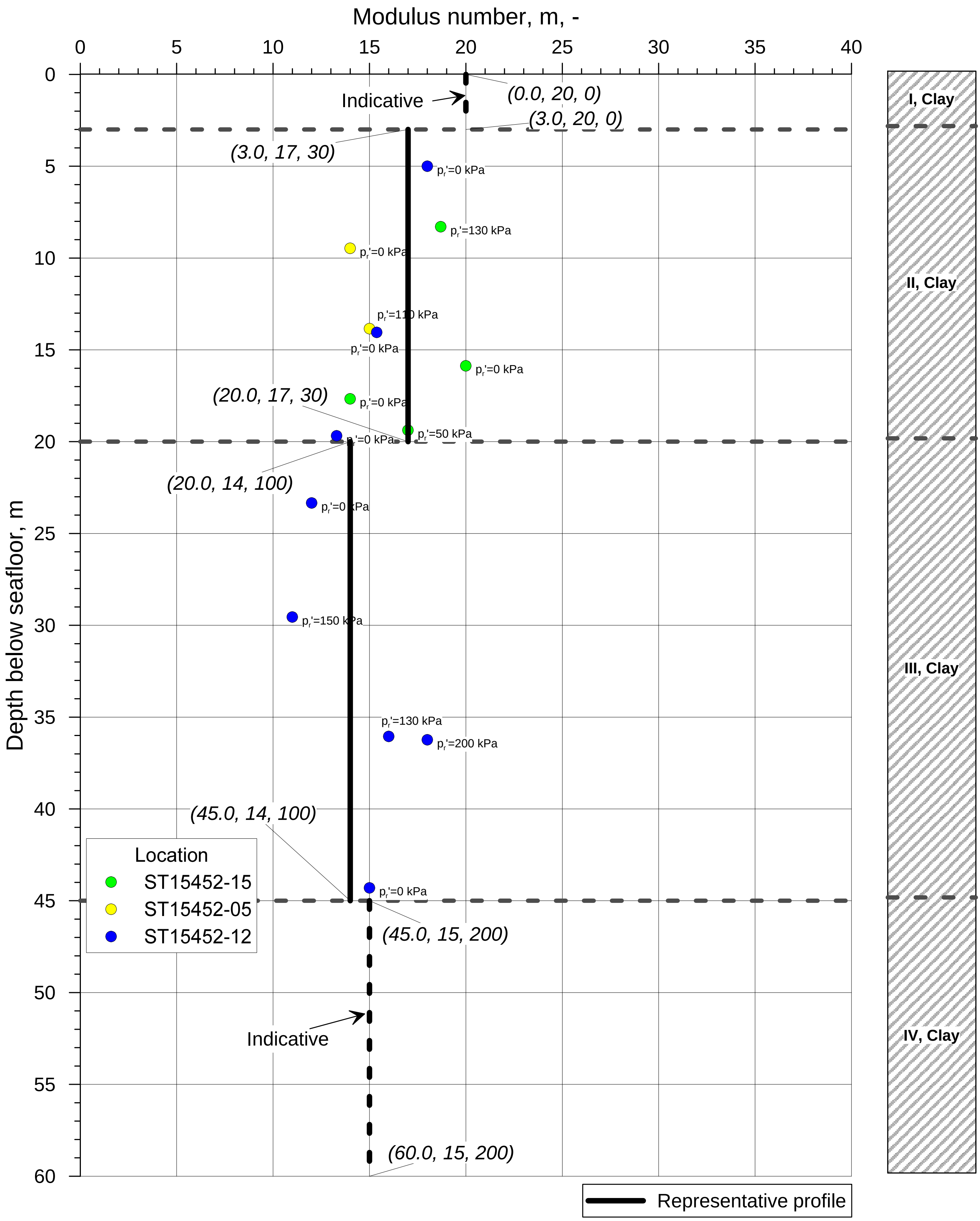

Label: *(depth, m, p_r')*

Date/Rev.: 2015-01-21/01

P:\2014\08\20140857\Leveransedokumenter\Rapport\20140857-02-R Data interpretation and evaluation\Figures\Section F\Figure F_05_03_07, modulus number versus depth_Fieldcentre.grf

ST15452 Flemish Pass Geotechnical Investigation	Document No. 20140857-02-R
Modulus number and reference stress versus depth Field Centre	Figure No. F5.3.7
	Date 2016-04-03 / Drawn by VDa

NGI

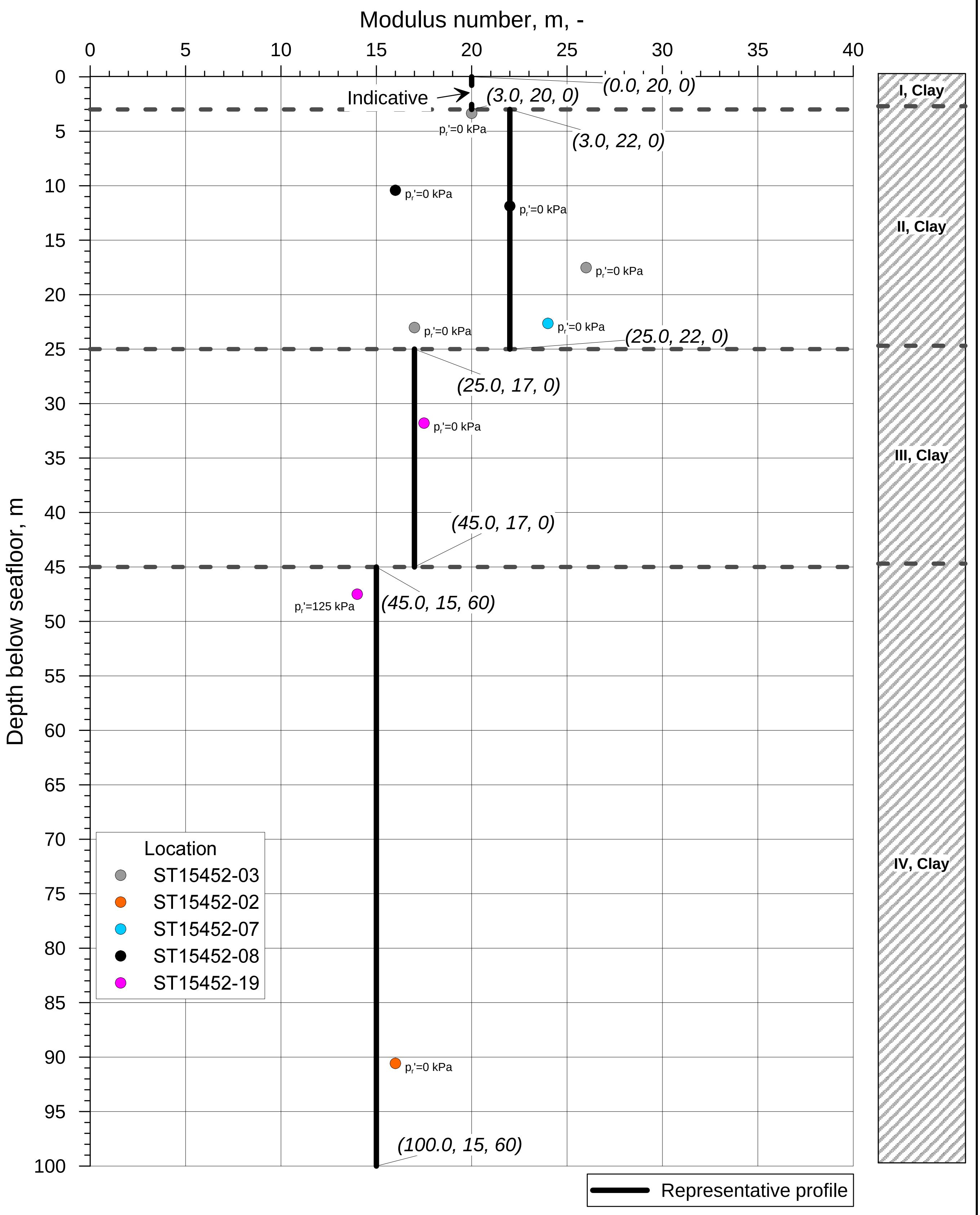

Label: *(depth, m, p_r')*

ST15452 Flemish Pass Geotechnical Investigation	Document No. 20140857-02-R
Modulus number and reference stress versus depth West Slope	Figure No. F5.3.8
	Date 2016-04-03 / Drawn by VDa
	NGI

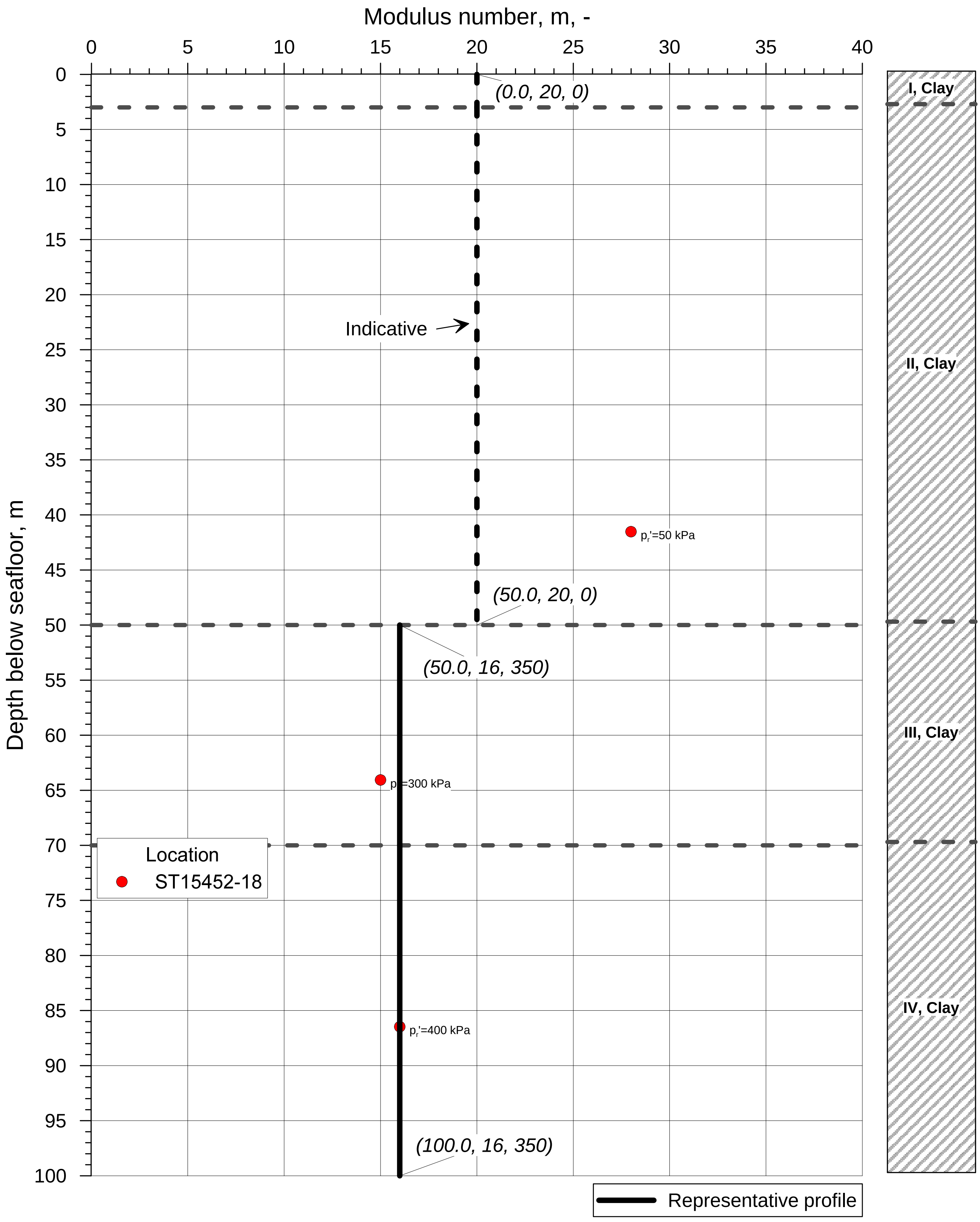

Label: *(depth, m, p_r')*

Date/Rev.: 2015-01-21/01

ST15452 Flemish Pass Geotechnical Investigation	Document No. 20140857-02-R
Modulus number and reference stress versus depth East Slope	Figure No. F5.3.9
	Date 2016-04-03 / Drawn by VDa

P:\2014\08\20140857\Leveransedokumenter\Rapport\20140857-02-R Data interpretation and evaluation\Figures\Section F\Figure F_05_03_09, modulus number versus depth_East.grf

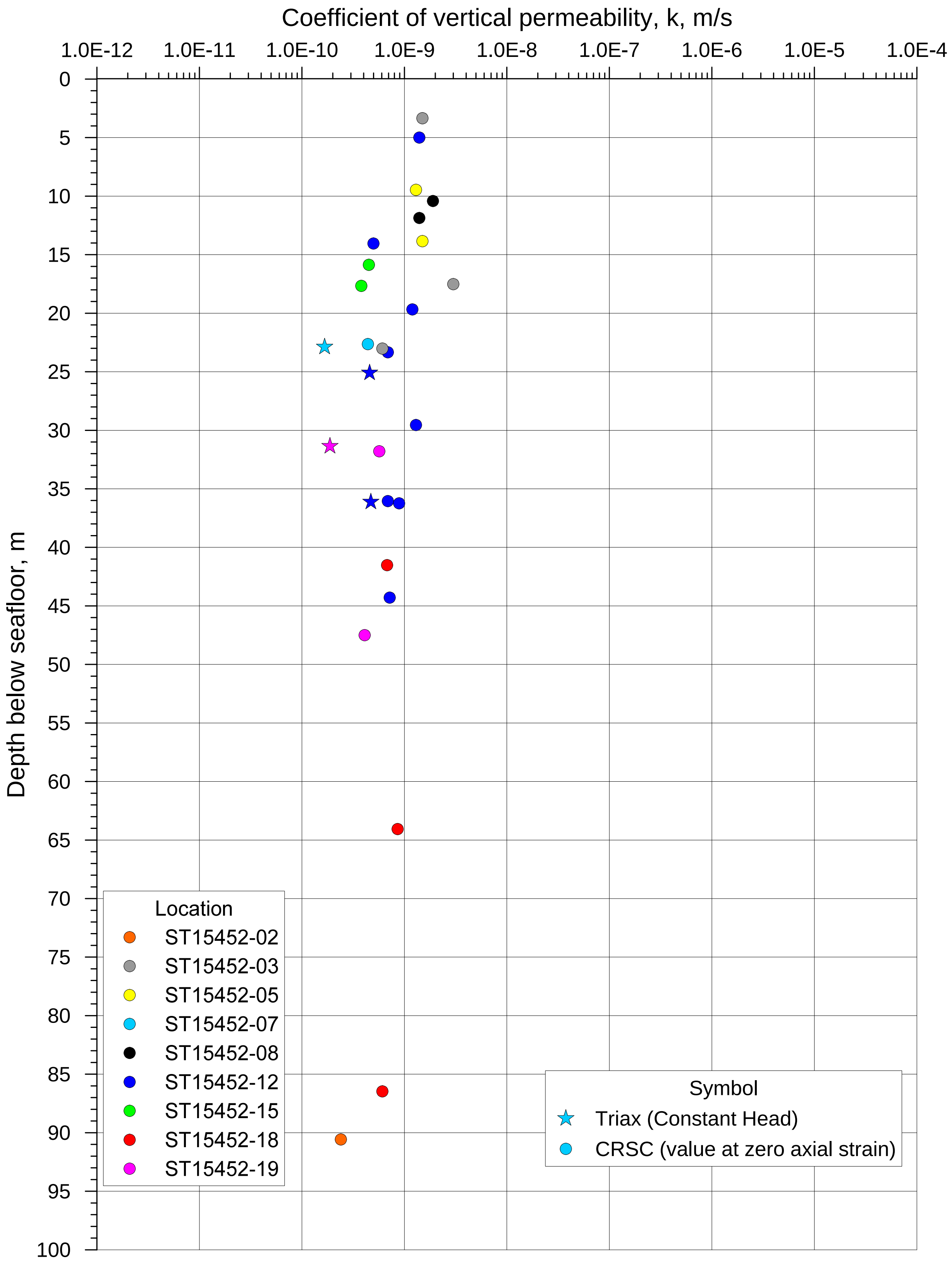

P:\2014\08\20140857\Leveranse dokumenter\Rapport\20140857-02-R Data interpretation and evaluation\Figures\Section F\Figure F_05_04_01, Coefficient of vertical permeability versus depth.grf

Date/Rev.: 2015-01-21/01

ST15452 Flemish Pass Geotechnical Investigation	Document No. 20140857-02-R
Coefficient of vertical permeability versus depth All locations	Figure No. F5.4.1
	Date 2016-04-03 / Drawn by VDa
	NGI

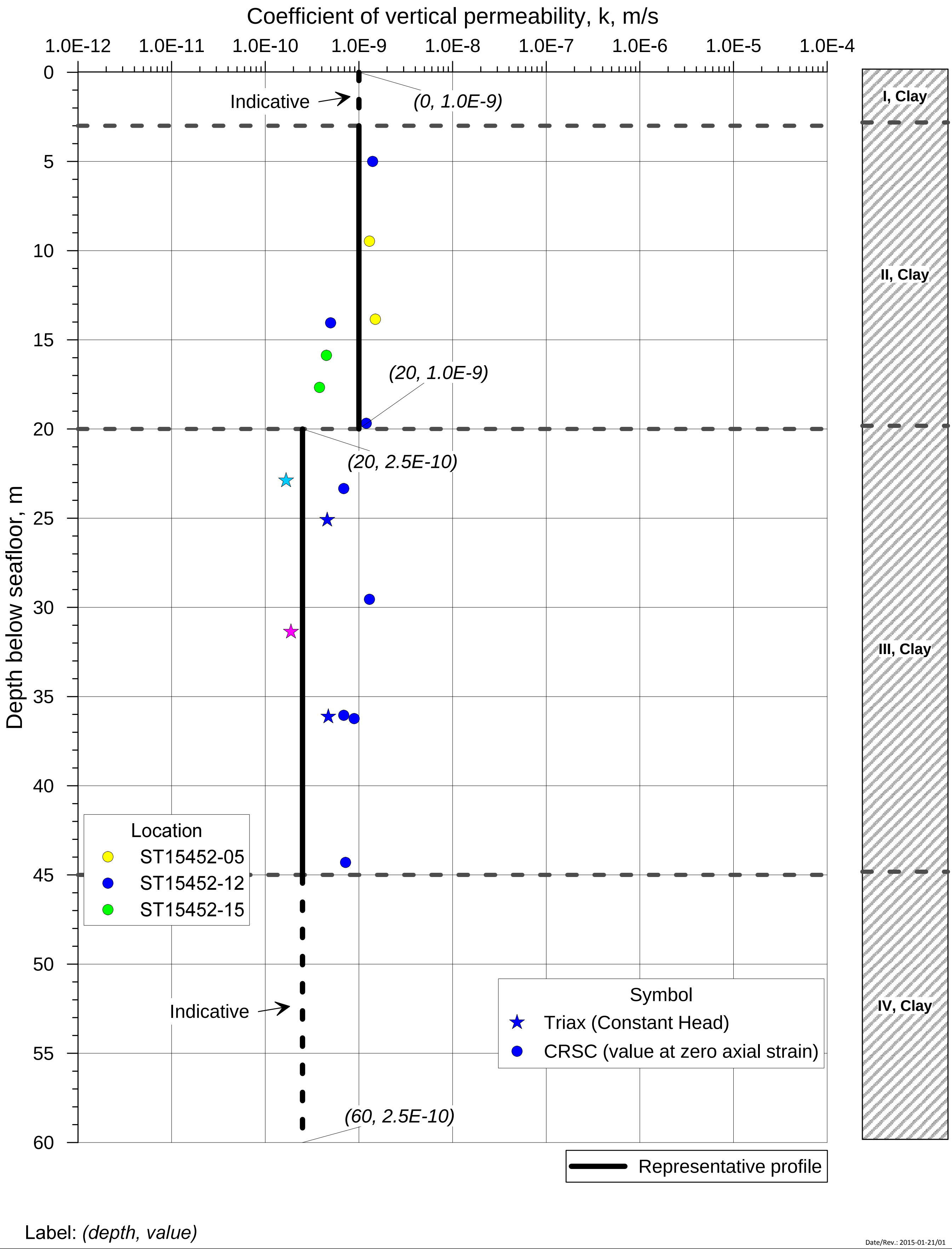

ST15452 Flemish Pass Geotechnical Investigation	Document No. 20140857-02-R	
Coefficient of vertical permeability versus depth Field Centre	Figure No. F5.4.2	
	Date 2016-04-03	Drawn by VDa
	NGI	

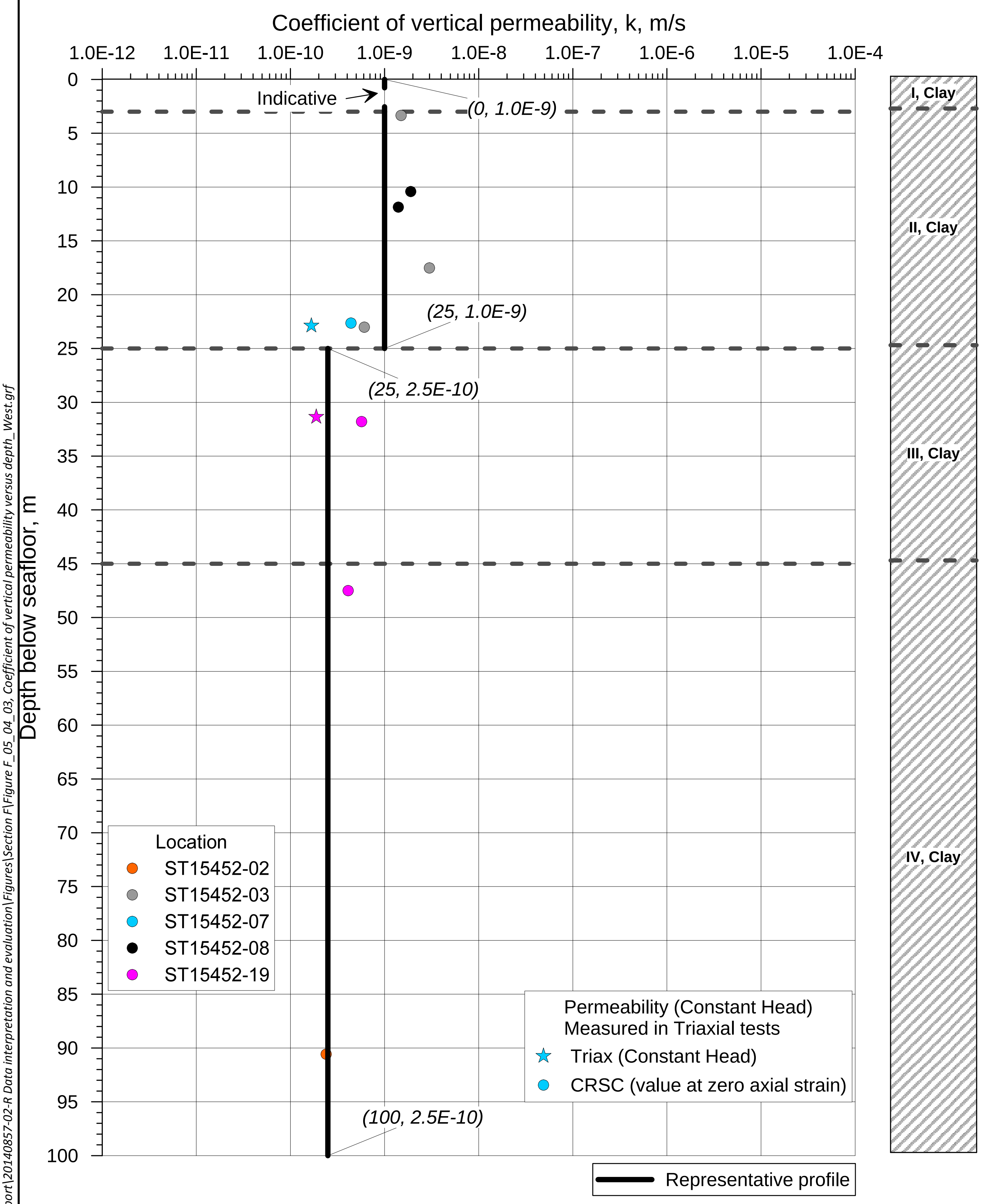

Label: *(depth, value)*

P:\2014\08\20140857\Leveransedokumenter\Rapport\20140857-02-R Data interpretation and evaluation\Figures\Section F\Figure F_05_04_03, Coefficient of vertical permeability versus depth_West.grf

Date/Rev.: 2015-01-21/01

ST15452 Flemish Pass Geotechnical Investigation	Document No. 20140857-02-R
Coefficient of vertical permeability versus depth West Slope	Figure No. F5.4.3
	Date 2016-04-03 / Drawn by VDa

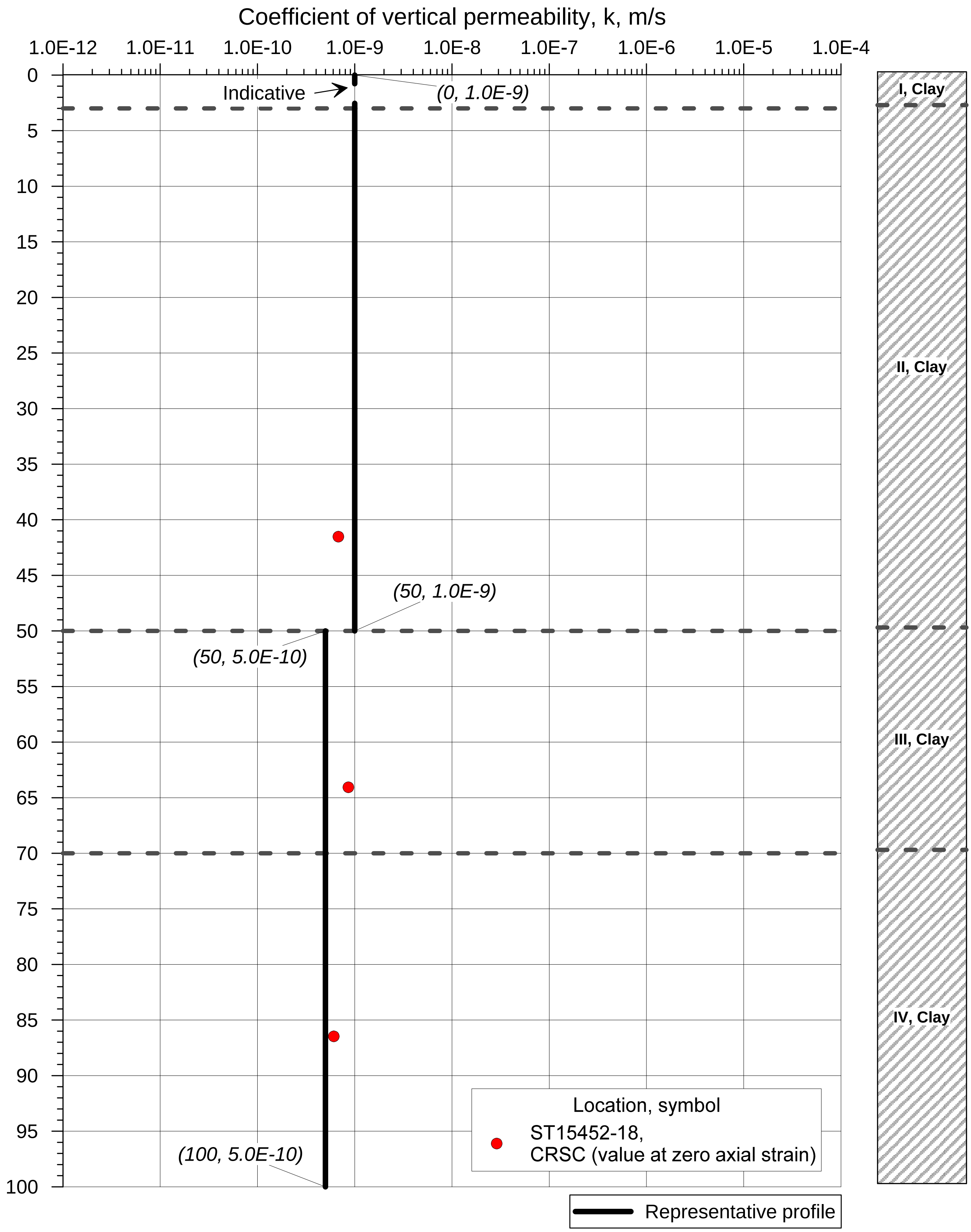

Label: *(depth, value)*

Date/Rev.: 2015-01-21/01

P:\2014\08\20140857\Leveransedokumenter\Rapport\20140857-02-R Data interpretation and evaluation\Figures\Section F\Figure F_05_04_04, Coefficient of vertical permeability versus depth_East.grf

ST15452 Flemish Pass Geotechnical Investigation	Document No. 20140857-02-R
Coefficient of vertical permeability versus depth East Slope	Figure No. F5.4.4
	Date 2016-04-03 / Drawn by VDa
	NGI

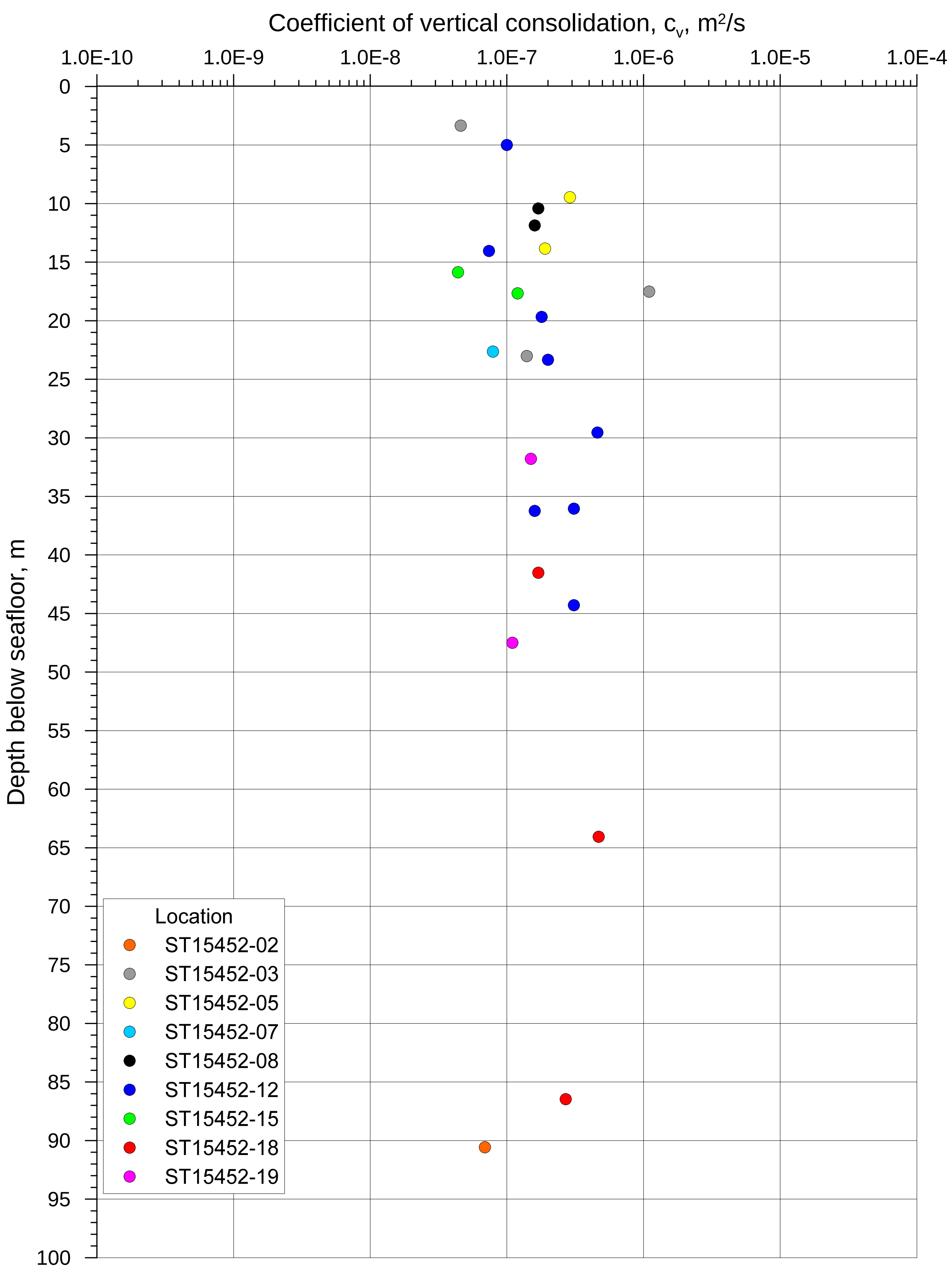

P:\2014\08\20140857\Leveransedokumenter\Rapport\20140857-02-R Data interpretation and evaluation\Figures\Section F\Figure F_05_05_01, Coefficient of vertical consolidation versus depth.grf

Date/Rev.: 2015-01-21/01

ST15452 Flemish Pass Geotechnical Investigation	Document No. 20140857-02-R	
Coefficient of vertical consolidation versus depth All locations	Figure No. F5.5.1	
	Date 2016-04-03	Drawn by VDa

NGI

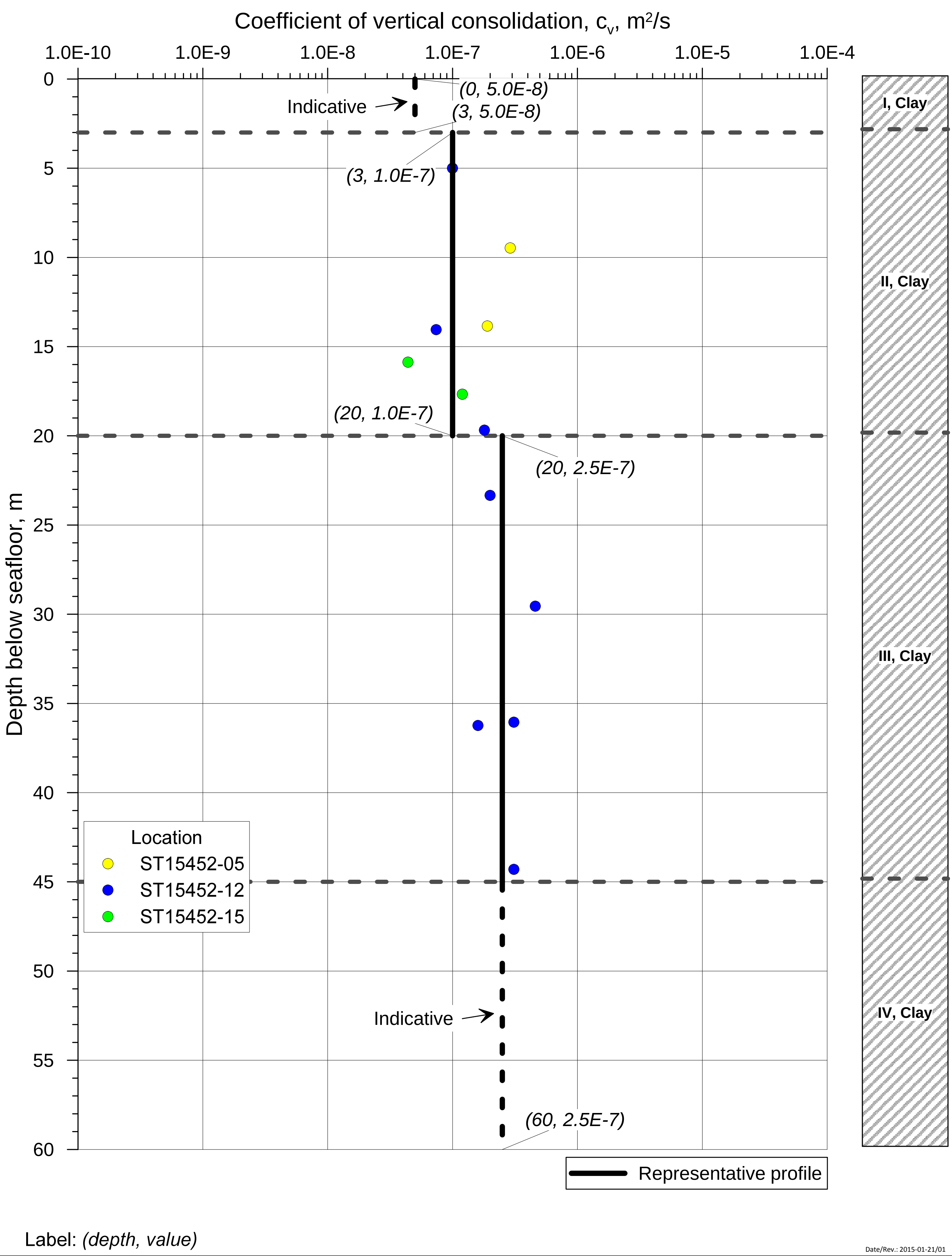

ST15452 Flemish Pass Geotechnical Investigation

Coefficient of vertical consolidation versus depth
Field Centre

Document No.	20140857-02-R
Figure No.	F5.5.2
Date	2016-04-03
Drawn by	VDa

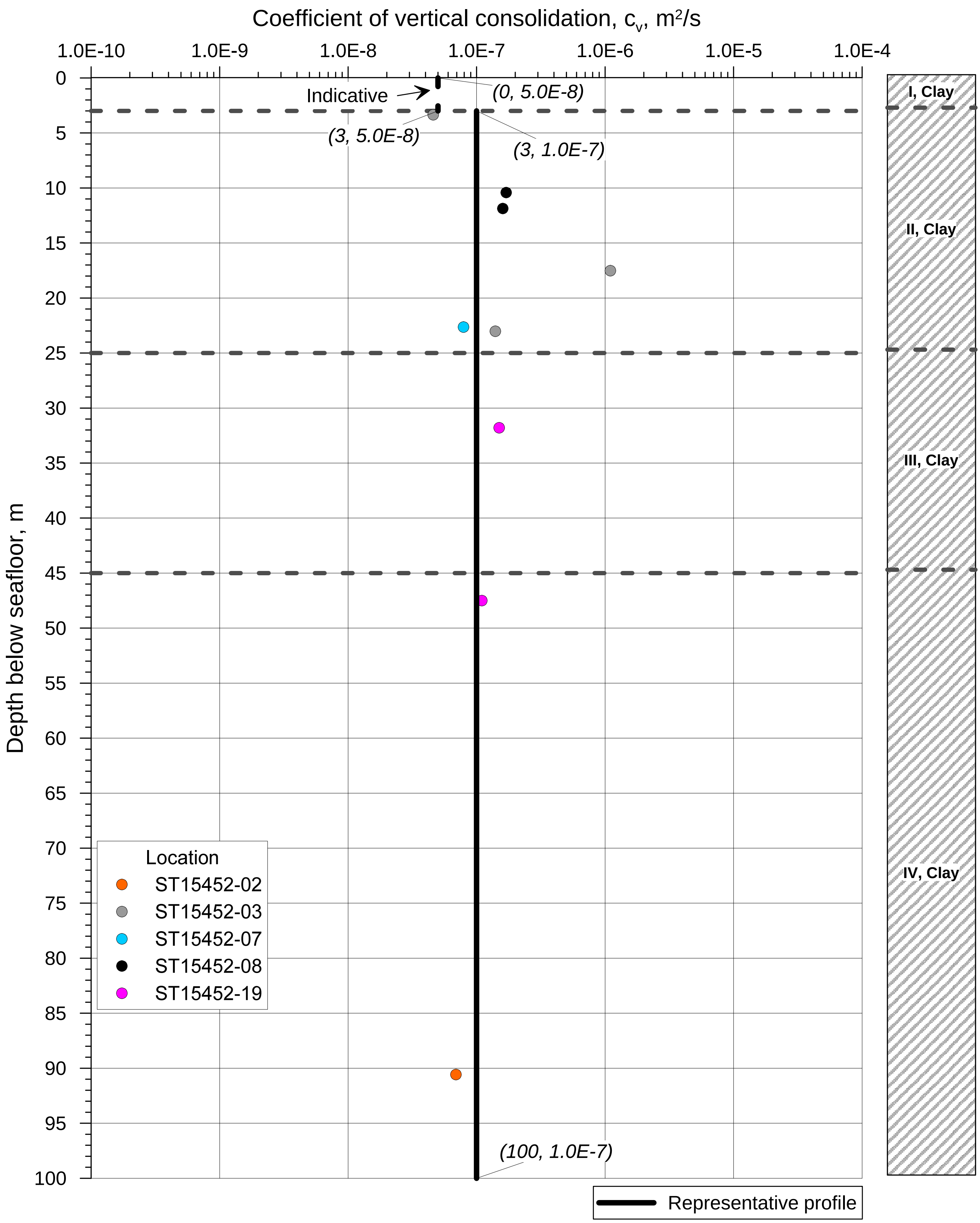

Label: *(depth, value)*

Date/Rev.: 2015-01-21/01

ST15452 Flemish Pass Geotechnical Investigation

Coefficient of vertical consolidation versus depth
West Slope

Document No. 20140857-02-R	
Figure No. F5.5.3	
Date 2016-04-03	Drawn by VDa

P:\2014\08\20140857\Leveransedokumenter\Rapport\20140857-02-R Data interpretation and evaluation\Figures\Section F\Figure F_05_05_03, Coefficient of vertical consolidation versus depth_West.grf

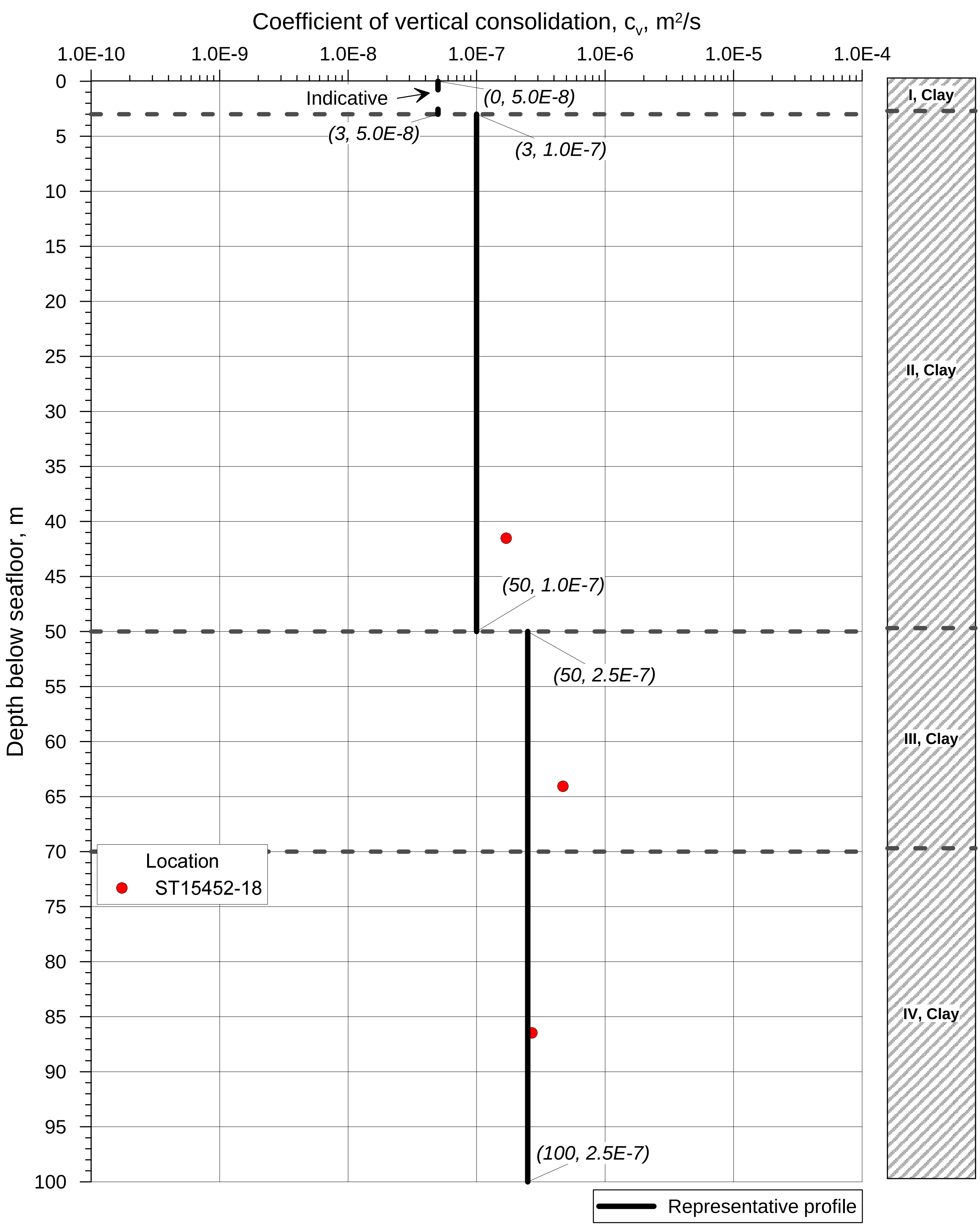

Label: *(depth, value)*

Date/Rev.: 2015-01-21/01

P:\2014\08\20140857\Leveranse dokumenter\Rapport\20140857-02-R Data interpretation and evaluation\Figures\Section F\Figure F_05_05_04, Coefficient of vertical consolidation versus depth_East.grf

ST15452 Flemish Pass Geotechnical Investigation	Document No. 20140857-02-R	
Coefficient of vertical consolidation versus depth East Slope	Figure No. F5.5.4	
	Date 2016-04-03	Drawn by VDa
	NGI	

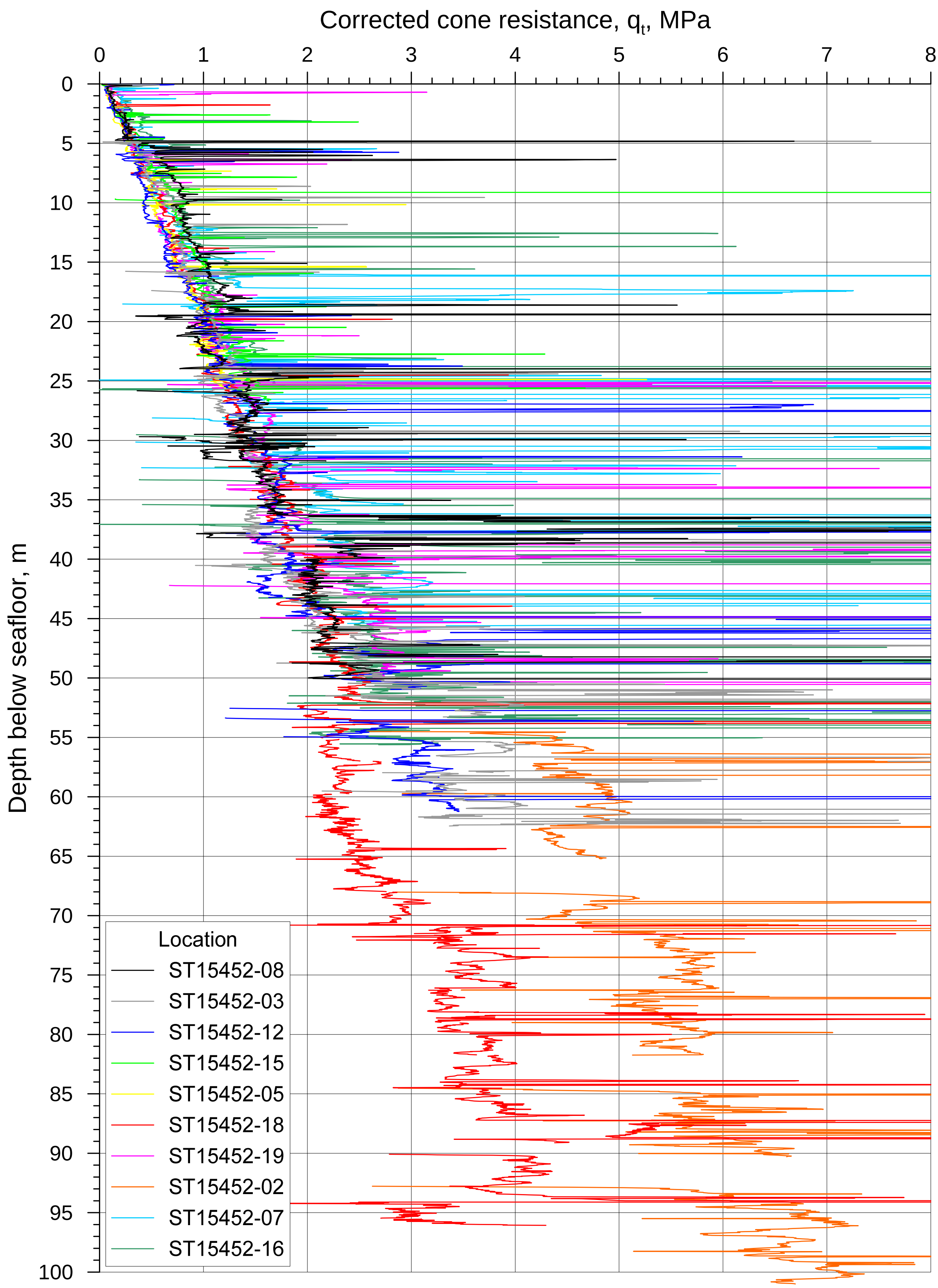

P:\2014\08\20140857\Leveransedokumenter\Rapport\20140857-02-R Data interpretation and evaluation\Figures\Section F\Figure F_06_02_01, qt versus depth.grf

Date/Rev.: 2015-01-21/01

ST15452 Flemish Pass Geotechnical Investigation	Document No. 20140857-02-R	
Corrected cone resistance versus depth All locations	Figure No. F6.2.1	
	Date 2016-04-03	Drawn by VBS
	NGI	

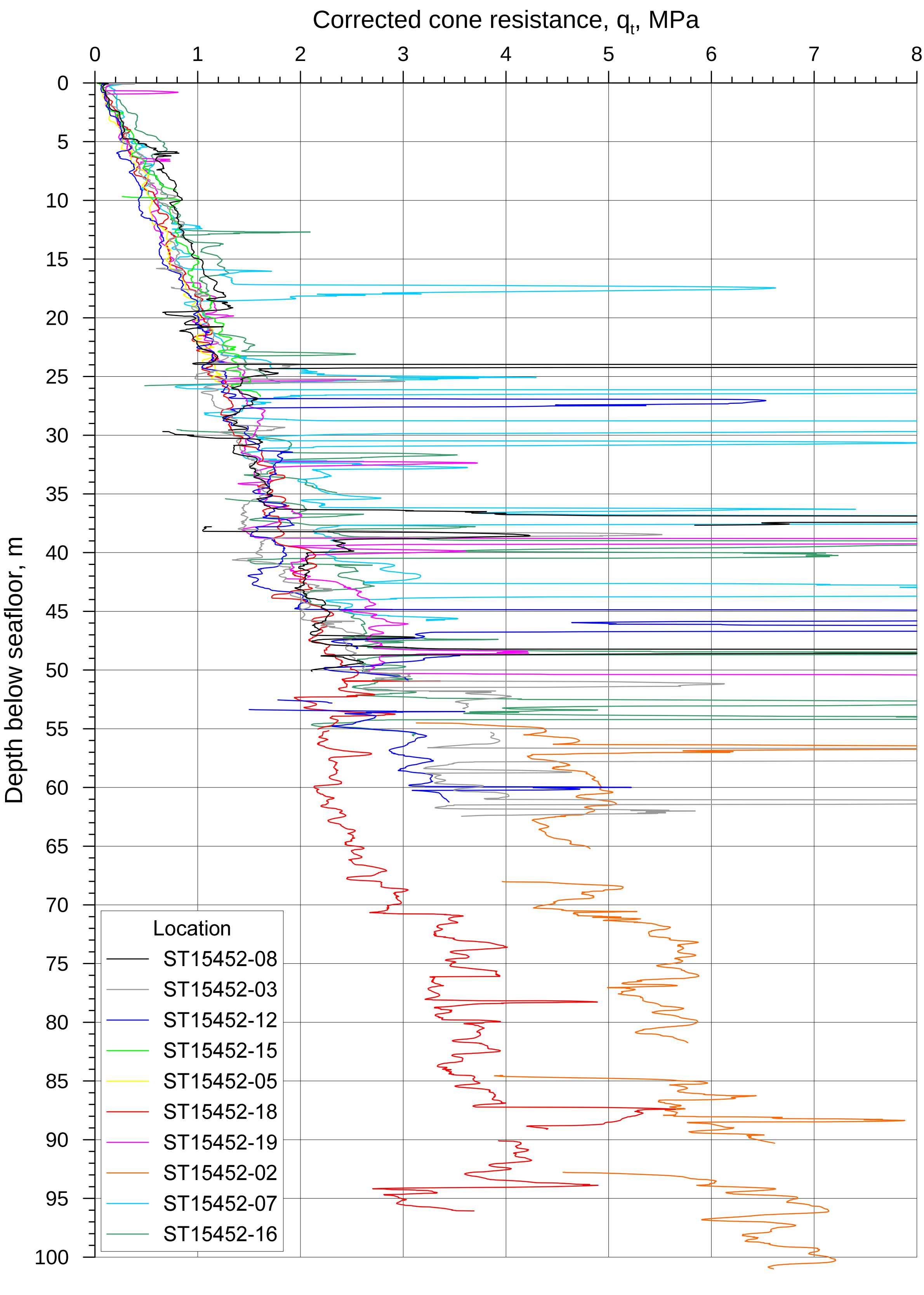

Data has been filtered by applying a Gausian moving average over a depth range of 0.5 m

ST15452 Flemish Pass Geotechnical Investigation

Corrected cone resistance versus depth
All locations
Data has been filtered for clarity. Allways refer to the full dataset

Document No. 20140857-02-R	
Figure No. F6.2.2	
Date 2016-05-20	Drawn by VBS

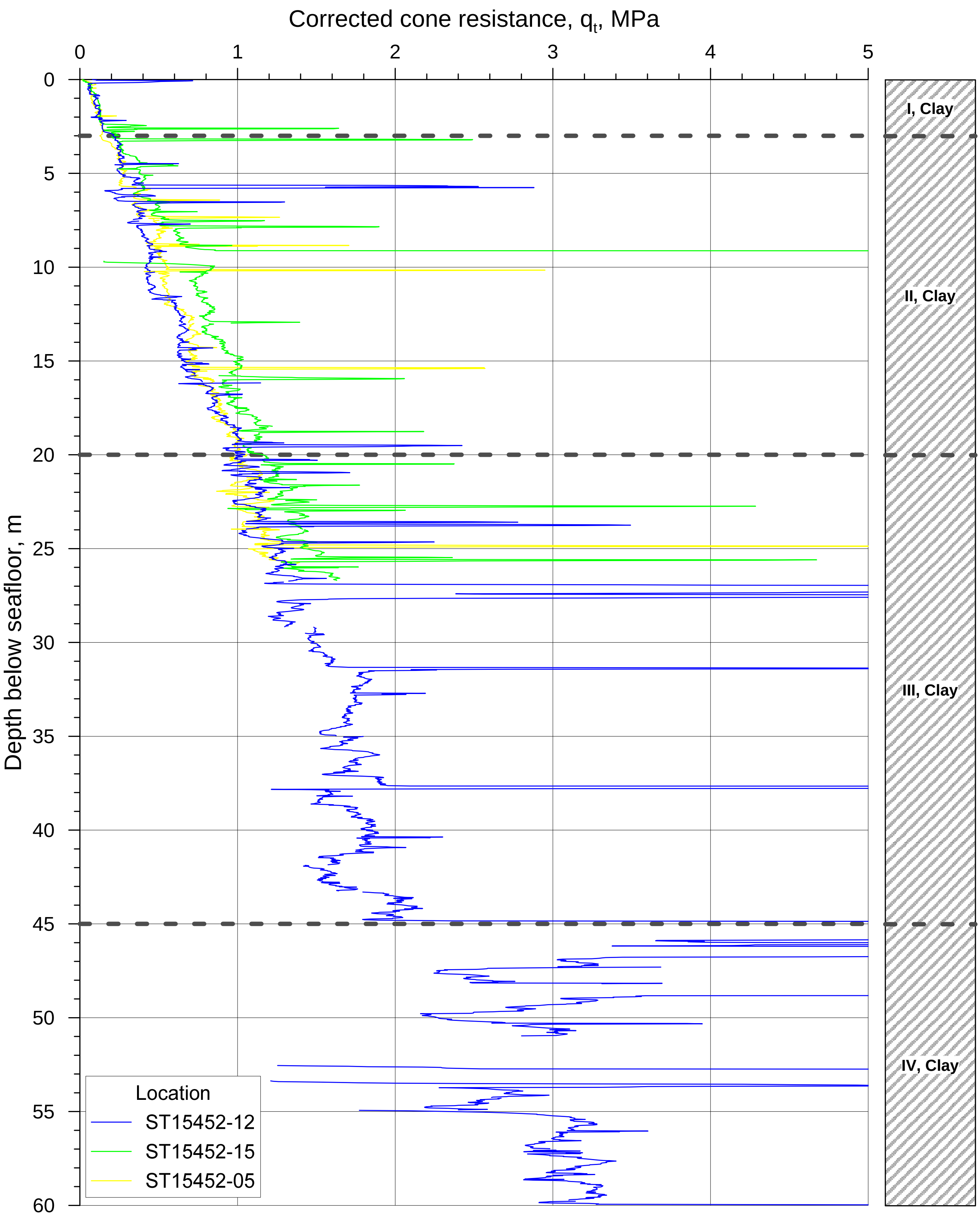

P:\2014\08\20140857\Leveransedokumenter\Rapport\20140857-02-R Data interpretation and evaluation\Figures\Section F\Figure F_06_02_03, qt versus depth-Fieldcentre.grf

Date/Rev.: 2015-01-21/01

ST15452 Flemish Pass Geotechnical Investigation	Document No. 20140857-02-R
Corrected cone resistance versus depth Field Centre	Figure No. F6.2.3
	Date 2016-04-03
	Drawn by VBS

NGI

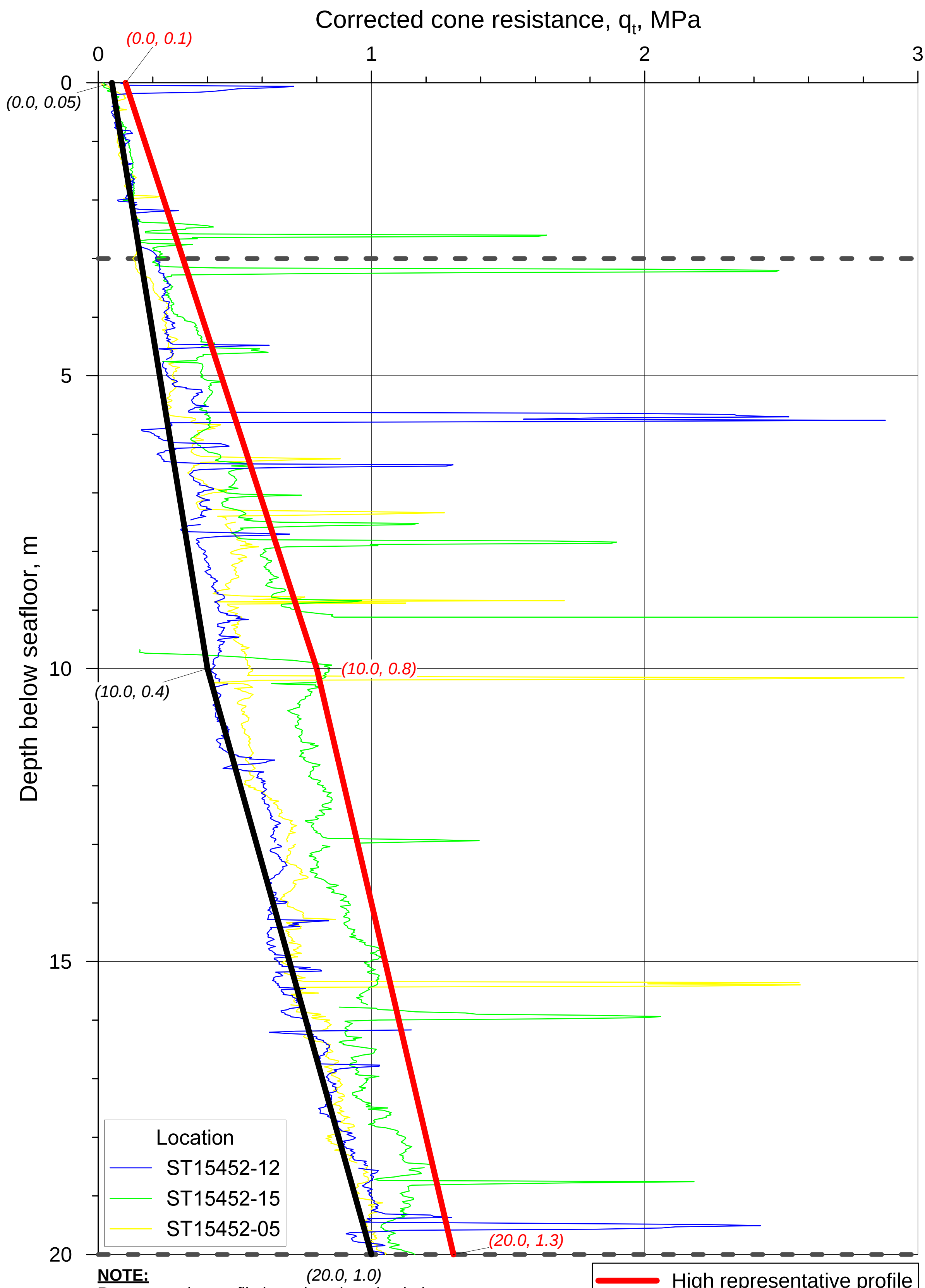

NOTE:
Representative profile based engineering judgement.

Label: *(depth, value)*

Date/Rev.: 2015-01-21/01

ST15452 Flemish Pass Geotechnical Investigation	Document No. 20140857-02-R	
Corrected cone resistance versus depth Field Centre, 0-20 m depth	Figure No. F6.2.4	
	Date 2016-04-03	Drawn by VBS
	NGI	

P:\2014\08\20140857\Leveransedokumenter\Rapport\20140857-02-R Data interpretation and evaluation\Figures\Section F\Figure F_06_02_04, qt versus depth-Fieldcentre 0-20m.grf

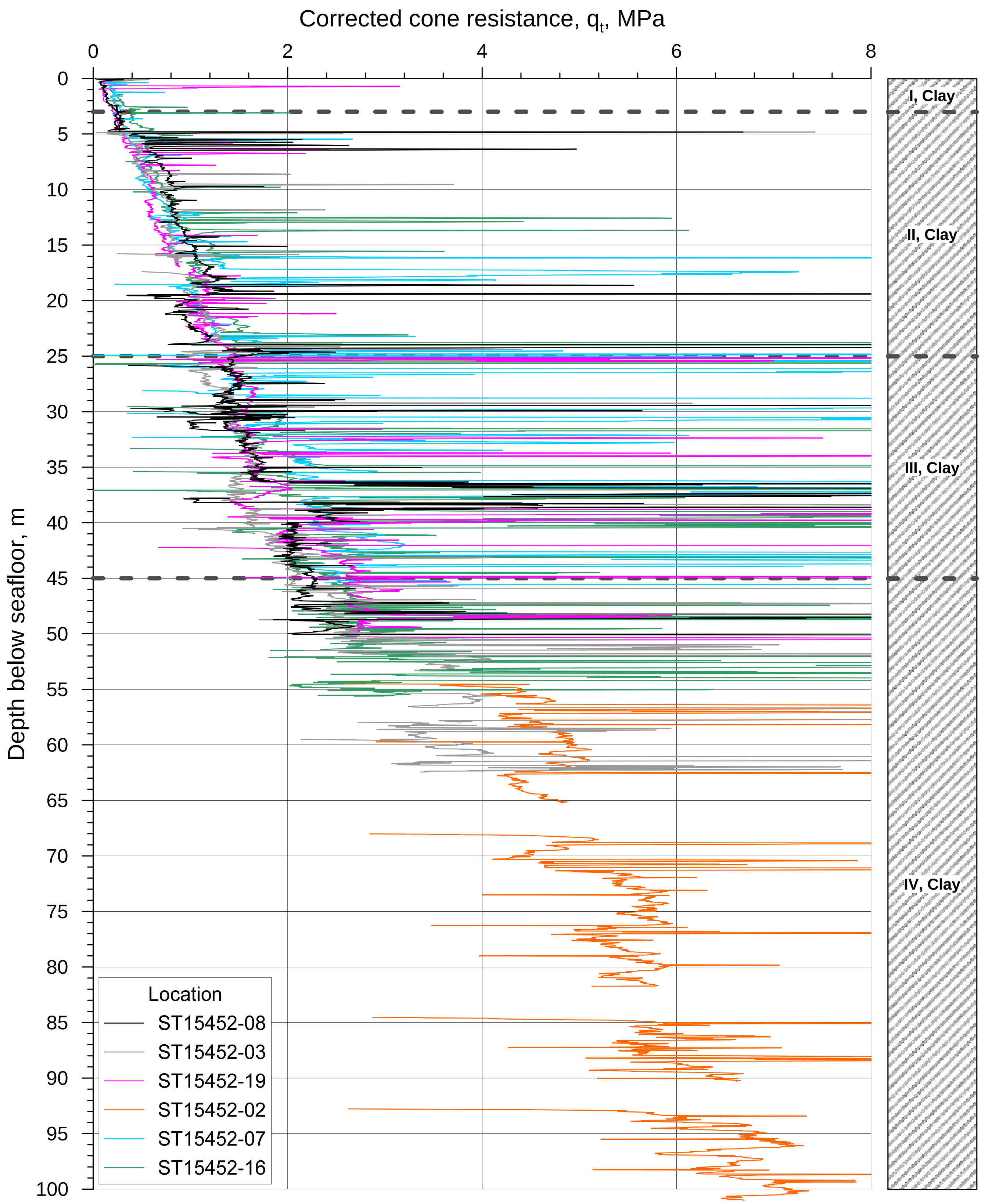

P:\2014\08\20140857\Leveransedokumenter\Rapport\20140857-02-R Data interpretation and evaluation\Figures\Section F\Figure F_06_02_05, qt versus depth-West.grf

Date/Rev.: 2015-01-21/01

ST15452 Flemish Pass Geotechnical Investigation	Document No. 20140857-02-R
Corrected cone resistance versus depth West Slope	Figure No. F6.2.5
	Date 2016-04-03 / Drawn by VBS
	NGI

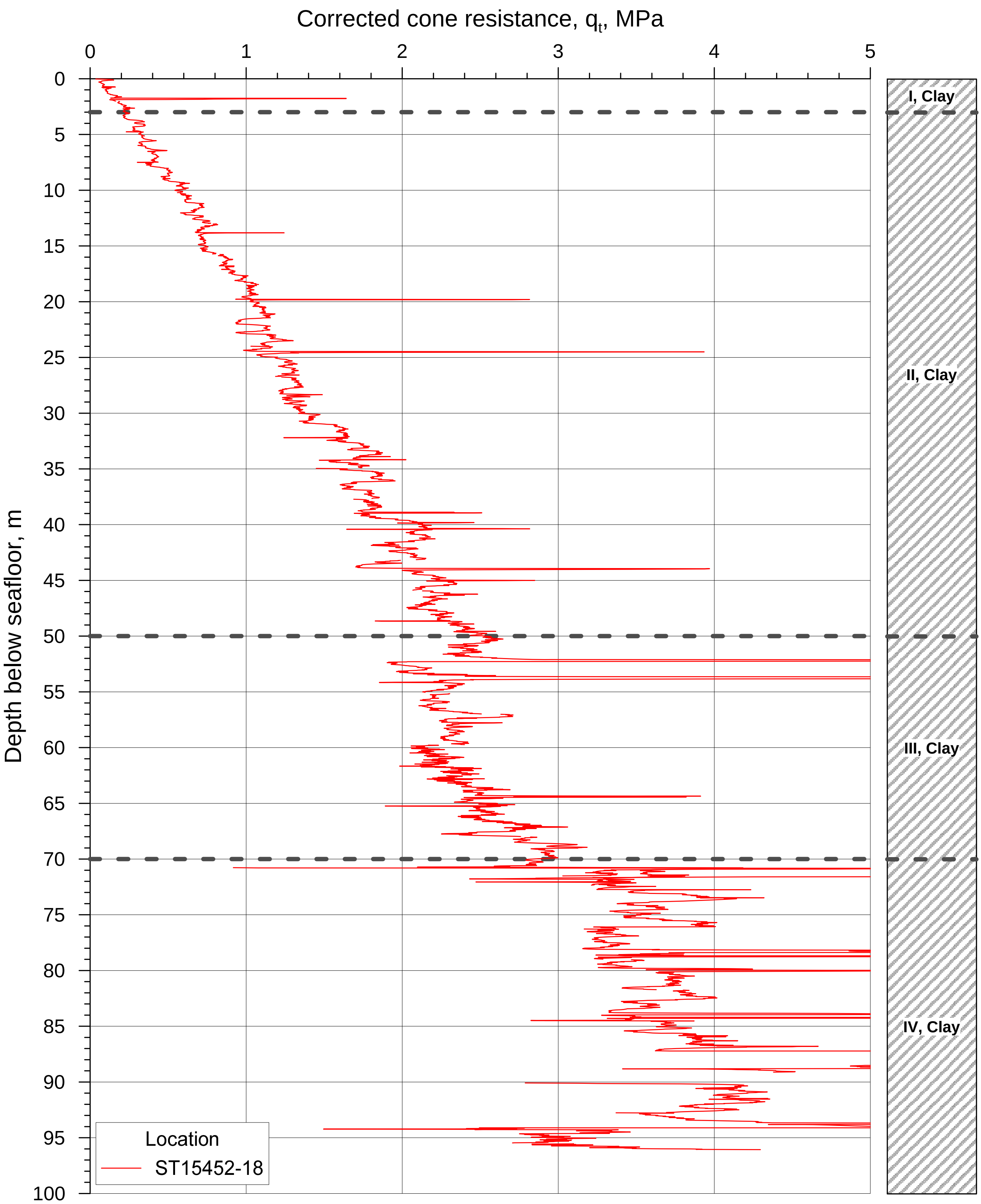

P:\2014\08\20140857\Leveransedokumenter\Rapport\20140857-02-R Data interpretation and evaluation\Figures\Section F\Figure F_06_02_06, qt versus depth-East.grf

Date/Rev.: 2015-01-21/01

ST15452 Flemish Pass Geotechnical Investigation	Document No. 20140857-02-R
Corrected cone resistance versus depth East Slope	Figure No. F6.2.6
	Date 2016-04-03 / Drawn by VBS

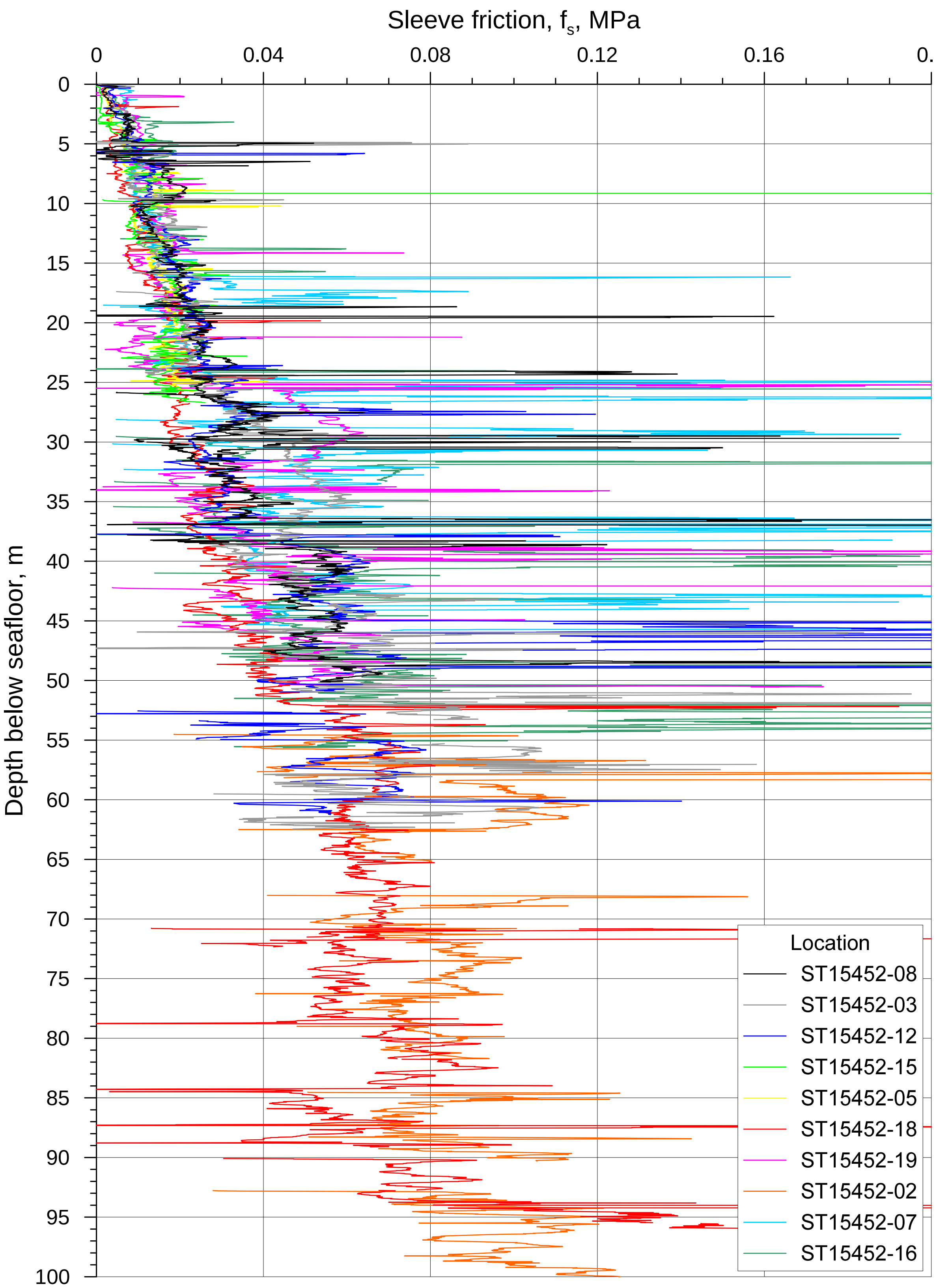

P:\2014\08\20140857\Leveransedokumenter\Rapport\20140857-02-R Data interpretation and evaluation\Figures\Section F\Figure F_06_02_07_fs versus depth.grf

Date/Rev.: 2015-01-21/01

ST15452 Flemish Pass Geotechnical Investigation	Document No. 20140857-02-R
Sleeve friction versus depth All locations	Figure No. F6.2.7
	Date 2016-04-04 / Drawn by VBS

NGI

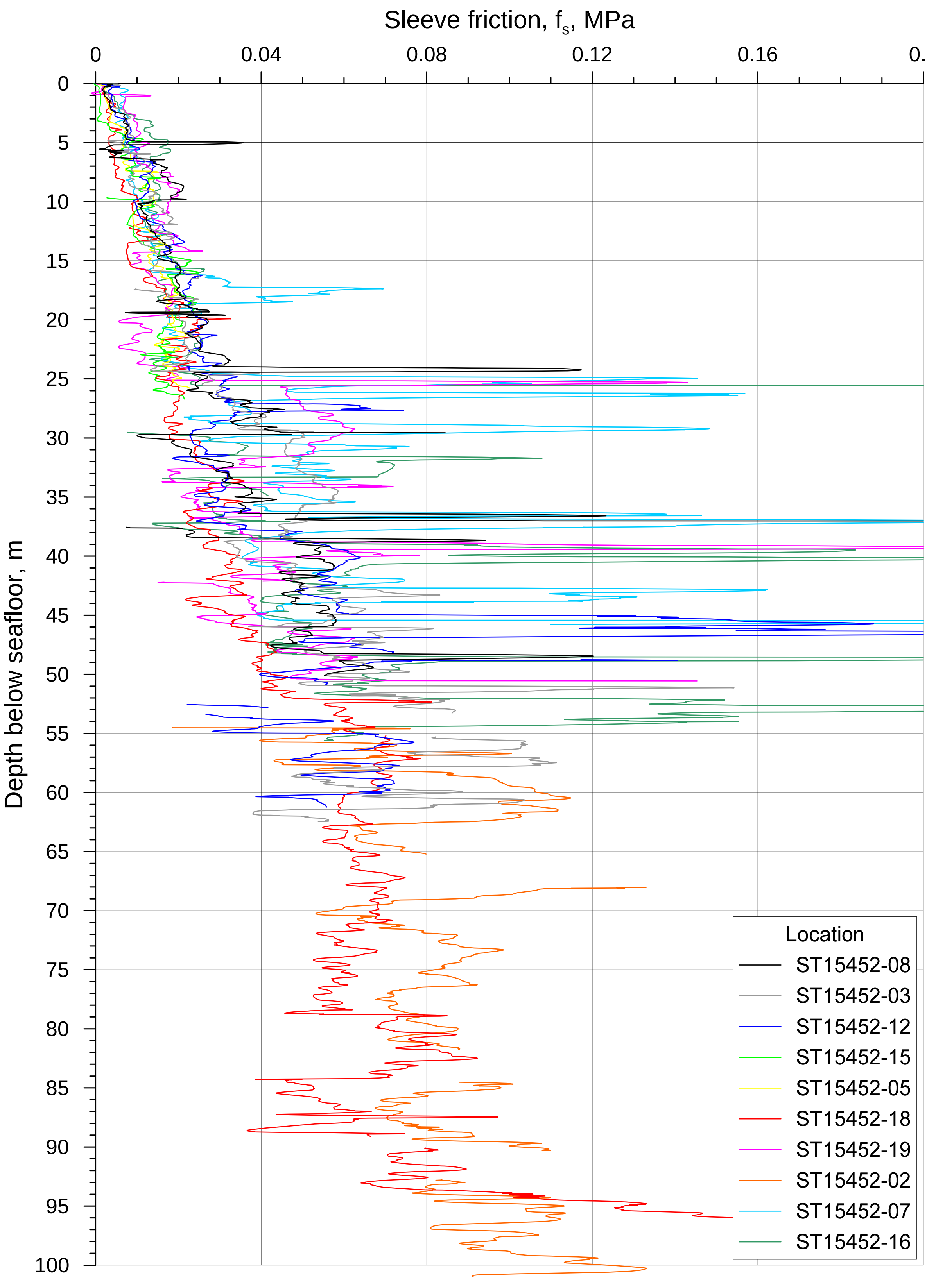

Data has been filtered by applying a Gausian moving average over a depth range of 0.5 m

Date/Rev.: 2015-01-21/01

ST15452 Flemish Pass Geotechnical Investigation	Document No. 20140857-02-R
Sleeve friction versus depth All locations Data has been filtered for clarity. Allways refer to the full dataset	Figure No. F6.2.8
	Date 2016-04-04 / Drawn by VBS

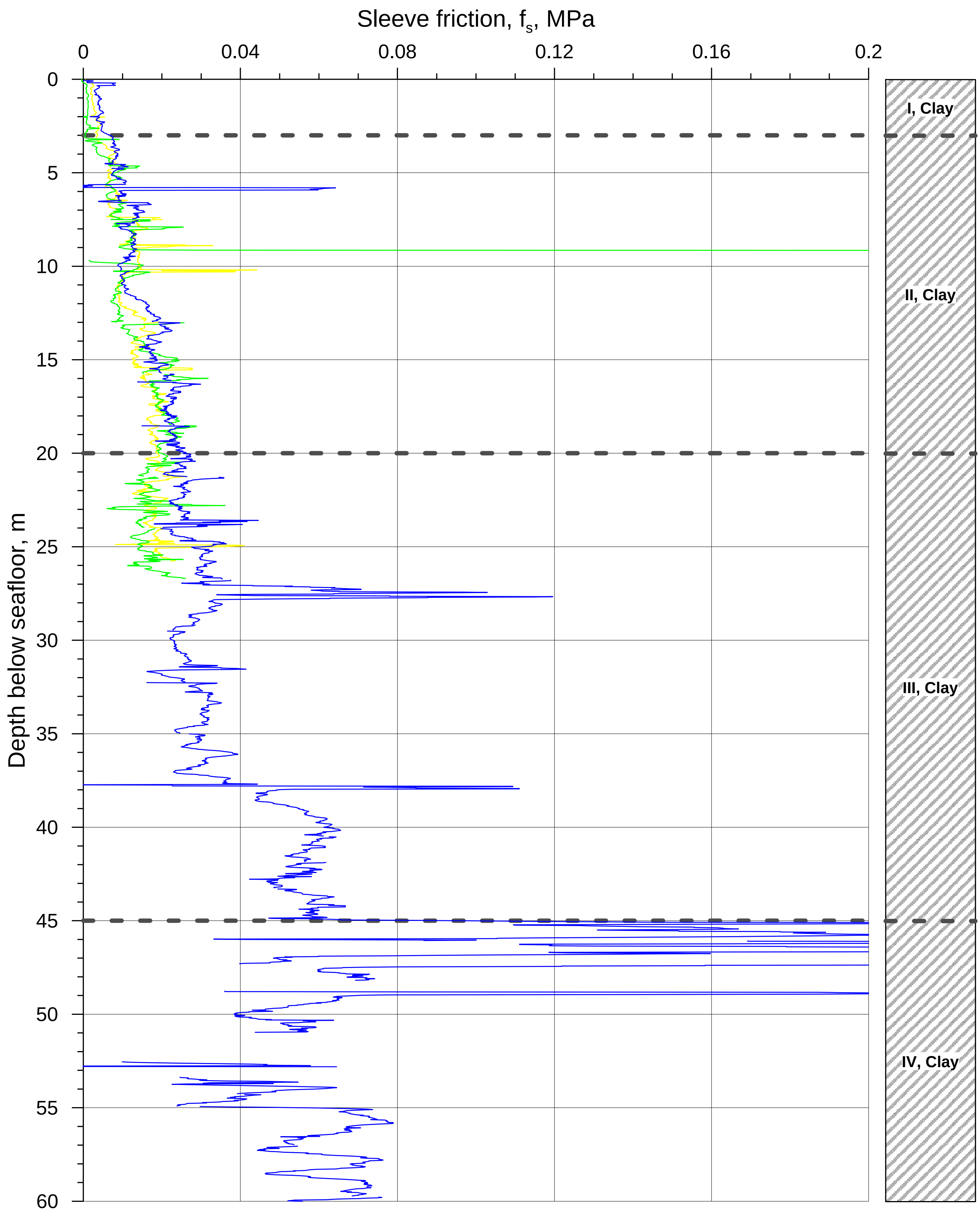

ST15452 Flemish Pass Geotechnical Investigation	Document No. 20140857-02-R
Sleeve friction versus depth Field Centre	Figure No. F6.2.9
	Date 2016-04-04 / Drawn by VBS

NGI

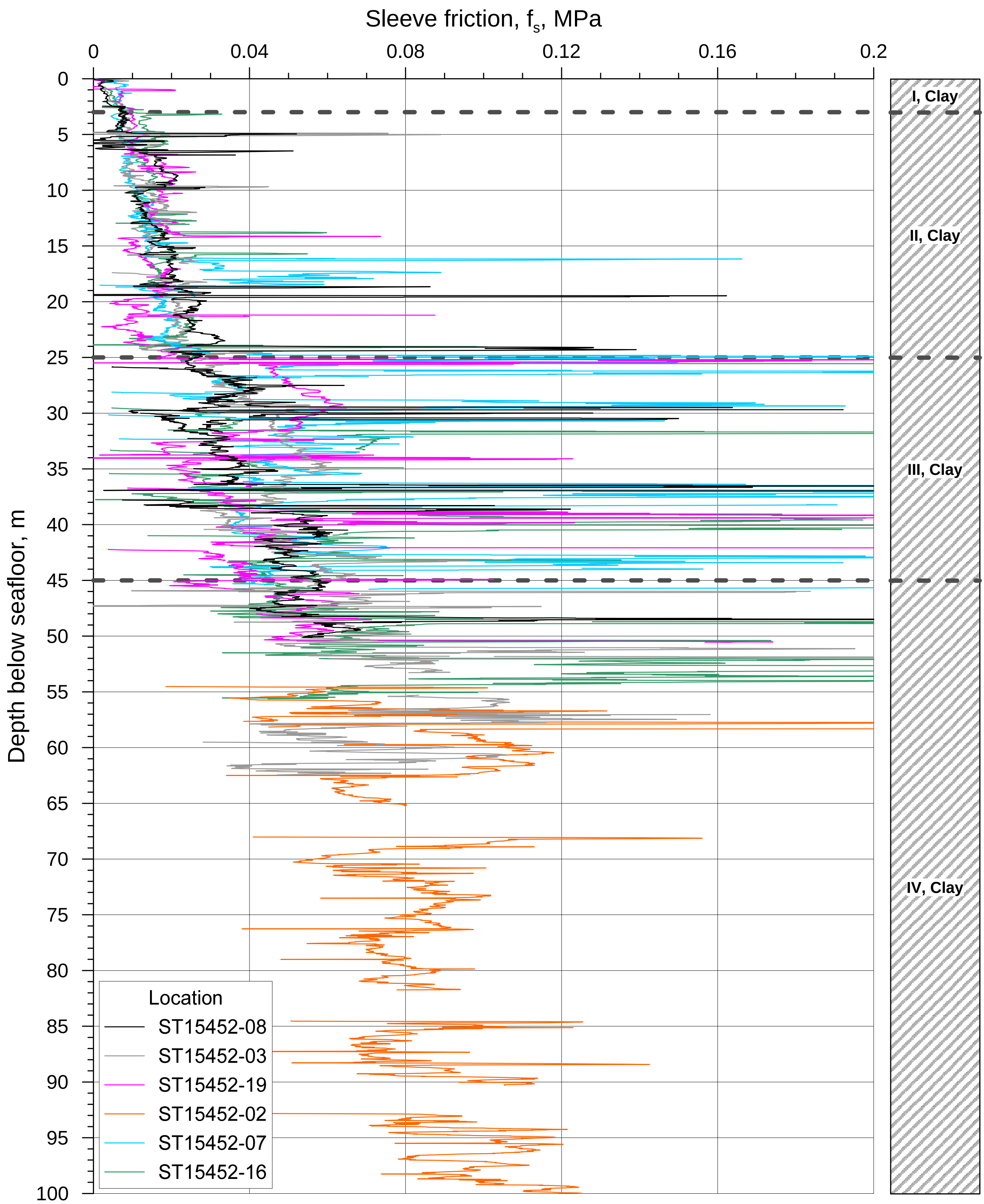

P:\2014\08\20140857\Leveransedokumenter\Rapport\20140857-02-R Data interpretation and evaluation\Figures\Section F\Figure F_06_02_10, fs versus depth-West.grf

Date/Rev.: 2015-01-21/01

ST15452 Flemish Pass Geotechnical Investigation	Document No. 20140857-02-R
Sleeve friction versus depth West Slope	Figure No. F6.2.10
	Date 2016-04-04 / Drawn by VBS

NGI

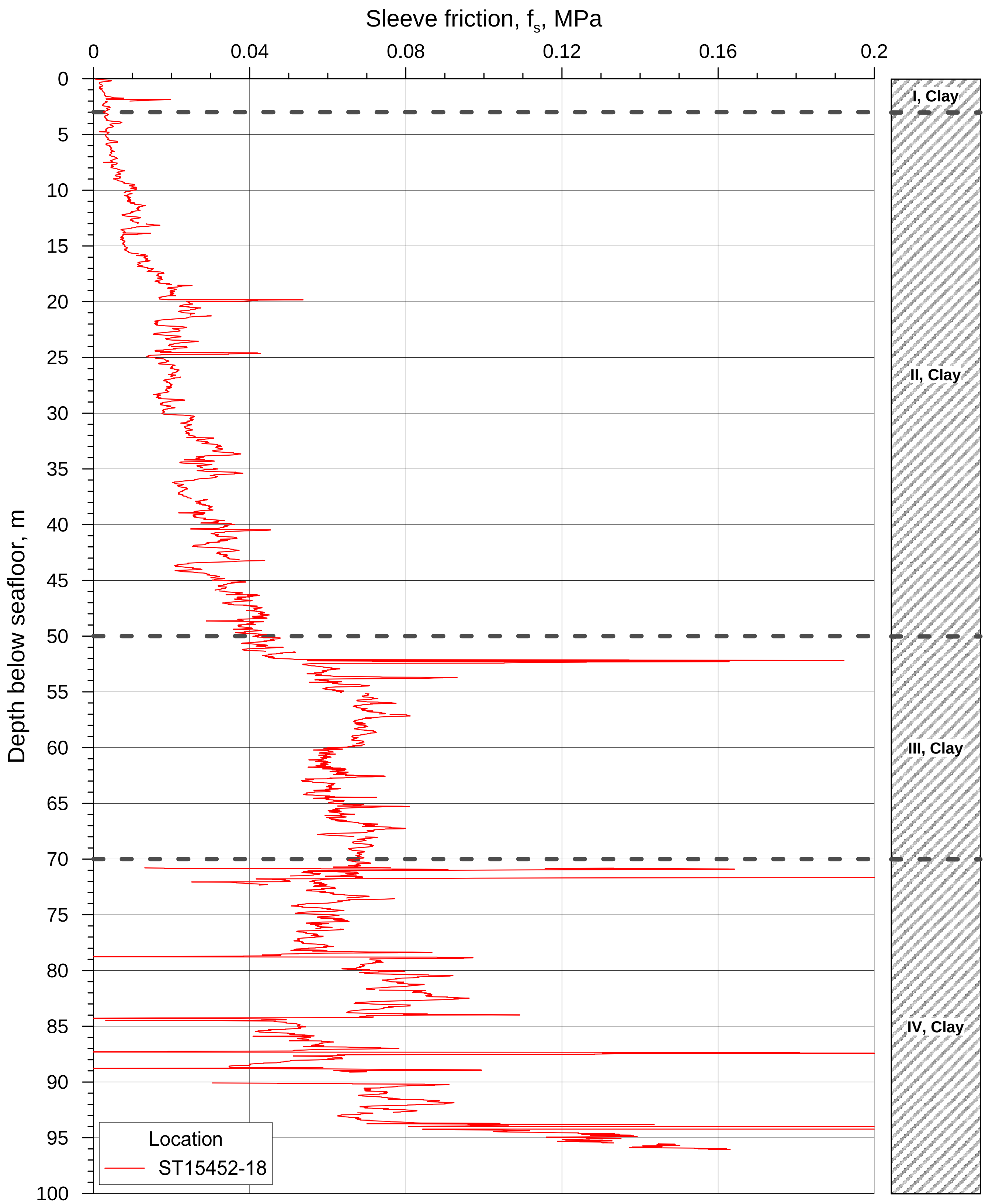

Date/Rev.: 2015-01-21/01

ST15452 Flemish Pass Geotechnical Investigation	Document No. 20140857-02-R
Sleeve friction versus depth East Slope	Figure No. F6.2.11
	Date 2016-04-04 / Drawn by VBS
	NGI

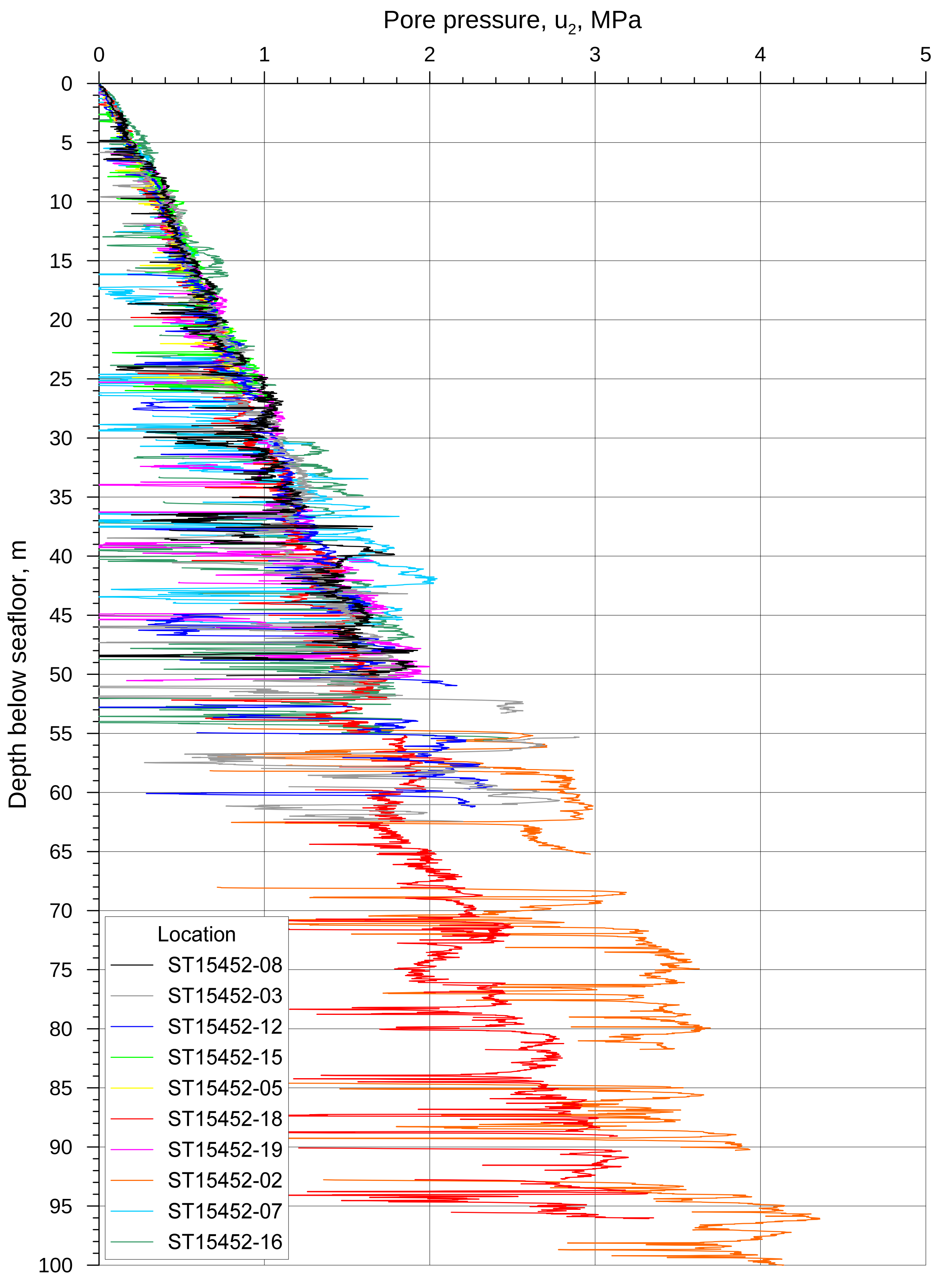

P:\2014\08\20140857\Leveransedokumenter\Rapport\20140857-02-R Data interpretation and evaluation\Figures\Section F\Figure F_06_02_12, u2 versus depth.grf

Date/Rev.: 2015-01-21/01

ST15452 Flemish Pass Geotechnical Investigation	Document No. 20140857-02-R
Pore pressure versus depth All locations	Figure No. F6.2.12
	Date 2016-04-03 / Drawn by VBS
	NGI

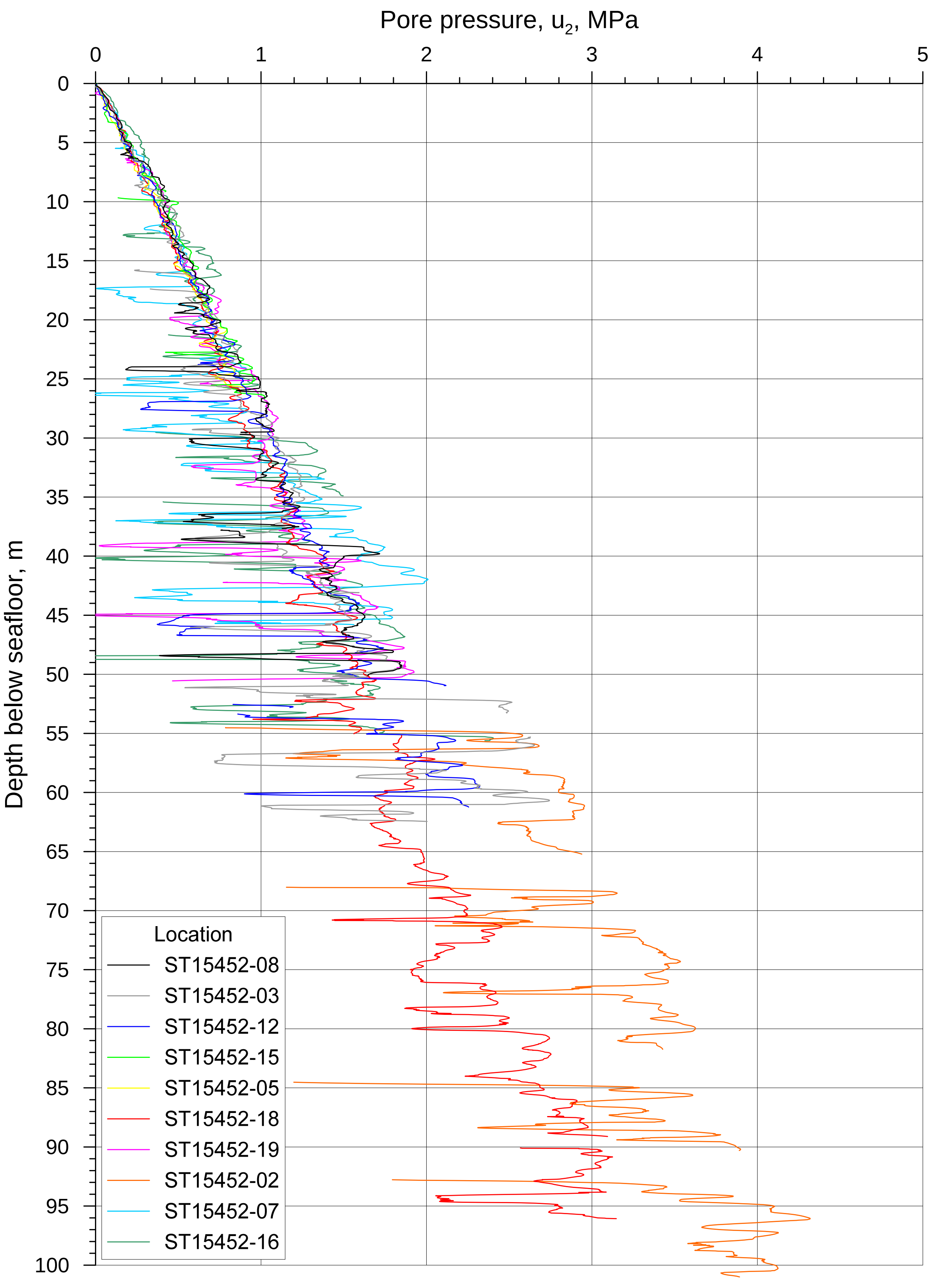

Data has been filtered by applying a Gausian moving average over a depth range of 0.5 m

Date/Rev.: 2015-01-21/01

ST15452 Flemish Pass Geotechnical Investigation	Document No. 20140857-02-R	
Pore pressure versus depth All locations Data has been filtered for clarity. Allways refer to the full dataset	Figure No. F6.2.13	
	Date 2016-04-03	Drawn by VBS

P:\2014\08\20140857\Leveransedokumenter\Rapport\20140857-02-R Data interpretation and evaluation\Figures\Section F\Figure F_06_02_13, u2 versus depth-Filtered.grf

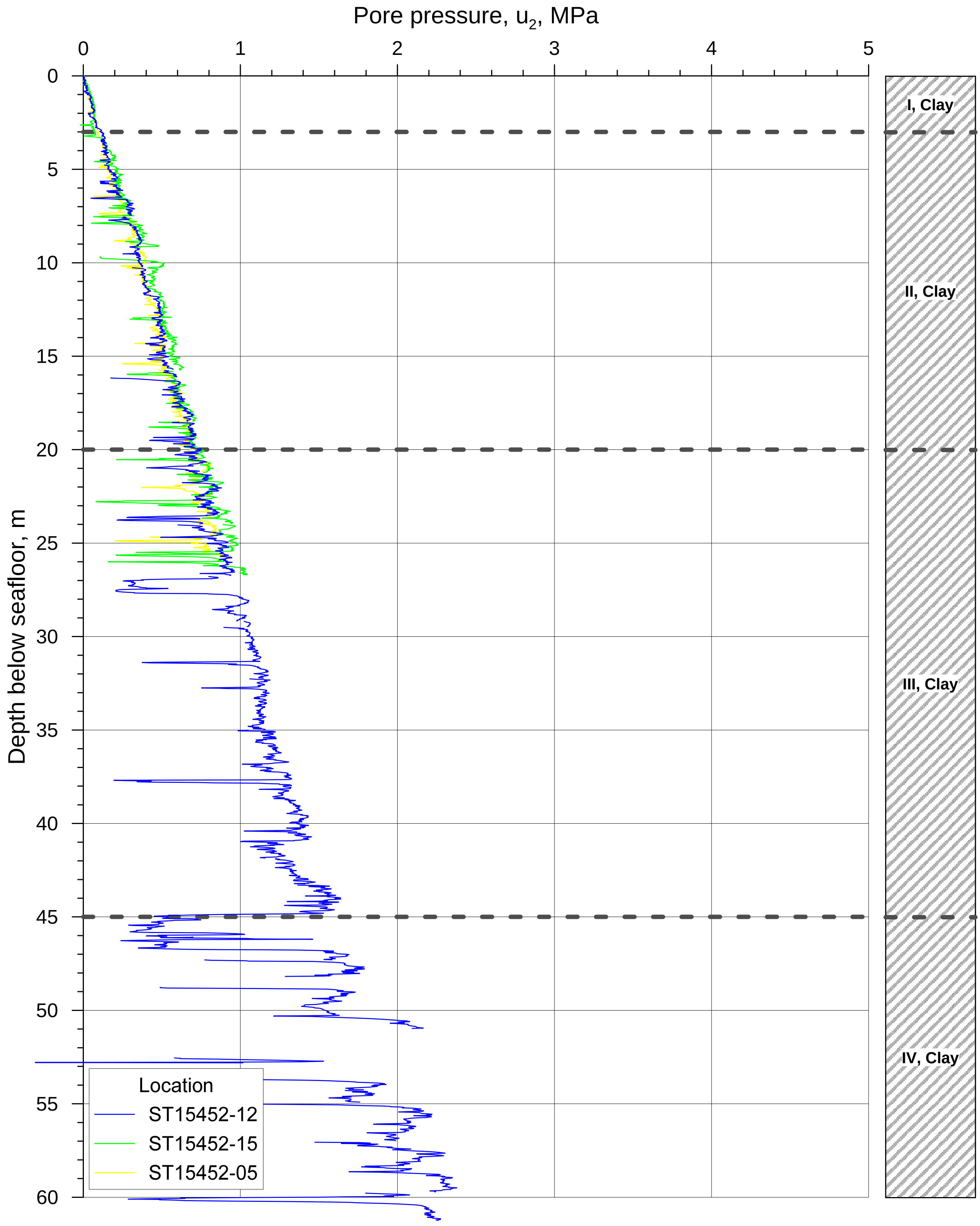

P:\2014\08\20140857\Leveransedokumenter\Rapport\20140857-02-R Data interpretation and evaluation\Figures\Section F\Figure F_06_02_14, u2 versus depth-Fieldcentre.grf

Date/Rev.: 2015-01-21/01

ST15452 Flemish Pass Geotechnical Investigation

Pore pressure versus depth
Field Centre

Document No. 20140857-02-R	
Figure No. F6.2.14	
Date 2016-05-23	Drawn by VBS

NGI

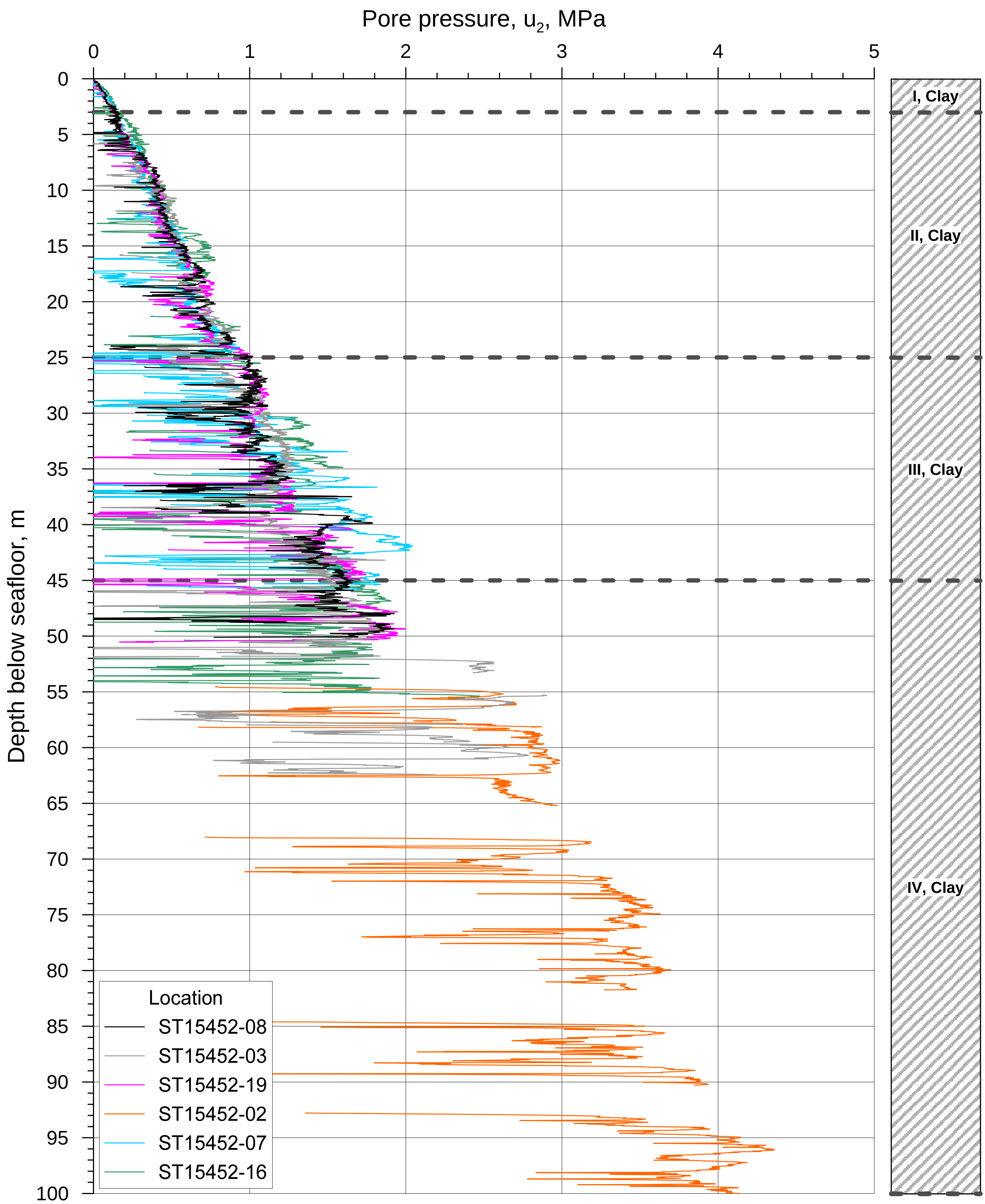

P:\2014\08\20140857\Leveransedokumenter\Rapport\20140857-02-R Data interpretation and evaluation\Figures\Section F\Figure F_06_02_15, u2 versus depth-West.grf

Date/Rev.: 2015-01-21/01

ST15452 Flemish Pass Geotechnical Investigation	Document No. 20140857-02-R
Pore pressure versus depth West Slope	Figure No. F6.2.15
	Date 2016-05-23 / Drawn by VBS
	NGI

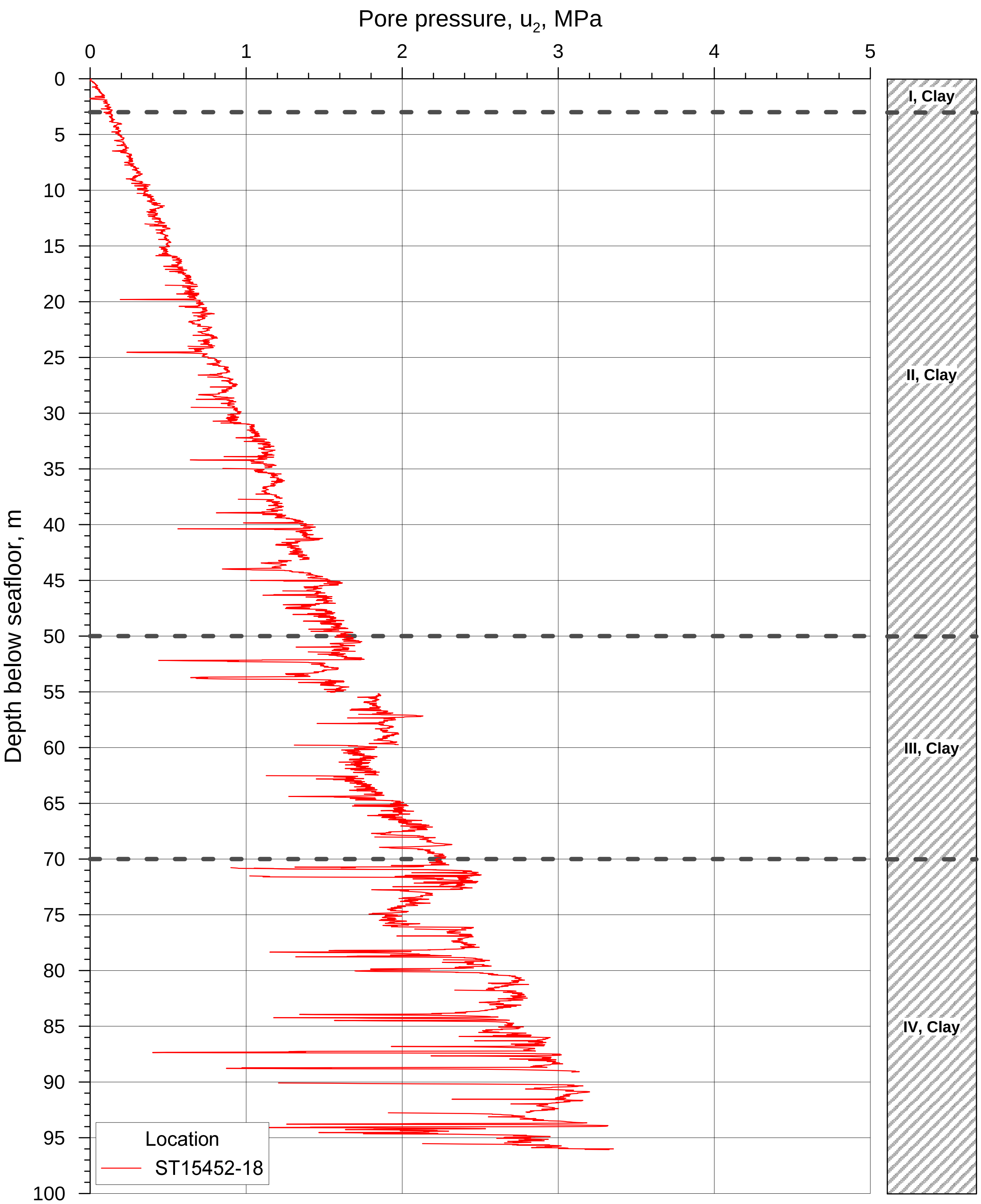

P:\2014\08\20140857\Leveransedokumenter\Rapport\20140857-02-R Data interpretation and evaluation\Figures\Section F\Figure F_06_02_16, u2 versus depth-East.grf

Date/Rev.: 2015-01-21/01

ST15452 Flemish Pass Geotechnical Investigation	Document No. 20140857-02-R	
Pore pressure versus depth East Slope	Figure No. F6.2.16	
	Date 2016-05-23	Drawn by VBS
	NGI	

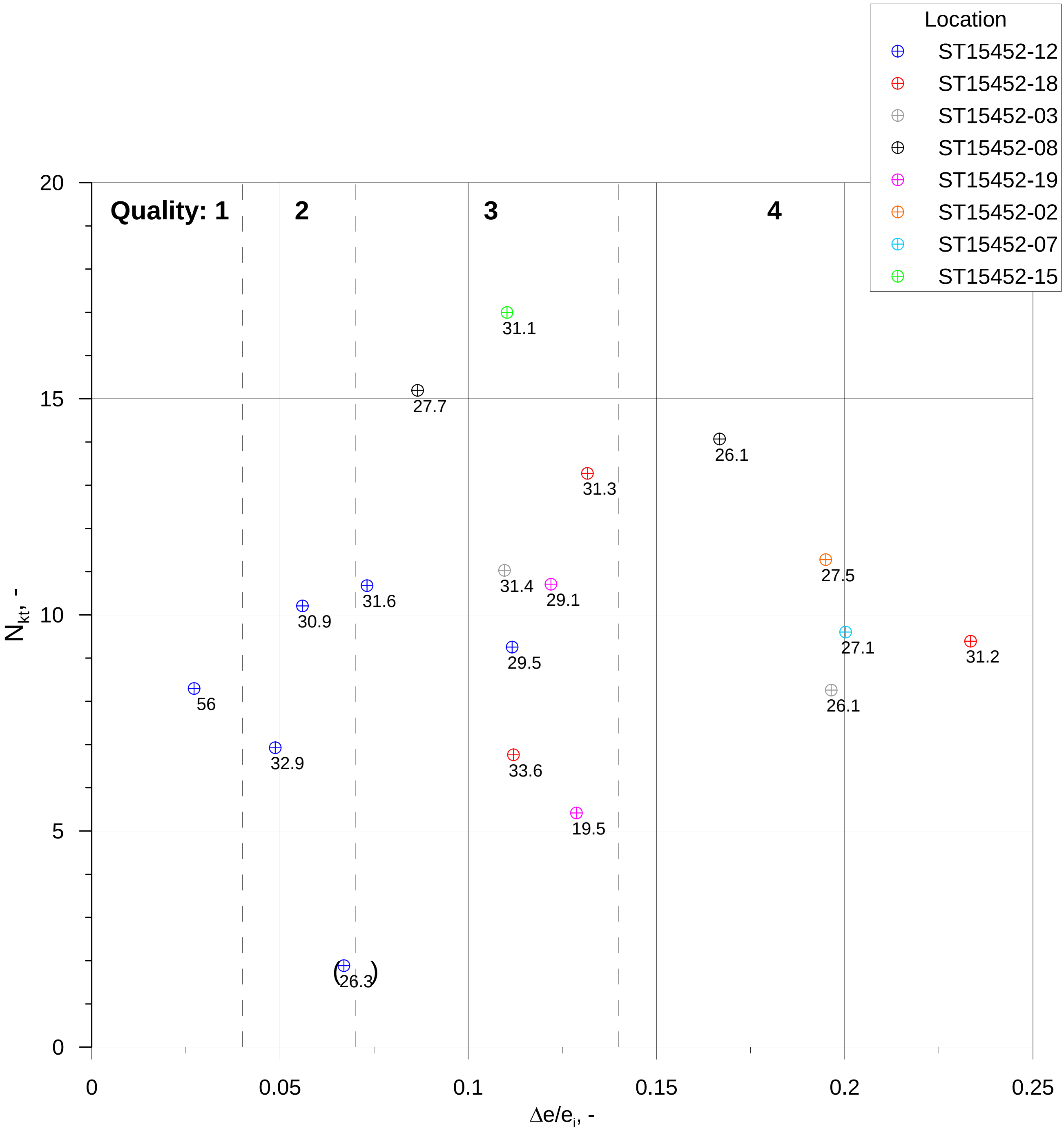

NOTE:
Values plotted are the cone factors giving the best match between q_t and an undrained triaxial CAUC strength (s_{uC}).

Point-Label (Water content)

Date/Rev.: 2015-01-21/01

ST15452 Flemish Pass Geotechnical Investigation

N_{kt} versus $\Delta e/e_0$

Document No.	20140857-02-R
Figure No.	F6.3.1
Date	2016-04-03
Drawn by	VBS

P:\2014\08\20140857\Leveransedokumenter\Rapport\20140857-02-R Data interpretation and evaluation\Figures\Section F\Figure F_06_03_01, Nkt versus e_e0.grf

Location

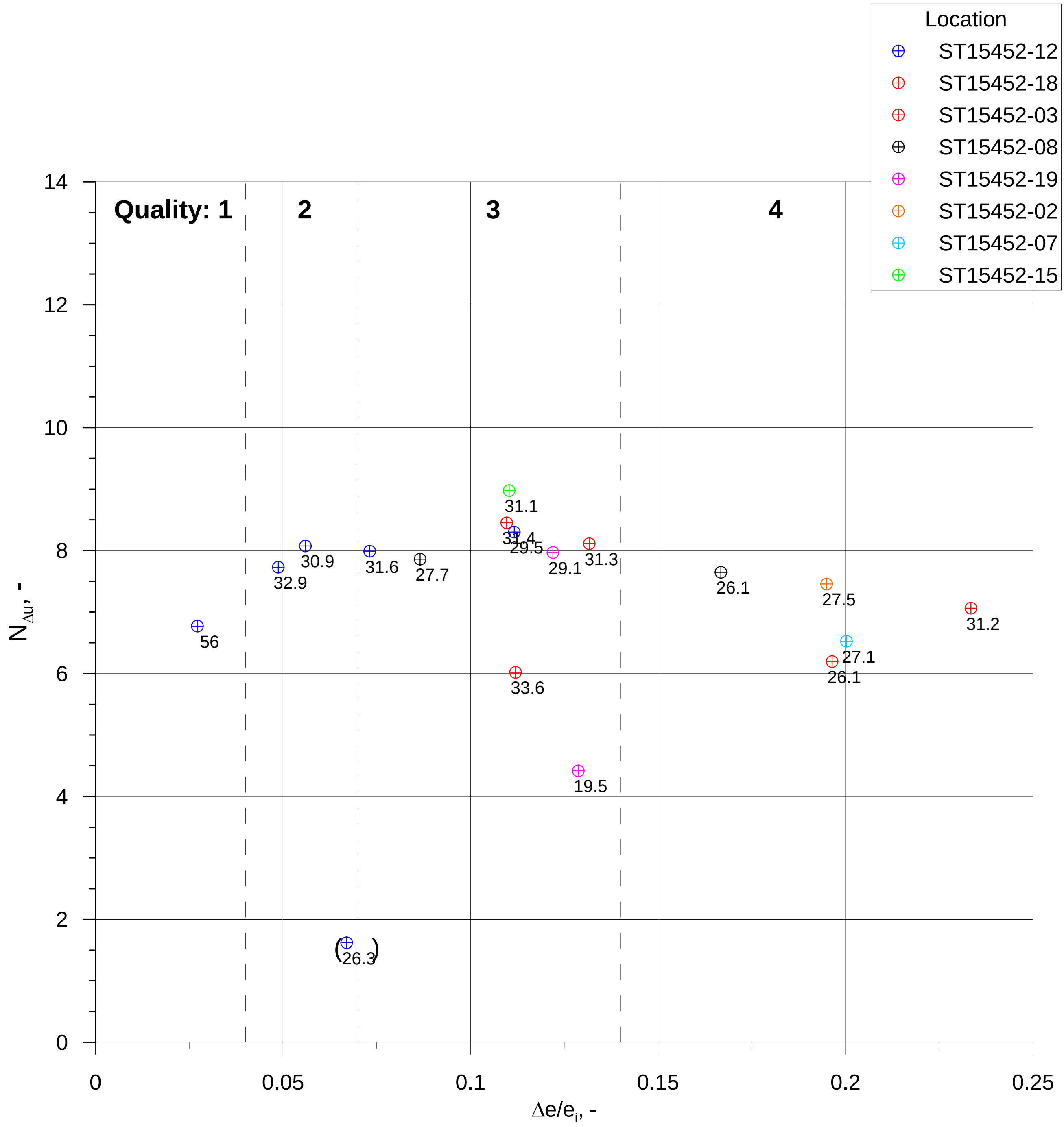

NOTE:
Values plotted are the cone factors giving the best match between u_2 and an undrained triaxial CAUC strength (s_{uC}).

Point-Label (water content)

Date/Rev.: 2015-01-21/01

ST15452 Flemish Pass Geotechnical Investigation	Document No. 20140857-02-R	
$N_{\Delta u}$ versus $\Delta e/e_0$	Figure No. F6.3.2	
	Date 2016-04-04	Drawn by VBS

NGI

P:\2014\08\20140857\Leveransedokumenter\Rapport\20140857-02-R Data interpretation and evaluation\Figures\Section F\Figure F_06_03_02, Ndu versus e_e0.grf

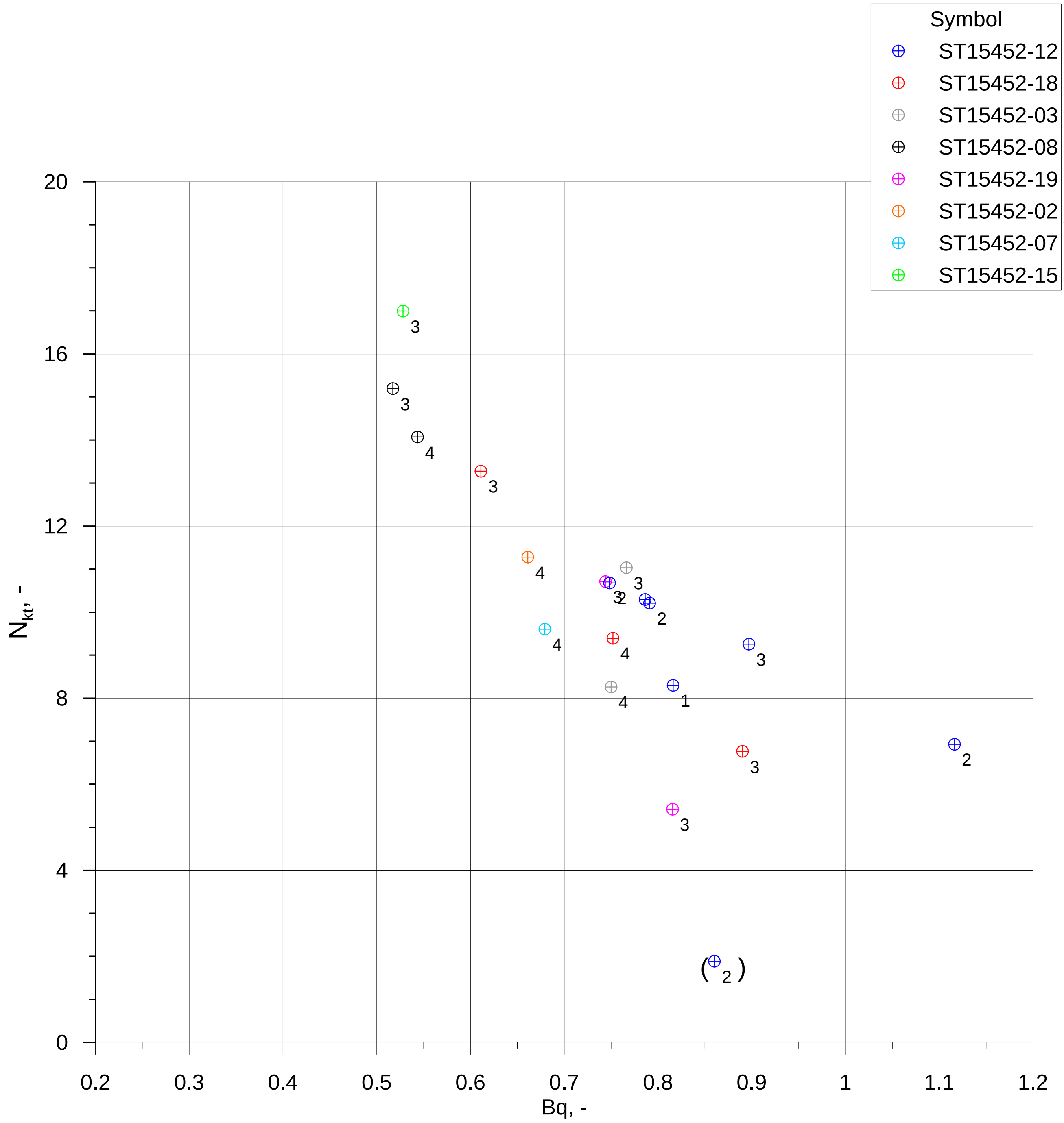

NOTE:
Values plotted are the cone factors giving the best match between q_t and an undrained triaxial CAUC strength (s_{uC}).

Point-Label (sample quality)

Date/Rev.: 2015-01-21/01

ST15452 Flemish Pass Geotechnical Investigation	Document No. 20140857-02-R
N_{kt} versus B_q	Figure No. F6.3.3
	Date 2016-04-03 / Drawn by VBS

NGI

P:\2014\08\20140857\Leveransedokumenter\Rapport\20140857-02-R Data interpretation and evaluation\Figures\Section F\Figure F_06_03_03, Nkt versus Bq.grf

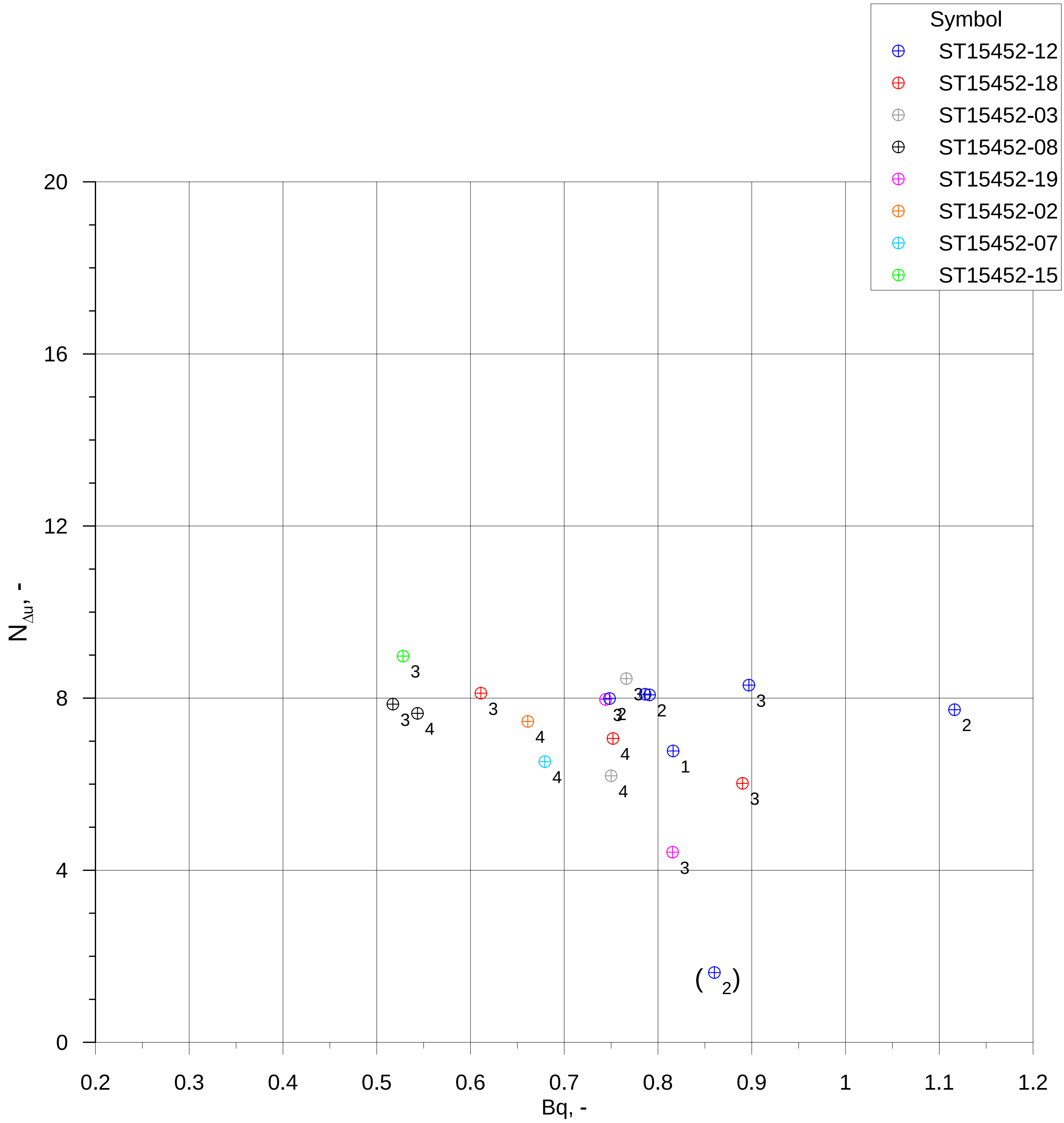

NOTE:
Values plotted are the cone factors giving the best match between u_2 and an undrained triaxial CAUC strength (s_{uC}).

Point-Label (sample quality)

Date/Rev.: 2015-01-21/01

ST15452 Flemish Pass Geotechnical Investigation

$N_{\Delta u}$ versus B_q

Document No.	20140857-02-R
Figure No.	F6.3.4
Date	2016-04-03
Drawn by	VBS

NGI

P:\2014\08\20140857\Leveransedokumenter\Rapport\20140857-02-R Data interpretation and evaluation\Figures\Section F\Figure F_06_03_04, Ndu versus Bq.grf

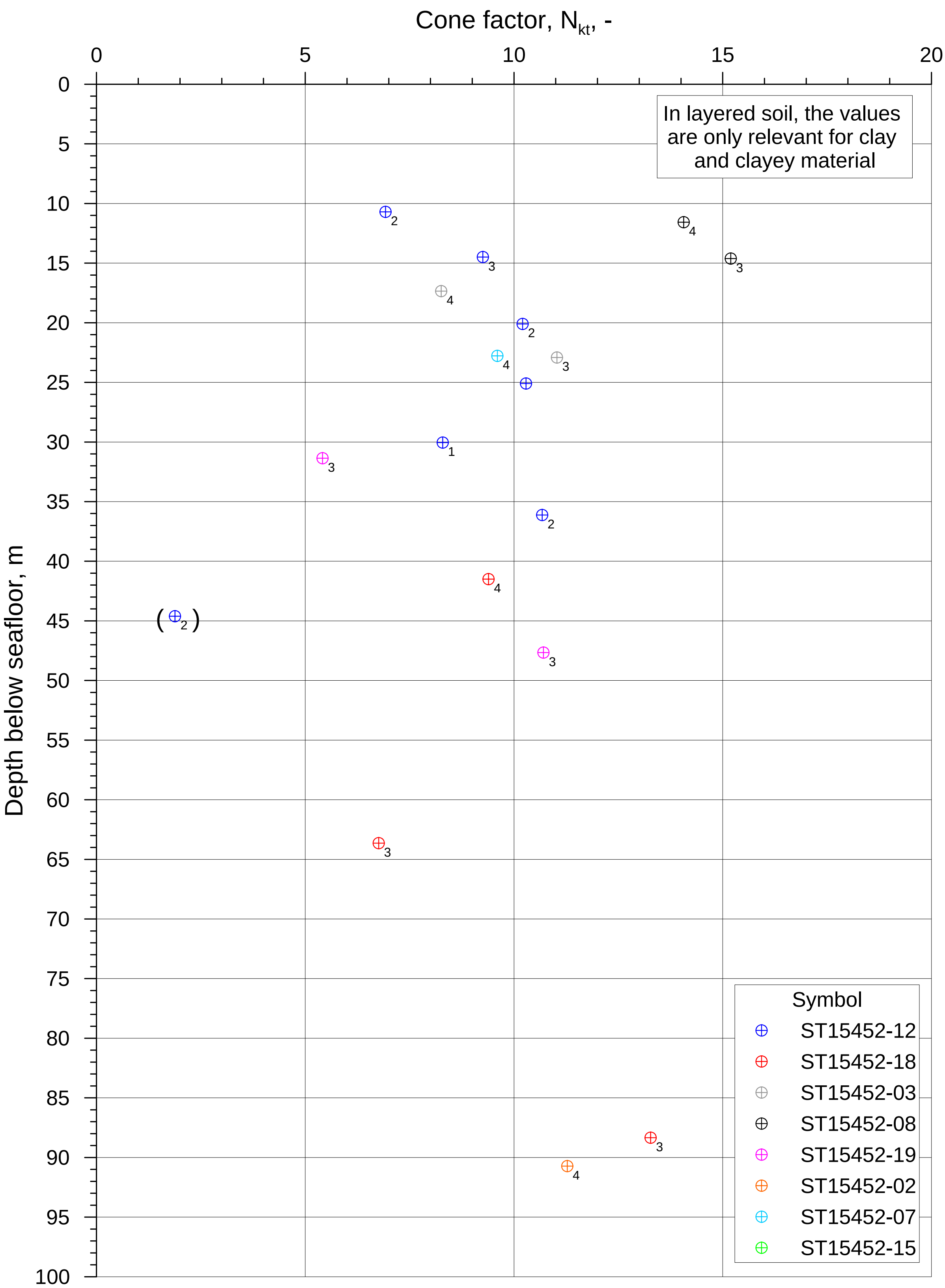

NOTE:
Values plotted are the cone factors giving the best match between q_{t2} and an undrained triaxial CAUC strength (s_{uC}).

ST15452 Flemish Pass Geotechnical Investigation

N_{kt} versus depth

Document No.	20140857-02-R
Figure No.	F6.3.5
Date	2016-04-03
Drawn by	VBS

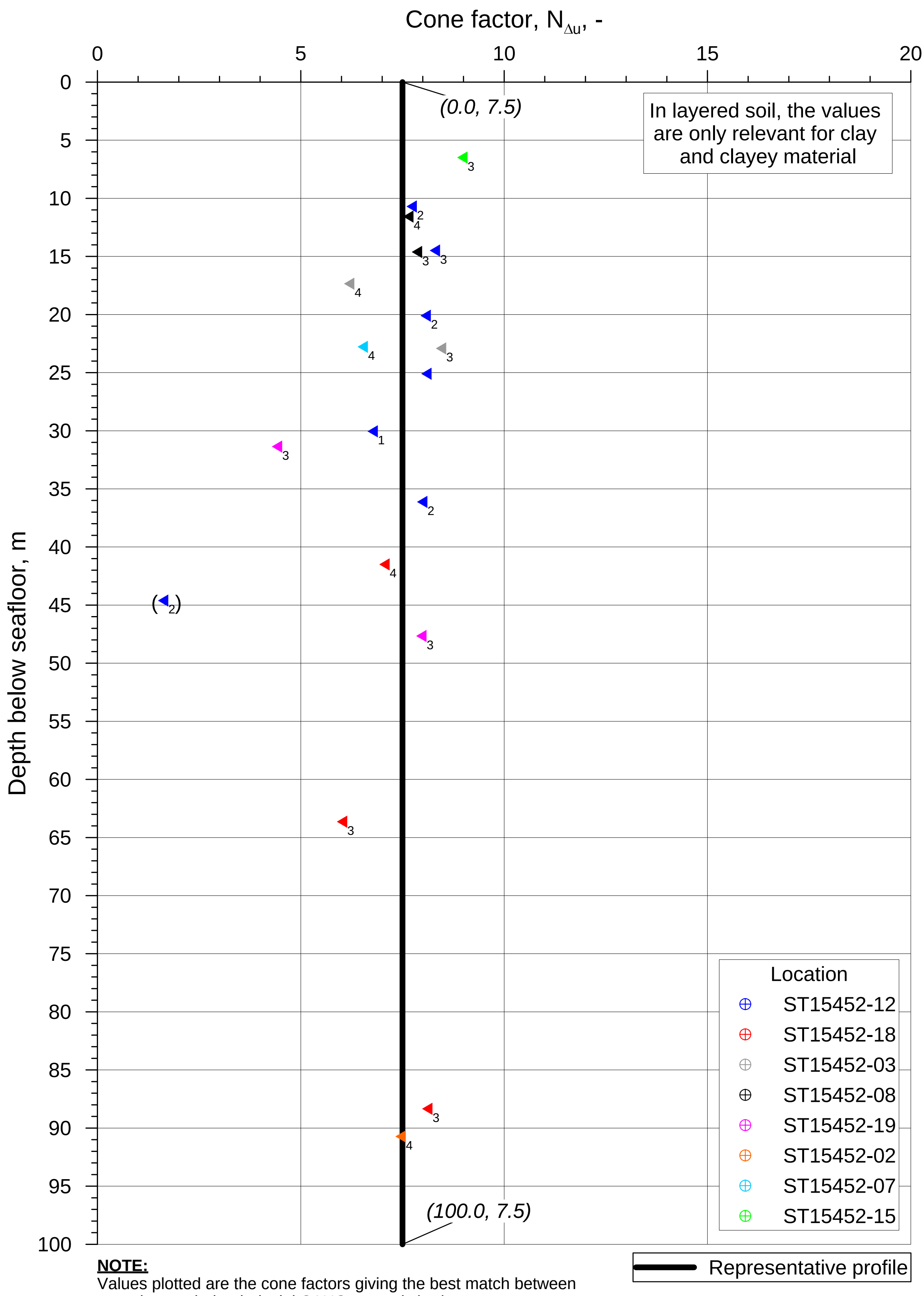

NOTE:
Values plotted are the cone factors giving the best match between u_2 and an undrained triaxial CAUC strength (s_{uC}).

Profile-Label: *(depth, value)* *Point-Label (sample quality)*

Date/Rev.: 2015-01-21/01

ST15452 Flemish Pass Geotechnical Investigation

$N_{\Delta u}$ versus depth

Document No.	
20140857-02-R	
Figure No. F6.3.6	
Date 2016-04-03	Drawn by VBS

NGI

P:\2014\08\20140857\Leveransedokumenter\Rapport\20140857-02-R Data interpretation and evaluation\Figures\Section F\Figure F_06_03_06, Ndu versus depth.grf

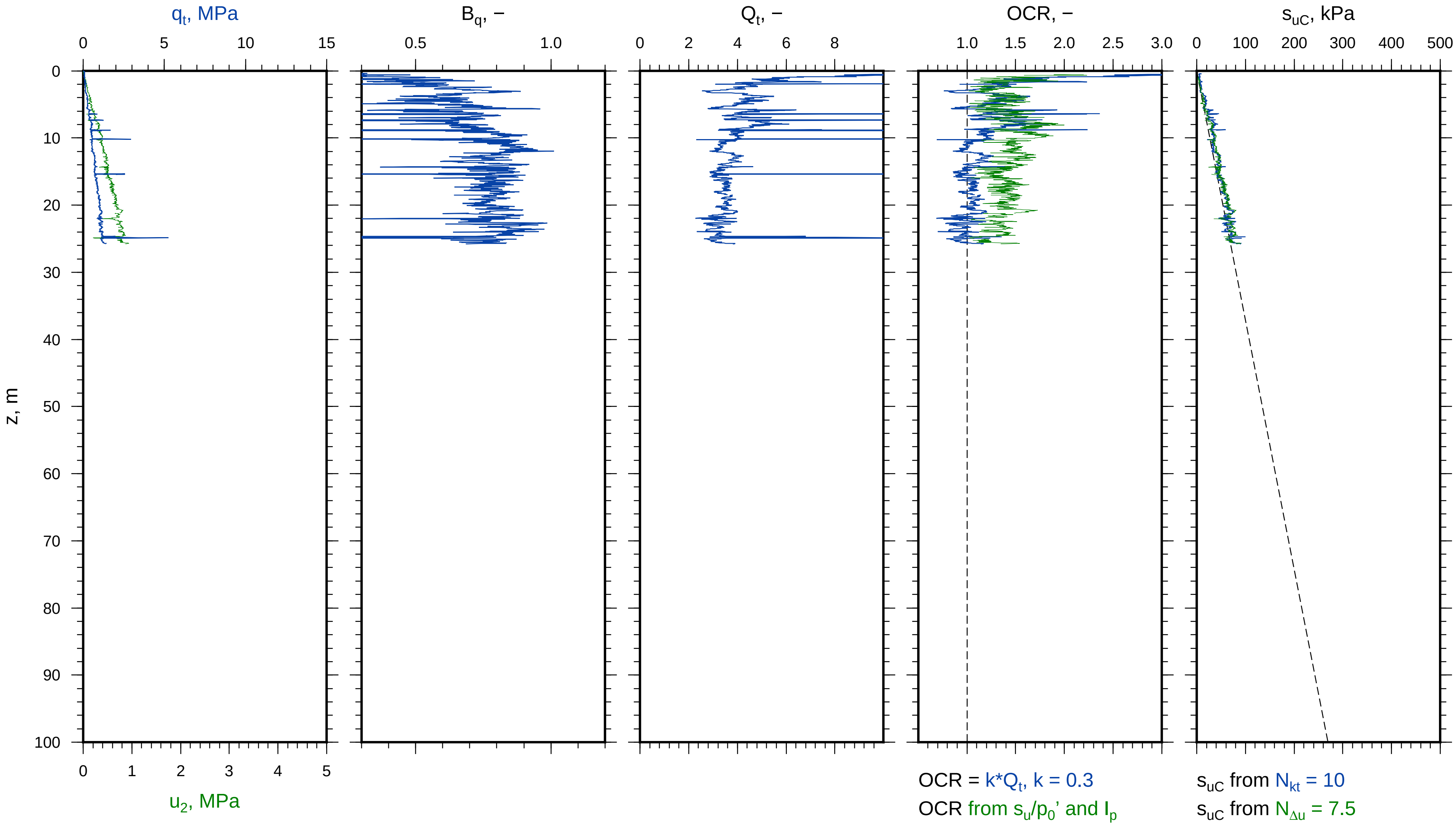

trepak:/grouphome/gmtapp/20140857_Flemish/CPT/Composites/CollatedCPTUdataFiltered/01−ST15452−05.ps

ST15452 Flemish Pass Geotechnical Investigation	Document No. 20140857−02−R	
	Figure No. F6.3.7	
CPTU data and derived parameters CPTU data: ST15452−05	Date 2016−04−05	Drawn by VBS/MVa
	NGI	

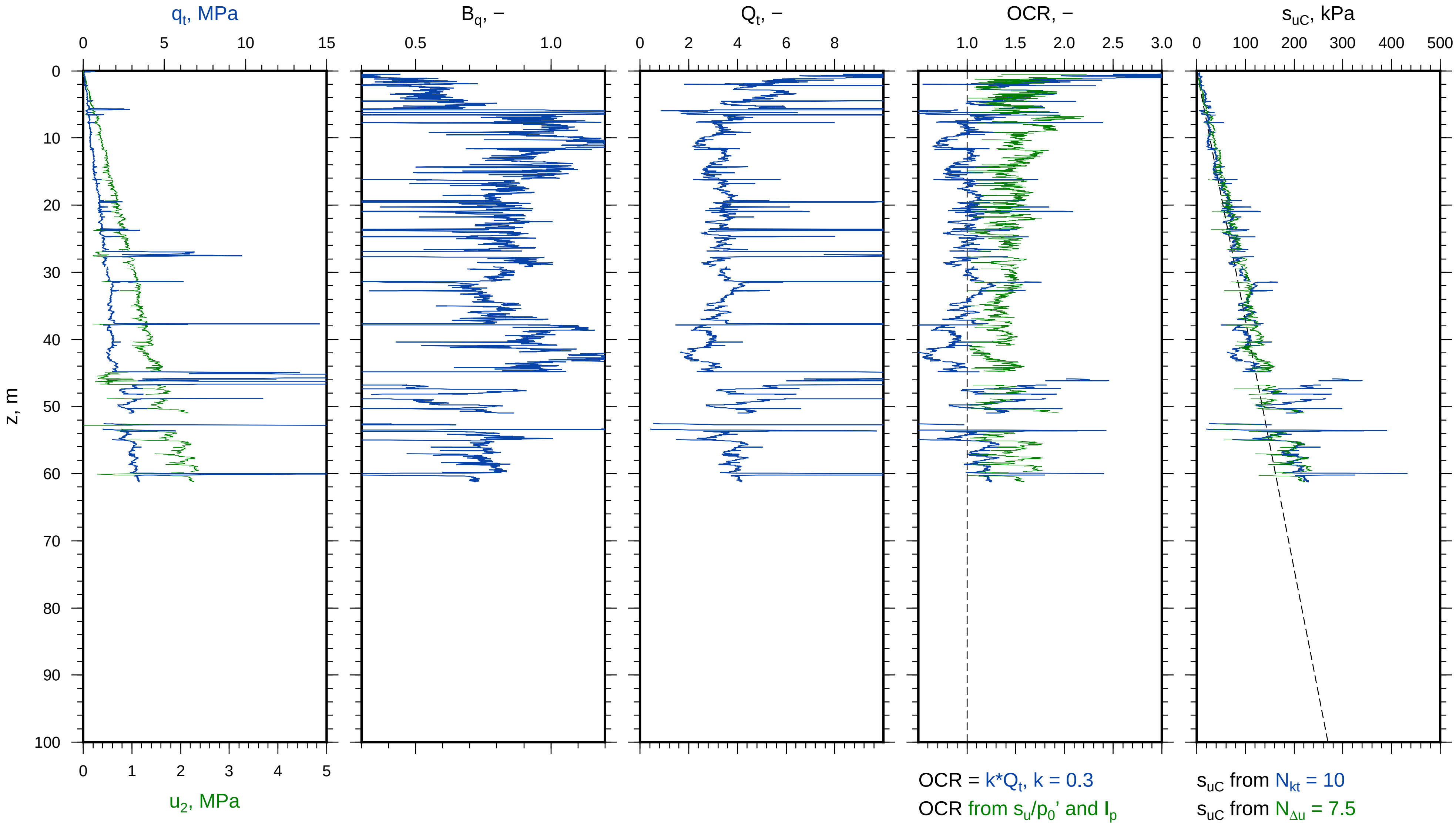

OCR = k^*Q_t, k = 0.3
OCR from s_u/p_0' and I_p

s_{uC} from N_{kt} = 10
s_{uC} from $N_{\Delta u}$ = 7.5

ST15452 Flemish Pass Geotechnical Investigation	Document No. 20140857−02−R	
	Figure No. F6.3.8	
CPTU data and derived parameters CPTU data: ST15452−12	Date 2016−04−05	Drawn by VBS/MVa
	NGI	

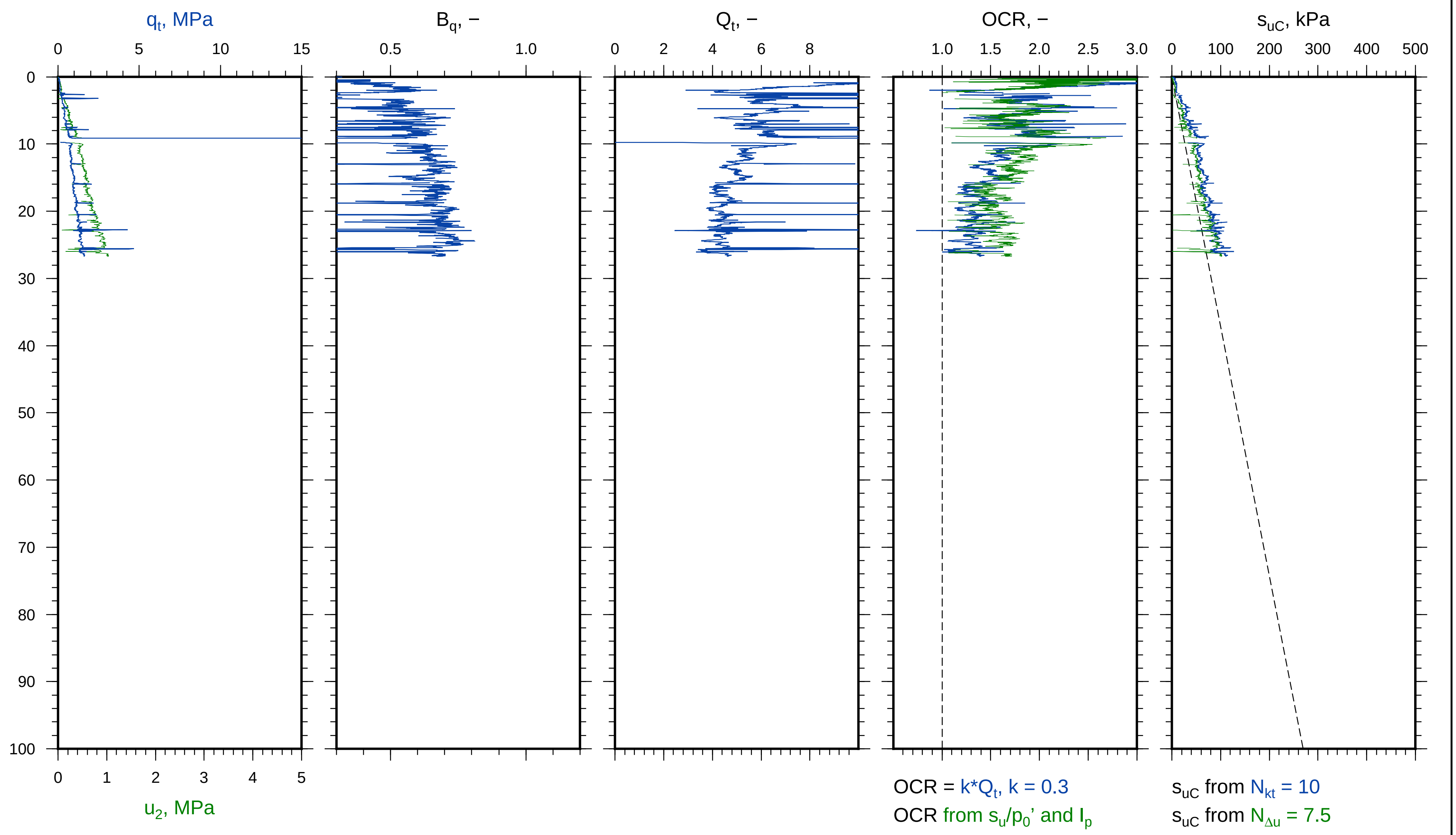

ST15452 Flemish Pass Geotechnical Investigation

CPTU data and derived parameters

CPTU data: ST15452−15

Document No.	20140857−02−R
Figure No.	F6.3.9
Date	2016−04−05
Drawn by	VBS/MVa

NGI

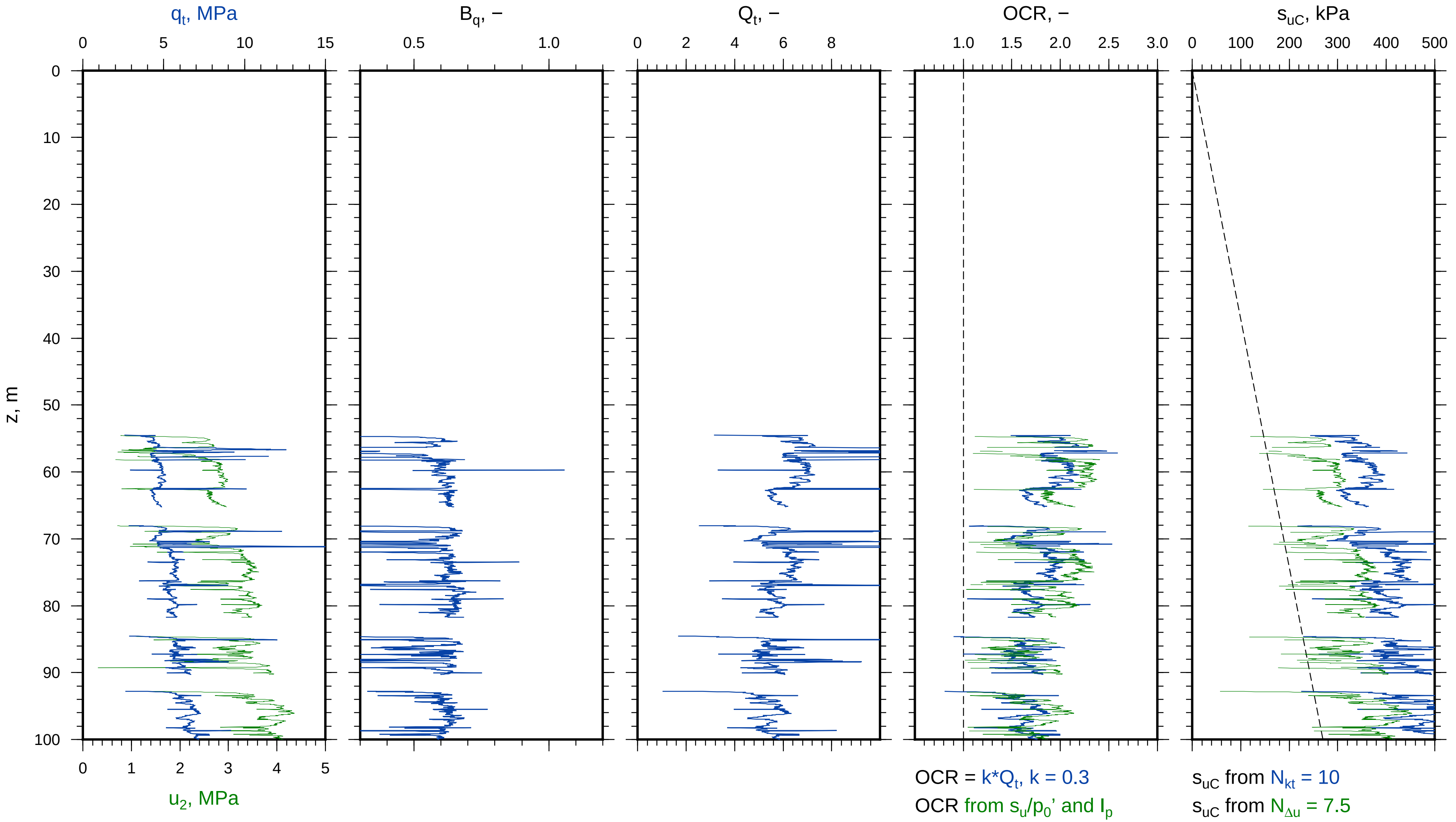

ST15452 Flemish Pass Geotechnical Investigation

CPTU data and derived parameters

CPTU data: ST15452−02

Document No.	20140857−02−R
Figure No.	F6.3.10
Date	2016−04−05
Drawn by	VBS/MVa

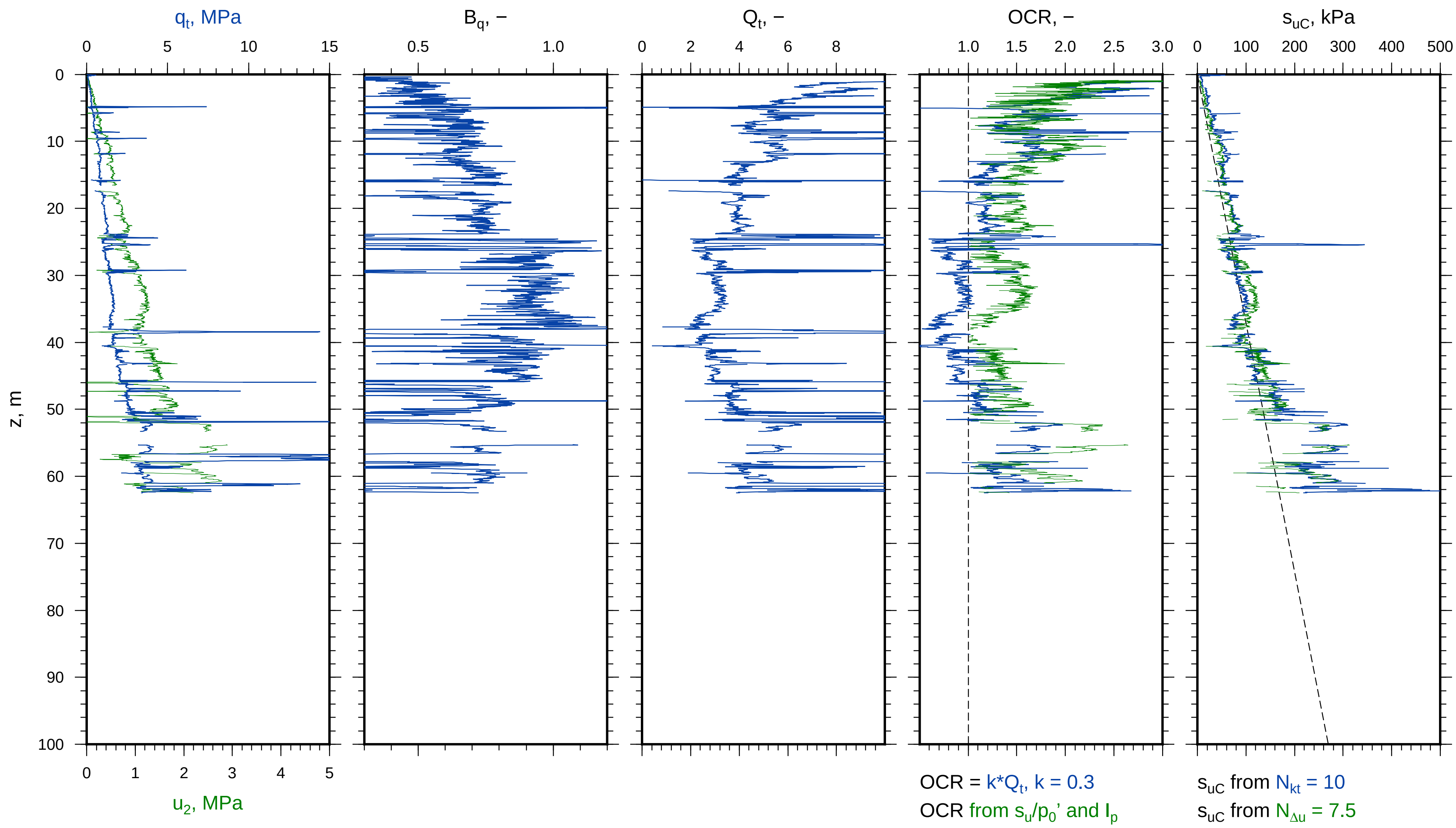

trepak:/grouphome/gmtapp/20140857_Flemish/CPT/Composites/CollatedCPTUdataFiltered/05−ST15452−03.ps

ST15452 Flemish Pass Geotechnical Investigation	Document No. 20140857−02−R	
	Figure No. F6.3.11	
CPTU data and derived parameters CPTU data: ST15452−03	Date 2016−04−05	Drawn by VBS/MVa
	NGI	

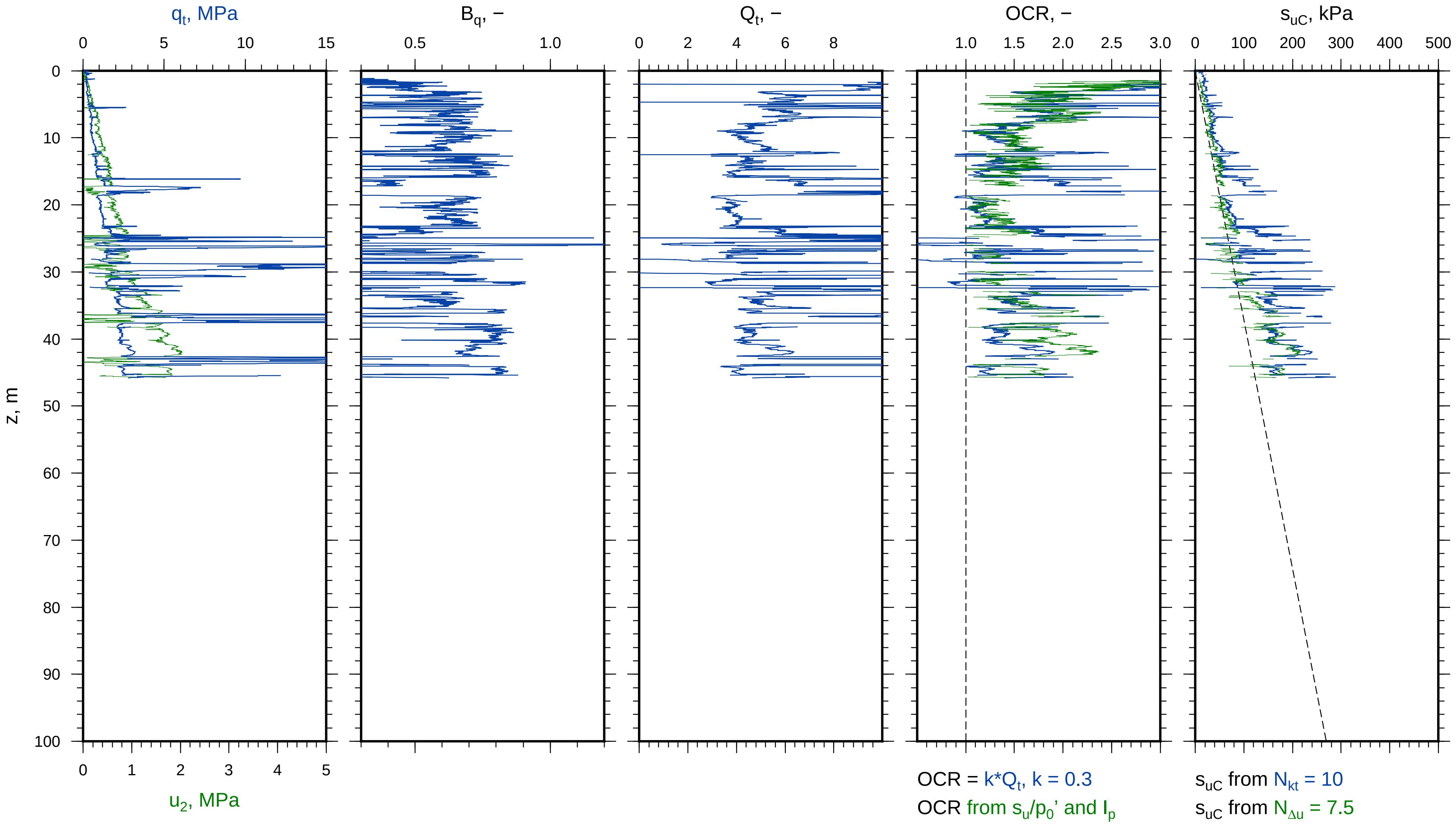

ST15452 Flemish Pass Geotechnical Investigation	Document No. 20140857−02−R	
	Figure No. F6.3.12	
CPTU data and derived parameters CPTU data: ST15452−07	Date 2016−04−05	Drawn by VBS/MVa
	NGI	

trepak:/grouphome/gmtapp/20140857_Flemish/CPT/Composites/CollatedCPTUdataFiltered/06−ST15452−07.ps

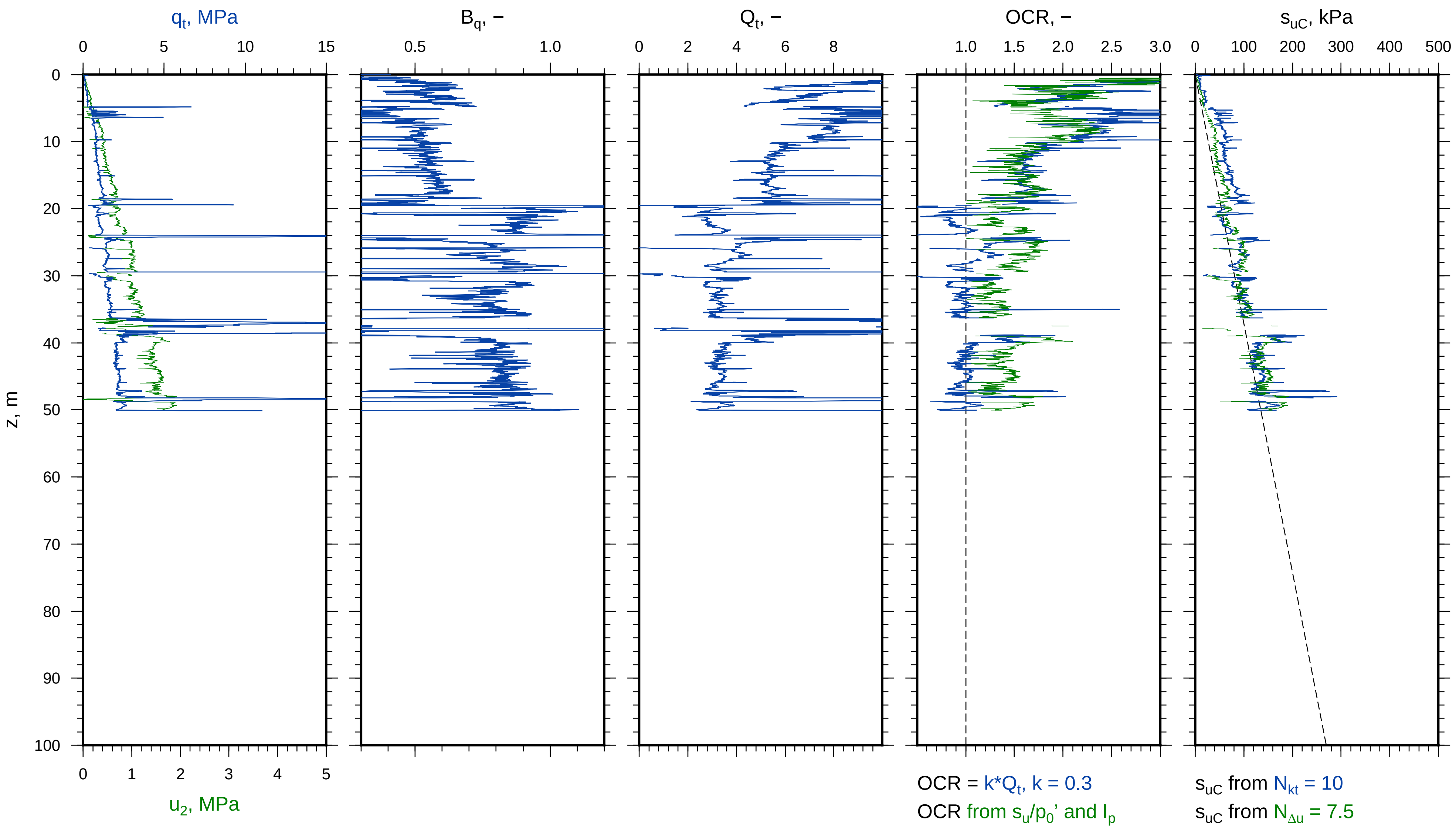

trepak:/grouphome/gmtapp/20140857_Flemish/CPT/Composites/CollatedCPTUdataFiltered/07−ST15452−08.ps

ST15452 Flemish Pass Geotechnical Investigation

CPTU data and derived parameters
CPTU data: ST15452−08

Document No.	20140857−02−R
Figure No.	F6.3.13
Date	2016−04−05
Drawn by	VBS/MVa

NGI

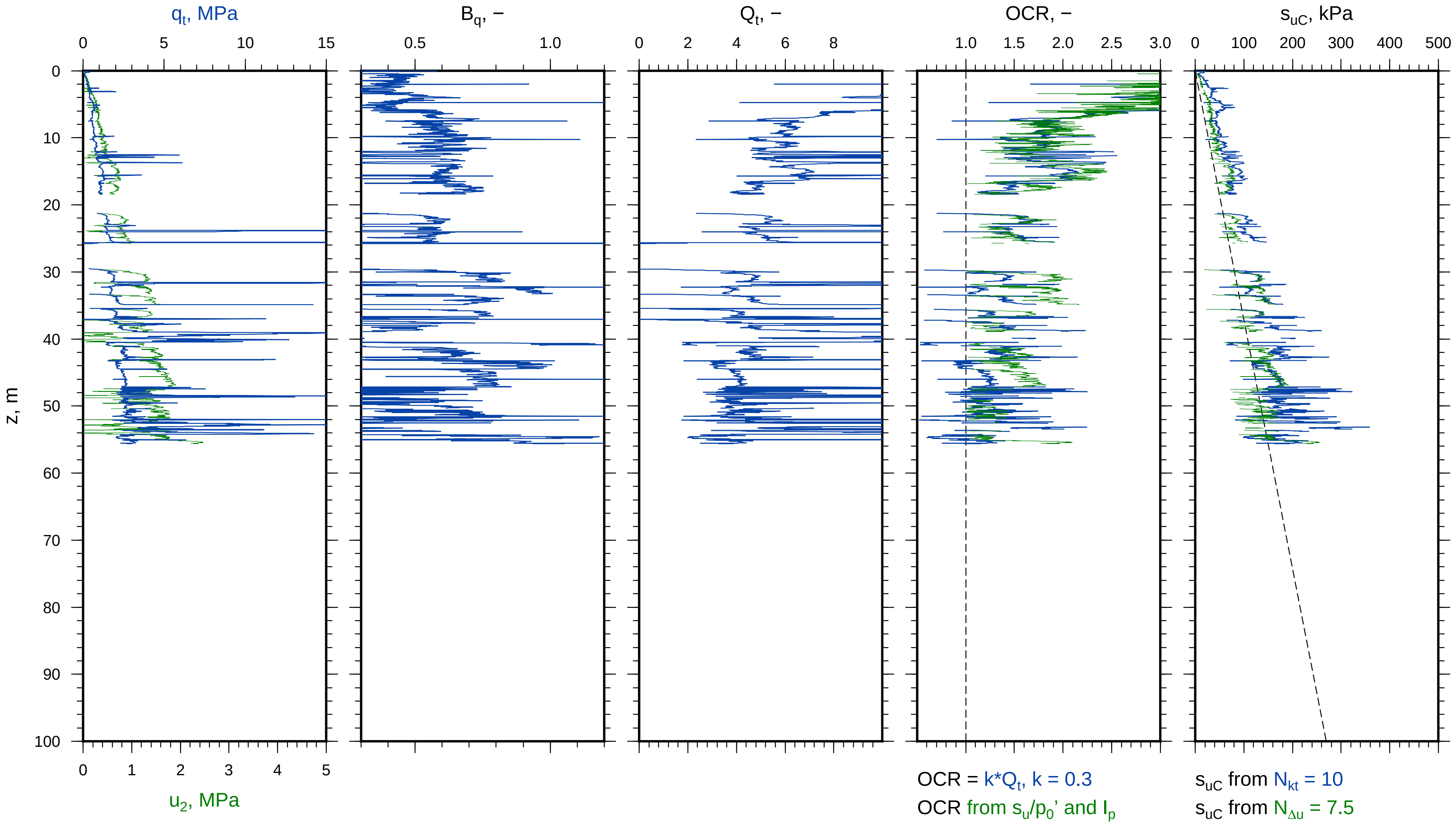

ST15452 Flemish Pass Geotechnical Investigation

CPTU data and derived parameters

CPTU data: ST15452−16

Document No.	20140857−02−R
Figure No.	F6.3.14
Date	2016−04−05
Drawn by	VBS/MVa

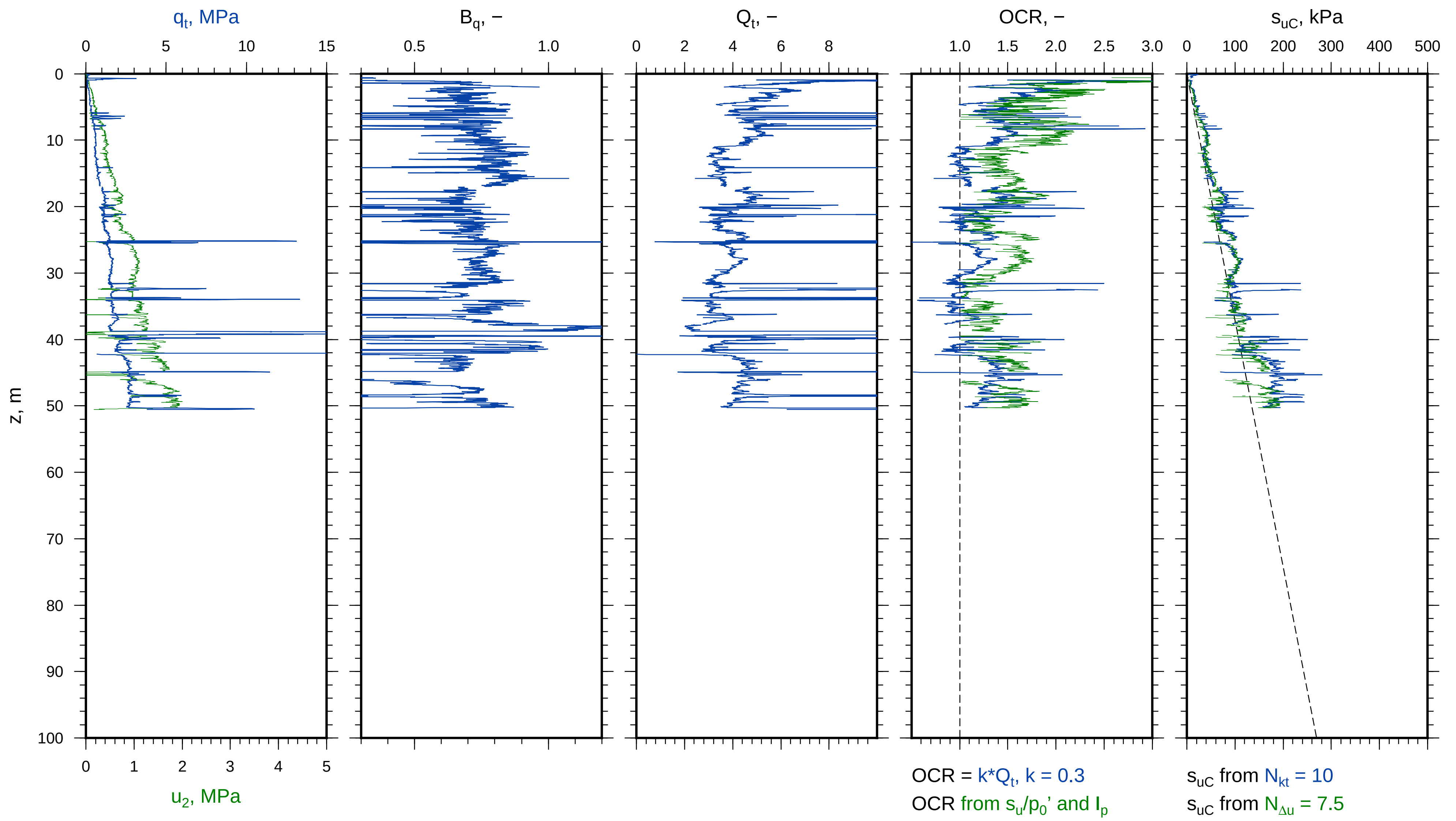

trepak:/grouphome/gmtapp/20140857_Flemish/CPT/Composites/CollatedCPTUdataFiltered/09−ST15452−19.ps

ST15452 Flemish Pass Geotechnical Investigation	Document No. 20140857−02−R	
	Figure No. F6.3.15	
CPTU data and derived parameters CPTU data: ST15452−19	Date 2016−04−05	Drawn by VBS/MVa
	NGI	

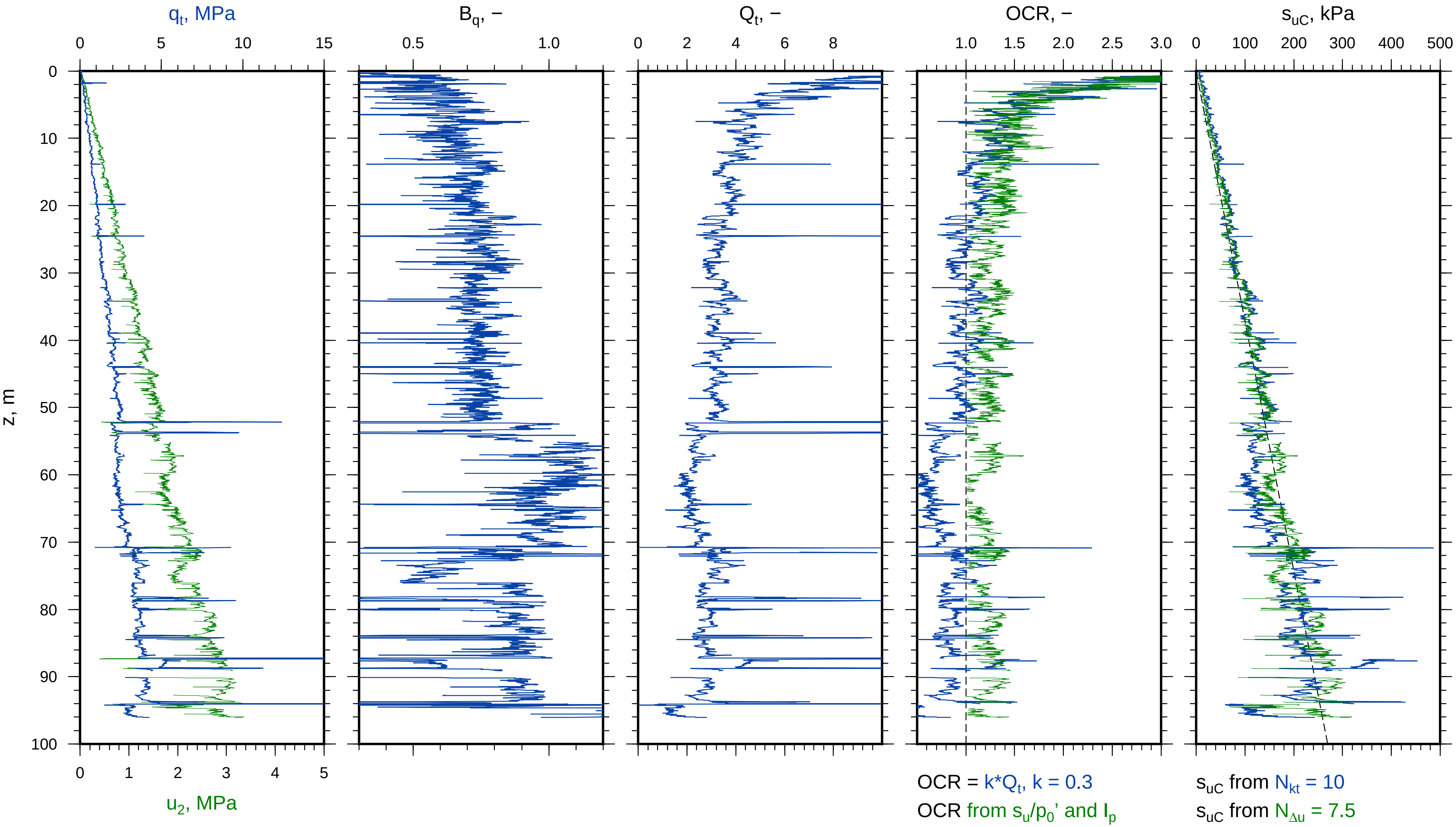

trepak:/grouphome/gmtapp/20140857_Flemish/CPT/Composites/CollatedCPTUdataFiltered/10-ST15452-18.ps

ST15452 Flemish Pass Geotechnical Investigation

CPTU data and derived parameters

CPTU data: ST15452−18

Document No.	20140857−02−R
Figure No.	F6.3.16
Date	2016−04−05
Drawn by	VBS/MVa

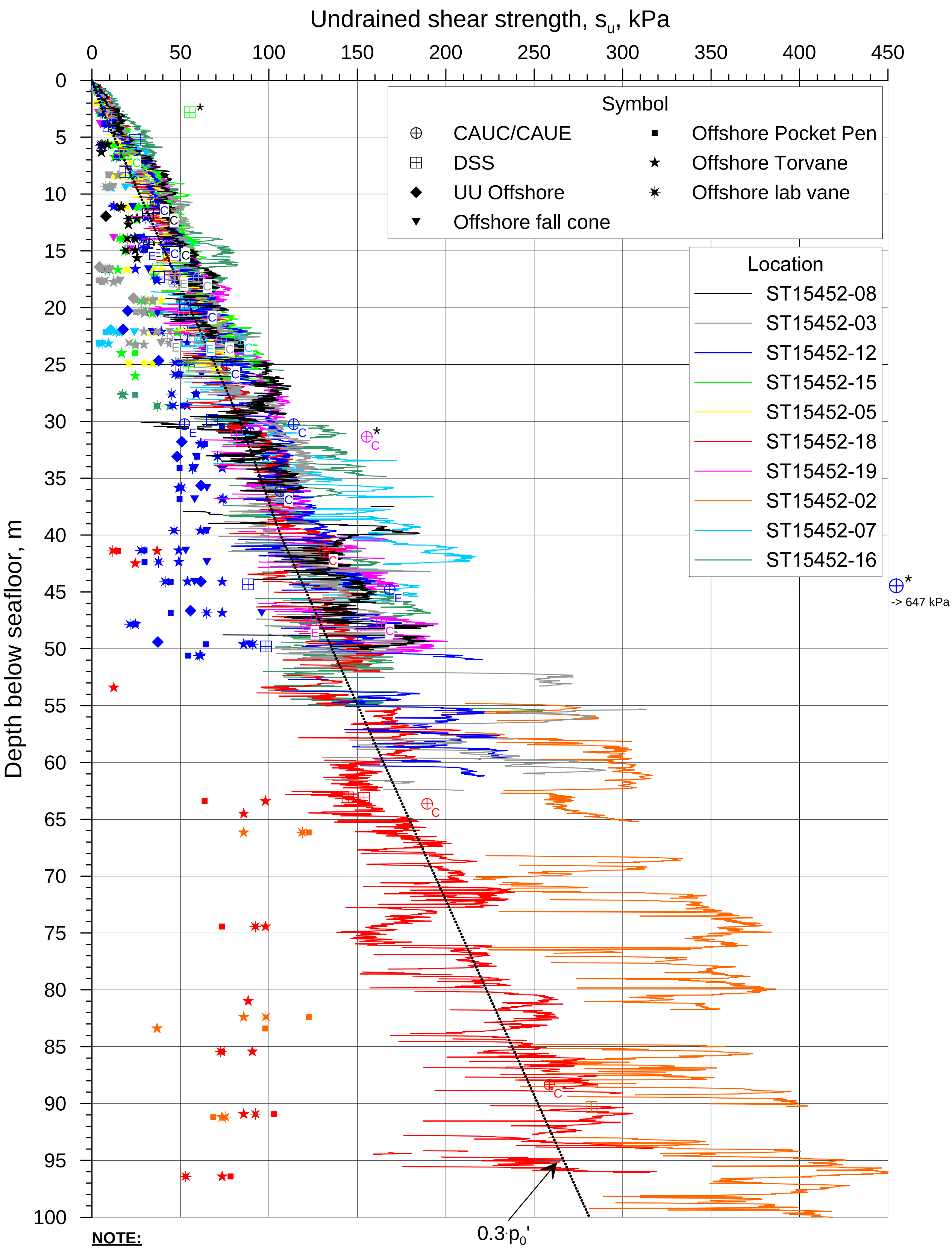

NOTE:
u_2 is used for interpretation of s_{uC} from CPTU using $N_{\Delta u}$ = 7.5

* Test representative of silty/sandy layer and not given weight in s_u interpretation

Date/Rev.: 2015-01-21/01

P:\2014\08\20140857\Leveransedokumenter\Rapport\20140857-02-R Data interpretation and evaluation\Figures\Section F\Figure F_06_03_17, su versus depth.grf

ST15452 Flemish Pass Geotechnical Investigation	Document No. 20140857-02-R	
Undrained shear strength versus depth All locations	Figure No. F6.3.17	
	Date 2016-04-04	Drawn by VBS

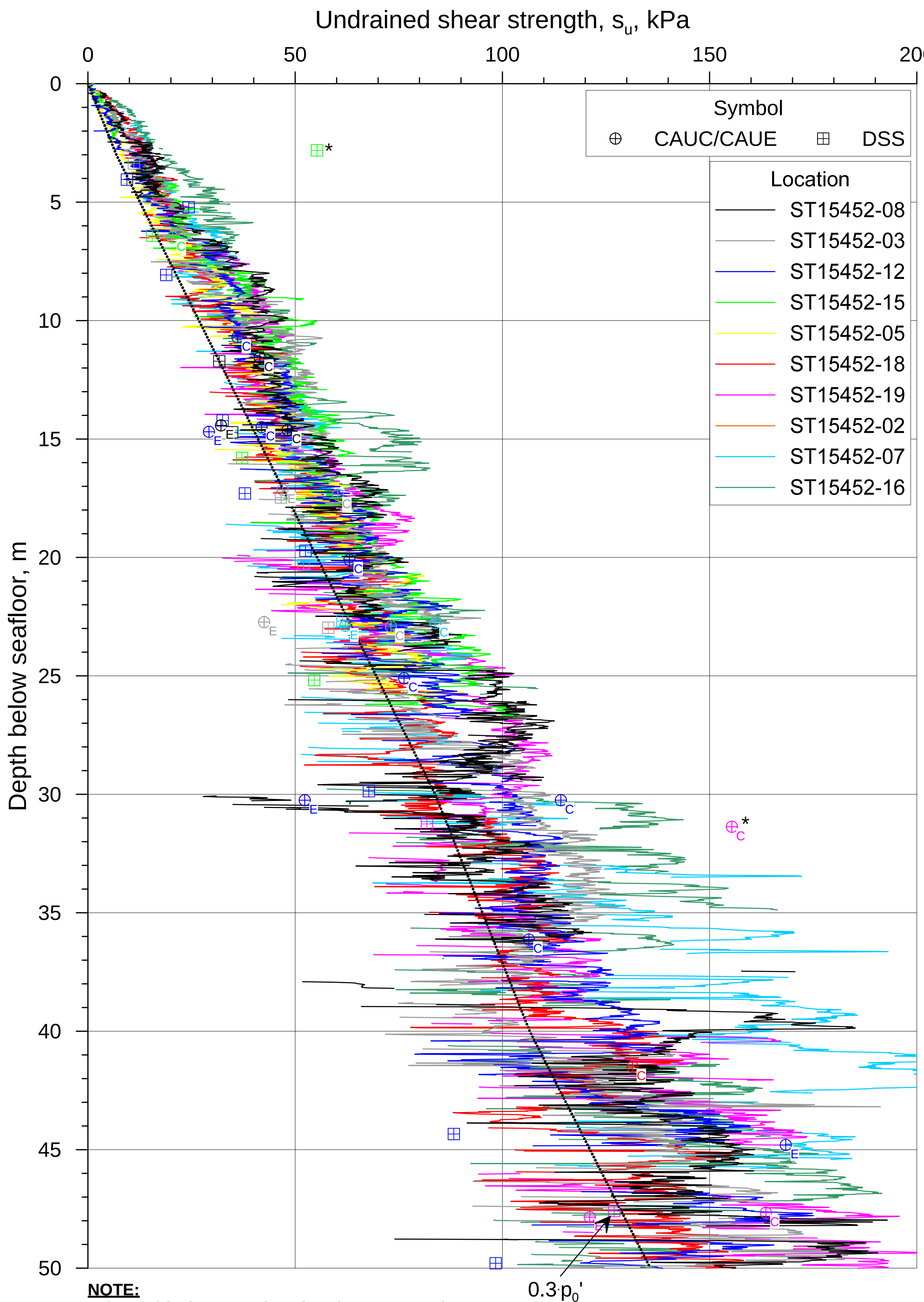

NOTE:
u_2 is used for interpretation of s_{uC} from CPTU using $N_{\Delta u}$ = 7.5

* Test representative of silty/sandy layer and not given weight in s_u interpretation

Date/Rev.: 2015-01-21/01

ST15452 Flemish Pass Geotechnical Investigation

Undrained shear strength versus depth
All locations, 0 - 50 m depth
Index data removed

Document No.	20140857-02-R
Figure No.	F6.3.18
Date	2016-04-04
Drawn by	VBS

P:\2014\08\20140857\Leveranseddokumenter\Rapport\20140857-02-R Data interpretation and evaluation\Figures\Section F\Figure F_06_03_18, su versus depth 0-50 m.grf

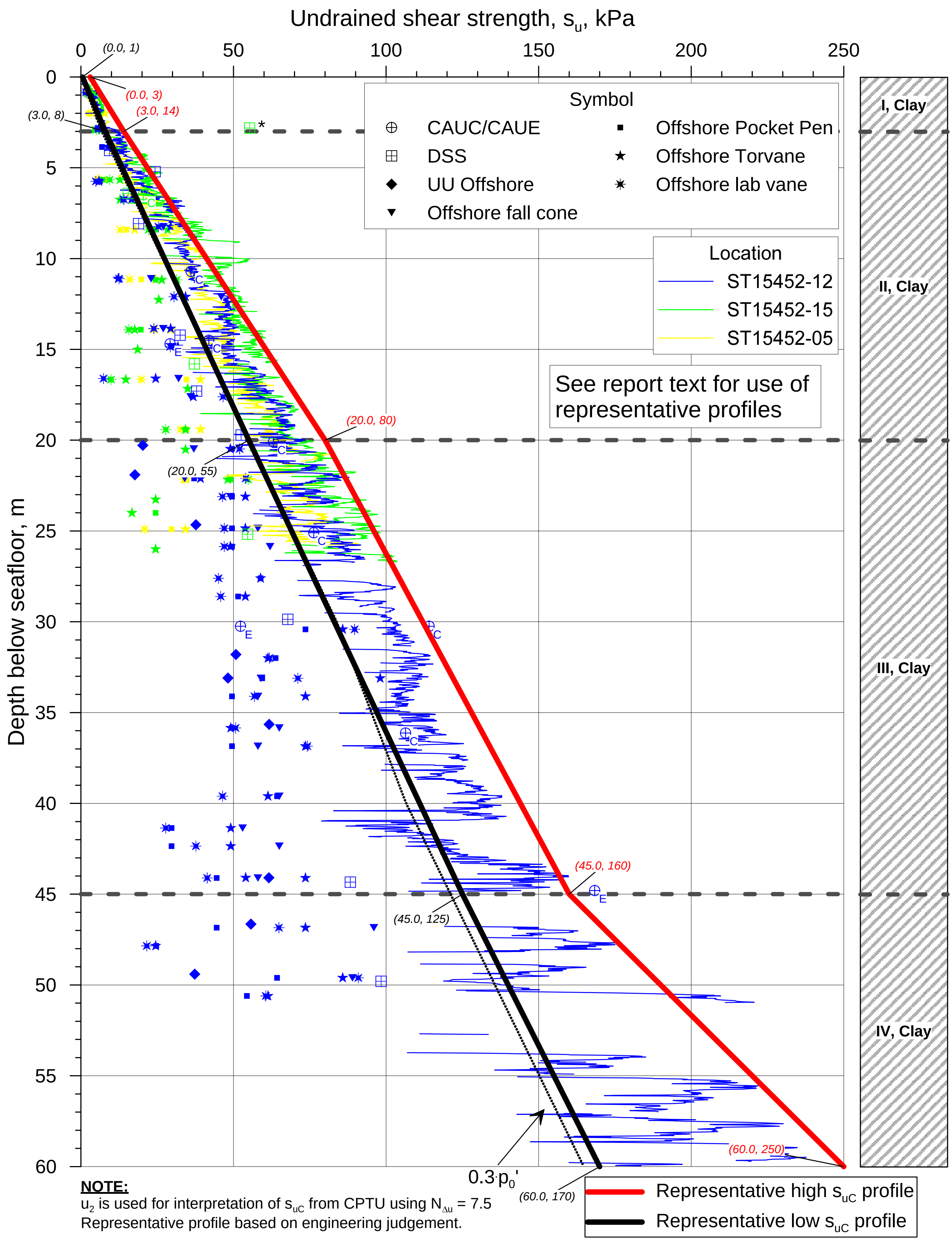

NOTE:
u_2 is used for interpretation of s_{uC} from CPTU using $N_{\Delta u}$ = 7.5
Representative profile based on engineering judgement.

* Test representative of silty/sandy layer and not given weight in s_u interpretation

Label: *(depth, value)* Date/Rev.: 2015-01-21/01

ST15452 Flemish Pass Geotechnical Investigation	Document No. 20140857-02-R
Undrained shear strength versus depth Field Centre	Figure No. F6.3.19
	Date 2016-04-03 / Drawn by VBS

P:\2014\08\20140857\Leveransedokumenter\Rapport\20140857-02-R Data interpretation and evaluation\Figures\Section F\Figure F_06_03_19, su versus depth-Fieldcentre.grf

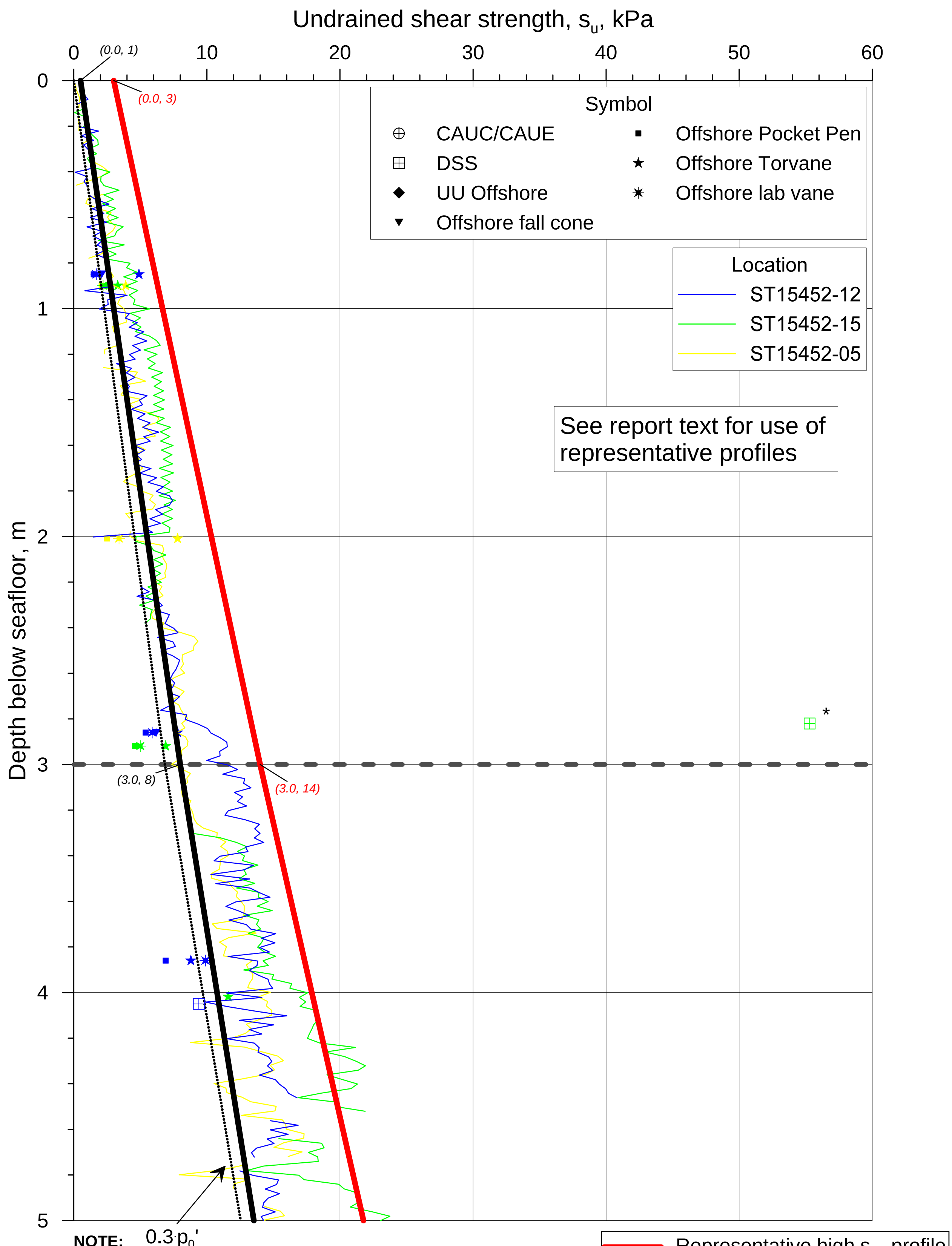

NOTE:
u_2 is used for interpretation of s_{uC} from CPTU using $N_{\Delta u}$ = 7.5
Representative profile based on engineering judgement.

Representative high s_{uC} profile
Representative low s_{uC} profile

* Test representative of silty/sandy layer and not given weight in s_u interpretation

Label: *(depth, value)*

Date/Rev.: 2015-01-21/01

P:\2014\08\20140857\Leveransedokumenter\Rapport\20140857-02-R Data interpretation and evaluation\Figures\Section F\Figure F_06_03_20, su versus depth-Fieldcentre 0-5m.grf

ST15452 Flemish Pass Geotechnical Investigation	Document No. 20140857-02-R
Undrained shear strength versus depth Field Centre, 0 - 5 m depth	Figure No. F6.3.20
	Date 2016-04-03 / Drawn by VBS
	NGI

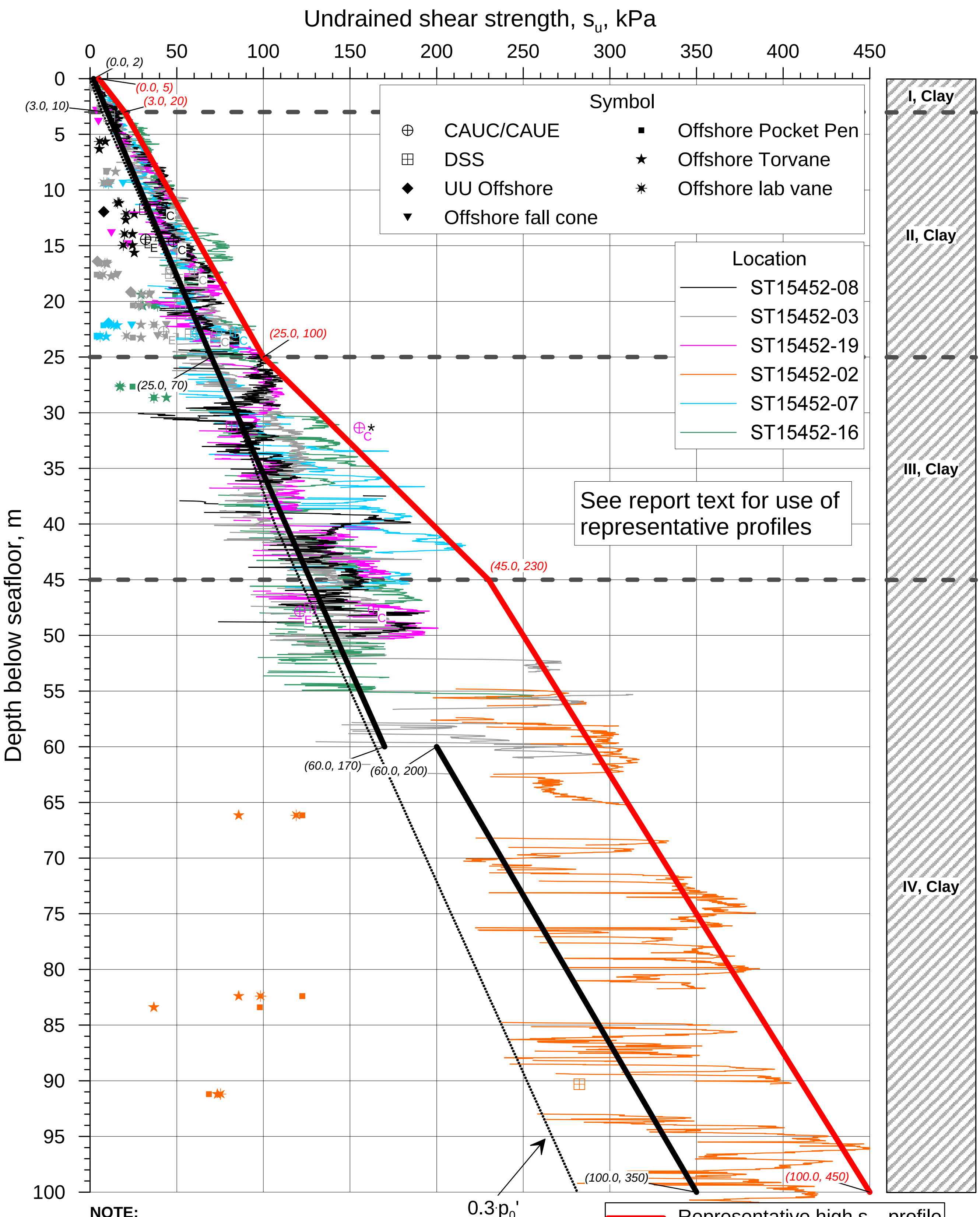

NOTE:
u_2 is used for interpretation of s_{uC} from CPTU using $N_{\Delta u}$ = 7.5
Representative profile based on engineering judgement.

Representative high s_{uC} profile
Representative low s_{uC} profile

* Test representative of silty/sandy layer and not given weight in s_u interpretation

Label: *(depth, value)*

Date/Rev.: 2015-01-21/01

P:\2014\08\20140857\Leveransedokumenter\Rapport\20140857-02-R Data interpretation and evaluation\Figures\Section F\Figure F_06_03_21, su versus depth-West.grf

ST15452 Flemish Pass Geotechnical Investigation	Document No. 20140857-02-R
Undrained shear strength versus depth West Slope	Figure No. F6.3.21
	Date 2016-04-03 / Drawn by VBS
	NGI

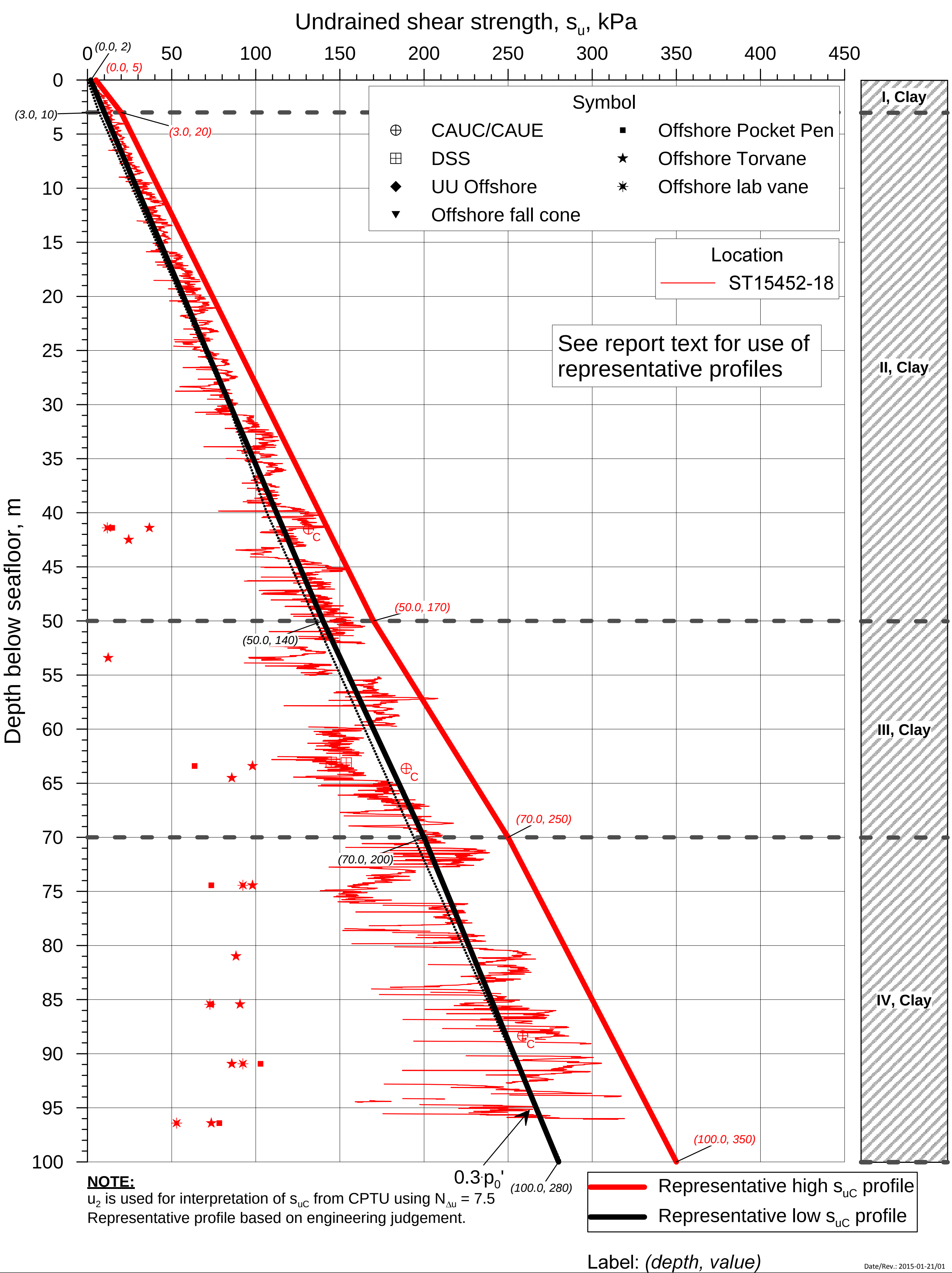

Date/Rev.: 2015-01-21/01

ST15452 Flemish Pass Geotechnical Investigation

Undrained shear strength versus depth
East Slope

Document No.	20140857-02-R
Figure No.	F6.3.22
Date	2016-04-03
Drawn by	VBS

NGI

P:\2014\08\20140857\Leveransedokumenter\Rapport\20140857-02-R Data interpretation and evaluation\Figures\Section F\Figure F_06_03_22, su versus depth-East.grf

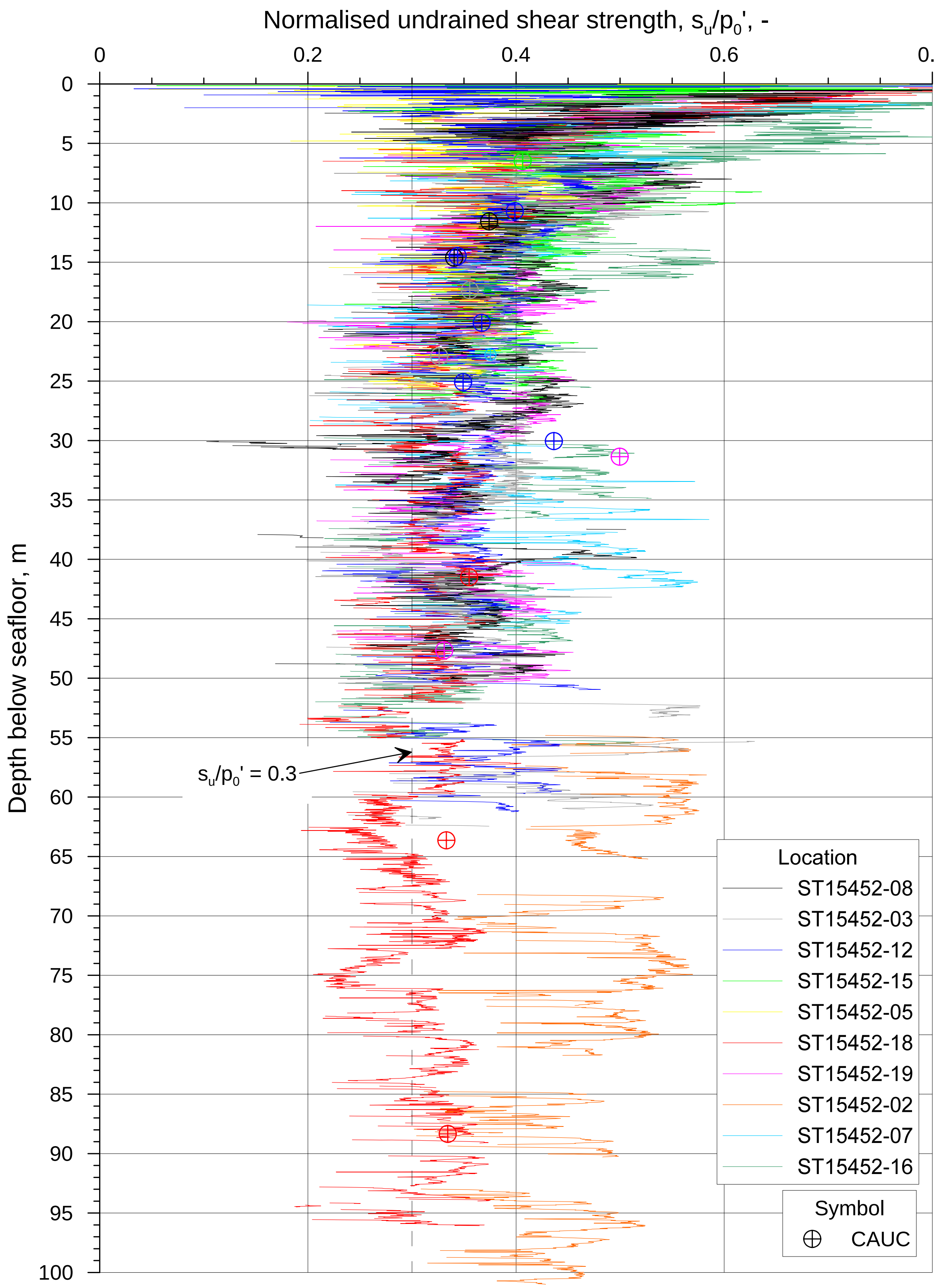

NOTE:
u_2 is used for interpretation of s_{uC} from CPTU using
$N_{\Delta u}$ = 7.5 and γ = 19 kN/m³

Date/Rev.: 2015-01-21/01

ST15452 Flemish Pass Geotechnical Investigation

Normalized undrained shear strength versus depth
All locations

Document No.	20140857-02-R
Figure No.	F6.3.23
Date	2016-04-04
Drawn by	VBS

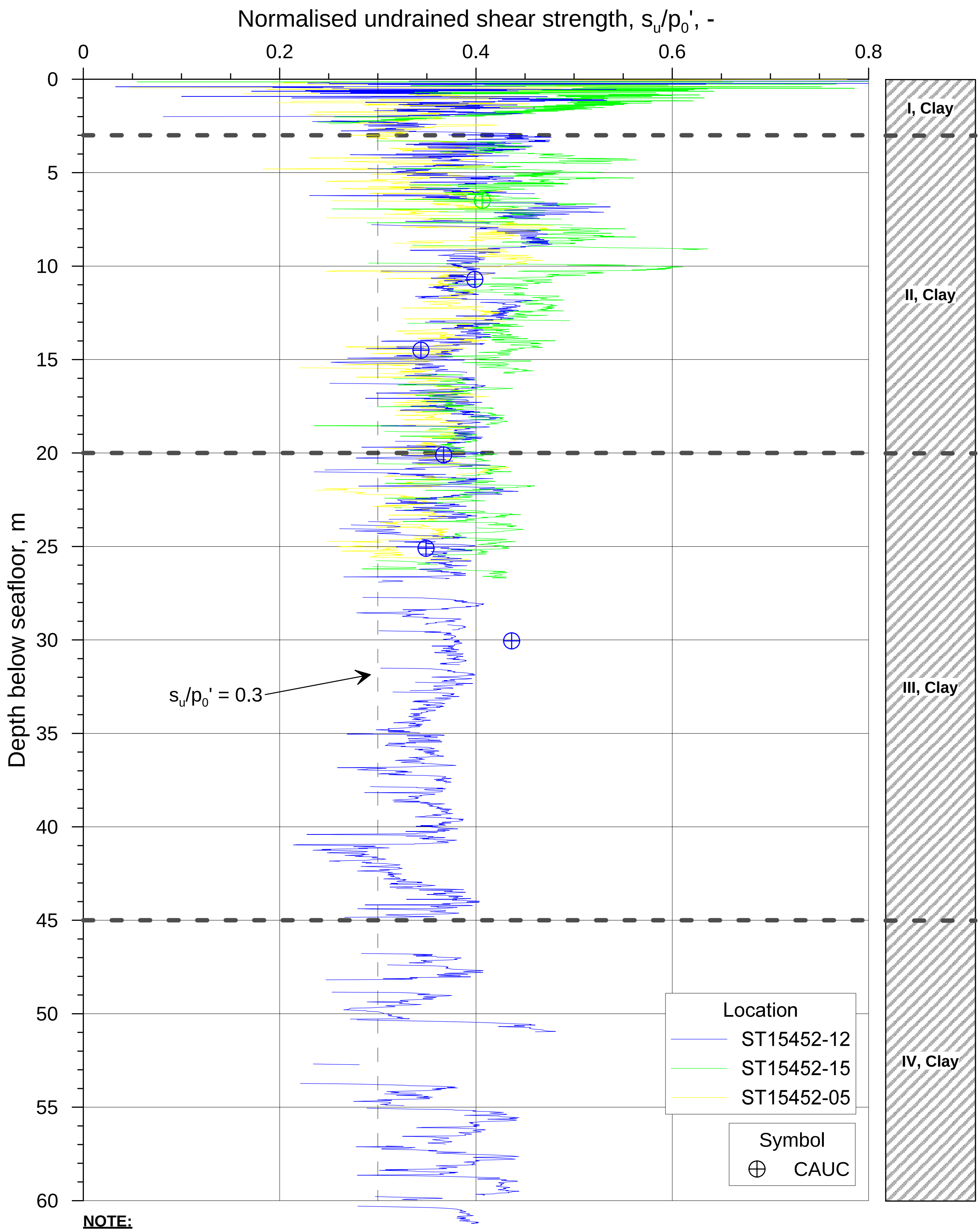

NOTE:
u_2 is used for interpretation of s_{uC} from CPTU using
$N_{\Delta u}$ = 7.5 and γ = 19 kN/m³

ST15452 Flemish Pass Geotechnical Investigation

Normalized undrained shear strength versus depth
Field Centre

Document No. 20140857-02-R	
Figure No. F6.3.24	
Date 2016-04-04	Drawn by VBS

NGI

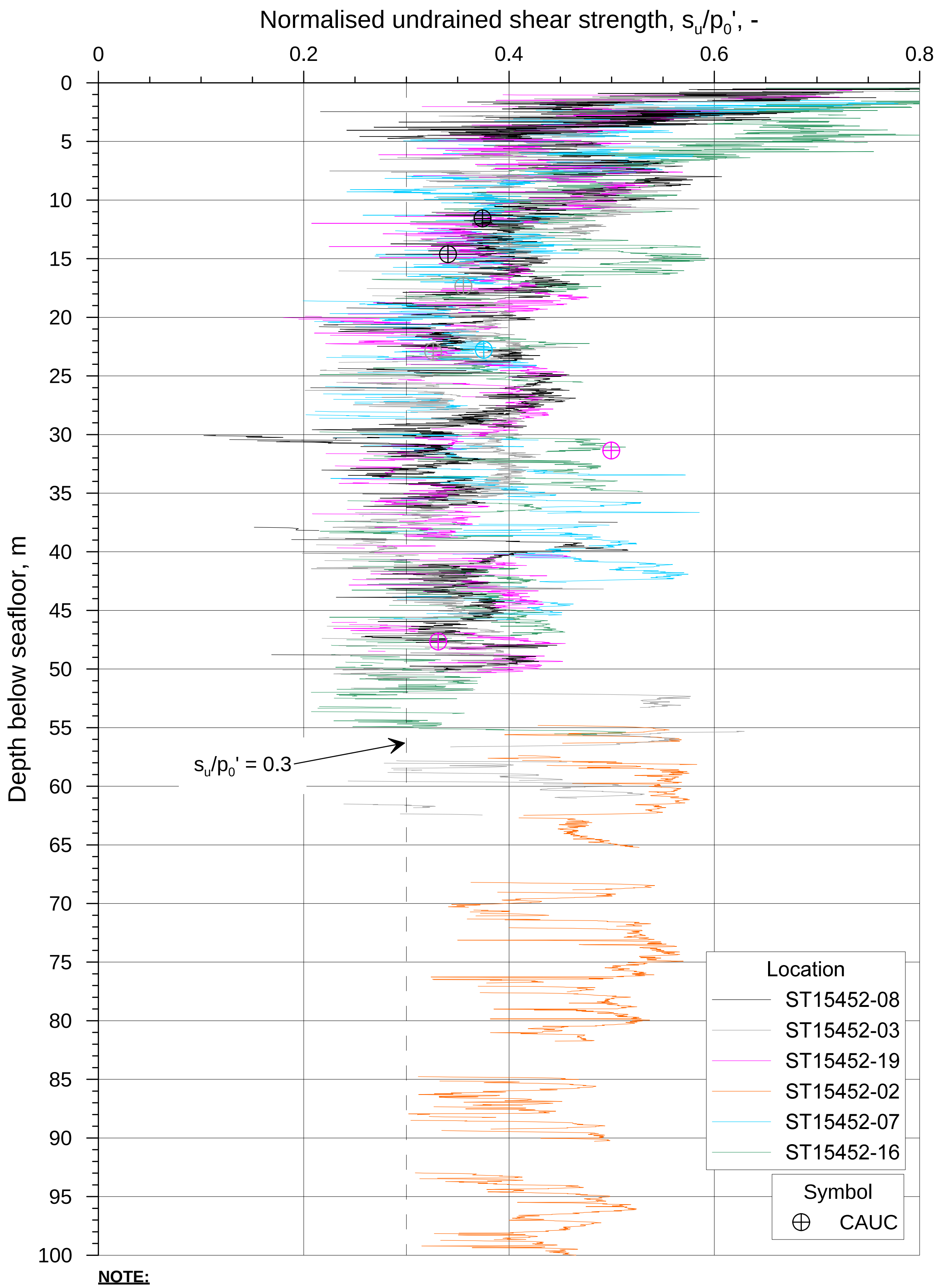

NOTE:
u_2 is used for interpretation of s_{uC} from CPTU using
$N_{\Delta u}$ = 7.5 and γ = 19 kN/m³

Date/Rev.: 2015-01-21/01

P:\2014\08\20140857\Leveranseddokumenter\Rapport\20140857-02-R Data interpretation and evaluation\Figures\Section F\Figure F_06_03_25, su-normalised versus depth-West.grf

ST15452 Flemish Pass Geotechnical Investigation

Normalized undrained shear strength versus depth
West Slope

Document No. 20140857-02-R	
Figure No. F6.3.25	
Date 2016-04-04	Drawn by VBS

NGI

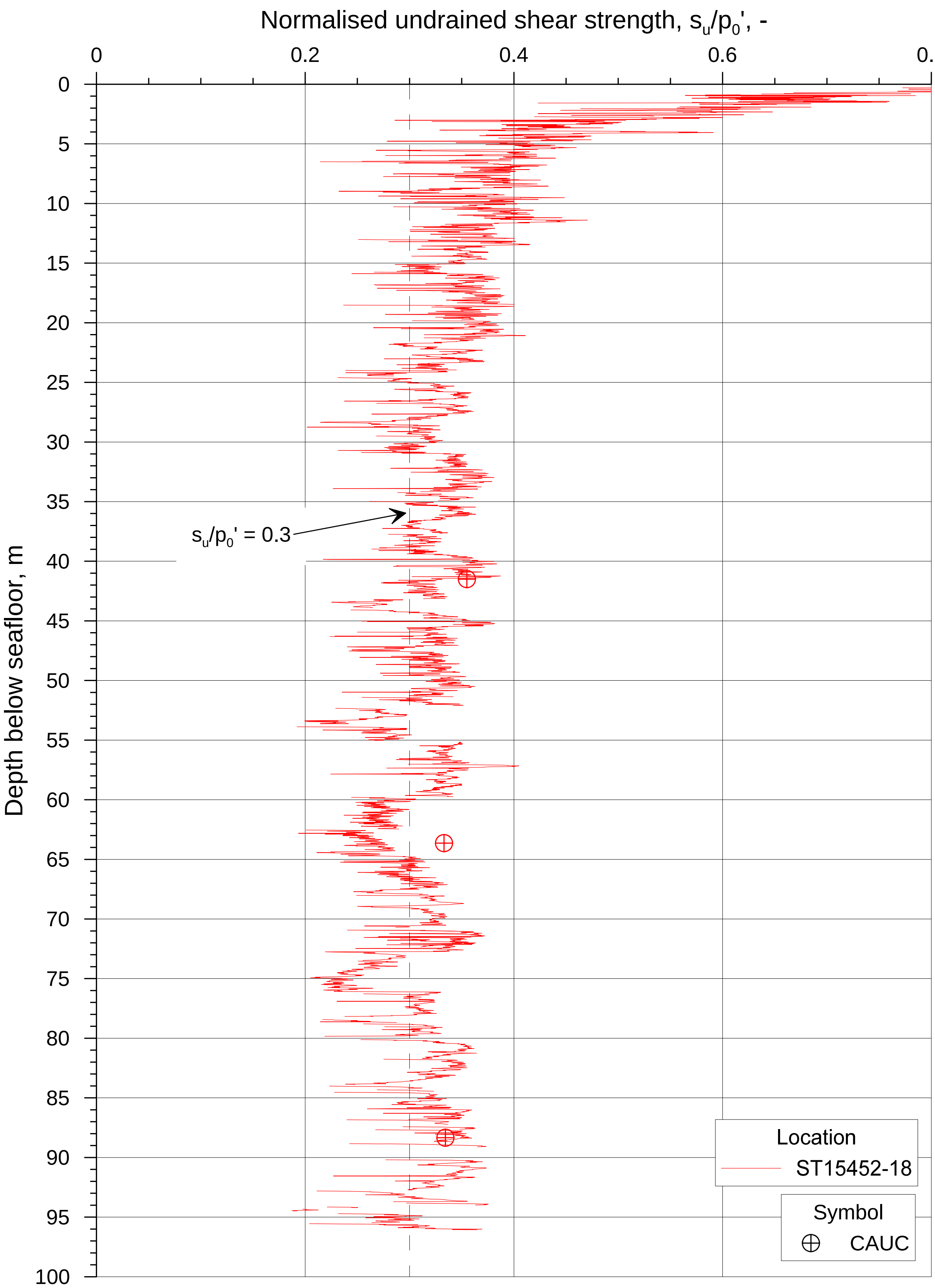

NOTE:
u_2 is used for interpretation of s_{uC} from CPTU using
$N_{\Delta u}$ = 7.5 and γ = 19 kN/m³

Date/Rev.: 2015-01-21/01

ST15452 Flemish Pass Geotechnical Investigation	Document No. 20140857-02-R	
Normalized undrained shear strength versus depth East Slope	Figure No. F6.3.26	
	Date 2016-04-04	Drawn by VBS

P:\2014\08\20140857\Leveransedokumenter\Rapport\20140857-02-R Data interpretation and evaluation\Figures\Section F\Figure F_06_03_26, su-normalised versus depth-East.grf

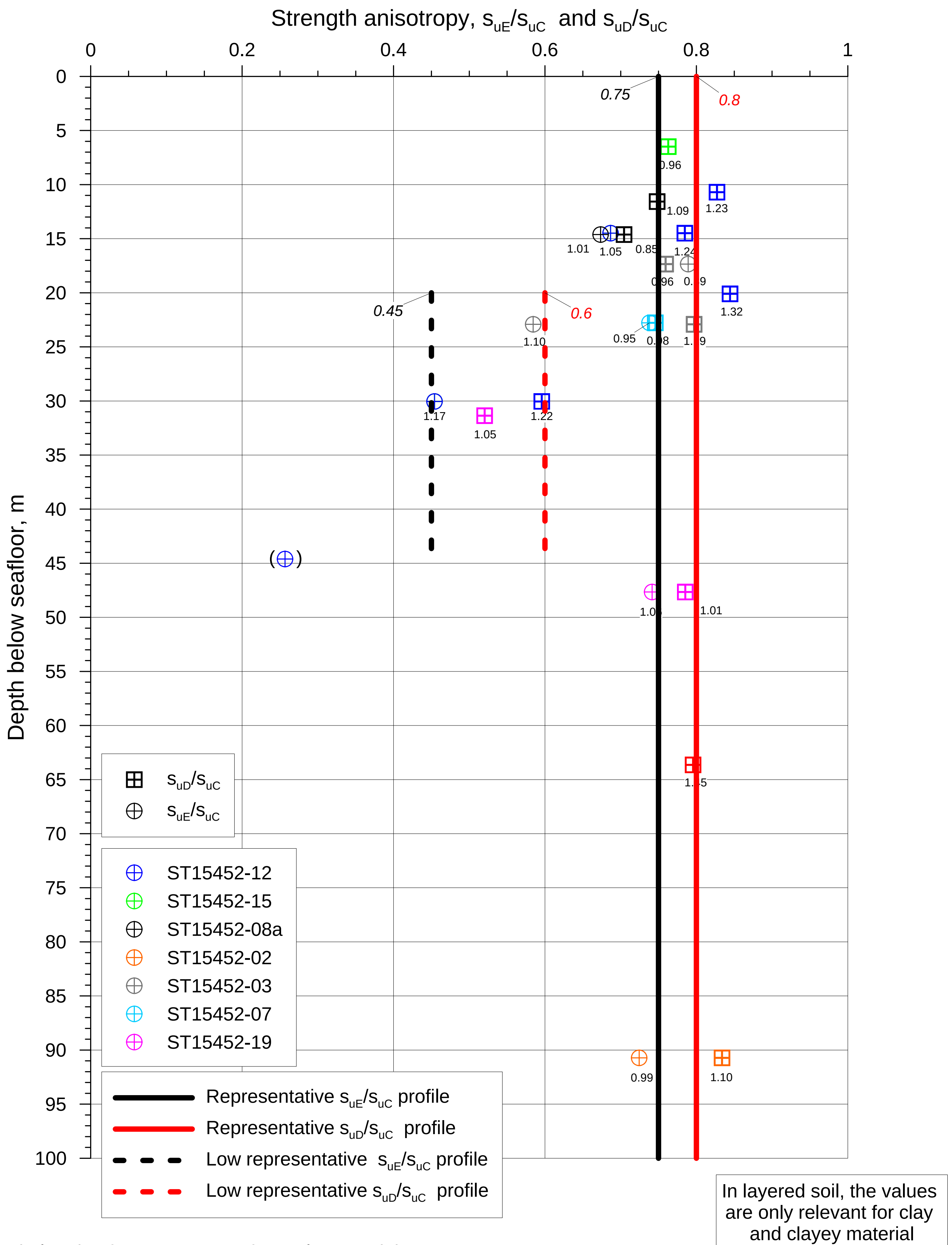

Label: ratio of water content of actual test and the nearest CAUC test

Date/Rev.: 2015-01-21/01

ST15452 Flemish Pass Geotechnical Investigation	Document No. 20140857-02-R	
Strength Anisotropy versus depth All locations Effect of the low representative profiles should be assessed by the designer	Figure No. F6.3.27	
	Date 2016-04-03	Drawn by VBS

P:\2014\08\20140857\Leveransedokumenter\Rapport\20140857-02-R Data interpretation and evaluation\Figures\Section F\Figure F_06_03_27, Strength anisotropy.grf

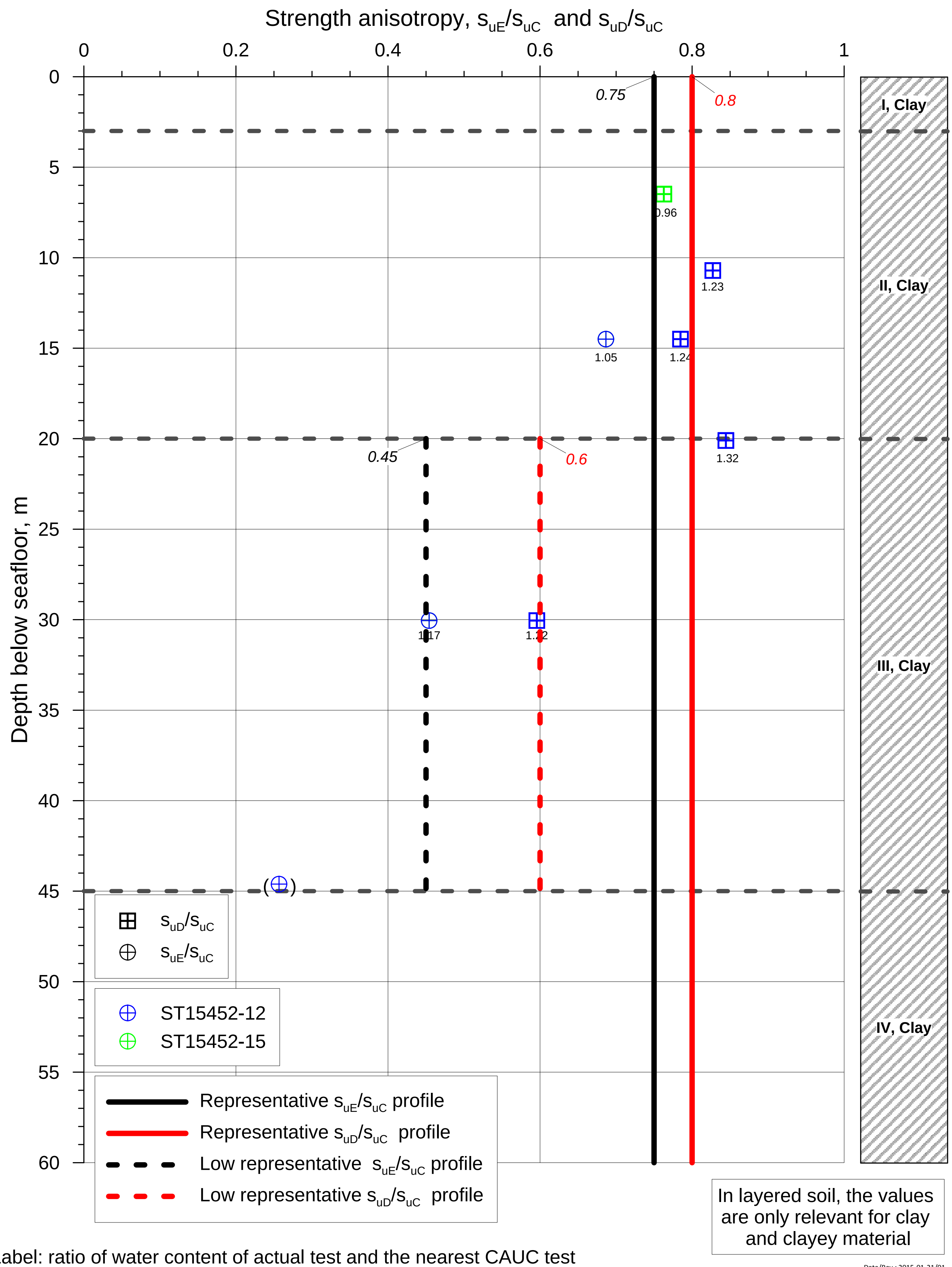

Label: ratio of water content of actual test and the nearest CAUC test

Date/Rev.: 2015-01-21/01

P:\2014\08\20140857\Leveransedokumenter\Rapport\20140857-02-R Data interpretation and evaluation\Figures\Section F\Figure F_06_03_28, Strength anisotropy,Field Centre.grf

ST15452 Flemish Pass Geotechnical Investigation

Strength Anisotropy versus depth
Field Centre
Effect of the low representative profiles should be assessed by the designer

Document No. 20140857-02-R	
Figure No. F6.3.28	
Date 2016-04-03	Drawn by VBS

NGI

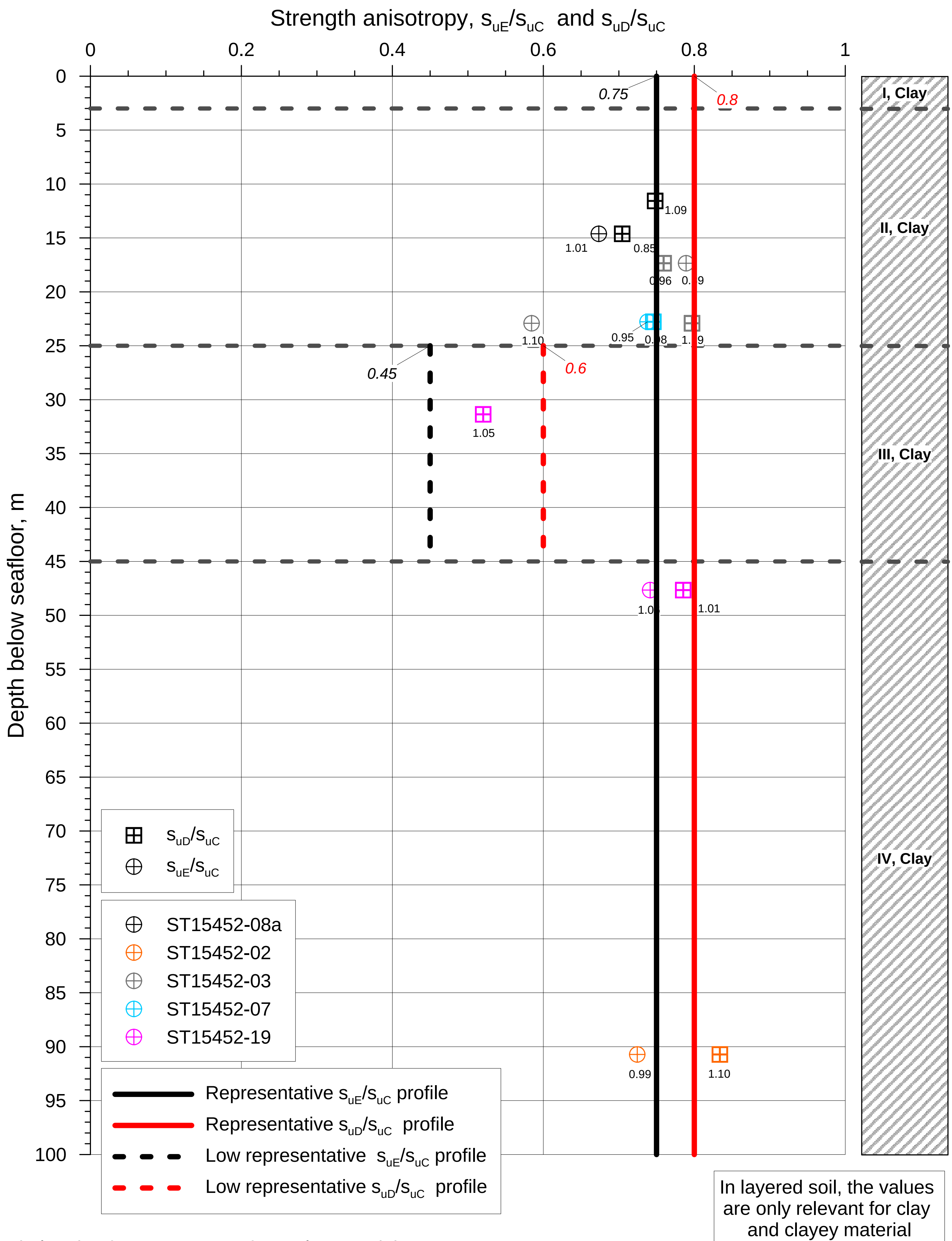

Label: ratio of water content of actual test and the nearest CAUC test

Date/Rev.: 2015-01-21/01

ST15452 Flemish Pass Geotechnical Investigation	Document No. 20140857-02-R
Strength Anisotropy versus depth West Slope Effect of the low representative profiles should be assessed by the designer	Figure No. F6.3.29
	Date 2016-04-03 / Drawn by VBS
	NGI

P:\2014\08\20140857\Leveransedokumenter\Rapport\20140857-02-R Data interpretation and evaluation\Figures\Section F\Figure F_06_03_29, Strength anisotropy, West Slope.grf

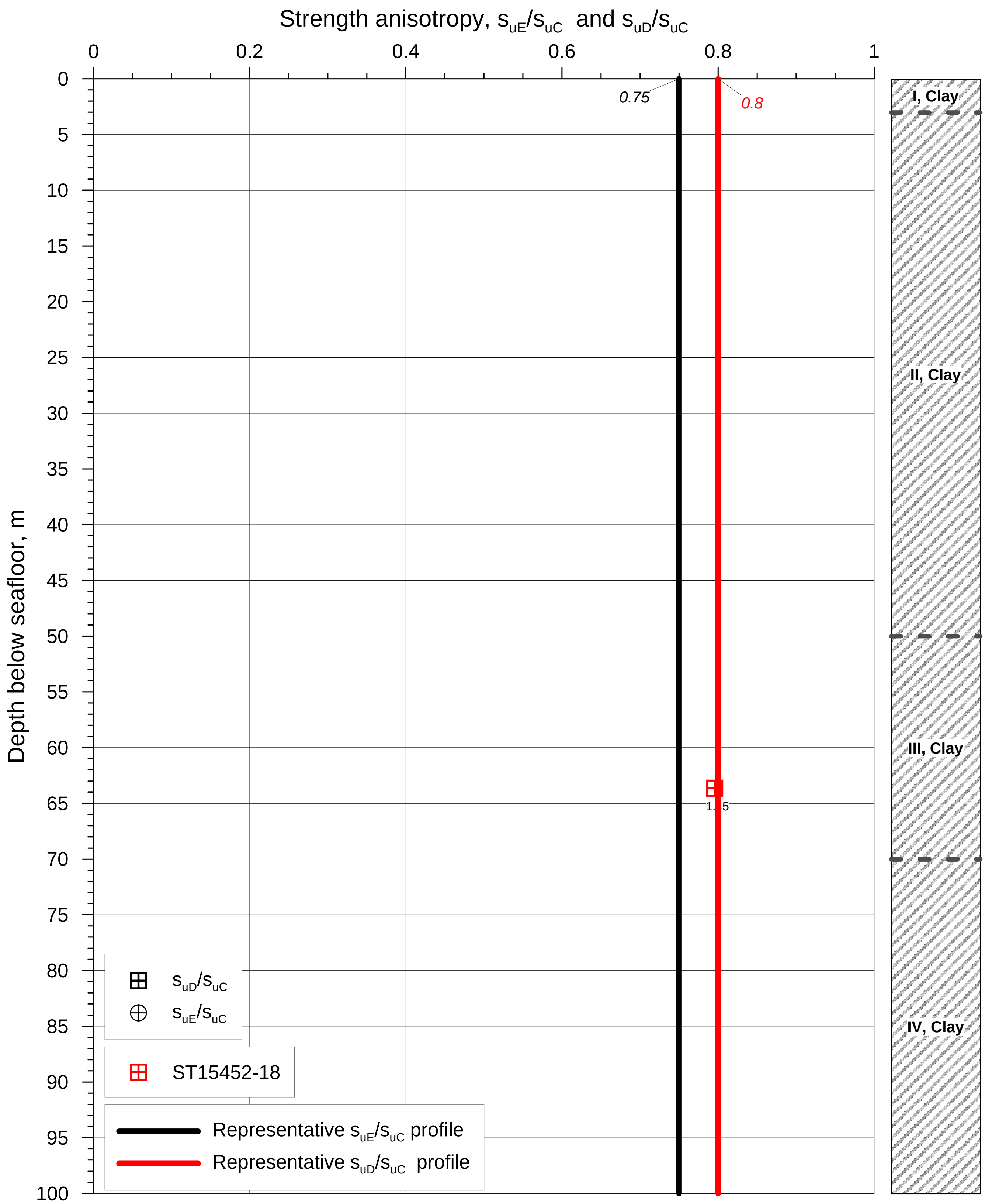

In layered soil, the values are only relevant for clay and clayey material

Label: ratio of water content of actual test and the nearest CAUC test

Date/Rev.: 2015-01-21/01

ST15452 Flemish Pass Geotechnical Investigation

Strength Anisotropy versus depth
East Slope

Document No.	20140857-02-R
Figure No.	F6.3.30
Date	2016-04-04
Drawn by	VBS

NGI

P:\2014\08\20140857\Leveransedokumenter\Rapport\20140857-02-R Data interpretation and evaluation\Figures\Section F\Figure F_06_03_30, Strength anisotropy,East Slope.grf

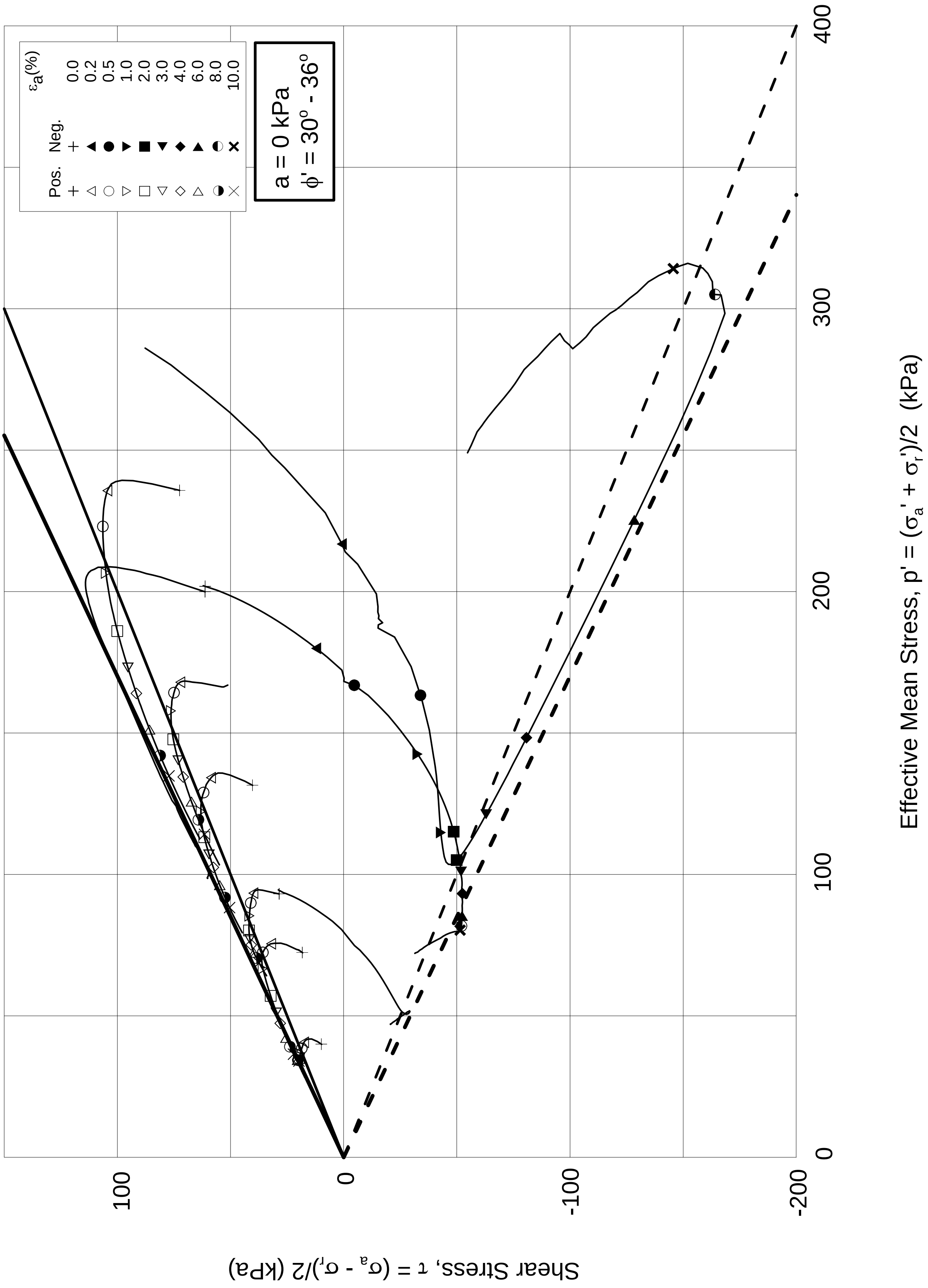

P:\2014\08\20140857\Leveransedokumenter\Rapport\20140857-02-R Data interpretation and evaluation\Figures\Section F\Figure F_06_04_01, CAU-stres_paths_field_centre.grf

Date/Rev.: 2015-01-21/01

ST15452 Flemish Pass Geotechnical Investigation	Document No. 20140857-02-R	
CAU triaxial stress paths, Field Centre	Figure No. F6.4.1	
	Date 2016-05-19	Drawn by VDa
	NGI	

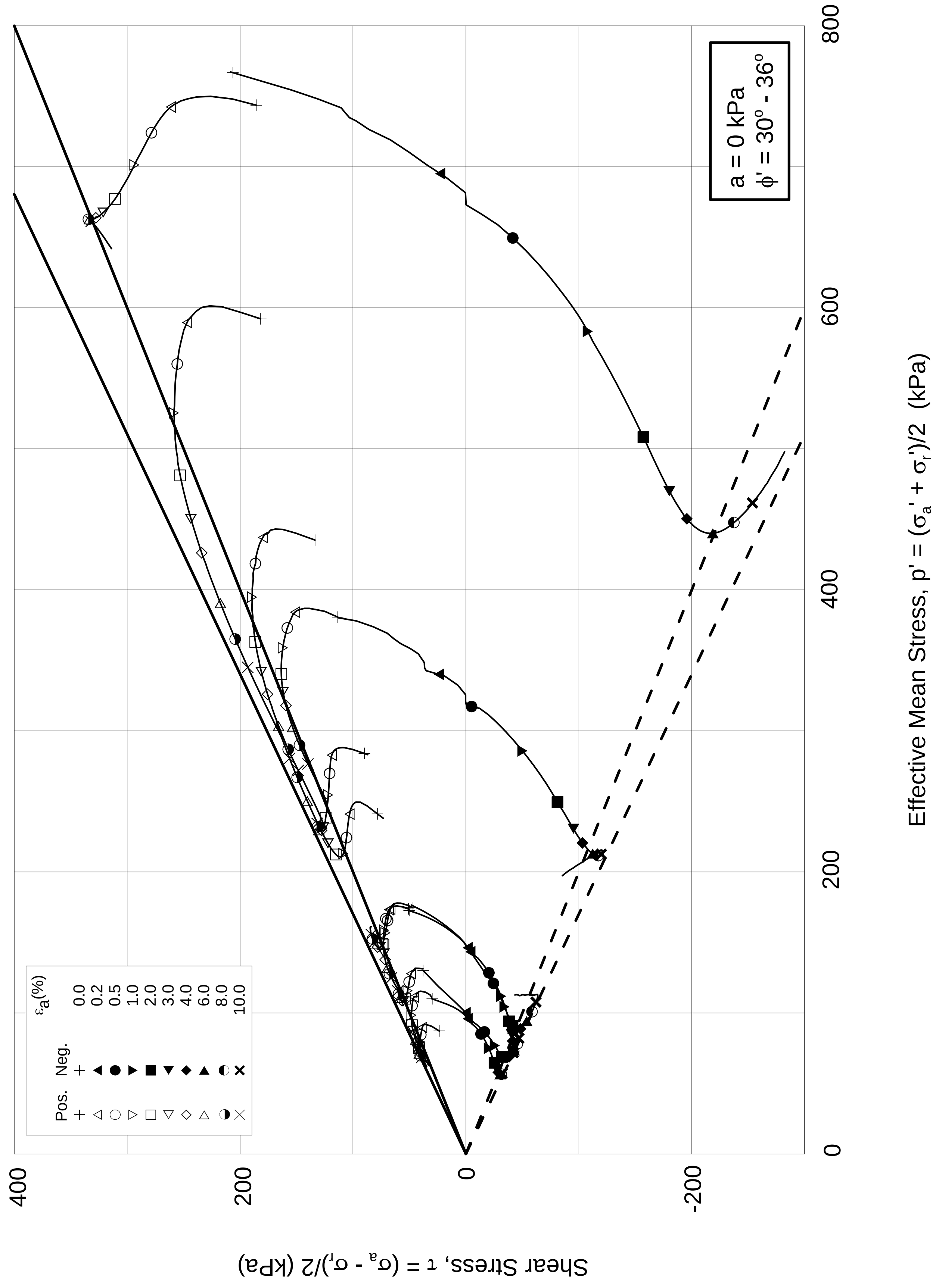

P:\2014\08\20140857\Leveransedokumenter\Rapport\20140857-02-R Data interpretation and evaluation\Figures\Section F\Figure F_06_04_02, CAU-stres_paths_slopes.grf

Date/Rev.: 2015-01-21/01

ST15452 Flemish Pass Geotechnical Investigation	Document No. 20140857-02-R
CAU triaxial stress paths, East and West Slopes	Figure No. F6.4.2
	Date 2016-05-19 — Drawn by VDa

NGI

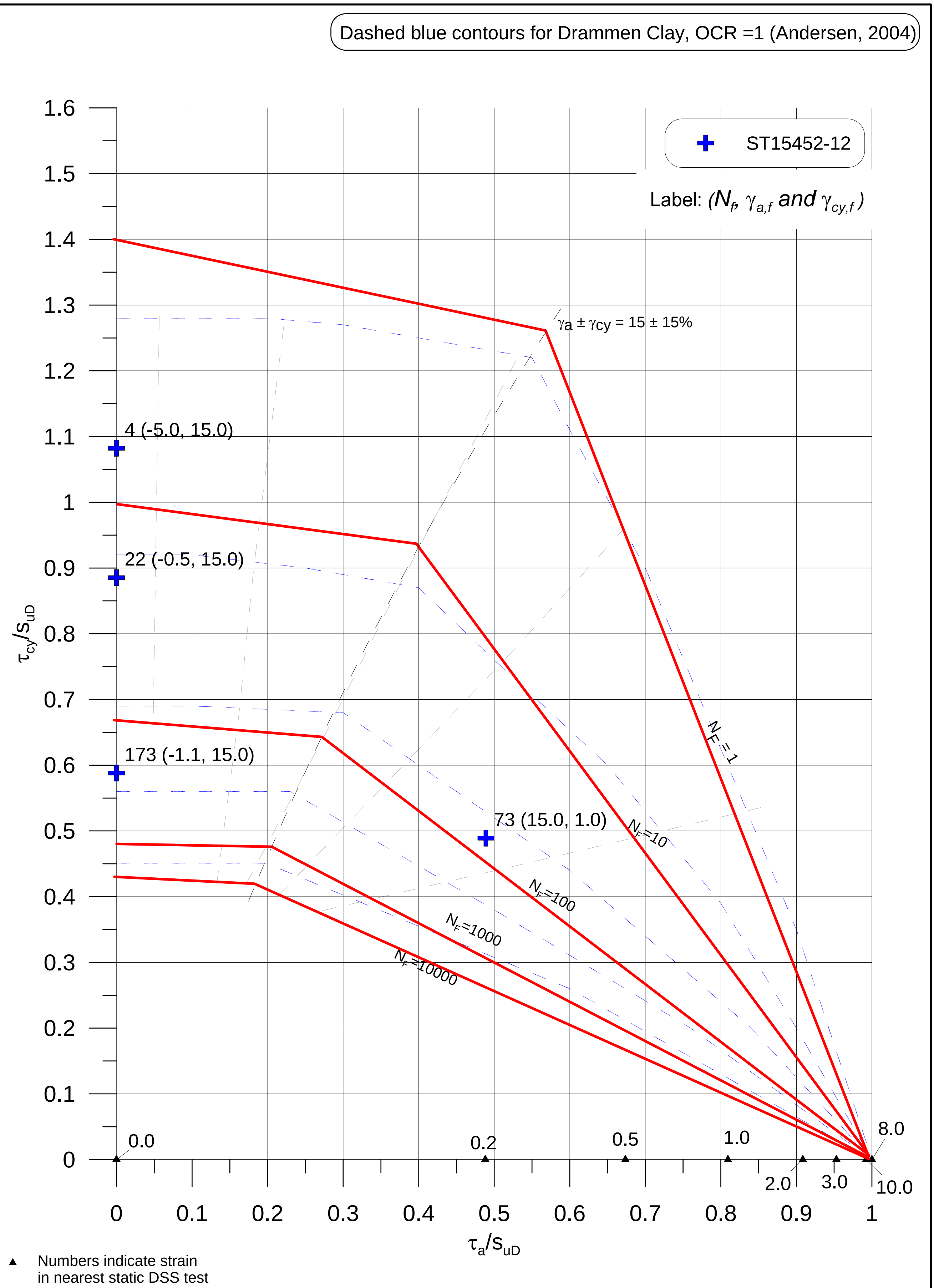

Date/Rev.: 2015-01-21/01

P:\2014\08\20140857\Leveransedokumenter\Rapport\20140857-02-R Data interpretation and evaluation\Figures\Section F\Figure F_07_02_01, DSS contour_field_centre.grf

ST15452 Flemish Pass Geotechnical Investigation	Document No. 20140857-02-R
Cyclic DSS Tests, Average and Cyclic Shear Stress normalised to s_{uD} Field Centre For Structural design	Figure No. F7.2.1 Date 2016-04-03 / Drawn by VDa

NGI

P:\2014\08\20140857\Leveransedokumenter\Rapport\20140857-02-R Data interpretation and evaluation\Figures\Section F\Figure F_07_02_02, Cyclic DSS t_cy vs N taua=0_field_centre.grf

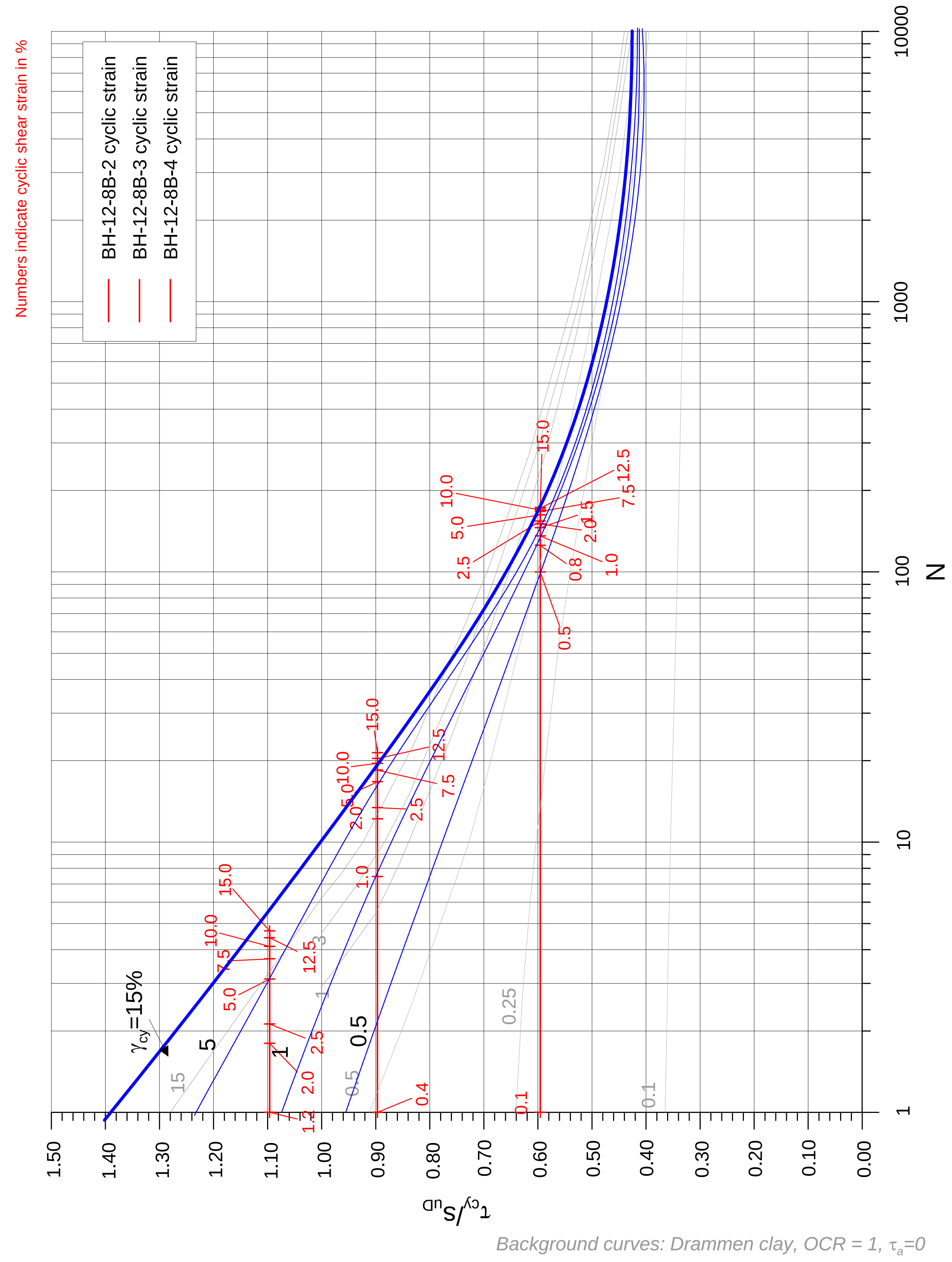

Date/Rev.: 2015-01-21/01

ST15452 Flemish Pass Geotechnical Investigation	Document No. 20140857-02-R	
Normalised cyclic shear stress vs Number of cycles. τ_a/s_{uD} = 0.0 Field Centre For Structural design	Figure No. F7.2.2	
	Date 2016-04-03	Drawn by VDa
	NGI	

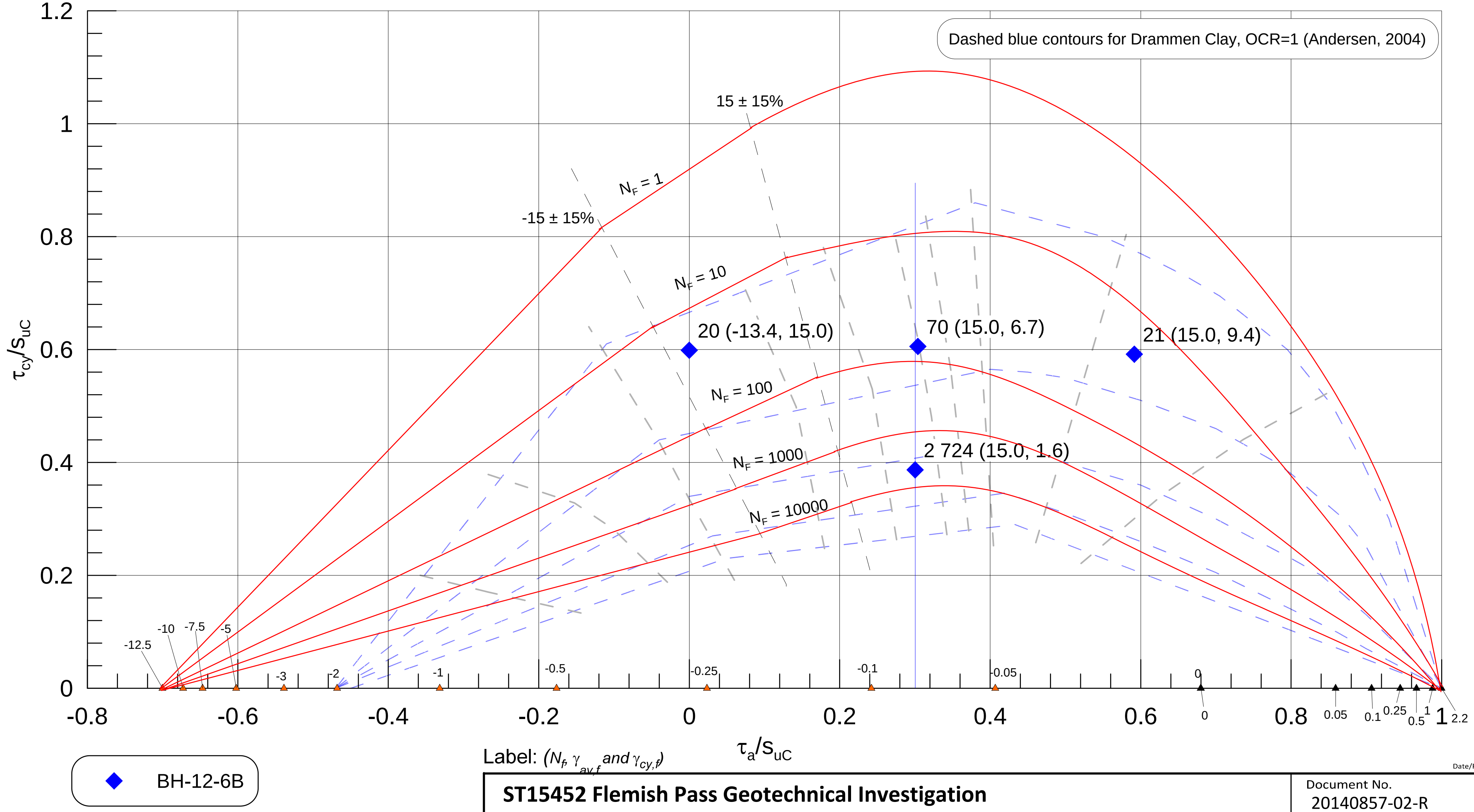

P:\2014\08\20140857\Leveransedokumenter\Rapport\20140857-02-R Data interpretation and evaluation\Figures\Section F\Figure F_07_02_03, CAU contour_field_centre.grf

Date/Rev.: 2015-01-21/01

ST15452 Flemish Pass Geotechnical Investigation	Document No. 20140857-02-R
Cyclic CAU Tests, Average and Cyclic Shear Stress normalised to s_{uC} Field Centre For Structural design	Figure No. F7.2.3
	Date 2016-04-03 / Drawn by VDa/KS

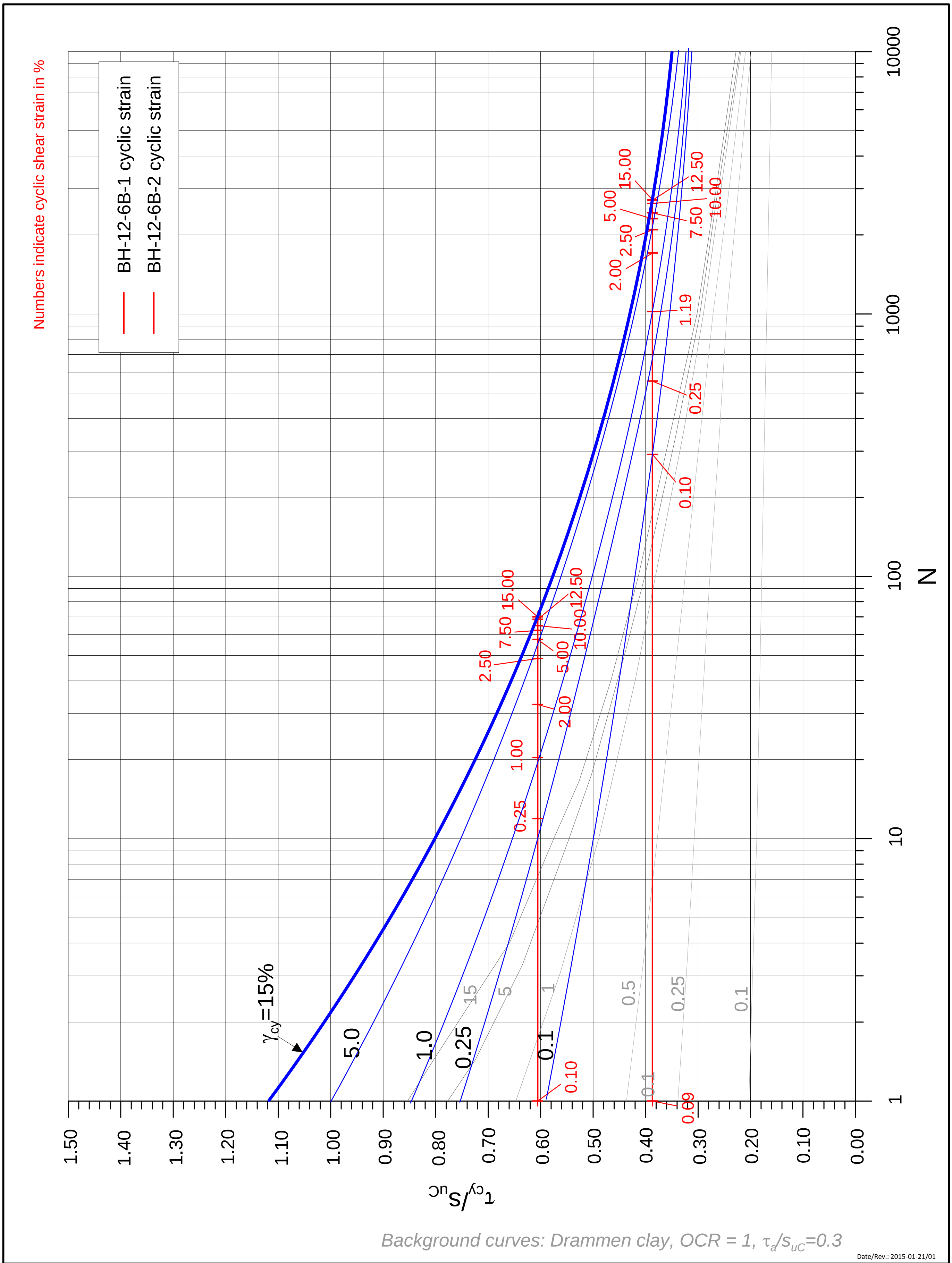

Date/Rev.: 2015-01-21/01

ST15452 Flemish Pass Geotechnical Investigation	Document No. 20140857-02-R
Normalised cyclic shear stress vs number of cycles. τ_a/s_{uC} = 0.3 Field Centre For Structural design	Figure No. F7.2.4
	Date 2016-05-27 / Drawn by VDa/VBS

NGI

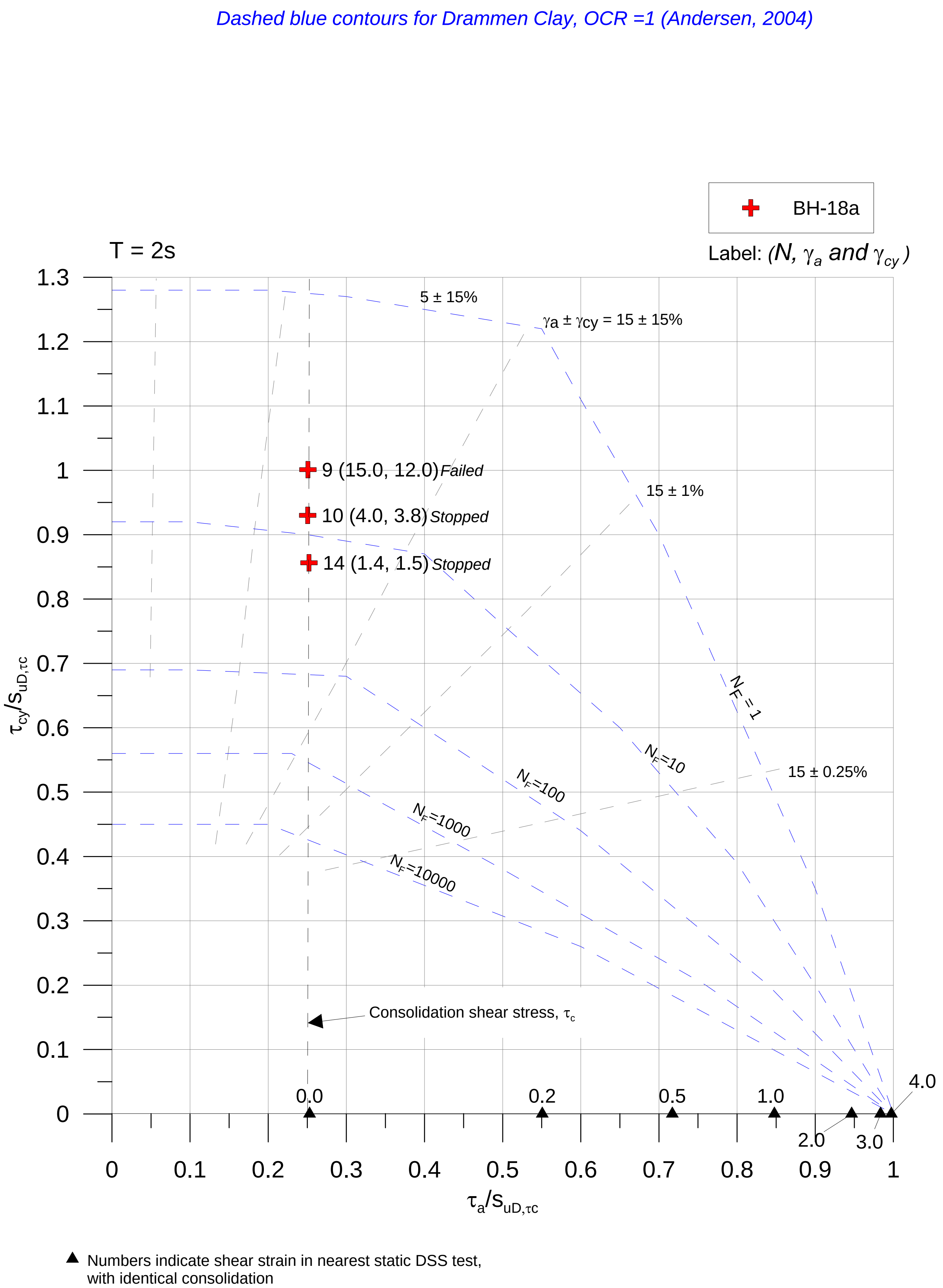

▲ Numbers indicate shear strain in nearest static DSS test, with identical consolidation

P:\2014\08\20140857\Leveransedokumenter\Rapport\20140857-02-R Data interpretation and evaluation\Figures\Section F\Figure F_07_03_01_DSS contour_slopes.grf

Date/Rev.: 2015-01-21/01

ST15452 Flemish Pass Geotechnical Investigation	Document No. 20140857-02-R
Cyclic DSS tests East Slope Average and cyclic shear stress normalised ot the nearest static DSS The closest static DSS consolidated with a shear stress	Figure No. F7.3.1 Date 2016-04-03 Drawn by VDa

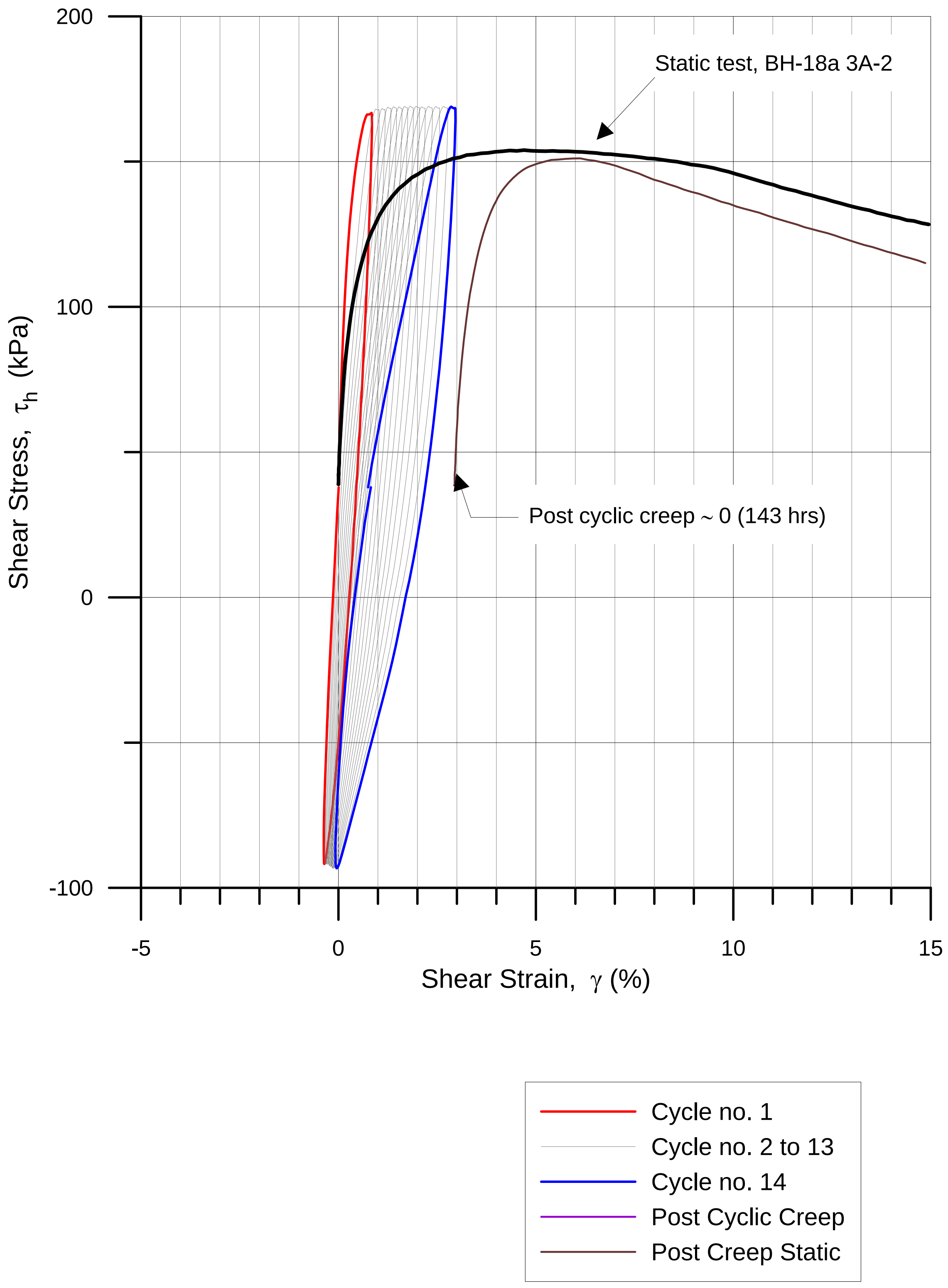

P:\2014\08\20140857\Leveransedokumenter\Rapport\20140857-02-R Data interpretation and evaluation\Figures\Section F\Figure F_07_03_02 cyclic-staticDSS.grf

Date/Rev.: 2015-01-21/01

ST15452 Flemish Pass Geotechnical Investigation	Document No. 20140857-02-R	
Comparison of cyclic DSS BH-18-3A-4 to static DSS Cyclic, creep and static phase of one DSS test compared to closes static DSS	Figure No. F7.3.2	
	Date 2016-04-03	Drawn by KS

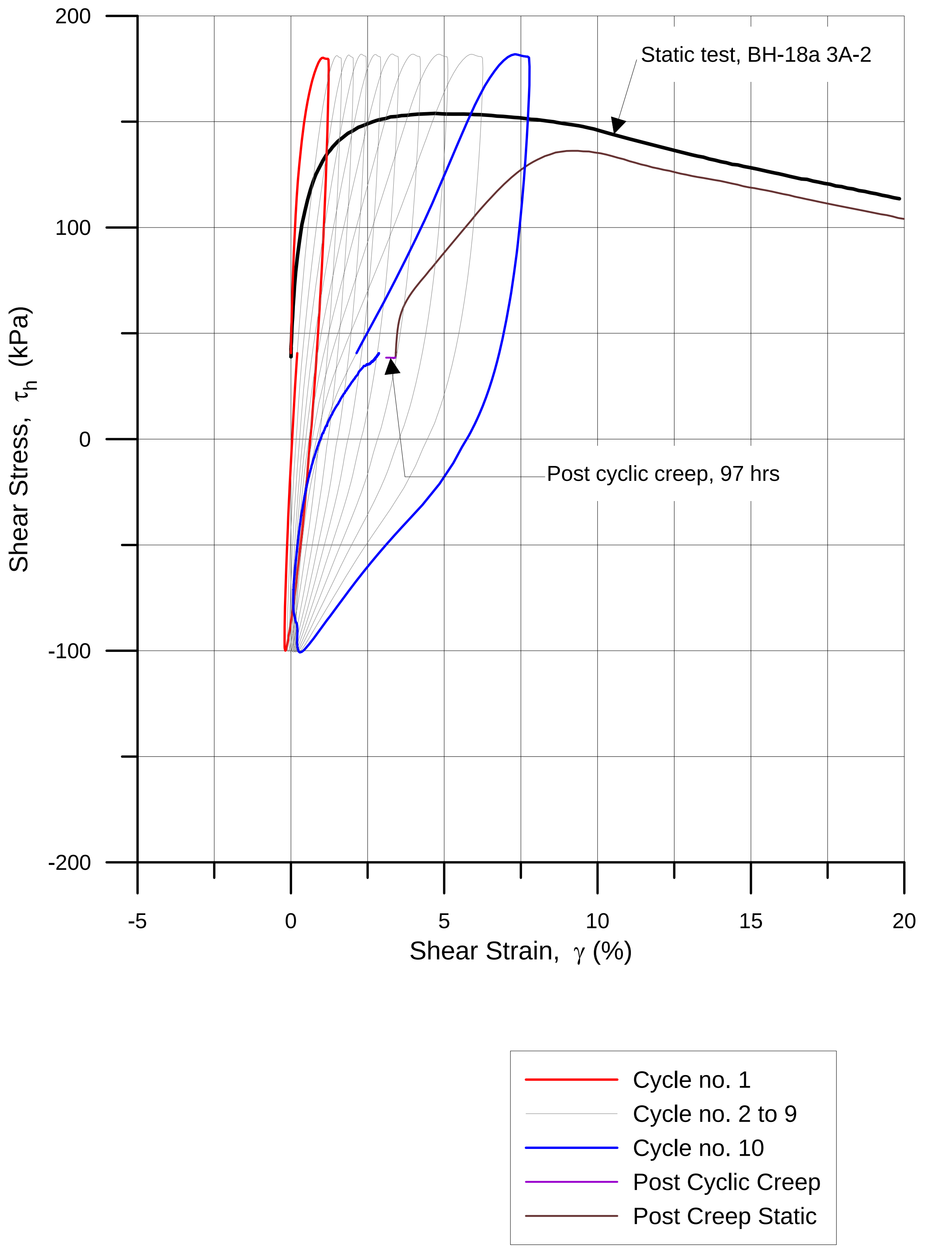

P:\2014\08\20140857\Leveransedokumenter\Rapport\20140857-02-R Data interpretation and evaluation\Figures\Section F\Figure F_07_03_03 cyclic-staticDSS.grf

Date/Rev.: 2015-01-21/01

ST15452 Flemish Pass Geotechnical Investigation	Document No. 20140857-02-R	
Comparison of cyclic DSS BH-18-3A-5 to static DSS	Figure No. F7.3.3	
	Date 2016-04-03	Drawn by KS
Cyclic, creep and static phase of one DSS test compared to closes static DSS	NGI	

P:\2014\08\20140857\Leveransedokumenter\Rapport\20140857-02-R Data interpretation and evaluation\Figures\Section F\Figure F_07_03_04, Creep tests, tau cy versus gamma, East Slope.grf

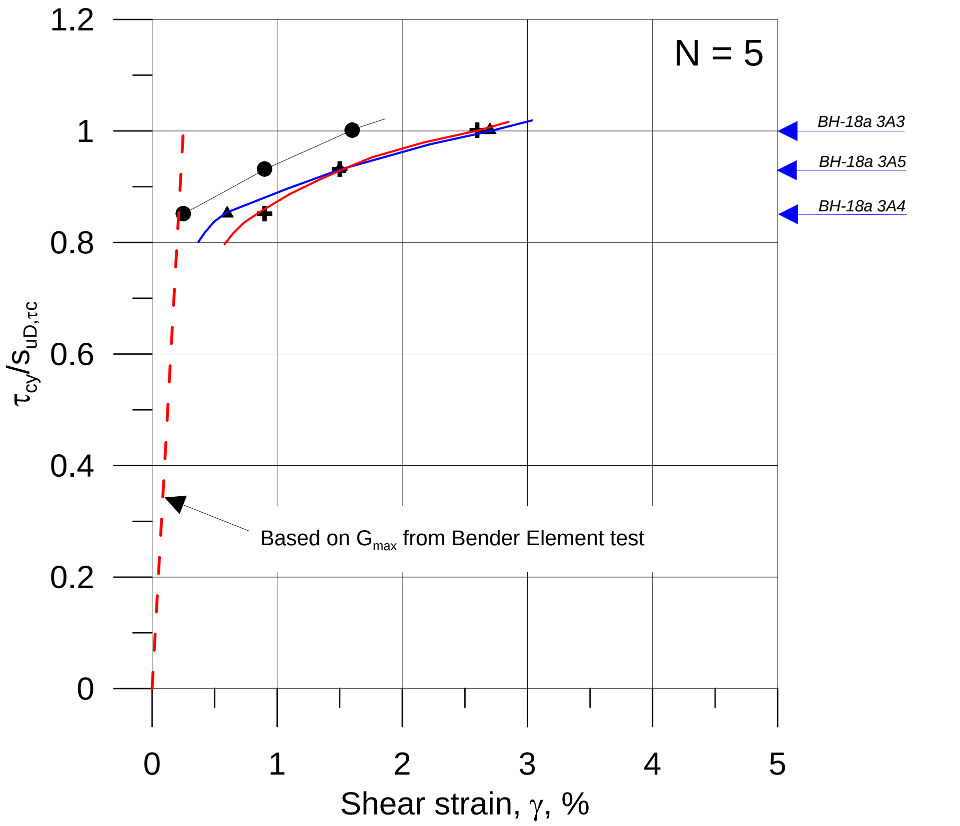

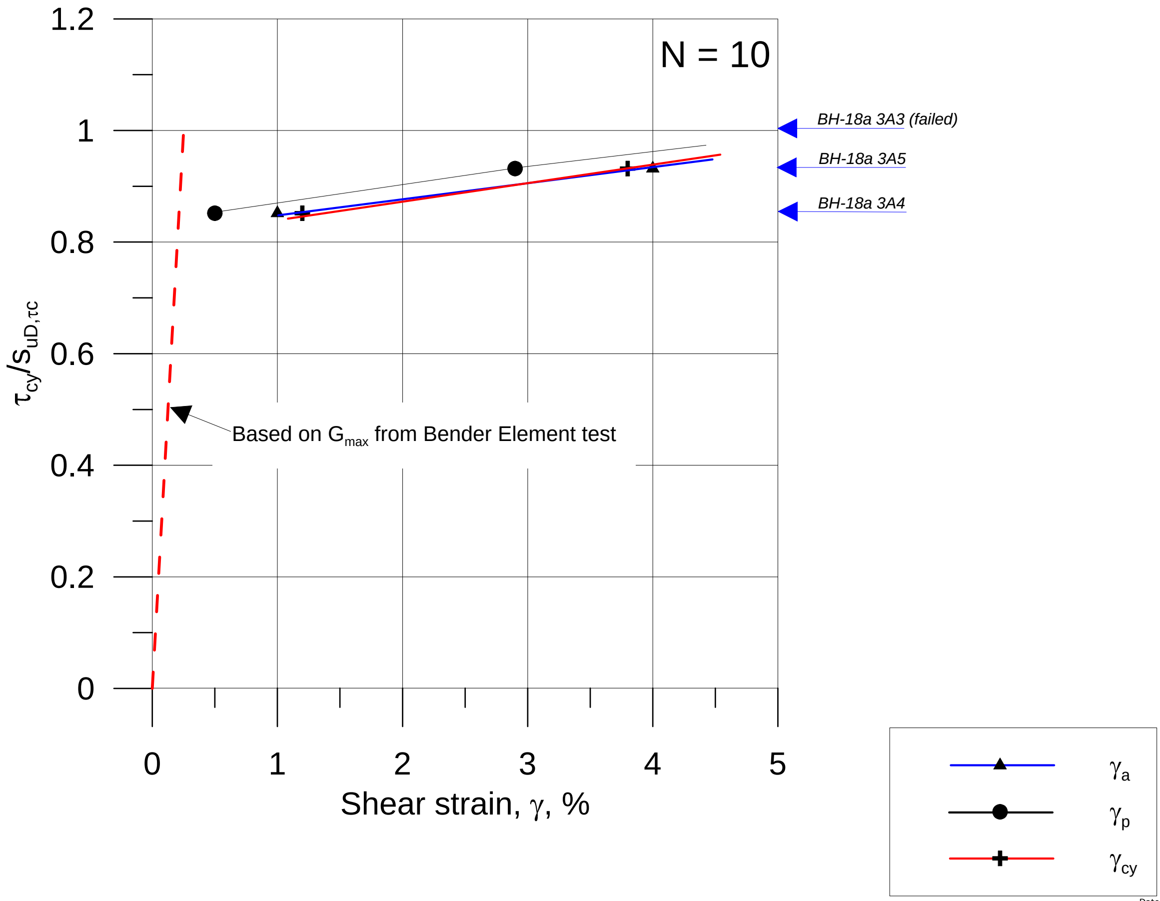

Date/Rev.: 2015-01-21/01

ST15452 Flemish Pass Geotechnical Investigation	Document No. 20140857-02-R	
Cyclic DSS tests East Slope Cyclic shear stress normalised to closest static DSS versus shear strain	Figure No. F7.3.4	
	Date 2016-04-03	Drawn by VDa
	NGI	

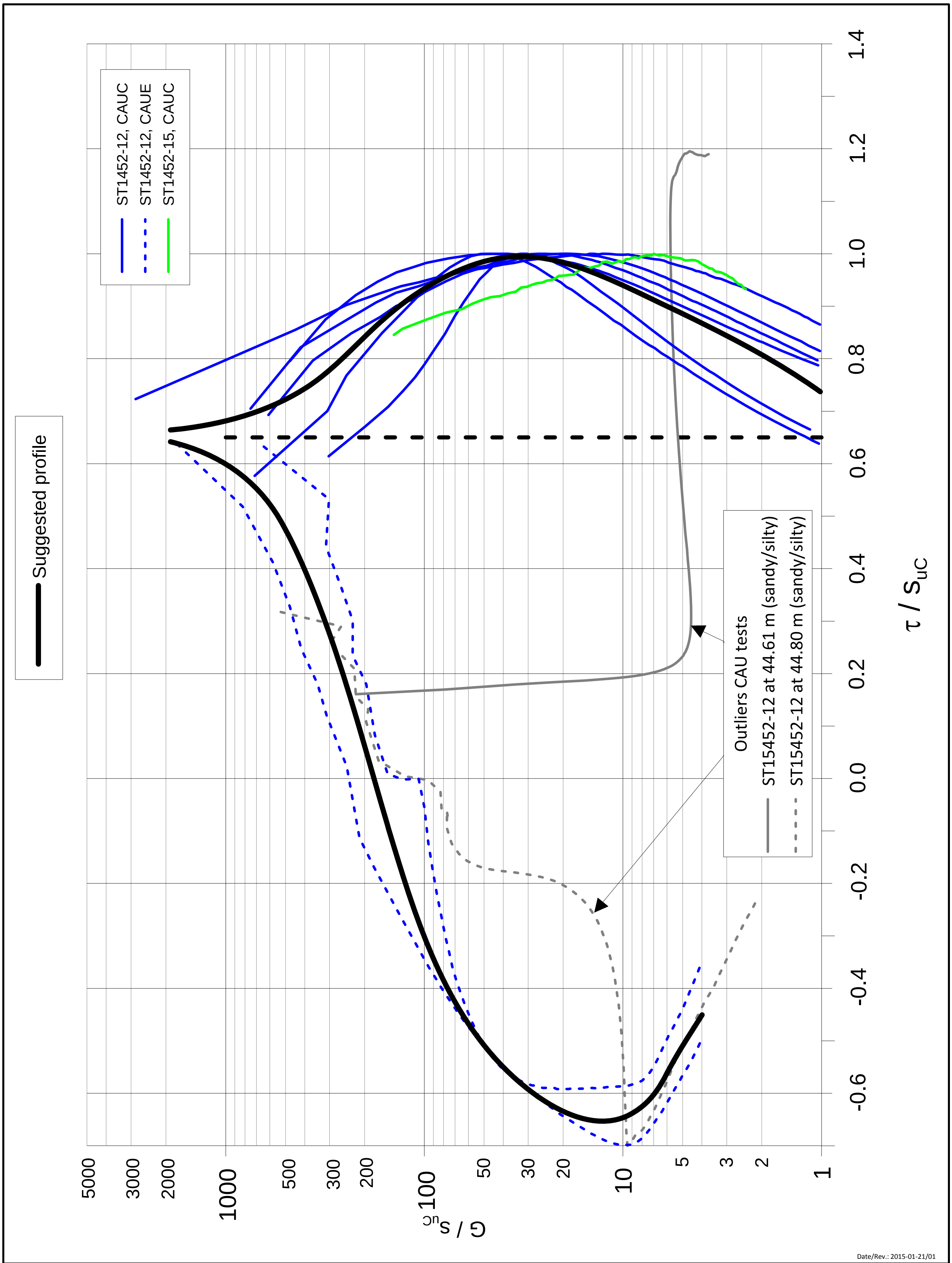

P:\2014\08\20140857\Leveransedokumenter\Rapport\20140857-02-R Data interpretation and evaluation\Figures\Section F\Figure F_08_02_01, G_su_triax vs tau_su_triax_Field_Centre.grf

ST15452 Flemish Pass Geotechnical Investigation	Document No. 20140857-02-R	
G/s_{uC} versus τ/s_{uC} from CAU triaxial tests. Ratio τ_c/s_{uC} = 0.65 Field Centre	Figure No. F8.2.1	
	Date 2016-04-04	Drawn by VDa
	NGI	

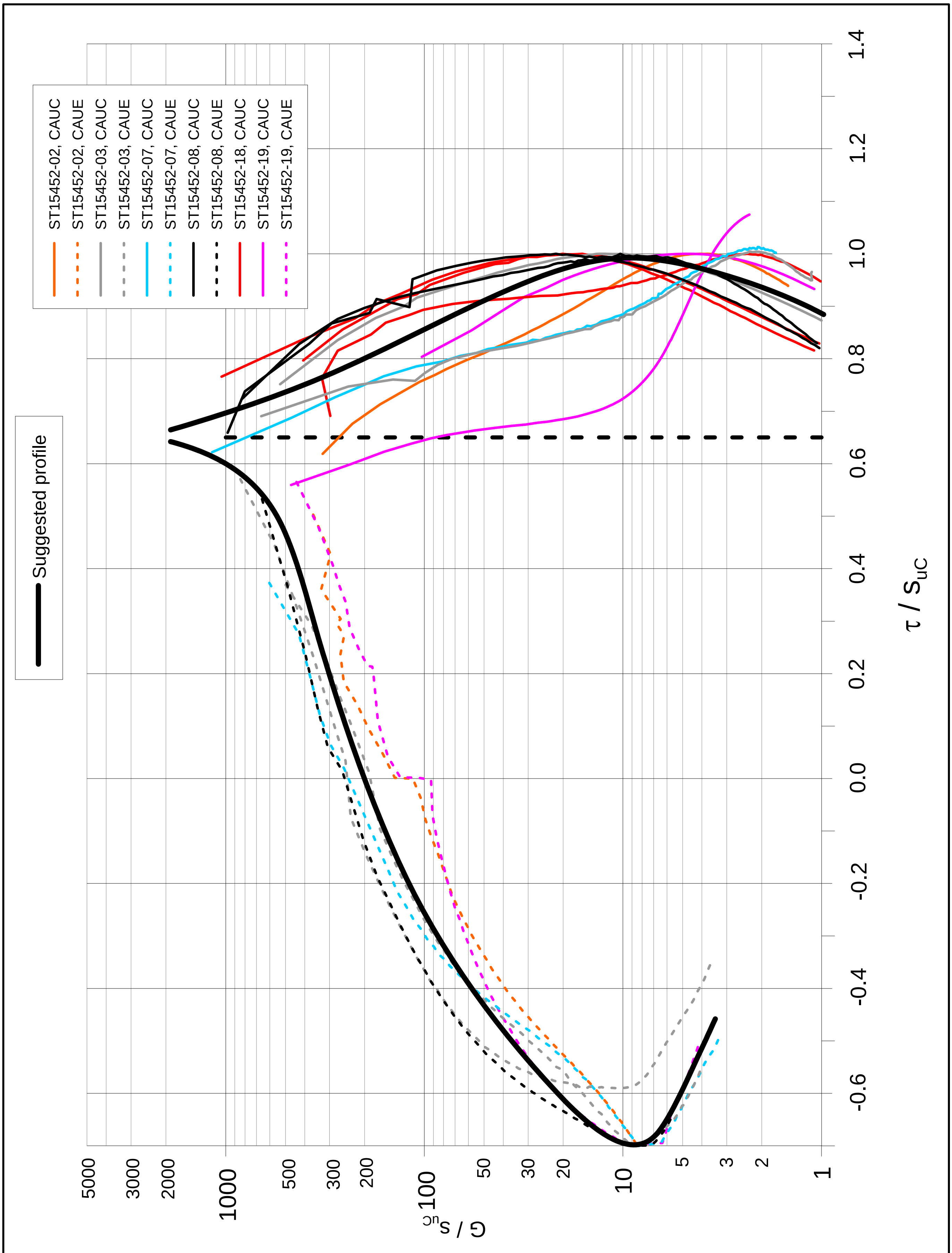

Date/Rev.: 2015-01-21/01

P:\2014\08\20140857\Leveransedokumenter\Rapport\20140857-02-R Data interpretation and evaluation\Figures\Section F\Figure F_08_02_02, G_su_triax vs tau_su_triax_Slopes.grf

ST15452 Flemish Pass Geotechnical Investigation

G/s_{uC} versus τ/s_{uC} from CAU triaxial tests. Ratio τ_c/s_{uC} = 0.65
West Slope and East Slope

Document No. 20140857-02-R	
Figure No. F8.2.2	
Date 2016-04-04	Drawn by VDa

P:\2014\08\20140857\Leveransedokumenter\Rapport\20140857-02-R Data interpretation and evaluation\Figures\Section F\Figure F_08_02_03, G_su_DSS vs tau_su_DSS_field_centre.grf

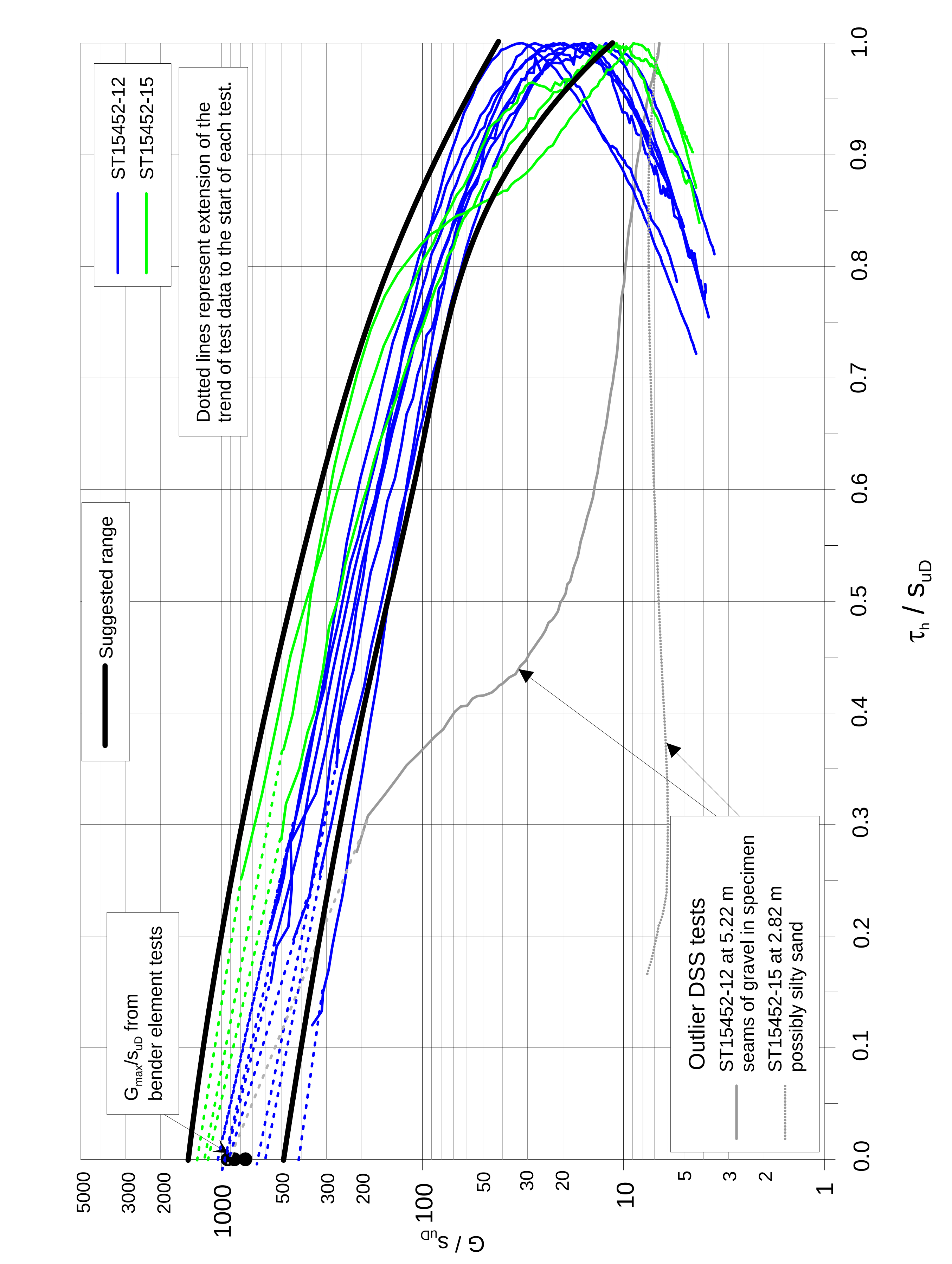

Date/Rev.: 2015-01-21/01

ST15452 Flemish Pass Geotechnical Investigation	Document No. 20140857-02-R
G/s_{uD} versus τ/s_{uD} from DSS tests Field Centre	Figure No. F8.2.3
	Date 2016-04-04 · Drawn by VDa

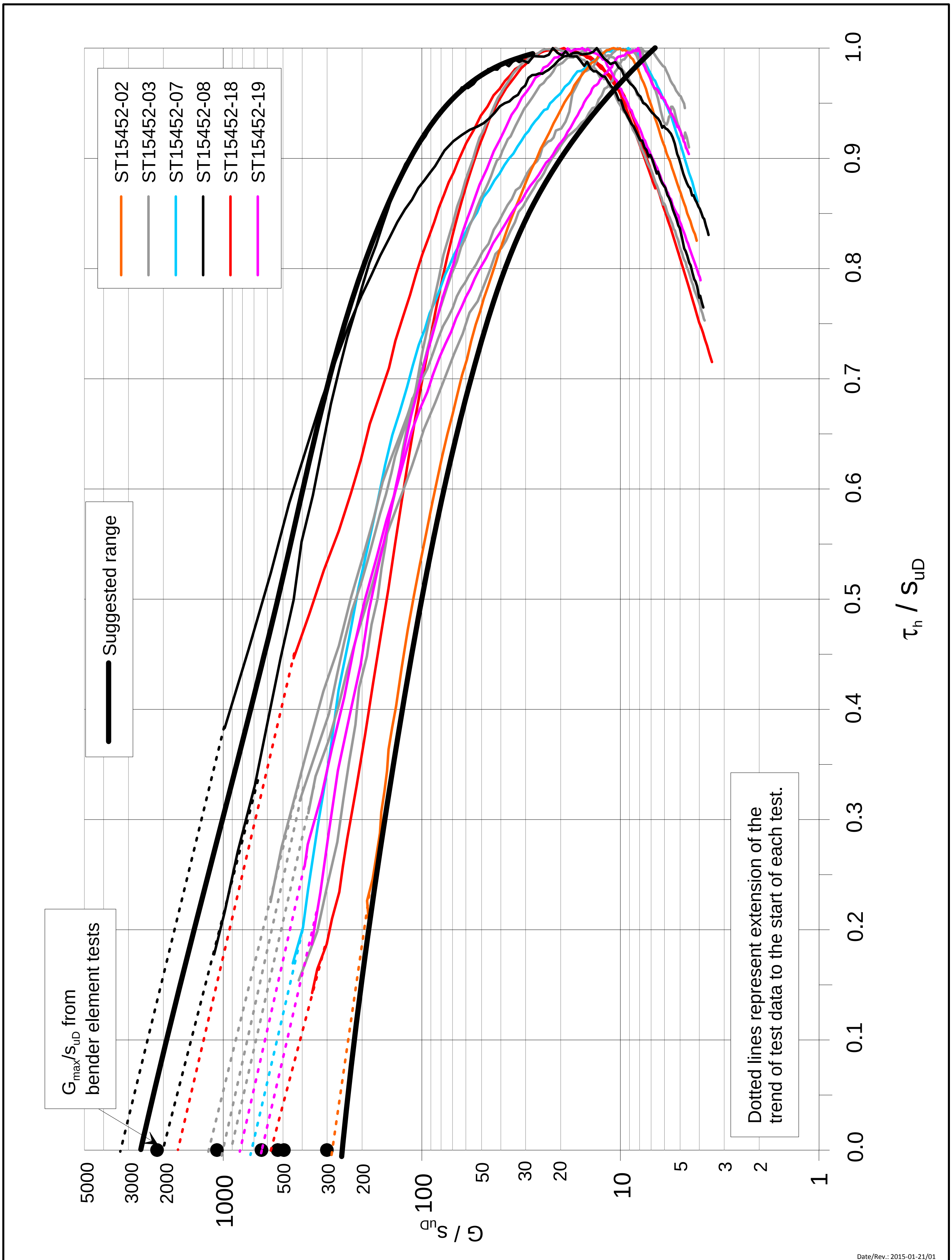

P:\2014\08\20140857\Leveransedokumenter\Rapport\20140857-02-R Data interpretation and evaluation\Figures\Section F\Figure F_08_02_04, G_su_DSS vs tau_su_DSS_Slopes.grf

Date/Rev.: 2015-01-21/01

ST15452 Flemish Pass Geotechnical Investigation	Document No. 20140857-02-R
G/s_{uD} versus τ/s_{uD} from DSS tests West Slope and East Slope	Figure No. F8.2.4
	Date: 2016-04-03 · Drawn by: VDa
	NGI

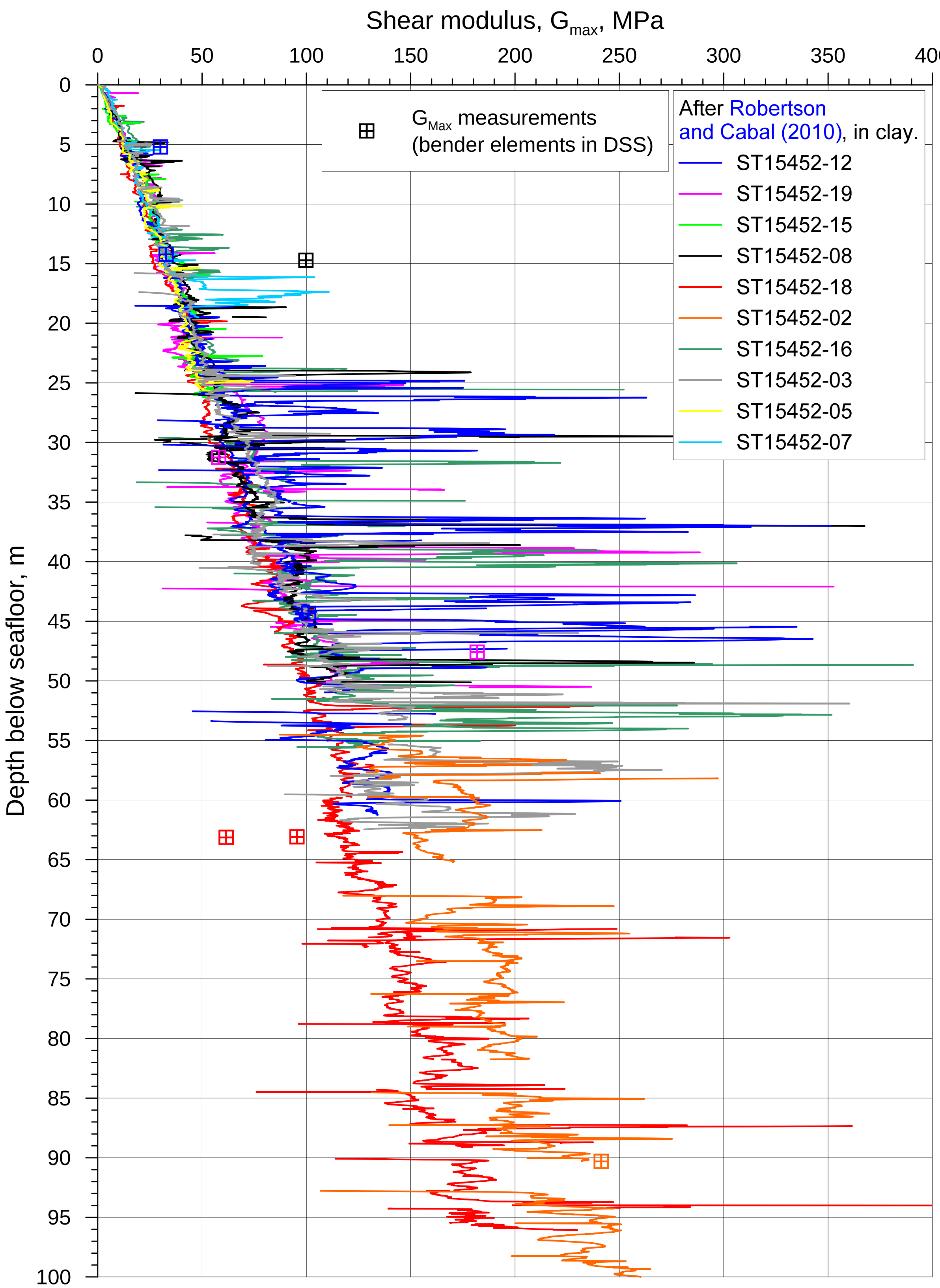

P:\2014\08\20140857\Leveransedokumenter\Rapport\20140857-02-R Data interpretation and evaluation\Figures\Section F\Figure F_08_03_01, Gmax versus depth_all.grf

Date/Rev.: 2015-01-21/01

ST15452 Flemish Pass Geotechnical Investigation	Document No. 20140857-02-R
Maximum shear modulus versus depth All locations	Figure No. F8.3.1
	Date 2016-04-03 / Drawn by VDa

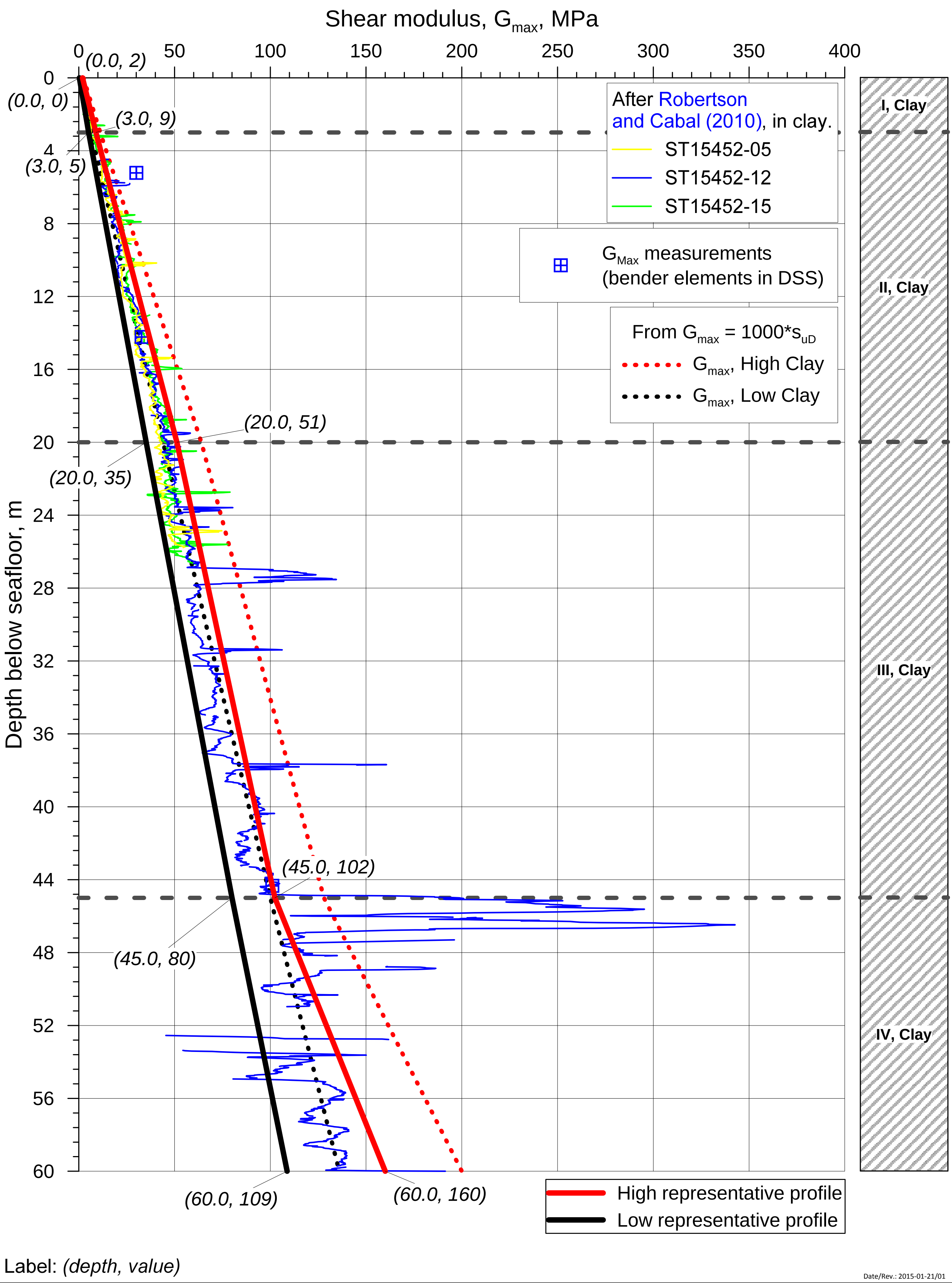

P:\2014\08\20140857\Leveransedokumenter\Rapport\20140857-02-R Data interpretation and evaluation\Figures\Section F\Figure F_08_03_02, Gmax versus depth_Field_Centre.grf

Date/Rev.: 2015-01-21/01

ST15452 Flemish Pass Geotechnical Investigation	Document No. 20140857-02-R
Maximum shear modulus versus depth Field Centre	Figure No. F8.3.2
	Date 2016-04-03 / Drawn by VDa

NGI

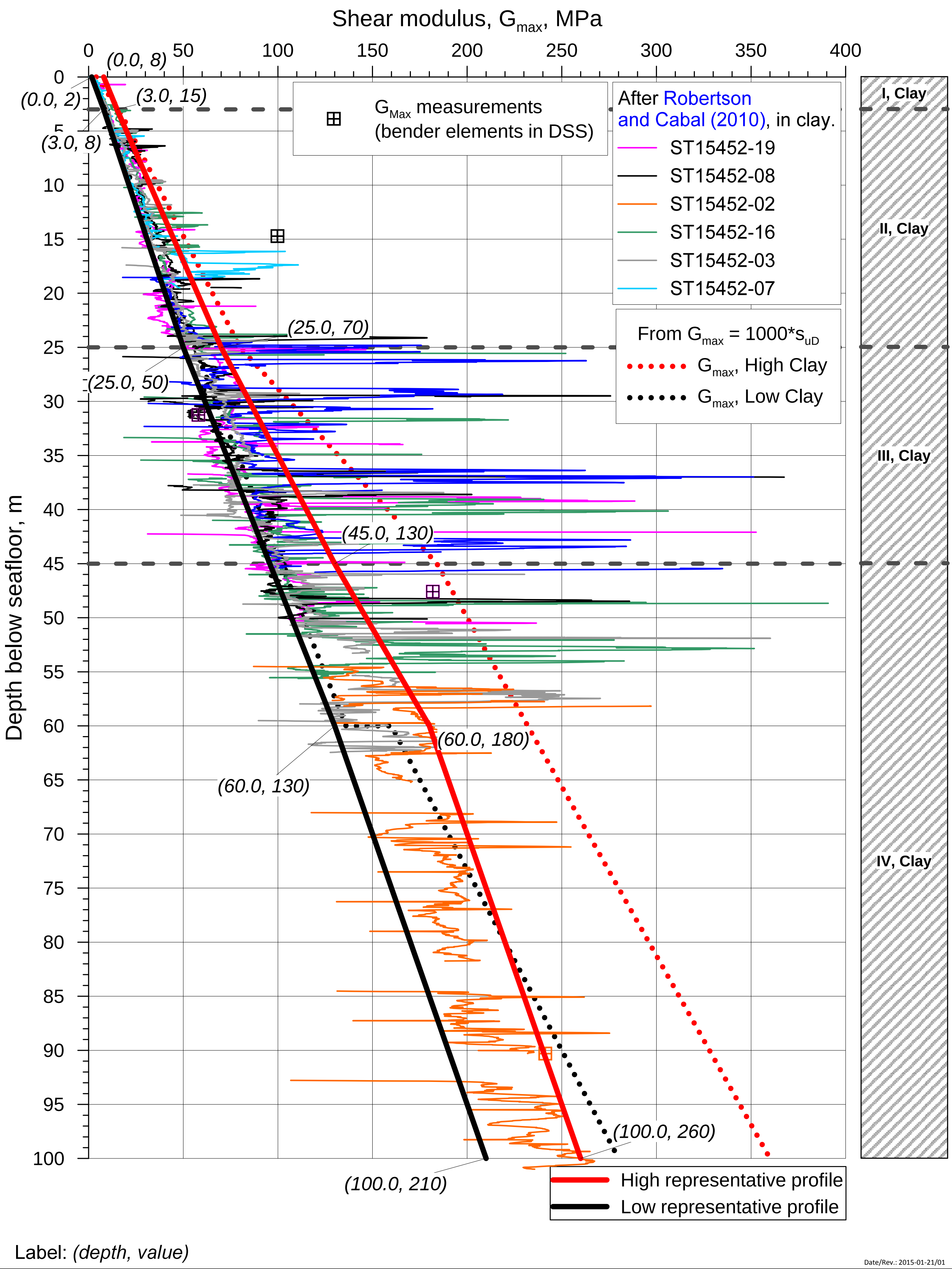

P:\2014\08\20140857\Leveransedokumenter\Rapport\20140857-02-R Data interpretation and evaluation\Figures\Section F\Figure F_08_03_03, Gmax versus depth_Westslope.grf

Date/Rev.: 2015-01-21/01

ST15452 Flemish Pass Geotechnical Investigation	Document No. 20140857-02-R
Maximum shear modulus versus depth West Slope	Figure No. F8.3.3
	Date 2016-04-03 / Drawn by VDa

NGI

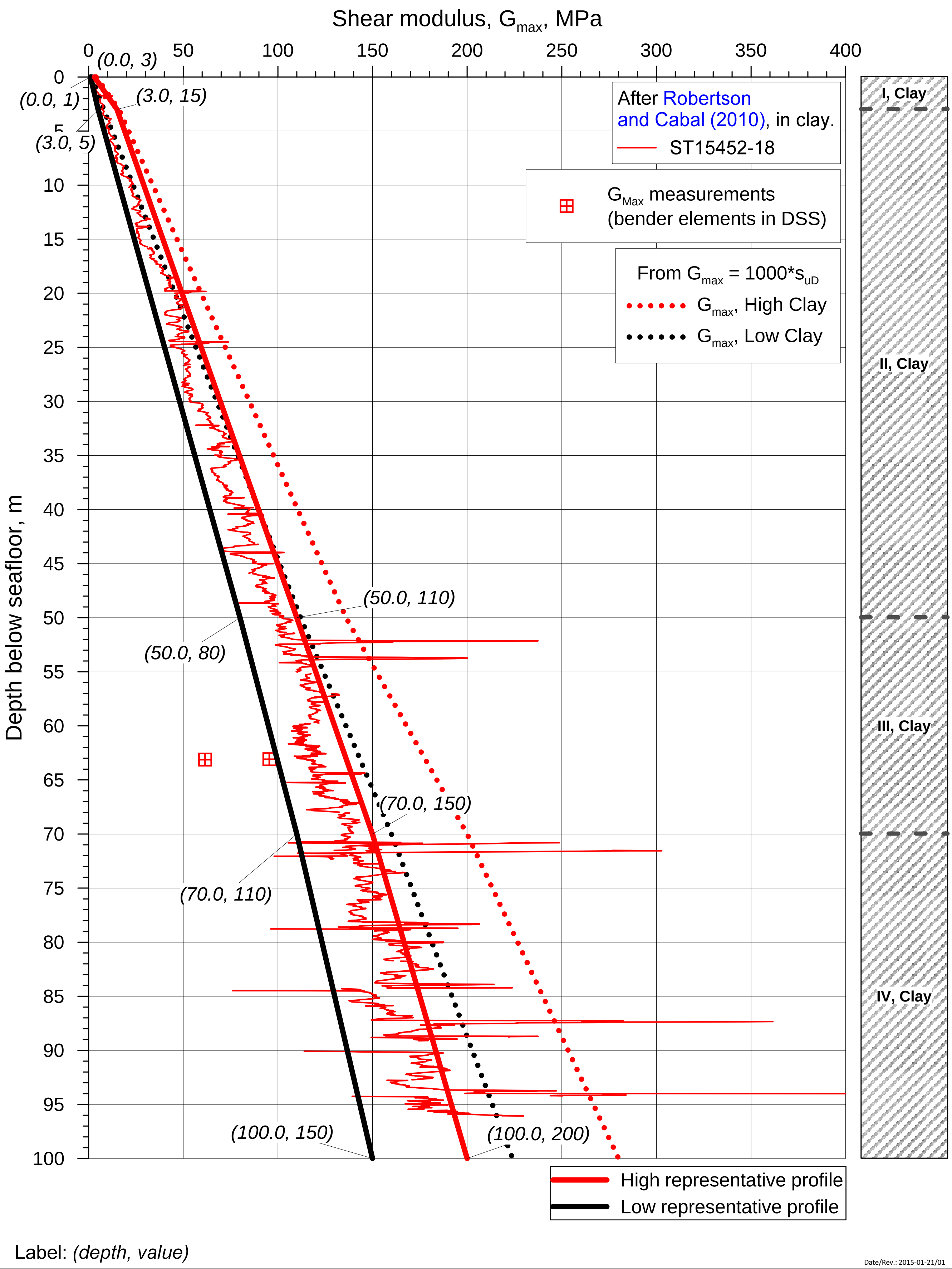

P:\2014\08\20140857\Leveranse dokumenter\Rapport\20140857-02-R Data interpretation and evaluation\Figures\Section F\Figure F_08_03_04, Gmax versus depth_Eastslope.grf

Date/Rev.: 2015-01-21/01

ST15452 Flemish Pass Geotechnical Investigation	Document No. 20140857-02-R
Maximum shear modulus versus depth East Slope	Figure No. F8.3.4
	Date 2016-04-03 / Drawn by VDa
	NGI

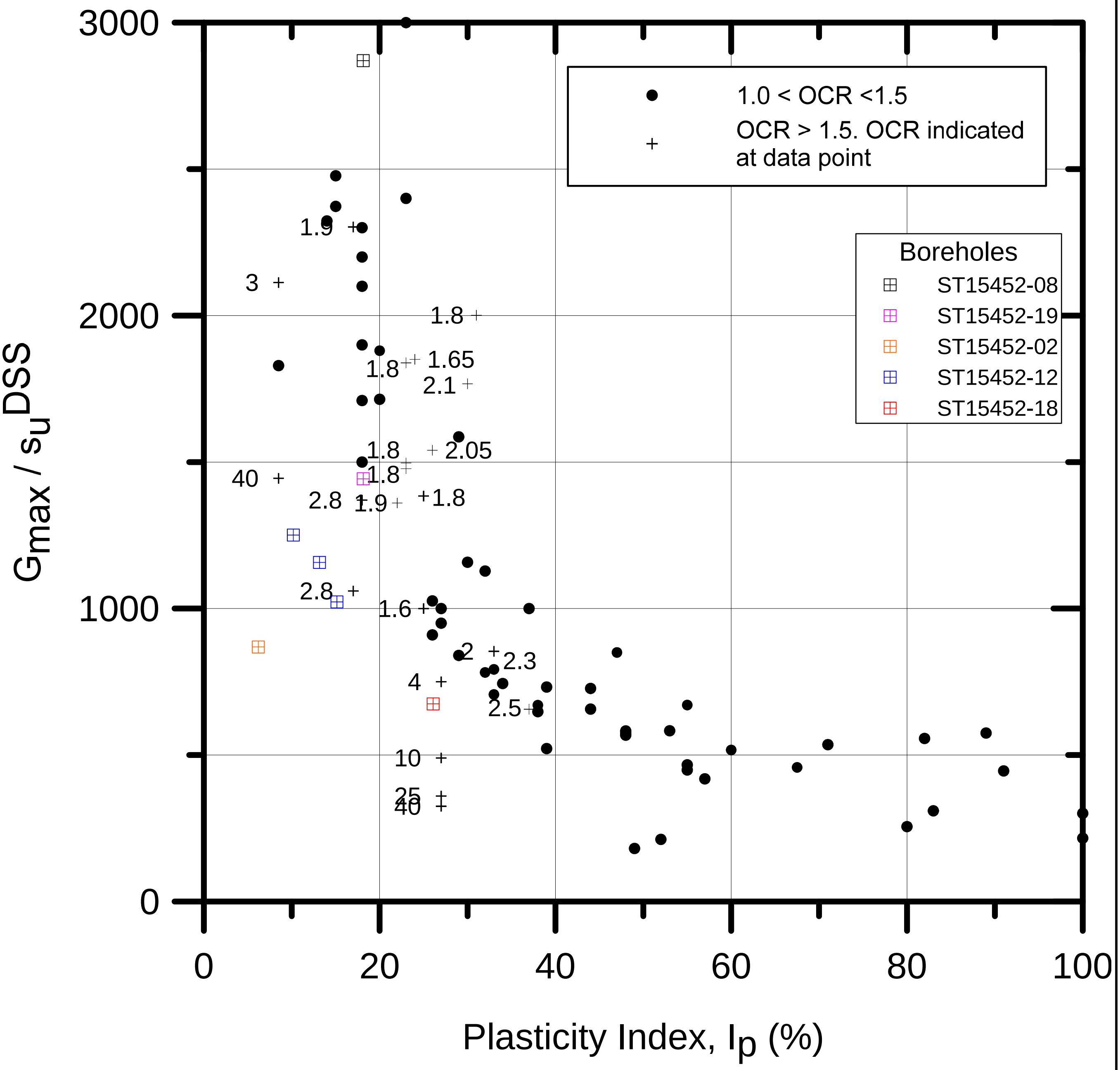

(Figure from Andersen et al., 2008)

Date/Rev.: 2015-01-21/01

ST15452 Flemish Pass Geotechnical Investigation

G/s_{uD} versus I_p from DSS tests
All locations

Document No.	20140857-02-R
Figure No.	F8.3.5
Date	2016-04-04
Drawn by	VDa

P:\2014\08\20140857\Leveransedokumenter\Rapport\20140857-02-R Data interpretation and evaluation\Figures\Section F\Figure F_08_03_05, Gmax_su_DSS vs_Ip_all.grf

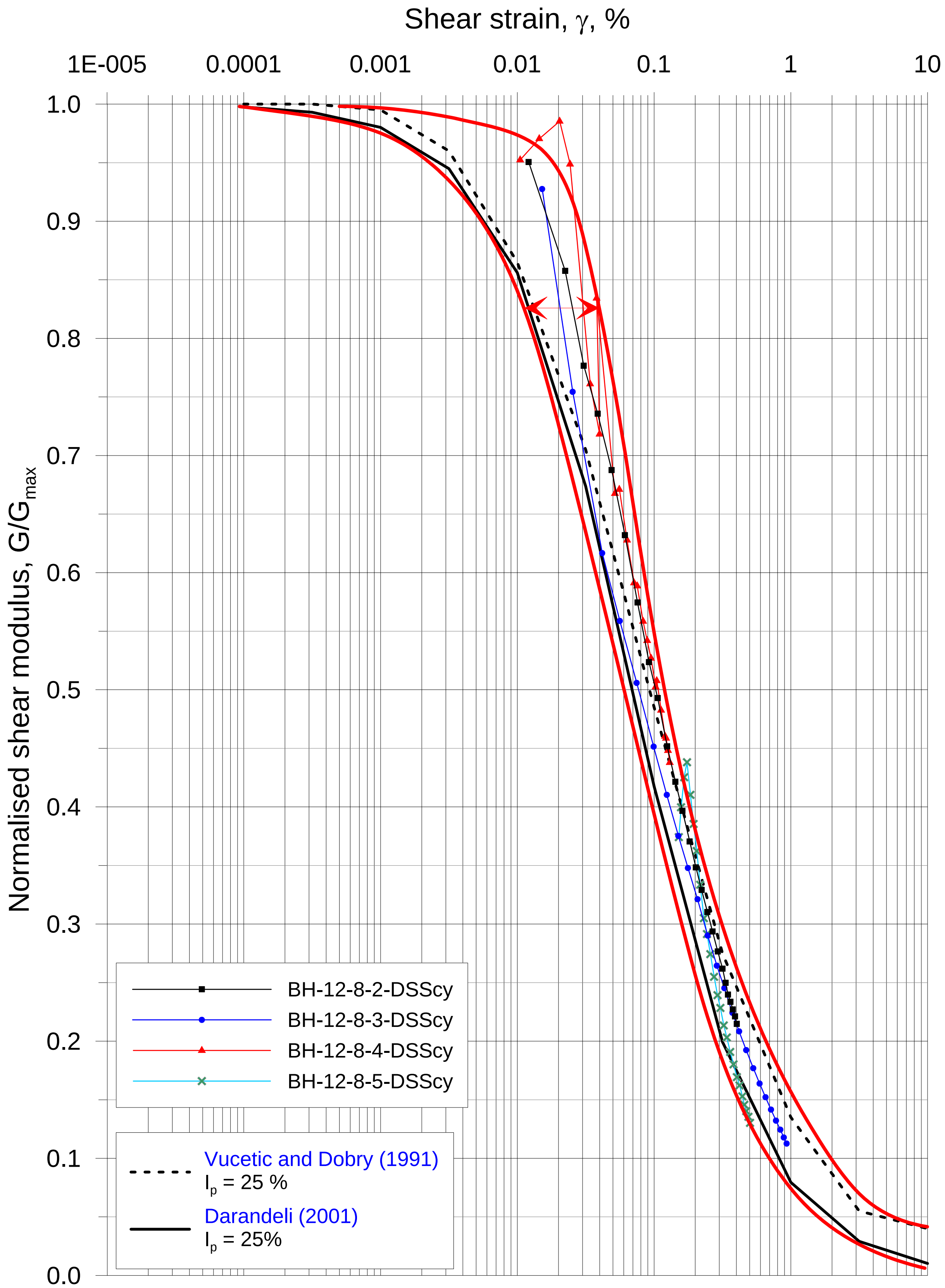

Note: For DSS tests, the G_{max} values are evaluated using Robertson and Cabbal, (2010) equation.

Suggested range of G/G_{max}

G_{max} = 39.3 MPa

Date/Rev.: 2015-01-21/01

P:\2014\08\20140857\Leveransedokumenter\Rapport\20140857-02-R Data interpretation and evaluation\Figures\Section F\Figure F_08_04_01, NormalizedGmax versus shear strain_N=1_Field_centre.grf

ST15452 Flemish Pass Geotechnical Investigation	Document No. 20140857-02-R	
Normalised shear modulus, G/G_{max}, versus shear strain from DSS tests Field Centre N=1 cycle	Figure No. F8.4.1	
	Date 2016-04-03	Drawn by VDa
	NGI	

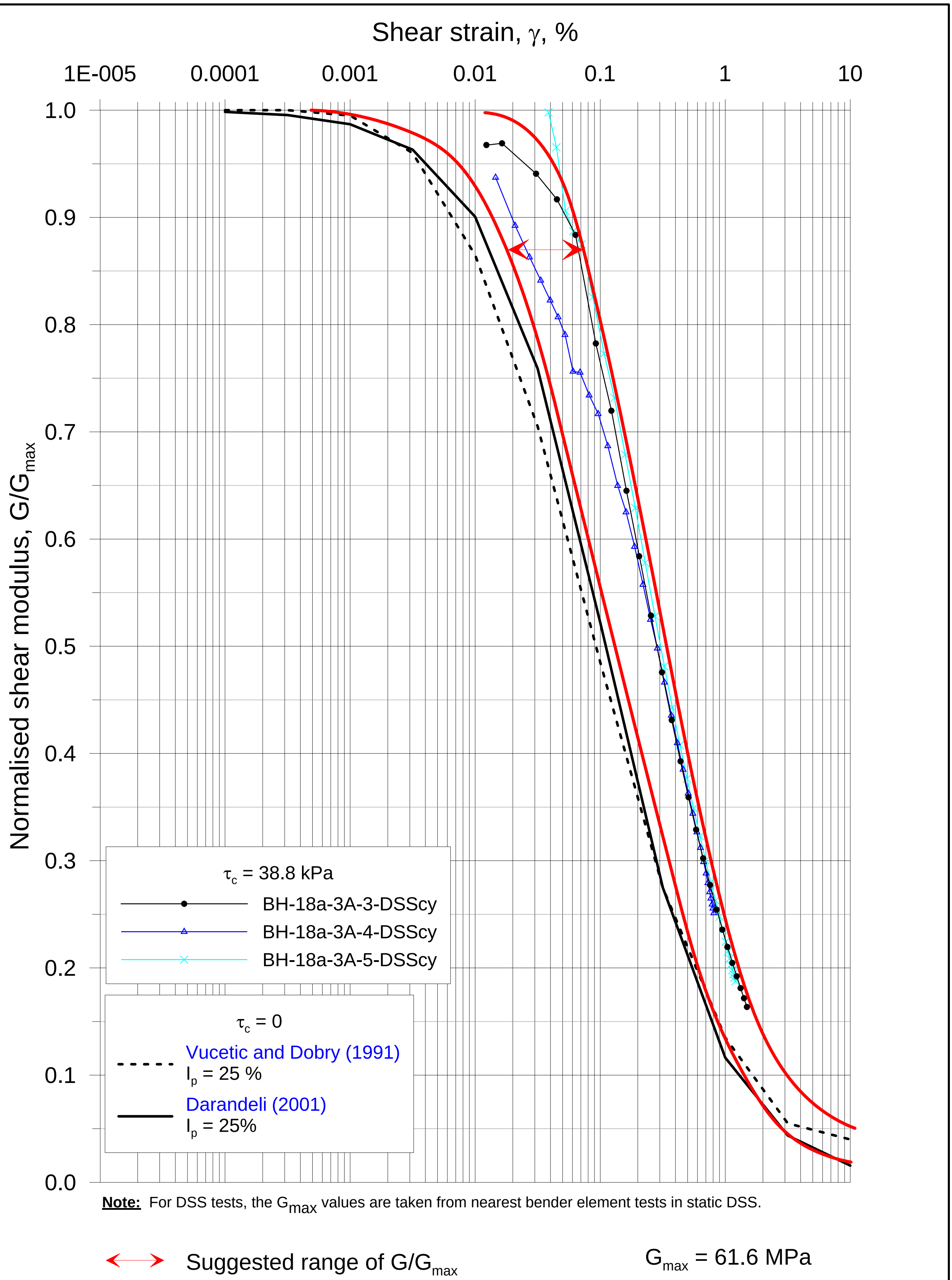

Date/Rev.: 2015-01-21/01

ST15452 Flemish Pass Geotechnical Investigation	Document No. 20140857-02-R
Normalised shear modulus, G/G_{max}, versus shear strain East Slope N=1 cycle	Figure No. F8.4.2
	Date: 2016-04-03 / Drawn by: VDa

NGI

P:\2014\08\20140857\Leveranse dokumenter\Rapport\20140857-02-R Data interpretation and evaluation\Figures\Section F\Figure F_08_05_01, Damping versus shear strain_Field_centre.grf

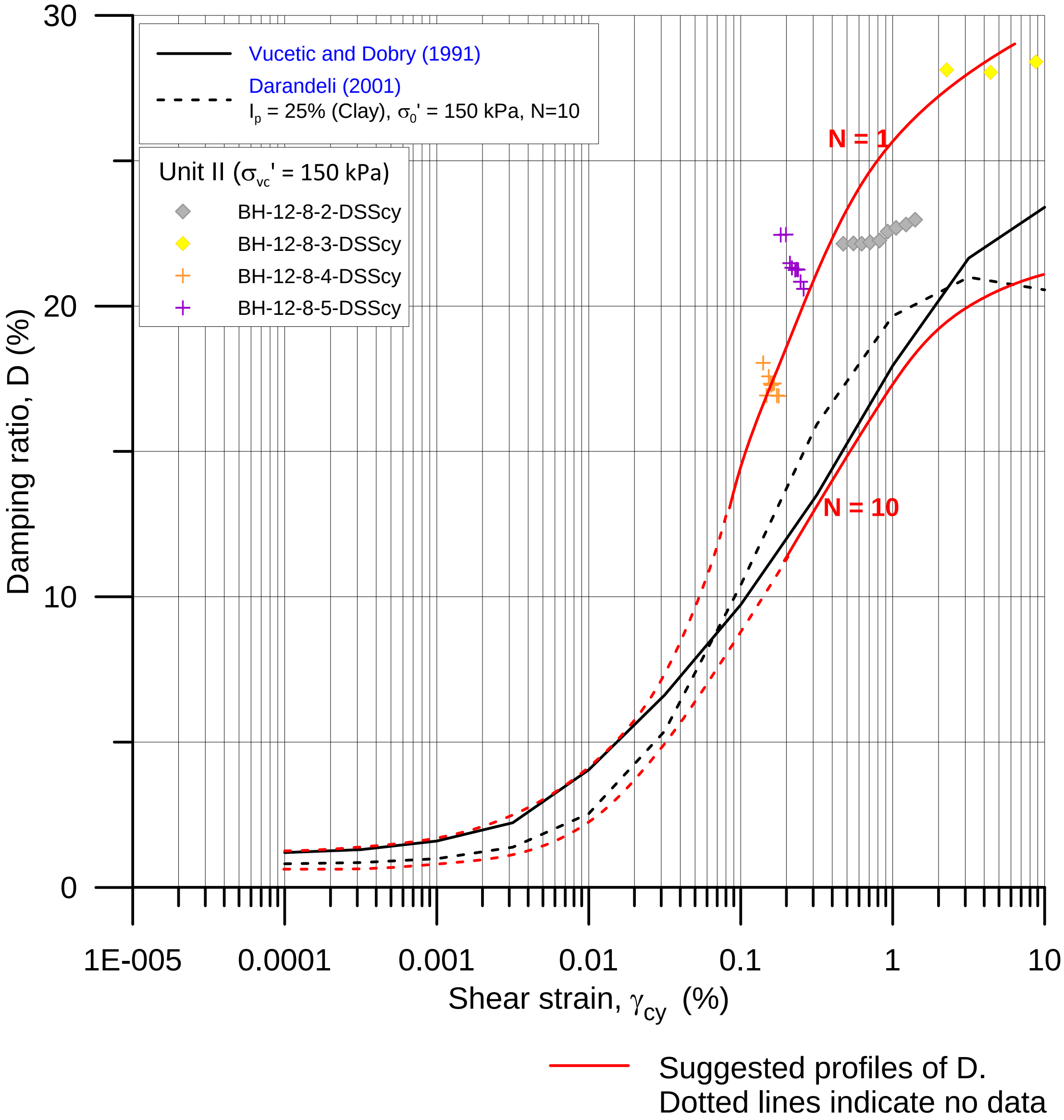

Date/Rev.: 2015-01-21/01

ST15452 Flemish Pass Geotechnical Investigation	Document No. 20140857-02-R	
Damping ratio, D, versus cyclic shear strain from symmetric cyclic DSS tests Field Centre	Figure No. F8.5.1	
	Date 2016-04-03	Drawn by VDa

NGI

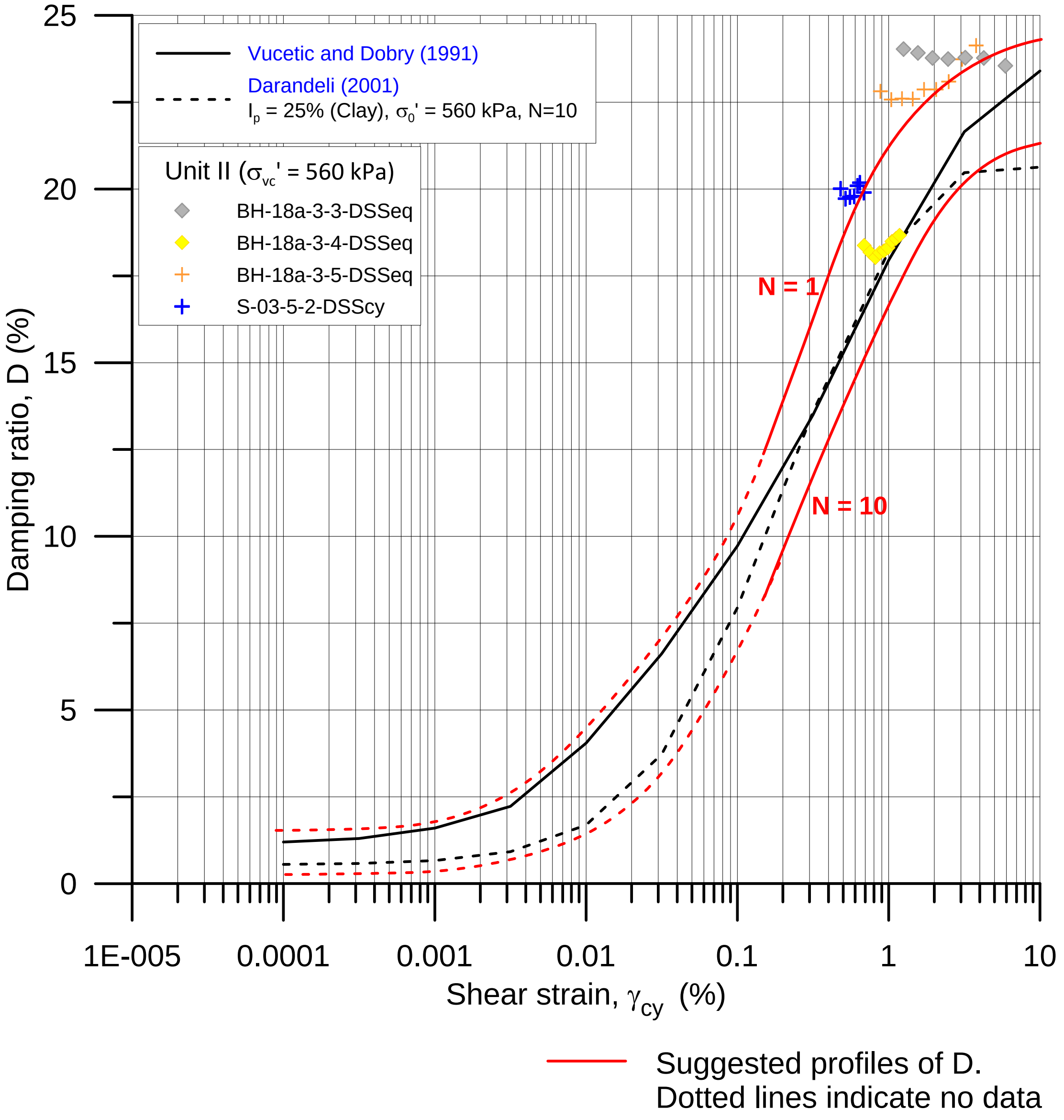

P:\2014\08\20140857\Leveransedokumenter\Rapport\20140857-02-R Data interpretation and evaluation\Figures\Section F\Figure F_08_05_02, Damping versus shear strain_East_slope.grf

Date/Rev.: 2015-01-21/01

ST15452 Flemish Pass Geotechnical Investigation	Document No. 20140857-02-R	
Damping ratio, D, versus cyclic shear strain from symmetric cyclic DSS tests East Slope	Figure No. F8.5.2	
	Date 2016-04-03	Drawn by VDa

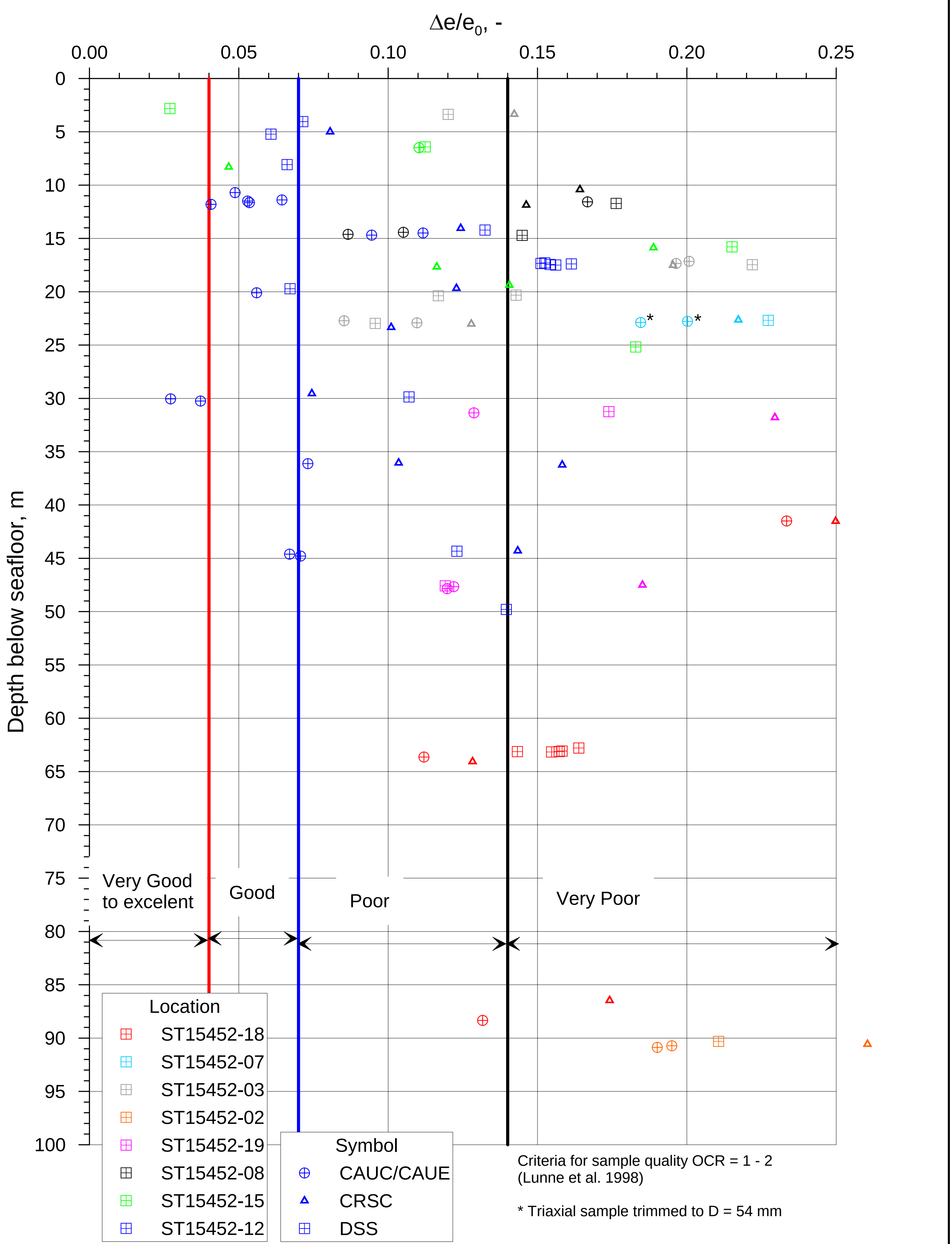

P:\2014\08\20140857\Leveransedokumenter\Rapport\20140857-02-R Data interpretation and evaluation\Figures\Section F\Figure F_09_01_01, e_e0 versus depth.grf

Date/Rev.: 2015-01-21/01

ST15452 Flemish Pass Geotechnical Investigation

Sample quality assessed from CAU, DSS and CRSC tests
All locations

Document No.
20140857-02-R

Figure No.
F9.1.1

Date
2016-04-03

Drawn by
VBS

NGI

Section G

RECOMMENDED REPRESENTATIVE GEOTECHNICAL PARAMETERS, FIELD CENTRE

Contents

Tables

Figures

G1 General

This section presents the representative soil parameters for the Flemish Pass Field Centre.

The main purpose of the geotechnical testing and parameters given for the Field Centre in this section is to provide parameters for FEED design of structures. This includes anchors, templates, pipelines etc.

The representative soil parameters are based on interpretation of the available data and test results reported and referred to in Section F and NGI (2016).

The soil is layered giving high variability over short depth ranges. The soil conditions are, however relatively consistent between the Field Centre locations. The figures presented herein show representative profiles including measured values in the background to illustrate the available information and spread in data.

The water depth at the boreholes investigated at the Field Centre location was between 1163 m and 1173 m.

G2 Soil layering

At the Field Centre the soil from seafloor down to a depth of 61 m can in general be divided into four clay units. Table G2-1 presents the depths to the units and the descriptions for the Field Centre locations. The units are in line with the geophysical interpretation presented in Section E.

Table G2-1 Summary of the generalised soil conditions encountered at the Field Centre locations

Unit	Depth below seafloor, m (indicative values)	Soil description
I	0 – 3.0	CLAY, silty, extremely low to low strength, traces of fine to medium sand partings and few shell fragments, greenish grey. Sandy in the upper 20 cm in some locations
II	3.0 – 20.0	CLAY, low to medium strength, low to medium plasticity, sand seams at different locations, few drop stones, gravel or larger, and pockets of sands, greenish grey to dark gray.
III	20.0 – 45.0[1)]	CLAY, medium to high strength, medium plasticity, traces of fine sub-angular to sub-rounded gravels and coarse shell fragments, dark gray, gas in solution.
IV	45.0 – 61.2[2)]	CLAY, medium to high strength, medium plasticity, drop stones, gravel or larger. Possibly mass transport deposit, dark gray.

1) End of borehole for ST15452 –S-05 is at 26.7 m and for ST15452 –S-15 is at 26.7 m.
2) End of borehole for ST15452 –BH-12 is at 61.2 m.

Table G2-2 presents a summary of the soil layering and representative characteristics for the Field Centre. Further details and discussion on classification data including profiles of recommended representative basic soil parameters are presented in Section F. The range of measured values are included in Table G2-2.

Table G2-2 Soil units and representative characteristics relevant for 0 – 61 m depth, Field Centre locations. The range of measured data is given in brackets to show variability.

Unit	Typical depth below seafloor, m	Soil type	Water content, w, %	Total unit weight, γ, kN/m^3	Plasticity index[2)], I_p, %	Fines content[3)], %	Corrected cone resistance[4)], q_t, MPa	Undrained shear strength[4)], s_{uC}, kPa
I	0 – 3.0	CLAY	55 (31-76)	16.5 (15.3 – 19.0)	22 (20 – 24)	92 - 96 (42 - 46)	0.05 – 0.1	1 – 8
II	3.0 – 20.0	CLAY	35 (15 – 72)	18.5 (15.0 – 22.5)	12 (6 – 30)	55 - 94 (18 - 44)	0.1 - 1	8 -55
III	20.0 – 45.0	CLAY	27-40 (17 – 73)	18.0-19.6 (15.5 – 22.0)	20 (9 – 35)	60 - 96 (19 - 50)	1 - 2	55 – 125
IV	45.0 – 61.2[1)]	CLAY	27 (20-33)	19.6 (17.8 – 20.8)	14 (14 – 16)	79 - 81 (34 - 36)	2.2 – 3.5	125 - 170

[1)] End of borehole for ST15452 –BH-12 is at 61.2 m
[2)] Only relevant for clay material
[3)] Range of values (range of clay content in brackets)
[4)] Low representative values or range of values

G3 Classification soil parameters

The figures presented herein show representative profiles including measured values in the background to illustrate the available information and spread in data.

G3.1 Water content

The representative water content profile for the Field Centre is presented in Figure G3.1.

G3.2 Total unit weight

The representative total unit weight profile for the Field Centre is presented in Figure G3.2.

G3.3 Plasticity data

The representative profile of plasticity index for the Field Centre is presented in Figure G3.3.

G3.4 Unit weight of solid particles

The representative profile of unit weight of solid particles is presented in Figure G3.4.

G3.5 Grain size distribution

Figure G3.5 presents the values of clay content and fines content with depth. No representative profile nor trend lines have been drawn due to the variability of the soil.

G3.6 Remoulded shear strength

For the purpose of skirt penetration analysis it is suggested to use a skirt wall friction equal to the remoulded undrained shear strength as measured in the laboratory tests. Figure G3.6 shows the measured remoulded shear strength together with a low and high representative profile.

G3.7 Sensitivity

Sensitivity has been determined from index shear strength tests on intact and remoulded clay samples. The sensitivity is calculated as $S_t = s_u/s_{ur}$, where s_u and s_{ur} are the shear strengths for the intact and the remoulded samples, respectively. The representative sensitivity profile is shown in Figure G3.7. It is taken as $S_t = s_{uD}^{avg}/s_{ur}^{avg}$. See Section F for further explanation.

G4 In situ stresses and stress history

G4.1 In situ effective vertical stress

The representative profile of effective vertical stress, p_0', is presented in Figure G4.1. The profile is derived from the representative total unit weight profile in Figure G3.2 assuming hydrostatic pore pressure in situ.

The in situ effective vertical stress, p_0' (in kPa), based on the average depth to each soil unit can be calculated as:

$0 < z < 3.0$ m:	$p_0' = 6.5z$
$3.0 < z < 20.0$ m:	$p_0' = -6 + 8.5z$
$20.0 < z < 30.0$ m:	$p_0' = -16 + 9z$
$30.0 < z < 40.0$ m:	$p_0' = 14 + 8z$
$40.0 < z < 60.0$ m:	$p_0' = -50 + 9.6z$

where z is depth below seafloor in metres.

G4.2 Preconsolidation stress and overconsolidation ratio

The interpretation of preconsolidation stress, p_c', and overconsolidation ratio, OCR, is based on results from oedometer tests using various interpretation methods and on the CAUC test results and the CPTU results using the method of Andresen et al. (1979). The representative profiles of p_c' and OCR are presented in Figures G4.2 and G4.3, respectively.

G4.3 Coefficient of earth pressure at rest

Horizontal in situ effective stresses are derived using the coefficient of earth pressure at rest, K_0. The representative K_0 profile is shown in Figure G4.4.

G5 Consolidation parameters

G5.1 Immediate settlements

Immediate settlements may be estimated by elasticity theory using the shear modulus, G. The G-value will typically vary from soil element to soil element and depends on the degree of strength mobilization, the degree of overconsolidation, the strength and the general soil characteristics.

Based on the laboratory tests carried out, the normalised secant shear moduli have been presented as a function of strength mobilisation. Figure G8.1 shows suggested values of

G/s_{uC} versus τ/s_{uC} for all different units tested based on the compression and extension CAU-triaxial tests carried out. Figure G8.2 gives similar suggestions in terms of G/s_{uD} versus τ_h/s_{uD} based on the DSS tests carried out.

G5.2 Primary consolidation settlements

The soil parameters necessary for evaluating the primary consolidation settlements and its time dependency are the constrained modulus, M, the coefficient of vertical consolidation, c_v, and the drainage length, H.

The primary consolidation settlements are generally influenced by the relationship between the stress increase imposed by the structure, the initial in situ stresses, and the preconsolidation stress, p_c'. Stress increases that exceed p_c' will usually yield much larger settlements.

The consolidation settlements can be calculated using the Janbu modulus concept (Janbu, 1963). The representative profile of the constrained modulus, M_0 is presented in Figure G5.1. Figure G5.2 presents the suggested representative profile of the modulus number and reference stress (m and p_r').

The soil parameters, k_v and c_v necessary for evaluating the speed of the primary consolidation settlement are presented in Figures G5.3 and G5.4, respectively.

G6 Static soil strength parameters

G6.1 CPTU measurements

Summary diagrams of the corrected cone resistance, q_t, are presented in Figures G6.1 and G6.2, at two different depth scales.

Summary plot of the sleeve friction, f_s, is presented in Figure G6.3.

Summary plot of the measured pore water pressure, u_2 versus depth is presented in Figure G6.4.

G6.2 Undrained static shear strength parameters

Static undrained shear strength parameters were evaluated based on CPTUs, triaxial tests, DSS tests and a number of index shear strength tests. All these tests were carried out as undrained tests relevant for short term loading, and the results are presented and discussed in Section F.

The representative high and low profiles of undrained shear strength are presented in two different scales in Figures G6.5 and G6.6. The low profile should be used for geotechnical analyses where a low strength is conservative and the upper profile for geotechnical analyses where a high strength is conservative. The designer should evaluate the effect of softer layers by adding a 1 m thick layer with strength 10 % below the low representative strength at any level below 5 m depth.

The representative strength anisotropy ratios are:

Soil Units I, II*, III and IV: $s_{uD}/s_{uC} = 0.80$
Soil Units I, II*, III and IV: $s_{uE}/s_{uC} = 0.75$

*There are data from approximately 30 m depth indicating lower values of anisotropy in Unit II of $s_{uD}/s_{uC} = 0.6$ and $s_{uE}/s_{uC} = 0.45$. A designer can take the representative profiles as a baseline and should assess the effect of applying the low representative profiles.

G6.3 Effective shear strength parameters

The triaxial tests have been interpreted in terms of effective stresses.

Summary of effective stress paths from CAUC and CAUE triaxial tests on intact samples are presented in Section F with the Mohr-Coulomb failure envelopes representing the recommended effective friction angles (ϕ'_u) and attraction (a) obtained from these undrained tests.

A range of a = 0 kPa and ϕ' between 30° and 36° is suggested appropriate for the tested material.

For further details see Section F.

G7 Cyclic soil strength parameters

The behaviour of Soil Unit II subjected to cyclic wave loading has been investigated by both cyclic triaxial and cyclic DSS tests. Figures G7.1 and G7.2 give parameters for cyclic behaviour of Soil Unit II. For further discussion on the applicability of the different parameters for different strata of soil, reference is made to Section F.

G8 Stiffness and damping parameters for dynamic analysis

The normalised secant shear moduli have been presented as a function of strength mobilisation. Figure G8.1 shows suggested values of G/s_{uC} versus τ/s_{uC} for all units tested based on the compression and extension CAU-triaxial tests carried out. Figure G8.2 gives similar suggestions in terms of G/s_{uD} versus τ_h/s_{uD} based on the DSS tests carried out.

G_{max} measurements were performed on specimens in the laboratory using piezo-ceramic bender elements in connections with DSS tests. The high and low representative profiles with depth are presented in Figure G8.3.

The suggested range in normalised shear modulus, G/G_{max}, versus shear strain is presented in Figures G8.4.

The suggested profiles of damping ratio, D, versus cyclic shear strain for N = 1 and N = 10 are presented in Figure G8.5 for soil Unit II.

For more details reference is made to Section F.

G9 Skirt penetration resistance

For a structure with skirts, the following geotechnical parameters are considered relevant for calculation of skirt penetration resistance and bearing capacity:

- Unit weight, see Figure G3.2
- Undrained shear strength in clay, see Figures G6.5 and G6.6 (two different depth scales)
- Remoulded shear strength profile, see Figure G3.6

Figures G6.5 and G6.6 give a good indication of the trend and variation of strength with depth. For the user of strength profiles it is important to note that some advanced data plot well above the given representative high profile. These are tests of material that is significantly more silty or sandy than the bulk of material. It is important to note that they are real measurements, and that may be important for installation analyses. Layers of sand typically 0.5 – 1 m thickness are found in various depths and boreholes. Some are up to 2 m thick. They are shown in terms of q_t in Figure G6.2. The designer should consider the background information presented in the report and use soil parameters relevant for the selected design approach and method(s).

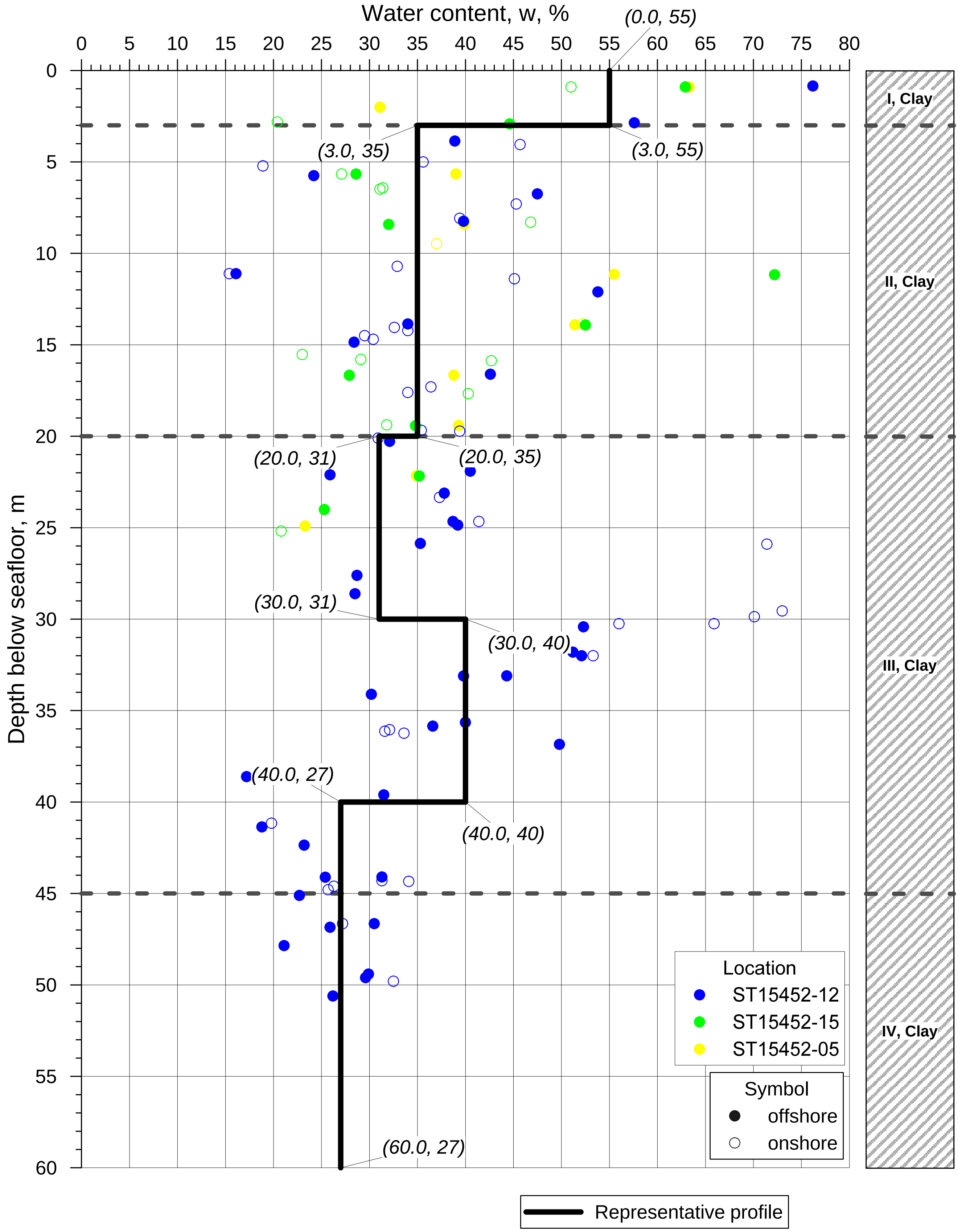

Label: *(depth, value)*

Date/Rev.: 2015-01-21/01

P:\2014\08\20140857\Leveransedokumenter\Rapport\20140857-02-R Data interpretation and evaluation\Figures\Section G\Figure G_03_01, water content versus depth-Fieldcentre.grf

ST15452 Flemish Pass Geotechnical Investigation	Document No. 20140857-02-R
Water content versus depth Field Centre	Figure No. G3.1
	Date 2016-04-03 / Drawn by VBS

NGI

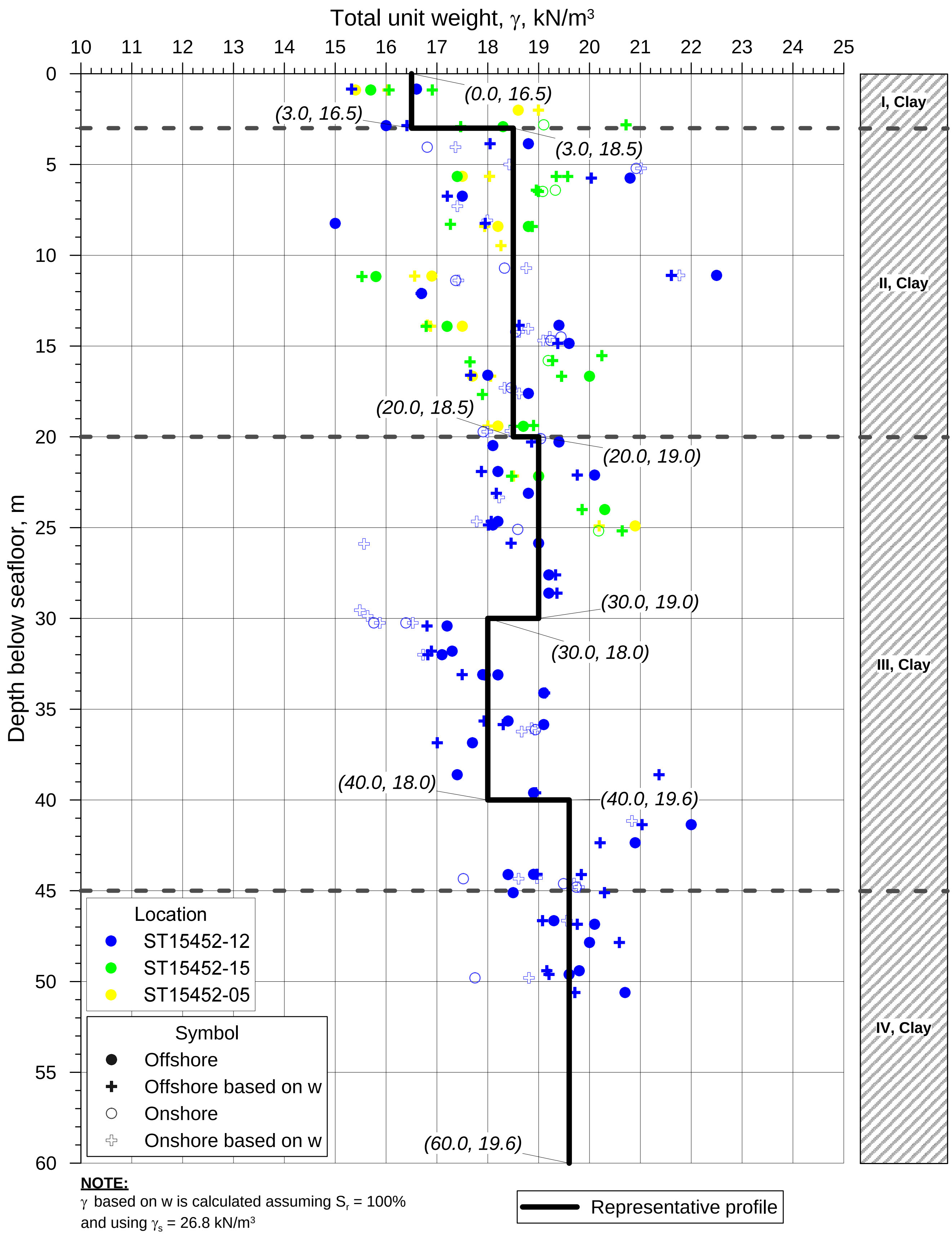

NOTE:
γ based on w is calculated assuming S_r = 100% and using γ_s = 26.8 kN/m³

Label: *(depth, value)*

Date/Rev.: 2015-01-21/01

P:\2014\08\20140857\Leveransedokumenter\Rapport\20140857-02-R Data interpretation and evaluation\Figures\Section G\Figure G_03_02, total unit weight versus depth-Fieldcentre.grf

ST15452 Flemish Pass Geotechnical Investigation	Document No. 20140857-02-R
Total unit weight versus depth Field Centre	Figure No. G3.2
	Date 2016-04-03 / Drawn by VBS

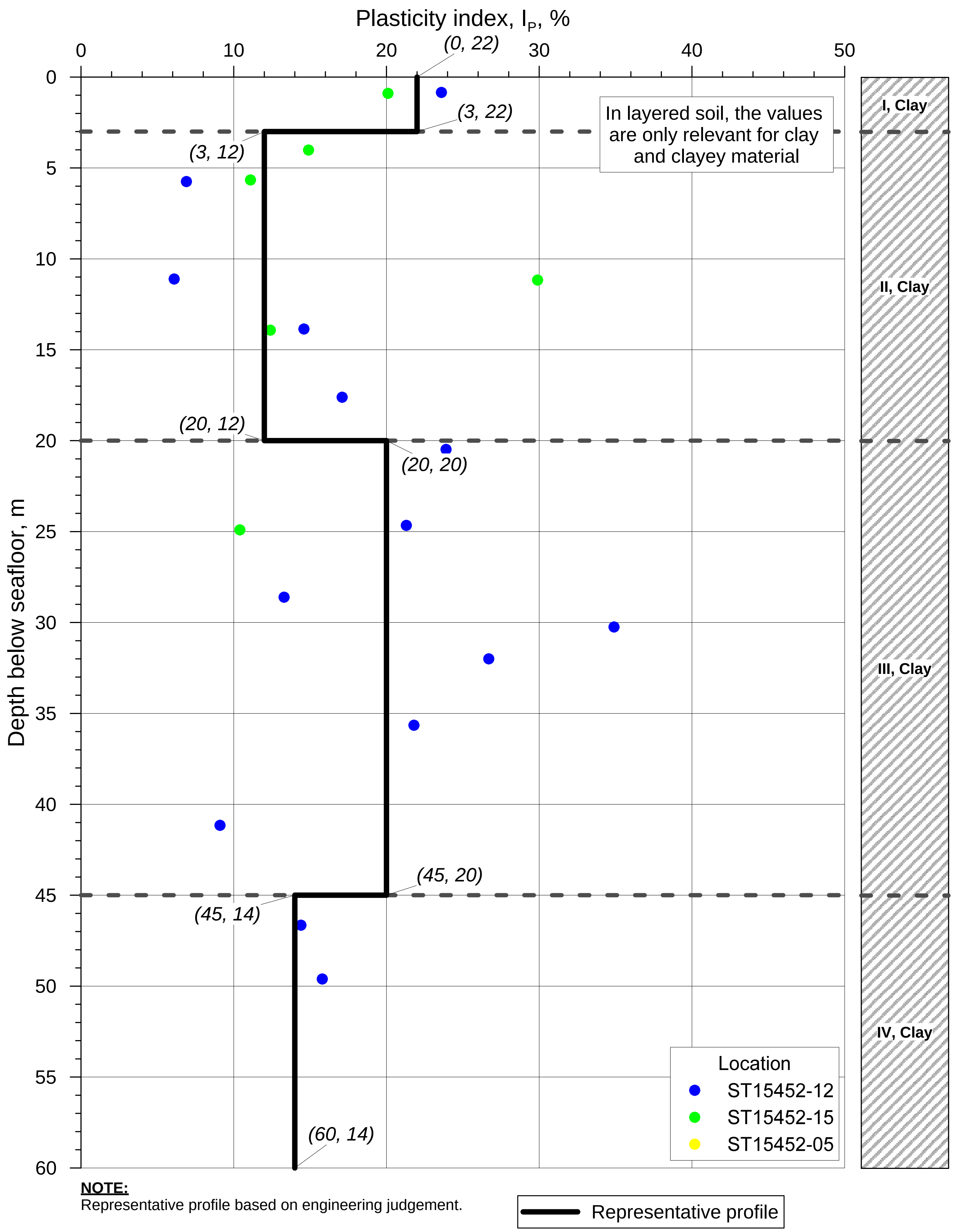

NOTE:
Representative profile based on engineering judgement.

Representative profile

Label: *(depth, value)*

Date/Rev.: 2015-01-21/01

P:\2014\08\20140857\Leveransedokumenter\Rapport\20140857-02-R Data interpretation and evaluation\Figures\Section G\Figure G_03_03, plasticity index versus depth-Fieldcentre.grf

ST15452 Flemish Pass Geotechnical Investigation	Document No. 20140857-02-R
Plasticity index versus depth Field Centre	Figure No. G3.3
	Date 2016-04-03 / Drawn by VBS
	NGI

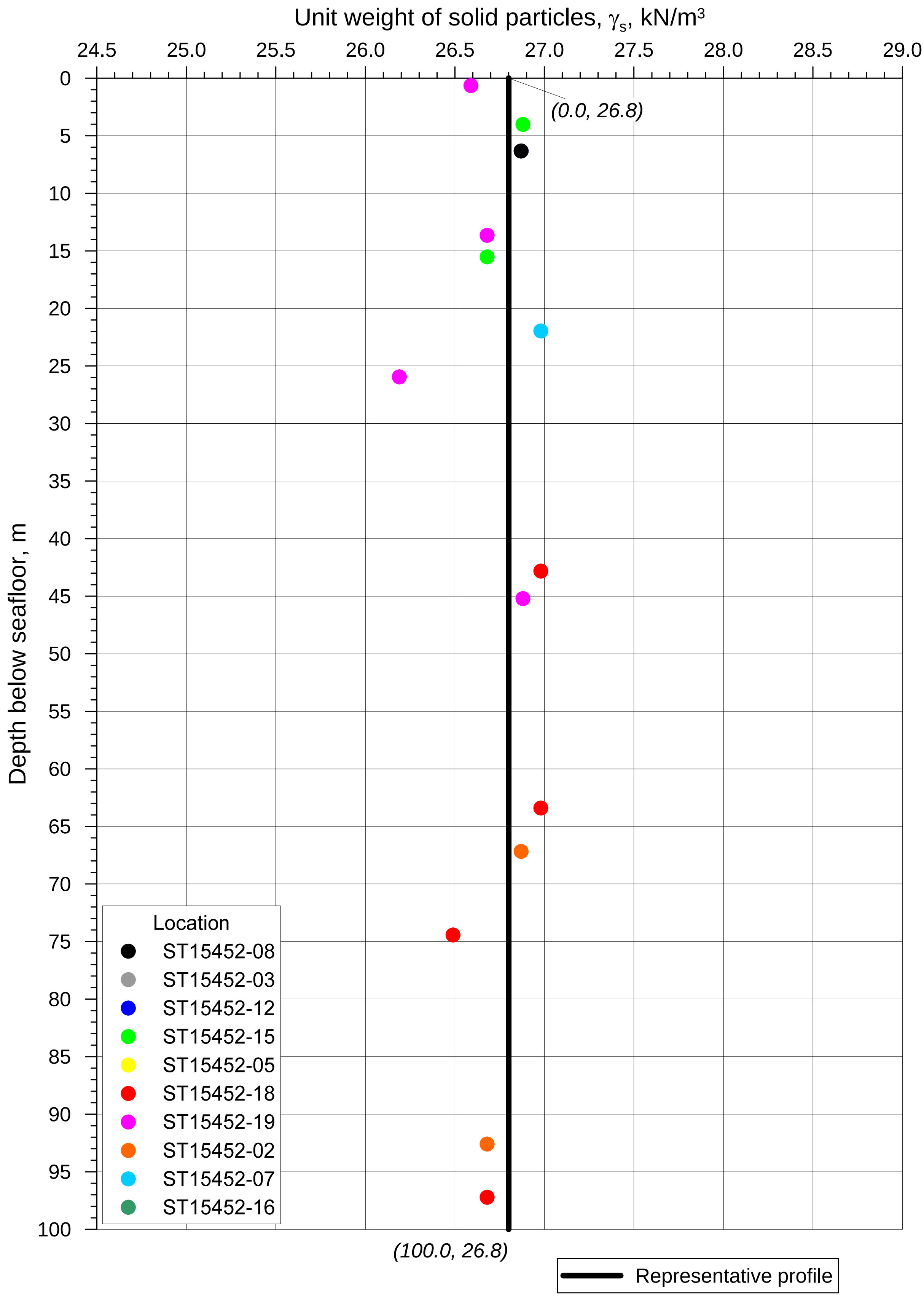

Label: *(depth, value)*

P:\2014\08\20140857\Leveransedokumenter\Rapport\20140857-02-R Data interpretation and evaluation\Figures\Section G\Figure G_03_04, unit weight of solid particles versus depth.grf

Date/Rev.: 2015-01-21/01

ST15452 Flemish Pass Geotechnical Investigation	Document No. 20140857-02-R
Unit weight of solid particles versus depth All locations	Figure No. G3.4
	Date 2016-04-03 / Drawn by VBS
	NGI

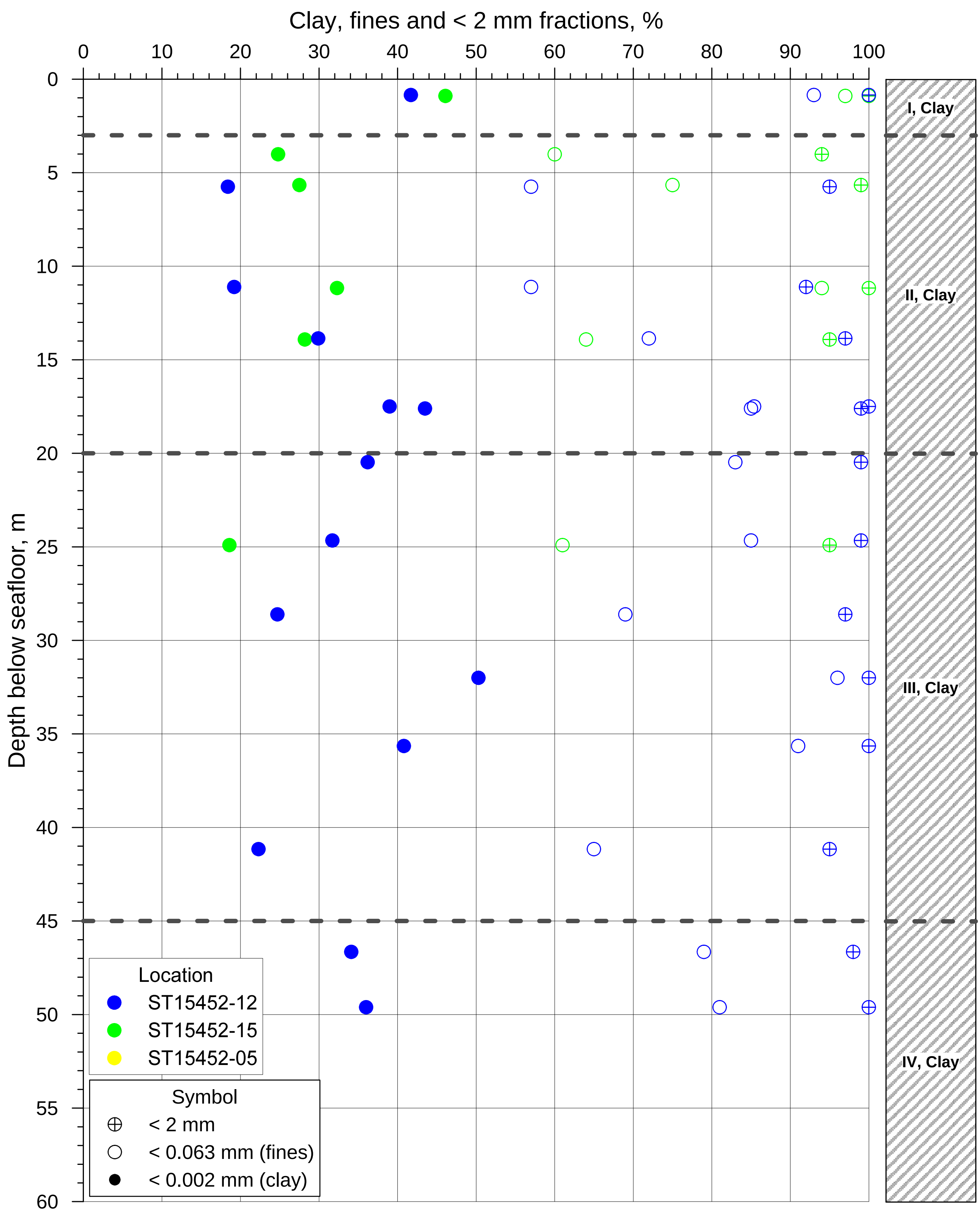

P:\2014\08\20140857\Leveransedokumenter\Rapport\20140857-02-R Data interpretation and evaluation\Figures\Section G\Figure G_03_05, grain size versus depth-Fieldcentre.grf

Date/Rev.: 2015-01-21/01

ST15452 Flemish Pass Geotechnical Investigation	Document No. 20140857-02-R
Clay, fines and <2 mm fractions versus depth Field Centre	Figure No. G3.5
	Date 2016-04-03 / Drawn by VBS
	NGI

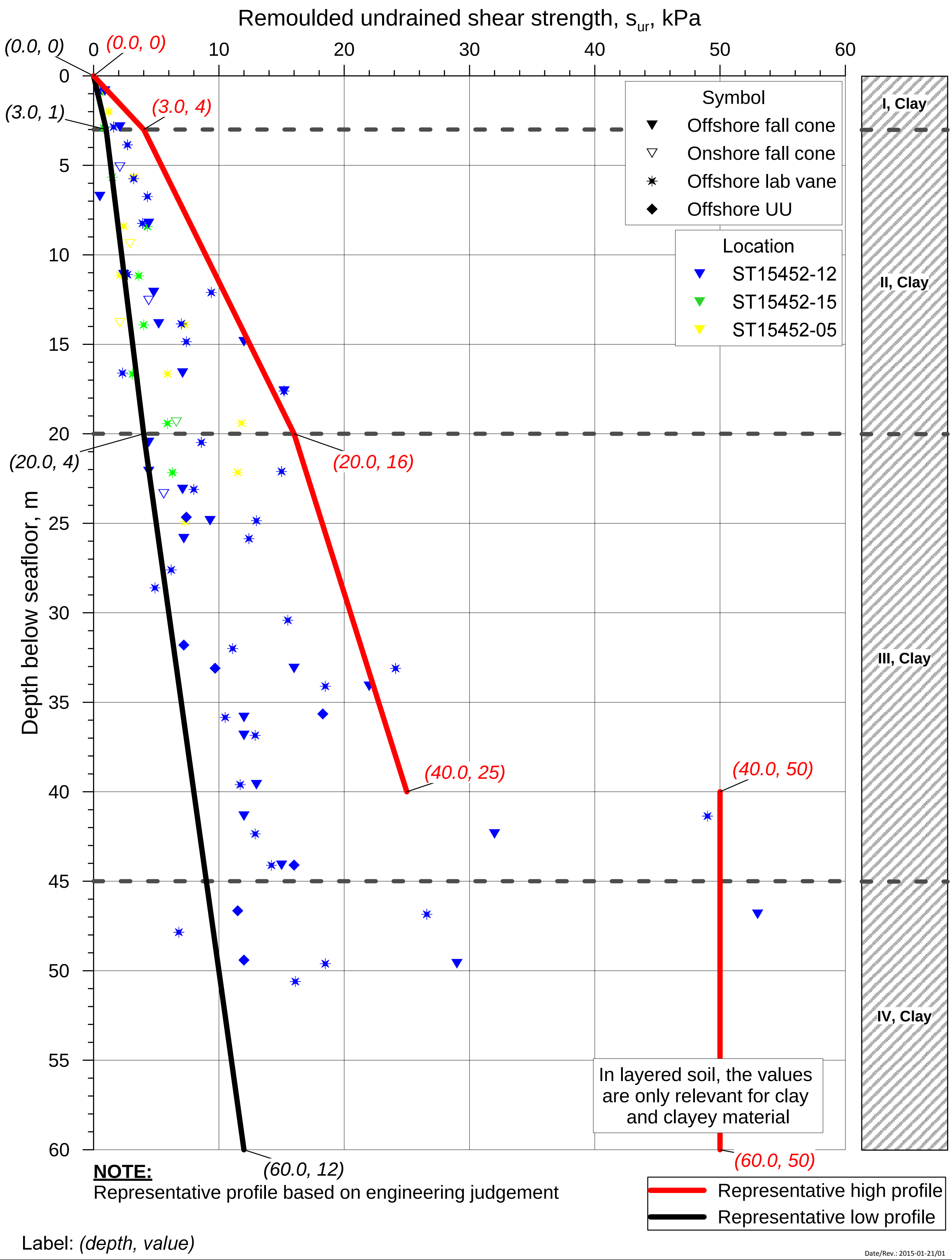

ST15452 Flemish Pass Geotechnical Investigation	Document No. 20140857-02-R
Remoulded undrained shear strength versus depth Field Centre	Figure No. G3.6
	Date 2016-04-04 / Drawn by VBS
	NGI

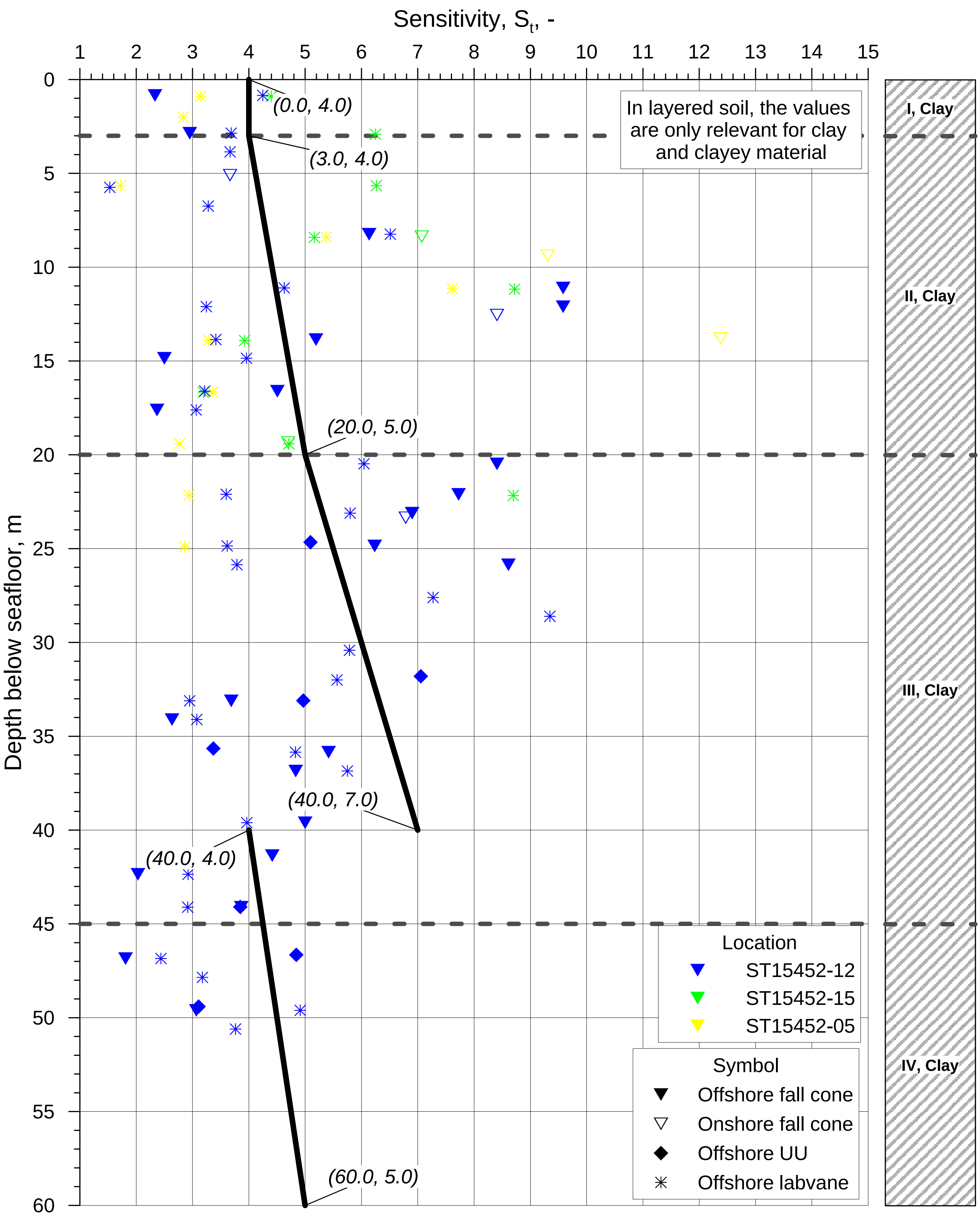

NOTE:
Representative profile taken as $S_t = s_{uD}^{avg}/s_{ur}^{avg}$

Representative profile

Label: *(depth, value)*

Date/Rev.: 2015-01-21/01

P:\2014\08\20140857\Leveransedokumenter\Rapport\20140857-02-R Data interpretation and evaluation\Figures\Section G\Figure G_03_07, sensitivity versus depth-Fieldcentre.grf

ST15452 Flemish Pass Geotechnical Investigation	Document No. 20140857-02-R
Sensitivity versus depth Field Centre	Figure No. G3.7
	Date 2016-04-04 / Drawn by VBS
	NGI

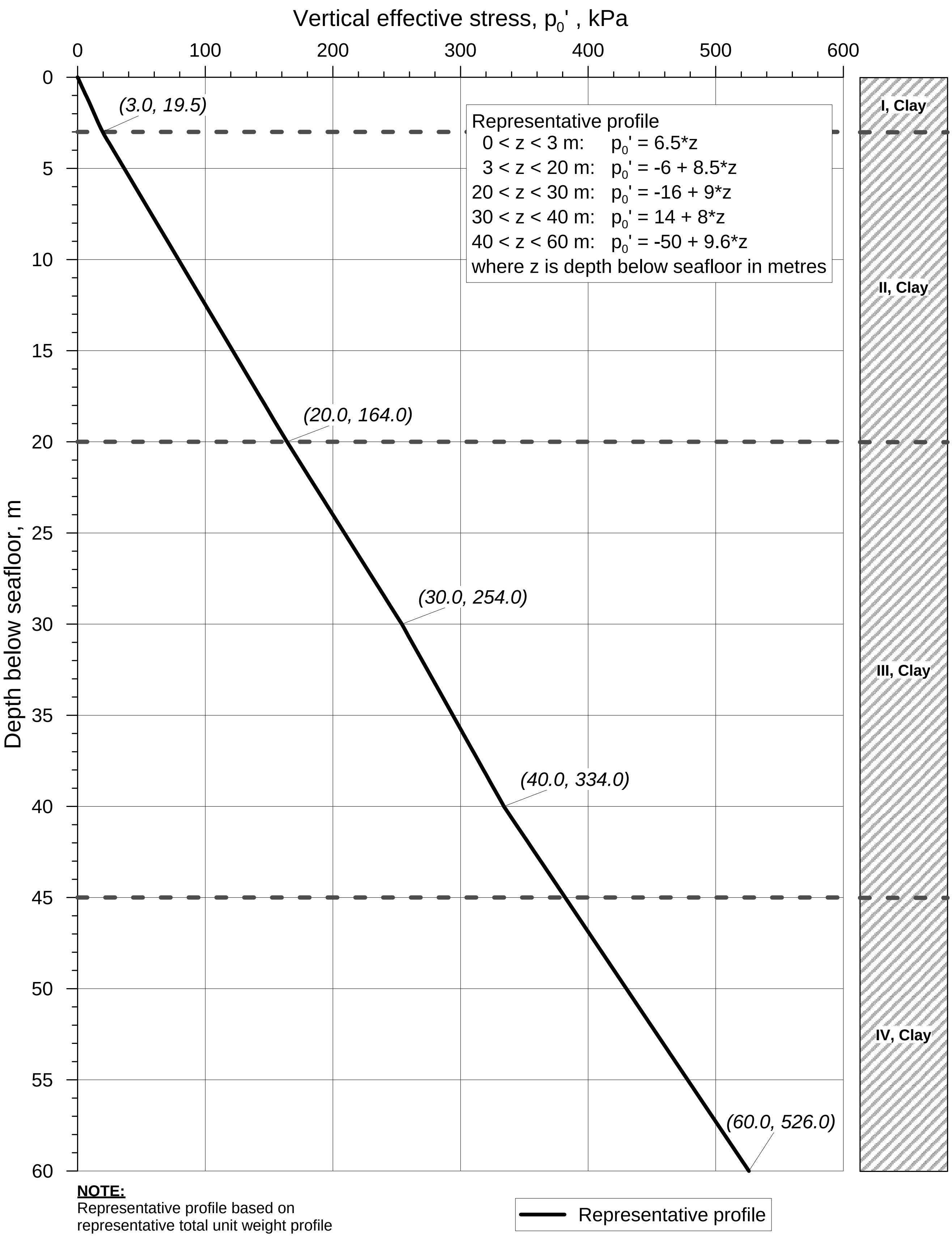

Label: *(depth, value)*

Date/Rev.: 2015-01-21/01

ST15452 Flemish Pass Geotechnical Investigation

Vertical effective stress versus depth
Field Centre

Document No. 20140857-02-R	
Figure No. G4.1	
Date 2016-04-03	Drawn by VBS

NGI

P:\2014\08\20140857\Leveransedokumenter\Rapport\20140857-02-R Data interpretation and evaluation\Figures\Section G\Figure G_04_01, p0 versus depth-Fieldcentre.grf

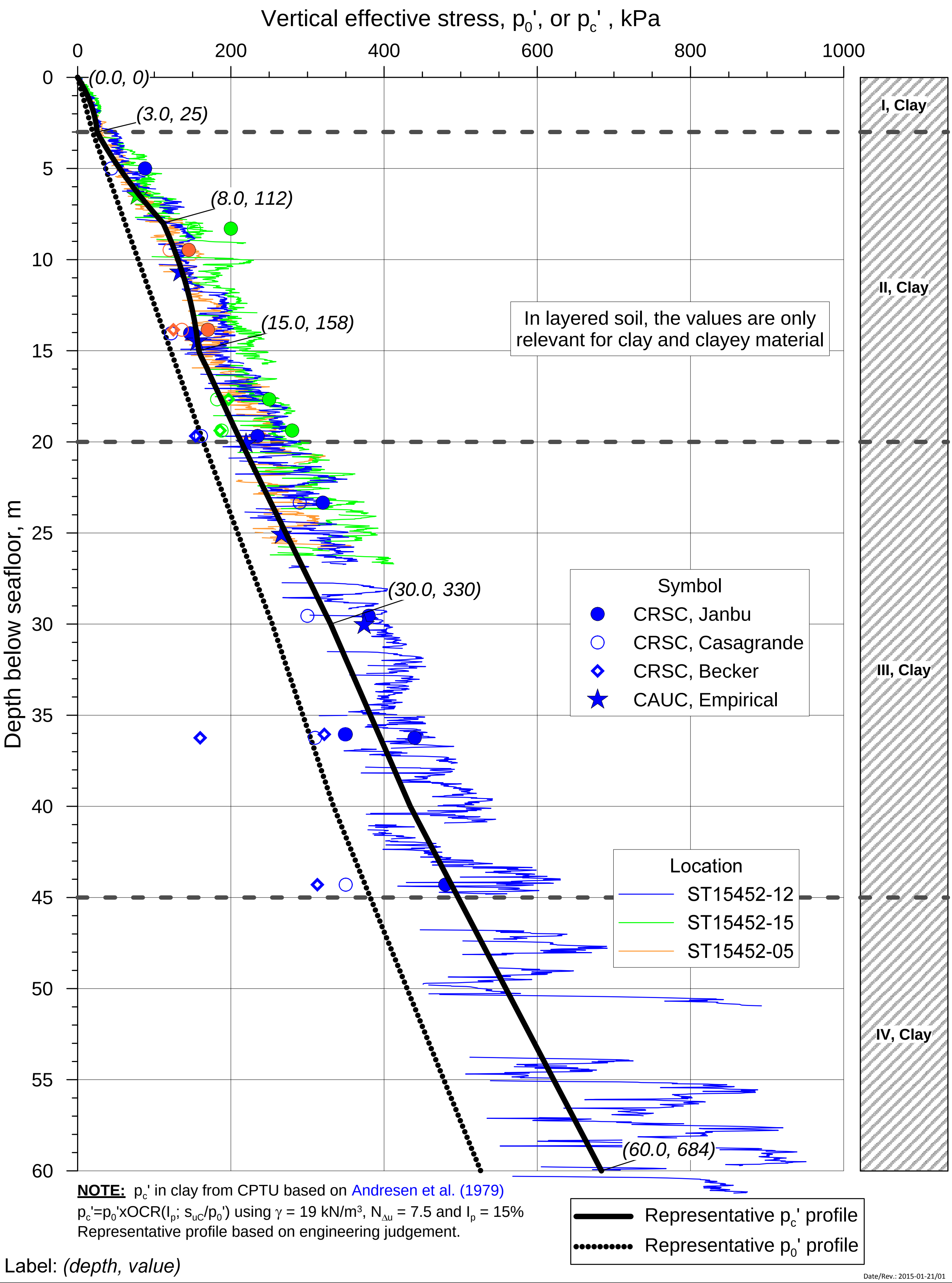

NOTE: p_c' in clay from CPTU based on Andresen et al. (1979)
$p_c'=p_0'xOCR(I_p;\ s_{uC}/p_0')$ using γ = 19 kN/m³, $N_{\Delta u}$ = 7.5 and I_p = 15%
Representative profile based on engineering judgement.

Representative p_c' profile
Representative p_0' profile

Label: *(depth, value)*

Date/Rev.: 2015-01-21/01

P:\2014\08\20140857\Leveransedokumenter\Rapport\20140857-02-R Data interpretation and evaluation\Figures\Section G\Figure G_04_02, pc' versus depth-Fieldcentre.grf

ST15452 Flemish Pass Geotechnical Investigation

Preconsolidation stress versus depth
Field Centre

Document No.	20140857-02-R
Figure No.	G4.2
Date	2016-04-03
Drawn by	SK

NGI

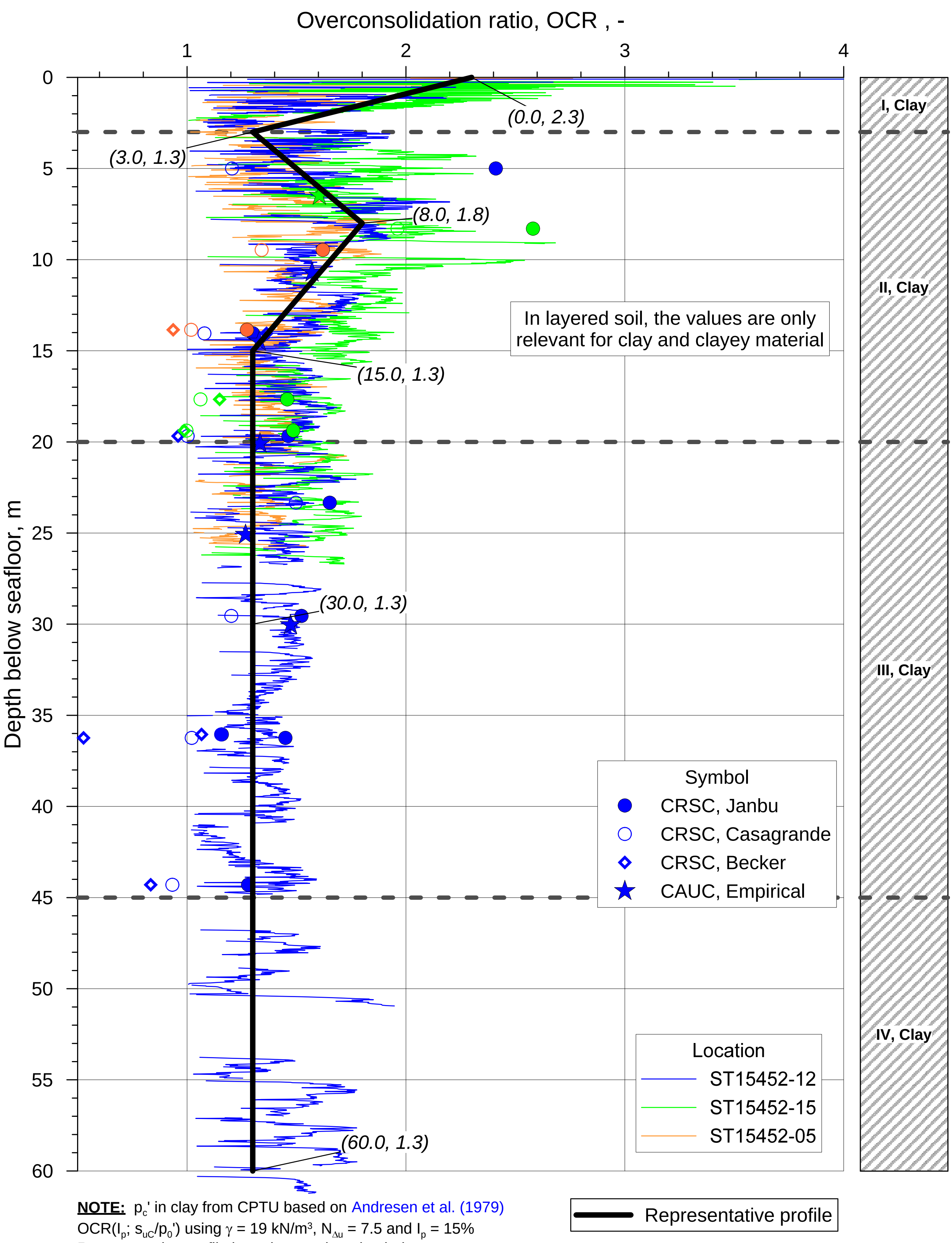

NOTE: p_c' in clay from CPTU based on Andresen et al. (1979)
OCR(I_p; s_{uC}/p_0') using γ = 19 kN/m³, $N_{\Delta u}$ = 7.5 and I_p = 15%
Representative profile based on engineering judgement.

Label: *(depth, value)*

Date/Rev.: 2015-01-21/01

ST15452 Flemish Pass Geotechnical Investigation	Document No. 20140857-02-R	
Overconsolidation ratio versus depth Field Centre	Figure No. G4.3	
	Date 2016-04-03	Drawn by KS/SK

P:\2014\08\20140857\Leveransedokumenter\Rapport\20140857-02-R Data interpretation and evaluation\Figures\Section G\Figure G_04_03, OCR versus depth-Fieldcentre.grf

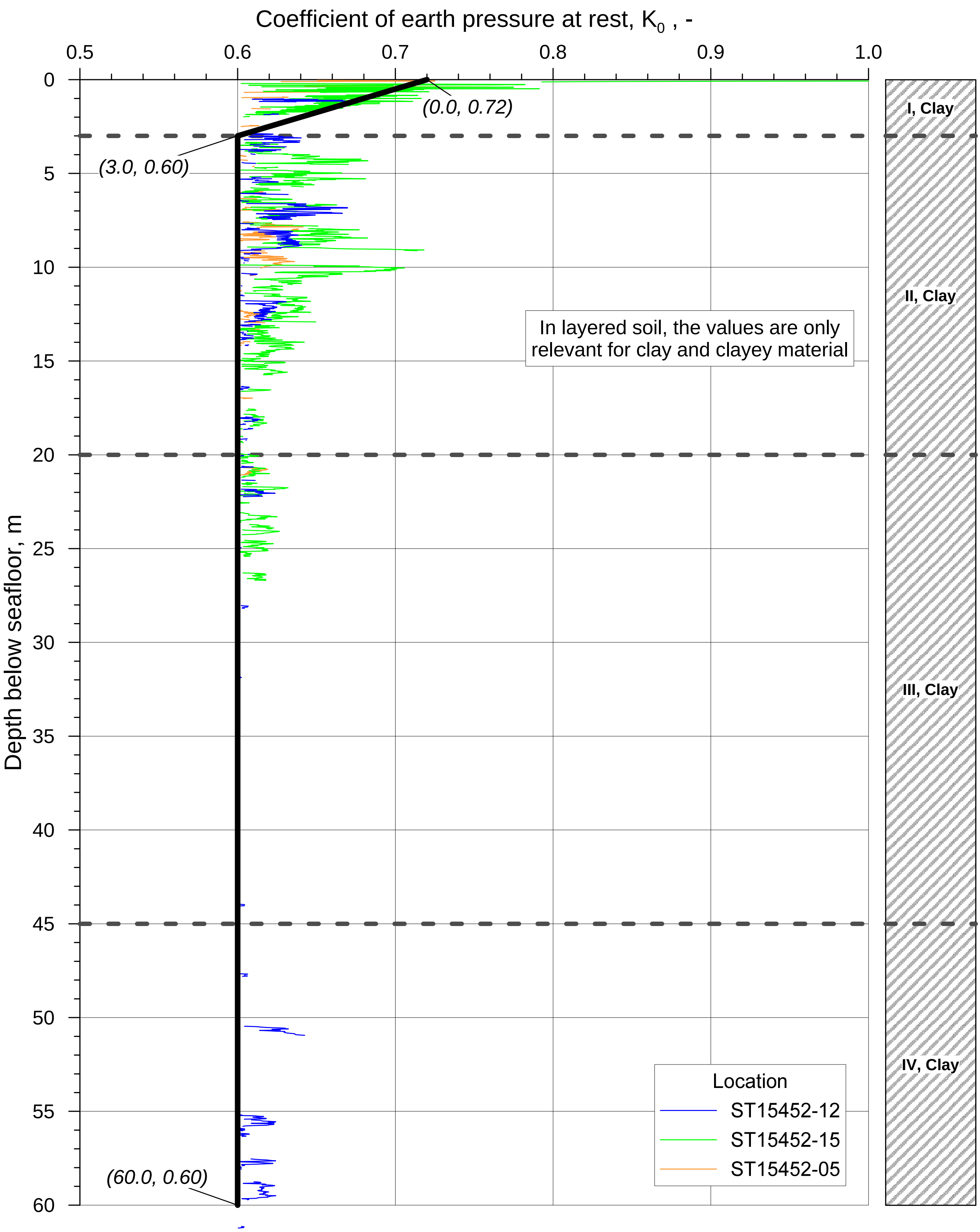

NOTE: K_0 in clay from CPTU using Brooker and Ireland (1965).
$K_0(I_p; s_{uC}/p_0')$ using γ = 19 kN/m³, $N_{\Delta u}$ = 7.5 and I_p = 15%.
Representative profile based on engineering judgement.

Representative profile

Label: *(depth, value)*

Date/Rev.: 2015-01-21/01

P:\2014\08\20140857\Leveransedokumenter\Rapport\20140857-02-R Data interpretation and evaluation\Figures\Section G\Figure G_04_04, K0 versus depth-Fieldcentre.grf

ST15452 Flemish Pass Geotechnical Investigation	Document No. 20140857-02-R
Coefficient of earth pressure at rest versus depth Field Centre	Figure No. G4.4
	Date 2016-04-03 / Drawn by SK
	NGI

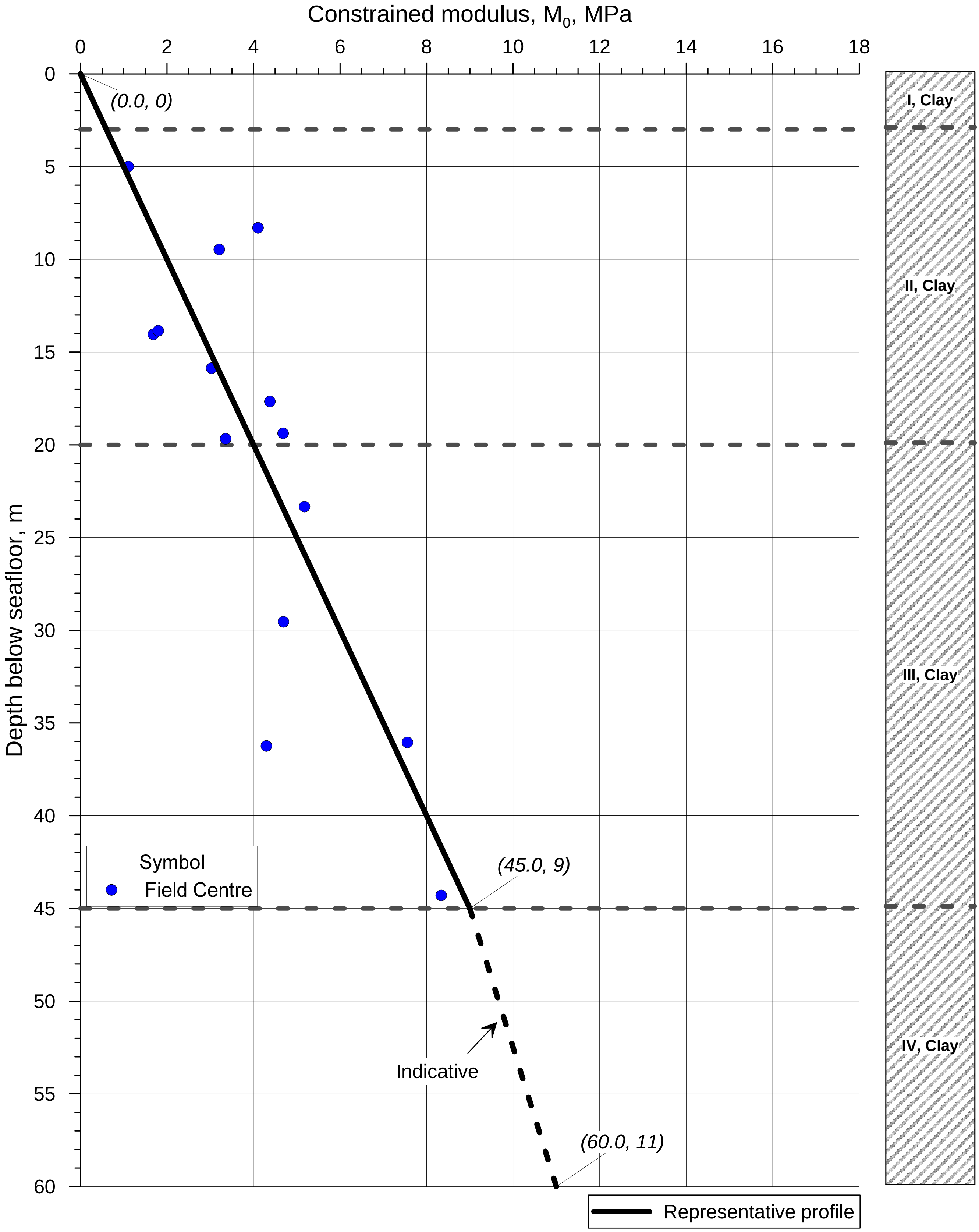

Label: *(depth, value)*

Date/Rev.: 2015-01-21/01

ST15452 Flemish Pass Geotechnical Investigation

Constrained modulus at in-situ vertical effective stress versus depth
Field Centre

Document No. 20140857-02-R	
Figure No. G5.1	
Date 2016-04-04	Drawn by VDa

P:\2014\08\20140857\Leveransedokumenter\Rapport\20140857-02-R Data interpretation and evaluation\Figures\Section G\Figure G_05_01, Constrained modulus versus depth_Fieldcentre.grf

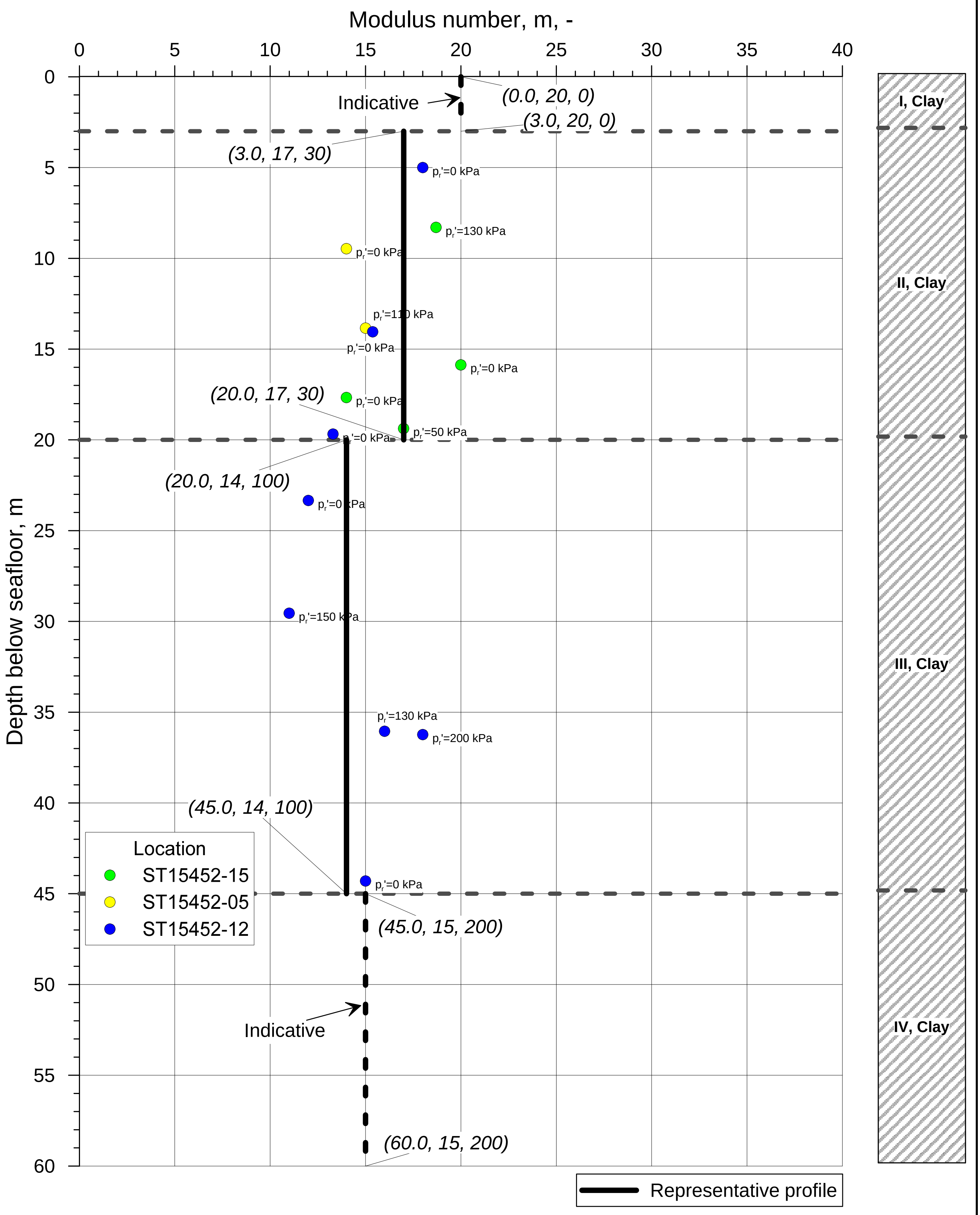

Label: *(depth, m, p_r')*

Date/Rev.: 2015-01-21/01

P:\2014\08\20140857\Leveransedokumenter\Rapport\20140857-02-R Data interpretation and evaluation\Figures\Section G\Figure G_05_02, modulus number versus depth_Fieldcentre.grf

ST15452 Flemish Pass Geotechnical Investigation	Document No. 20140857-02-R
Modulus number and reference stress versus depth Field Centre	Figure No. G5.2
	Date 2016-04-04 / Drawn by VDa

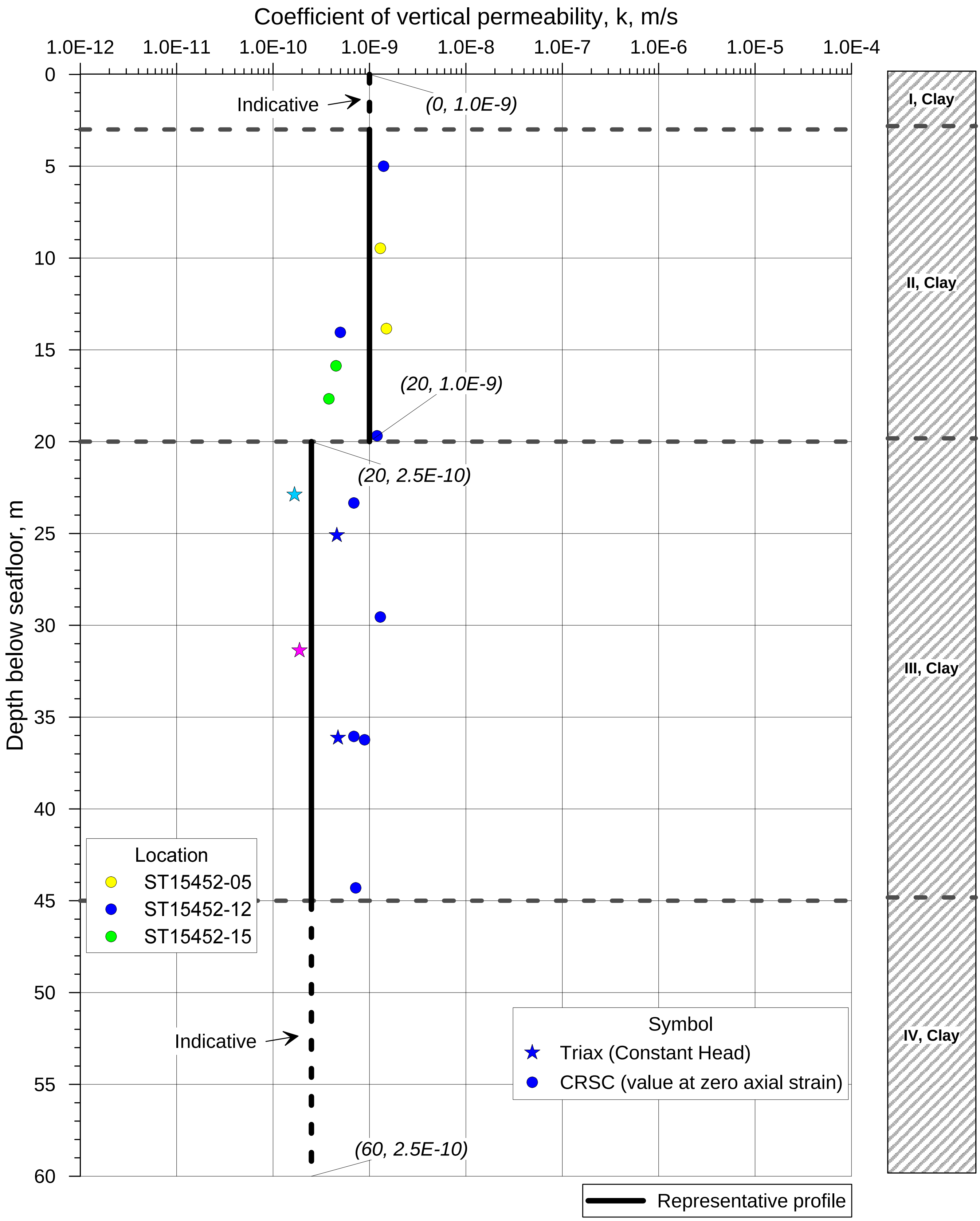

Label: *(depth, value)*

Date/Rev.: 2015-01-21/01

ST15452 Flemish Pass Geotechnical Investigation	Document No. 20140857-02-R
Coefficient of vertical permeability versus depth Field Centre	Figure No. G5.3
	Date 2016-04-04 / Drawn by VDa

NGI

P:\2014\08\20140857\Leveranseedokumenter\Rapport\20140857-02-R Data interpretation and evaluation\Figures\Section G\Figure G_05_03, Coefficient of vertical permeability versus depth_Fieldcentre.grf

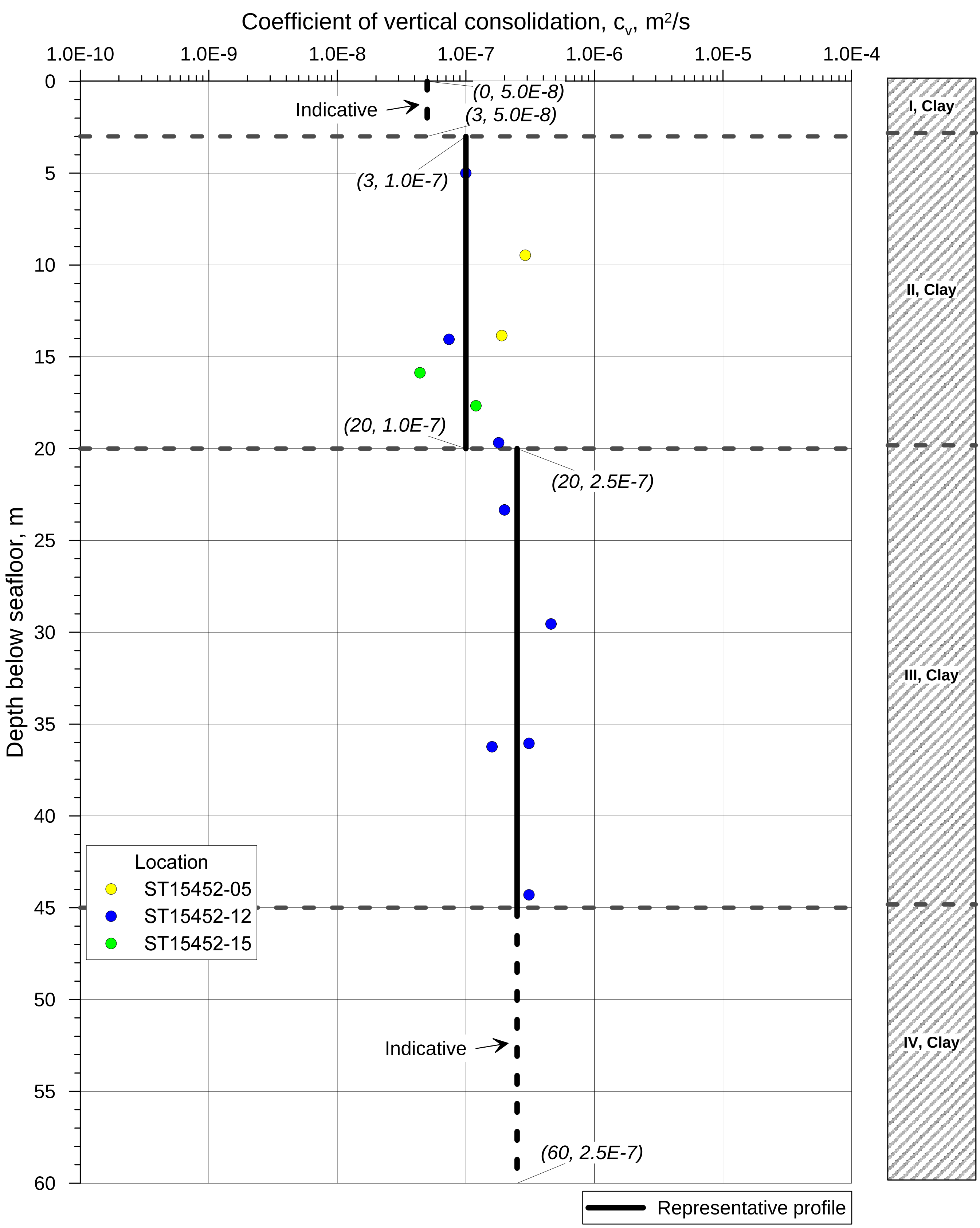

Label: *(depth, value)*

Date/Rev.: 2015-01-21/01

P:\2014\08\20140857\Leveransedokumenter\Rapport\20140857-02-R Data interpretation and evaluation\Figures\Section G\Figure G_05_04, Coefficient of vertical consolidation versus depth_Fieldcentre.grf

ST15452 Flemish Pass Geotechnical Investigation	Document No. 20140857-02-R
Coefficient of vertical consolidation versus depth Field Centre	Figure No. G5.4
	Date 2016-04-04 / Drawn by VDa

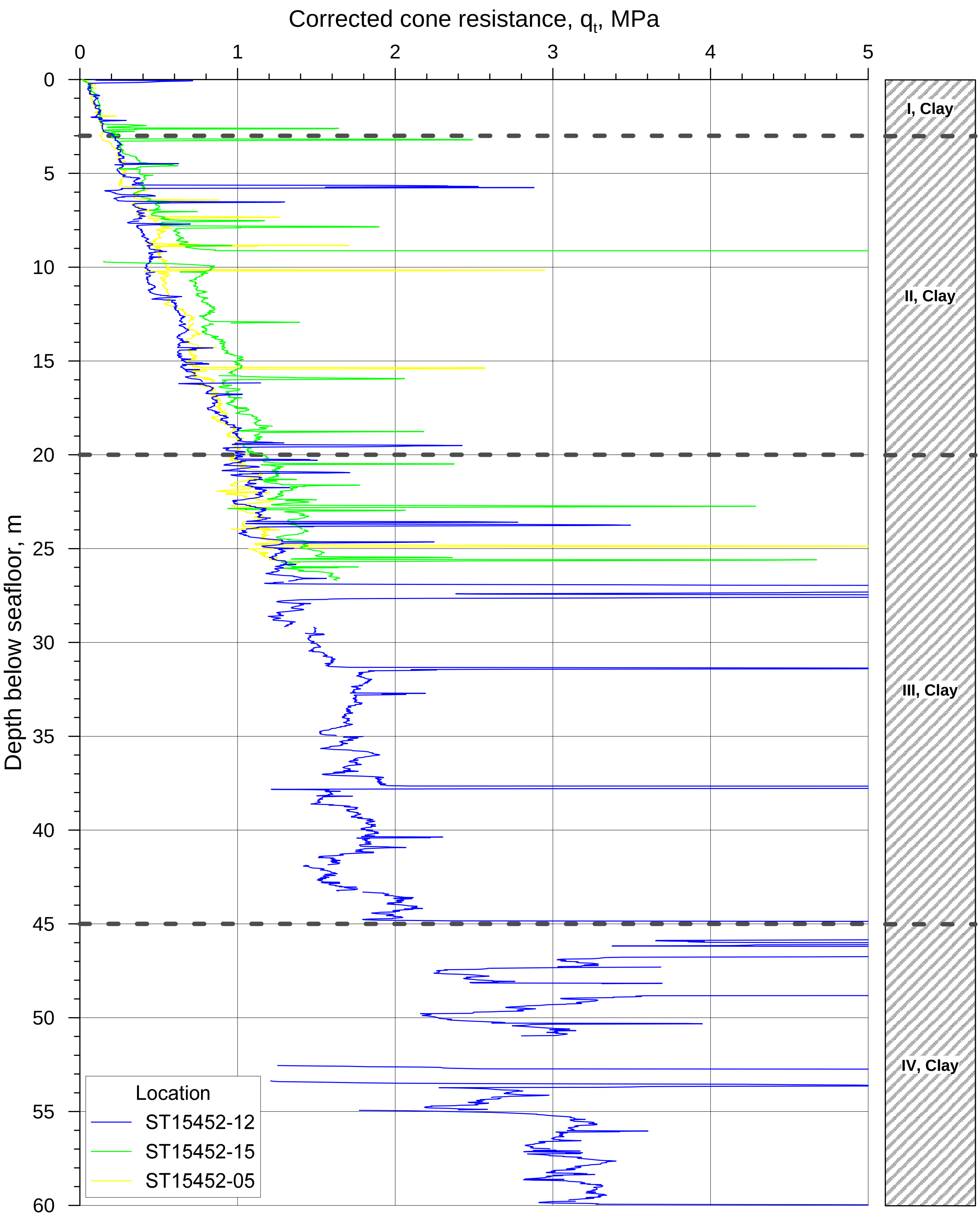

Date/Rev.: 2015-01-21/01

ST15452 Flemish Pass Geotechnical Investigation	Document No. 20140857-02-R	
Corrected cone resistance versus depth Field Centre	Figure No. G6.1	
	Date 2016-04-03	Drawn by VBS
	NGI	

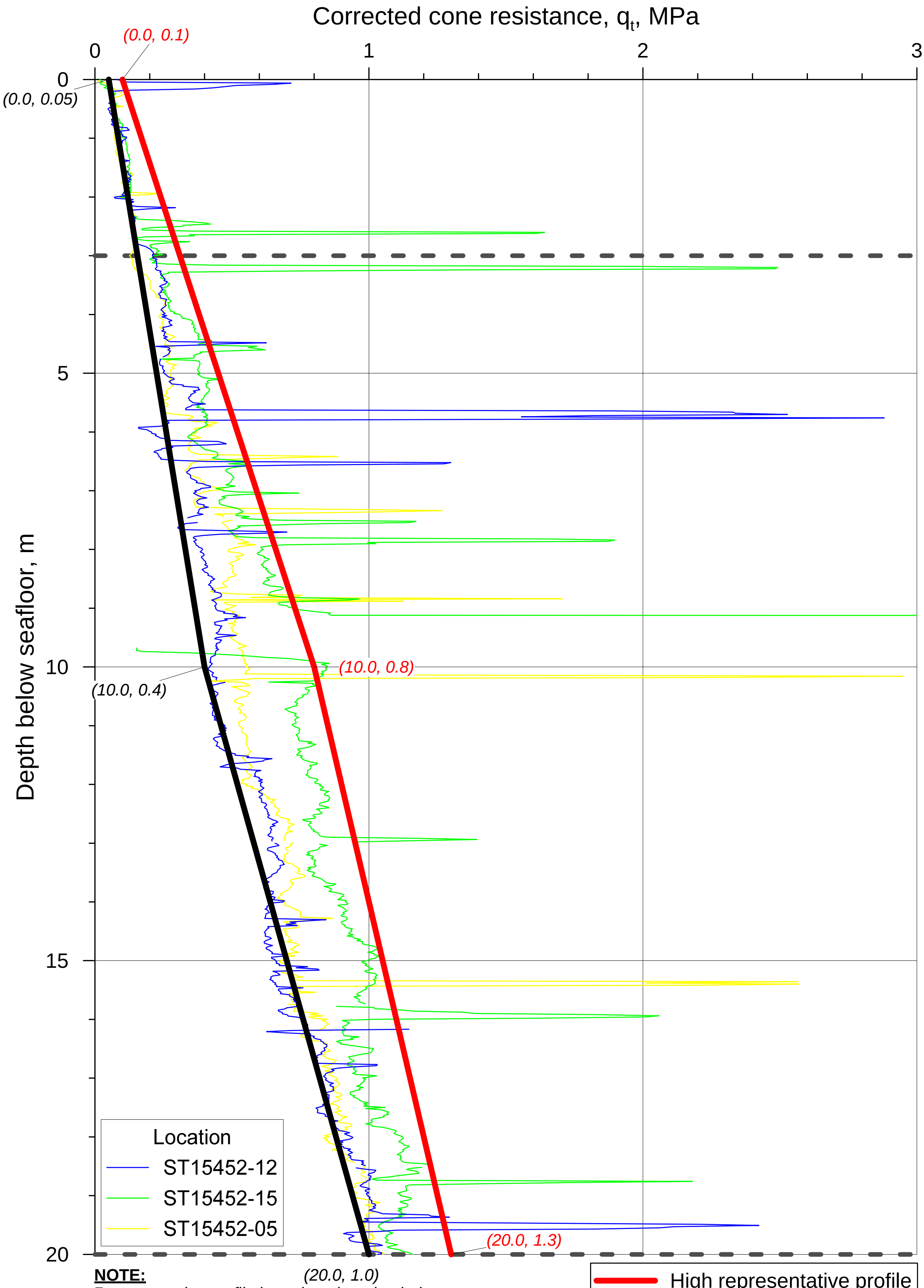

NOTE:
Representative profile based engineering judgement.

Label: *(depth, value)*

P:\2014\08\20140857\Leveransedokumenter\Rapport\20140857-02-R Data interpretation and evaluation\Figures\Section G\Figure G_06_02, qt versus depth-Fieldcentre 0-20m.grf

Date/Rev.: 2015-01-21/01

ST15452 Flemish Pass Geotechnical Investigation

Corrected cone resistance versus depth
Field Centre, 0-20 m depth

Document No.	
20140857-02-R	
Figure No. G6.2	
Date 2016-04-03	Drawn by VBS

NGI

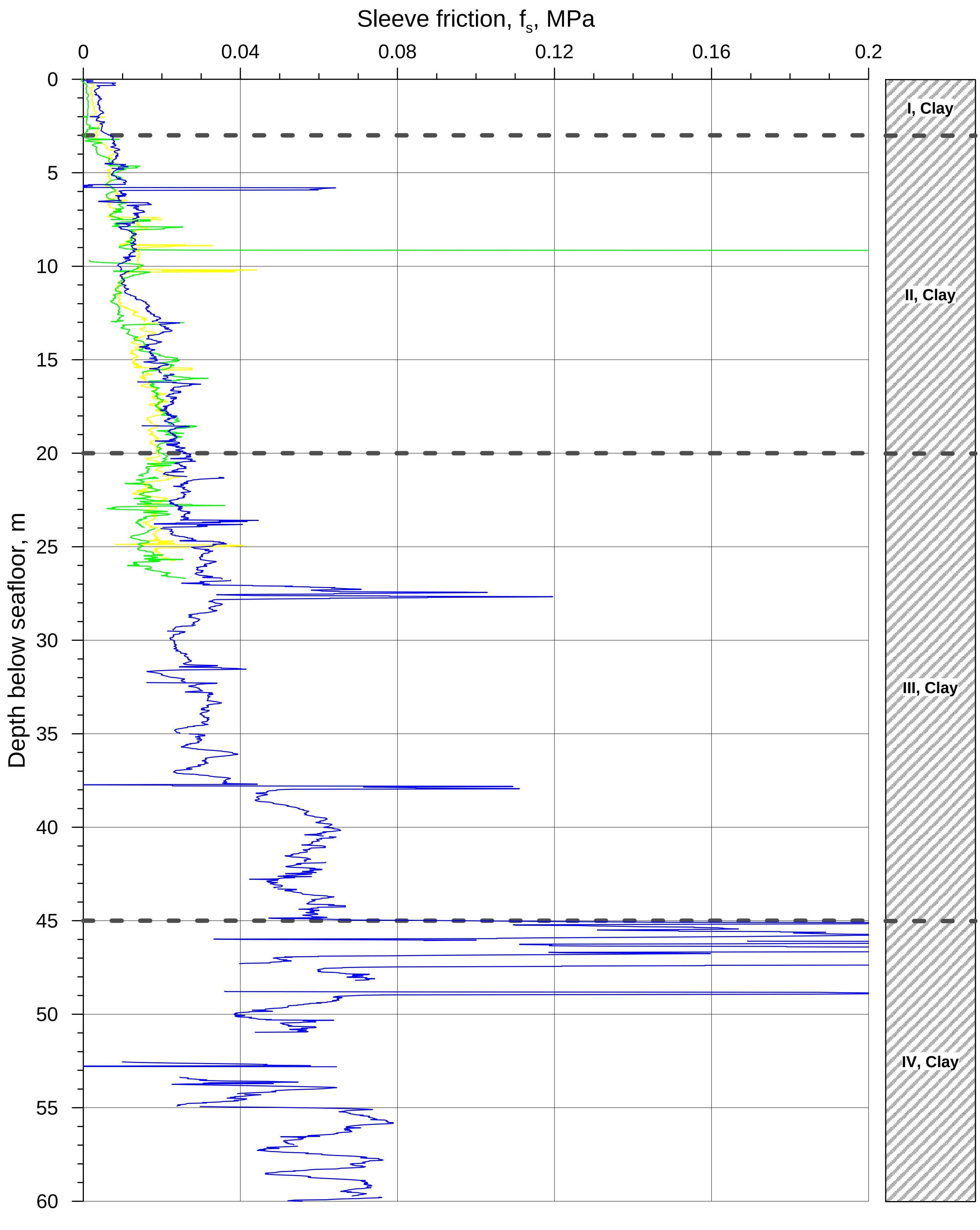

P:\2014\08\20140857\Leveransedokumenter\Rapport\20140857-02-R Data interpretation and evaluation\Figures\Section G\Figure G_06_03, fs versus depth-Fieldcentre.grf

Date/Rev.: 2015-01-21/01

ST15452 Flemish Pass Geotechnical Investigation	Document No. 20140857-02-R
Sleeve friction versus depth Field Centre	Figure No. G6.3
	Date 2016-04-04 / Drawn by VBS
	NGI

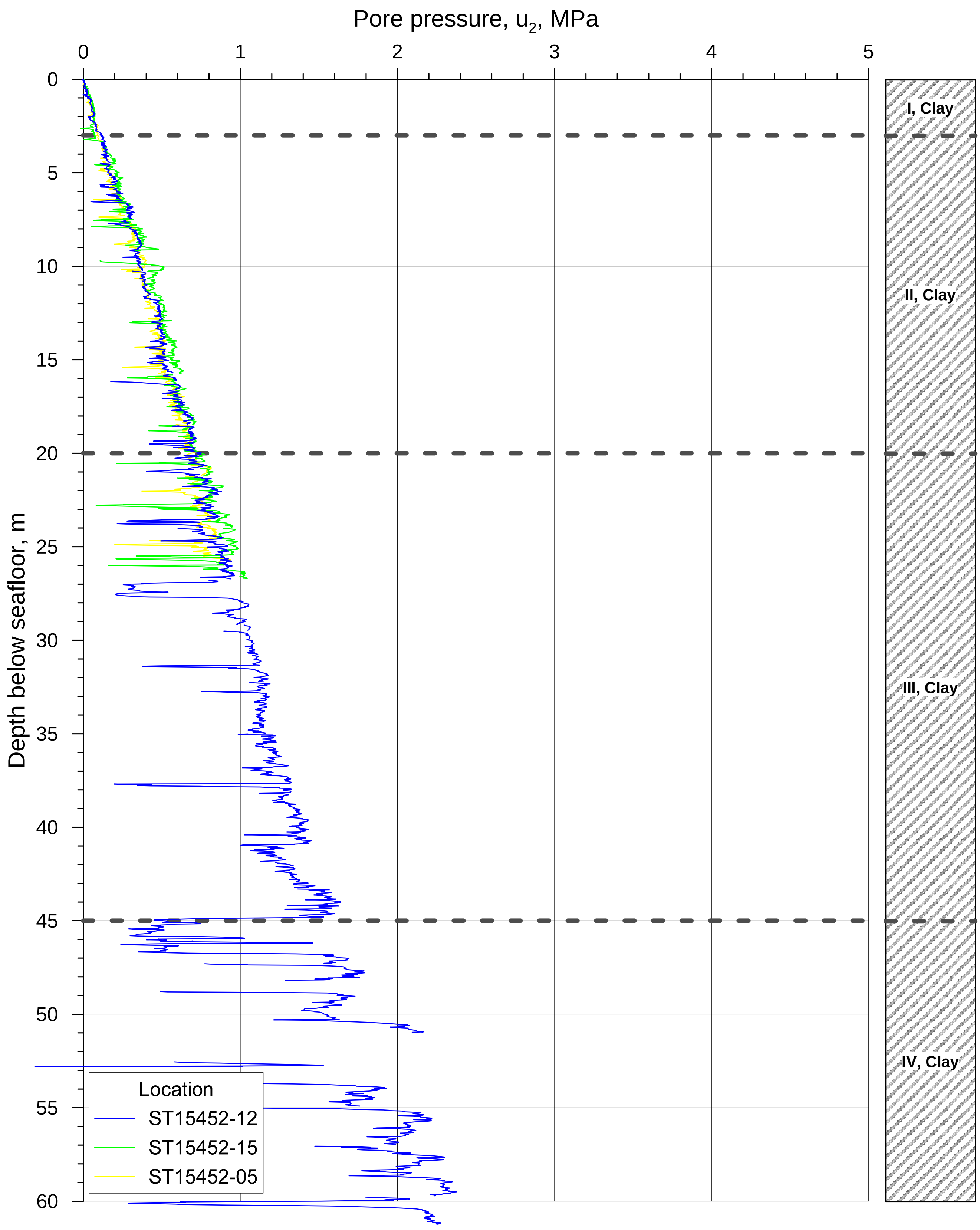

P:\2014\08\20140857\Leveransedokumenter\Rapport\20140857-02-R Data interpretation and evaluation\Figures\Section G\Figure G_06_04, u2 versus depth-Fieldcentre.grf

Date/Rev.: 2015-01-21/01

ST15452 Flemish Pass Geotechnical Investigation	Document No. 20140857-02-R
Pore pressure versus depth Field Centre	Figure No. G6.4
	Date 2016-04-03 / Drawn by VBS

NGI

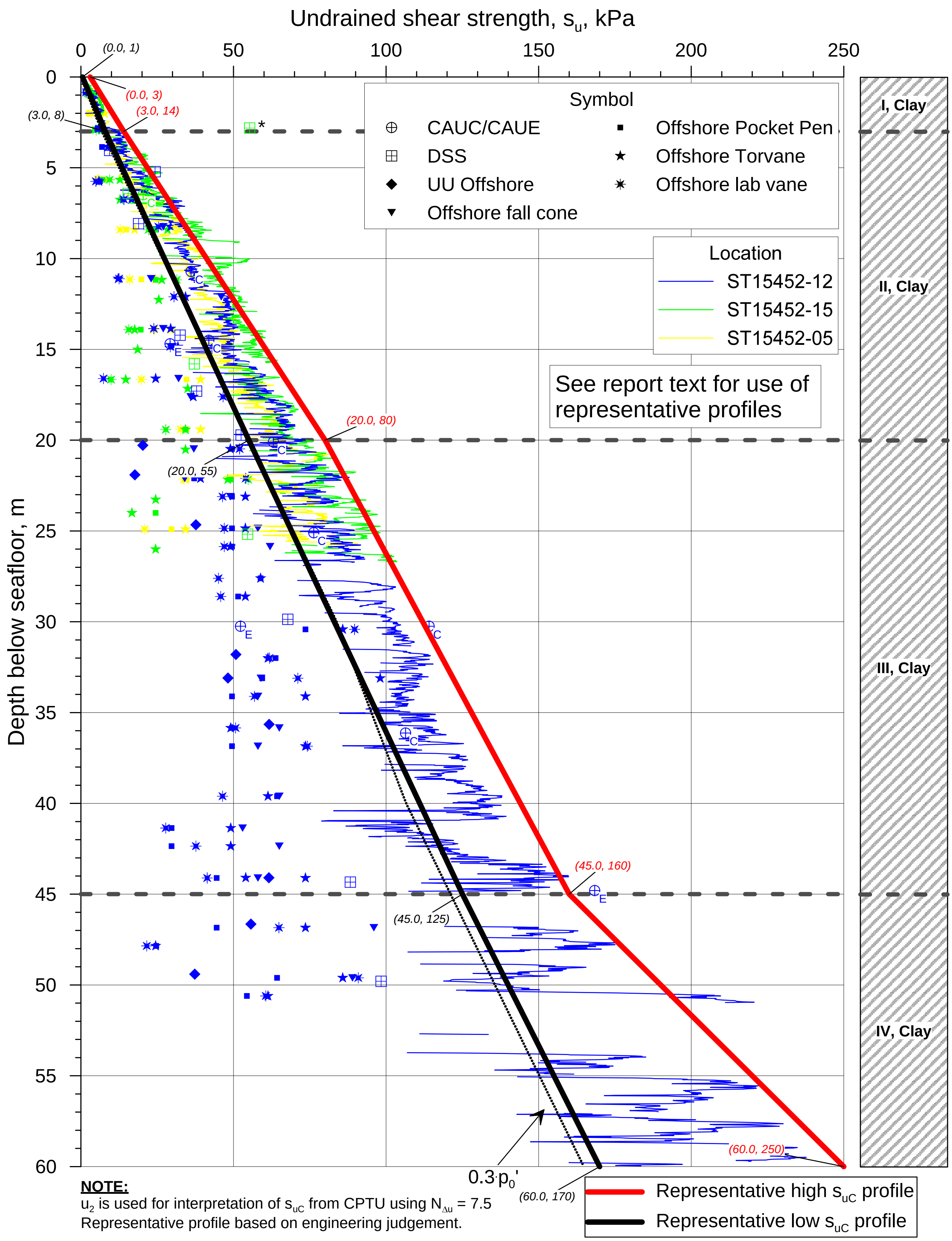

NOTE:
u_2 is used for interpretation of s_{uC} from CPTU using $N_{\Delta u} = 7.5$
Representative profile based on engineering judgement.

* Test representative of silty/sandy layer and not given weight in s_u interpretation

Label: *(depth, value)*

Date/Rev.: 2015-01-21/01

P:\2014\08\20140857\Leveransedokumenter\Rapport\20140857-02-R Data interpretation and evaluation\Figures\Section G\Figure G_06_05, su versus depth-Fieldcentre.grf

ST15452 Flemish Pass Geotechnical Investigation

Undrained shear strength versus depth
Field Centre

Document No.	20140857-02-R
Figure No.	G6.5
Date	2016-04-04
Drawn by	VBS

NGI

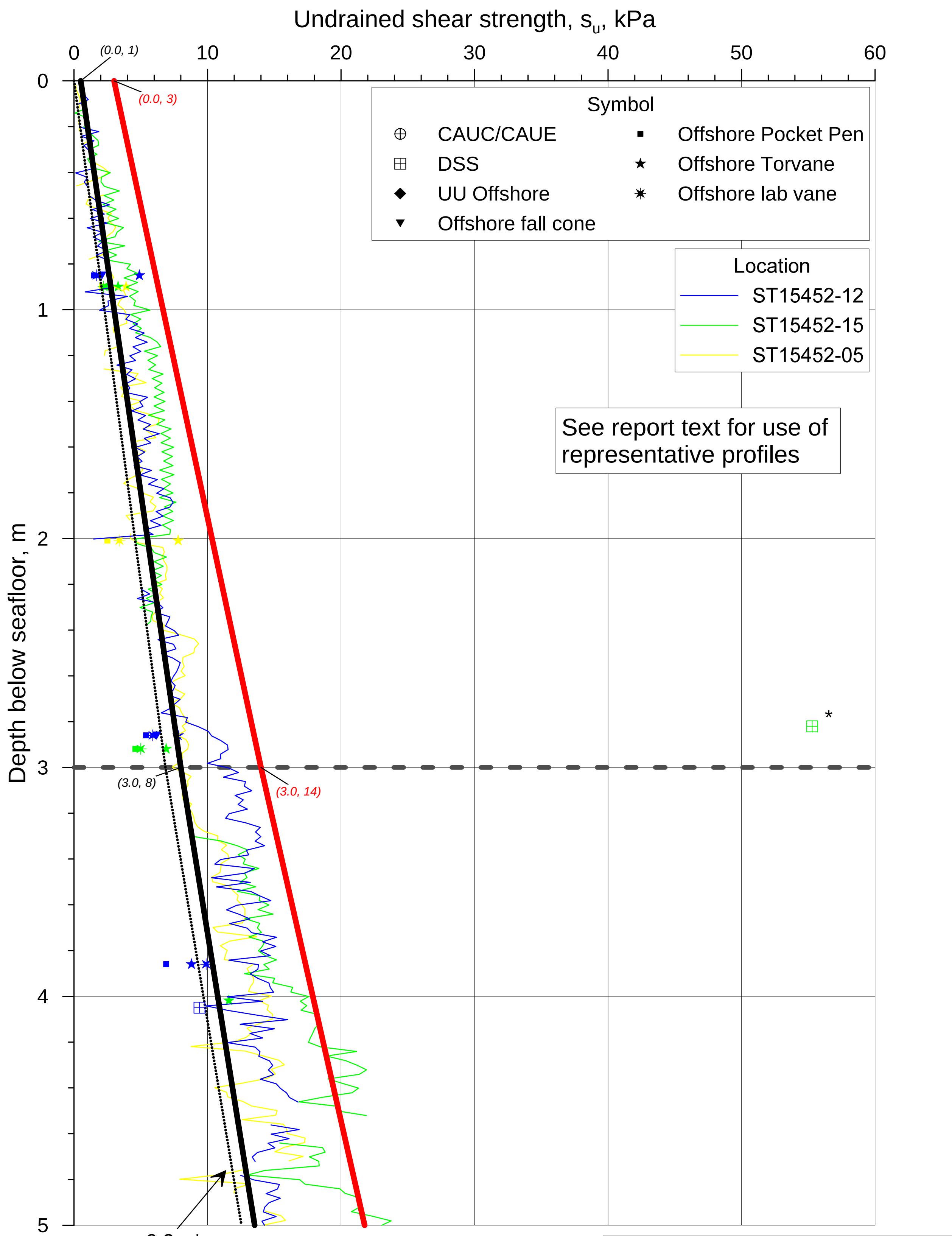

NOTE:
u_2 is used for interpretation of s_{uC} from CPTU using $N_{\Delta u}$ = 7.5
Representative profile based on engineering judgement.

* Test representative of silty/sandy layer and not given weight in s_u interpretation

Label: *(depth, value)*

Date/Rev.: 2015-01-21/01

P:\2014\08\20140857\Leveransedokumenter\Rapport\20140857-02-R Data interpretation and evaluation\Figures\Section G\Figure G_06_06, su versus depth-Fieldcentre 0-5m.grf

ST15452 Flemish Pass Geotechnical Investigation	Document No. 20140857-02-R
Undrained shear strength versus depth Field Centre, 0 - 5 m depth	Figure No. G6.6
	Date 2016-04-04 / Drawn by VBS
	NGI

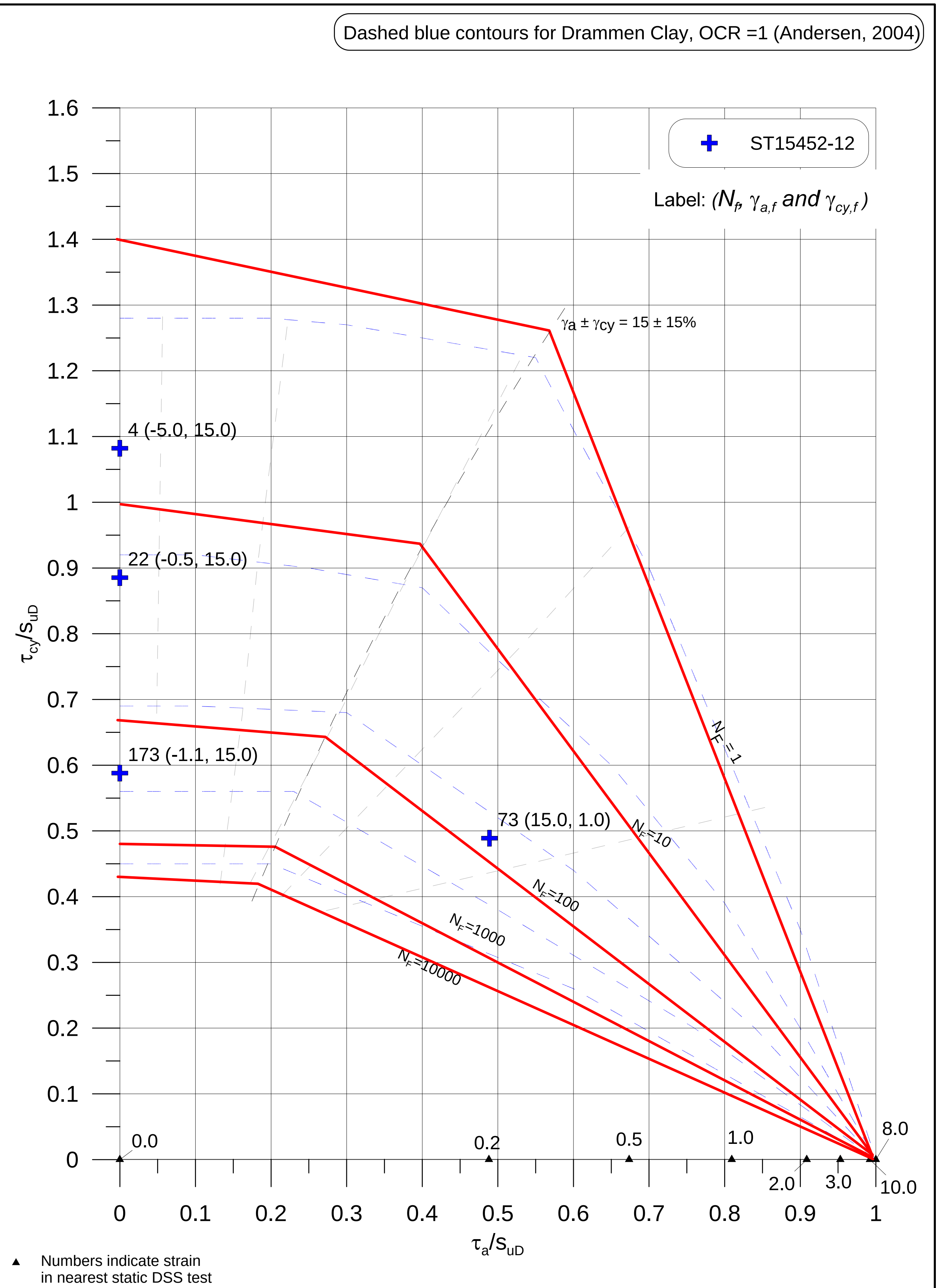

P:\2014\08\20140857\Leveransedokumenter\Rapport\20140857-02-R Data interpretation and evaluation\Figures\Section G\Figure G_07_01, DSS contour_field_centre.grf

Date/Rev.: 2015-01-21/01

ST15452 Flemish Pass Geotechnical Investigation	Document No. 20140857-02-R
Cyclic DSS Tests, Average and Cyclic Shear Stress normalised to s_{uD} Field Centre For Structural design	Figure No. G7.1 Date 2016-04-03 Drawn by VDa

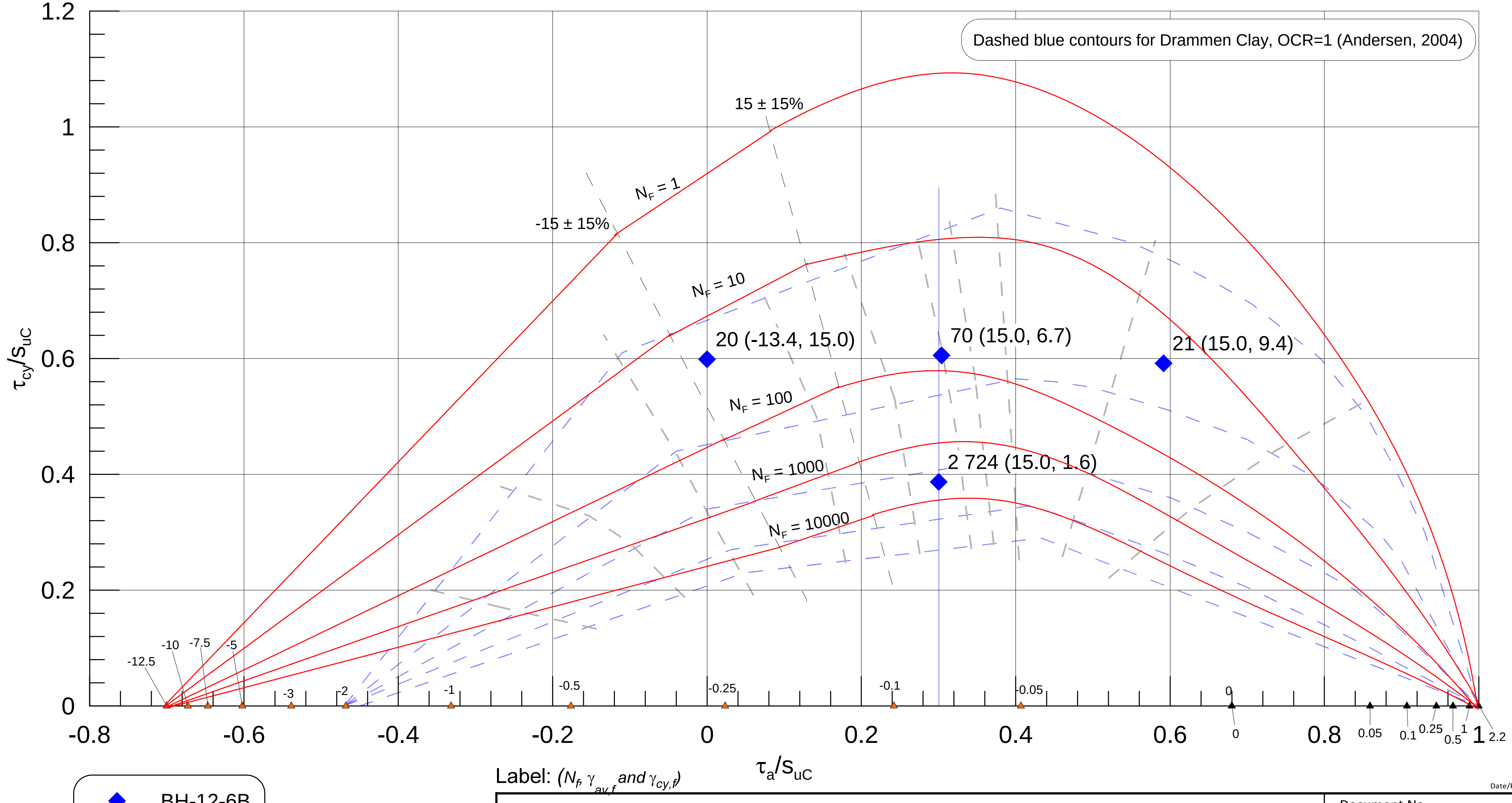

BH-12-6B

▲ Numbers indicate shear strain in nearest static extension test

▲ Numbers indicate shear strain in nearest static compression test

Date/Rev.: 2015-01-21/01

ST15452 Flemish Pass Geotechnical Investigation	Document No. 20140857-02-R	
Cyclic CAU tests, average and cyclic shear stress normalised to s_{uC} Field Centre For Structural design	Figure No. G7.2	
	Date 2016-04-03	Drawn by VDa/KS

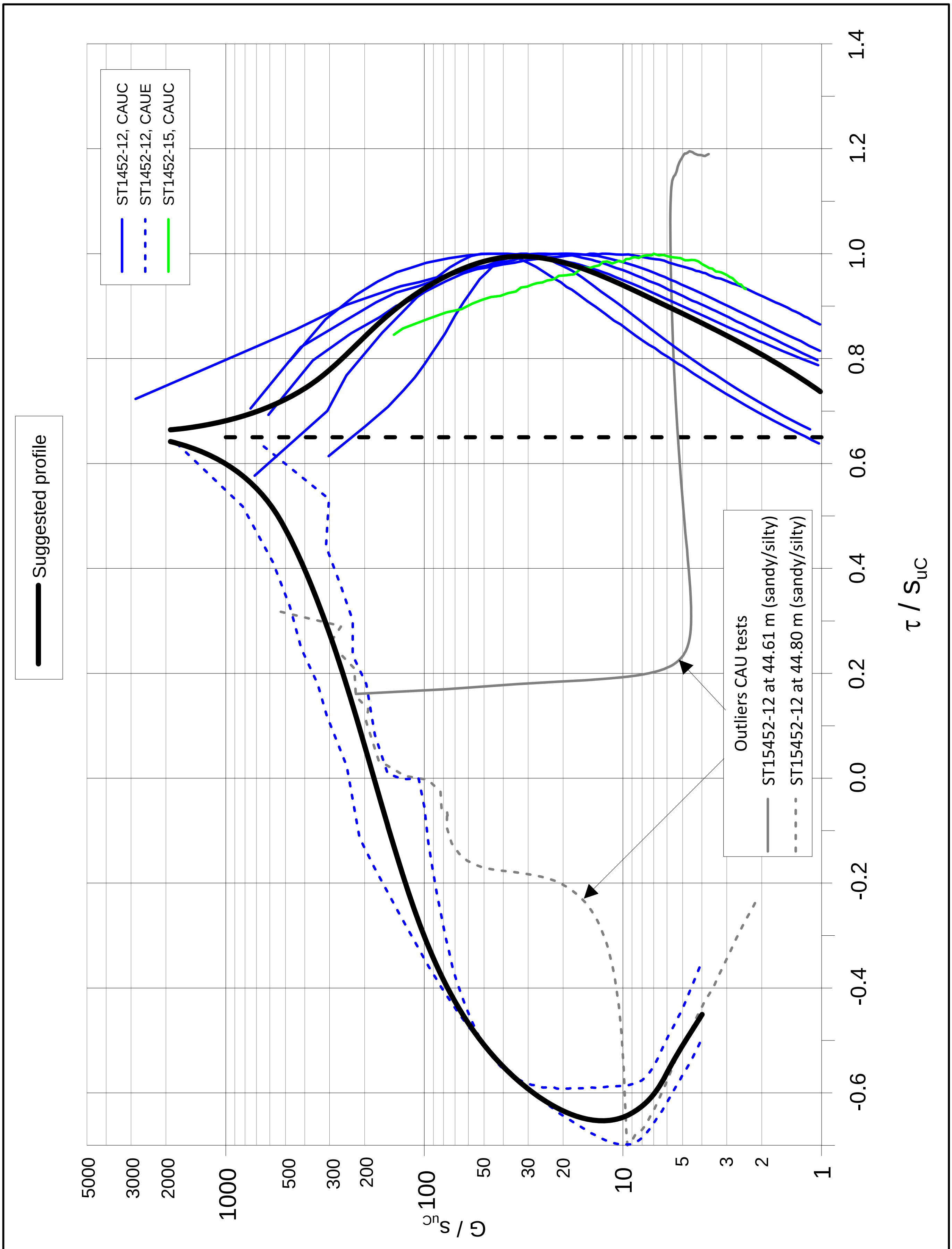

Date/Rev.: 2015-01-21/01

ST15452 Flemish Pass Geotechnical Investigation

G/s_{uC} versus τ/s_{uC} from CAU triaxial tests. Ratio τ_c/s_{uC} = 0.65
Field Centre

Document No.	20140857-02-R
Figure No.	G8.1
Date	2016-04-04
Drawn by	VDa

P:\2014\08\20140857\Leveranse dokumenter\Rapport\20140857-02-R Data interpretation and evaluation\Figures\Section G\Figure G_08_01, G_su_triax vs tau_su_triax_Field_Centre.grf

P:\2014\08\20140857\Leveransedokumenter\Rapport\20140857-02-R Data interpretation and evaluation\Figures\Section G\Figure G_08_02, G_su_DSS vs tau_su_DSS_field_centre.grf

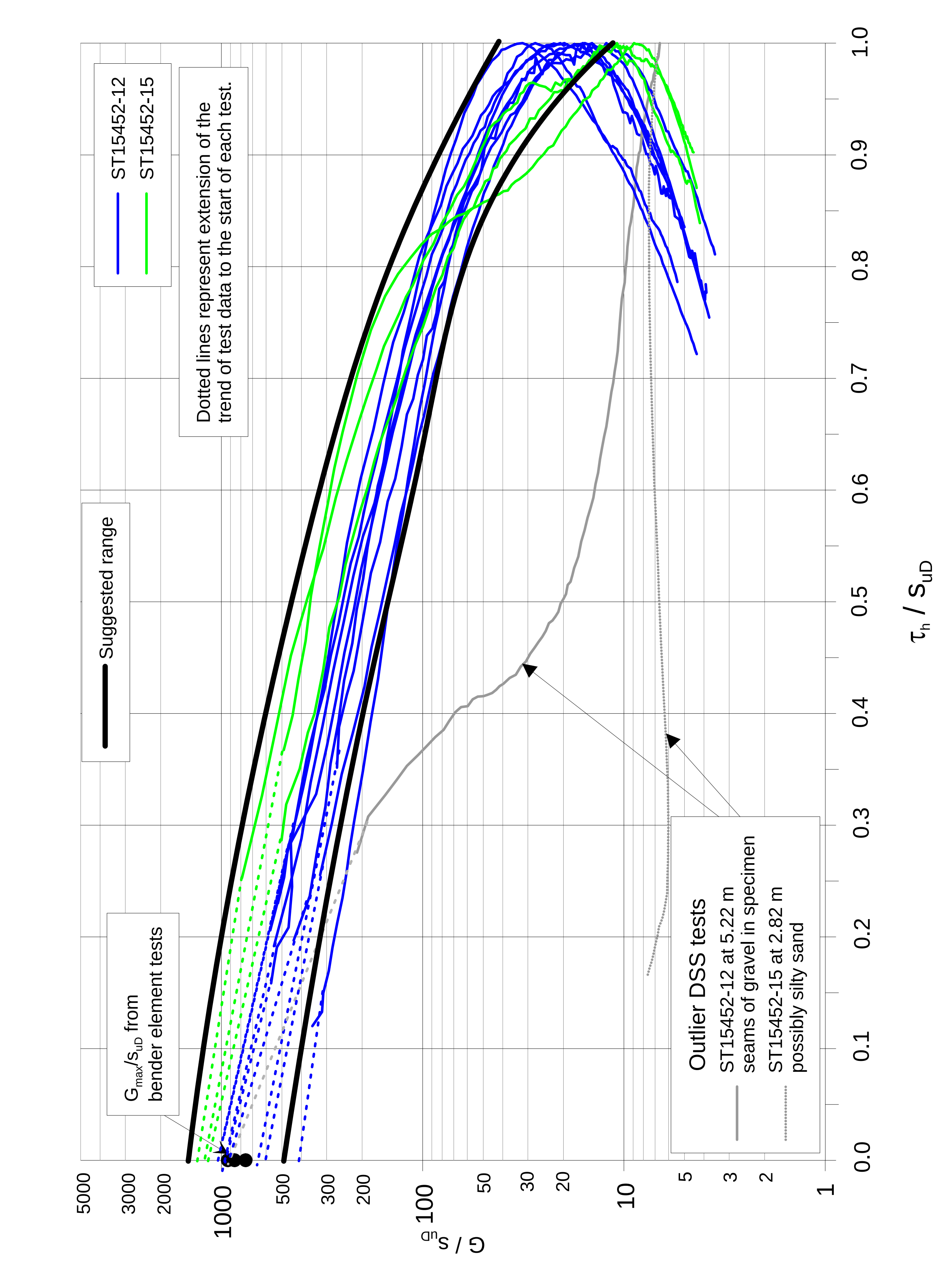

Date/Rev.: 2015-01-21/01

ST15452 Flemish Pass Geotechnical Investigation	Document No. 20140857-02-R
G/s_{uD} versus τ/s_{uD} from DSS tests Field Centre	Figure No. G8.2
	Date 2016-04-04
	Drawn by VDa

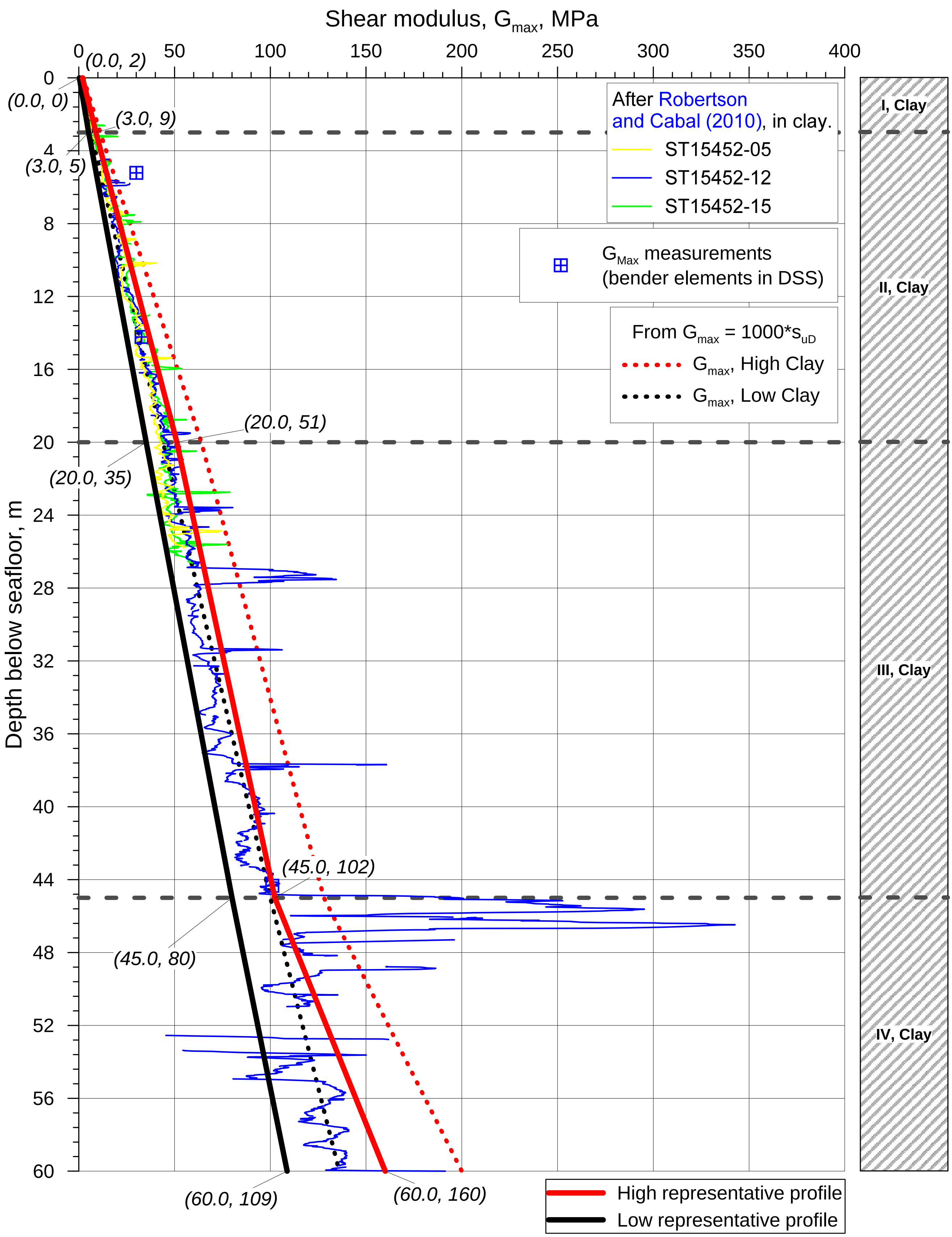

Label: *(depth, value)*

Date/Rev.: 2015-01-21/01

ST15452 Flemish Pass Geotechnical Investigation	Document No. 20140857-02-R
Maximum shear modulus versus depth Field Centre	Figure No. G8.3
	Date 2016-04-03 / Drawn by VDa

P:\2014\08\20140857\Leveransedokumenter\Rapport\20140857-02-R Data interpretation and evaluation\Figures\Section G\Figure G_08_03, Gmax versus depth_Field_Centre.grf

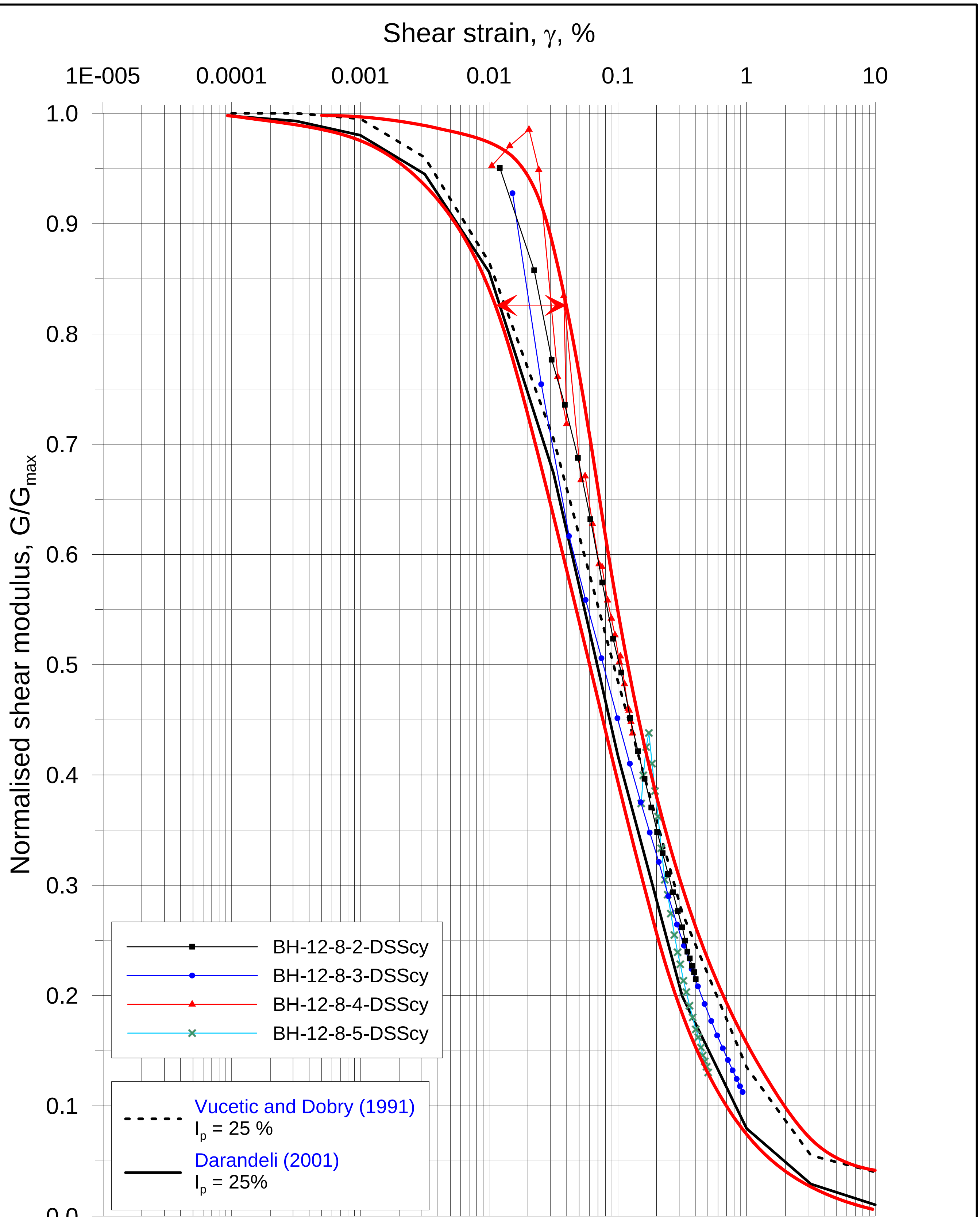

Note: For DSS tests, the G_{max} values are evaluated using Robertson and Cabbal, (2010) equation.

Suggested range of G/G_{max} G_{max} = 39.3 MPa

Date/Rev.: 2015-01-21/01

P:\2014\08\20140857\Leveransedokumenter\Rapport\20140857-02-R Data interpretation and evaluation\Figures\Section G\Figure G_08_04, NormalizedGmax versus shear strain_N=1_Field_centre.grf

ST15452 Flemish Pass Geotechnical Investigation

Normalised shear modulus, G/G_{max}, versus shear strain
from DSS tests
Field Centre
N=1 cycle

Document No. 20140857-02-R	
Figure No. G8.4	
Date 2016-04-03	Drawn by VDa

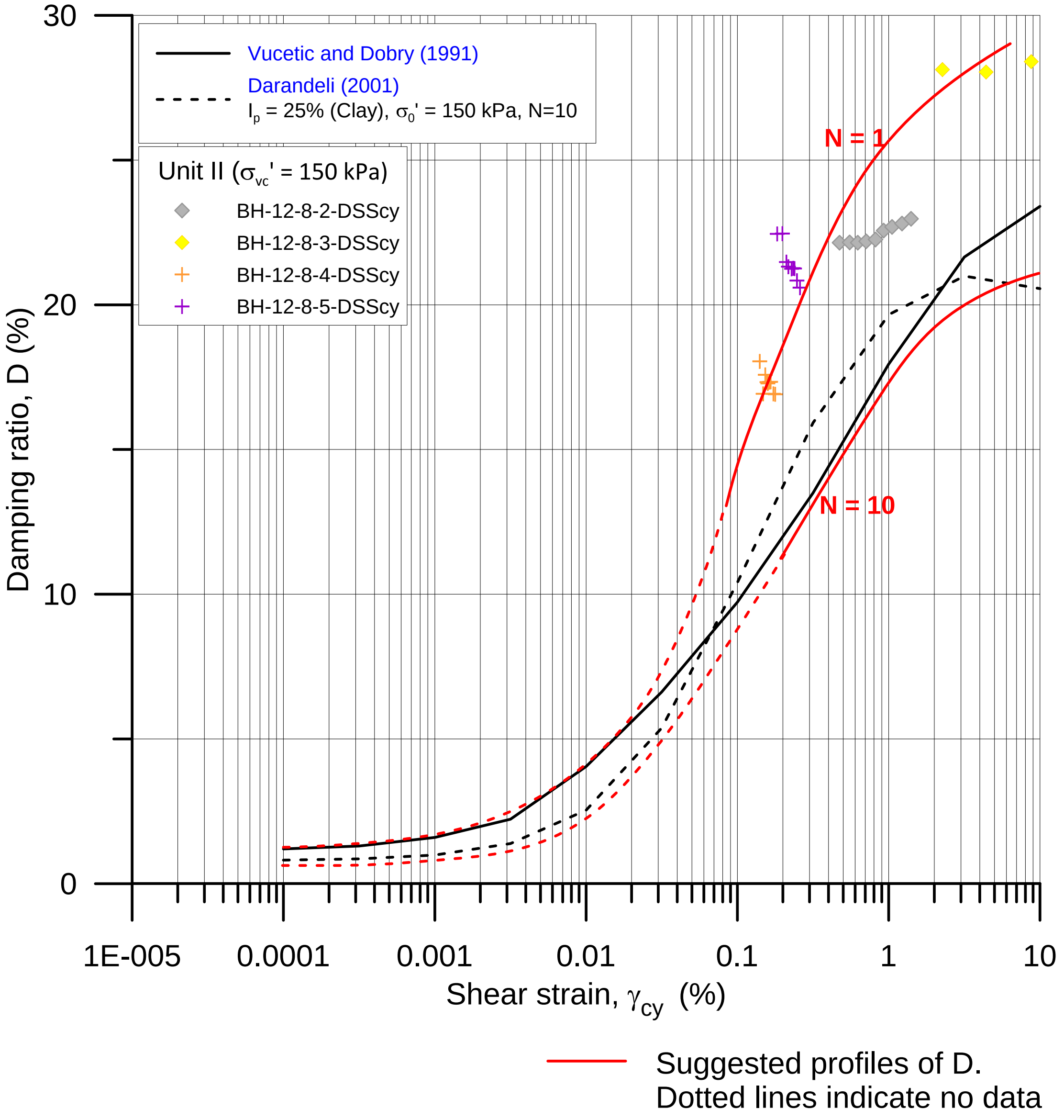

P:\2014\08\20140857\Leveransedokumenter\Rapport\20140857-02-R Data interpretation and evaluation\Figures\Section G\Figure G_08_05, Damping versus shear strain_Field_centre.grf

Date/Rev.: 2015-01-21/01

ST15452 Flemish Pass Geotechnical Investigation	Document No. 20140857-02-R	
Damping ratio, D, versus cyclic shear strain from symmetric cyclic DSS tests Field Centre	Figure No. G8.5	
	Date 2016-04-03	Drawn by VDa

Section H

RECOMMENDED REPRESENTATIVE GEOTECHNICAL PARAMETERS, SLOPES

Contents

Tables

Figures

H1 General

This section presents the representative soil parameters for the Flemish Pass West Slope and East Slope.

The main purpose of the geotechnical testing and parameters given for the Slopes in this section is to provide parameters for geohazard evaluations including slope stability, and for FEED design of structures like pipelines.

The representative soil parameters are based on interpretation of the available data and test results reported and referred to in Section F and NGI (2016).

The soil is layered giving high variability over short depth ranges. The soil conditions are, however relatively consistent between the different locations The figures presented herein show representative profiles including measured values in the background to illustrate the available information and spread in data.

The figures presented herein show representative profiles including measured values in the background to illustrate the available information and spread in data.

The two slope areas both extend from a water depth of about 300 m to 1200 m. The water depth at the borehole locations investigated at the West Slope varied between 675 m and 875 m. At the boreholes at the East Slope location the water depth was 1004 m.

H2 Soil layering

At the West Slope locations the soil from seafloor down to a depth of 101 m can in general be divided into four clay units. Table H2-1 presents the depths to the units and the descriptions for the West Slope locations. The units are in line with the geophysical interpretation presented in Section E.

At the East Slope location the soil from seafloor down to a depth of 98.2 m can in general be divided into four clay units. Table H2-2 presents the depths to the units and the descriptions for the East Slope location. The units are in line with the geophysical interpretation presented in Section E.

Table H2-1 Summary of the generalised soil conditions encountered at the West Slope locations

Unit	Depth below seafloor, m (indicative values)	Soil description
I	0 – 3.0	CLAY, silty, extremely low to low strength, traces of fine to medium sand partings, medium to coarse sub-angular gravels and few shell fragments, greenish gray. Sandy in the upper 20 cm in some locations
II	3.0 – 25.0	CLAY, silty, low to medium strength, low to medium plasticity, sand seams at different locations, few drop stones, gravel or larger, and pockets of sands, greenish grey to dark gray.
III	25.0 – 45.0	CLAY, medium to high strength clay, medium plasticity, traces of fine sub-angular to sub-rounded gravels and coarse shell fragments, dark gray, gas in solution.
IV	45.0 – 101.0[1)]	CLAY, medium to high strength, medium plasticity, drop stones, gravel or larger. Possibly mass transit deposit, dark gray.

1) End of borehole for ST15452 –02 = 101.0 m; ST15452 –03 = 62.5 m; ST15452 – 07 = 45.8 m; ST15452 –08 = 62.5 m; ST15452 –16 = 55.6 m; ST15452 –19 = 50.6 m.

Table H2-2 Summary of the generalised soil conditions encountered at the East Slope location

Unit	Depth below seafloor, m (indicative values)	Soil description
I	0 – 3.0	CLAY, silty, extremely low to low strength.
II	3.0 – 50.0	CLAY, low to medium strength, low to medium plasticity, sand seams at different locations, few drop stones, gravel or larger, and pockets of sands.
III	50.0 – 70.0	CLAY, medium to high strength clay, medium plasticity, traces of fine sub-angular to sub-rounded gravels and coarse shell fragments, dark gray, gas in solution.
IV	70.0 – 98.2[1)]	CLAY, medium to high strength, medium plasticity, drop stones, gravel or larger. Possibly mass transit deposit, dark greenish gray.

1) End of borehole for ST15452 –18 = 98.2 m.

Table H2-3 presents a summary of the soil layering and representative characteristics for the West Slope locations. Further details on classification data including profiles of recommended representative basic soil parameters are presented in Section F.

Table H2-3 Soil units and representative characteristics relevant for 0 – 101 m depth. West Slope locations. The range of measured data is given in brackets to show variability.

Unit	Typical depth below seafloor, m	Soil type	Water content, w, %	Total unit weight, γ, kN/m^3	Plasticity index[2], I_p, %	Fines content[3], %	Corrected cone resistance[4], q_t, MPa	Undrained shear strength[4], s_{uC}, kPa
I	0 – 3.0	Clay	35 (29-38)	18.5 (18.2-19.2)	12 (6-12)	67-76 (19-34)	0.1-0.2	0.2 - 10
II	3.0 – 25.0	Clay	25 (18-48)	20 (17.2-22.8)	15 (4-18)	50-86 (10-46)	0.2-1	10-70
III	25.0 – 45.0	Clay	20 (15-42)	21 (17.5-23.0)	15 (8-24)	52-87 (20-33)	1-2	70-125
IV	45.0 – 101 [1]	Clay	25 (19-33)	20 (18.5-21.0)	12 (5-17)	63-90 (15-32)	2-7	125-350

[1] End of borehole for ST15452 –02 = 101.0 m
[2] Only relevant for clay material
[3] Range of values (range of clay content in brackets)
[4] Low representative values or range of values

Table H2-4 presents a summary of the soil layering and representative characteristics for the East Slope location. Further details on classification data including profiles of recommended representative basic soil parameters are presented in Section F.

Table H2-4 Soil units and representative characteristics relevant for 0 – 98 m depth. East Slope location. The range of measured data is given in brackets to show variability.

Unit	Typical depth below seafloor, m	Soil type	Water content, w, %	Total unit weight, γ, kN/m^3	Plasticity index[2], I_p, %	Fines content[3], %	Corrected cone resistance[4], q_t, MPa	Undrained shear strength[4], s_{uC}, kPa
I	0 – 3.0	Clay	25 (n.a)	20.0 (n.a)	15 (n.a.)	n.a. (n.a.)	0.08-0.2	0.2 - 10
II	3.0 – 50.0	Clay	25 (18-36)	20.0 (18.3-21.0)	15 (n.a.)	91 (38)	0.2-2.3	10-140
III	50.0 – 70.0	Clay	31 (22-50)	19.0 (17.0-20.9)	10 (6-28)	49-94 (15-55)	2.1-2.8	140-200
IV	70.0 – 98.2[1]	Clay	31 (22-36)	19.0 (17.9-20.5)	15 (5-18)	65-91 (9-30)	3-4	200-280

[1] End of borehole for ST15452 –18 = 98.2 m
[2] Only relevant for clay material
[3] Range of values (range of clay content in brackets)
[4] Low representative values or range of values

H3 Classification soil parameters

The figures presented herein show representative profiles including measured values in the background to illustrate the available information and spread in data.

H3.1 Water content

The representative water content profiles for the West Slope and the East Slope are presented in Figures H3.1 and H3.2 respectively.

H3.2 Total unit weight

The representative total unit weight profiles for the West Slope and the East Slope are presented in Figures H3.3 and H3.4 respectively.

H3.3 Plasticity data

The representative profiles of plasticity index for the West Slope and the East Slope are presented in Figures H3.5 and H3.6 respectively.

H3.4 Unit weight of solid particles

The representative profile of unit weight of solid particles is presented in Figure H3.7.

H3.5 Grain size distribution

Figures H3.8 and H3.9 present the values of clay content and fines content with depth the West Slope and the East Slope respectively. No representative profiles nor trend lines have been drawn due to the variability of the soil.

H3.6 Remoulded shear strength

Remoulded strength is used for installation analyses and for slope stability analyses for runout analyses. For both, it is suggested to use remoulded strength equal to the remoulded undrained shear strength as measured in the laboratory tests. Figures H3.10 and H3.11 show the measured remoulded shear strength together with low and high representative profiles the West Slope and the East Slope respectively.

The profiles of remoulded strength are based on the measured data. It is possible that the variability in remoulded strength is large over short depth intervals so that the low representative profile should only be applied over short depth ranges, with the values in between being higher. The designer should consider such possibilities.

H3.7 Sensitivity

Sensitivity has been determined from index shear strength tests on intact and remoulded clay samples. The sensitivity is calculated as $S_t = s_u/s_{ur}$, where su and sur are the shear strengths for the intact and the remoulded samples, respectively. The representative sensitivity profiles are shown in Figures H3.12 and H3.13 for the West Slope and the East Slope respectively, and taken as $S_t = s_{uD}^{avg}/s_{ur}^{avg}$. See Section F for discussion.

H4 In situ stresses and stress history

H4.1 In situ effective vertical stress

The representative profile of effective vertical stress, p_0', is presented in Figures H4.1 and H4.2 for the West Slope and the East Slope respectively. The profiles are derived from the relevant total unit weight profiles (Figures H3.3 and H3.4) assuming hydrostatic pore pressure in situ.

The in situ effective vertical stress, p_0' (in kPa), based on the average depth to each soil unit can be calculated as:

West Slope

$0 < z < 3.0$ m: $p_0' = 5.5z$
$3.0 < z < 25.0$ m: $p_0' = -4.5 + 10z$
$25.0 < z < 45.0$ m: $p_0' = -29.5 + 11z$
$45.0 < z < 100.0$ m: $p_0' = 15.5 + 10z$

East Slope

$0 < z < 50.0$ m: $p_0' = 10z$
$50.0 < z < 100.0$ m: $p_0' = 50 + 9z$

where z is depth below seafloor in metres.

H4.2 Preconsolidation stress and overconsolidation ratio

The interpretation of preconsolidation stress, p_c', and overconsolidation ratio, OCR, is based on results from oedometer tests using various interpretation methods and on the CAUC test results and the CPTU results using the method of Andresen et al. (1979). The representative profiles of p_c' and OCR are presented in Figures H4.3 to H4.6 for the West Slope and the East Slope.

H4.3 Coefficient of earth pressure at rest

Horizontal in situ effective stresses are derived using the coefficient of earth pressure at rest, K_0. The representative K_0 profile is shown in Figures H4.7 and H4.8 for the West Slope and the East Slope respectively.

H5 Consolidation parameters

H5.1 Immediate settlements

Immediate settlements may be estimated by elasticity theory using the shear modulus, G. The G-value will typically vary from soil element to soil element and depends on the degree of strength mobilization, the degree of overconsolidation, the strength and the general soil characteristics.

Based on the laboratory tests carried out, the normalised secant shear moduli have been presented as a function of strength mobilisation. Figure H8.1 shows suggested values of G/s_{uC} versus τ/s_{uC} for all units tested based on the compression and extension CAU-triaxial tests carried out. The figure represents both West Slope and East Slope locations. Similarly, Figure H8.2 gives similar suggestions in terms of G/s_{uD} versus τ_h/s_{uD} based on the DSS tests carried out on both West Slope and East Slope locations.

H5.2 Primary consolidation settlements

The soil parameters necessary for evaluating the primary consolidation settlements and its time dependency are the constrained modulus, M, the coefficient of vertical consolidation, c_v, and the drainage length, H.

The primary consolidation settlements are generally influenced by the relationship between the stress increase imposed by the structure, the initial in situ stresses, and the preconsolidation stress, p_c'. Stress increases that exceed p_c' will usually yield much larger settlements.

The consolidation settlements can be calculated using the Janbu modulus concept (Janbu, 1963). The representative profiles of the constrained modulus, M_0 are presented in Figures H5.1 and H5.2 for the West Slope and the East Slope respectively. Similarly, Figures H5.3 and H5.4 present the suggested representative profiles of the modulus number and reference stress (m and p_r').

The soil parameters, k_v and c_v necessary for evaluating the primary consolidation settlement are presented in Figures H5.5 to H5.8, for the West Slope and the East Slope.

H6 Static soil strength parameters

H6.1 CPTU parameters

Summary plots of the corrected cone resistance, q_t, are presented in Figures H6.1 and H6.2 for the West Slope and the East Slope respectively.

Summary plots of the sleeve friction, f_s, are presented in Figures H6.3 and H6.4.

Summary diagrams of the measured pore water pressure, u_2, are presented in Figures H6.5 and H6.6 for the two areas respectively.

H6.2 Undrained static shear strength parameters

Static undrained shear strength parameters were evaluated based on CPTUs, triaxial tests, DSS tests and a number of index shear strength tests. All these tests were carried out as undrained tests relevant for short term loading, and the results are presented and discussed in Section F.

The representative high and low profiles of undrained shear strength are presented in Figures H6.7 and H6.8 for the West Slope and the East Slope respectively. The low profile should be used for geotechnical analyses where a low strength is conservative and the upper profile for geotechnical analyses where a high strength is conservative. The designer should evaluate the effect of softer layers by adding a 1 m thick layer with strength 10 % below the low representative strength at any level below 5 m depth.

The representative strength anisotropy ratios are:

Soil Units I, II*, III and IV:	$s_{uD}/s_{uC} = 0.80$
Soil Units I, II*, III and IV:	$s_{uE}/s_{uC} = 0.75$

*There are data from approximately 30 m depth indicating lower values of anisotropy in Unit II of $s_{uD}/s_{uC} = 0.6$ and $s_{uE}/s_{uC} = 0.45$. A designer can take the representative profiles as a baseline and should assess the effect of applying the low representative profiles.

H6.3 Effective shear strength parameters

The triaxial tests have been interpreted in terms of effective stresses.

Summary of effective stress paths from CAUC and CAUE triaxial tests on intact samples are presented in Section F with the Mohr-Coulomb failure envelopes representing the recommended effective friction angles (ϕ'_u) and attraction (a) obtained from these undrained tests.

A range of a = 0 kPa and ϕ' between 30° and 36° is suggested appropriate for the tested material.

See Section F for more details.

H7 Cyclic soil strength parameters

A special type of cyclic DSS tests were performed on samples from East Slope location. The objective of these tests was to determine the soil behavior subjected to earthquake loading and to quantify the cyclic and post-cyclic strength for slope stability analysis. Three cyclic DSS tests were performed with a cyclic period of T = 2s. Figure H7.1 illustrates the loading and effect of the special cyclic tests with a cyclic period of 2 s together with failure contours from literature (T = 10 s).

Figure H7.2 shows the results. The upper graph illustrates the strain developed after 5 cycles as a function of the cyclic shear stress normalised to the static strength, $\tau_{cy}/s_{uD,\tau c}$, where $s_{uD,\tau c}$ is the strength of a static test consolidated with a shear stress as explained above. The fact that 5 cycles with a cyclic shear stress equal to the static strength generates less than 3% strain is attributed to rate effect. A cyclic test with a period of 2 s, has a rate of shear stress of the order of 10^4 faster than a standard static DSS test. The lower graph in Figure H7.2 shows the measured strains after 10 cycles. In both graphs the initial slope of the stress-strain relationship is illustrated by the G_{max} from a bender element test performed on the static reference test.

Based on the limited number of cyclic tests performed, one conclusion may to be that in order to avoid large shear strains after 10 cycles, the cyclic shear stress ratio $\tau_{cy}/s_{uD,\tau c}$, should be less than 0.8. See Section F for further discussion

H8 Stiffness and damping parameters

The normalised secant shear moduli have been presented as a function of strength mobilisation. Figure H8.1 shows suggested values of G/s_{uC} versus τ/s_{uC} for all units tested based on the compression and extension CAU-triaxial tests carried out. Figure H8.2 gives similar suggestions in terms of G/s_{uD} versus τ_h/s_{uD} based on the DSS tests carried out.

G_{max} measurements were performed on specimens in the laboratory using piezo-ceramic bender elements in connections with DSS tests. The high and low representative profiles with depth are presented in Figures H8.3 - H8.4 for West and East Slopes respectively.

The suggested range in normalised shear modulus, G/G_{max}, versus shear strain is presented in Figure H8.5.

The suggested profiles of damping ratio, D, versus cyclic shear strain for N = 1 and N = 10 is presented in Figure H8.6 for soil Unit II.

For more details reference is made to Section F.

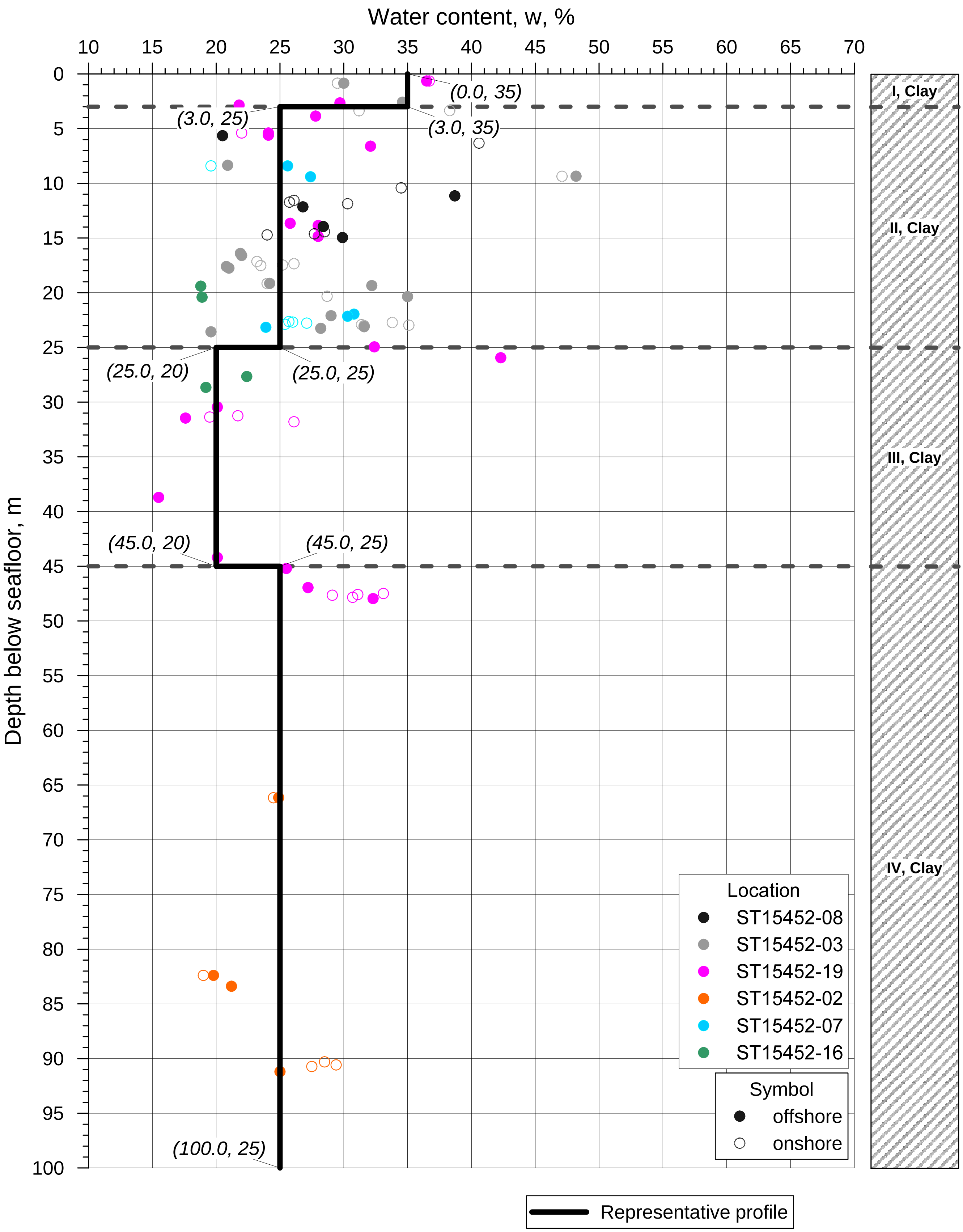

Label: *(depth, value)*

Date/Rev.: 2015-01-21/01

ST15452 Flemish Pass Geotechnical Investigation	Document No. 20140857-02-R
Water content versus depth West Slope	Figure No. H3.1
	Date 2016-04-03 / Drawn by VBS
	NGI

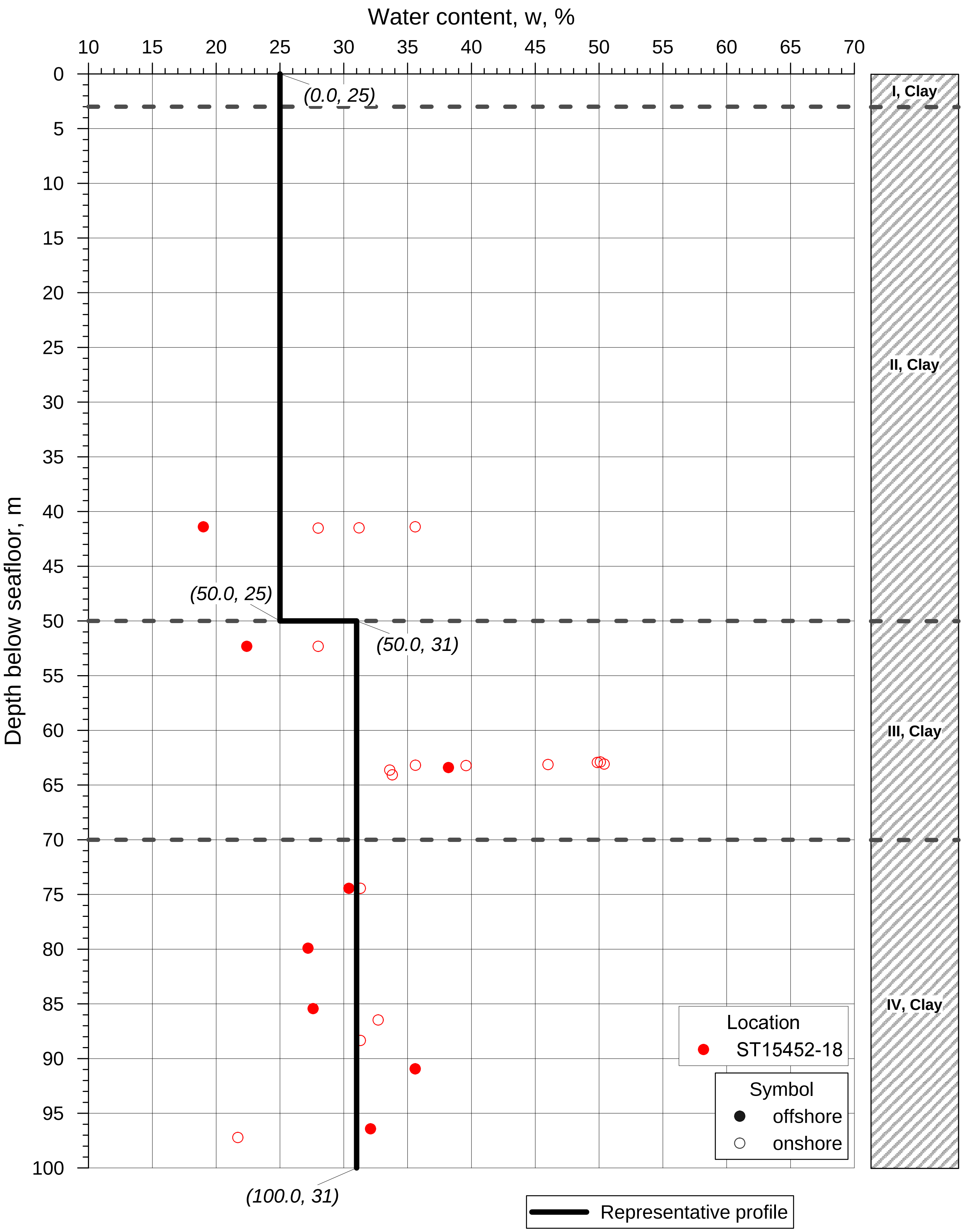

Label: *(depth, value)*

Date/Rev.: 2015-01-21/01

P:\2014\08\20140857\Leveransedokumenter\Rapport\20140857-02-R Data interpretation and evaluation\Figures\Section H\Figure H_03_02, water content versus depth-East.grf

ST15452 Flemish Pass Geotechnical Investigation	Document No. 20140857-02-R
Water content versus depth East Slope	Figure No. H3.2
	Date 2016-04-03 / Drawn by VBS

NGI

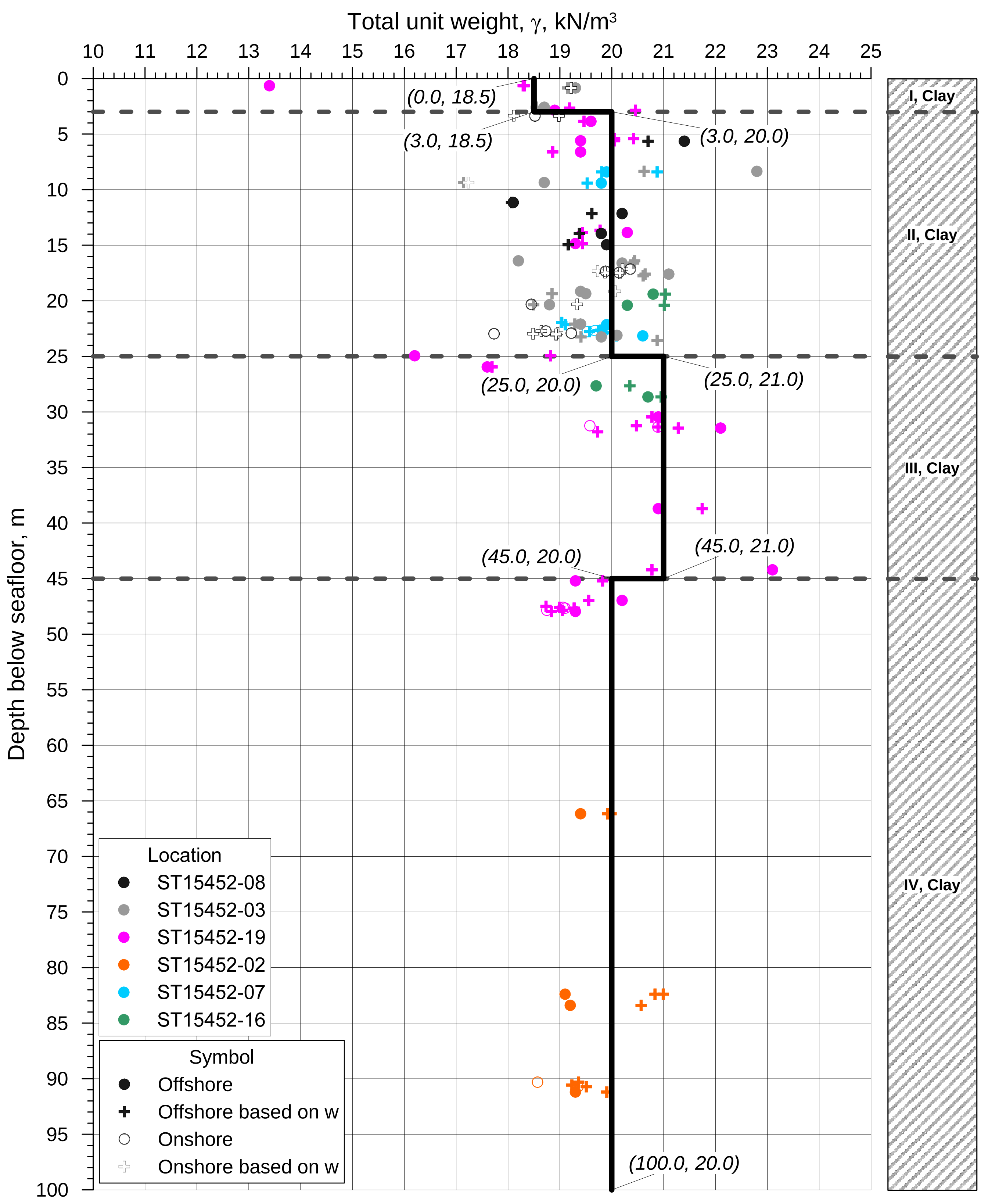

NOTE:
γ based on w is calculated assuming S_r = 100%
and using γ_s = 26.8 kN/m³

Label: *(depth, value)*

Date/Rev.: 2015-01-21/01

P:\2014\08\20140857\Leveransedokumenter\Rapport\20140857-02-R Data interpretation and evaluation\Figures\Section H\Figure H_03_03, total unit weight versus depth-West.grf

ST15452 Flemish Pass Geotechnical Investigation	Document No. 20140857-02-R
Total unit weight versus depth West Slope	Figure No. H3.3
	Date 2016-04-03 / Drawn by VBS
	NGI

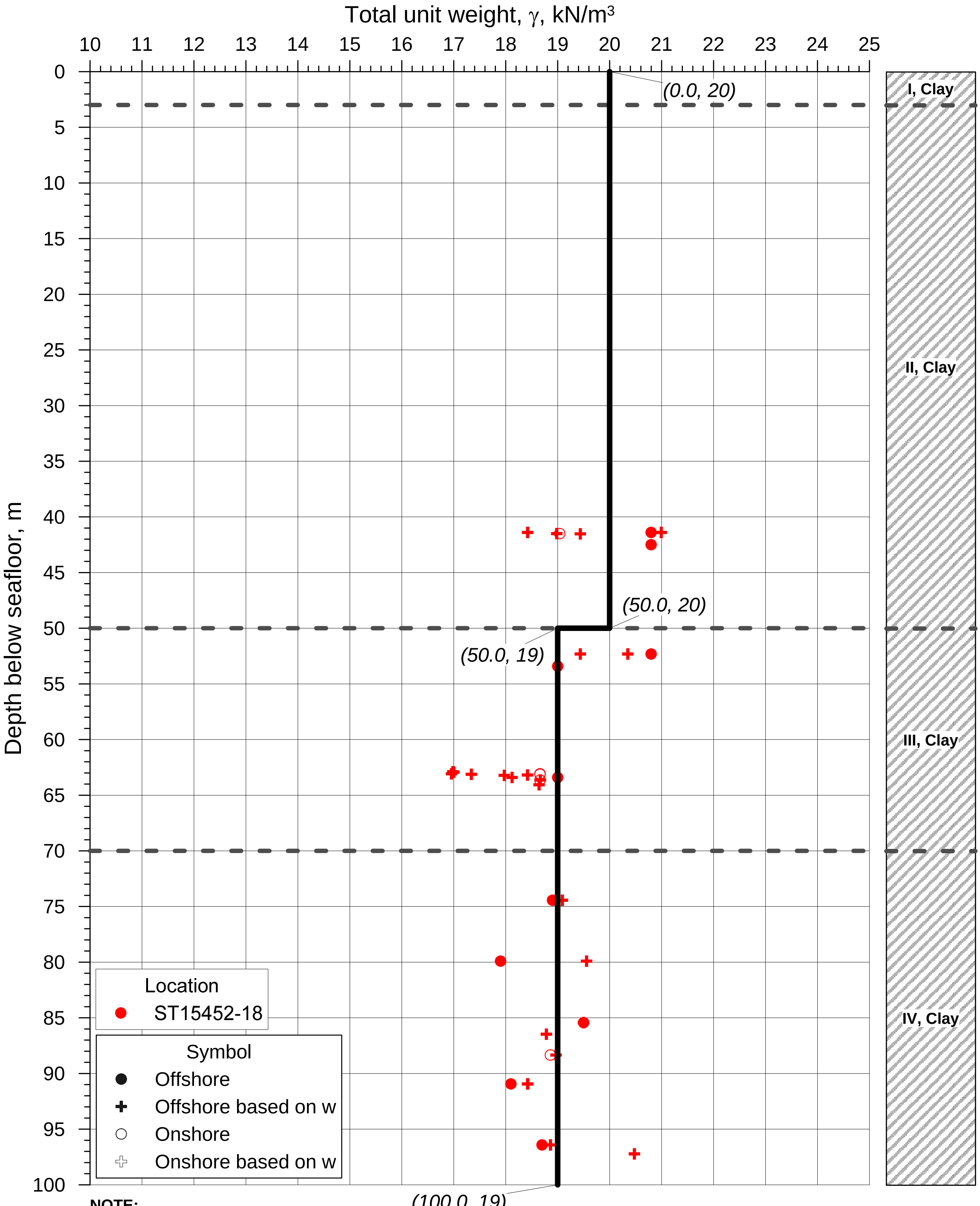

NOTE:
γ based on w is calculated assuming S_r = 100%
and using γ_s = 26.8 kN/m³

Label: *(depth, value)*

P:\2014\08\20140857\Leveransedokumenter\Rapport\20140857-02-R Data interpretation and evaluation\Figures\Section H\Figure H_03_04, total unit weight versus depth-East.grf

Date/Rev.: 2015-01-21/01

ST15452 Flemish Pass Geotechnical Investigation	Document No. 20140857-02-R
Total unit weight versus depth East Slope	Figure No. H3.4
	Date 2016-04-03 / Drawn by VBS

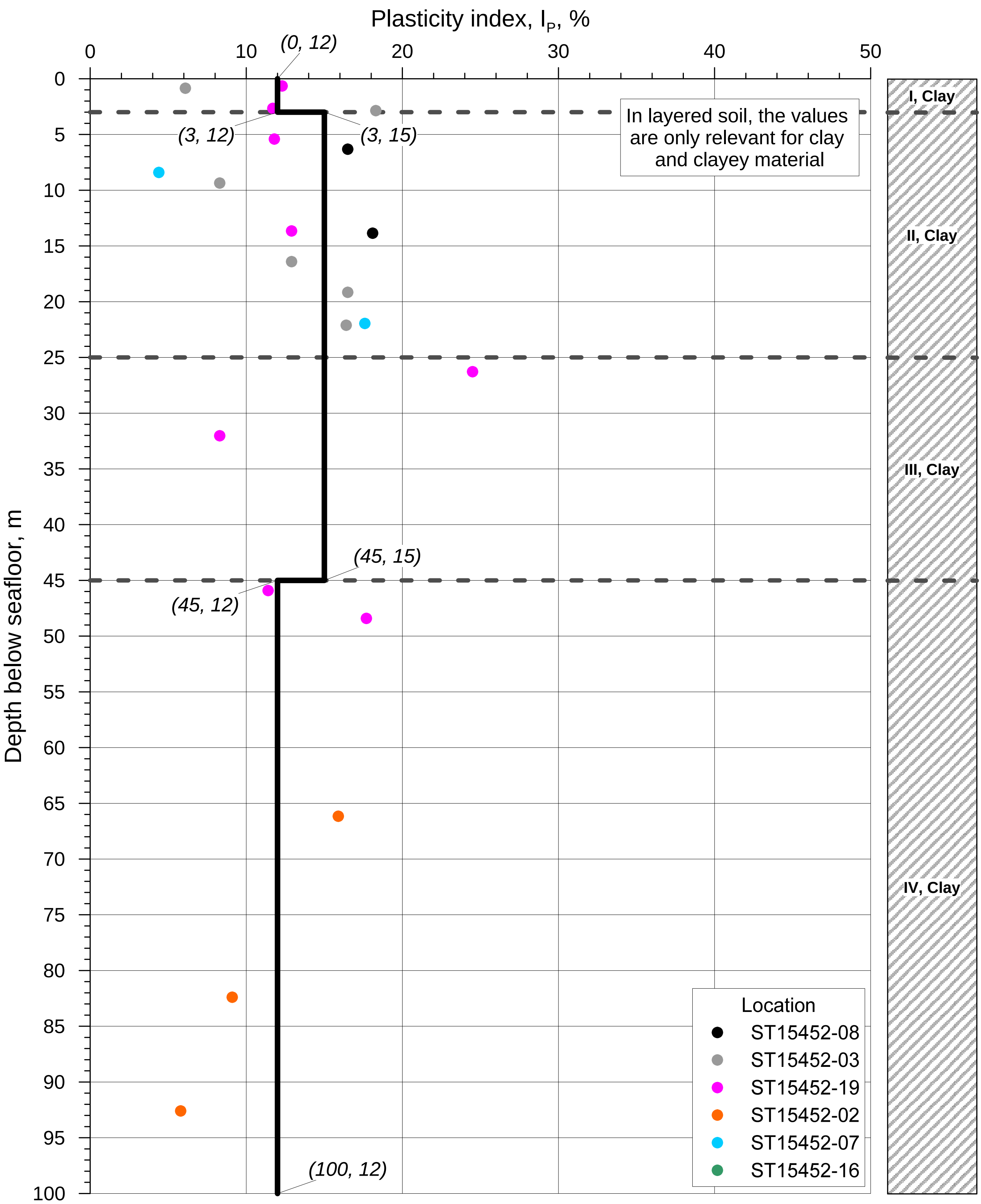

NOTE:
Representative profile based on engineering judgement.

Representative profile

Label: *(depth, value)*

Date/Rev.: 2015-01-21/01

ST15452 Flemish Pass Geotechnical Investigation	Document No. 20140857-02-R
Plasticity index versus depth West Slope	Figure No. H3.5
	Date 2016-04-03 — Drawn by VBS
	NGI

P:\2014\08\20140857\Leveransedokumenter\Rapport\20140857-02-R Data interpretation and evaluation\Figures\Section H\Figure H_03_05, plasticity index versus depth-West.grf

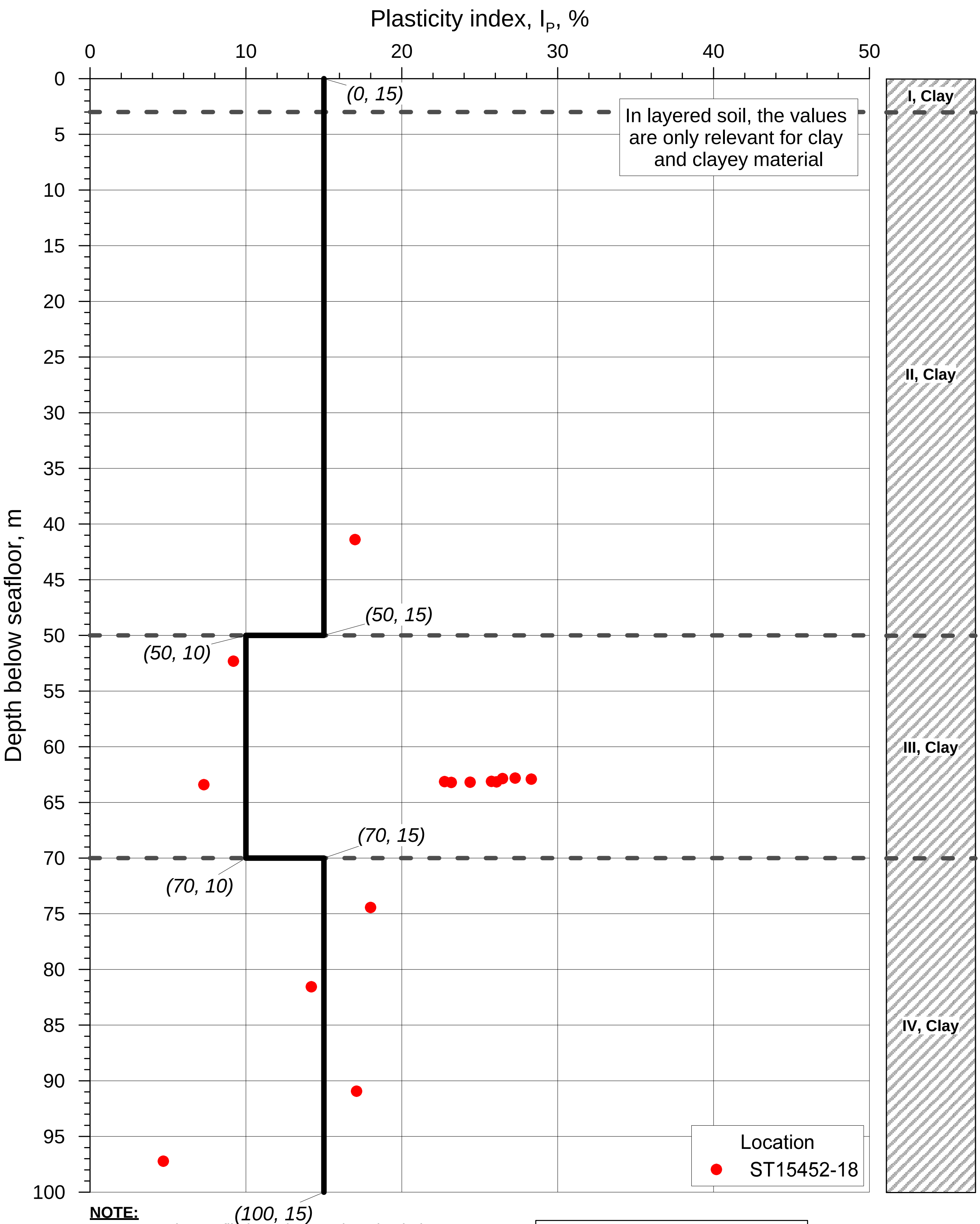

NOTE:
Representative profile based on engineering judgement.

Representative profile

Label: *(depth, value)*

ST15452 Flemish Pass Geotechnical Investigation

Plasticity index versus depth
East Slope

Document No. 20140857-02-R	
Figure No. H3.6	
Date 2016-04-03	Drawn by VBS

NGI

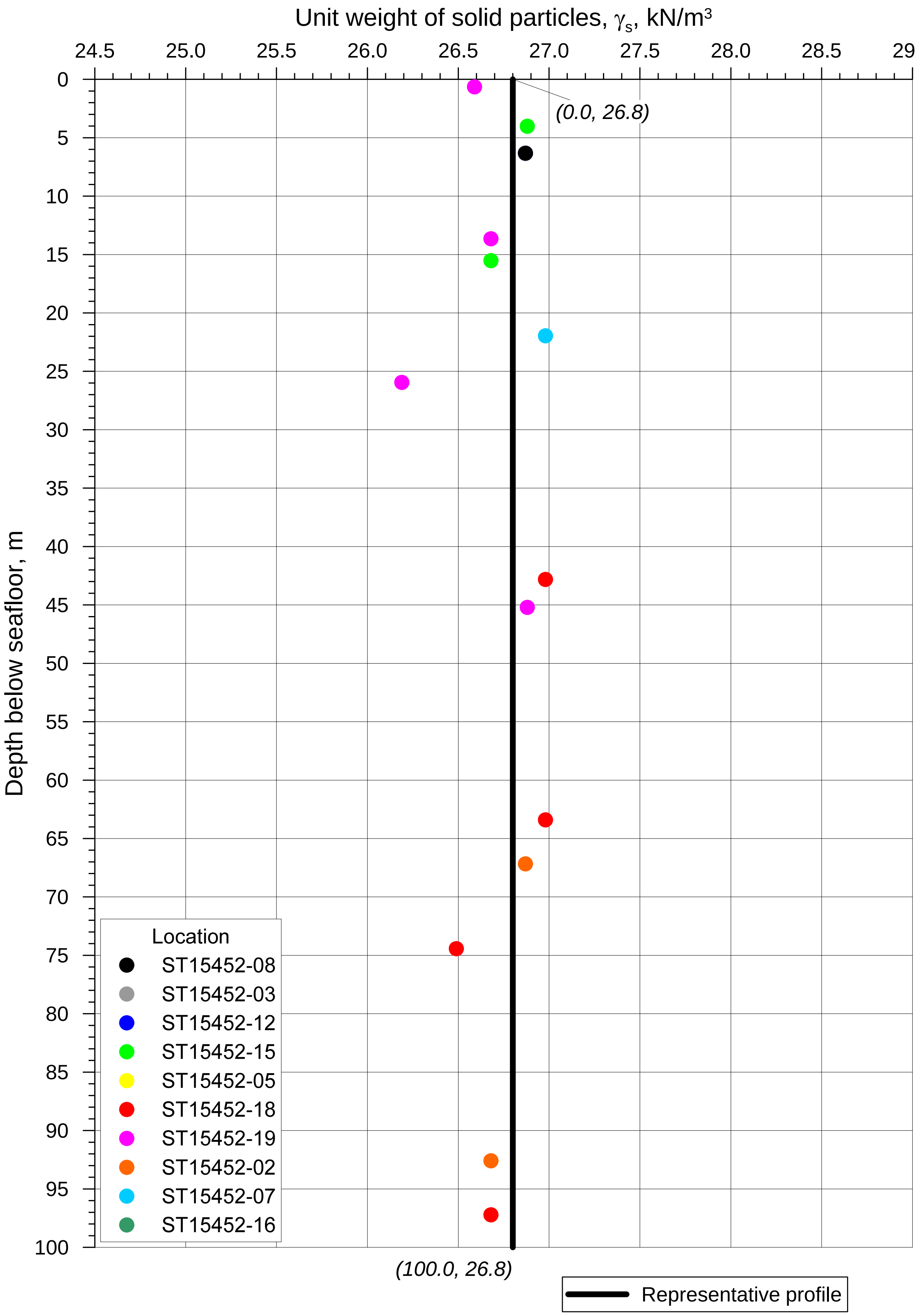

Label: *(depth, value)*

Date/Rev.: 2015-01-21/01

ST15452 Flemish Pass Geotechnical Investigation

Unit weight of solid particles versus depth
All locations

Document No.	20140857-02-R
Figure No.	H3.7
Date	2016-04-03
Drawn by	VBS

NGI

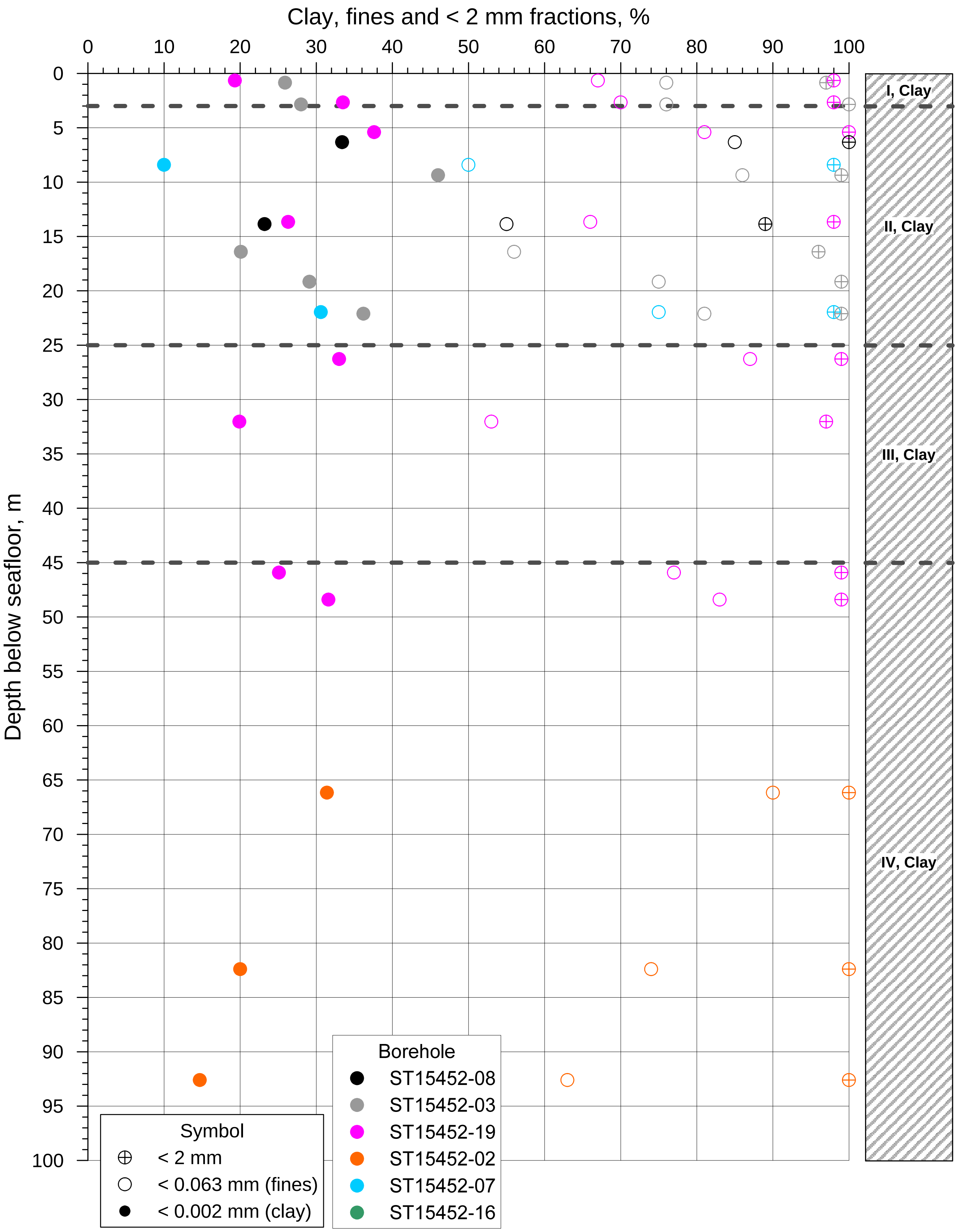

Date/Rev.: 2015-01-21/01

ST15452 Flemish Pass Geotechnical Investigation	Document No. 20140857-02-R
Clay, fines and <2 mm fractions versus depth West Slope	Figure No. H3.8
	Date 2016-04-03 / Drawn by VBS
	NGI

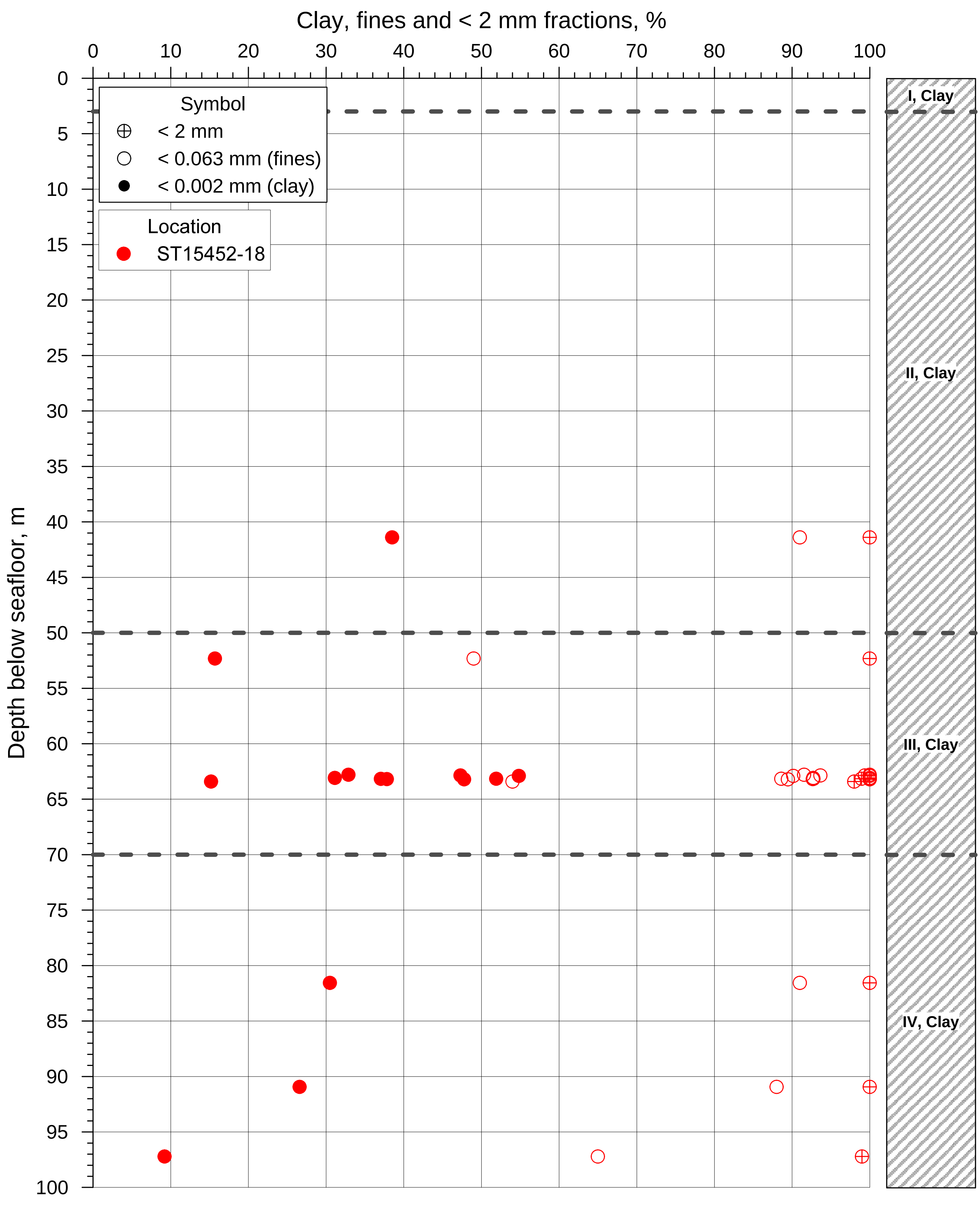

P:\2014\08\20140857\Leveransedokumenter\Rapport\20140857-02-R Data interpretation and evaluation\Figures\Section H\Figure H_03_09, grain size versus depth-East.grf

Date/Rev.: 2015-01-21/01

ST15452 Flemish Pass Geotechnical Investigation	Document No. 20140857-02-R
Clay, fines and <2 mm fractions versus depth East Slope	Figure No. H3.9
	Date 2016-04-03 / Drawn by VBS

NGI

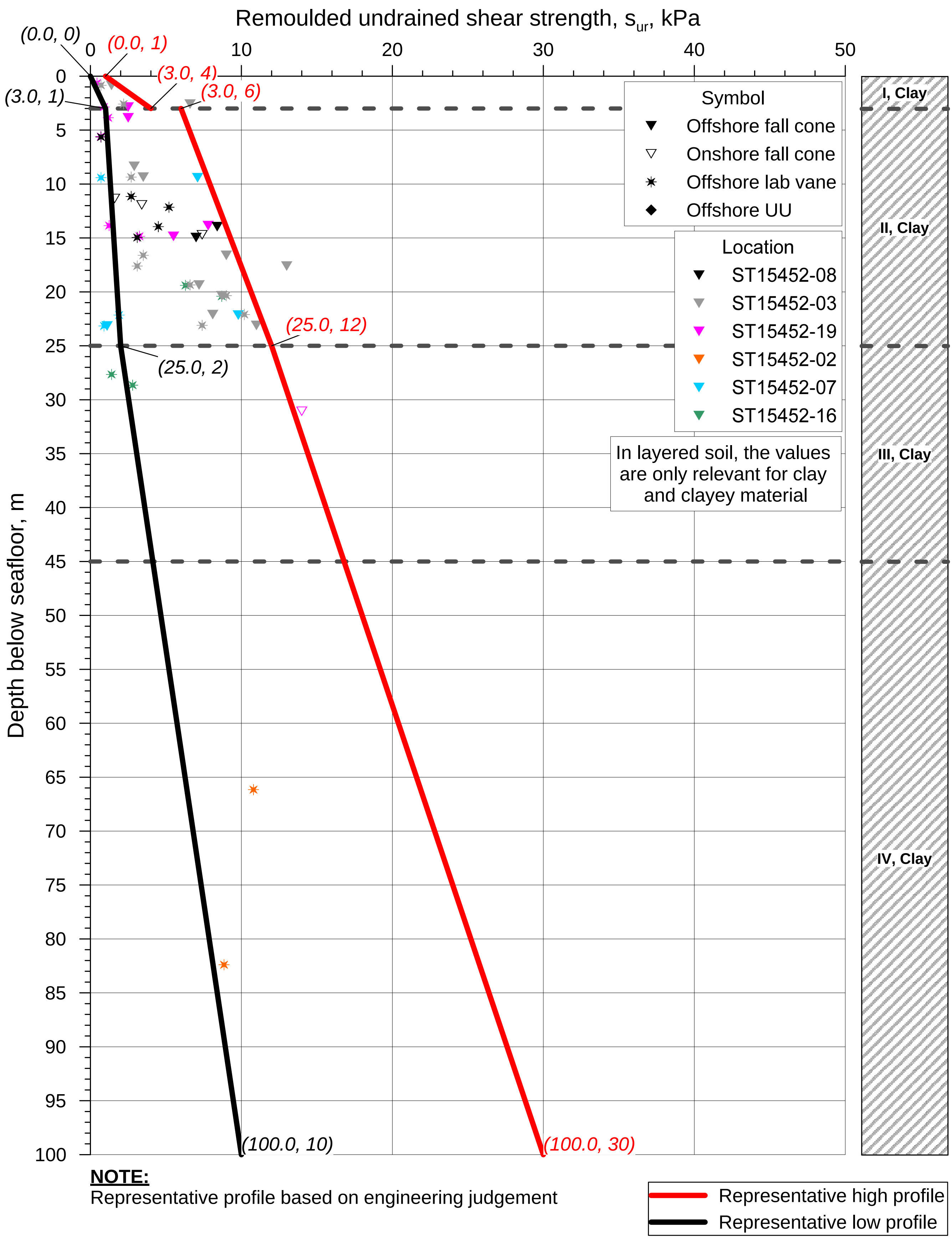

NOTE:
Representative profile based on engineering judgement

Label: *(depth, value)*

P:\2014\08\20140857\Leveransedokumenter\Rapport\20140857-02-R Data interpretation and evaluation\Figures\Section H\Figure H_03_10, su_rem versus depth-West.grf

Date/Rev.: 2015-01-21/01

ST15452 Flemish Pass Geotechnical Investigation	Document No. 20140857-02-R
Remoulded undrained shear strength versus depth West Slope	Figure No. H3.10
	Date 2016-04-04 / Drawn by VBS
	NGI

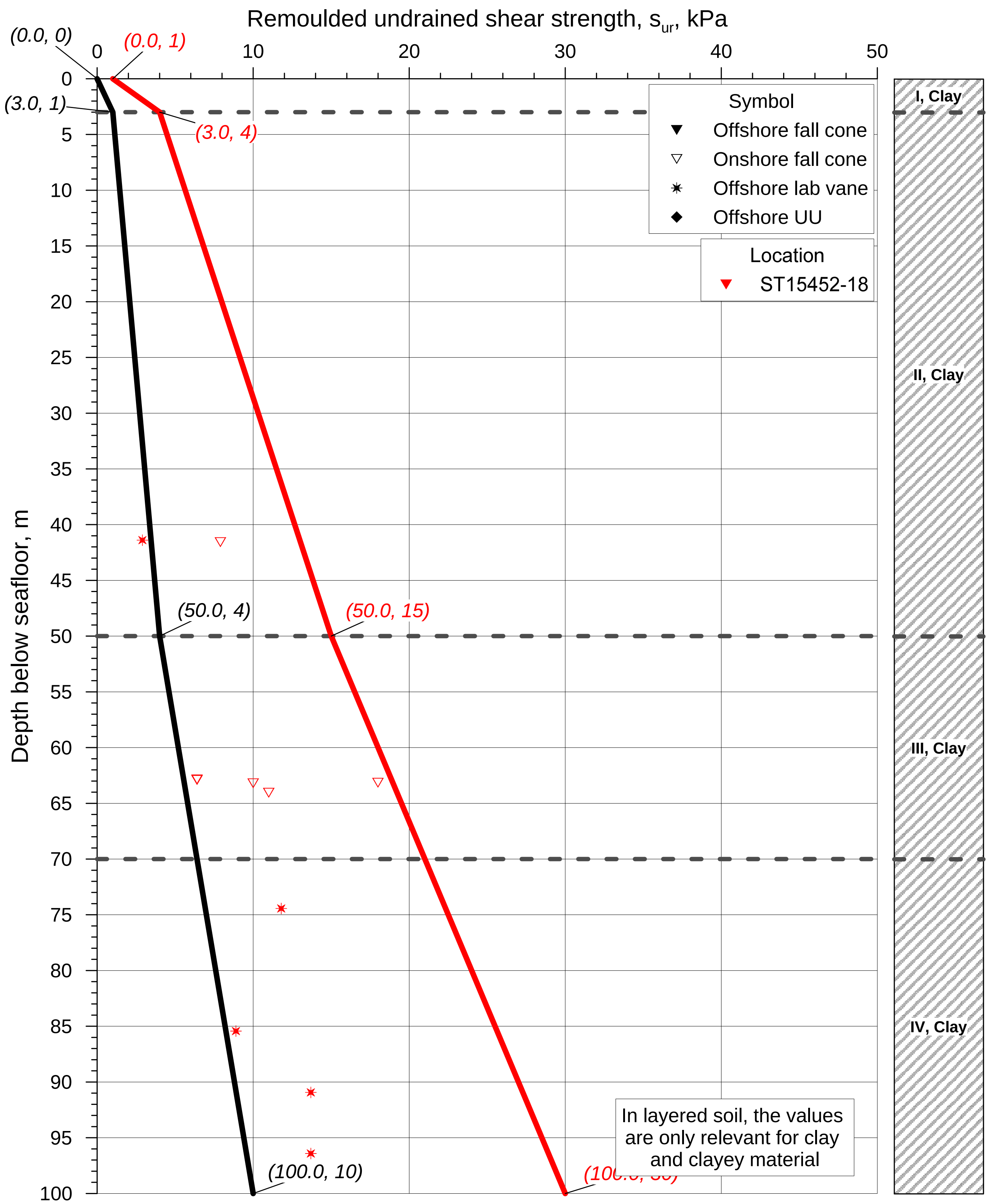

NOTE:
Representative profile based on engineering judgement

Representative high profile
Representative low profile

Label: *(depth, value)*

Date/Rev.: 2015-01-21/01

P:\2014\08\20140857\Leveransedokumenter\Rapport\20140857-02-R Data interpretation and evaluation\Figures\Section H\Figure H_03_11, su_rem versus depth-East.grf

ST15452 Flemish Pass Geotechnical Investigation	Document No. 20140857-02-R
Remoulded undrained shear strength versus depth East Slope	Figure No. H3.11
	Date 2016-04-04 / Drawn by VBS
	NGI

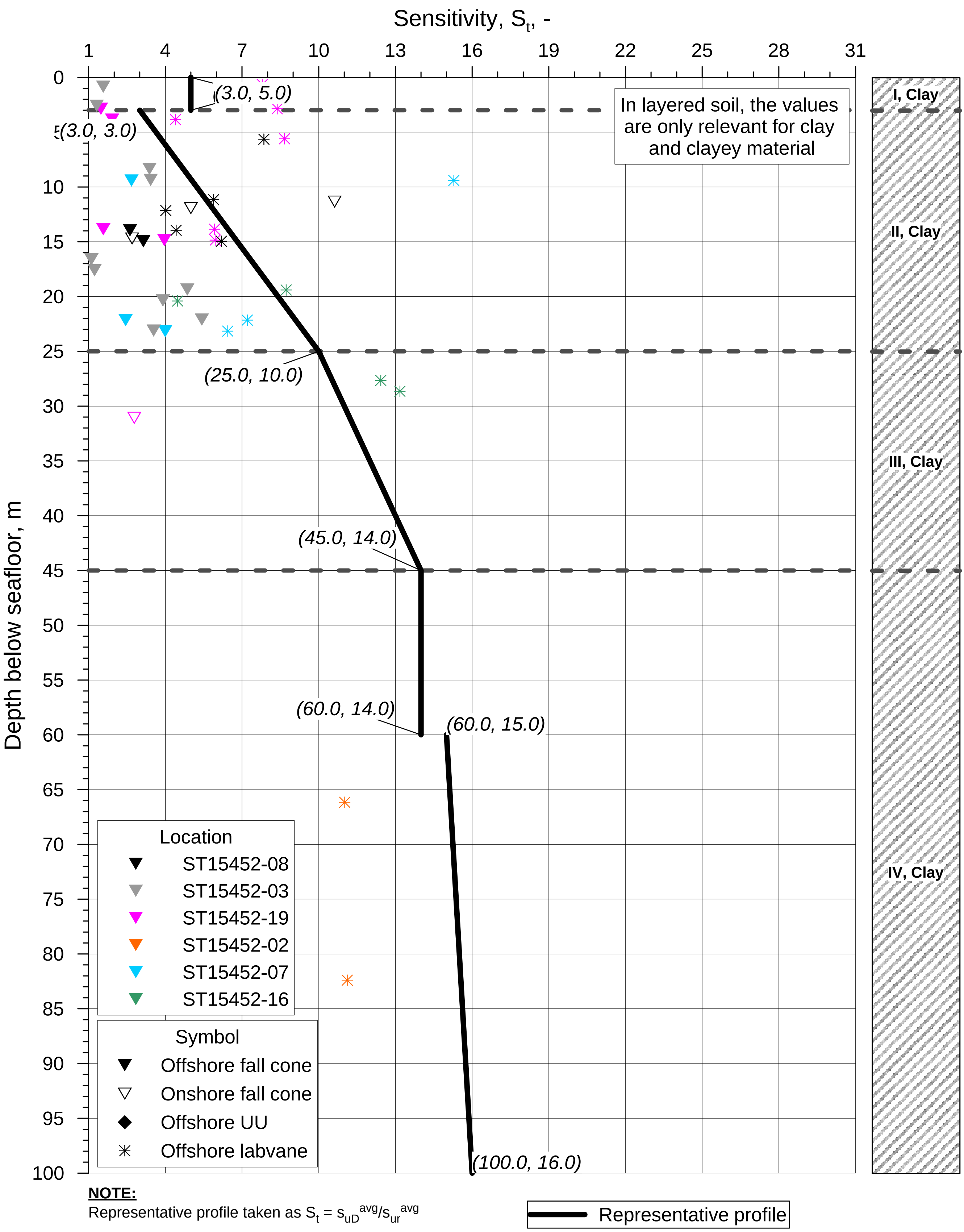

NOTE:
Representative profile taken as $S_t = s_{uD}^{avg}/s_{ur}^{avg}$

Label: *(depth, value)*

P:\2014\08\20140857\Leveransedokumenter\Rapport\20140857-02-R Data interpretation and evaluation\Figures\Section H\Figure H_03_12, sensitivity versus depth-West.grf

Date/Rev.: 2015-01-21/01

ST15452 Flemish Pass Geotechnical Investigation	Document No. 20140857-02-R
Sensitivity versus depth West Slope	Figure No. H3.12
	Date 2016-04-04 / Drawn by VBS

NGI

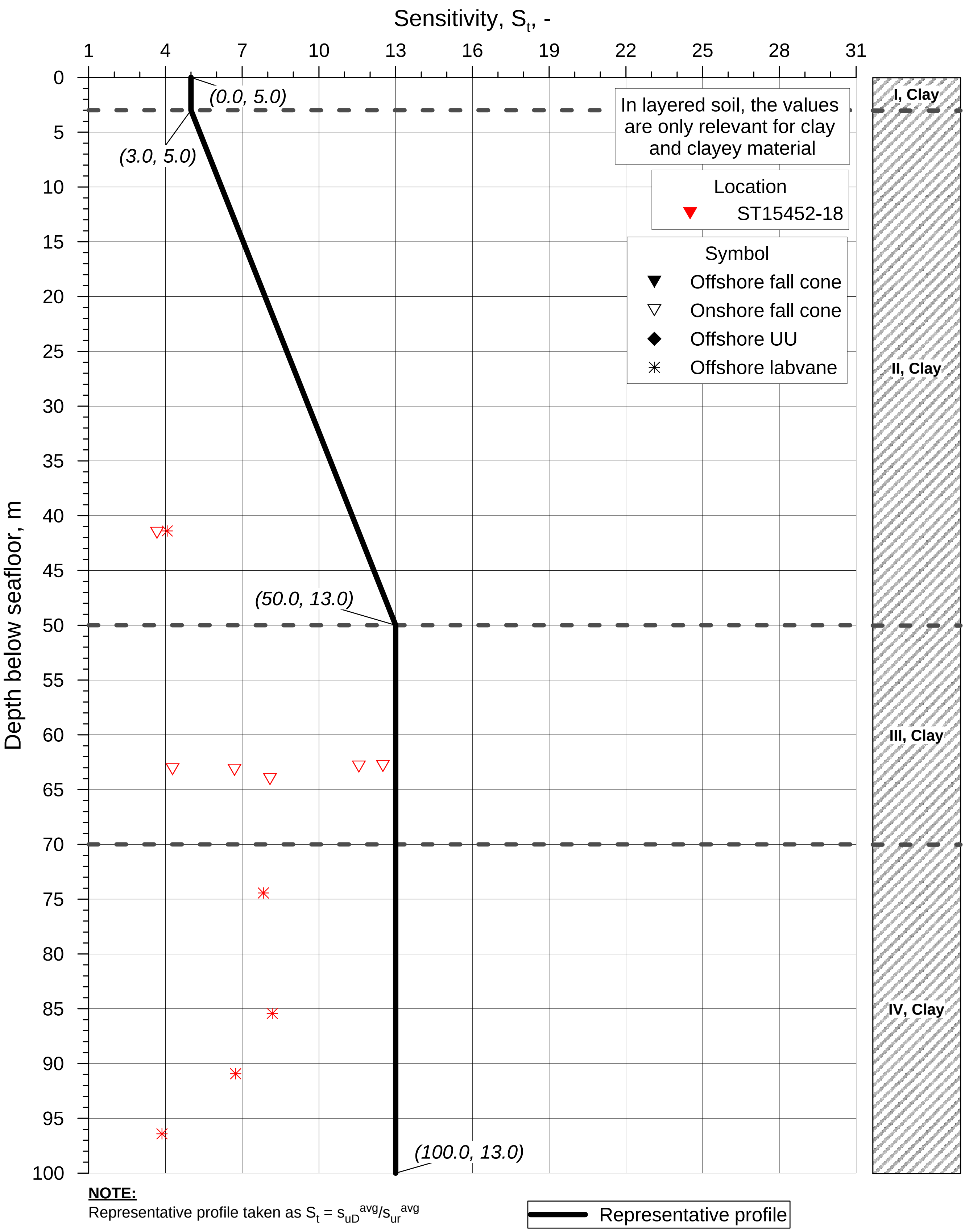

NOTE:
Representative profile taken as $S_t = s_{uD}^{avg}/s_{ur}^{avg}$

Label: *(depth, value)*

Date/Rev.: 2015-01-21/01

ST15452 Flemish Pass Geotechnical Investigation	Document No. 20140857-02-R
Sensitivity versus depth East Slope	Figure No. H3.13
	Date 2016-04-04 / Drawn by VBS

NGI

P:\2014\08\20140857\Leveransedokumenter\Rapport\20140857-02-R Data interpretation and evaluation\Figures\Section H\Figure H_03_13, sensitivity versus depth-East.grf

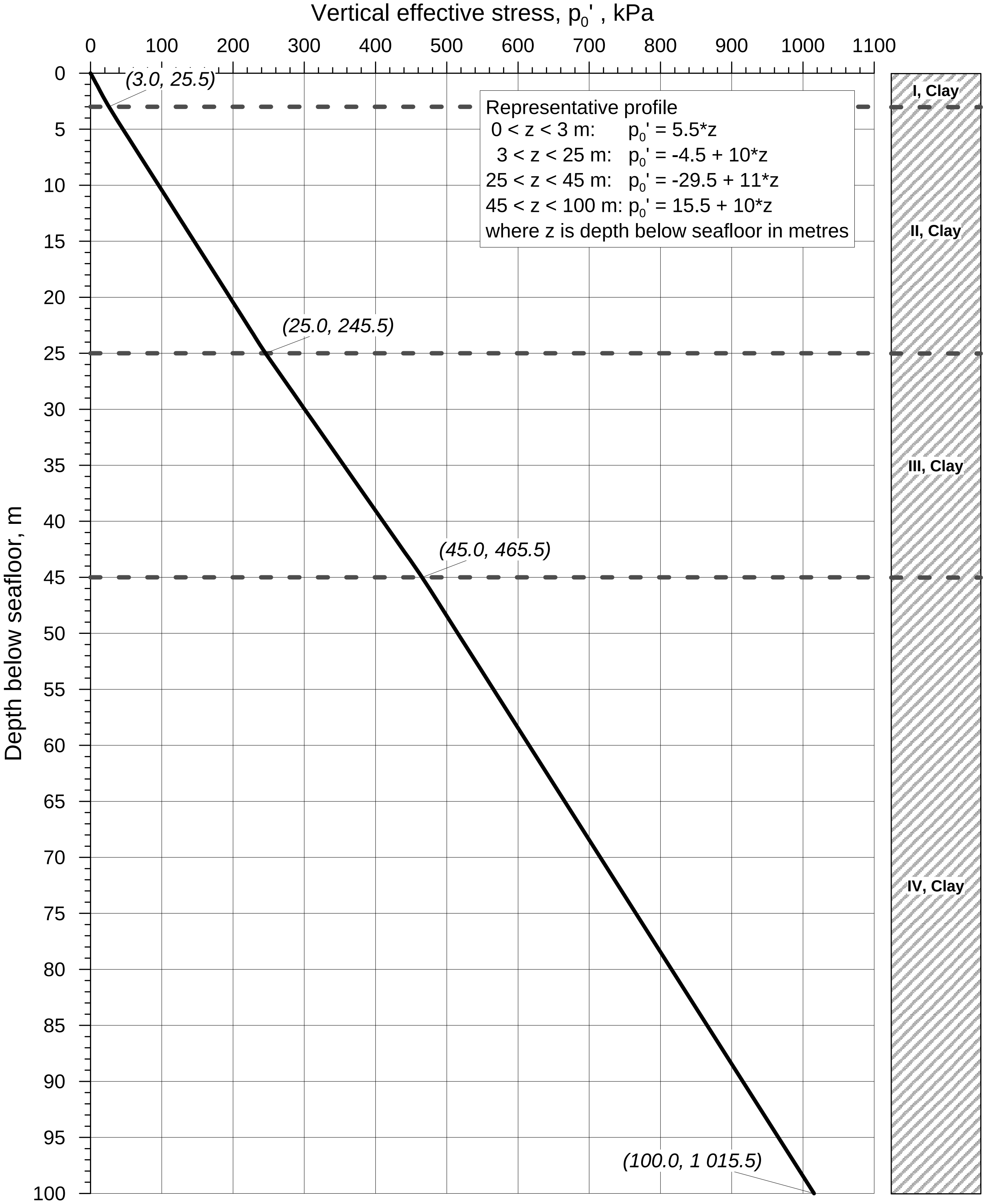

NOTE:
Representative profile based on representative total unit weight profile

Label: *(depth, value)*

Date/Rev.: 2015-01-21/01

P:\2014\08\20140857\Leveransedokumenter\Rapport\20140857-02-R Data interpretation and evaluation\Figures\Section H\Figure H_04_01, p0 versus depth-West.grf

ST15452 Flemish Pass Geotechnical Investigation

Vertical effective stress versus depth
West Slope

Document No. 20140857-02-R	
Figure No. H4.1	
Date 2016-04-03	Drawn by VBS

NGI

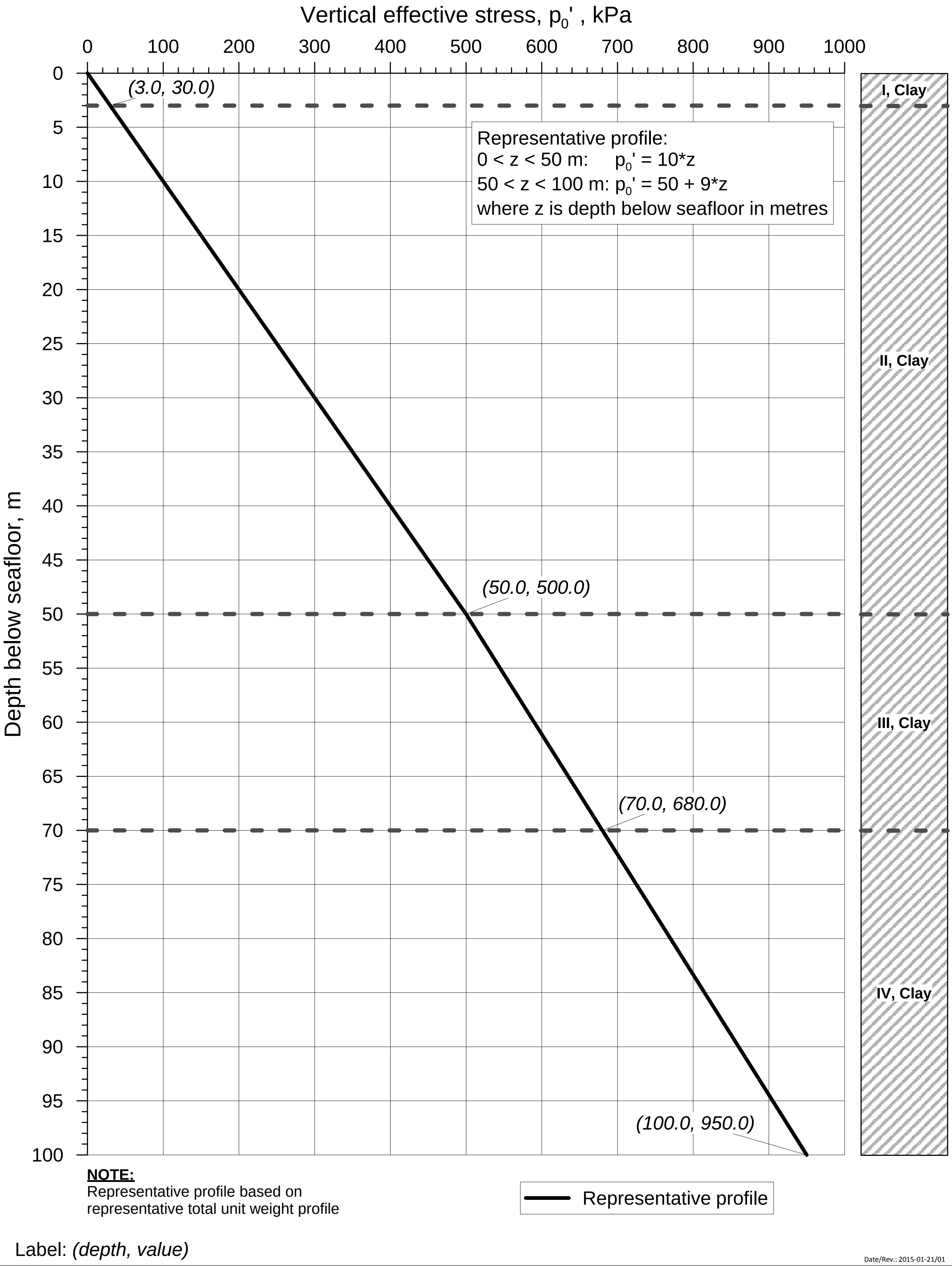

Date/Rev.: 2015-01-21/01

ST15452 Flemish Pass Geotechnical Investigation

Vertical effective stress versus depth
East Slope

Document No. 20140857-02-R	
Figure No. H4.2	
Date 2016-04-03	Drawn by VBS

P:\2014\08\20140857\Leveransedokumenter\Rapport\20140857-02-R Data interpretation and evaluation\Figures\Section H\Figure H_04_02, p0 versus depth-East.grf

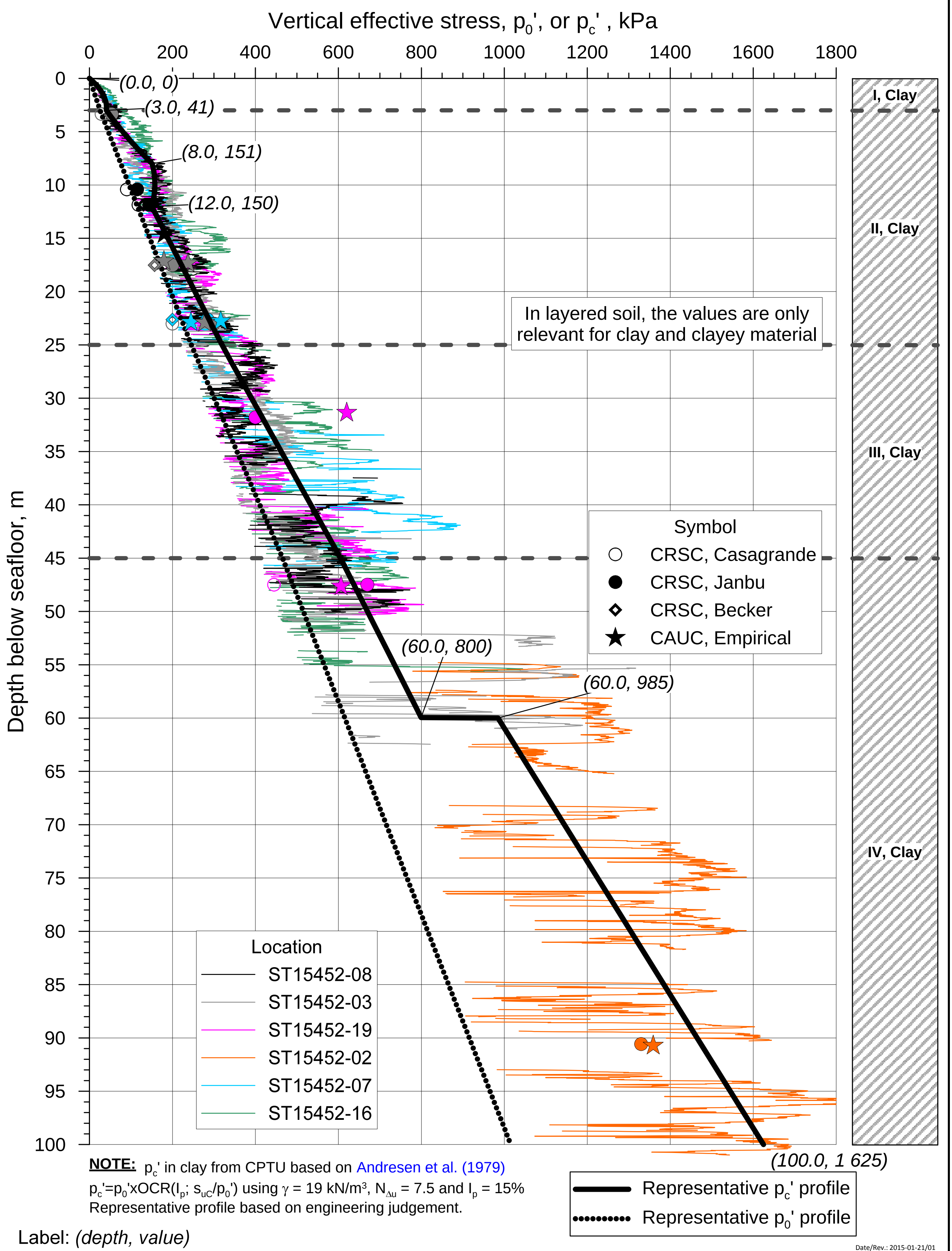

P:\2014\08\20140857\Leveranser\dokumenter\Rapport\20140857-02-R Data interpretation and evaluation\Figures\Section H\Figure H_04_03, pc versus depth-West.grf

ST15452 Flemish Pass Geotechnical Investigation

Preconsolidation stress versus depth
West Slope

Document No. 20140857-02-R	
Figure No. H4.3	
Date 2016-04-03	Drawn by SK

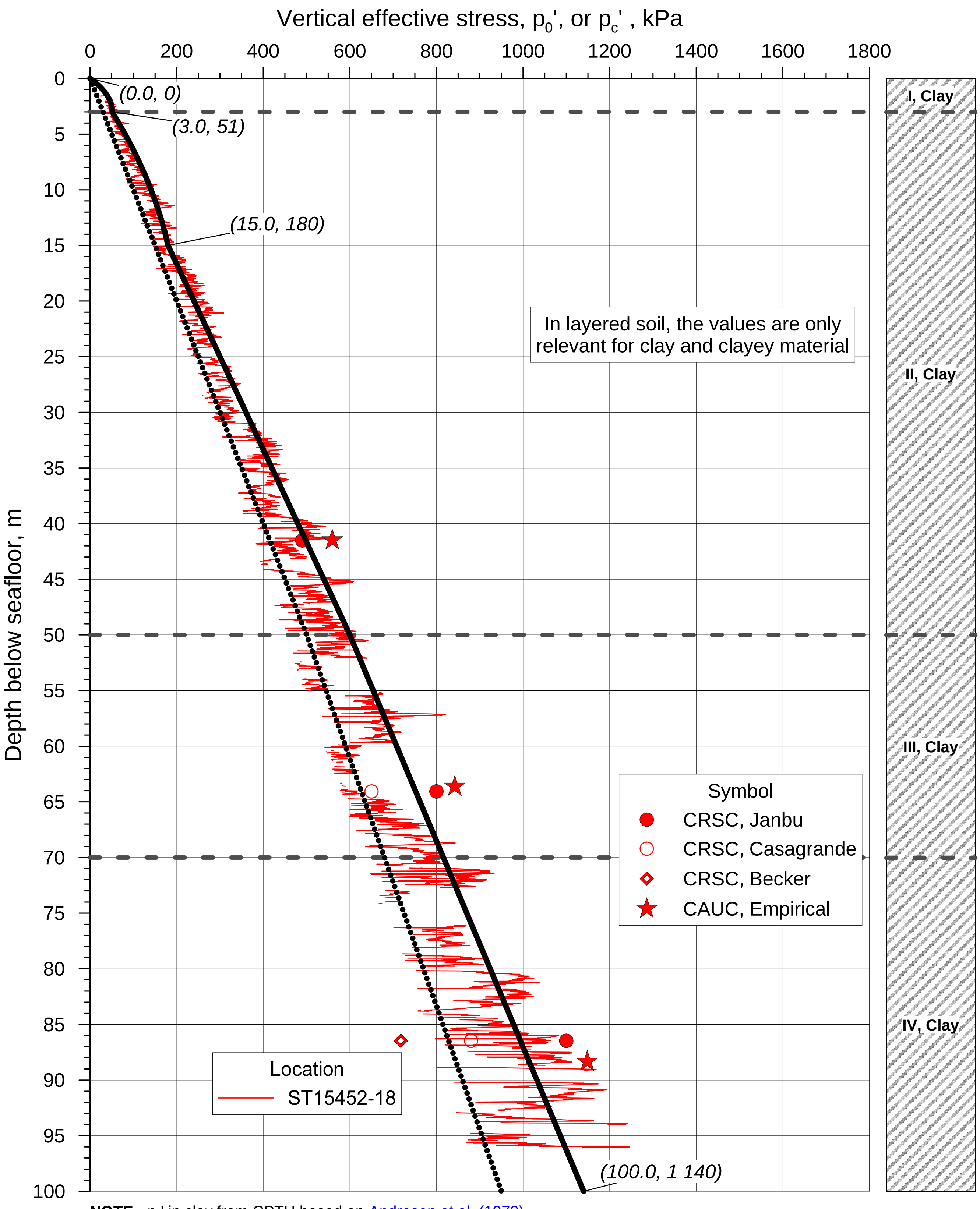

NOTE: p_c' in clay from CPTU based on Andresen et al. (1979)
p_c'=p_0'xOCR(I_p; s_{uC}/p_0') using γ = 19 kN/m³, $N_{\Delta u}$ = 7.5 and I_p = 15%
Representative profile based on engineering judgement.

Representative p_c' profile
Representative p_0' profile

Label: *(depth, value)*

Date/Rev.: 2015-01-21/01

P:\2014\08\20140857\Leveransedokumenter\Rapport\20140857-02-R Data interpretation and evaluation\Figures\Section H\Figure H_04_04, pc versus depth-East.grf

ST15452 Flemish Pass Geotechnical Investigation	Document No. 20140857-02-R	
Preconsolidation stress versus depth East Slope	Figure No. H4.4	
	Date 2016-04-03	Drawn by SK
	NGI	

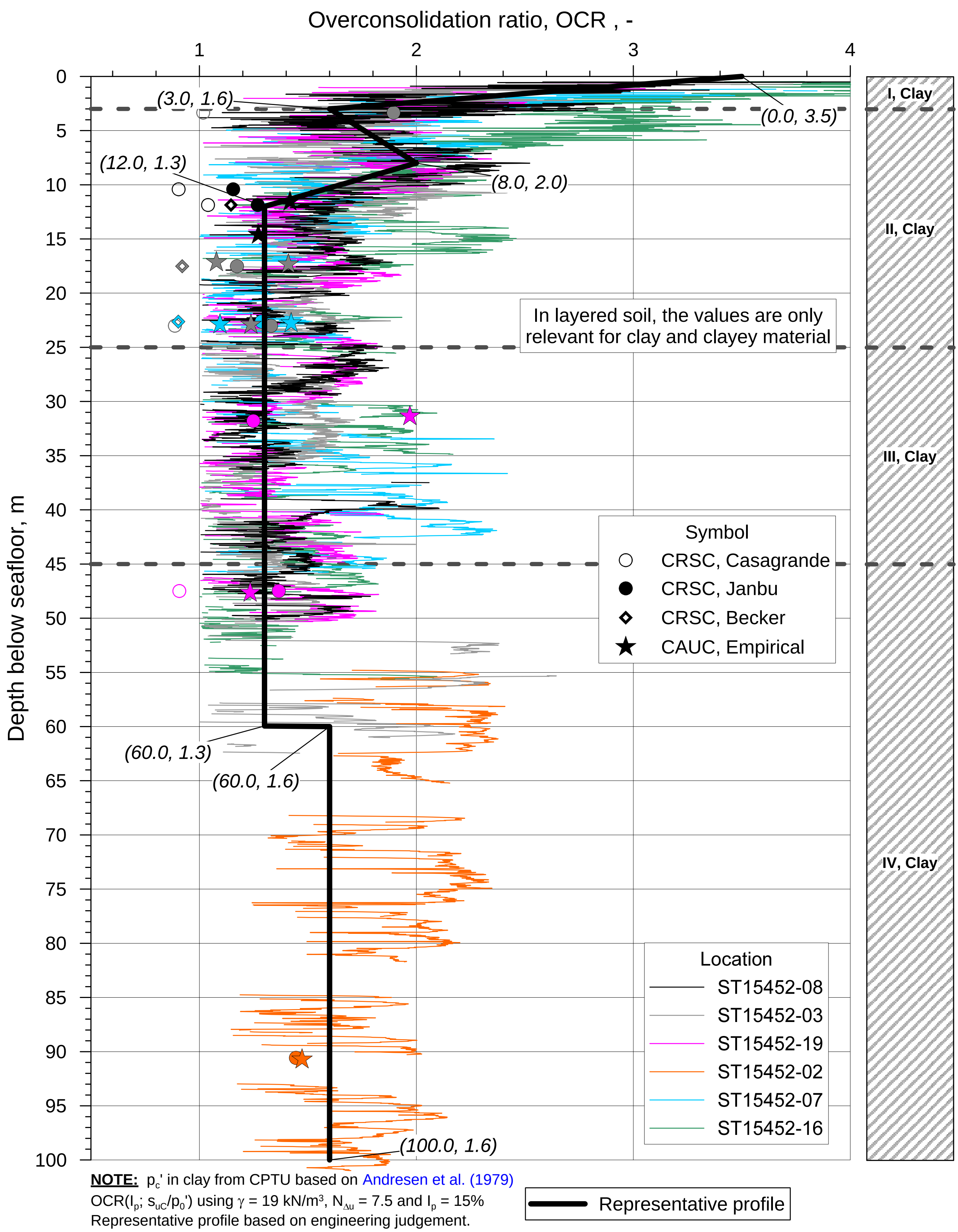

NOTE: p_c' in clay from CPTU based on Andresen et al. (1979)
OCR(I_p; s_{uC}/p_0') using γ = 19 kN/m³, $N_{\Delta u}$ = 7.5 and I_p = 15%
Representative profile based on engineering judgement.

Label: *(depth, value)*

Date/Rev.: 2015-01-21/01

P:\2014\08\20140857\Leveransedokumenter\Rapport\20140857-02-R Data interpretation and evaluation\Figures\Section H\Figure H_04_05, OCR versus depth-West.grf

ST15452 Flemish Pass Geotechnical Investigation	Document No. 20140857-02-R
Overconsolidation ratio versus depth West Slope	Figure No. H4.5
	Date 2016-04-03 / Drawn by KS/SK

NGI

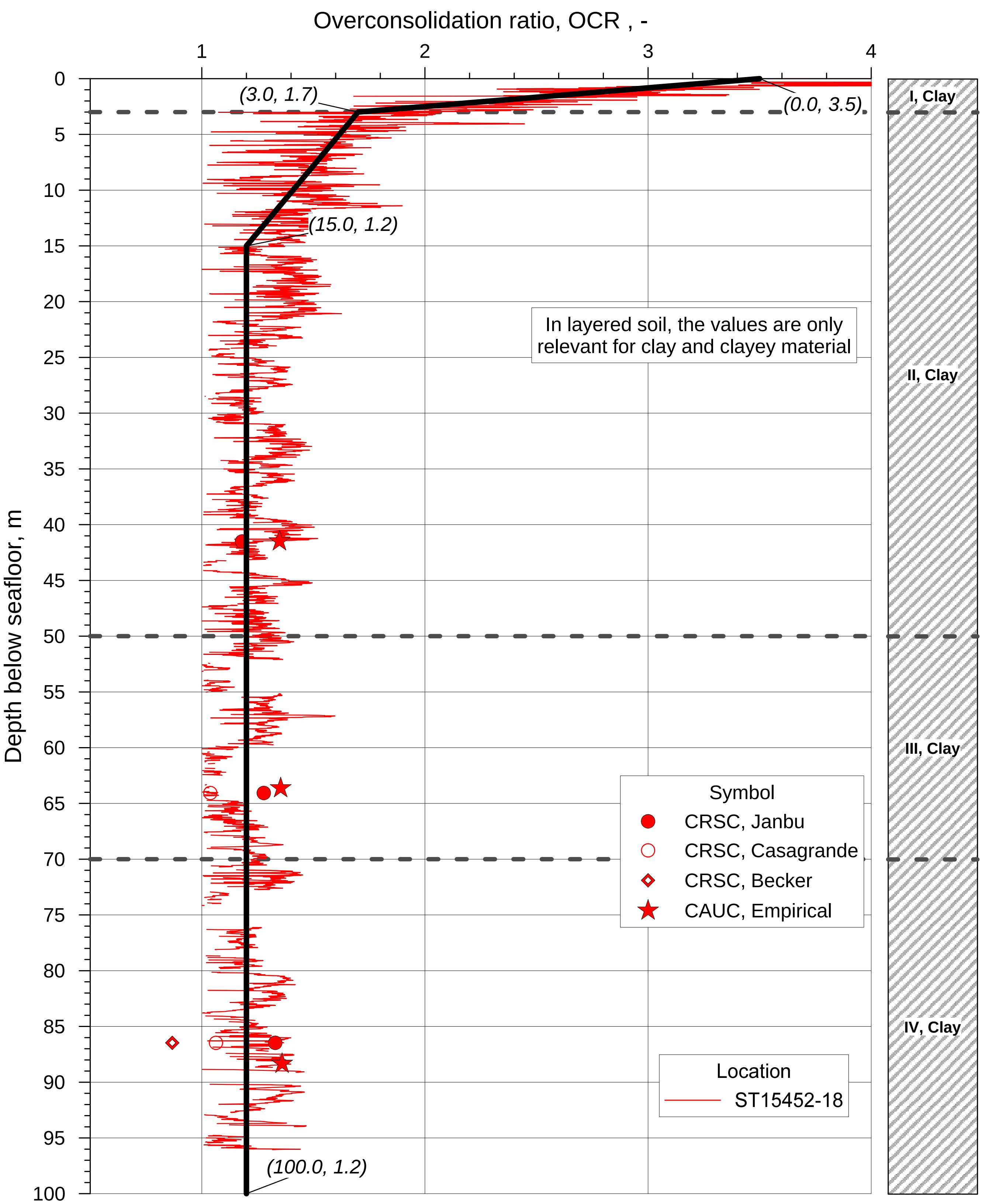

NOTE: p_c' in clay from CPTU based on Andresen et al. (1979)
OCR(I_p; s_{uC}/p_0') using γ = 19 kN/m³, $N_{\Delta u}$ = 7.5 and I_p = 15%
Representative profile based on engineering judgement.

Label: *(depth, value)*

Date/Rev.: 2015-01-21/01

ST15452 Flemish Pass Geotechnical Investigation

Overconsolidation ratio versus depth
East Slope

Document No.	20140857-02-R
Figure No.	H4.6
Date	2016-04-03
Drawn by	KS/SK

P:\2014\08\20140857\Leveransedokumenter\Rapport\20140857-02-R Data interpretation and evaluation\Figures\Section H\Figure H_04_06, OCR versus depth-East.grf

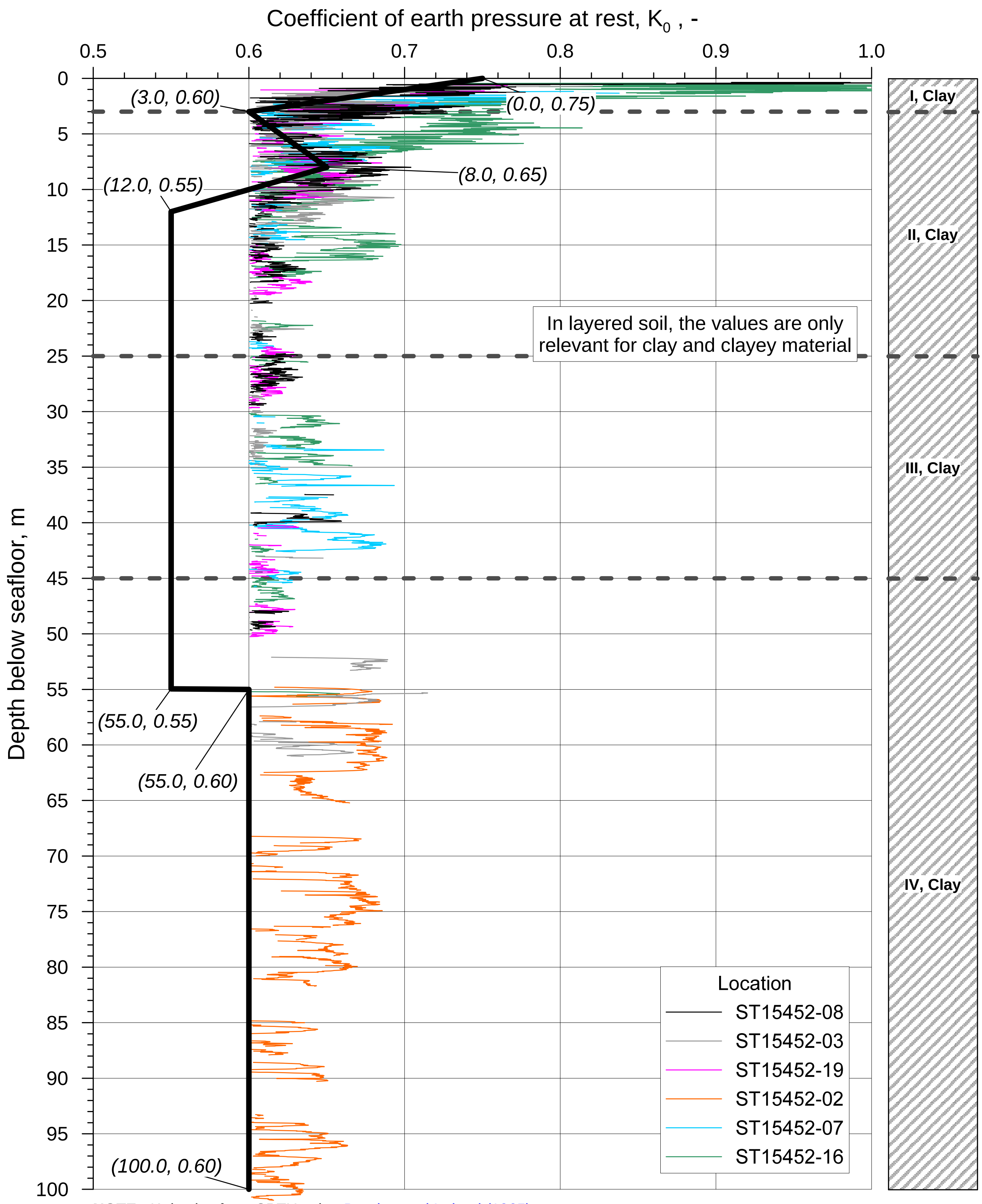

NOTE: K_0 in clay from CPTU using Brooker and Ireland (1965).
$K_0(I_p;\ s_{uC}/p_0')$ using γ = 19 kN/m³, $N_{\Delta u}$ = 7.5 and I_p = 15%.
Representative profile based on engineering judgement.

Representative profile

Label: *(depth, value)*

Date/Rev.: 2015-01-21/01

ST15452 Flemish Pass Geotechnical Investigation	Document No. 20140857-02-R
Coefficient of earth pressure at rest versus depth West Slope	Figure No. H4.7
	Date 2016-04-03 / Drawn by SK

NGI

P:\2014\08\20140857\Leveransedokumenter\Rapport\20140857-02-R Data interpretation and evaluation\Figures\Section H\Figure H_04_07, K0 versus depth-West.grf

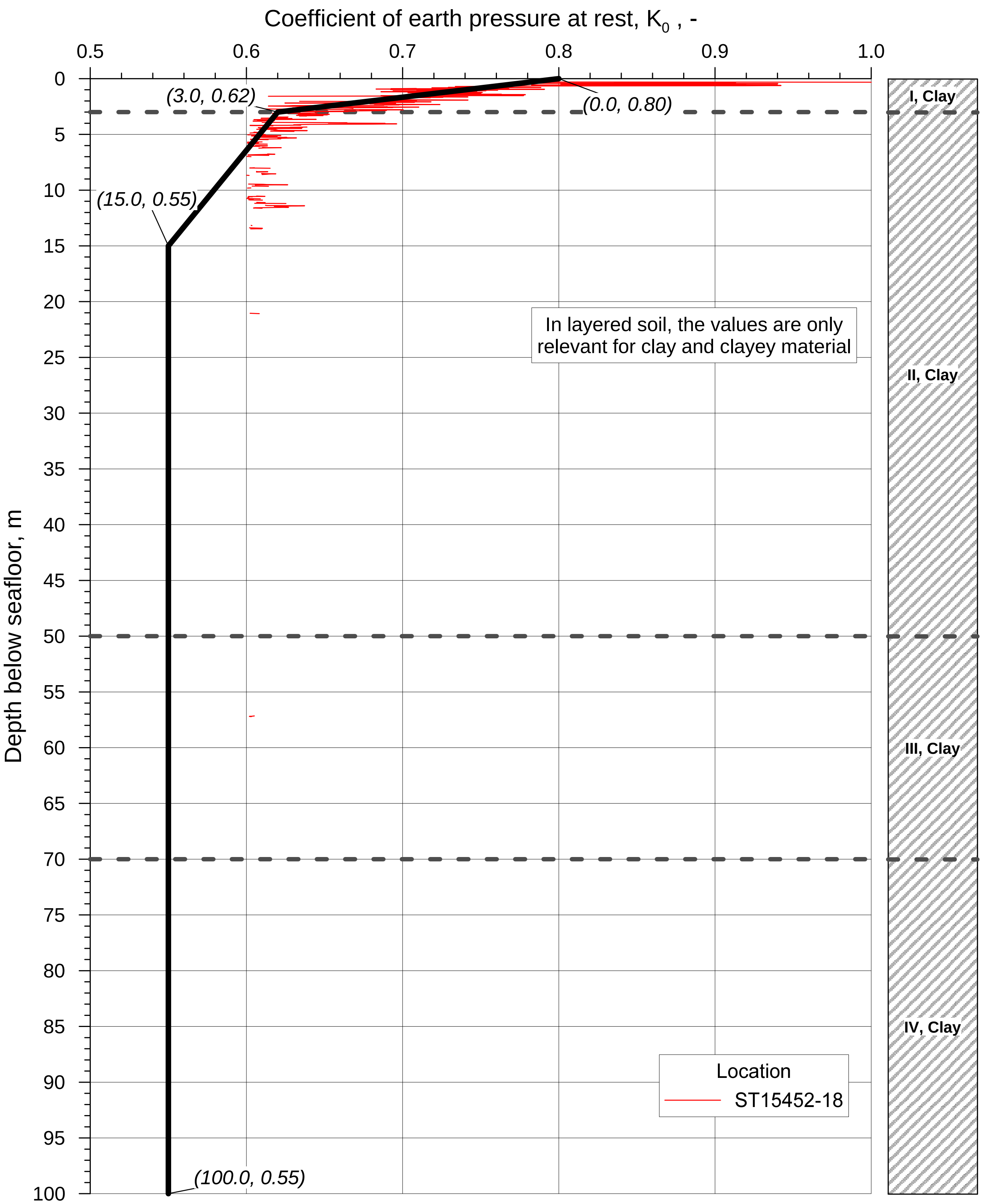

NOTE: K_0 in clay from CPTU using Brooker and Ireland (1965).
$K_0(I_p; s_{uC}/p_0')$ using γ = 19 kN/m³, $N_{\Delta u}$ = 7.5 and I_p = 15%.
Representative profile based on engineering judgement.

Representative profile

Label: *(depth, value)*

Date/Rev.: 2015-01-21/01

ST15452 Flemish Pass Geotechnical Investigation	Document No. 20140857-02-R	
Coefficient of earth pressure at rest versus depth East Slope	Figure No. H4.8	
	Date 2016-04-03	Drawn by KS/SK
	NGI	

P:\2014\08\20140857\Leveransedokumenter\Rapport\20140857-02-R Data interpretation and evaluation\Figures\Section H\Figure H_04_08, K0 versus depth-East.grf

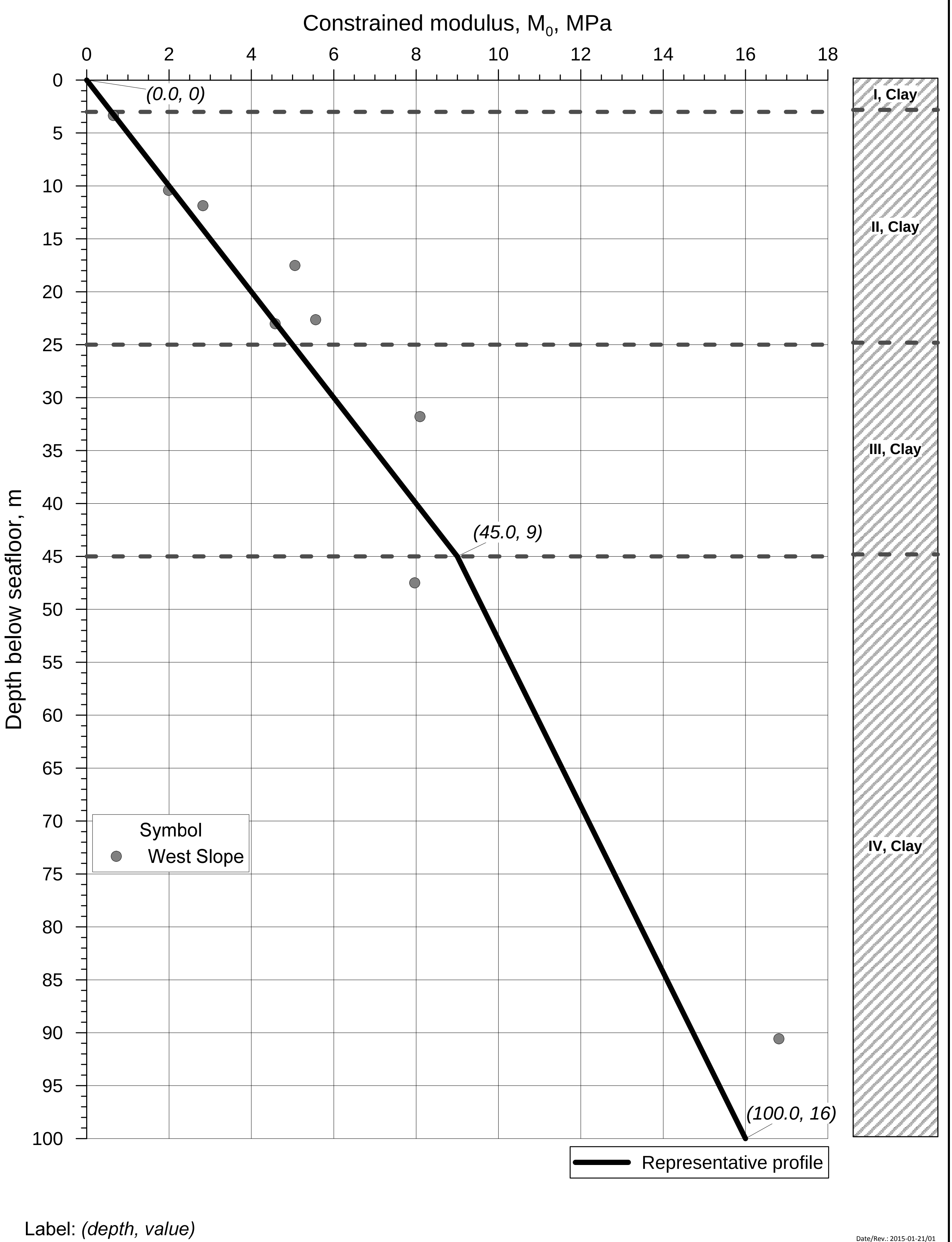

P:\2014\08\20140857\Leveransedokumenter\Rapport\20140857-02-R Data interpretation and evaluation\Figures\Section H\Figure H_05_01, Constrained modulus versus depth_West.grf

Date/Rev.: 2015-01-21/01

ST15452 Flemish Pass Geotechnical Investigation	Document No. 20140857-02-R
Constrained modulus at in-situ vertical effective stress versus depth West Slope	Figure No. H5.1
	Date 2016-04-03 — Drawn by VDa

NGI

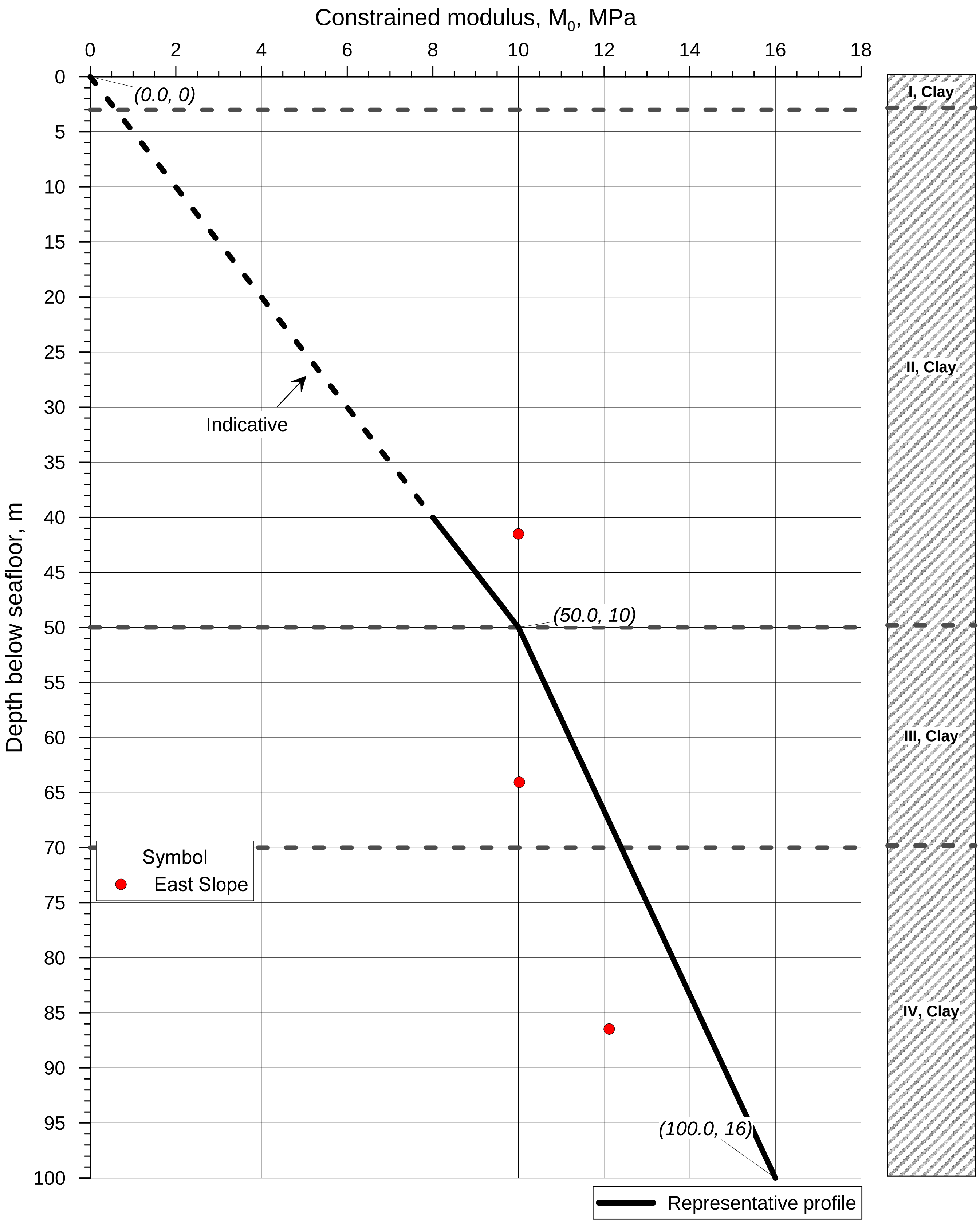

Label: *(depth, value)*

Date/Rev.: 2015-01-21/01

ST15452 Flemish Pass Geotechnical Investigation

Constrained modulus at in-situ vertical effective stress versus depth
East Slope

Document No. 20140857-02-R	
Figure No. H5.2	
Date 2016-04-03	Drawn by VDa

P:\2014\08\20140857\Leveransedokumenter\Rapport\20140857-02-R Data interpretation and evaluation\Figures\Section H\Figure H_05_02, Constrained modulus versus depth_East.grf

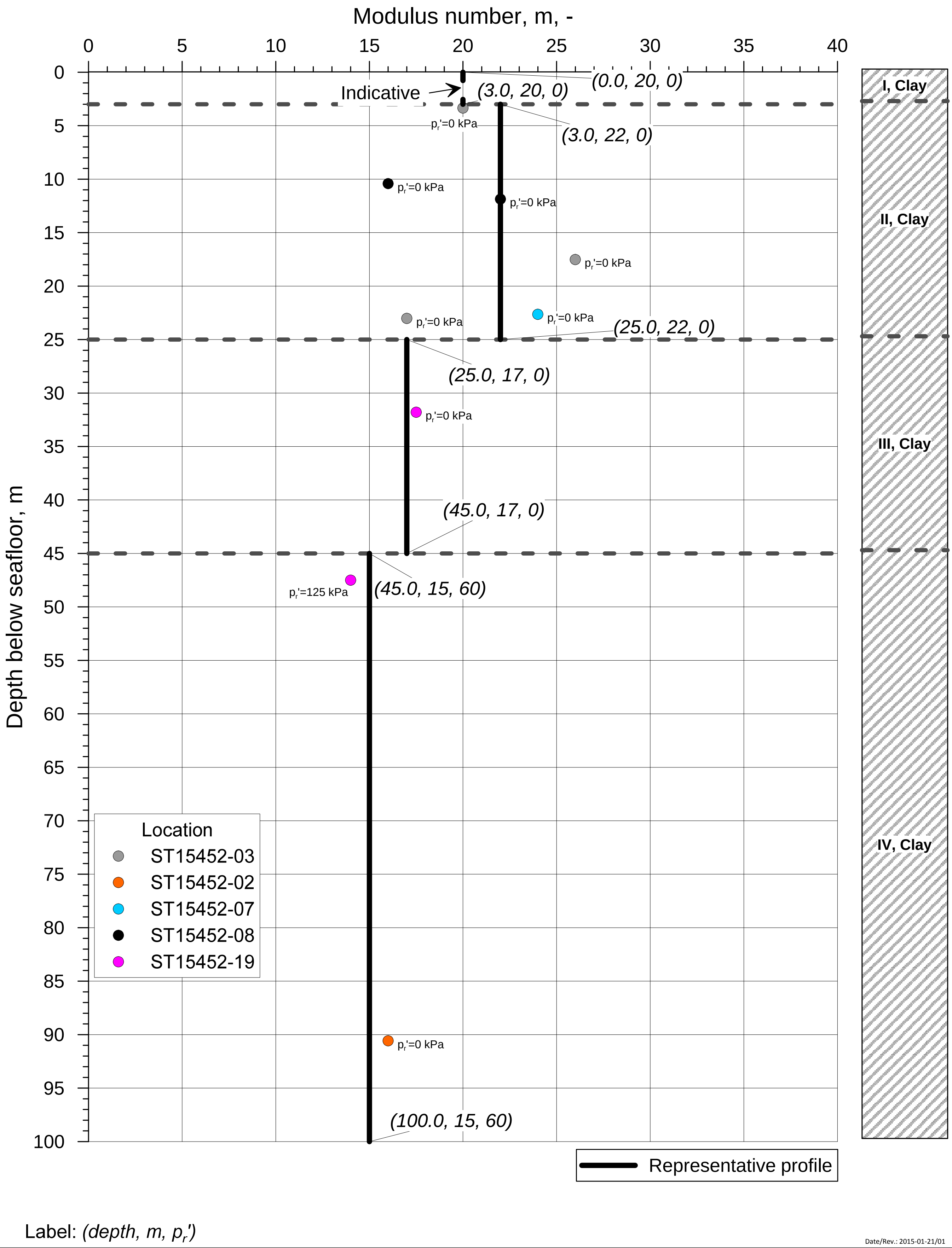

Date/Rev.: 2015-01-21/01

P:\2014\08\20140857\Leveransedokumenter\Rapport\20140857-02-R Data interpretation and evaluation\Figures\Section H\Figure H_05_03, modulus number versus depth_West.grf

ST15452 Flemish Pass Geotechnical Investigation

Modulus number and reference stress versus depth
West Slope

Document No. 20140857-02-R	
Figure No. H5.3	
Date 2016-04-03	Drawn by VDa

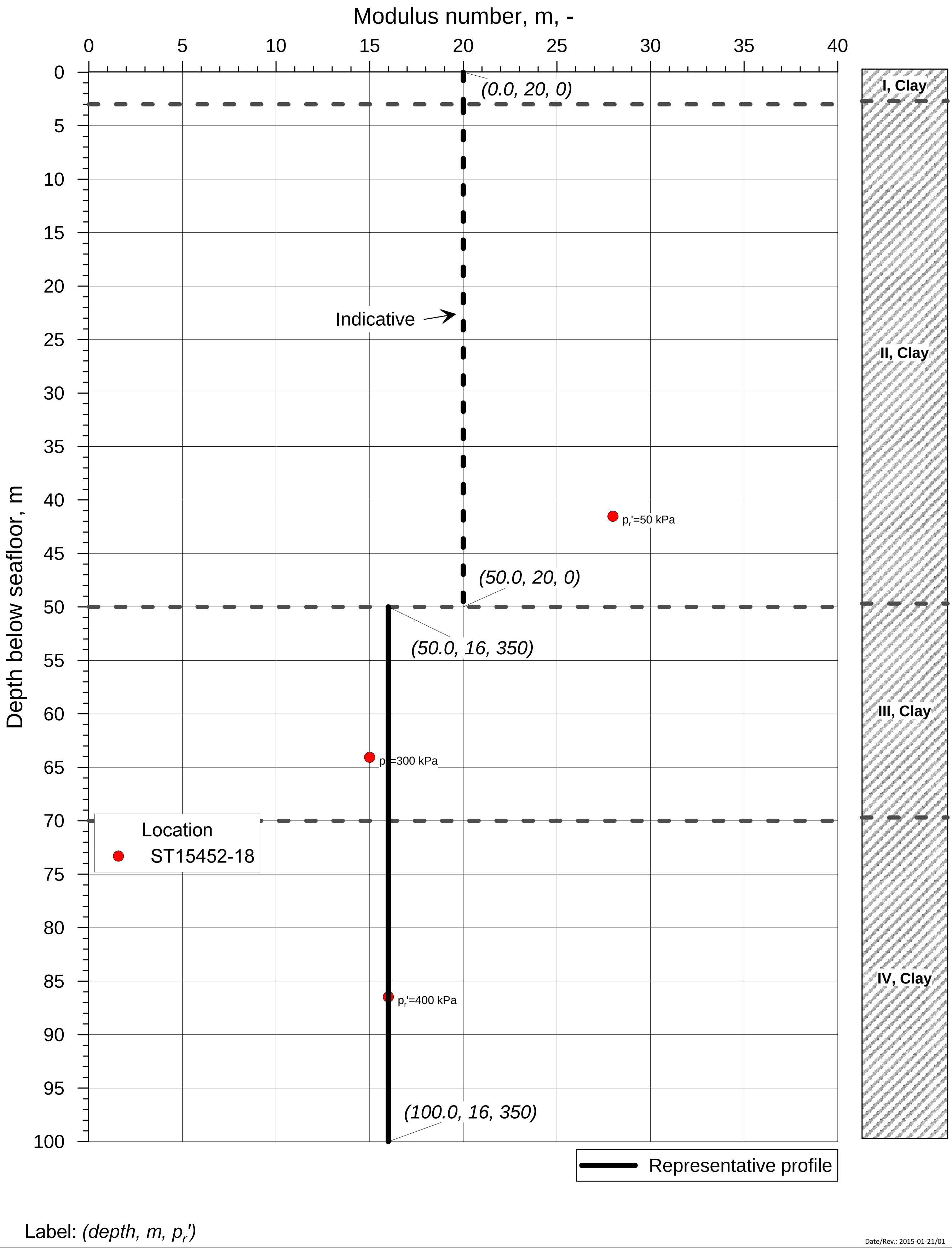

Date/Rev.: 2015-01-21/01

P:\2014\08\20140857\Leveransedokumenter\Rapport\20140857-02-R Data interpretation and evaluation\Figures\Section H\Figure H_05_04, modulus number versus depth_East.grf

ST15452 Flemish Pass Geotechnical Investigation

Modulus number and reference stress versus depth
East Slope

Document No.	
20140857-02-R	
Figure No.	
H5.4	
Date	Drawn by
2016-04-03	VDa

NGI

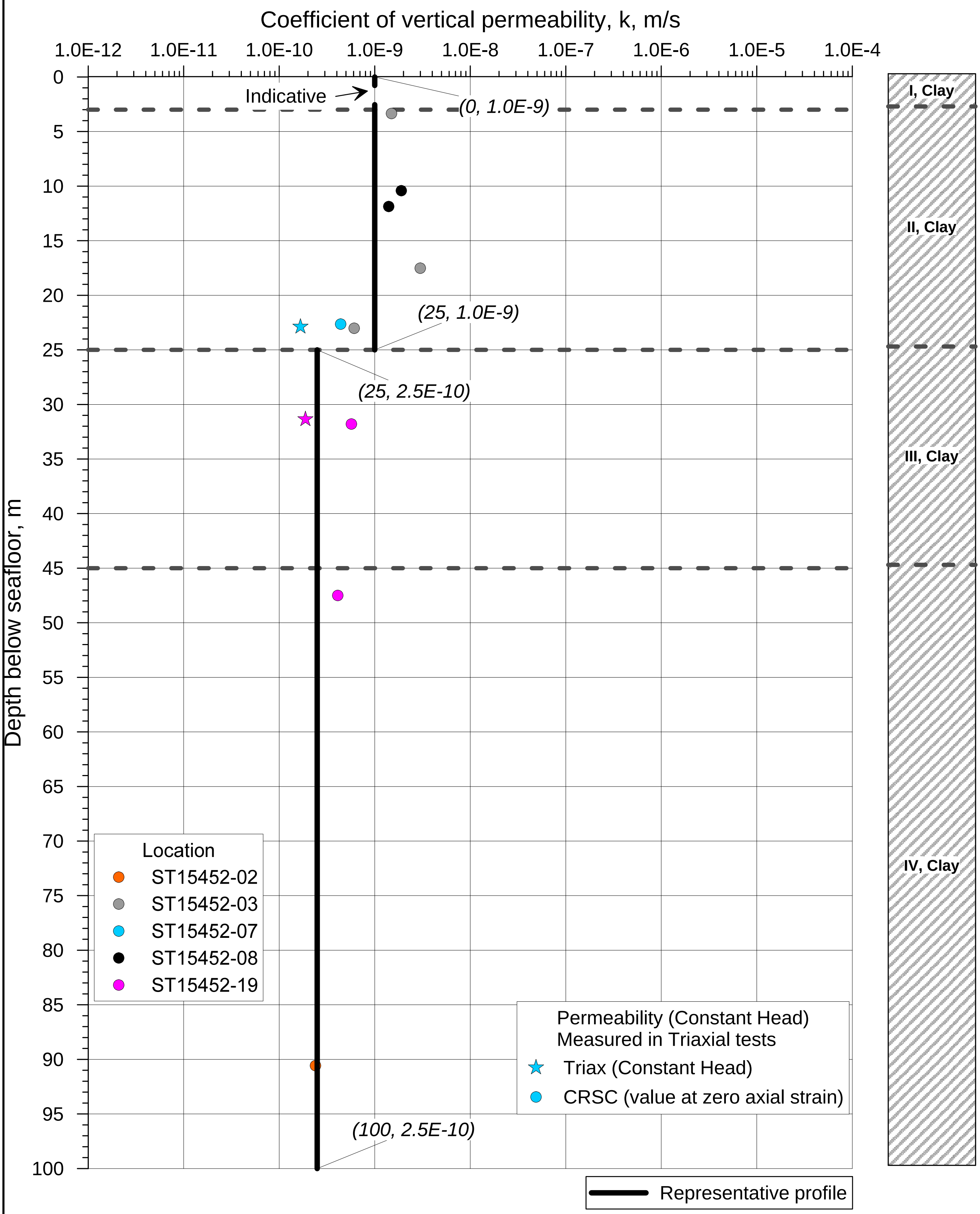

Label: *(depth, value)*

Date/Rev.: 2015-01-21/01

ST15452 Flemish Pass Geotechnical Investigation

Coefficient of vertical permeability versus depth
West Slope

Document No.
20140857-02-R

Figure No.
H5.5

Date
2016-04-03

Drawn by
VDa

NGI

P:\2014\08\20140857\Leveransedokumenter\Rapport\20140857-02-R Data interpretation and evaluation\Figures\Section H\Figure H_05_05, Coefficient of vertical permeability versus depth_West.grf

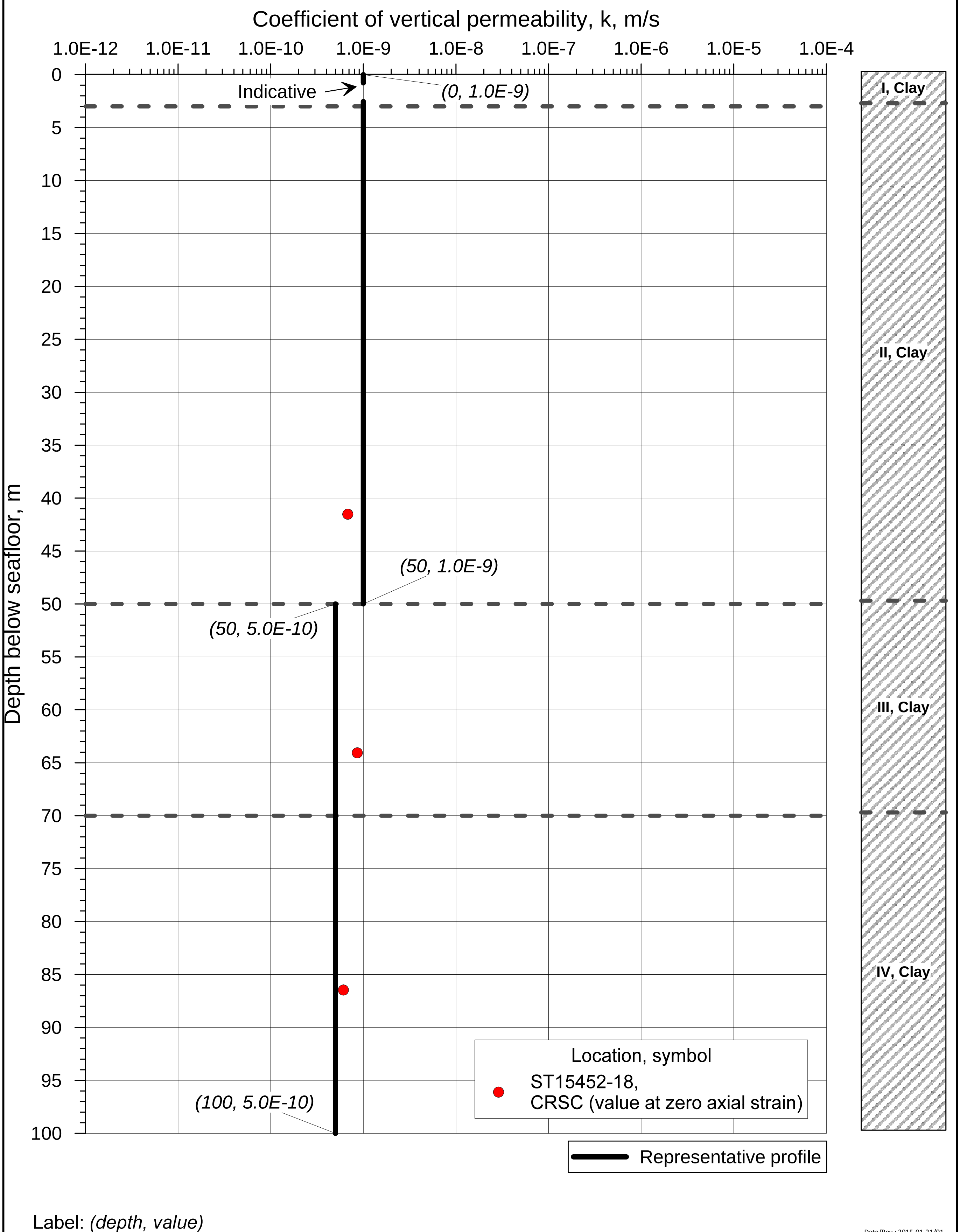

Date/Rev.: 2015-01-21/01

ST15452 Flemish Pass Geotechnical Investigation

Coefficient of vertical permeability versus depth
East Slope

Document No.	20140857-02-R
Figure No.	H5.6
Date	2016-04-03
Drawn by	VDa

NGI

P:\2014\08\20140857\Leveransedokumenter\Rapport\20140857-02-R Data interpretation and evaluation\Figures\Section H\Figure H_05_06, Coefficient of vertical permeability versus depth_East.grf

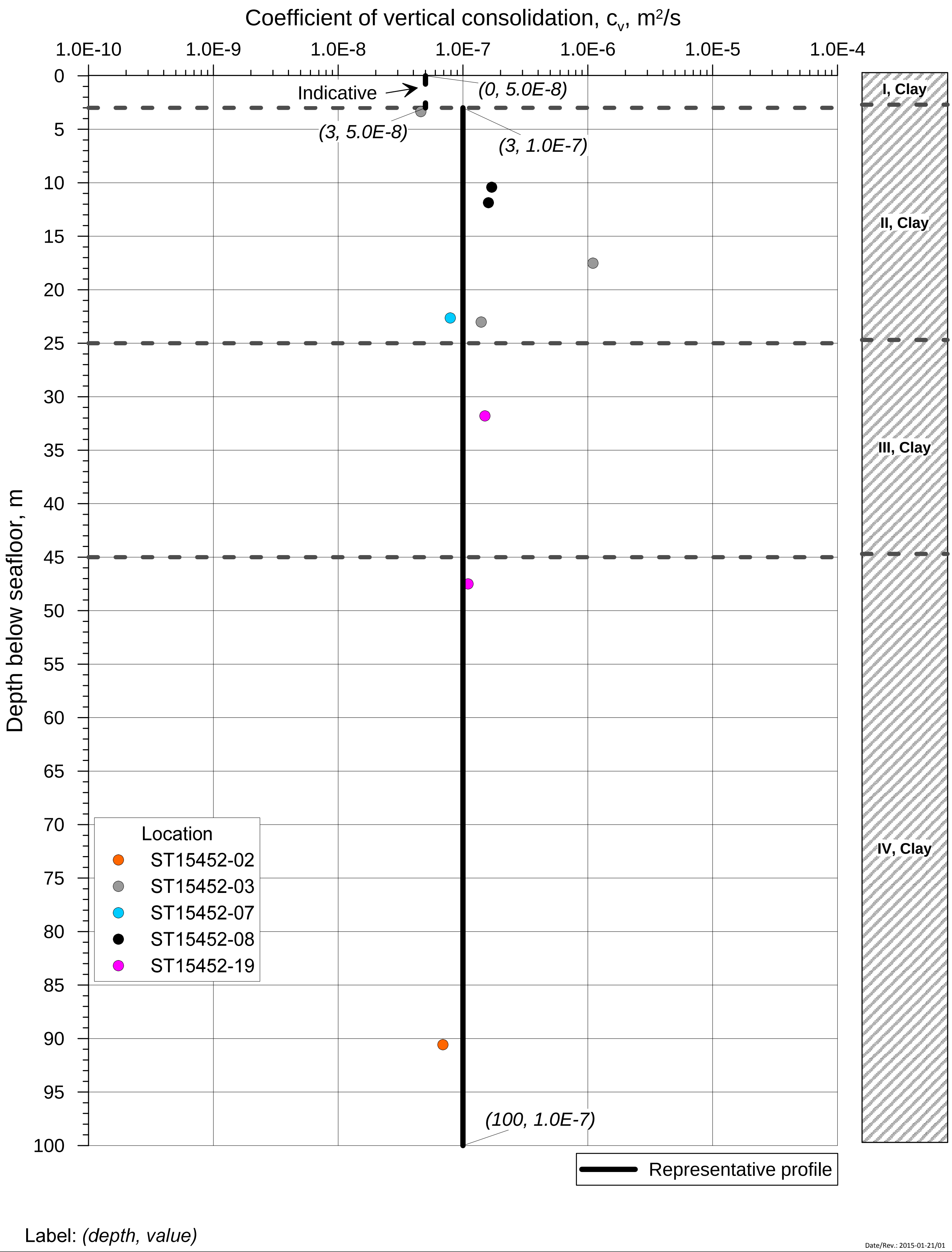

ST15452 Flemish Pass Geotechnical Investigation	Document No. 20140857-02-R
Coefficient of vertical consolidation versus depth West Slope	Figure No. H5.7
	Date 2016-04-03 / Drawn by VDa
	NGI

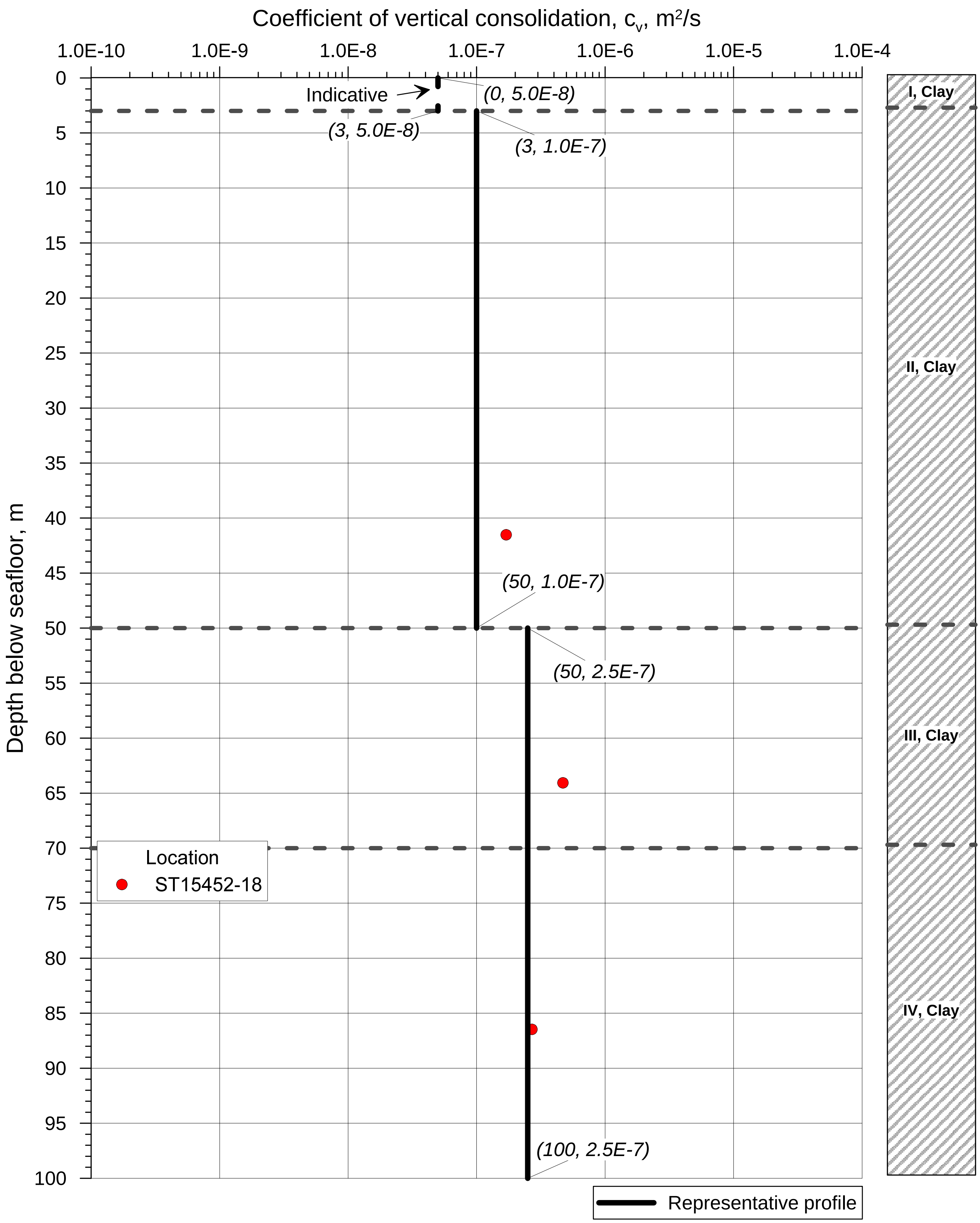

Label: *(depth, value)*

Date/Rev.: 2015-01-21/01

P:\2014\08\20140857\Leveransedokumenter\Rapport\20140857-02-R Data interpretation and evaluation\Figures\Section H\Figure H_05_08, Coefficient of vertical consolidation versus depth_East.grf

ST15452 Flemish Pass Geotechnical Investigation	Document No. 20140857-02-R
Coefficient of vertical consolidation versus depth East Slope	Figure No. H5.8
	Date 2016-04-03 / Drawn by VDa

NGI

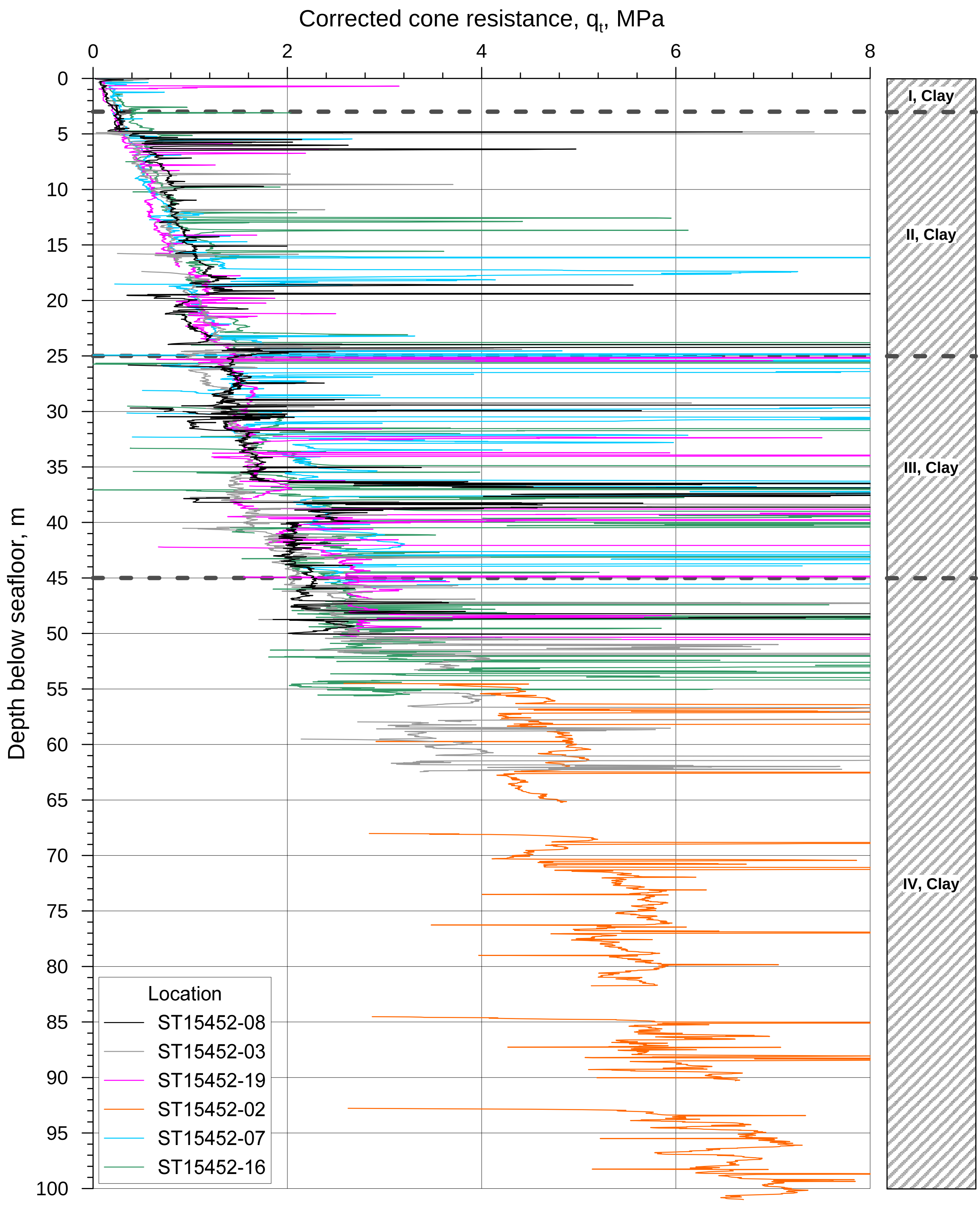

P:\2014\08\20140857\Leveransedokumenter\Rapport\20140857-02-R Data interpretation and evaluation\Figures\Section H\Figure H_06_01, qt versus depth-West.grf

Date/Rev.: 2015-01-21/01

ST15452 Flemish Pass Geotechnical Investigation	Document No. 20140857-02-R
Corrected cone resistance versus depth West Slope	Figure No. H6.1
	Date 2016-04-03 / Drawn by VBS

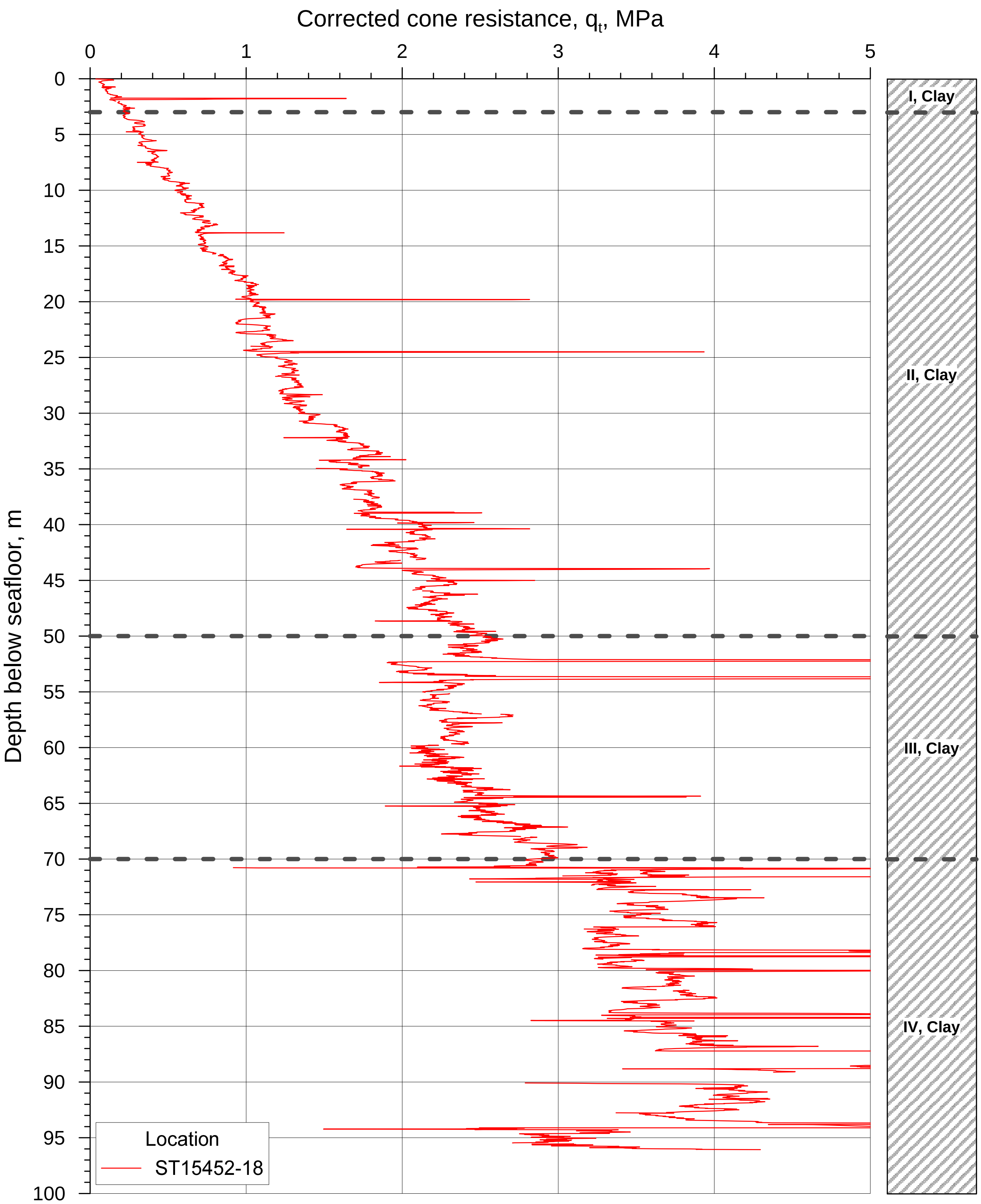

P:\2014\08\20140857\Leveransedokumenter\Rapport\20140857-02-R Data interpretation and evaluation\Figures\Section H\Figure H_06_02, qt versus depth-East.grf

Date/Rev.: 2015-01-21/01

ST15452 Flemish Pass Geotechnical Investigation	Document No. 20140857-02-R
Corrected cone resistance versus depth East Slope	Figure No. H6.2
	Date 2016-04-03 / Drawn by VBS
	NGI

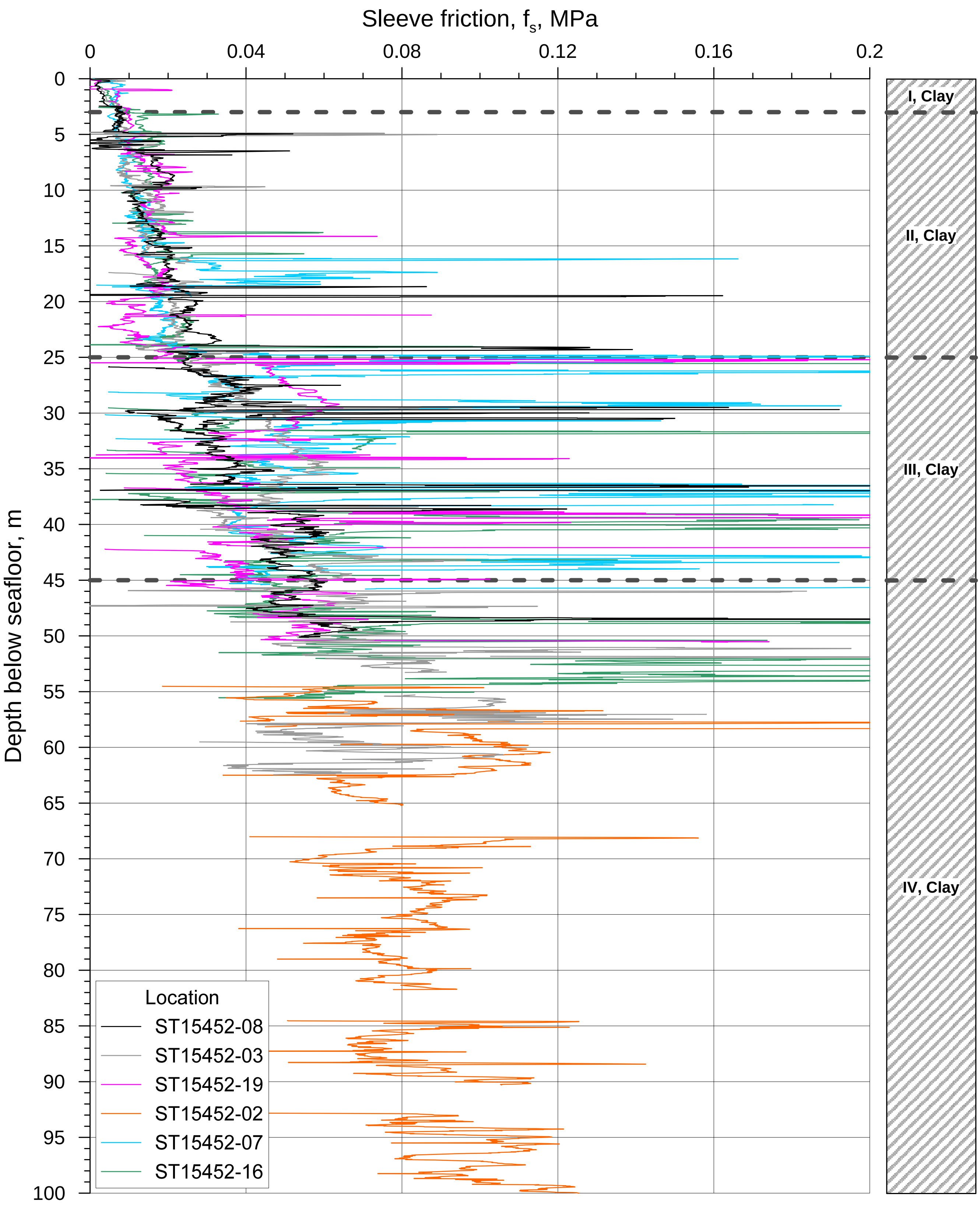

ST15452 Flemish Pass Geotechnical Investigation	Document No. 20140857-02-R
Sleeve friction versus depth West Slope	Figure No. H6.3
	Date 2016-04-04 / Drawn by VBS

NGI

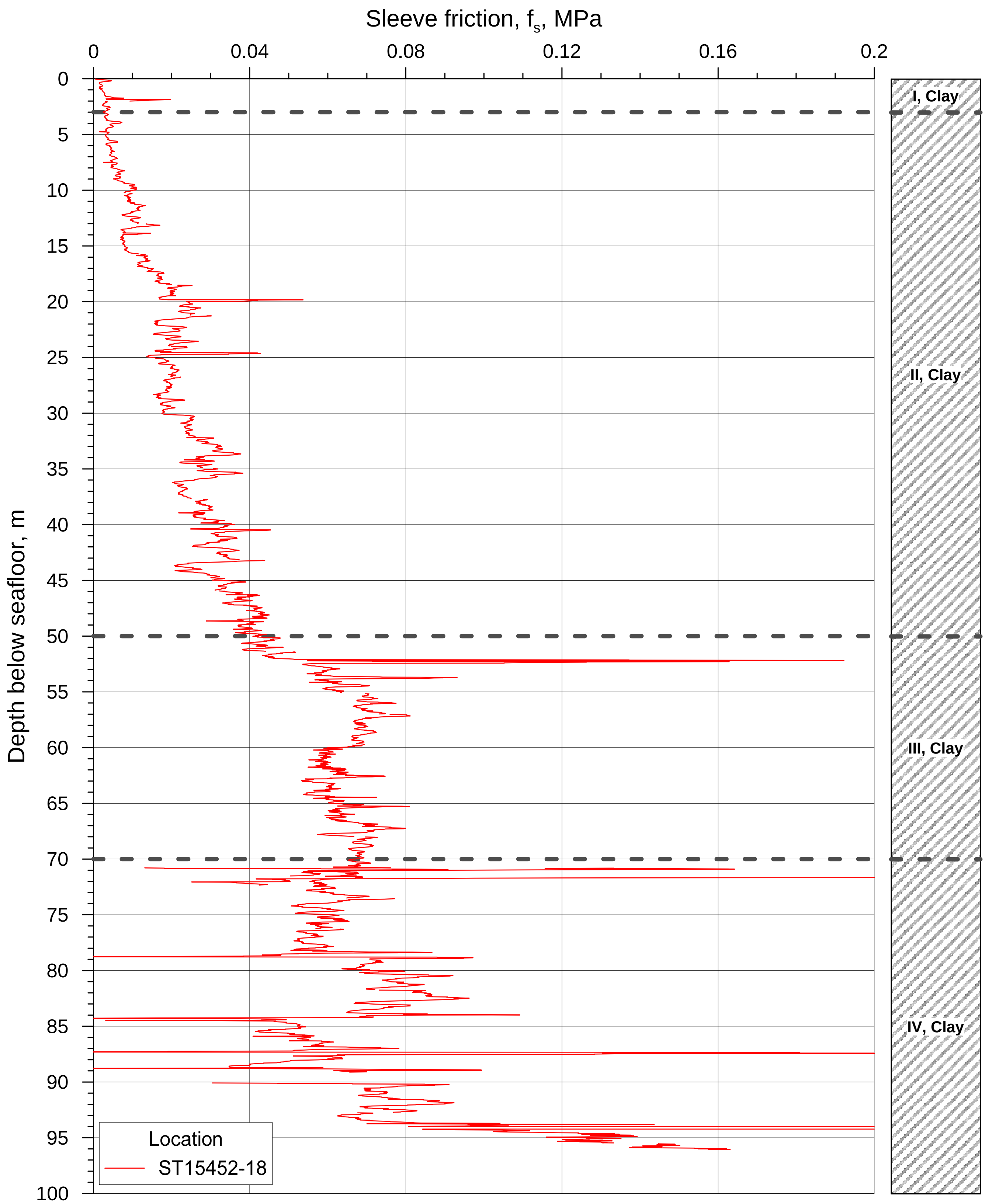

Date/Rev.: 2015-01-21/01

ST15452 Flemish Pass Geotechnical Investigation

Sleeve friction versus depth
East Slope

Document No.	
20140857-02-R	
Figure No.	
H6.4	
Date	Drawn by
2016-04-04	VBS

NGI

P:\2014\08\20140857\Leveransedokumenter\Rapport\20140857-02-R Data interpretation and evaluation\Figures\Section H\Figure H_06_04, fs versus depth-East.grf

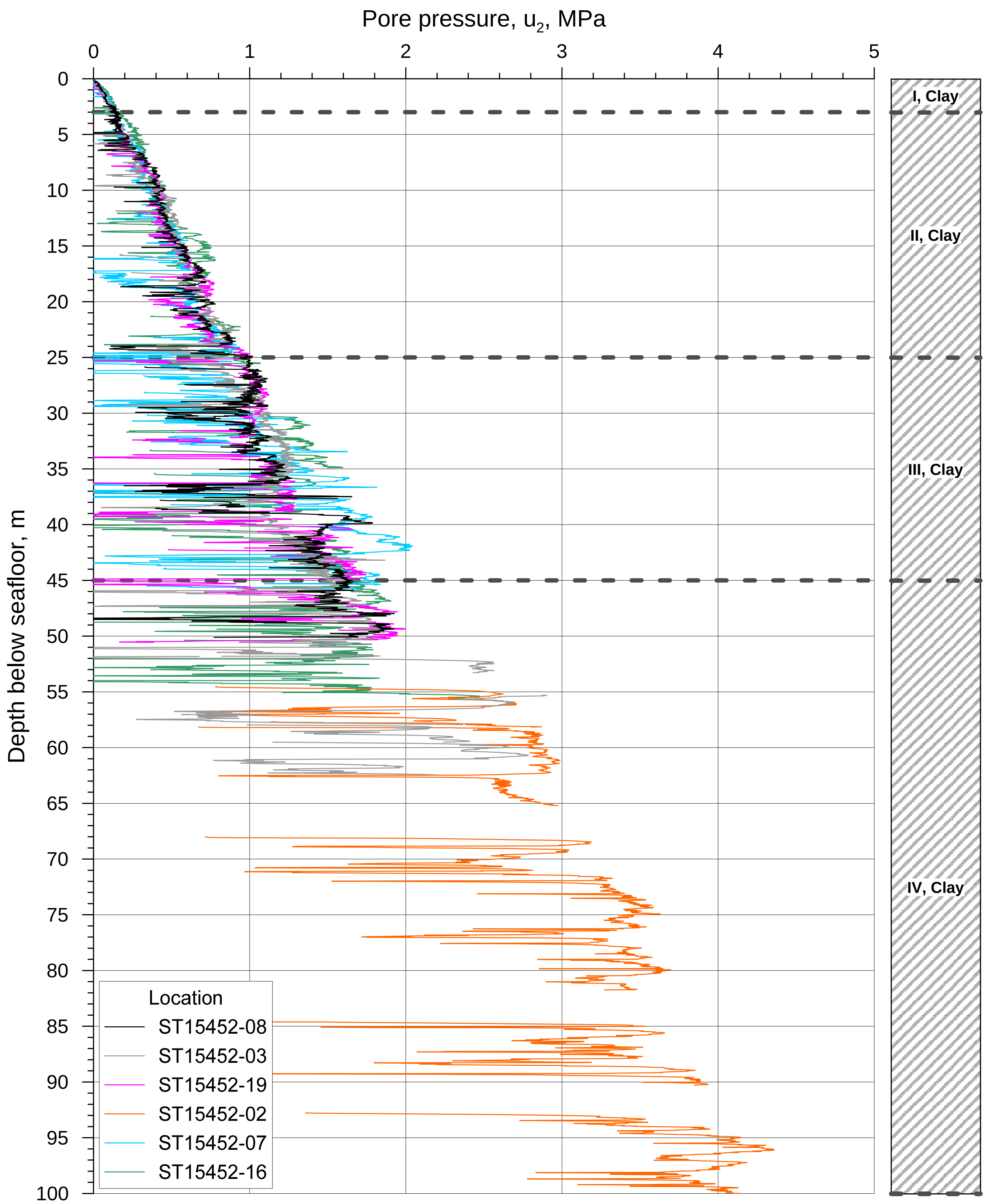

P:\2014\08\20140857\Leveransedokumenter\Rapport\20140857-02-R Data interpretation and evaluation\Figures\Section H\Figure H_06_05, u2 versus depth-West.grf

Date/Rev.: 2015-01-21/01

ST15452 Flemish Pass Geotechnical Investigation	Document No. 20140857-02-R
Pore pressure versus depth West Slope	Figure No. H6.5
	Date 2016-04-03 / Drawn by VBS

NGI

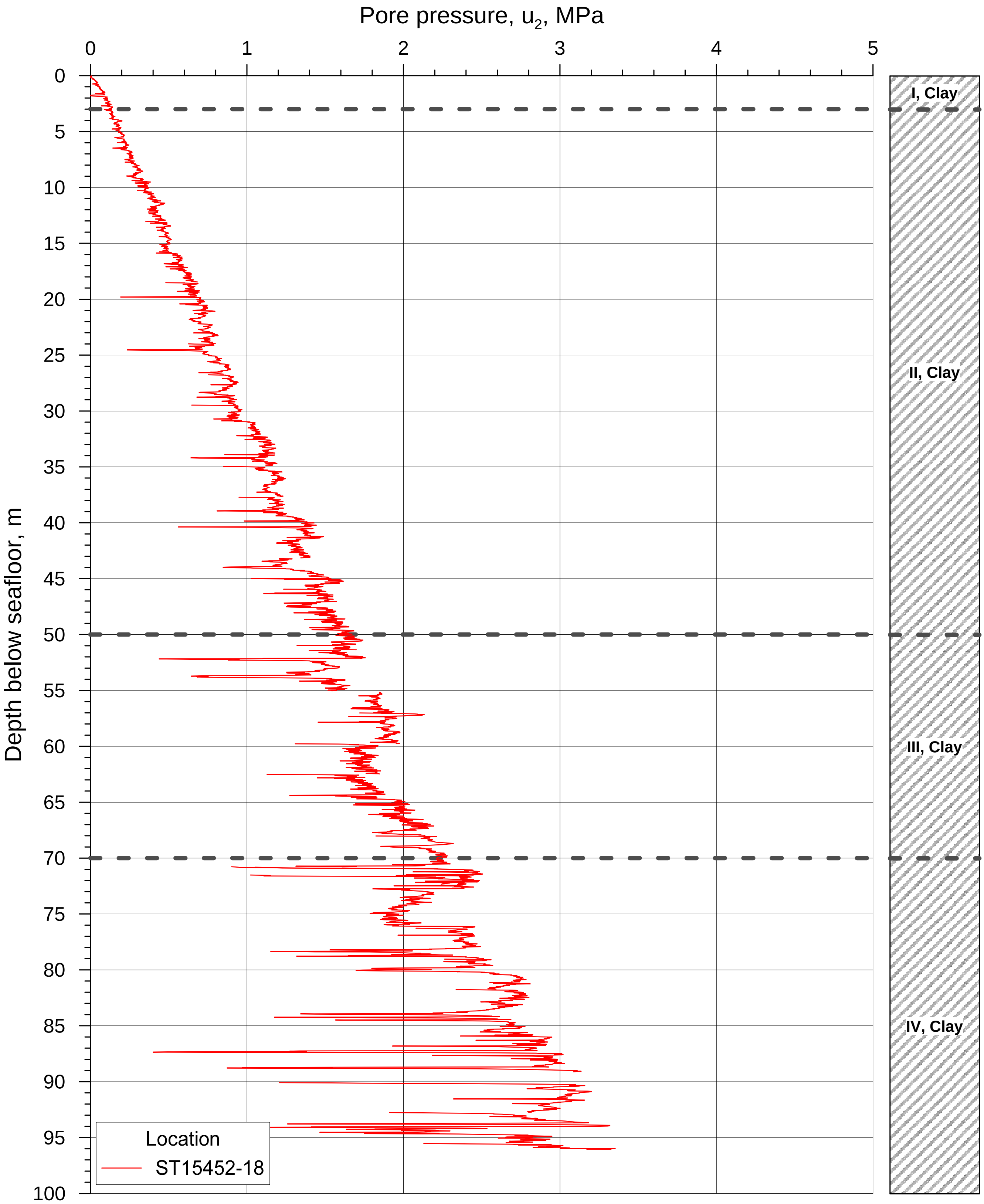

Date/Rev.: 2015-01-21/01

ST15452 Flemish Pass Geotechnical Investigation

Pore pressure versus depth
East Slope

Document No. 20140857-02-R	
Figure No. H6.6	
Date 2016-04-03	Drawn by VBS

NGI

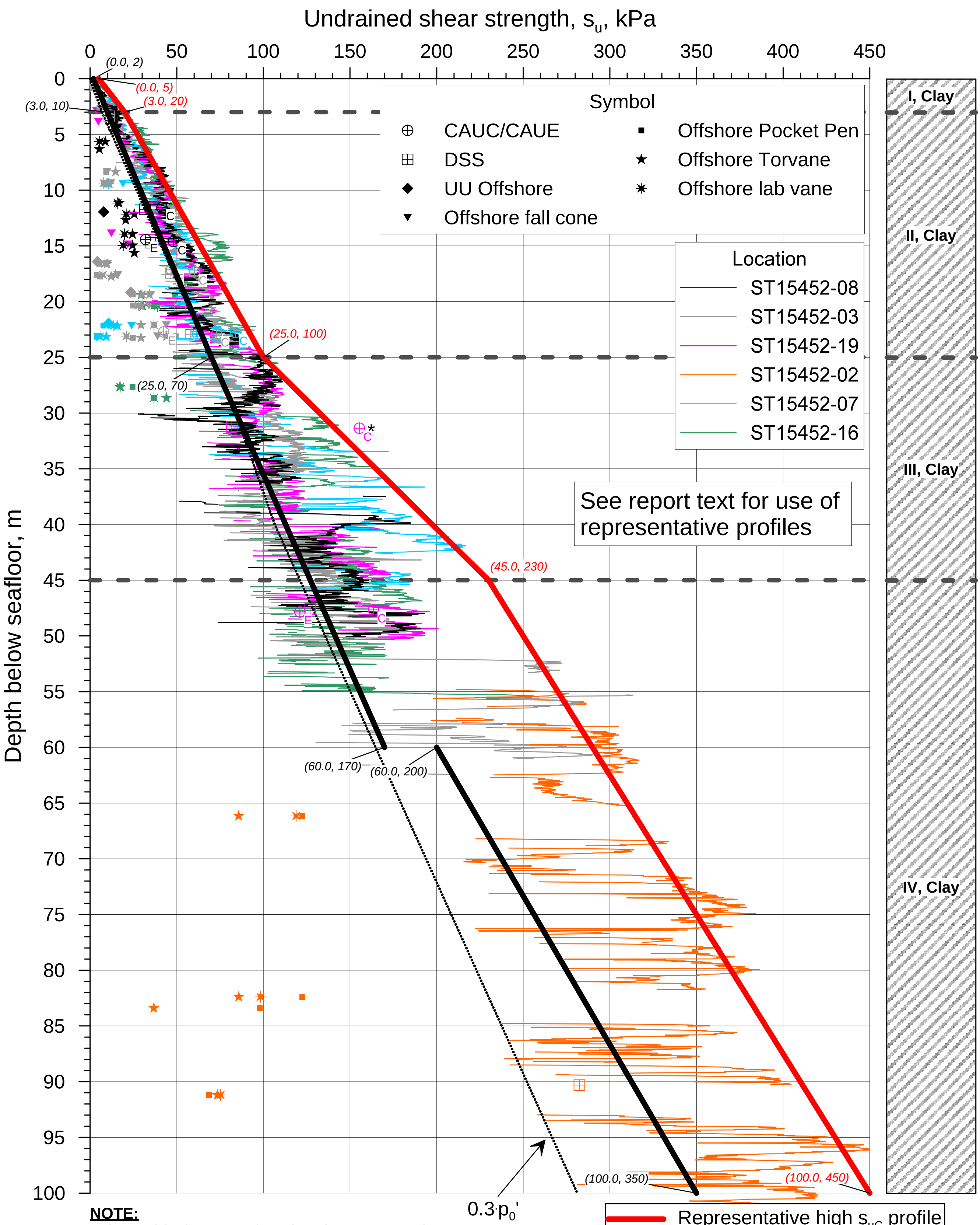

Representative high s_{uC} profile
Representative low s_{uC} profile

NOTE:
u_2 is used for interpretation of s_{uC} from CPTU using $N_{\Delta u}$ = 7.5
Representative profile based on engineering judgement.

* Test representative of silty/sandy layer and not given weight in s_u interpretation

Label: *(depth, value)*

Date/Rev.: 2015-01-21/01

P:\2014\08\20140857\Leveransedokumenter\Rapport\20140857-02-R Data interpretation and evaluation\Figures\Section H\Figure H_06_07, su versus depth-West.grf

ST15452 Flemish Pass Geotechnical Investigation	Document No. 20140857-02-R
Undrained shear strength versus depth West Slope	Figure No. H6.7
	Date 2016-04-04 / Drawn by VBS

NGI

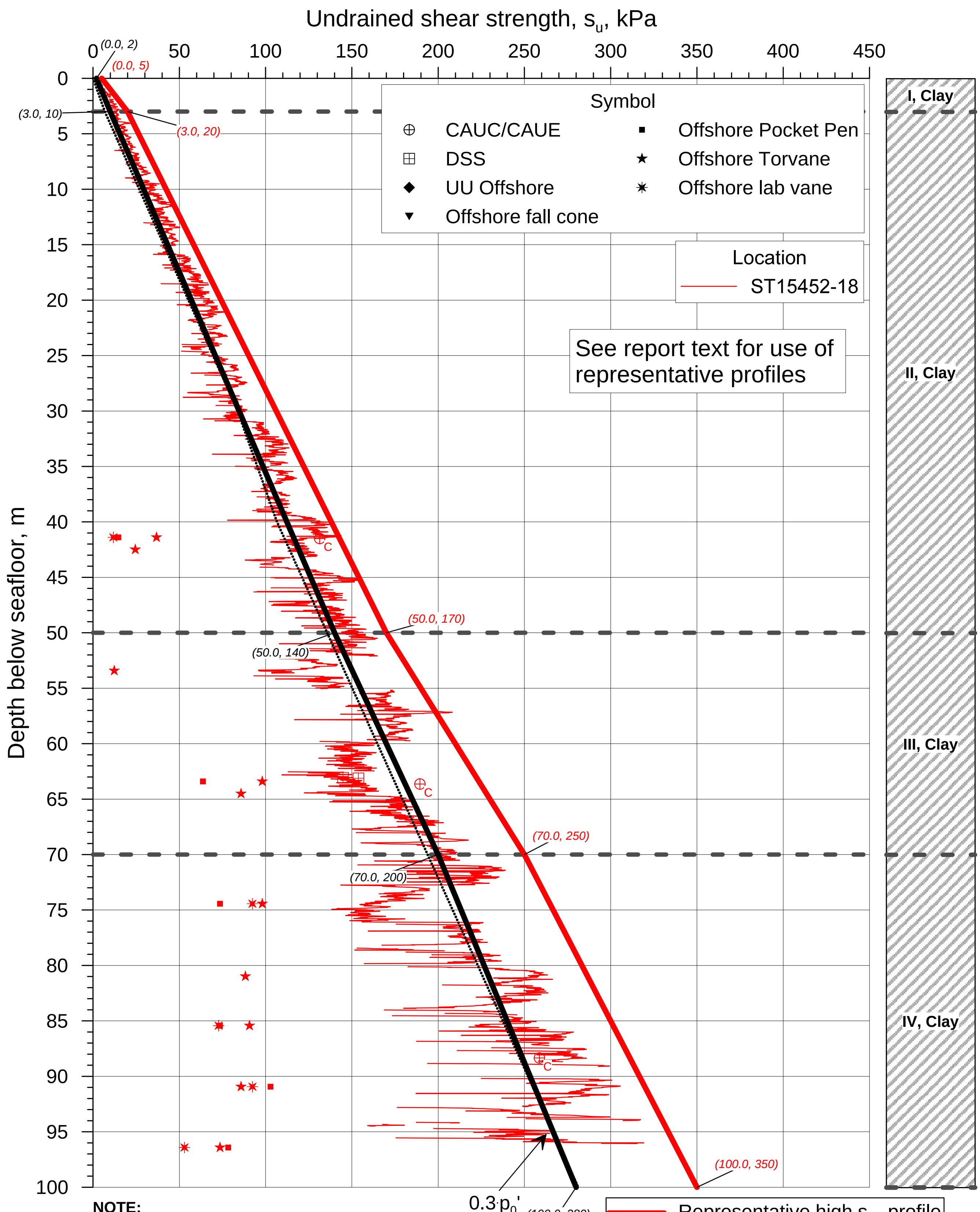

NOTE:
u_2 is used for interpretation of s_{uC} from CPTU using $N_{\Delta u}$ = 7.5
Representative profile based on engineering judgement.

Representative high s_{uC} profile
Representative low s_{uC} profile

Label: *(depth, value)*

Date/Rev.: 2015-01-21/01

P:\2014\08\20140857\Leveransedokumenter\Rapport\20140857-02-R Data interpretation and evaluation\Figures\Section H\Figure H_06_08, su versus depth-East.grf

ST15452 Flemish Pass Geotechnical Investigation	Document No. 20140857-02-R
Undrained shear strength versus depth East Slope	Figure No. H6.8
	Date 2016-04-04 / Drawn by VBS
	NGI

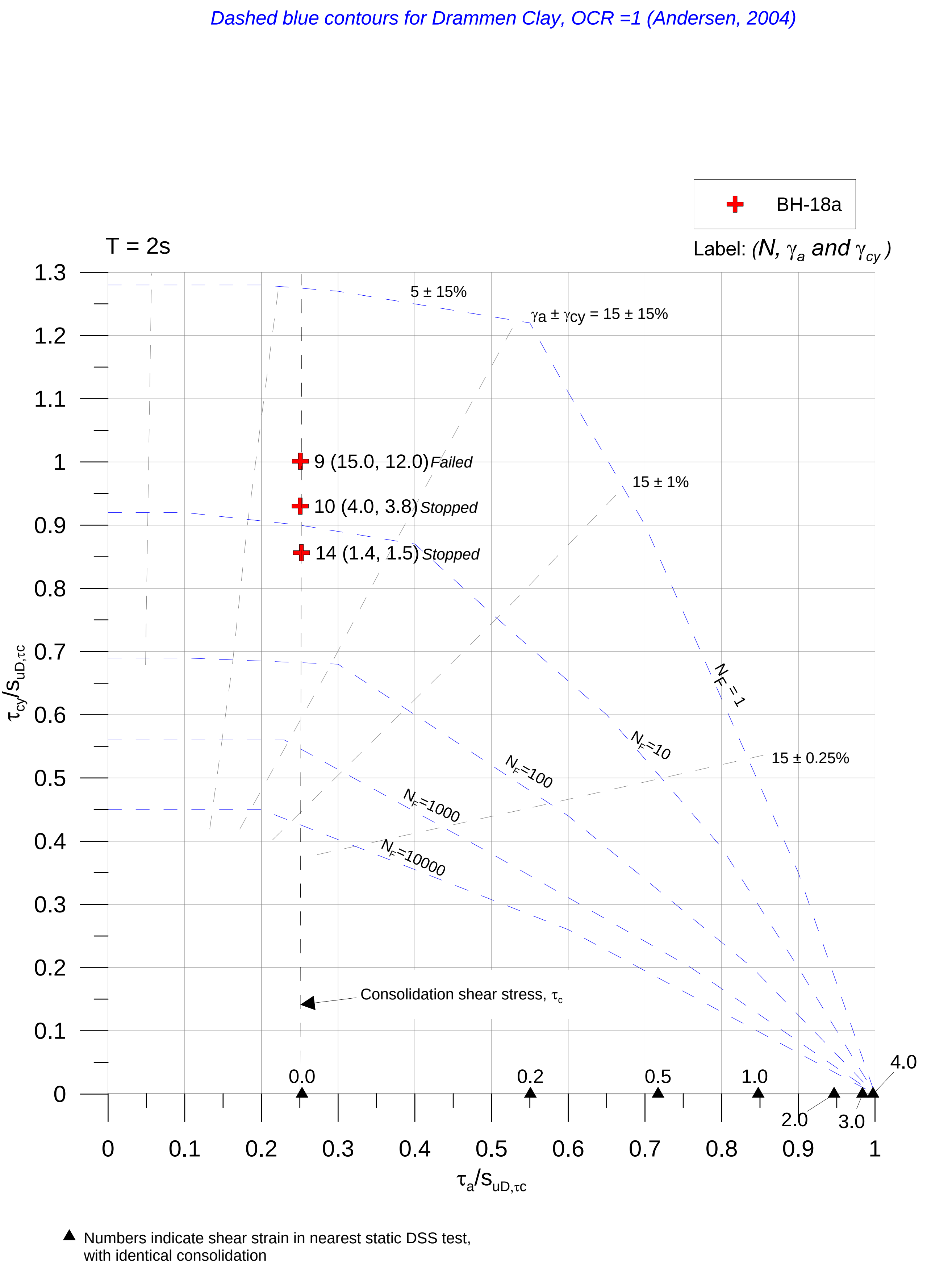

ST15452 Flemish Pass Geotechnical Investigation

Cyclic DSS tests East Slope
Average and cyclic shear stress normalised to the nearest static DSS
The closest static DSS consolidated with a shear stress

Document No.	20140857-02-R
Figure No.	H7.1
Date	2016-04-03
Drawn by	VDa

NGI

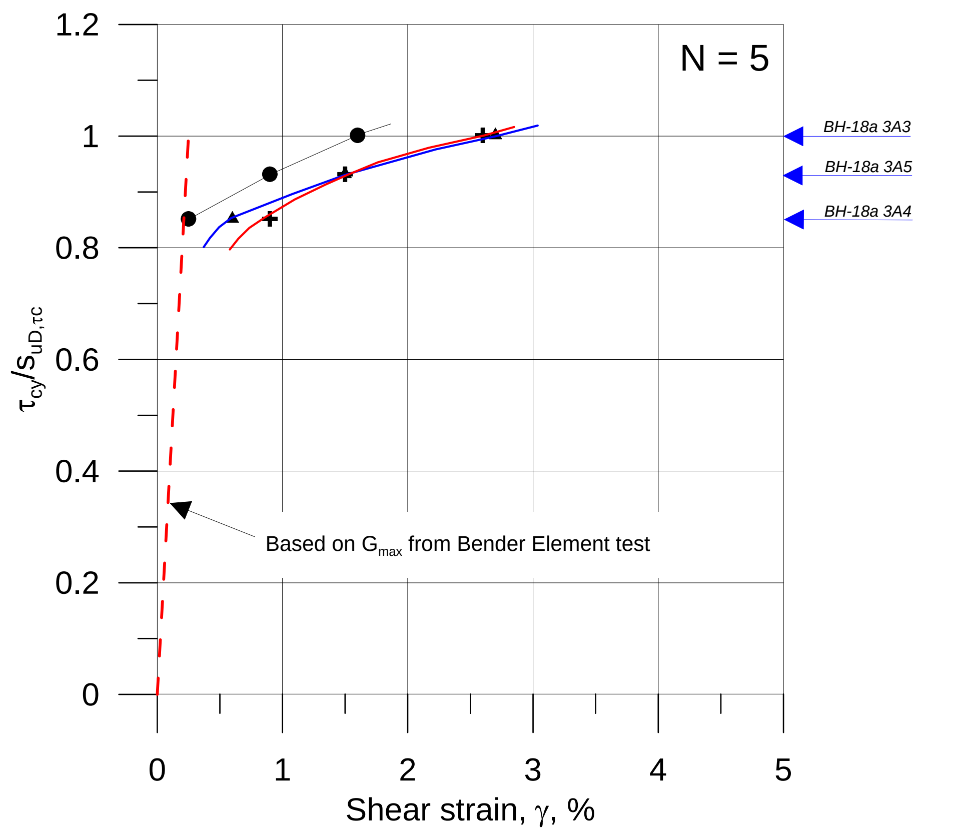

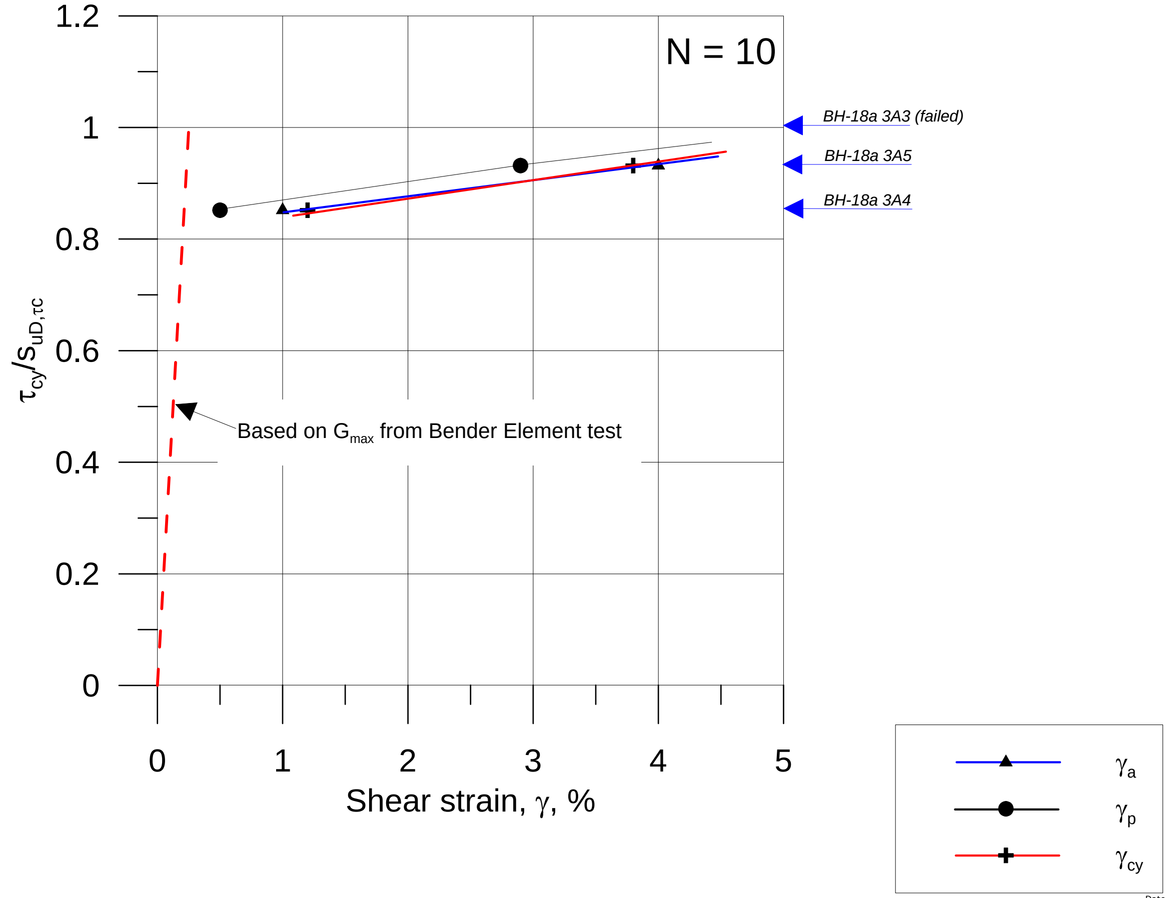

Date/Rev.: 2015-01-21/01

ST15452 Flemish Pass Geotechnical Investigation	Document No. 20140857-02-R	
Cyclic DSS tests East Slope Cyclic shear stress normalised to the nearest static DSS versus shear strain	Figure No. H7.2	
	Date 2016-04-03	Drawn by VDa
	NGI	

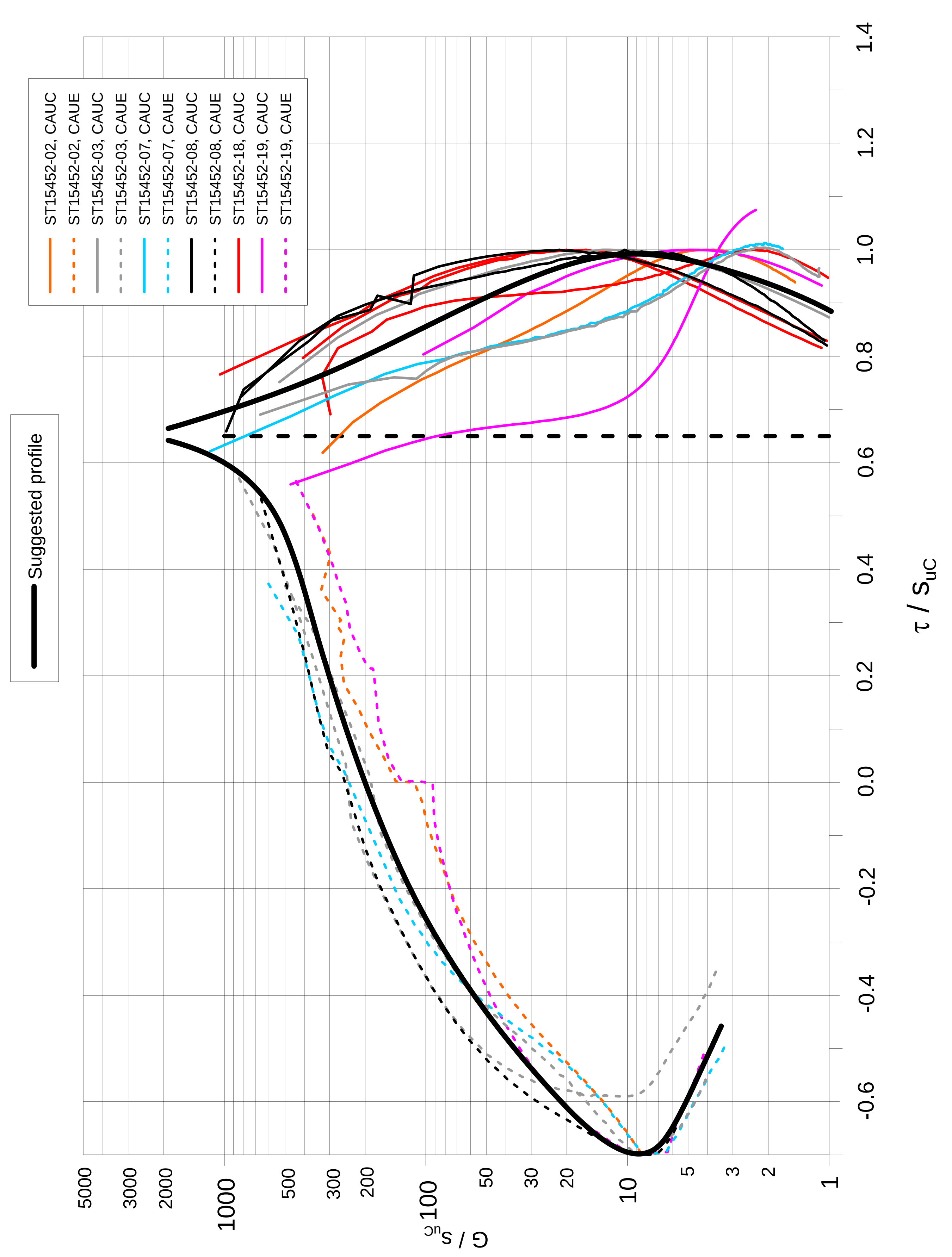

Date/Rev.: 2015-01-21/01

ST15452 Flemish Pass Geotechnical Investigation

G/s_{uC} versus τ/s_{uC} from CAU triaxial tests. Ratio τ_c/s_{uC} = 0.65
West Slope and East Slope

Document No.	20140857-02-R
Figure No.	H8.1
Date 2016-04-04	Drawn by VDa

P:\2014\08\20140857\Leveransedokumenter\Rapport\20140857-02-R Data interpretation and evaluation\Figures\Section H\Figure H_08_01, G_su_triax vs tau_su_triax_Slopes.grf

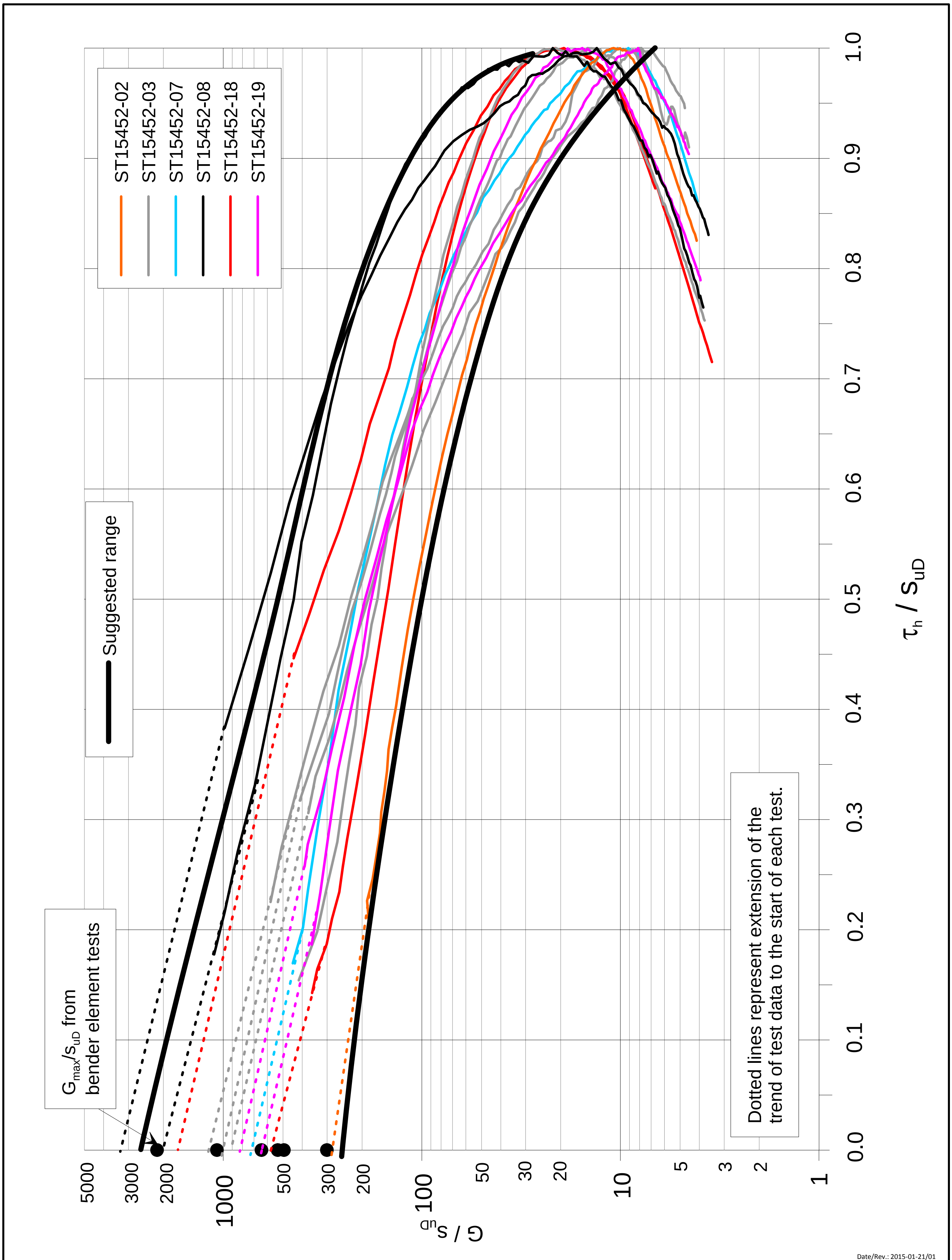

Date/Rev.: 2015-01-21/01

ST15452 Flemish Pass Geotechnical Investigation

G/s_{uD} versus τ/s_{uD} from DSS tests
West Slope and East Slope

Document No.	20140857-02-R
Figure No.	H8.2
Date	2016-04-03
Drawn by	VDa

NGI

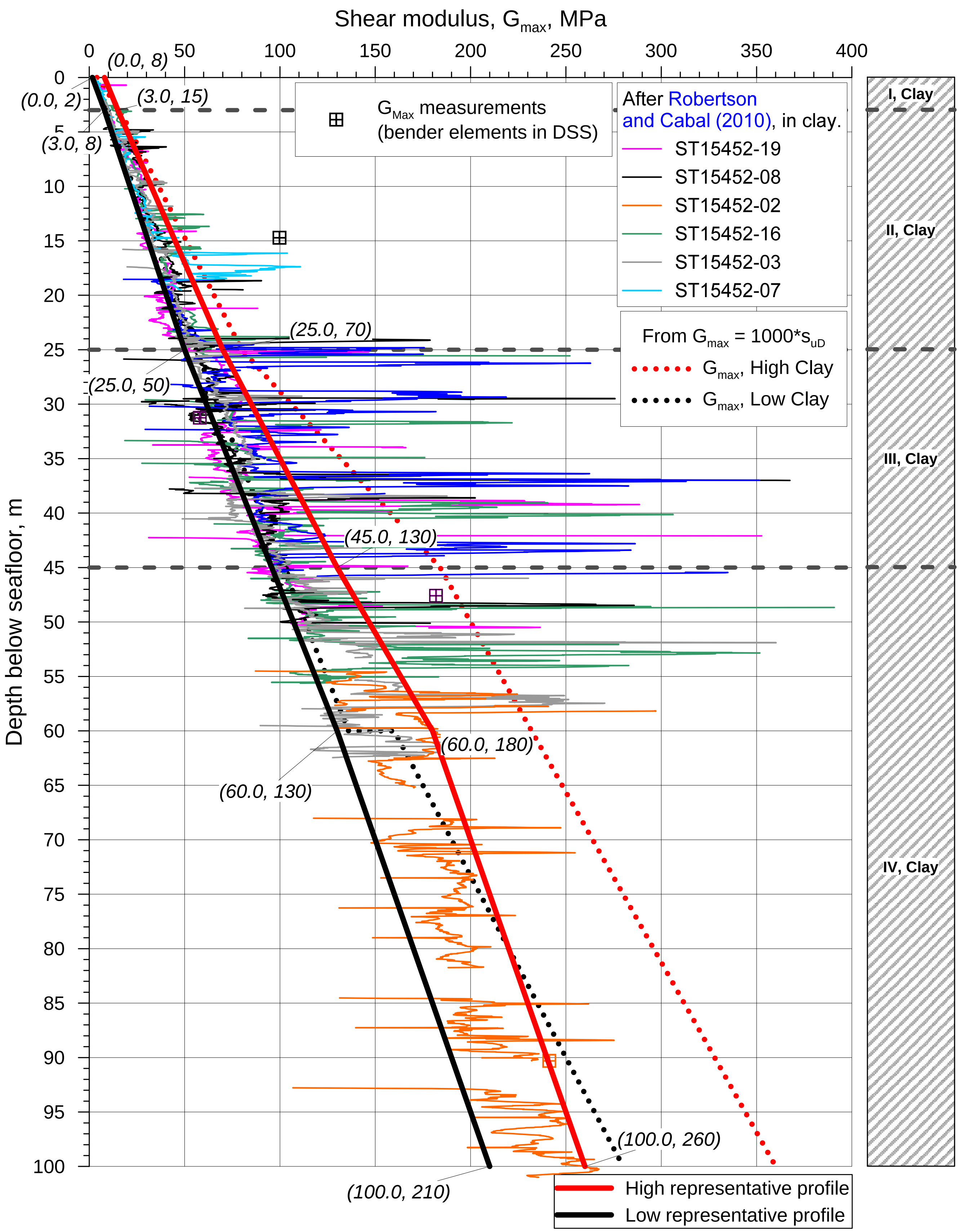

Label: *(depth, value)*

Date/Rev.: 2015-01-21/01

P:\2014\08\20140857\Leveransedokumenter\Rapport\20140857-02-R Data interpretation and evaluation\Figures\Section H\Figure H_08_03, Gmax versus depth_Westslope.grf

ST15452 Flemish Pass Geotechnical Investigation	Document No. 20140857-02-R	
Maximum shear modulus versus depth West Slope	Figure No. H8.3	
	Date 2016-04-03	Drawn by VDa
	NGI	

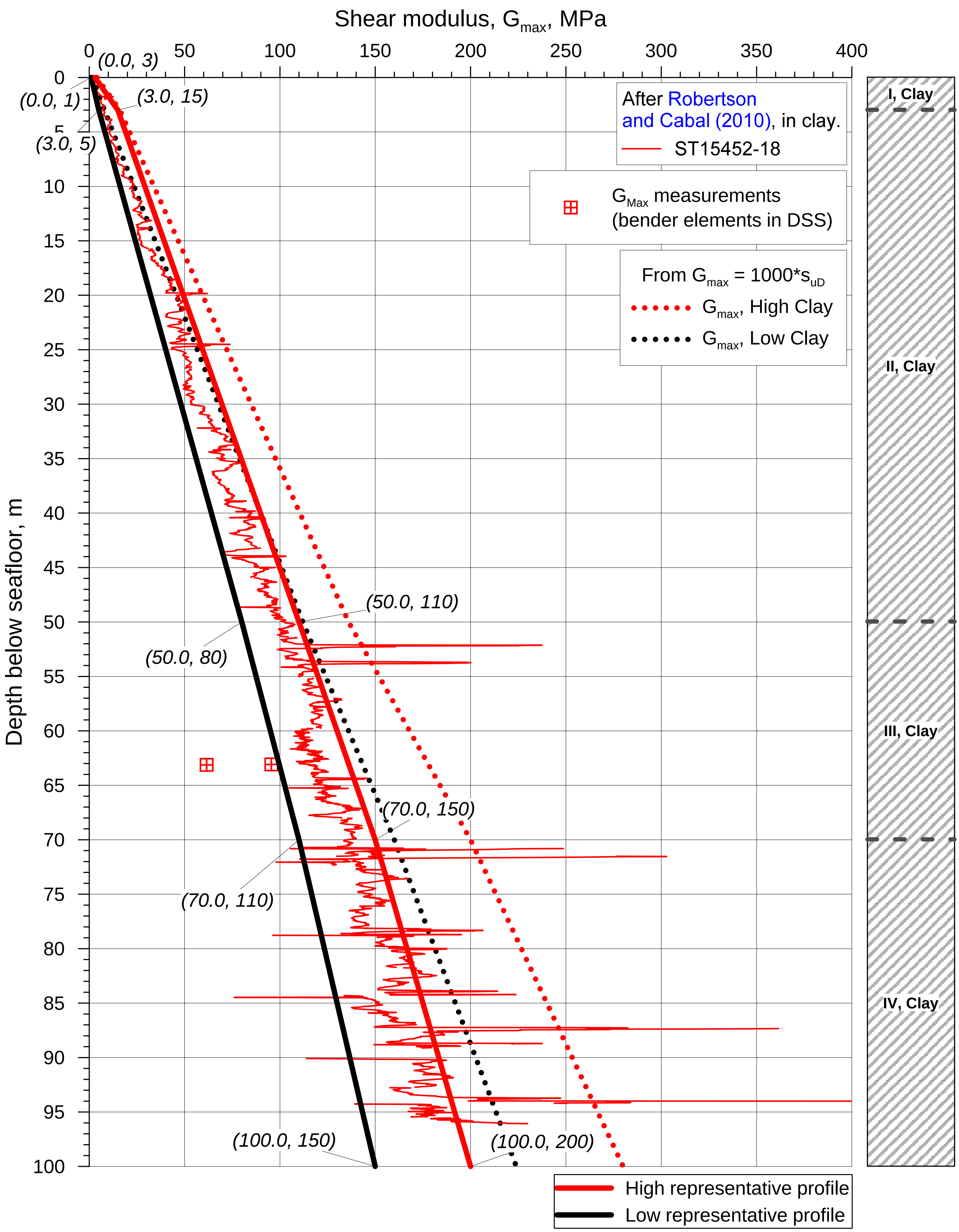

Label: *(depth, value)*

Date/Rev.: 2015-01-21/01

ST15452 Flemish Pass Geotechnical Investigation	Document No. 20140857-02-R
Maximum shear modulus versus depth East Slope	Figure No. H8.4
	Date 2016-04-03 / Drawn by VDa

NGI

P:\2014\08\20140857\Leveransedokumenter\Rapport\20140857-02-R Data interpretation and evaluation\Figures\Section H\Figure H_08_04, Gmax versus depth_Eastslope.grf

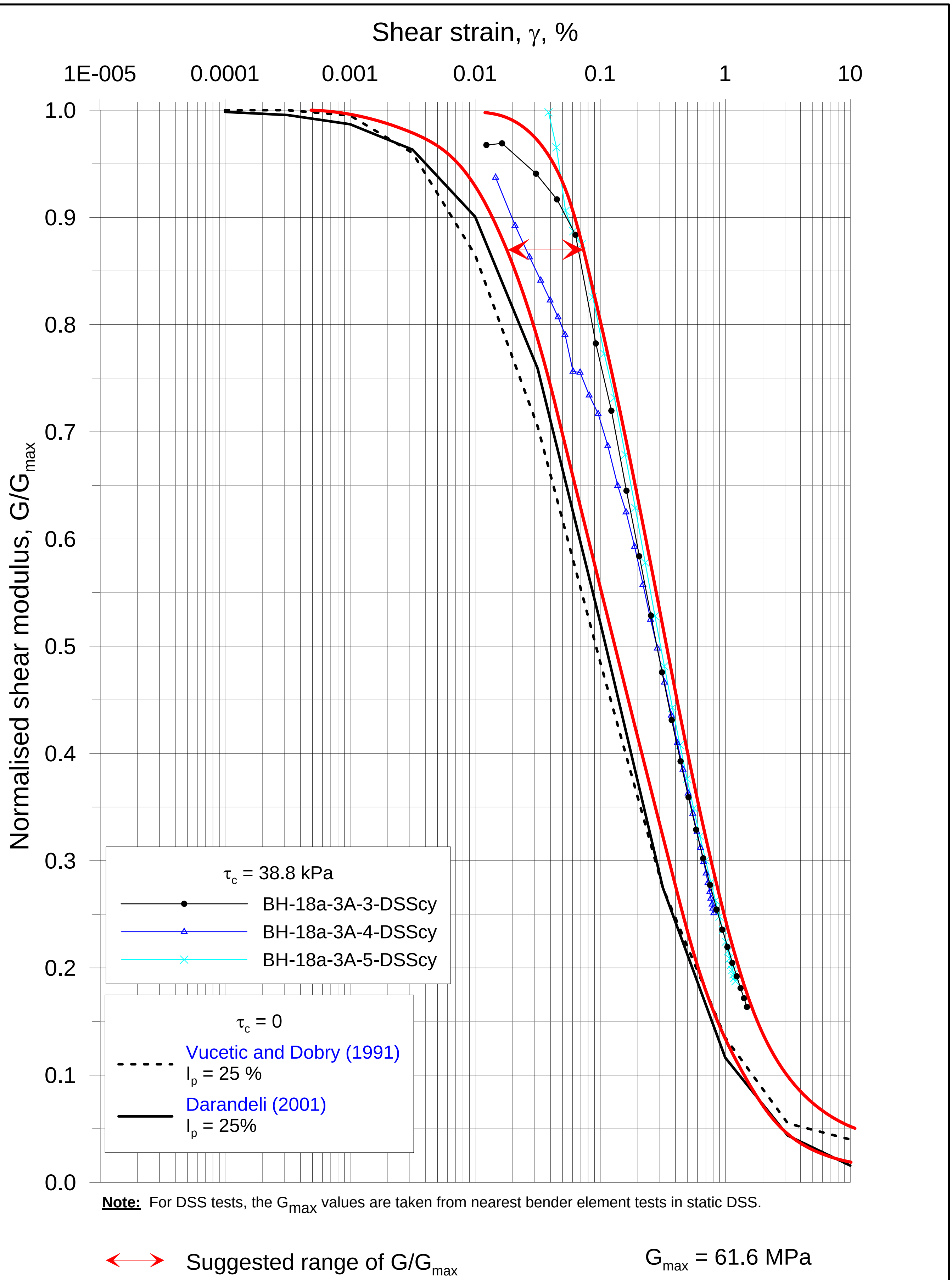

Date/Rev.: 2015-01-21/01

P:\2014\08\20140857\Leveransedokumenter\Rapport\20140857-02-R Data interpretation and evaluation\Figures\Section H\Figure H_08_05, NormalizedGmax versus shear strain_N=1_East_slope.grf

ST15452 Flemish Pass Geotechnical Investigation	Document No. 20140857-02-R	
Normalised shear modulus, G/G_{max}, versus shear strain East Slope N=1 cycle	Figure No. H8.5	
	Date 2016-04-03	Drawn by VDa
	NGI	

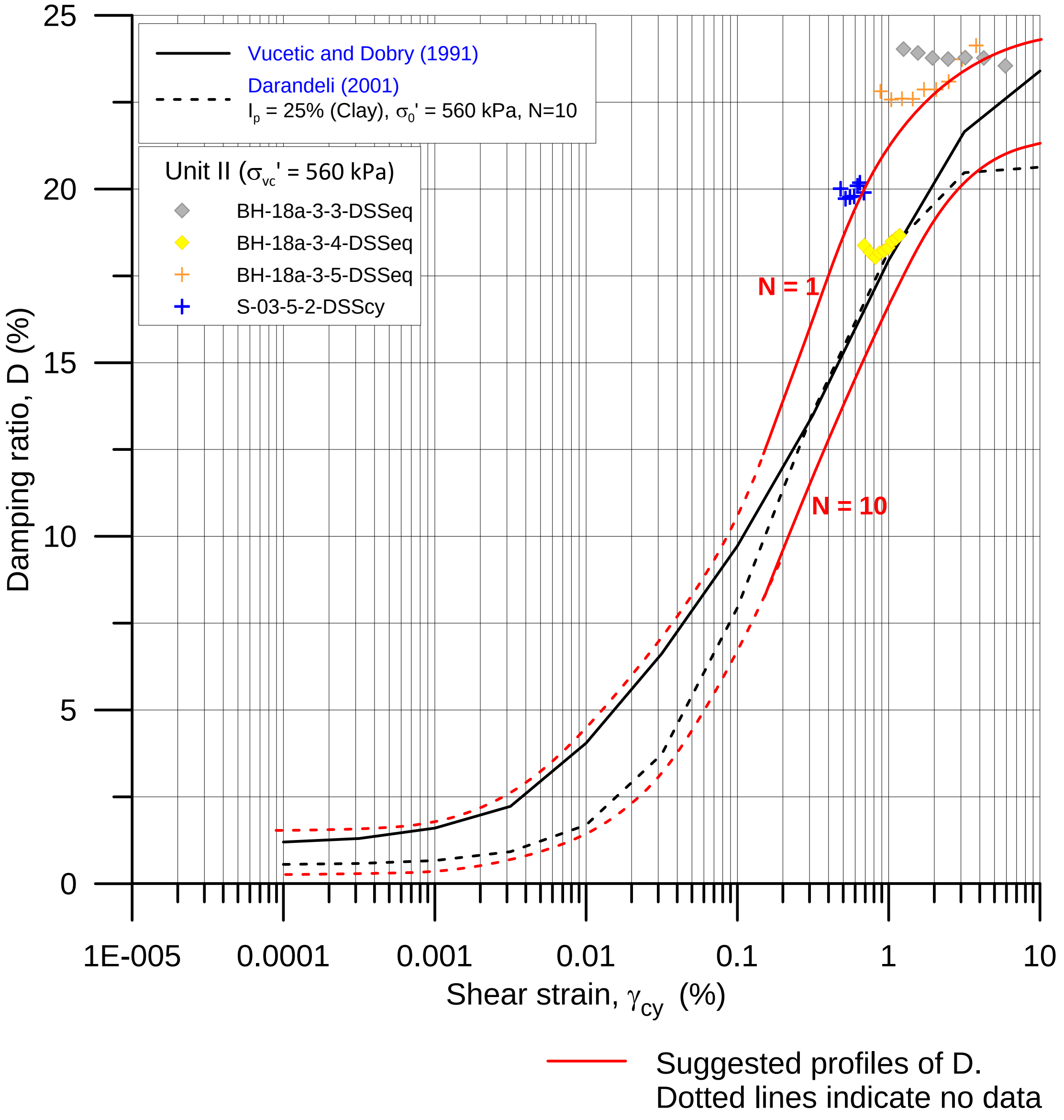

P:\2014\08\20140857\Leveransedokumenter\Rapport\20140857-02-R Data interpretation and evaluation\Figures\Section H\Figure H_08_06, Damping versus shear strain_East_slope.grf

Date/Rev.: 2015-01-21/01

ST15452 Flemish Pass Geotechnical Investigation	Document No. 20140857-02-R
Damping ratio, D, versus cyclic shear strain from symmetric cyclic DSS tests East Slope	Figure No. H8.6
	Date 2016-04-03 / Drawn by VDa

NGI

Section I

RECOMMENDATIONS ON ADDITIONAL DATA

Contents

I1 General

This section contains information on what parts of the data presented in the report would benefit from further investigation, additional sampling or other additional work. The data and recommendations given in previous sections are valid as they stand, and recommendations given here are intended as informative.

I2 Additional data

The soil variation over short depth ranges may be of importance for many analyses. The variation at specific locations and testing of specific layers should be part of a second investigation giving input to design. It is then possible to target testing towards layers that are believed to be of special importance. The soil parameters presented in this report should also be confirmed at locations where there are limited or no data in certain depth intervals.

The thixotropy results are outside of the range of published data. Only two test were performed. If strength regain of the magnitude indicated by the two test are to be used in design, it is recommended that further thixotropy tests are performed. Another way to investigate the same phenomenon is to perform DSS test on remoulded material that is consolidated back to the relevant stress in the DSS cell. It is recommended that such tests are done, especially for anchor design.

There are clear indications of gas in the samples based on cracking of samples, and from testing of gas found in the cracks. The amount of gas found in situ can be investigated by the use of an in situ probe similar to the BAT probe to sample the pore water directly.

The cyclic program performed is limited to Unit II and should be complemented by more extensive testing, both in Unit II and other units for detailed structural design. Depending on the outcomes of a future geo-hazard study, further testing for earth quake susceptibility may be relevant.

The sample quality leaves some uncertainty about the interpreted data. Sample quality should be focus of a later additional sampling campaign at Flemish Pass taking the apparently difficult conditions into account. The area ratio of the sampler is one factor playing a role in the quality of the samples (e.g. Tjelta & Yetginer, 2010 and NGI 2010) that should be considered in a future investigation. If soil strength is to be derived directly from SHANSEP results, a more thorough program of testing should be performed in order to understand the influence of the layering on the stress dependence of the soil strength.

It is suggested that the use of seismic CPT (SCPT) will give additional valuable data in terms of V_s and G_{max}.

There is the possibility to develop area specific correlations between measured CPT sleeve friction (f_s) and remoulded shear strength and sensitivity and normalized friction ratio ($F_r = f_s/q_{net}$). The estimates of sensitivity can also be found from $S_t = N_S/F_r$ where N_s is an empirical constant that has to be determined.

Further age dating tests by Amino acid racemisation will become available in the near future. If these tests are successful and results are coherent with results presented herein, the established age model will likely be sufficiently reliable.

Section J

REFERENCES

Contents

J1 References

References in Section E are listed at the end of the section.

American Society for Testing and Materials (2004)
ASTM Standard D 2487-00
Standard test method for classification of soils for engineering purposes.

Andresen, A., T. Berre, A. Kleven and T. Lunne (1979)
Procedures used to obtain soil parameters for foundation engineering in the North Sea.
Marine Geotechnology, Vol. 3, No. 3, pp. 201-266. Also publ. in: Norwegian Geotechnical Institute, Publication, 129.

Andersen, K.H. (2004)
Cyclic clay data for foundation design of structures subjected to wave loading.
Invited lecture: International Conference on Cyclic Behaviour of Soils and Liquefaction Phenomena, Bochum, Germany (19 pages).

Andersen, K. H., T. Lunne, T. J. Kvalstad and C. F. Forsberg (2008)
Deep Water Geotechnical Engineering
Proceedings of the XXIV Nat. Conf. of the Mexican Soc. of Soil Mechanics, Agualscalientes, 26-29 Nov. 2008

Andersen, K.H. and K. Schjetne (2013)
Database of friction angles of sand and consolidation characteristics of sand, silt and clay.
ASCE J. of Geotechnical and Environmental Engrg., Vol. 139, No. 7, July 1, 2013.

Andersen, K.H (2015)
The Third ISSMGE McClelland Lecture - Cyclic soil parameters for offshore foundation design.
Third International Symposium on Frontiers in Offshore Geotechnics (ISFOG 2015), 10-12 June, Oslo, Norway.

Becker, D.E., J.H. Crooks, K. Been and M.G. Jefferies (1987)
Work as a criterion for determining in situ and yield stresses in clay.
Canadian Geotechnical Journal, Vol. 24, pp. 549

Benthic (2015a)
ST15452 Flemish Pass Geotechnical Investigation, Field Report – Volume 1: Geotechnical Data
Document No. 12399-RP-1-0, dated 13 November 2015

Benthic (2015b)
ST15452 Flemish Pass Geotechnical Investigation, Field Report – Volume 2: Operations
Document No. 12399-RP-1-0, dated 13 November 2015

Brooker, E.W. and H.O. Ireland (1965)
Earth pressures at rest related to stress history. Canadian
Geotechnical Journal, Vol. 2, No. 1, pp. 1-15.

Casagrande, A. (1936)
The determination of the pre-consolidation load and its practical significance.
International Conference on Soil Mechanics and Foundation Engineering, 1.
Cambridge, Mass. 1936. Proceedings, Vol. 3, pp.60-64.

Darandeli, M.B (2001)
Development of a new family of normalized modulus reduction and material damping curves. Ph.D. Dissertation. The University of Texas at Austin. August, 2001.

DeGroot, D.J., Lunne, T., Andersen, K.H., Boscardin, A.G. (2012)
Laboratory measurement of the remoulded shear strength of clays with application to design of offshore infrastructure.
Offshore Site Investigation and Geotechnics, SUT Conference, London 12-14 September 2012, Proc. 7th International Conference, pp. 355-364.

ISO 14688-1 (2002)
Geotechnical investigation and testing - Identification and classification of soil
Part 1: Identification and description

ISO 14688-2 (2004)
Geotechnical investigation and testing - Identification and classification of soil
Part 2: Principles for a classification

ISO 19901-8 (2014)
Petroleum and natural gas industries - Specific requirements for offshore structures - Part 8: Marine soil investigations

Janbu, N. (1963)
Soil compressibility as determined by oedometer and triaxial tests.
European Conference on Soil Mechanics and Foundation Engineering, Wiesbaden, Proceedings, Vol. 1, pp. 19-25.

Janbu, N. (1970)
Grunnlag i geoteknikk
Tapir forlag, 1970

Johansen, Ø. (1975)
Thermal conductivity of soils. Ph.D diss., Norwegian Technical Univ., Trondheim; also U.S. Army cold Reg. Res. Eng. Lab. Transl. 637, July 1977.

Karlsrud, K., Lunne, T., Kort, D.A. and Strandvik, S. (2005)
CPTU correlations for clays.
International Conference on Soil Mechanics and Foundation Engineering, 16. Osaka 2005. Proceedings, Vol. 2, pp. 693-702.

Lunne, T., P.K. Robertson and J.J.M. Powell (1997)
Cone Penetration Testing in Geotechnical Practice.
Blackie Academic & Professional. London, 1997.

Lunne, T., T. Berre and S. Strandvik (1998)
Sample disturbance effects in deepwater soil investigations.
SUT Conference on Soil Investigations and Foundation Behaviour.
London Sept. 1998. Proceedings pp. 199-220.

NGI (2010)
Luva 2009 Soil Investigation. Geotechnical report.
NGI Report No. 20091764-00-3-R, dated 30 August 2010.

NGI (2016)
ST15452 Flemish Pass Geotechnical Investigation. Measured and derived geotechnical parameters and final results.
NGI Doc. no. 20140857-01-R, 8 April 2016.

Norwegian Geotechnical Society (NGF). (2011)
Veiledning for symboler og definisjoner i geoteknikk.
Identifisering og klassifisering av jord.

Robertson, P. K. (1990)
Soil Classification using the CPT
Canadian Geotechnical Journal, 1991, Vol. 28, pp. 113-126

Robertson, P. K. and Cabal, K.L. (2010)
Guide to Cone Penetration Testing for Geotechnical Engineering, Gregg Drilling & Testing, Inc., 4th Edition, 2010.

Tjelta, T.I. and A.G. Yetginer (2010)
Luva deepwater site investigation programme and findings.
Second International Symposium on Frontiers in Offshore Geotechnics (ISFOG 2010), 8-10 November, Perth, Australia.

Vucetic, M. and R. Dobry (1991)
Effect of Soil Plasticity on Cyclic Response.
Journal of Geotechnical Engineering, ASCE, Vol. 117(1), pp 89-107.

Kontroll- og referanseside/ Review and reference page

Dokumentinformasjon/*Document information*		
Dokumenttittel/*Document title* Data interpretation and evaluation		**Dokumentnr./*Document no.*** 20140857-02-R
Dokumenttype/*Type of document* Rapport / Report	**Distribusjon/*Distribution*** Begrenset/Limited	**Dato/*Date*** 2016-05-24 **Rev.nr.&dato/Rev.no.&date** 1 / 2016-05-30
Oppdragsgiver/*Client* Benthic – Statoil Canada ltd.		
Emneord/*Keywords* Slope stability, laboratory testing, soil investigation		

Stedfesting/*Geographical information*	
Land, fylke/*Country* Canada	**Havområde/*Offshore area***
Kommune/*Municipality*	**Feltnavn/*Field name***
Sted/*Location*	**Sted/*Location***
Kartblad/*Map*	**Felt, blokknr./*Field, Block No.***
UTM-koordinater/*UTM-coordinates* **Zone: East: North:**	

Dokumentkontroll/*Document control*
Kvalitetssikring i henhold til/*Quality assurance according to NS-EN ISO9001*

Rev/ *Rev.*	Revisjonsgrunnlag/*Reason for revision*	Egenkontroll av/ *Self review by:*	Sidemanns-kontroll av/ *Colleague review by:*	Uavhengig kontroll av/ *Independent review by:*	Tverrfaglig kontroll av/ *Inter-disciplinary review by:*
0	Draft	2016-04-04 Victor Smith	2016-04-04 Tom Lunne		
0	Original document	2016-05-19 Victor Smith	2016-05-23 Tom Lunne		
1	Comments from Client	2016-05-30 Victor Smith	2016-05-30 Tom Lunne		

Dokument godkjent for utsendelse/ *Document approved for release*	Dato/*Date*	Prosjektleder/*Project Manager*
	30 May 2016	Victor Smith

NGI (Norwegian Geotechnical Institute) is a leading international centre for research and consulting within the geosciences. NGI develops optimum solutions for society and offers expertise on the behaviour of soil, rock and snow and their interaction with the natural and built environment.

NGI works within the following sectors: Offshore energy – Building, Construction and Transportation – Natural Hazards – Environmental Engineering.

NGI is a private foundation with office and laboratories in Oslo, a branch office in Trondheim and daughter companies in Houston, Texas, USA and in Perth, Western Australia

www.ngi.no

NGI (Norges Geotekniske Institutt) er et internasjonalt ledende senter for forskning og rådgivning innen ingeniørrelaterte geofag. Vi tilbyr ekspertise om jord, berg og snø og deres påvirkning på miljøet, konstruksjoner og anlegg, og hvordan jord og berg kan benyttes som byggegrunn og byggemateriale.

Vi arbeider i følgende markeder: Offshore energi – Bygg, anlegg og samferdsel – Naturfare – Miljøteknologi.

NGI er en privat næringsdrivende stiftelse med kontor og laboratorier i Oslo, avdelingskontor i Trondheim og datterselskaper i Houston, Texas, USA og i Perth, Western Australia.

www.ngi.no

OSLO
TRONDHEIM
HOUSTON
PERTH

NORWEGIAN GEOTECHNICAL INSTITUTE
NGI.NO

Main office
PO Box 3930 Ullevaal St.
NO-0806 Oslo
Norway

Trondheim office
PO Box 5687 Sluppen
NO-7485 Trondheim
Norway

T (+47)22 02 30 00
F (+47)22 23 04 48
NGI@ngi.no

BIC NO. DNBANOKK
IBAN NO26 5096 0501 281
COMPANY NO
958 254 318MVA

ISO 9001/14001
CERTIFIED BY BSI
FS 32989/EMS 612006